



JRC CONFERENCE AND WORKSHOP REPORT

Proceedings of the 24th International Transport and Air Pollution (TAP) Conference

Edited by:
Hausberger, S.
Minarik, S.
Fontaras, G.

2022



International Transport and Air
Pollution Conference

Joint
Research
Centre

This publication is a Conferences and Workshops report by the Joint Research Centre (JRC), the European Commission's science and knowledge service. It aims to provide evidence-based scientific support to the European policymaking process. The scientific output expressed does not imply a policy position of the European Commission. Neither the European Commission nor any person acting on behalf of the Commission is responsible for the use that might be made of this publication. For information on the methodology and quality underlying the data used in this publication for which the source is neither Eurostat nor other Commission services, users should contact the referenced source. The designations employed and the presentation of material on the maps do not imply the expression of any opinion whatsoever on the part of the European Union concerning the legal status of any country, territory, city or area or of its authorities, or concerning the delimitation of its frontiers or boundaries.

Contact information

Name: Georgios Fontaras

Address: European Commission, Joint Research Centre (JRC), via E. Fermi 2479, TP-230 I – 21027 Ispra (VA) /Italy

Email: georgios.fontaras@ec.europa.eu

Tel.: +39 0332 786425

EU Science Hub

<https://ec.europa.eu/jrc>

JRC126978

PDF

ISBN 978-92-76-43803-8

doi:10.2760/019404

Luxembourg: Publications Office of the European Union, 2022

© European Union, 2022



The reuse policy of the European Commission is implemented by the Commission Decision 2011/833/EU of 12 December 2011 on the reuse of Commission documents (OJ L 330, 14.12.2011, p. 39). Except otherwise noted, the reuse of this document is authorised under the Creative Commons Attribution 4.0 International (CC BY 4.0) licence (<https://creativecommons.org/licenses/by/4.0/>). This means that reuse is allowed provided appropriate credit is given and any changes are indicated. For any use or reproduction of photos or other material that is not owned by the EU, permission must be sought directly from the copyright holders.

All content © European Union, 2022

Figures and tables –Source © : International Transport and Air Pollution Conference, 2021

How to cite this report: Hausberger S., Minarik S., Fontaras G., *Proceedings of the 24th International Transport and Air Pollution (TAP) Conference*, Publications Office of the European Union, Luxembourg, 2022, ISBN 978-92-76-43803-8, doi:10.2760/019404, JRC126978.

Contents

Acknowledgements	1
Abstract	2
1. Introduction	3
1.1 Message of the chairman	4
1.2 Organisation	5
1.3 Organisers	5
1.4 Scientific Committee	6
2. Conference Papers	
2.1 Roadmap to zero carbon road transport	7
2.2 Study on a test track of dust resuspension induced by a vehicle	13
2.3 Beyond car efficiency and electrification: Examining the role of demand reduction, public transit, and active travel measures to reduce GHG emissions in transport	26
2.4 Emission behaviour of recent EURO VI HDVs from chassis dyno and PEMS Tests	35
2.5 Bus emissions measurement in operational conditions using PEMS: comparison between different Euro technologies and fuels	48
2.6 On-road emission measurements beyond type approval PEMS	59
2.7 Insights for post-Euro 6, based on analysis of Euro 6d-TEMP PEMS data	66
2.8 Validation of low cost sensors for gases and particulate matter in the city centre of Wuppertal, Germany	75
2.9 Using modelling to improve air quality: The Concawe urban air quality studies	86
2.10 Operational GRAL urban street-canyon air quality forecast: Model assessment and COVID- 19 restrictions impact in air quality	96
2.11 Design of a program for the identification and correction of high emitting vehicles in Europe using remote sensing devices	107
2.12 Environmental assessment of different transport modes for all lifecycle stages	118
2.13 Effect of auxiliary usage on bus CO ₂ emissions through vehicle simulation	126
2.14 Understanding the fuel consumption gap using self-reported user and smartphone application datasets	135
2.16 Using a simulation approach to reconstruct the lab values with real-world driving data	161
2.17 Conventional engine vehicles model parametrization for real-world fuel consumption estimation	172
2.18 RDE of NRMM - Comparing portable and stationary measurement methods	182
2.19 Emissions of passenger cars in special driving situations	188
2.20 Particulate matter emissions in railway operation – in-situ measurements in an Austrian railway tunnel	199
2.21 Monitoring of ship emissions to enforce environmental regulations. The SCIPPER project	208
2.22 ‘Real Sailing Emissions’ for maritime vessels using sensors and satellite data transmission	218
2.23 Emission estimation and uncertainty analysis of nonroad construction machinery	228

2.24	A novel real driving emissions mapping model at a road-segment scale	239
2.25	Lower emissions from existing cars: personalised advice based on emission maps.....	255
2.26	Portable, on-board FTIR spectrometers: A universal tool for real-world monitoring of greenhouse gases, reactive nitrogen compounds, and other gaseous pollutants?.....	267
2.27	A virtual PEMS for Eco Driver training.....	277
2.28	Impact on mobility and environment in six European cities due to the introduction of Electrified L-category Vehicles (EL-Vs) – The ELVITEN project.....	285
2.29	Emission reduction benefits from PHEVs.....	287
2.30	Impacts to emissions and air quality of electric vehicles in Denmark in 2030.....	296

Acknowledgements

The editors would like to thank all the people involved in the successful organisation of the 24th International Transport and Air Pollution conference, and in particular the members of the Scientific and Organizing Committees for their invaluable efforts. We would like to thank Mrs Nadia Mesi for her valuable help in the final editing of the proceedings. Above all we would like to thank all authors for their high quality contributions to the conference proceedings.

Abstract

The 24th Transport and Air Pollution (TAP) conference collected the important research results in transport emissions and efficiency research. The papers presented focus on existing and future road vehicle EURO emission standards, CO₂ emissions targets, and the corresponding real-world emissions of regulated and non-regulated pollutants from all transport modes. The main topic are options for emission reduction through improved vehicle and engine technology, traffic management and behavioural change. Specific topics include electrification of transport, clean maritime shipping, and renewable fuels and decarbonisation of energy supply. The impact of emissions is analysed using improved air quality models and novel measurement systems and methods. The publication is aimed at researchers, engineers and policy makers, and anyone interested in developing a more efficient and cleaner transport system.

1 Introduction

The International Transport and Air Pollution Conference (TAP) has been held since 1986 in Graz (Austria), Zurich (Switzerland), Avignon, Reims, Toulouse and Lyon (France), Boulder (Colorado, USA) and Thessaloniki (Greece) and has turned into a key event of dialogue and networking in the areas of transport and air pollution, between scientists, researchers, transport users and decision-makers.

The 24th Transport and Air Pollution (TAP) conference took place in Graz, Austria from March 30, to April 1, 2021. It was organized by the Institute for Internal Combustion Engines and Thermodynamics of Graz, University of Technology, with the support of the Joint Research Centre of the European Commission.

The topics of this TAP conference include energy consumption and GHG emissions from vehicles, open issues for pollutant emissions, such as tampering, retrofits of software and hardware and non-regulated pollutants, emissions from non-road mobile machinery and other transport modes and measurements and simulation of traffic-related environmental impacts and air quality.

In the context of the conference, forty-five (45) scientific papers were presented in the form of oral presentations. The conference was attended by one hundred and twenty-seven (127) participants.

The present report includes the proceedings of this 24th TAP conference (2021), i.e. the collection of all the papers that were presented in the framework of the conference. The remainder of the report is organised as follows:

Chapter 1 includes an introductory message from the Chairman at the 24th TAP conference (2021) and information related to the organisation of the conference. Chapter 2 provides the full text of all the papers presented at the conference.

1.1 Message of the Chairman

A main strength of the TAP conferences is the coverage of the whole chain of impacts from transport emissions from the vehicle towards the air quality effects. This holistic approach of the TAP conferences provides a unique overview of current research in transport, air pollution and global warming. Emission-related topics cover life cycle assessments and measurement and simulation of real world emissions from all transport modes, including in-depth analysis of remaining issues, such as deterioration, tampering, loopholes in emission regulations, etc. Air quality related presentations dealt with improved air quality models and novel measurement systems and evaluation methods.

Besides analysing the current transport modes and systems, the assessment of possible options to reduce the environmental impacts was a central topic of the conference. Toolboxes and methods are presented in the papers to quantify the efficiency of different emission reduction measures, allowing robust assessments based on simulations. Such a scientifically sound analysis of options is an important basis for discussions and decisions by policymakers.

In the wake of the ambitious European Green Deal targets and the pressure to significantly reduce greenhouse gas emissions at the global level, important decisions must be made as soon as possible as to which of the available, and usually very drastic, measures should be taken in order to achieve the targets most efficiently. I sincerely hope the proceedings of the conference, the related research and the contacts you made during the conference will prove helpful and a good basis for such decisions and indeed for any associated studies!

Of course, I regret that the TAP could only be held as a web conference. Nevertheless, I am satisfied with the result, the exchange of information through the presentations worked very well from my point of view. Unfortunately, discussions during coffee breaks and dinners with good Austrian food were not possible this time, which has always been an important part of the TAP conferences. I, therefore, wish the coming conferences a live event and good and healthy success in order to continue the TAP tradition at the high level of the past years.

Stefan Hausberger

Chairman at 24th TAP conference (2021)

1.2 Organisation

Conference
Logo



Conference
Title

24th International Transport and Air Pollution Conference

Date

March 30 – April 1, 2021

Venue

On-line, Graz University of Technology , Austria

1.3 Organisers



IVT / Institute of Internal Combustion Engines and Thermodynamics



FVT



Graz University of Technology (TU GRAZ)



with the support of the:
European Commission (EC), Joint Research Centre (JRC)

1.4 Scientific Committee

The Scientific Committee (SC) of TAP 2021 contributed to the overall organisation of the conference, the review of the received papers, the formulation of the program, the oral sessions' chairing and the in-situ evaluation of the presented papers. The members of the Scientific Committee, as well as their affiliations, are provided below:

- Stefan Hausberger, IVT TUGraz (AT), (Chairman)
- Martin Rexeis, IVT TUGraz (AT)
- Peter Sturm, IVT TUGraz (AT)
- Leonidas Ntziachristos, Laboratory of Heat Transfer and Environmental Engineering / Aristotle University of Thessaloniki (GR)
- Zissis Samaras, Laboratory of Applied Thermodynamics / Aristotle University of Thessaloniki (GR)
- Nicolas Moussiopoulos, Laboratory of Heat Transfer and Environmental Engineering/ Aristotle University of Thessaloniki (GR)
- Jon Andersson, Ricardo (UK)
- Nicolas Hill, Ricardo (UK)
- Jens Borken-Kleefeld, International Institute for Applied Systems Analysis
- Miriam Elser, Empa (CH)
- Asif Faiz, Faiz & Associates LLC (US)
- James Tate, ITS/UNL, (UK)
- Georgios Fontaras, European Commission, Joint Research Centre
- Chris Frey, NC State University (US)
- Salah Khardi, IFSTTAR (FR)
- Norbert Ligterink, Netherlands Organisation for Applied Scientific Research - TNO (NL)
- Robin Vermeulen, Netherlands Organisation for Applied Scientific Research - TNO (NL)
- Åke Sjödin, IVL (SE)
- Robin Smit, University of Queensland (AU)
- Till Riedel, Karlsruhe Institute of Technology (DE)
- Carol Wong, Hong Kong Environmental Protection Department (HK)
- Ye Wu, Tsinghua University (CN)

2. Conference papers

2.1 Roadmap to zero carbon road transport

J. Horváth^{1,2*}, J. Szemesová², L. Zetochová²

¹ Faculty of Ecology and Environmental Sciences, Technical University Zvolen,

² Slovak Hydrometeorological Institute

jan.horvath@shmu.sk

Abstract

With the signing of the Paris Agreement (PA) in 2015, most of the countries has committed themselves to mitigate and even stop the global warming.

The European Union, and with it Slovakia, have committed themselves to reduce greenhouse gas emissions by 55% by 2030 compared to 1990 and to achieve carbon neutrality by 2050. These targets are being reviewed and incorporated into the European Green Deal. In total, transport accounts for 18% of total greenhouse gas emissions in Slovakia. One of the main source is road transport, which represents 96% of all greenhouse gas emissions from transport in Slovakia.

Slovakia must therefore prepare plans to change its economy in order to limit greenhouse gas emissions as much as possible. In road transport, the current highest target, and at the same time the obligation for car manufacturers, is to reduce emissions of new vehicles by 37.5% by 2030 compared to 2021. This work will outline a possible path that should lead to a reduction in greenhouse gas emissions by 2050. Slovakia has in the moment the second highest CO₂ emissions (g/km) from new registered vehicles in the EU, according to the database of the European Environmental Agency (EEA).

The policies and measures used in each scenario come from the national strategies, action plans and international regulations and agreements. Set of scenarios was prepared with an atypical approach. The snowball effect was used, where each additional scenario includes new measures in addition to the previous one. In this way, the effect of a set of new measures can be monitored individually. Based on historical data and estimates according to the Sybil baseline, all emissions scenarios for CO₂ were modelled in the COPERT model. The results of the presently prepared scenarios show that there is not a single scenario that brings the satisfactory reduction of CO₂ emissions, to which Slovakia has committed itself to reach carbon neutrality in 2050.

The growing trend presented in WEM scenario is due to increasing demand in road transport and high average survival rate of old vehicles with high CO₂ emissions. The breaking year is 2035 but the CO₂ emissions are higher than those in the presented in the latest National Inventory Report 2021.

In the case of WAM scenarios, the reduction starts at 0.95% and ends at 74.37% compared to the WEM scenario. These results show that even stronger support and efforts to achieve a high share of electric cars is not enough to significantly reduce CO₂ emissions. Nevertheless there is a significant reduction in emissions, but this reduction is still not close to the assumptions of zero-carbon or carbon-neutral road transport. Therefore, a more significant intervention in the fleet composition is needed and shall be introduced in the future.

Introduction

With the signing of the Paris Agreement (PA) in 2015 (UNFCCC, 2015), most of the countries has committed themselves to mitigate and even stop the global warming. The European Union, and with it Slovakia, have committed themselves to reach carbon neutrality by 2050 (except of Poland). Each Member State is aware to take these goals into account and plan its national strategies accordingly. Countries are required to prepare and regularly report mitigation contributions that will keep the average global temperature increase above 2°C by 2050.

The targets set by the European Union call for a drastic reduction in greenhouse gas emissions through vigorous actions in all sectors including the transport sector. These targets are being reviewed and incorporated into the European Green Deal (European Commission, 2018). In total, transport accounts for 18% of all greenhouse gas emissions in Slovakia (Szemesová et al, 2020). One of the main source is road transport, which represents 96% of all greenhouse gas emissions from transport in Slovakia.

Slovakia must therefore prepare plans to change its economy in order to limit greenhouse gas emissions as much as possible. In road transport, the current target, and at the same time the obligation for car manufacturers, is to reduce emissions of new vehicles by 37.5% by 2030 compared to 2021 (European Union, 2019). This work will outline a

possible path that should lead to a reduction in greenhouse gas emissions by 2050. Slovakia has in the moment the second highest CO₂ emissions (g/km) from new registered vehicles in the EU according to the EEA database. The aim of this work is to present an overview of possible scenarios for most feasible level of decarbonisation of the road transport.

Methodologies

Complex emission projections require a detailed analysis of historical data and the most accurate estimate of the development of input data and parameters. The main inputs for road transport projections are:

- a. Development of national vehicle fleet
- b. Development of fleet activity (mileage)
- c. Technological changes within the vehicle fleet

Input data and models

The fleet database for emission projections consists of two main parts:

- The historical time series, which is based on the Information System of Vehicle Registry of the Police of the Slovak Republic (IS EVO);
- The future modelled estimates of the development of the vehicle fleet.

The historical data of the time series are prepared annually for the needs of emissions inventories of Slovakia according to the methodology of the COPERT model (Emisia, 2020).

The development of the vehicle fleet is based on Sybil baseline dataset. This dataset includes basic estimates of vehicles until 2050. Estimates up to 2050 are made on the basis of knowledge of the historical series, newly registered vehicles, annually scrapped vehicles and the survival rate of vehicles within individual categories. This calculation does not take into account vehicles older than 30 years. Thanks to these data, it is possible to create a general matrix of the age structure of the vehicle fleet and apply or adapt it to any development of the vehicle fleet within Slovakia. Creating an age structure for each year by 2050 is the most important part of model preparation.

The calculation itself is done by the model COPERT via the CLI (Command Line Interface), which allows to introduce any new vehicle category and technology into the model. It is necessary to complete all the basic data for these categories such as emission factors, energy consumption and circulation data (share of urban, rural and highway driving). After input, the model calculates the fuels consumption and emissions in the same way as for the emissions inventories. The estimated emissions are afterwards recalculated by the technological efficiency factor. This factor indicates the technological evolution of vehicle fleet up to 2050.

Scenarios

The policies and measures used in each scenario come from the national strategies, action plans and international regulations and agreements. Set of scenarios was prepared with an atypical approach. The snowball effect was used, where each additional scenario includes new measures in addition to the previous one. In this way, the effect of a set of new measures can be monitored individually. The WEM scenario is based on already existing measures, which were put in force by the end of 2020. All measures are directly listed in the Low Carbon Strategy and subsequently in the National Energy and Climate Plan (NECP) (MH SR, 2021); or direct referenced to other relevant strategies.

The **WEM scenario** contains only two known measures that interfere with the energy mix and the baseline fleet. These measures are:

1. Higher biofuel share according to act no. 277/2020, which is national transposition of Directive (EU) 2018/2001 of the European Parliament and of the Council on the promotion of the use of energy from renewable sources. The specific objectives on the shares of biofuels are also set in the NECP:
 - 5.8% in 2017,
 - 5.8% in 2018,
 - 6.9% in 2019, of which 0.1% are advanced biofuels,
 - 7.6% in 2020 of which 0.5% are advanced biofuels,
 - 8.0% in 2021, of which 0.5% are advanced biofuels,
 - 8.2% between 2022 and 2030, with the share of advanced biofuels to be 0.75% from 2025

2. Electromobility – slow growth in the number of electric cars and subsidies for electromobility are also captured in the WEM scenario. The growing trend of electric vehicle market penetration based on the survival and lifetime of electric vehicles (PHEV and EV) is expected to last until 2050 and no further new measures will be introduced. The current share of electric vehicles is 0.1% and for plug-in hybrid vehicles 0.09%, with the final number of pure electric vehicles being around 1,749,000, which will cover only about 45% of all passenger cars in 2050.

As for the WAM scenarios there were prepared three sets of scenarios, each more ambition than the previous one. Measures in these scenarios are only planned for the future:

1. WAM 1 scenario: "Bonus Malus"
2. WAM 2 scenario: "Modal shift"
3. WAM 3 scenario: "100in50"

The WAM "Bonus Malus" scenario is an initial scenario with additional measures and includes only a limited number of measures.

- First measure is stricter technical control with the combination of new taxes for internal combustion engine (ICE) vehicles which can support intention to buy low-emissions vehicles. Slovakia has in the moment the second highest CO₂ emissions (g/km) from new registered vehicles in the EU. It is assumed that this measure can reach to replace not more than 2 000 vehicles a year older than 15 years. This is 0.04% share of passenger cars older than 15 years.
- Second measure assumes more efficient penetration of electric vehicles into the passenger cars segment than in the WEM scenario. It is expected that further more significant subsidy schemes will be introduced and the share of electric vehicles will increase up to 79% between the years 2025 to 2050, which is an increase of 34% compared to the WEM.

The WAM 2 "Modal shift" scenario should have a more significant effect on reducing emissions than the WAM "Bonus Malus" scenario, as it introduces new measures to those already in place. These new measures represent a combination of measures from the Strategic Transport Development Plan for 2030.

- First measure expects transfer of passengers from individual transport mode to public transportation service. It should result into increase of passenger car occupancy by 50%, which will reduce, in particular, the number of kilometres travelled up to 33% by 2050. This modal shift will take place between passenger cars and railways and passenger car and public bus transportation. A slight increase of mileage in public bus transportation is expected in this context.
- The second measure includes the changes in transfer of goods. Currently, the freight transport is the main emissions source in Slovakia. The measure proposed, that the volume of freight transport will be reduced by 65% by 2050. As a result, there will be a reduction in the activity of these vehicles and ultimately a reduction in the number of trucks and transit transport.

The WAM 3 scenario "100in50" represents the scenario with the maximum degree of decarbonisation at maximum effort. This scenario included all measures included in the scenarios presented above and a set of new ones, which can be described as phasing out measures.

- The most significant measure in this scenario is prohibition of registration of new fossil fuel passenger cars (diesel and petrol). Starting 2030 only alternative fuel-powered new vehicles will be allowed to register. Also phasing out of light-duty vehicles is expected as part of the decarbonisation of the "last mile". These vehicles will be substituted by electric light-duty vehicles.
- Hydrogen powertrains will be introduced to the vehicle fleet by the end of 2030. Maximum possible penetration is assumed according to the European hydrogen strategy. For passenger cars, this strategy assumes that 20% of the passenger vehicles will be powered by hydrogen. As for trucks, the highest assumption is not more than 16%.
- Phasing out diesel trucks and their substitution to LNG is also assumed. Until 2030, LNG will be only fossil based, but from 2030 LNG will be prepared from bio-methane. The substitution of fossil based LNG to biomass based LNG bring additional reduction and soft the possible negative effect of methane emissions.

Results and discussion

Despite the impact of the corona pandemic, rise of emissions in the road transport sector is expected at least until 2030. The growing trend presented in the WEM scenario (fig. 1) is due to increasing demand in road transport and high average survival rate of old vehicles with high level CO₂ emissions per kilometre. The breaking year for this assumption is 2035 however the CO₂ emissions are still higher than those reported in the National Inventory Report 2020 (Szemesová et al, 2020).

The “Bonus Malus” scenario can reduce emissions by 2050, but this reduction does not even reach the 1990 emissions level. This scenario is able to reduce additional emissions on the level about 1 600 kt of CO₂ in 2050 what represents 21.99% (table 1). This outcome means that phasing out old passenger cars and electrification of the passenger cars segment will be not enough to meet the targets set by the European Green Deal.

On the contrary, the “Modal shift” scenario, where activity in the form of mileage is reduced in the vehicle fleet has the potential to significantly reduce emissions by 2050. This reduction is based on decreasing of fuel consumption as lower mileage need. Measures supporting the transfer of passenger cars to public transportation should be strongly supported, and in addition also the movement of goods over longer distances by rail. This scenario already reduced emissions in 2050 well below 1990 emissions level, but still does not meet the reduction targets set in the European Green Deal. The reduction potential of this scenario in 2050 is only at most 60%.

The “100in50” scenario is the only one scenario that meets at least the 2030 target, however with an 11-years delay. The target is met in 2041 on the level of reduction at 55.24%. This delay is probably caused by the survival rate of vehicles. Phasing out of the fossil fuels based engines is crucial to achieve any goal. Slovakia has to introduce as soon as possible absolute prohibition of fossil fuels engines to meet the 2050 targets.

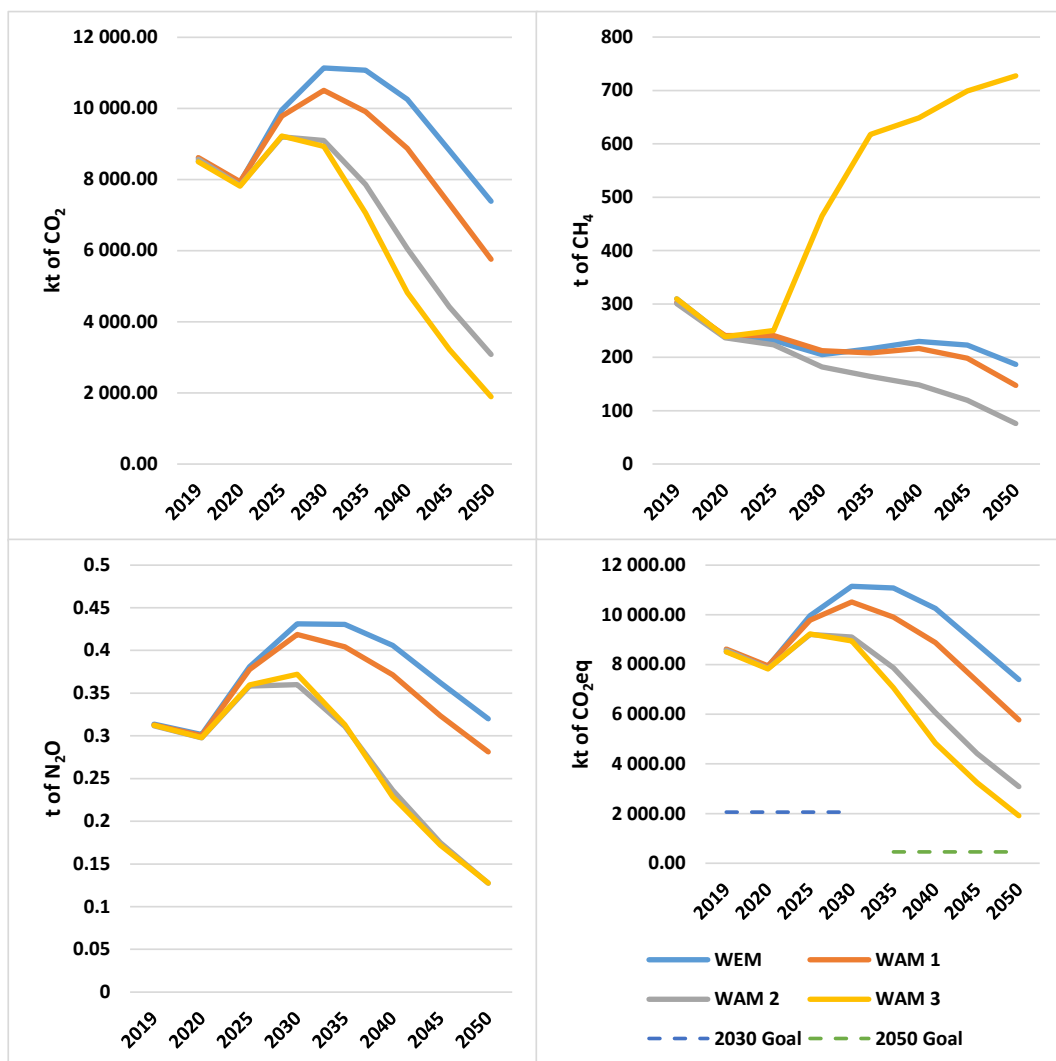


Figure 1: GHG emission projections for each scenario.

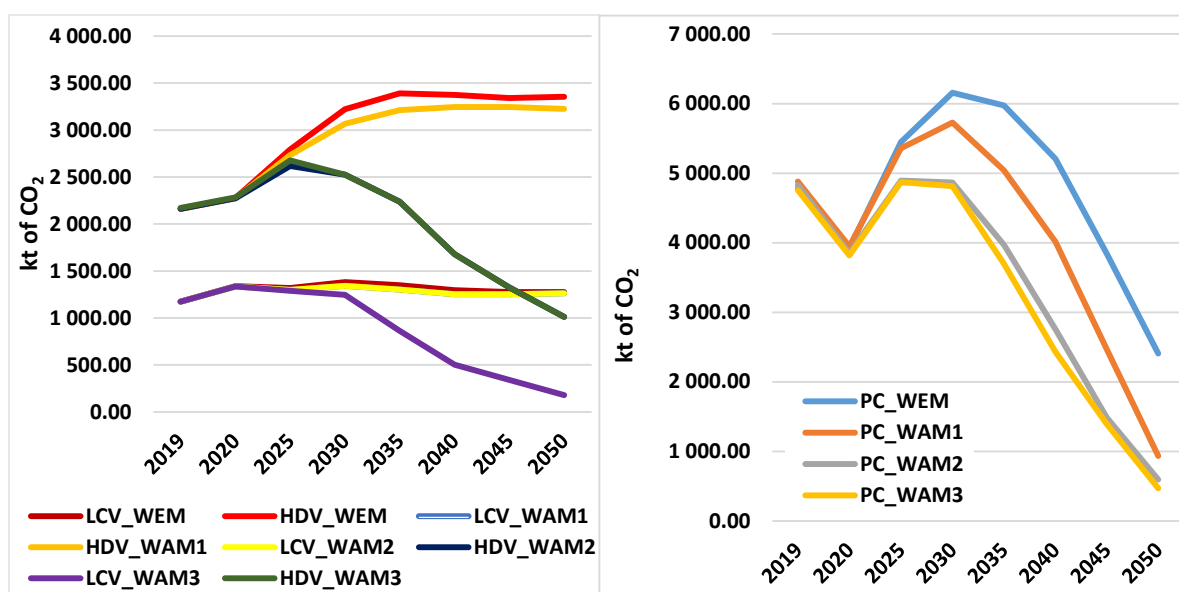
Table 1: WEM scenario CO₂ emissions (in kt) and the possible reduction according to each WAM scenario.

Scenario	2020	2025	2030	2035	2040	2045	2050
WEM	7 914.16	9 952.79	11 137.82	11 074.95	10 251.36	8 820.97	7 383.66
WAM 1	0.26%	-1.75%	-5.68%	-10.58%	-13.41%	-17.04%	-21.99%
WAM 2	-0.95%	-7.59%	-18.31%	-29.07%	-40.94%	-49.92%	-58.27%
WAM 3	-1.26%	-7.32%	-19.80%	-36.33%	-52.97%	-63.46%	-74.37%

According to the measures set in any presented scenario, Slovakia is unable to meet its commitment to reduce GHG emissions by 55% until 2030. This goal could only be achieved by an immediate, very significant change in the vehicle fleet.

Phasing out of diesel trucks and their substitution with bio-methane based LNG is significantly important measure to reduce emissions under 2 000 kt of CO₂ equivalents from this category. The LNG trucks are important in the emission reduction. However these vehicles have high methane emission compared to other technologies. This can be seen also in the projections of methane in on figure 1. Methane emission are rising only if the LNG trucks are introduced into the vehicle fleet. However, this increase of methane emissions does not affect the reduction needed.

The identified reduction potential were identified mostly in the freight transportation of goods (fig. 2). There is still a high share of GHG emissions from the trucks segment. The reduction can be achieved by the electrification of this segment. Electricity powered trucks have a drawback in the form of low maximum range of 600 km. Natural phasing out of fossil fuelled vehicles is already reality as it started already in 2020. The results show that reaching the European Green Deal targets at least for 2050 and a zero-carbon road transport needs immediate response and bringing new strict measures into force even before 2030.

**Figure 2:** Possible gaps for potential emission reduction in heavy-duty trucks (HDV), light-duty vehicles (LCV) and passenger cars (PC).

Conclusion

Signing the Paris Agreement by the most of the countries is the result of effort to mitigate the global temperature most possible below the 2°C until the end of century. Slovakia, as a Member State of the European Union, also signed this agreement and committed itself to reach carbon neutrality by 2050. A major problem are rising emissions from the transport sector across the world. Preparation of detailed emission projections and implementation of new policies and measures in the road transport is vital for the emissions reduction needed. Slovakia has sufficient potential to achieve carbon neutrality as well as low-carbon or zero-carbon transport however the immediate introduction of efficient policies and measure in transport is needed. The possibilities of the used policies and measures were considered in the prepared emission projections. There are still gaps in the policies but these gaps can be filled in with measures that support new carbon-free technologies. In the heavy-duty trucks segment, these technologies are electric vehicles with range extenders, more supported hydrogen fuelled vehicles, where the hydrogen is not natural gas based. Additional 15% reduction of emissions is needed to achieve at least the targets set in the European Union Green Deal.

References

- European Union., „Regulation (EU) 2019/631 of the European Parliament and of the Council on setting CO2 emission performance standards for new passenger cars and for new light commercial vehicles, and repealing Regulations (EC) No 443/2009 and (EU) No 510/2011, vol. 2019, 2019.
- Szemesová, J., Zetochová, L. a Dančová, M. (eds). National Inventory Report of the Slovak Republic 2020, 2020
- UNFCCC. Conference of the Parties (COP), Paris Climate Change Conference–November 2015, COP 21, 2015.
- European Union., Regulation (EU) 2018/1999 of the European Parliament and of the Council on the Governance of the Energy Union and Climate Action, Official Journal of European Union, vol. 2018, 2018.
- COPERT 5 Computer programme to calculate emissions from road transport, EMISIA, S.A.
- EUROPEAN COMMISSION. Regulation (EC) No 443/2009 - setting emission performance standards for new passenger. Official Journal of European Communities, vol. 2009
- EUROPEAN COMMISSION. Directive (EU) 2018/2001 of the European Parliament and of the Council on the promotion of the use of energy from renewable sources. Official Journal of European Union, vol. 2018
- EUROPEAN COMMISSION. Regulation (EU) 2019/631 of the European Parliament and of the Council of 17 April 2019 setting CO2 emission performance standards for new passenger cars and for new light commercial vehicles, and repealing Regulations (EC) No 443/2009 and (EU) No 510/201. Official Journal of European Union, vol. 2019
- FUEL CELLS AND HYDROGEN JOINT UNDERTAKING. Hydrogen roadmap Europe, Luxembourg, Publications Office of the European Union, 2019, ISBN 978-92-9246-332-8
- MINISTERSTVO HOSPODÁRSTVA SR. Integrovaný národný energeticko-klimatický plán. [Online] Available: <https://www.mhsr.sk/uploads/files/zsrwR58V.pdf> [ref.: March 21, 2021]
- MINISTERSTVO ŽIVOTNÉHO PROSTREDIA SR. Low-Carbon Development Strategy of the Slovak Republic until 2030 with a View to 2050. [Online] Available: <https://www.minzp.sk/files/oblasti/politika-zmeny-klimy/ets/its-sk-eng.pdf> [ref.: March 21, 2021]

2.2 Study on a test track of dust resuspension induced by a vehicle

M. Le Vern^{1*}, A. Razakamanantsoa¹, F. Murzyn², F. Larrarte³, V. Cerezo⁴

¹ University Gustave Eiffel, GERS-GIE, Allée des Ponts et Chaussées, 44344, Bouguenais, France

² ESTACA West Campus, Department of Mechanical Engineering, Rue Georges Charpak, 53000, Laval, France

³ University Gustave Eiffel, GERS-SRO, Boulevard Newton, 77447, Champs sur Marne, France

⁴ University Gustave Eiffel, AME-EASE, 25 Avenue François Mitterrand, 69675, Bron, France

mickael.le-vern@univ-eiffel.fr

Abstract

An experimental campaign was carried out on a test track to assess resuspension of dust by vehicle traffic. Two vehicles were driven on a road covered by four different types of particles representing a wide range of fine soils. Each test consisted of running one of the vehicles at a given speed (30, 45 or 60 km.h⁻¹) over one of the type of particles previously spread on the road at a given mass per unit area (200, 400 or 600 g.m⁻²). The concentration of resuspended particles was measured by suction of the dust plume behind the rear tire using a particle counter. The influence of physical (type and quantity of particles, vehicle geometry) and mechanical (vehicle speed, tire/surface interface, dynamical behavior) parameters on particle lift are discussed. In terms of particle mass concentrations, results indicate that doubling the vehicle speed leads to 1.5 to 5.7 times higher PM₁₀ emissions. The lift of fine clay particles is 2 to 9 times more important than that of coarser soils. Significant differences are also observed between the emissions of the two vehicles, pointing out the key role of ground clearance and mud flaps in particles resuspension. It is believed that the present results may be extended to earthworks sites where solutions are expected to reduce dust emissions without watering.

Introduction

Dust emissions lead to a reduction of visibility and the worsening of air quality (Pope and Dockery, 2006; Baddock et al., 2014). This phenomenon occurs during the circulation of cars and haul trucks on unpaved roads and earthworks runways (Kuhns et al., 2003; Muleski et al., 2005). The particles on the surface of the road can be re-suspended by the passage of a vehicle due to the shear stress at the tire/road interface combined with the 3D turbulent flow generated in the wake (Gillies et al., 2005; Kuhns et al., 2010). This problem is also present on paved roads due to non-exhaust emissions including tire, brake and road related wear (Hussein et al., 2008; Hichri et al., 2019).

Studies on unpaved roads (USEPA, 1995; Etyemezian et al., 2003; Gillies et al., 2005; Kuhns et al., 2010) have shown that dust emissions are dependent on vehicle weight and speed as well as on the silt content (% of particles < 75 µm) of the road. These roads are built from compacted soils that degrade as vehicles travel, resulting in the accumulation of particles on the surface (Le Vern et al., 2020a; Le Vern et al., 2020b). However, no study has investigated dust emissions as a function of the level of degradation of the unpaved road surface yet. Similarly, Gillies et al. (2005) found that vehicle type did not influence emissions. Nevertheless, the use of accessories to control particle lift (such as mud flaps) has not been studied to date.

The main objective of this study is to analyze the effect of the level of surface degradation of an unpaved road on the dust emission. The degradation is characterized by the dust loading on the surface, i.e. the mass of particles per unit area. Different amounts of particles had been poured on a test track before vehicles were driven on it. Several types of particles were studied in order to identify the convenient parameter governing dust lift. The effect of vehicle type and mud flaps on this phenomenon is also studied. For this purpose, a light passenger car and a 4x4 equipped with mud flaps were driven at different speeds over the particles. An analysis of the mechanical parameters of tire/surface contact is also performed by means of a dynamometric wheel fitted to the passenger car.

The results of the study apply to the topic of unpaved roads but can be extended to the problem of particulate contamination of asphalt roads.

The methodology used for this study is described in the second part of this paper, followed by a presentation of the results and a discussion. This paper ends with the different conclusions that can be drawn from the experiments.

Methodology

Vehicles used and dynamometric wheel

Two vehicles were used during the tests: a Renault Clio III and a 4x4 Ford Ranger. The first one was chosen because it is one of the best-selling cars in Europe and is representative of small passenger cars. The 4x4 is much more massive (unladen weight of about 2 tons against 1 ton for the Clio) and has larger dimensions. Moreover, it is more likely to be used on unpaved roads and earthworks runways. Figure 1 shows these two vehicles. The Clio has about half the ground clearance of the 4x4 (120 mm vs. 229 mm). From a dimensionless point of view, the ratio of ground clearance to empty height (H/G as shown in Figure 1) is also different between the two vehicles (0.08 for the Clio and 0.13 for the 4x4).

The Clio was also instrumented with a Kistler RoadDyn S625 dynamometer wheel. This device was mounted on the right front wheel of the vehicle (see its location in Figure 3-a). It allows the continuous measurement of longitudinal, vertical and transverse forces and torques applied to the wheel using Wheatstone bridge-mounted strain gauges. Its acquisition frequency is 100 Hertz.

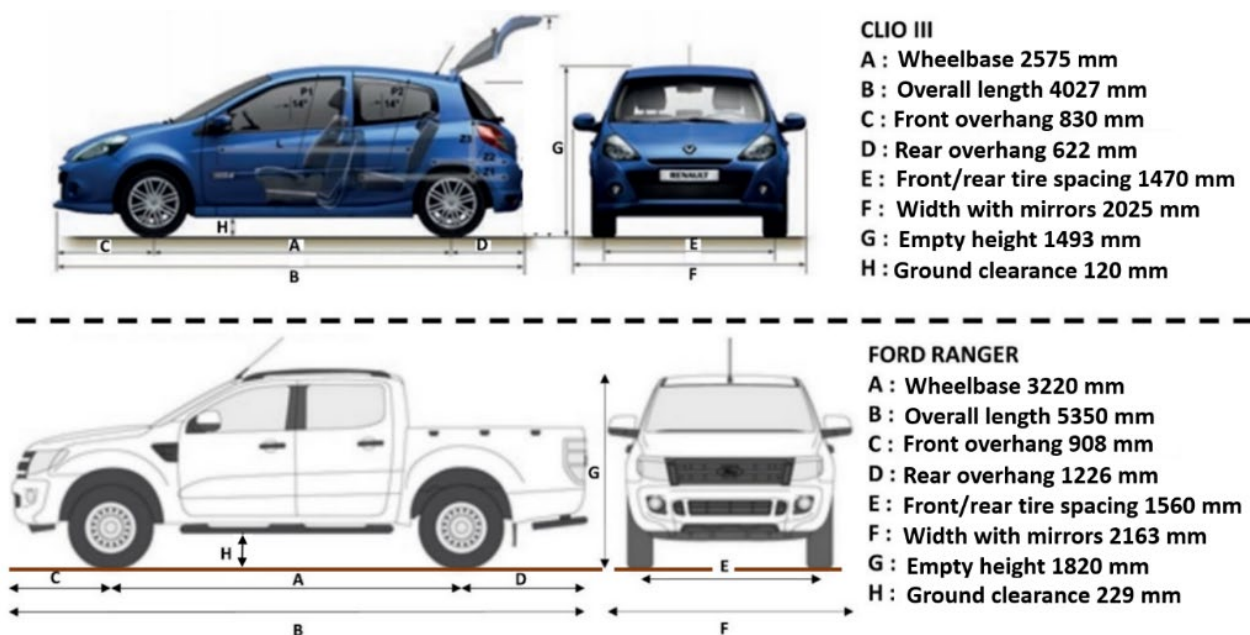


Figure 1: Dimensions of the two vehicles.

Particles under study

In previous studies about dust generation during vehicle traffic on unpaved roads, there is often only one geotechnical criterion for characterizing the soil: the percentage of particles smaller than 75 μm (USEPA, 1995; Etyemezian et al., 2003; Gillies et al., 2005; Muleski et al., 2005; Kuhns et al., 2010). The United Soil Classification System designates this percentage as the “silt content”. Results have shown that the higher the silt content, the more dust will be emitted, all other things being equal. For this study we have chosen to work with particles having approximately the same percentage below 75 μm . Thus, we will be able to verify if this criterion is sufficient to characterize particle lift (if so we will measure similar dust emissions with the different soils) or if it is required to take into account other geotechnical parameters.

Four types of particles were used for the tests: a clay mixture composed with montmorillonite and illite (cosmetic green clay CATTIER) and three silty soils sampled from different earthwork sites in Europe: Val d'Europe and Strasbourg in France, Marche les Dames in Belgium. These soils have been selected because they have similar silt contents (between 95 and 100%) but their other geotechnical properties differ, as shown in Figure 2. In this Figure, the Liquid Limit and Plastic Limit are parameters that quantify the cohesion of the soil. They have been measured according to ISO 17892-12:2018 (ISO, 2018). Together with the granulometric properties (passing at 2 μm and 75 μm), they allow the classification of the particles. In Figure 2, we present their classification according to the American Society for Testing Material standard (ASTM, 2017) and the French Guide for road earthworks (GTR, 2000).

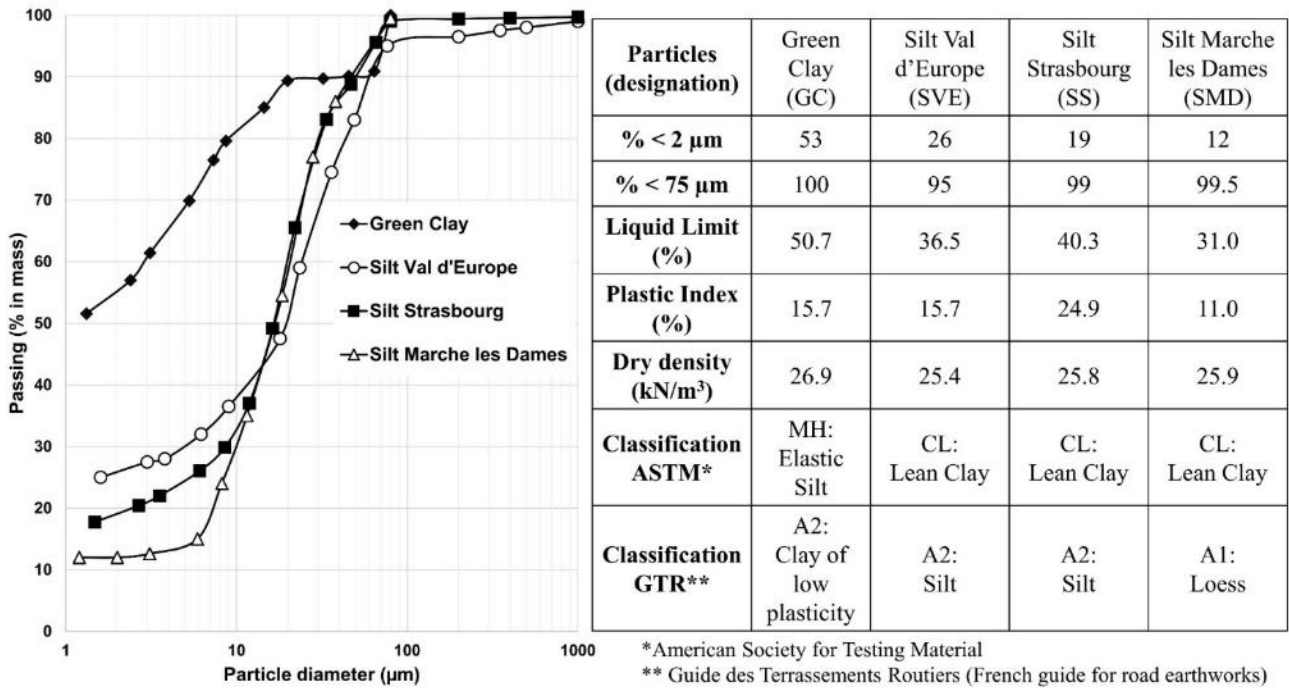


Figure 2: Particle size distributions and geotechnical properties of the soils.

Experimental protocol

In order to ensure particles being free of moisture during the tests, they were previously dried in an oven at 105°C for 24 hours. They were then sieved to break up any aggregates and packed in plastic bags. Before each test, the particles were spread homogeneously on the track along two lines each 3 m long and 0.3 m wide and spaced apart from each other by a distance corresponding to the spacing between the two tires of the vehicle (1.47 m for the Clio and 1.56 m for the 4x4). The width of the lines was chosen to be greater than the width of the vehicle tires (20 cm for the Clio and 25 cm for the 4x4). The length was chosen for practical reasons related to the quantities of particles available. Three quantities of particles per unit area were tested: 200, 400 and 600 g.m⁻². These quantities correspond to three distinct soil degradation states (low, medium and high) highlighted in a previous study (Le Vern et al., 2020b). The two lines were delimited by markings on the ground on which wooden frames were placed. The necessary quantity of particles was poured into these frames and then spread evenly with a brush. A weather station was on the side of the road to measure temperature, relative humidity as well as wind speed and direction. The tests took place after 9 days without precipitations, under conditions of relative humidity ranging from 50 to 80% and temperature ranging from 17 to 25°C. Figure 3 shows the experimental layout.

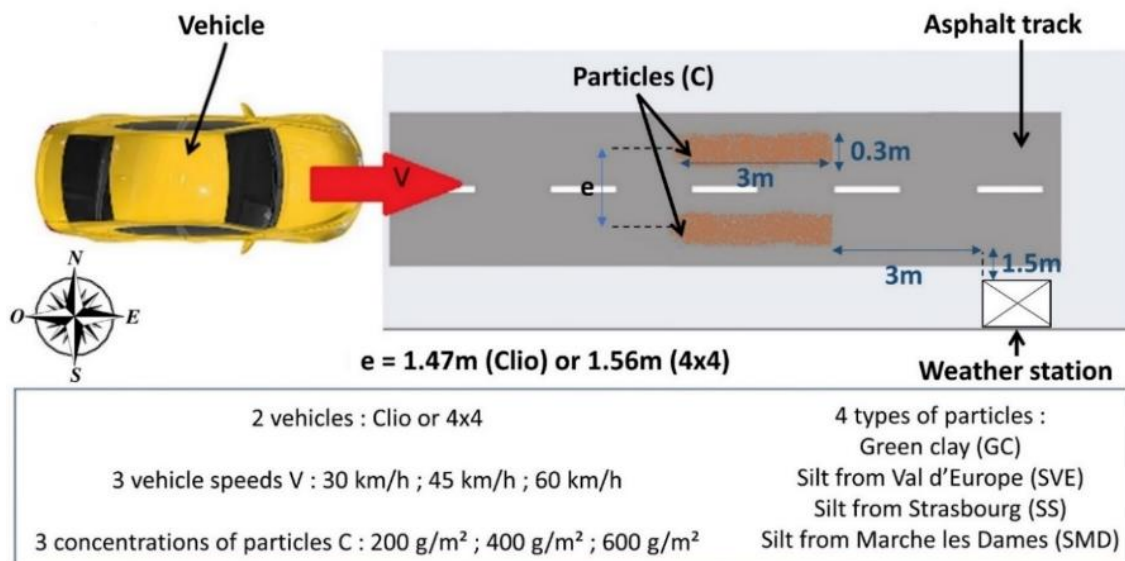


Figure 3: Experimental layout of the tests on the track (diagram not to scale).

Each test consisted in running one of the two vehicles at a predefined speed (30, 45 or 60 km.h⁻¹) over one type of particles previously poured on the ground at a given mass per unit area (200, 400 or 600 g.m⁻²). The speed of 30 km/h corresponds to the traffic conditions generally imposed when the risk of dust is important (especially on construction sites). The speed of 45 km/h is a speed frequently reached in cities or on construction sites. Working at 60 km/h allows to study the effect of doubling the speed compared to 30 km/h.

The test track was made of asphalt concrete to ensure that the vehicle blew away only the particles that had been poured on the surface. Conducting the tests on an unpaved road would not have controlled this parameter. This experimental configuration makes it possible to extend the results obtained to the problem of particle emission due to contaminations of asphalt mixes. These contaminations nevertheless generate smaller quantities of particles than those studied here.

During the tests, an optical particle counter measured the concentrations of suspended dust by particle aspiration directly behind the right rear tire of the vehicle. It is a dust analyzer PALAS Fidas Mobile equipped with a pump that sucks the particles contained in the ambient air. These particles pass through a beam of LED light which is then scattered at an angle that depends on the size of the particle (Mie scattering theory). The estimation of the particle size is performed with a photomultiplier that measures the scattered light. Combined with a counting algorithm, the mass concentration of particles per unit volume ($\mu\text{g}/\text{m}^3$) can be estimated.

Figure 4 shows the two vehicles (Figure 4-a for the Clio III and 3-b for the 4x4) as well as the installation of the particle counter in the 4x4 (Figure 4-c). For these measurements, the inlet of the suction pipe for particle aspiration was located in the median plane of the right rear wheel, 30 cm from the rear edge of the tire and 20 cm above the ground (Figure 4-d). The distance between the pipe and the tire was the same for the measurements with the Clio III, except that the pipe was 10 cm above the ground. These pipe positions are related to practical considerations due to the vehicles' geometry.

After each test, the particles remaining on the ground were blown to the sides of the road using a leaf blower. A manual sweep of the road was also performed to ensure that the particles in the asphalt voids were removed.

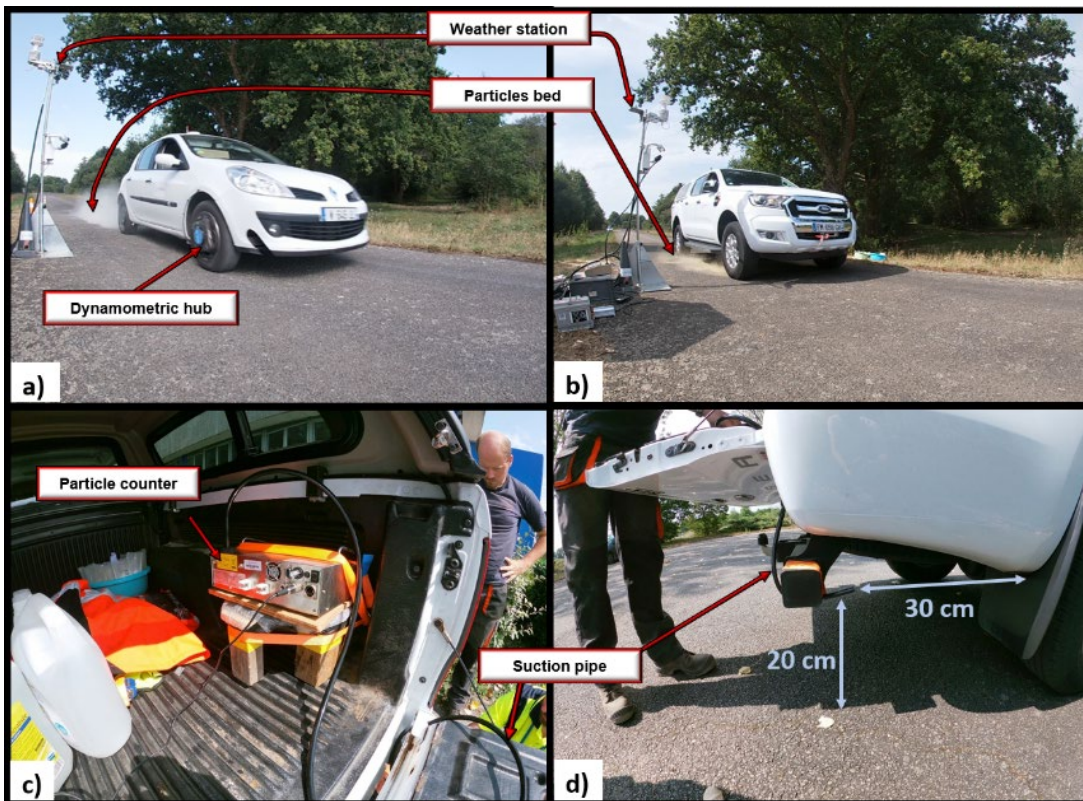


Figure 4: Vehicles used for the experiments: a) Renault Clio III and b) 4x4 Ford Ranger; On-board measurements with c) installation of the particle counter in the 4x4 and d) suction of particles directly behind the tire.

A total of 47 tests were carried out over three days by varying the different parameters (vehicle type and speed, particle type and mass per unit area). Table 1 shows all the tests carried out. Not all the possible configurations of parameters could be tested for practical reasons of time and quantity of particles available. Some configurations were tested several times for two reasons:

- To check the repeatability of the measurements by performing the same test twice in a row;
- To highlight the effect of meteorological parameters on dust emission by performing the same test in the morning and afternoon.

Table 1: Configurations of the tests.

Vehicle	Particles*	Speed	Concentration	Vehicle	Particles*	Speed	Concentration		
Clio III	GC	30 km/h	400 g/m ²	4x4 Ford Ranger	GC	30 km/h	400 g/m ²		
		60 km/h	200 g/m ²			45 km/h	400 g/m ²		
			400 g/m ²			60 km/h	200 g/m ²		
			600 g/m ²				400 g/m ²		
	SVE	30 km/h	400 g/m ²		SVE	30 km/h	400 g/m ²		
		60 km/h	200 g/m ²			60 km/h	200 g/m ²		
			400 g/m ²				400 g/m ²		
			600 g/m ²				600 g/m ²		
	SS	30 km/h	200 g/m ²		SS	30 km/h	400 g/m ²		
			400 g/m ²			45 km/h	400 g/m ²		
		60 km/h	200 g/m ²			60 km/h	200 g/m ²		
			400 g/m ²				400 g/m ²		
			600 g/m ²				600 g/m ²		
			600 g/m ²				600 g/m ²		
	SMD	30 km/h	200 g/m ²		SMD	30 km/h	400 g/m ²		
			400 g/m ²			60 km/h	400 g/m ²		
		60 km/h	200 g/m ²				60 km/h	400 g/m ²	
			400 g/m ²			400 g/m ²			
			600 g/m ²			600 g/m ²			
			600 g/m ²			600 g/m ²			
	* GC: Green Clay SVE: Silt from Val d'Europe SS: Silt from Strasbourg SMD: Silt from Marche les Dames								

Data processing

Analysis of particle counter measurements

The particle counter provides the evolution of the concentration of the different classes of particles (PM₁₀, PM₄, PM_{2.5} and PM₁) at a data rate of 1 Hertz. We did not analyse particles beyond PM₁₀ because it is the upper limit of the apparatus. Moreover, particles larger than 10 µm have high deposition velocities (Petroff and Zhang, 2010) and

therefore fall rapidly to the ground, within 100 meters from their emission source (Veranth et al., 2003). They are also much less hazardous to health than the finest particles (Astrup, 2010).

Figure 5-a shows an example of particle concentration measured during a test performed with the 4x4 at 30km/h on 400g/m² of Val d'Europe silt particles. Figure 5-b presents the parameters that are taken into account in the present study for each curve, namely: the area under the curve, the maximum value and the mean value. The area under the curve is determined by the trapezoidal method and allows the definition of an "emission coefficient" ϕ given in $\mu\text{g}\cdot\text{s}\cdot\text{m}^{-3}$. The mean value is assessed by considering the measurements between the beginning of the concentration rise before the peak and the return to a "normal" concentration (defined as the average of the PM₁₀ concentrations measured between two tests, i.e. 10 $\mu\text{g}\cdot\text{m}^{-3}$). It is arbitrarily considered that the peak concentration begins when the "normal" concentration is exceeded by a factor of 100 (that is PM₁₀ concentration larger than 1000 $\mu\text{g}\cdot\text{m}^{-3}$) and ends when it falls below 10 $\mu\text{g}\cdot\text{m}^{-3}$. According to this procedure, it is possible to highlight the moment when the vehicle is driving over the particles.

As the tests were carried out under subisokinetic conditions, the measurements underestimated the concentrations of the finest particles (Wilcox, 1956; Belyaev and Levin, 1974). We therefore focus our analysis on the coarsest particles, i.e. PM₁₀ concentrations. Moreover, it is the range of particles generally studied in the literature on dust emissions on unpaved roads (USEPA, 1995; Etyemezian et al., 2003; Gillies et al., 2005; Kuhns et al., 2010).

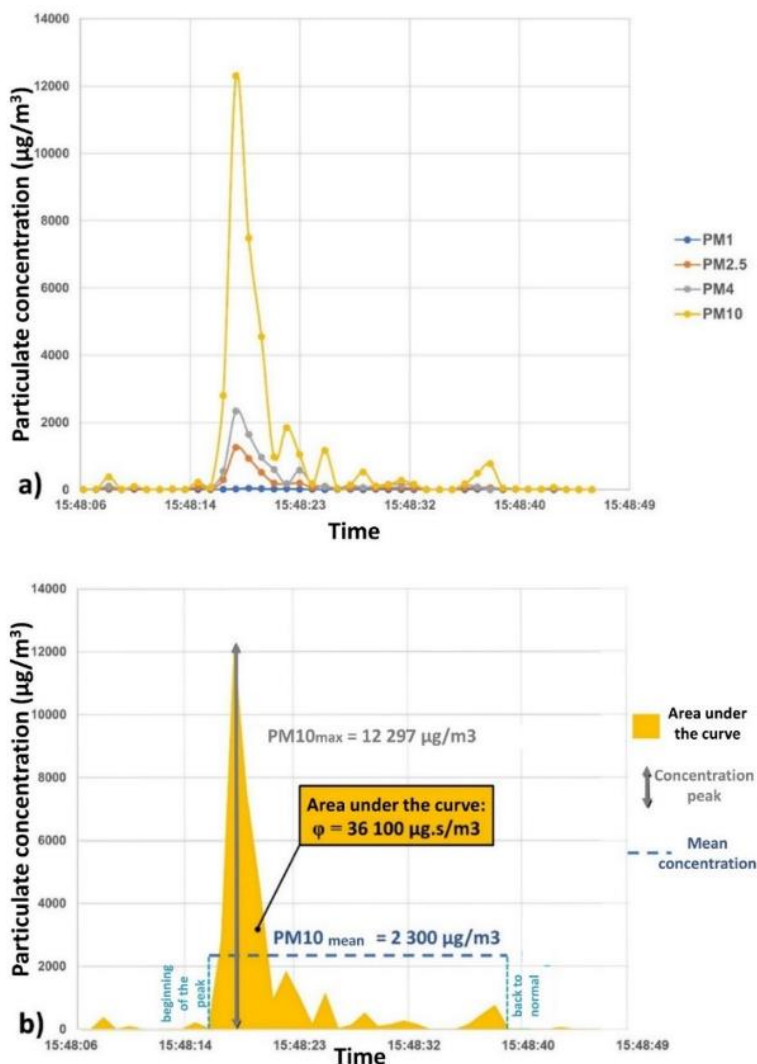


Figure 5: a) Evolution, for one of the tests, of the particle concentrations measured behind the tire as a function of time; b) Highlighting, for the PM₁₀ curve, of the parameters considered in the study.

Analysis of dynamometric wheel measurements

The dynamometric wheel allows real-time measurement of the forces and moments applied to the right front wheel of the Clio III. In the context of the study, the influencing parameters on the lift of the particles are:

- The longitudinal force F_x which characterizes the friction between the tire and the road;

- The vertical force F_z which characterizes the action of the vehicle weight in the tire/road contact mechanics;
- The moment M_y which also characterizes the tire/road friction.

The vertical force F_z did not vary much during the tests ($F_z \approx 3750 \text{ N} \pm 3\%$) since the masses of the Clio and its driver were always the same. In addition, the road smoothness was of good quality and the speed of the vehicle was constant so the dynamic variations were attenuated by the shock absorbers. The parameter F_z is therefore not taken into account in the analysis.

Figure 6-a shows an example of the evolution over time of the vehicle speed, F_x and M_y for one of the tests (Clio driving at 45 km/h over 200 g/m^2 of Marche les Dames silt particles). The figure shows the total duration of a test characterized by an evolution of the vehicle speed in three phases: acceleration, steady speed and then deceleration. During the acceleration and deceleration phases, the parameters F_x and M_y undergo significant variations due to gear changes and braking. For the analysis, the average values of these parameters ($F_{x_{\text{moy}}}$ and $M_{y_{\text{moy}}}$) are taken into account during the period when the tire is in contact with the particles (Figures 6-b and 6-c). This period takes place in the stable speed phase, which explains why the variations in F_x and M_y are less important than during the acceleration and deceleration phases.

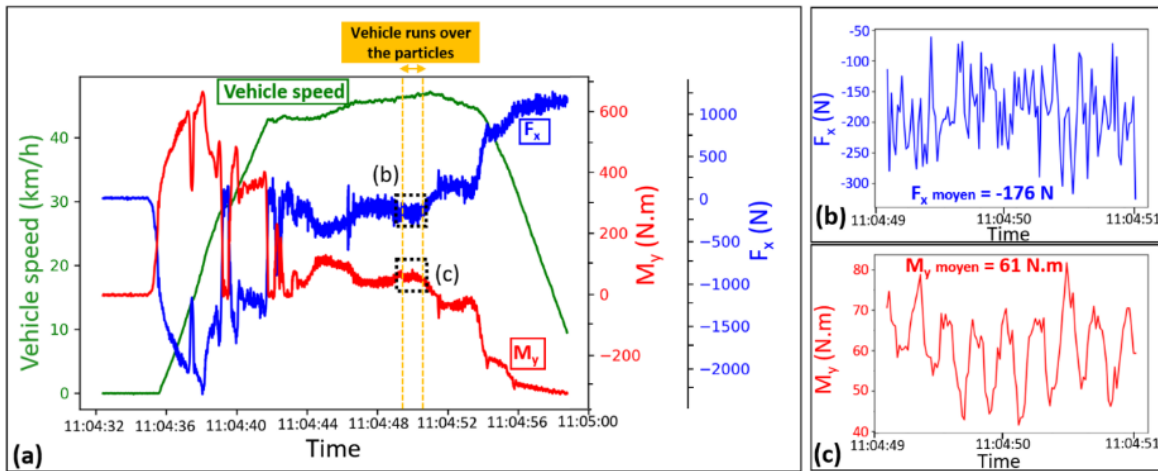


Figure 6: (a) Time evolution, for one of the tests, of the vehicle speed (green curve), the longitudinal force (blue curve) and the vertical moment (red curve) applied to the vehicle wheel. Curves (b) and (c) show respectively a zoom on the evolutions of the longitudinal force and the vertical moment during the passage of the vehicle on the particles.

Results and discussion

Repeatability of the results

Some configurations were tested several times to check the repeatability of the results (the acronyms are those used in Table 1):

- The SS-60km/h-200g/m²-Clio configuration was reproduced twice
- The SMD-60km/h-200g/m²-Clio configuration was reproduced four times
- The SMD-60km/h-400g/m²-Clio configuration was reproduced twice
- The GC-60km/h-200g/m²-Clio configuration was reproduced twice

Repeatability tests were done at 60 km/h because this is the speed for which there are the most disturbances and a priori the most lifted particles. For each configuration, the average value is determined for $\text{PM}_{10_{\text{max}}}$, ϕ and $\text{PM}_{10_{\text{mean}}}$. The minimum and maximum values are also considered. The average gap for each configuration is given by equation (1):

$$\text{average_gap}(\%) = \frac{\text{Value}_{\text{max}} - \text{Value}_{\text{min}}}{\text{Value}_{\text{mean}}} \times 100 \quad (1)$$

Figure 7 shows the corresponding results.

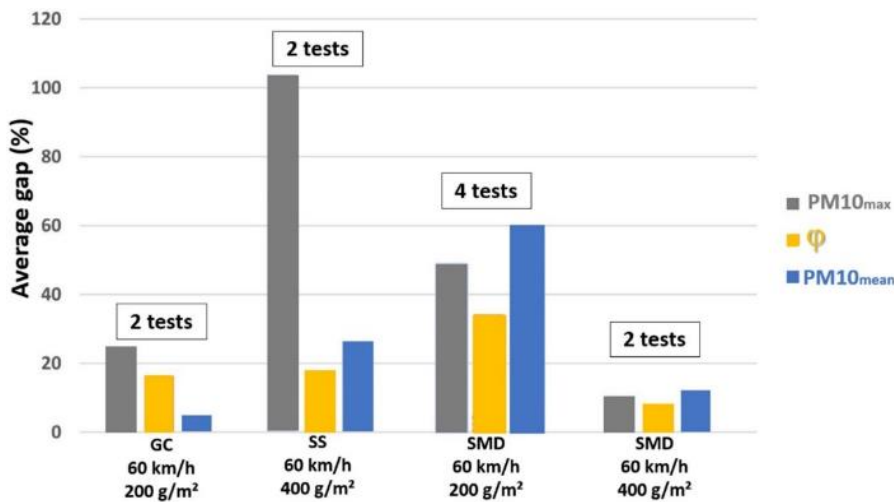


Figure 7: Average gaps for the repeatability tests.

The overall average gap is 47% for PM10_{max}, 19% for ϕ and 26% for PM10_{mean}. The large deviations observed for the peaks of concentration are due to the very strong dependence of this parameter on the particle aspiration kinematics. Indeed, their distribution in a dust plume is chaotic and more or less particles can be recorded at the same time in the particle counter. Thus, for the same dust plume, the concentration peak can vary significantly depending on the location of the aspiration. Therefore, it is more relevant to look at the evolution of the amount of particles sucked up as a function of time. As such, the parameter ϕ appears to be the most appropriate to characterize the dust plume generated. It is also the parameter with the best repeatability.

The observed variations are not due to the wind as it has no effect on the particles directly behind the vehicle tires. On the one hand, the wind speeds were low during the tests (between 2 and 9 km/h). On the other hand, it was visually observed during the experimental campaign that the effect of the wind appears several seconds after the particles are suspended, when they have reached a certain height (about 1 meter). Below this height, it is the aerodynamic phenomena related to the wake of the vehicles that entrap the particles, particularly in the counter-rotating vortices generated behind the wheels (Mercker and Berneburg, 1992).

Some tests were carried out both in the morning and in the afternoon with a strong variation in relative humidity (about 80% in the morning and 60% in the afternoon). However, small differences were observed for dust emissions between these tests (less than 8% for the ϕ parameter). This suggests that relative humidity does not appear to be a parameter influencing the lift of particles directly behind the tire for the presenting tests. Indeed, the vehicle was running on the dry particles few minutes after they were poured on the ground while moisture exchanges take hours or even days to take place between dry particles and the atmosphere (Ravi et al., 2006).

In the following, the results are presented with error bars that take into account the average gaps that were defined above.

Emission coefficients

For the sake of brevity, we focus the analysis on the parameter with the best repeatability: the emission coefficient ϕ . Figure 8 shows its evolution as a function of the vehicle speed and of the particle concentration for the Clio III tests. Overall, it appears that an increase in speed leads to an increase in ϕ . For the same concentration of particles on the ground, doubling the speed of the Clio III (from 30 to 60 km/h) leads to a multiplication of the emission coefficient by a factor ranging from 1.5 (for green clay at 400 g.m⁻², Figure 8-a) to 5.7 (for Strasbourg silt at 200 g.m⁻², Figure 8-c).

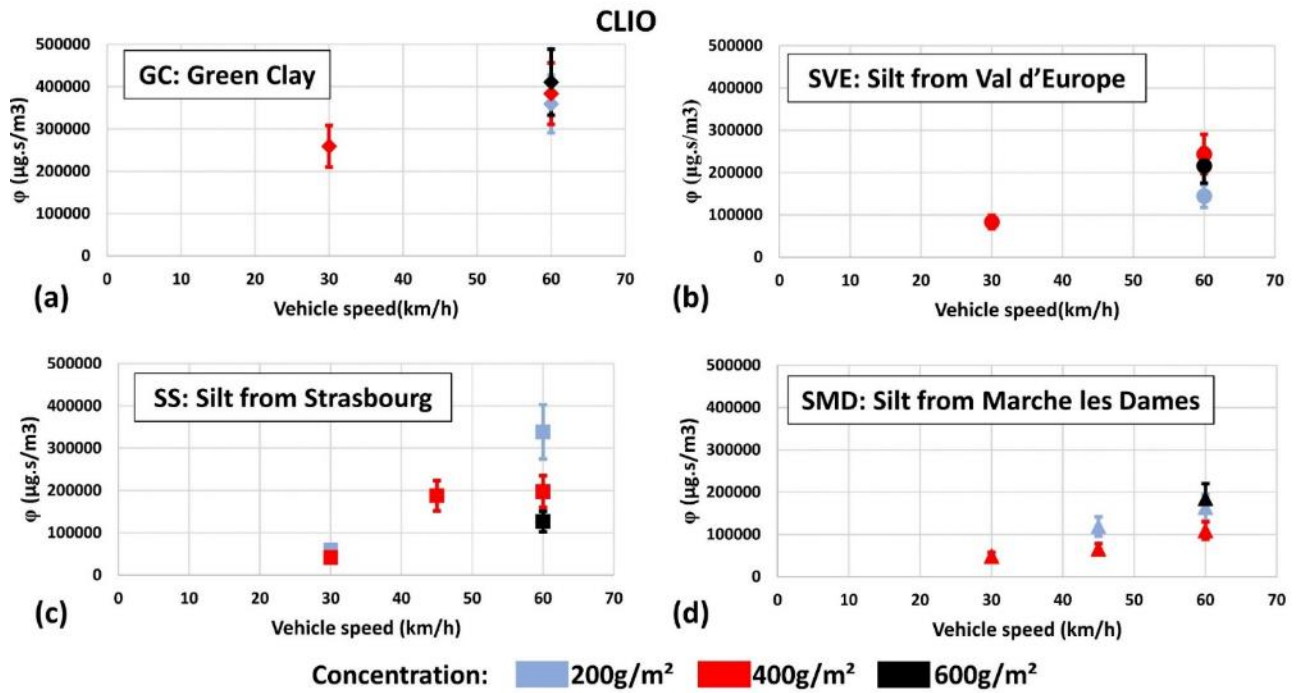


Figure 8: Emission coefficients for the Clío tests with particles of (a) green clay, (b) silt from Val d'Europe, (c) silt from Strasbourg and (d) silt from Marche les Dames.

For the same speed of the vehicle, an increase in the concentration of particles on the ground can lead to a decrease in the emission coefficient. Indeed, it is observed for the tests at 60 km/h on the Val d'Europe silt (Figure 8-b), for the tests at 30 and 60 km/h on the Strasbourg silt (Figure 8-c) and for the tests at 45 and 60 km/h on the Marche les Dames silt (Figure 8-d). It cannot be explained by the weather conditions as they do not affect the measurements as indicated in the previous section. To get a better understanding of the processes involved, a Principal Component Analysis (PCA) integrating the longitudinal force F_x and the vertical moment M_y is performed (Figure 9).

Figure 9-a shows that the emission coefficient ϕ is particularly correlated with the percentage of particles smaller than $2 \mu\text{m}$ ($R^2=0.77$) and with the vehicle speed ($R^2=0.60$). The variables F_x and M_y are highly correlated with each other ($R^2=0.78$) since they represent the same physical phenomenon. The correlation is not 100% because the F_x measurement is noisy due to slip-free rolling conditions. According to the Principal Component Analysis theory, the F1 and F2 axes allow to define the plane that maximizes the dispersion of the experimental data in order to visualize the cloud of results as well as possible. The circle of correlations is such that the abscissa axis F1 is highly correlated to F_x and M_y (correlations of 94% and 91% respectively). The F2 axis is highly correlated to ϕ ($R^2=0.93$). Thus, the analysis of the observations on these two axes (Figure 9-b) does not allow to conclude about the effect of the parameters F_x and M_y on the coefficient ϕ for concentrations of 200 g/m^2 and 400 g/m^2 . Indeed, the clouds of the blue and red symbols are too scattered. For the highest concentration (600 g/m^2 , black symbols in Figure 9-b), a decreasing trend of ϕ appears when F_x and M_y increase. This is probably a phenomenon of aggregation of the particles caused by the tire. Indeed, the tire compacts the bed of particles as it rolls over it, forming aggregates that are then torn off by shear force (Le Vern et al., 2020b). The greater the shear forces, the more numerous these aggregates are. Many of them have sizes greater than $10 \mu\text{m}$ and are therefore not measured by the particle counter (hence the decrease of the parameter ϕ which only takes into account PM_{10}). This mechanism seems to appear when the quantity of particles on the ground is large and is particularly marked for coarser particles (silts from Strasbourg and Marche les Dames). This phenomenon of aggregation has been previously highlighted for soil degradation by vehicles (Le Vern et al., 2020b).

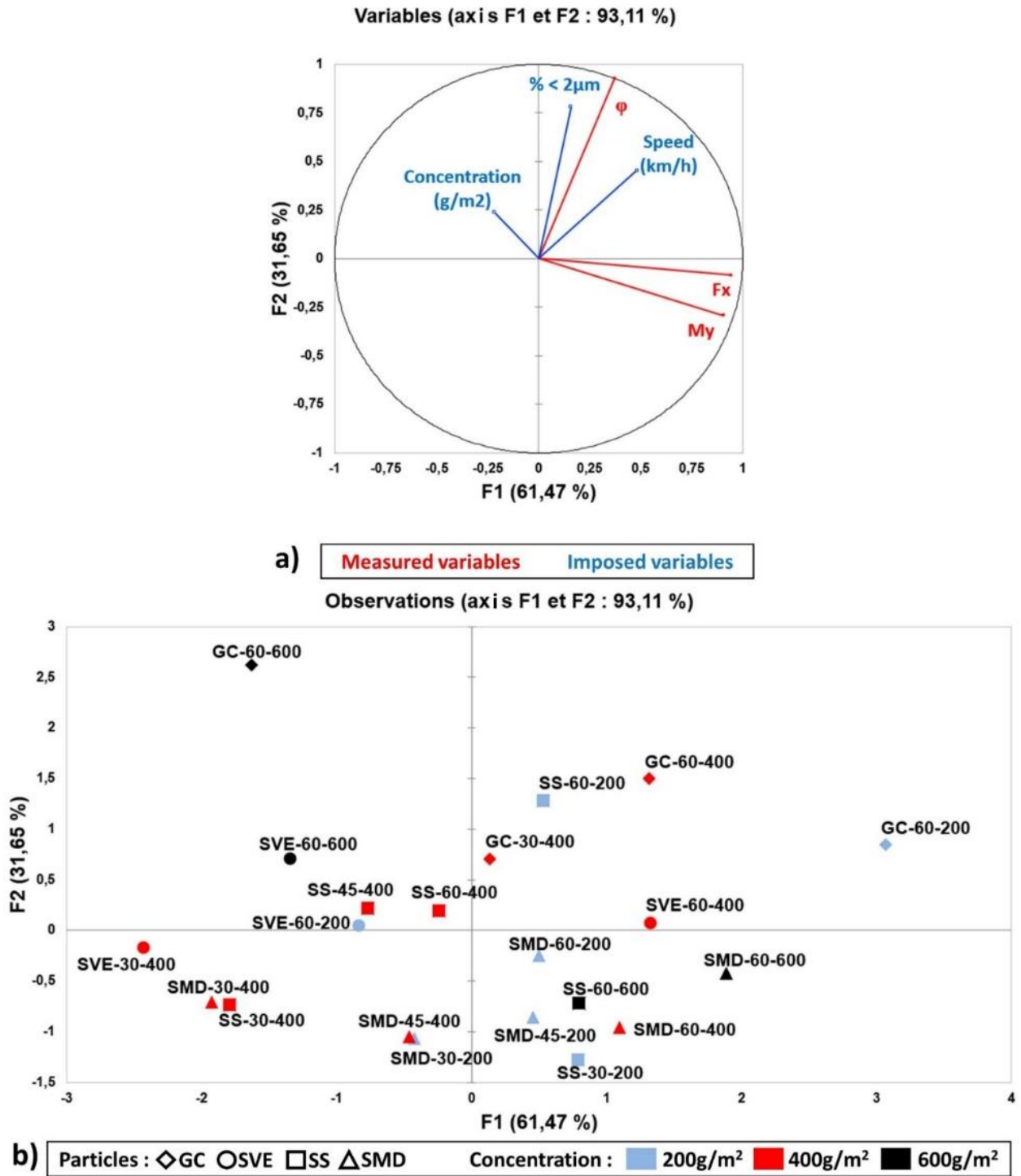


Figure 9: Principal Component Analysis of the Clio tests. a) Circle of correlations for the variables and b) visualization of the tests in the correlation space. Each test is designated by: Type of particles-vehicle speed-concentration.

Figure 10 shows the emission factors as a function of vehicle speed and particle concentration for the Ford Ranger 4x4 tests. By analyzing Figures 8 and 10, it can be seen that the orders of magnitude of the emissions are lower for the tests with the 4x4 compared to those carried out with the Clio. Since the 4x4 is more massive, one could theoretically have expected a higher generation of particles. This is not the case because semi-rigid mud flaps were present behind the tires of the 4x4 (visible in Figure 4-d). They may prevent dust resuspension.

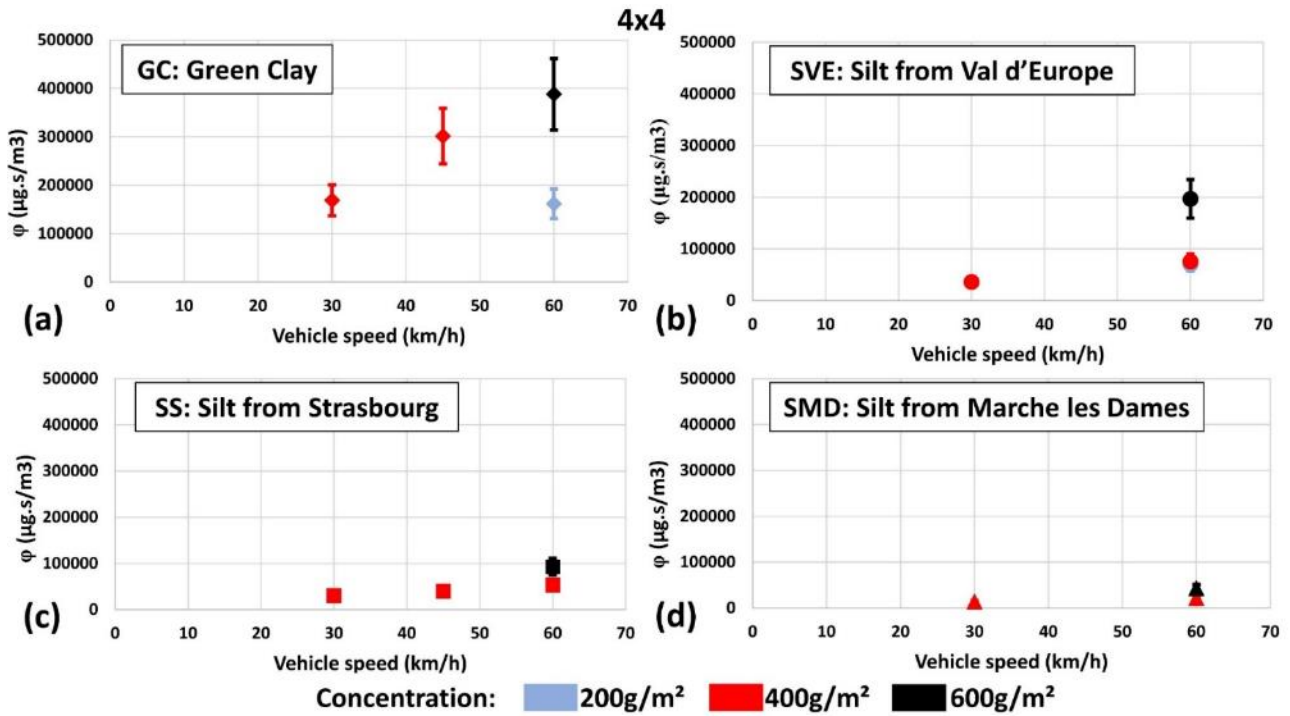


Figure 10: Emission coefficients for the 4x4 tests with particles of (a) green clay, (b) silt from Val d'Europe, (c) silt from Strasbourg and (d) silt from Marche les Dames.

In order to quantify the difference in dust emissions between the two vehicles, Figure 11 shows the comparison of the coefficient ϕ corresponding to the tests with the Clio and those with the 4x4. The gaps are calculated using equation (1). It can be seen that the average difference between the emissions of these two vehicles is all the greater the lower the clay content of the particles. The effect of mud flaps seems to be more marked for coarse particles than for very fine particles. For confirmation, it would be necessary to carry out the tests with the same vehicle with and without mud flaps.

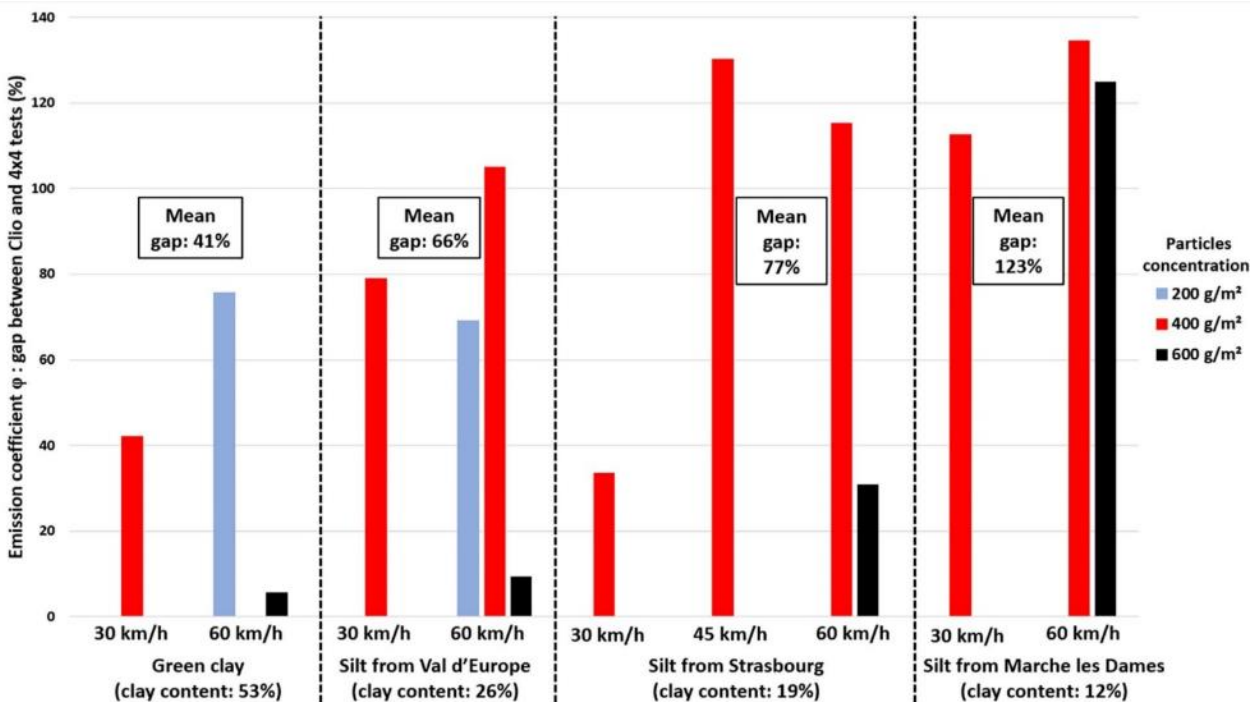


Figure 11: Emission coefficients: gap between Clio and 4x4 tests calculated using equation (1).

In general, Figures 8 and 10 show different dust emissions depending on the type of particle. However, the particles used in the study have almost the same percentages of particles below 75 μm (between 95% and 100%). It is therefore evident that this parameter, although often used in the literature, is not sufficient to characterize the dust emission related to vehicle traffic. Figures 9 and 11 suggest that the percentage of particles below 2 μm would be a more relevant parameter to quantify the lift of particles.

Conclusions

In this study, the dust emissions linked to the traffic of a Renault Clio III and a Ford Ranger 4x4 were studied. Four types of particles (green clay, silt from Val d'Europe, silt from Strasbourg and silt from Marche les Dames) were poured on a test track at different mass per unit area (200 g/m^2 , 400 g/m^2 and 600 g/m^2). Vehicles were driven over the particle beds at different speeds (30, 45 and 60 km/h) and the concentrations of suspended dust were measured directly behind the tire of the vehicle. Weather conditions were measured on the roadside.

The results of the study lead to the following conclusions:

- To quantify the lift of particles, it is not relevant to consider only their silt content (% < 75 μm). The percentage of particles < 2 μm seems to be a more appropriate parameter.
- Although it is often the sole data considered in the literature, the weight of the vehicle is not a sufficient criterion to characterize its dust emission potential. It appears from this study that the impact of accessories such as mud flaps behind the tires could be significant. Vehicle aerodynamics is also a relevant criterion that needs to be taken into account.
- The effect of vehicle speed on dust emission is not a linear process. Indeed, doubling the speed can lead to a multiplication of the emission coefficient by a factor of 5.7. The effect of speed depends on the type of vehicle and the type of particles.
- The results suggest that a phenomenon of particle aggregation by the tire may appear. It seems to be all the more marked as the concentration of particles on the ground is important. This phenomenon would be characterized by the suspension of coarser particles (larger than 10 μm). The measurement of the particle size distribution of all suspended aerosols would be necessary to validate this hypothesis.

Acknowledgement

The authors would like to express their gratitude to the Fédération Nationale des Travaux Publics (grant number RP2_E18101) and the Région Pays de la Loire (grant number GHPAI3) for their financial support. Special thanks to Ouardia Sediki, Erwann Rayssac, Sébastien Buisson and Daniel Bodenes for their help during the experiments.

References

ASTM (2017) ASTM D2487-17e1, Standard practice for classification of soils for engineering purposes (Unified Soil Classification System), *ASTM International, West Conshohocken, PA*

Autrup, H. (2010). Ambient air pollution and adverse health effects. *Procedia Social and Behavioral Sciences* **2**(5):7333-7338, doi: 10.1016/j.sbspro.2010.05.089

Baddock, M.C., Strong, C.L., Leys, J.F., Heidenreich, S.K., Tews, E.K., McTainsh, G.H. (2014). A visibility and total suspended dust relationship. *Atmospheric Environment* **89**:329-336, doi: 10.1016/j.atmosenv.2014.02.038

Belyaev, S.P., Levin, L.M. (1974). Techniques for collection of representative aerosol samples. *Journal of Aerosol Science*, **5**(4):325-338, doi: 10.1016/0021-8502(74)90130-X

Etyemezian, V., Kuhns, H., Gillies, J., Green, M., Pitchford, M., Watson, J. (2003). Vehicle-based road dust emission measurement: I—methods and calibration. *Atmospheric Environment* **37**(32):4559-4571, doi:10.1016/S1352-2310(03)00528-4

Gillies, J.A., Etyemezian, V., Kuhns, H., Nikolic, D., Gillette, D.A. (2005). Effect of vehicle characteristics on unpaved road dust emissions. *Atmospheric Environment* **39**(13):2341-2347, doi: 10.1016/j.atmosenv.2004.05.064

GTR (2000). *Guide français pour la Réalisation des remblais et des couches de forme*. IFSTTAR-CEREMA, Ministère de l'Écologie, du Développement durable et de l'Aménagement du territoire, 2^{ème} édition (in french)

Hichri, Y., Descartes, S., Cerezo, V., Do. M.-T. (2019). Understanding the behavior of fine particles at the tire/road interface. *Tribology International* **149**, 105635, doi: 10.1016/j.triboint.2019.02.043

Hussein, T., Johansson, C., Karlsson, H., Hansson, H.-C. (2008). Factors affecting non-tailpipe aerosol particle emissions from paved roads: On road measurements in Stockholm, Sweden. *Atmospheric Environment* **42**(4):688-702, doi: 10.1016/j.atmosenv.2007.09.064.

ISO (2018). ISO 17892-12/2018 – Laboratory testing of soil – Part 12: Determination of liquid and plastic limits. *International Organization of Standardization, Geneva, Switzerland*

Kuhns, H.D., Green, M., Etyemezian, V. (2003). Big Bend Regional Aerosol and Visibility Observational (BRAVO) study emissions inventory. *Report for the Desert Research Institute, Las Vegas, Nevada*, 56 p.

Kuhns, H.D., Gillies, J., Etyemezian, V., Nikolich, G., King, J., Zhu, D., Uppapalli, S., Engelbrecht, J., Kohl, S. (2010). Effect of Soil Type and Momentum on Unpaved Road Particulate Matter Emissions from Wheeled and Tracked Vehicles. *Aerosol Science and Technology* **44**(3):187-196, doi:10.1080/02786820903516844

Le Vern, M., Sediki, O., Razakamanantsoa, A.R., Murzyn, F., Larrarte, F. (2020a). Experimental study of particle lift initiation on roller compacted sand-clay mixtures. *Environmental Geotechnics*, doi:10.1680/jenge.19.00172

Le Vern, M., Sediki, O., Razakamanantsoa, A.R., Murzyn, F., Larrarte, F. (2020b). Experimental assessment of dust emissions on compacted soils degraded by traffic. *Atmosphere* **11**, 369, doi:10.3390/atmos11040369

Mercker, E., Berneburg, H. (1992). On the simulation of road driving of a passenger car in a wind tunnel using a moving belt and rotating wheels. *Proceedings of 3rd International Conference on Innovation and Reliability*, Florence, Italy

Muleski, G.E., Cowherd, C., Kinsey, J.S. (2005). Particulate emissions from construction activities. *Journal of Air and Waste Management Association*, **55**(6):772-783, doi:10.1080/10473289.2005.10464669

Petroff, A., Zhang, L. (2010). Development and validation of a size-resolved particle dry deposition scheme for application in aerosol transport models. *Geoscientific Model Development* **3**:753-769, doi: 10.5194/gmd-3-753-2010

Pope, C.A., Dockery, D.W. (2006). Health effects of fine particulate air pollution: Lines that connect. *Journal of the Air & Waste Management Association*, **56**(6):709-742, doi:10.1080/10473289.2006.10464485

Ravi, S., Zobeck, T.M., Over, T.M., Okin, G.S., D'Odorico, P. (2006). On the effect of moisture bonding forces in air-dry soils on threshold friction velocity of wind erosion. *Sedimentology* **53**:597-609, doi: 10.1111/j.1365-3091.2006.00775.x

U.S. Environmental Protection Agency. (1995) "Compilation of Air Pollutant Emission Factors, AP-42, Fifth Edition.", *Office of Air Quality Planning and Standards, Research Triangle Park*.

Veranth, J.M., Pardyjak, E.R., Seshadri, G. (2003). Vehicle-generated fugitive dust transport: analytic models and field study. *Atmospheric Environment* **37**:2295-2303, doi:10.1016/S1352-2310(03)00086-4

Wilcox, J.D. (1956). Isokinetic flow and sampling. *Journal of the Air Pollution Control Association*, **5**(4):226-245, doi:10.1080/00966665.1956.10467715

2.3 Beyond car efficiency and electrification: Examining the role of demand reduction, public transit, and active travel measures to reduce GHG emissions in transport

V. O’Riordan^{1,2*}, H. Daly^{1,2}, T. Mac Uidhir¹, B. Ó Gallachóir^{1,2}, F. Rogan^{1,2}

¹ Energy Policy and Modelling Group, MaREI Centre, Environmental Research Institute, Co. Cork, Ireland

² School of Engineering, University College Cork, Co. Cork, Ireland

vera.oriordan@ucc.ie

Abstract

This paper applies a data set of passenger kilometre transport demand by trip-purpose, mode type and trip-distance based on the outcomes of a National Travel Survey. The Irish Passenger Transport Emissions and Mobility (IPTeM) model enables a system-wide perspective on various measures which could be introduced to reduce passenger transport emissions. Combined with the LEAP Ireland 2050 energy systems simulation model, the carbon abatement potential of trip-purpose based policies, modal shift policies and technology improvements in public transport can be assessed. The results indicate that significant savings can be achieved from modal shift in Ireland, and that trip-purpose based targets and policies have a relevance in the effort to reduce Ireland’s energy related transport CO₂ emissions. The active mode scenarios, which focus on increased walking and cycling achieve a 0.2 – 1 MTCO₂ reduction in annual passenger transport emissions in 2030. The range of public transport scenarios, inspired by targets set out by the Irish Government’s Climate Action Plan achieve a between 0.001 – 0.3 MTCO₂ reduction in annual passenger transport emissions in 2030. In addition, traffic camera data is used to model the impact of COVID-19 travel restrictions on transport CO₂ emissions. The calculated reduction in transport CO₂ emissions is 3.9 MTCO₂ for 2020 and 2021. This study highlights the importance of factoring modal shift, trip distance and trip purpose into scenario analysis for transport emissions reduction, as it provides a framework for looking beyond only improving technologies in private vehicle transport.

Introduction

To date, solutions for decarbonizing transport have focused on altering the fuel and technology composition of the car fleet. For example, Ireland’s most recent Climate Action Plan outlines ambitions to have 845,000 EVs in Ireland by 2030 [1]. Ireland has also committed to an increased biofuel blending rate under the Biofuel Obligation Scheme for vehicles using petrol and diesel [2]. Under the EU Effort Sharing Decision, Ireland has agreed to ambitious targets of 20% emissions reduction below 2005 levels by 2020 and 30% by 2030 [3]. Past national transport emissions reductions policy analyses have focused on private vehicle emissions and the efficacy of an emissions-based vehicle motor tax to encourage a shift in purchases from to cars with a lower carbon intensity [4]–[6]. Other studies have focussed on the role of increased biofuel mixing for internal combustion engines and the role of increasing sales of electric vehicles [7], [8].

The Intergovernmental Panel on Climate Change (IPCC) has noted the rise in global transport greenhouse gas emissions, despite efficiency improvements, as transport activity has increased, while becoming more individual and motorized. The new framing is represented in transport by moves from the low-carbon approach, which focuses on fuel switching, to a comprehensive sustainability approach in the Avoid-Shift-Improve (ASI) framework, as recommended by the IPCC [9]. This approach involves moving through a hierarchy of actions: avoid – avoiding journeys where possible, through innovative spatial planning, compact development and demand management; shift – shifting mode to the more sustainable modes of walking, cycling and public transport; and lastly improve – improving the energy and carbon efficiency of vehicles, including improved designs, choosing smaller vehicles, and switching to alternative powertrains and renewable fuels.

The Irish Government’s Department for Transport, Tourism and Sport has also acknowledged that the ASI framework is the best practice approach. Building on this consensus, the next steps required are to ensure that appropriate evidence is made available to inform decision-making at each level in designing policies and understanding measures that can deliver effectively on each level of the Avoid-Shift-Improve framework [10].

Global energy systems optimization modelling identified the possible range of CO₂ emissions reductions from modal shift in transport. Cuenot et al. identified a need for national and localized studies to acutely identify the regional scope for emissions reduction through increased active travel and public transport [11]. Transport energy modelling studies up until now for Ireland have focused on the impacts of fuel-switching and the electrification of private vehicles [12]. This study aims to address this need.

Urban based studies of modal shift highlight the possibility for reduced carbon footprint through a switch to active modes [13], [14]. The methods in this paper aim to develop a national projection of how active modes of travel and modal shift can contribute to national efforts to reduce greenhouse gas emissions as pledged under the Paris Agreement.

This study aims to push beyond fuel switching and private car transport to investigate the role of modal shift and demand reduction measures in reducing Ireland's transport CO₂ emissions. This model will build on previous knowledge from the technology rich Irish Car Stock Model [15], and the Low Emissions Analysis Platform (LEAP) developed for the transport sector in Ireland [16]. Using information from the National Travel Survey [17], this study compiles a snapshot of mobility and modal choices in Ireland, giving an estimate of the passenger transport demand.

In 2009, the Irish Government published their "Smarter Travel" policy document, which aspired to achieve "10% of all trips for work to be completed by bike". Up until now, it was not possible to monitor the target, and neither was it possible to record the emission reduction implications of achieving such a target. The same document also aspired to have "10% of all journeys completed by bike" and a vision of 450,000 people walking and cycling to work or school each day in 2020, up from 240,000 in 2006" [18].

Comparisons of the abatement potential of technology-, trip- and mode-based measures can be compiled within the framework of the Irish Passenger Transport Emissions and Mobility (IPTeM) Model alongside LEAP Ireland energy systems simulation model. The results will be discussed in the context of Ireland's current transport emissions reduction target to 2030.

Policy areas to be explored in this study include: i) Increased walking and cycling rates and ii) Increased uptake and electrification of public transport.

Methods

The modelling framework used to model increased walking and cycling rates and increased uptake and electrification of public transport involves three elements_

- The Irish Car Stock Model
- The Irish Passenger Transport Emissions and Mobility (IPTeM) Model
- The Low Emissions Analysis Platform (LEAP) Ireland Model

An overview of the modelling space is highlighted in Figure 1 (below), followed by detailed descriptions of each of the modelling elements.

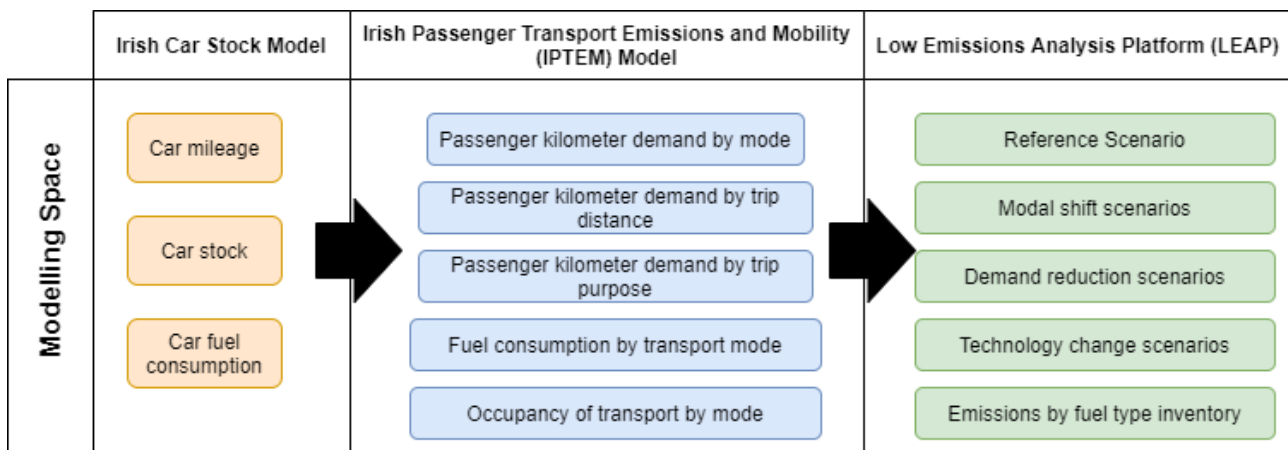


Figure 1: Overview of Transport Emissions Modelling Framework.

Irish Car Stock Model

The first element of the Transport Emissions Modelling Framework builds from a technological stock model of the Irish private car fleet, which was first developed in Daly & Ó Gallachóir, 2011a [16]. The car stock was disaggregated by fuel type, engine cc and age to produce a detailed look at private car activity and energy consumption over the period 2000 - 2018. The car stock simulation program developed for this paper is publicly available on Zenodo [19].

The total number of new private cars from 2000 – 2018 is based on the number of new vehicles registered, as recorded by the Central Statistics Office each year [19]. The car stock model then calculates survival rates of cars and import rates of second-hand cars to develop a picture of the entire car fleet in Ireland.

The Irish Passenger Transport Emissions and Mobility (IPTeM) Model

The Irish Passenger Transport Emissions and Mobility (IPTeM) Model factors in trip-purpose and modal shift in determining passenger transport demand. The IPTeM Model deduces passenger transport demand across all mode types based on responses from the National Travel Survey. By calibrating the passenger kilometres travelled by car with an estimated occupancy rate of 1.5 people and vehicle kilometres as calculated by the Irish Car Stock Model [17]. Combined with the system wide simulation model LEAP (Low Emissions Analysis Platform), these tools can investigate the role of cycling, walking, remote working, and public transport in low carbon passenger transport transitions [20].

Using the IPTeM model, we can observe how modal shift and trip purpose-based transport reductions can influence Irish passenger transport emissions. Passenger numbers, fuel consumption figures and occupancy rates for public transport are based on annual reports from Bus Éireann (nationwide intercity bus service), Dublin Bus (urban bus system operating in Dublin, Ireland), Irish Rail (heavy rail) and Luas (light rail operating in Dublin, Ireland) [21]–[24]. Passenger kilometres travelled in Ireland by mode type, as calculated within the IPTeM model, are shown in Figure 2 (below).

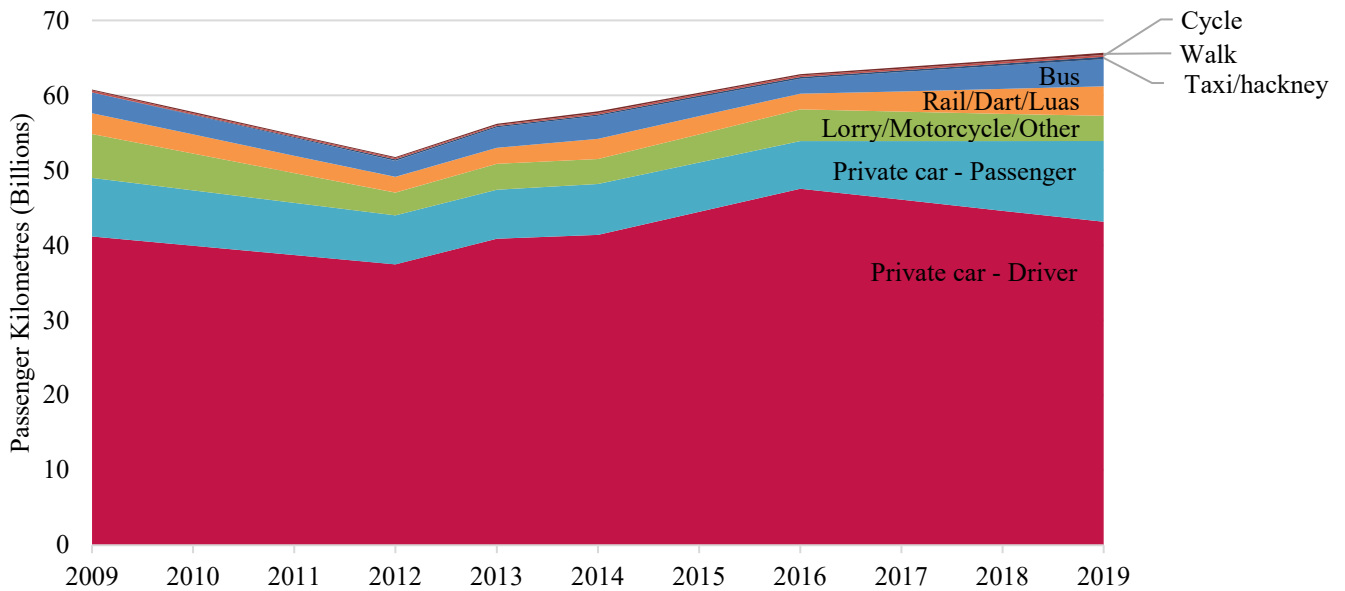


Figure 2: Passenger kilometres by mode type, 2009 – 2019.

The energy intensity of each mode type per passenger kilometre (Pkm) was calculated as follows in Equation 1:

$$\text{Energy Intensity} \left(\frac{\text{kWh}}{\text{pkm}} \right) = \frac{\text{Energy intensity per kWh}_{f,t} \times \text{Energy consumption per year}_{f,t}}{\text{Pkm}_t} \quad (1)$$

where f is the fuel type, and t represents the transit provider (Bus Éireann, Irish Rail, etc.).

The carbon intensity of each mode type per passenger kilometre (Pkm) was then calculated as follows in Equation 2:

$$\text{Carbon Intensity} \left(\frac{\text{gCO}_2}{\text{pkm}} \right) = \frac{\text{Carbon intensity per kWh}_{f,t} \times \text{Energy consumption per year}_{f,t}}{\text{Pkm}_t} \quad (2)$$

where f is the fuel type, and t represents the transit provider.

The carbon intensities of the energy sources are provided by the Sustainable Energy Authority of Ireland [25].

Low Emissions Analysis Platform (LEAP IE 2050)

The third element of the Transport Emissions Modelling Framework uses the LEAP (Low Emissions Analysis Platform) Ireland model. LEAP models use a hierarchical tree structure to define energy demand sectors. These tree structures are flexible and can be designed to incorporate large volumes of granular data. The LEAP transport sector is described by four main subsectors: private transport, freight, fuel tourism and navigation. Private transport further subdivides into distinct subcategories; road private cars, aviation, passenger rail, buses, and active modes of travel (cycling, walking etc.). Private passenger vehicles are defined by vintage (25 years), fuel types (petrol, diesel, electric, compressed natural gas (CNG), hybrid and plug-in hybrid electric), and engine sizes (ranging from less than 900 cc to greater than 2100 cc), based on outputs from the aforementioned Irish Car Stock Model. Passenger kilometres are calibrated against the Irish Passenger Transport Emissions and Mobility (IPTeM) Model.

The platform provides a basis for developing a “business-as-usual” reference scenario, defined by the modeler, and multiple alternate scenarios with variations for comparison. Simulation modelling is particularly useful as it can be easily reused and communicated for custom purposes. Energy consumption rates and net CO₂ emissions are handled within the platform by combining stated energy demands with the associated fuel consumption per unit of demand and the carbon intensity of the fuels. Further information on the Low Emissions Analysis Platform is available online [26]. Emissions savings are calculated as CO₂ emissions reductions of a stated scenario with respect to the reference, and these emissions savings are highlighted in the results section, as shown in Table 3, Table 4 and Figure 4 (below).

COVID-19 & Passenger Transport Demand

The COVID-19 pandemic resulted in blanket travel restrictions and ‘work-from-home’ resolutions in many countries, including Ireland. Transport is one of the main sources of carbon dioxide (CO₂) emissions globally. Our paper calculates the impact of travel restrictions on passenger transport demand and the associated CO₂ emissions for 2020 and 2021. We apply a novel approach, using road traffic data from traffic cameras nationwide to inform changes in an energy systems model. By comparing traffic volume levels before and during the pandemic, a snapshot of the changed transport mobility patterns was captured. These recorded mobility patterns were quantified in terms of the passenger kilometres by mode type.

At the beginning of the year, traffic counter data indicated a net increase in traffic volumes in 2020, with volumes 9.8% and 7.5% higher than January and February 2019, respectively. On introduction of the COVID-19 travel restrictions on the 12th March 2020 in Ireland, monthly traffic volumes for March 2020 fell 28% below 2019 traffic volumes.

Figure 3 (below) highlights the annual indexed fluctuations in transport demand by vehicle type across the road transport system. Bus and car traffic volumes have experienced the worst effects over the year, with net reductions 26% and 25% below 2019 levels, respectively. Caravans and articulated trucks (HGV_ART) were among the least impacted, with articulated trucks indicating a traffic volume increase of 2.5% when compared to 2019. Rigid heavy goods vehicles (HGV_RIG) and light good vehicles (LGV) traffic volume flows in 2020 were reduced by 11% and 8% respectively.

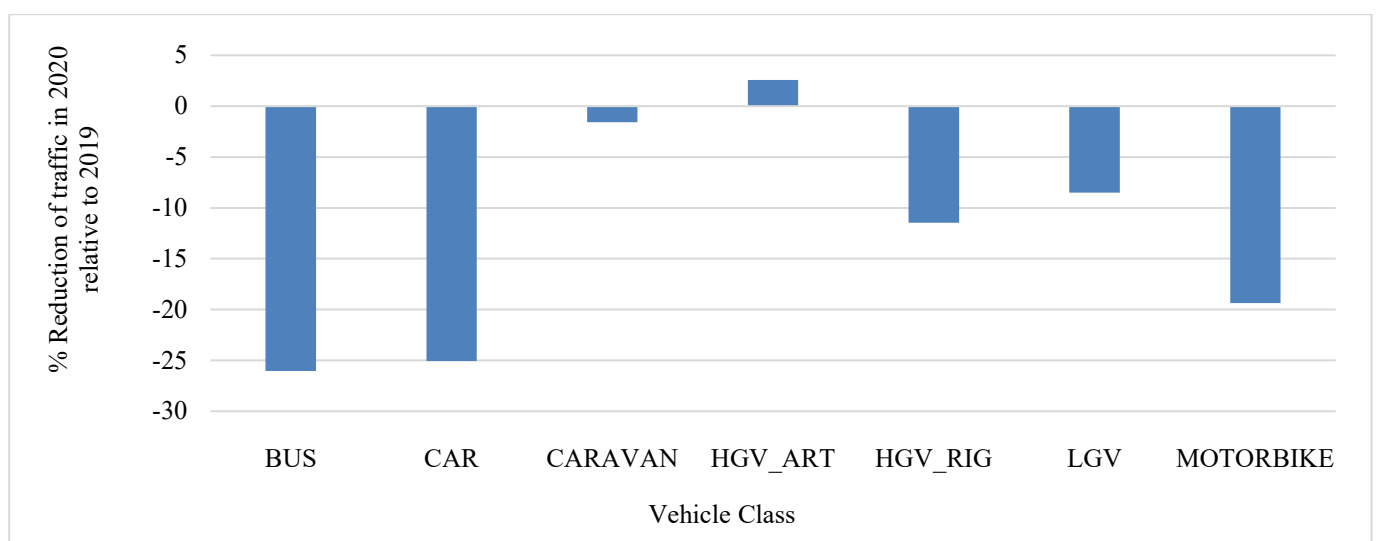


Figure 3: Index of traffic volumes by vehicle class in 2020 (January – November) with respect to 2019.

Cycling rates were estimated based on analysing bike counter data from a site on Grove Road in Co. Dublin, which recorded up to a 40% increase in cycling rates, and nation-wide reports of increased bike sale of 30% with a partial regression to pre-COVID levels in 2021 [reference].

Projections for passenger transport demand up to 2030

The Irish car stock is projected using income per adult and car per adult as the drivers. The growth rate of income per adult is taken from the National Transport Model [27]. This income per adult is further used to project the car per adult, using a Gompertz function as shown below (3) [28].

$$y = \alpha e^{-\beta * e^{-\gamma x}} \quad (3)$$

Where α is the saturation level (maximum number of cars per 1000 persons) is equal to 875; β and γ are estimated. Historical passenger kilometres from CSO's database and car per adult are then used in a regression model to finally project passenger kilometres. For the reference scenario, it is assumed that growth in car passenger kilometres corresponds with an equivalent growth in passenger kilometres of other transport modes.

Active Modes – Walking and Cycling Scenarios

An overview of the scenarios for active modes of travel ran in the LEAP IE model based on inputs from the Irish Passenger Transport Emissions and Mobility (IPTeM) Model is shown in Table 1 (below).

Table 1: Overview of scenarios for walking and cycling.

Scenario	Description
Reference	Assumes no change in share of transport modes from 2019 levels, and demand growth in line with population and economic growth drivers as calculated by Equation 3.
Cycling accounts for 10% of the shortest trips	Share of cycling passenger kilometres increases until it reaches the value of passenger kilometres that represents 10% of the shortest trips
Cycling and walking 450k trips per day	Walking and cycling trips increase proportionally to their current shares until 450k trips per day are either by walking or cycling
Cycling accounts for 10% of work passenger kilometres by 2030	Cycling rate increases for work related travel until 10% of passenger kilometres for work is by cycling
Cycling is 10% of work and education passenger kilometres	Cycling rate increases for work and education related travel until 10% of passenger kilometres for work and education is by cycling
Cycling accounts for 10% of trips of typical cycling journey length	Cycling accounts for 10% of trips of typical cycling length
Cycling accounts for 10% of ALL passenger kilometres	Cycling services 10% of ALL passenger kilometre demand each year.

Public Transport Scenarios

An overview of the scenarios for public transport ran in the LEAP IE model based on inputs from the Irish Passenger Transport Emissions and Mobility (IPTeM) Model is shown in Table 2 (below).

Table 2: Overview of scenarios for Public Transport.

Scenario	Description
Reference	Assumes no change in share of transport modes from 2019 levels, and demand growth in line with population and economic growth drivers as calculated by Equation 3.
Bus Connects	Based on Climate Action Plan Action No. 88 – “Implementation of Bus Connects services network” [1]. This scenario assumes a 20% of car passenger kilometres in Dublin switches to bus, based on studies from past success of mode switching with BRT from studies, which indicate mode shift potential of between 5 - 70% from car to bus following the introduction of a Bus Rapid Transit system [29].
Electrification of Rail	Based on Climate Action Plan No. 93 – Electrification of all railway lines in Ireland by 2030 [1].
Hybrid Rail Fleet	Based on the Climate Action Plan Action No.92 Hybrid fleet for rail, with hybrid fleet, with full hybridization by 2030, and a linear increase from 2023 to 2030. (20% electric, 80% diesel [2])
Extension of Luas line	Based on the Climate Action Plan Action No. 90, “Add additional capacity to Luas network”, Addition of Luas in Finglas to Dublin’s city center, a 4km Luas line expansion. The scenario assumes that the increase in passenger kilometres will increase. Exploratory scenarios using NTS modality shares for Dublin (using other red & green lines as a guide). Method will increase Luas passenger kilometre proportion, using past usage patterns with respect to line length as a guide for usage patterns with increased rail line length [1].

Results

The passenger transport emissions calculations from the various active modes scenarios as described in Table 1 is highlighted in Figure 4 (below). A summary of results is documented in Table 3 (below).

Active modes of travel

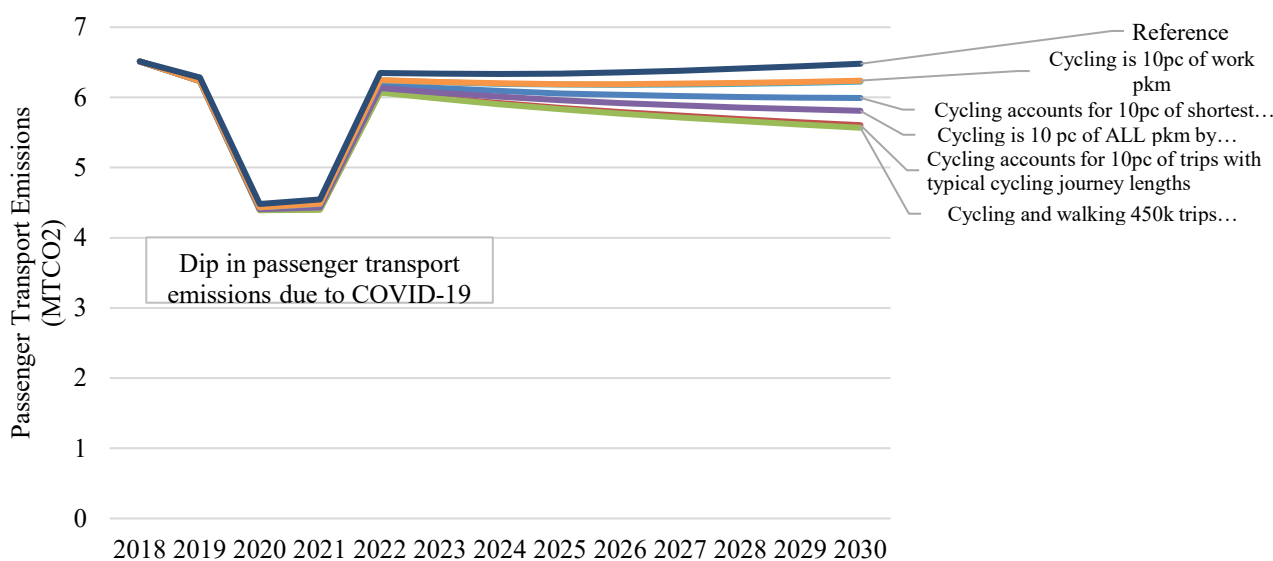


Figure 4: Scenario Comparisons for Energy Related Annual Passenger Transport CO₂ Emissions for Ireland (2018 – 2030).

Table 3: Summary of results for Active Travel Scenarios.

Scenario	Annual reduction in emissions by 2030 compared to 2019
	MTCO ₂
Cycling accounts for 10% of work passenger kilometres by 2030	0.2
Cycling accounts for 10% of work and education passenger kilometres by 2030	0.3
Cycling accounts for 10% of all trips, starting with the shortest	0.5
Cycling is 10% of all passenger kilometres by 2030 (this is the current rate of cycling in the Netherlands [30])	0.7
Cycling accounts for 10% of trips with typical cycling length	0.9
Cycling and walking increases proportional to current penetrations to 450,000 trips per day (Smarter Travel Target [18])	1

Public Transport Scenarios

A summary of results from calculations from the public transport scenarios as described in Table 2 is highlighted in Table 4 (below).

Table 4: Summary of results for Public Transport scenarios.

Scenario	Annual reduction in emissions by 2030 compared to 2019
	MTCO ₂
Electrification of all rail by 2030	0.3
Hybrid fleet of trains by 2030	0.2
Bus Rapid Transit in Ireland's capital city with "Dublin Bus Connects"	0.04
Extension of the light rail "Luas" (Light rail) line in Ireland's capital, Dublin	0.001

Discussion and Conclusion

The Irish Passenger Transport Emissions and Mobility (IPTeM) model, in conjunction with the simulation based Low Emissions Analysis Platform, LEAP Ireland can demonstrate how demand reduction and modal shift measures can achieve transport emissions reductions in Ireland. The scenarios draw from policies outlined by the Irish Government and illustrate the scale of the challenge to achieve a 7% annual reduction in CO₂ emissions from transport in Ireland, and a near 50% reduction in transport related CO₂ emissions by 2030. For passenger transport, a 7% annual reduction in CO₂ emissions would correspond with a reduction in annual passenger transport of between 3 – 4 MTCO₂ by 2030 compared to 2020.

Private car is the most common transport mode in Ireland - many more journeys could be via public transport or via active travel. The active travel policy scenarios highlight the potential of the targets originally outlined in the "Smarter Travel" policy document to achieve tangible CO₂ emissions reduction from passenger transport. Our results show that achieving the increased active travel passenger transport targets offers CO₂ emissions reductions of between 0.2 – 1 MT CO₂ by 2030 from 2019. The public transport measures in the Climate Action Plan (2019) do not achieve

a significant reduction in emissions by 2030. Our results indicate that they achieve between 0.001 – 0.3 MTCO₂ reduction by 2030 when compared with 2019. Some policies, such as the electrification of all rail, have a far greater impact than other measures, such as the extension of the Luas (light rail) line. The electrification of all rail lines achieves 300 times the CO₂ emissions reductions that extending the light-rail Luas does. However, both policies are included as individual actions in the Climate Action Plan, with no prioritization or any indication of their relative impact. Keeping the relative scale of emissions reduction savings in mind is particularly useful when assigning resources to achieving these targets.

Development of the remote working scenarios as noted in the 2020 Irish Program for Government, and future scenario analysis on passenger kilometre demand reduction and modal shift scenarios are areas for future work [31]. Further work should also focus on the interaction effect between different policy measures, as the process of achieving emissions reductions through modal shift may elevate or dampen the impacts of policy measures focusing on another part of the transportation system (e.g. simultaneously increasing the biofuel mixing percentage in fuels and active modes of travel).

In conclusion, this paper has provided a framework for calculating the system-wide emissions impacts of demand reduction from the COVID-19 pandemic and of modal shift policy targets. The framework enables modellers to carry out analysis beyond car efficiency and electrification measures and the study demonstrated the role of public transport, active modes of travel and demand reduction due to the COVID-19 pandemic in transport CO₂ emissions reduction.

Acknowledgements

The authors acknowledge the funding and support provided by the Climate and Energy Modelling Services to the Technical Research and Modelling (TRAM) Group: Services RFT2016/01213/12806.

References

- [1] Department of Communications Climate Action and Environment, “Climate Action Plan to Tackle Climate Breakdown,” *Dep. Commun. Clim. Action Environ.*, p. 150, 2019, doi: 10.5860/choice.46-0890.
- [2] National Oil Reserves Agency, “Biofuel Obligation Scheme.” [Online]. Available: <https://www.nora.ie/biofuels-obligation-scheme.141.html>. [Accessed: 13-Oct-2020].
- [3] REGULATION (EU) 2018/842 OF THE EUROPEAN PARLIAMENT AND OF THE COUNCIL of 30 May 2018. European Parliament.
- [4] F. Rogan, E. Dennehy, H. Daly, M. Howley, and B. P. Ó Gallachóir, “Impacts of an emission based private car taxation policy – first year ex-post analysis,” *Transp. Res. Part A Policy Pract.*, vol. 45, no. 7, pp. 583–597, 2011, doi: 10.1016/j.tra.2011.03.007.
- [5] S. Giblin and A. McNabola, “Modelling the impacts of a carbon emission-differentiated vehicle tax system on CO₂ emissions intensity from new vehicle purchases in Ireland,” *Energy Policy*, vol. 37, no. 4, pp. 1404–1411, 2009, doi: 10.1016/j.enpol.2008.11.047.
- [6] H. Hennessy and R. S. J. Tol, “The impact of tax reform on new car purchases in Ireland,” *Energy Policy*, vol. 39, no. 11, pp. 7059–7067, 2011, doi: 10.1016/j.enpol.2011.08.011.
- [7] E. Mulholland, F. Rogan, and B. P. Ó Gallachóir, “From technology pathways to policy roadmaps to enabling measures – A multi-model approach,” *Energy*, vol. 138, pp. 1030–1041, 2017, doi: 10.1016/j.energy.2017.07.116.
- [8] E. Mulholland, F. Rogan, T. Mac Uidhir, and B. Ó. Gallachóir, “Opportunities to Decarbonise the Irish Transportation Sector.” [Online]. Available: https://www.epa.ie/pubs/reports/research/climate/Research_Report_321.pdf. [Accessed: 19-May-2021].
- [9] IPCC, Climate Change 2014: Mitigation of Climate Change. Summary for Policymakers and Technical Summary, no. September 2014. 2014.
- [10] Department of Transport, “Oireachtas Joint Committee on Climate Action Wednesday 27 November 2019 Statement by the Department of Transport, Tourism and Sport,” vol. 11, no. 1. 2019.
- [11] F. Cuenot, L. Fulton, and J. Staub, “The prospect for modal shifts in passenger transport worldwide and impacts on energy use and CO₂,” *Energy Policy*, vol. 41, pp. 98–106, 2012, doi: 10.1016/j.enpol.2010.07.017.

- [12] H. Daly and B. P. Ó Gallachóir, “Modelling private car energy demand using a technological car stock model,” *Transportation Research Part D: Transport and Environment*, vol. 16, no. 2, pp. 93–101, 2011, doi: 10.1016/j.trd.2010.08.009.
- [13] C. Brand *et al.*, “The climate change mitigation impacts of active travel: Evidence from a longitudinal panel study in seven European cities,” vol. 67, no. September 2020, 2021, doi: 10.1016/j.gloenvcha.2021.102224.
- [14] S. Pye and H. Daly, “Urban transport modal shift: an energy systems approach,” in *International Energy Workshop*, 2015.
- [15] H. E. Daly and B. P. Ó Gallachóir, “Future energy and emissions policy scenarios in Ireland for private car transport,” *Energy Policy*, 2012, doi: 10.1016/j.enpol.2012.08.066.
- [16] F. Rogan *et al.*, “LEAPs and Bounds—an Energy Demand and Constraint Optimised Model of the Irish Energy System,” *Energy Effic.*, vol. 7, no. 3, pp. 441–466, 2014, doi: 10.1007/s12053-013-9231-9.
- [17] Central Statistic Office, “National Travel Survey 2019,” 2020. [Online]. Available: <https://www.cso.ie/en/releasesandpublications/ep/p-nts/nationaltravelsurvey2019/howwetravelled/>. [Accessed: 21-Nov-2020].
- [18] Department of Transport, “Smarter Travel: A Sustainable Transport Future,” 2009. [Online]. Available: http://www.smartertravel.ie/sites/default/files/uploads/2012_12_27_Smarter_Travel_english_PN_WEB%5B1%5D_0.pdf.
- [19] V. O’Riordan, E. Mulholland, F. Rogan, B. O. Gallachóir, and H. E. Daly, “Irish Car Stock Model V 2.4.” 2021, doi: 10.5281/zenodo.4651477.
- [20] T. Mac Uidhir, F. Rogan, and B. Ó. Gallachóir, “Develop a LEAP GHG Ireland Analytical Tool for 2050,” 2020.
- [21] Bus Éireann, “Annual Reports,” 2021. [Online]. Available: <https://www.buseireann.ie/inner.php?id=680>. [Accessed: 13-Apr-2021].
- [22] Dublin Bus, “Annual Reports,” 2021. [Online]. Available: <https://www.dublinbus.ie/About-Us/Reports/Annual-Reports/>. [Accessed: 13-Apr-2021].
- [23] Irish Rail, “Iarnród Éireann Annual Reports,” 2021. [Online]. Available: <https://www.irishrail.ie/en-ie/about-us/company-information/iarnrod-eireann-annual-reports>. [Accessed: 13-Apr-2021].
- [24] National Transport Authority, “Luas Performance Reports 2017 to 2020,” 2021. [Online]. Available: <https://www.nationaltransport.ie/publication/luas-performance-reports-2017-to-2020/>. [Accessed: 13-Apr-2021].
- [25] Sustainable Energy Authority of Ireland, “Conversion Factors | SEAI Statistics | SEAI,” 2020. [Online]. Available: <https://www.seai.ie/resources/seai-statistics/conversion-factors/>. [Accessed: 13-Oct-2020].
- [26] “Low Emissions Analysis Platform,” 2020. [Online]. Available: <https://leap.sei.org>. [Accessed: 10-Dec-2020].
- [27] AECOM Ireland Limited, “National Transport Model Update,” 2019. [Online]. Available: <https://www.tii.ie/tii-library/strategic-planning/national-transport-model/NTpM-Vol2-Data-Collection-Report.pdf>. [Accessed: 19-May-2021].
- [28] L. Lian, W. Tian, H. Xu, and M. Zheng, “Modeling and Forecasting Passenger Car Ownership Based on Symbolic Regression,” 2018, doi: 10.3390/su10072275.
- [29] T. Satiennam, S. Jaensirisak, W. Satiennam, and S. Detdamrong, “Potential for modal shift by passenger car and motorcycle users towards Bus Rapid Transit (BRT) in an Asian developing city,” *IATSS Res.*, vol. 39, no. 2, pp. 121–129, 2016, doi: 10.1016/j.iatssr.2015.03.002.
- [30] T. A. S. Nielsen, I. Mulalic, and H. Christiansen, “Drivers of cycling mode-share: analysis of danes travel behavior 1996-2013,” *Transp. Res. Procedia*, vol. 14, pp. 2284–2288, 2016, doi: 10.1016/j.trpro.2016.05.244.
- [31] Government of Ireland, “Programme for Government – Our Shared Future,” 2020. [Online]. Available: <https://assets.gov.ie/94092/50f892b9-a93e-43fc-81d1-778ff9954d9f.pdf>. [Accessed: 19-May-2021].

2.4 Emission behaviour of recent EURO VI HDVs from chassis dyno and PEMS Tests

K. Weller*, L. Landl, S. Lipp, C. Matzer, S. Hausberger

Institute of Internal Combustion Engines and Thermodynamics, Graz University of Technology, Austria

weller@ivt.tugraz.at

Abstract

The introduction of the emissions standard Euro VI D for Heavy-Duty Vehicles (HDV) [1] brought a decrease of the power threshold for moving average windows in In-Service-Conformity (ISC) tests from 20 to 10 percent. In addition to that, one valid moving average window has to be completely inside the urban part. The main aim of these requirements is to push manufacturers to improve the low load emission performance of Euro VI D vehicles.

The Institute for Internal Combustion Engines and Thermodynamics of Graz University of Technology (TUG) tested different Euro VI D vehicles on the chassis dyno and on-road to check their real world emission performance. The test program contains type approval compliant tests as well as tests which exceeded regulatory boundary conditions with main focus on low load and cold start tests. The campaign covered so far tests on 7 diesel driven vehicles and 1 vehicle powered by liquefied natural gas (LNG). The selected test vehicles cover different manufacturers and size classes. This creates a comprehensive picture about the real-world emission performance of Euro VI D heavy goods vehicles (HGV).

The main focus of this paper regarding regulated gaseous pollutants is on NO_x. Most diesel vehicles showed an improvement compared to vehicles up to Euro VI C in type approval tests. In motorway driving some trucks come up with NO_x emissions which are in the range of analysers' detection limit. But the spread between best and worst performing vehicles is large. One vehicle comes up with NO_x emissions even above the limit. The results show also that driving situations outside of the ISC boundary conditions (e.g. low load urban driving combined with cold start) lead to higher emission levels for all test vehicles. The tested LNG truck was in all test conditions on the level of the best performing diesel vehicles.

The analysis of the non-regulated gaseous emissions pushed N₂O in the focus. Although N₂O was measured by use of a FTIR only on the chassis dyno, WHVC and real world cycle tests allow an evaluation of the emission behaviour. N₂O emissions of diesel driven vehicles contributed to the total CO₂ equivalent emissions up to 5 % based on the N₂O global warming potential of 265 related to 100 years [2]. The results illustrate also a connection between low NO_x and high N₂O emissions and thus suggest the introduction of a regulative N₂O-limit in Euro 7.

This paper addresses also particulate emissions from Euro VI D HGVs. PN₂₃ and PN₁₀ were measured. By and large, the new vehicles have very low PN emission values. Increased particulate emissions only occur in special driving situations, such as in the cold start phase and during DPF regeneration. Analogous to the N₂O emissions, the PN₁₀ emissions should also be examined more closely with regard to future emission legislations.

Acknowledgement: All measurement data used in this paper were elaborated in the project "Projekt 91180: Realemissionen aus Fahrzeugen und Maschinen (real world emissions from vehicles and machinery)" funded by the German Environment Agency (UBA). We want to thank the UBA for the possibility to use the measurement data of the project for this paper.

Introduction

Continuous economic growth and further globalisation leads to an increasing goods transport all over the world and, of course, also in Europe. Predictions assume an increase of the demand in goods transport in Europe of 30 % in the next 10 years [3]. This will also affect the sector of road transport which accounts for more than half of the total volume of goods transported (in 2018 52.4 % of all goods). The most relevant alternatives are shipping (34.1 %) and rail traffic (13 %) [4]. A further increase of the transport sector will also raise the amount of trucks on the road, which are nearly all diesel powered, and thus impact air quality. As an example, heavy duty vehicles (HDV) including heavy goods vehicles (HGV), coaches (CO) and urban busses (CB), contribute currently 18 % of the total NO_x emissions from road traffic in Austria [5]. Consequently further air quality improvements can only be reached hand in hand with effective future emission standards.

Step A of the current emission standard Euro VI came along with a more demanding test cycle on the engine test bed, the World Harmonized Transient Cycle (WHTC), and on-road testing, so-called in-service conformity tests (ISC), became part of the regulatory framework. Further steps (B to E) modified valid ISC test conditions, e.g. Euro VI step C extended the possible payload from a range between 50 and 60 % to a range between 10 and 100 % [6]. In the meantime, vehicles with emissions standard Euro VI step D (introduction in September 2018 for new models and September 2019

for all vehicles) are part of the HGV fleet. The main adaptation by step D was the reduction of the average engine power for valid moving average windows (MAW)¹ from 20 to 10 % of the rated engine power [1]. Consequently, regulatory tests can become more challenging since keeping the temperature of the exhaust aftertreatment system in its optimal operating conditions for high NO_x conversion at low engine loads is a demanding task. Accordingly, increasing NO_x-emissions of vehicles with emission standard Euro VI A and B in such low load driving conditions were found [7]. Hence, vehicles with emission standard Euro VI D need special measures to increase the temperature of the exhaust gas in low load driving in order to stay below the emission limits in ISC tests.

Euro VI step E (introduction in January 2021 for new models and in January 2022 for all vehicles) will also include the cold start emissions above an engine coolant temperature of 30°C in the evaluation of an ISC test. Until Euro VI D they are excluded below a coolant temperature of 70°C. Moreover, particle number measurement will also be part of on-road tests. Up to Euro VI D, the measurement of particles was only a topic for the engine test bed in the laboratory. [8]

The work shown in this paper covers the measurements of 8 different HGVs with emission standard Euro VI D tested on the chassis dynamometer and on-road and gives an overview about the real world emission performance of these vehicles. In addition, the paper compares the emission behaviour to vehicles with emission standard Euro VI A, B and C and passenger cars with latest technology (Euro 6d-temp and Euro 6d) measurements. The main focus is on NO_x, N₂O and particle number.

Test setup

Figure 1 shows the schematic measurement setup on the HGV chassis dynamometer at TUG. The following measuring devices and sensors were used for the chassis dynamometer measurements:

- NO_x- and temperature sensors upstream diesel particulate filter (DPF) and downstream selective catalytic reduction (SCR) for NO_x-engine out (EO) concentration and temperature-EO as well as NO_x concentration and temperature end of tailpipe (standard HGV Continental NO_x sensors)
- AVL EFM (exhaust flow meter) or Sensors Semtech EFM for measuring the exhaust mass flow
- AVL M.O.V.E. PEMS (Gas+FID+PN) or Sensors Semtech DS
- Down to ten (DTT) PN measurement system consisting of a dilution system with 2 dilution stages, a catalytic stripper and 2 Condensation Particle Counter (CPC) with cut-off points at 23 and 10 nm (TSI CPC 3790 (23nm), Airmodus A23(23nm), AVL CPC (10nm))
- Standard laboratory IAG Fourier-Transform Infrared spectroscopy (FTIR) including a flame ionization detector (FID)
- Particle measurement programme (PMP) compliant dilution system with sampling from constant volume sampler (CVS) with a CPC with a cut-off point at 23nm (TSI CPC 3790)
- Particulate matter (PM) measurement sampling with secondary dilution from CVS

The on-board measurement setup is similar to the measurement setup on the chassis dynamometer, but without the laboratory instruments. The following measuring devices were used during on-board measurements:

- NO_x- and temperature sensors upstream DPF and downstream SCR for NO_x-EO concentration and temperature-EO as well as NO_x concentration and temperature end of tailpipe (standard HGV Continental NO_x sensors)
- AVL EFM (exhaust flow meter) or Sensors Semtech EFM for measuring the exhaust mass flow
- AVL M.O.V.E. PEMS (Gas+FID+PN) or Sensors Semtech DS
- DTT PN measurement system consisting of a dilution system with 2 dilution stages and a catalytic stripper and 2 CPC's with cut-off points at 23 and 10 nm (TSI CPC 3790 (23nm), Airmodus A23(23nm), AVL CPC (10nm))

¹ ISC tests are evaluated with the EMROAD tool, which uses the MAW principle. Every second a new MAW is started until the positive engine work in the window reaches the WHTC work. In Euro VI step D the average positive engine power in a MAW has to be higher than 10 percent of the rated engine power to make it valid. In total more than 50 percent of all windows have to be valid for a valid trip. In addition one valid window has to be inside the urban part. The final emission result is the 90 percentile of all valid windows. More details can be found in [9].

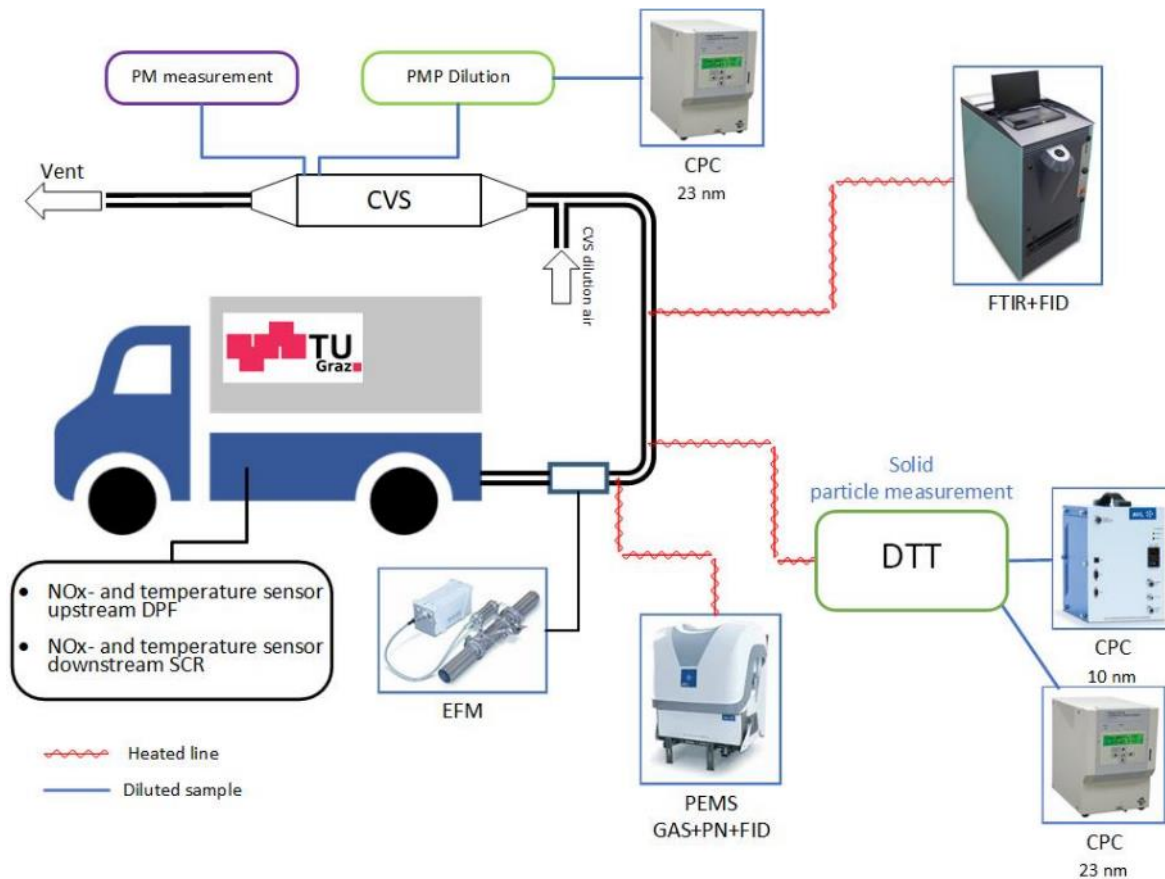


Figure 1: Scheme of the testing setup at **TUG** for the **HGV** tests on the chassis dynamometer.

The Measurement Campaign

This section describes the vehicles and test cycles covered by the test campaign.

Vehicles

The vehicle selection is based on following criteria to create a comprehensive picture of the emission performance of Euro VI D HGVs:

- Different vehicle categories: The vehicle selection contains 6 long haul and 2 rigid trucks. Consequently, the measurement data indicates if there may be a dependency between emission performance and truck size class.
- Different makes and models: The set of long haul trucks covers 5 of the 6 most popular manufacturers in Europe. The 2 rigid trucks are also from different brands. Hence, the data set shows if there are differences between the single manufacturers.
- Engine technology:
 - 1 long haul truck uses LNG in a positive ignition engine with three way catalyst (TWC). Although the market share of the LNG technology is today quite low, an increase of the share could be possible in future especially with regard on CO₂ reduction regulations [11], since the concept promises a noticeable CO₂ reduction potential [10]. This paper compares the emission performance of a LNG vehicle with diesel trucks.
 - All other 5 long haul trucks are diesel driven and equipped with the standard HDV exhaust aftertreatment system, which contains a diesel oxidation catalyst (DOC), a diesel particle filter (DPF) and a selective catalytic reduction catalyst (SCR). 4 of the 5 vehicles use also an external high pressure exhaust gas recirculation (EGR) to reduce NO_x engine out (EO) emissions.
 - The 2 rigid trucks are also diesel driven and equipped with the standard HDV exhaust aftertreatment technology and use external high pressure EGR.

All vehicles had a mileage between 5 000 and 50 000 kilometres at the time of the tests. Consequently, the results should not be impacted by special behaviour of completely new vehicles and also not by deterioration effects due to high mileage.

Test cycles

In order to get a comprehensive picture of the real world emission behaviour of the different vehicles, the test program was designed to cover on the one hand the typical normal driving situations of the specific vehicles and on the other very challenging driving situations, which are realistic to occur (e.g. low load urban driving). Of course, on-road tests suit well for this purpose since they include also real ambient conditions (e.g. traffic, weather, etc.), but the range of measureable emission components is limited by portable emission measurement systems (PEMS) to the regulated ones. For that reason, the program contains also tests on the chassis dyno to get information about non-regulated emission components by a FTIR system, which is currently only available in the lab.

The following points describe the test cycles more in detail:

- On-Board
 - ISC test: This test is the regulatory on-road test and represents therefore common driving of HDVs. The test starts with a cold start in urban driving, followed by rural and motorway driving. The time shares of the different road categories are defined depending on the vehicle class (e.g. N3: urban 30 %, rural 25 %, motorway 45 %) [1]. The total duration of an ISC test is about 3 to 3.5 hours. A test according to the regulation uses the tool EMROAD for the evaluation, which cuts off the cold start until the coolant temperature has reached 70°C for the first time or the first 15 minutes, whatever occurs primarily. Of course, the cold start has also an effect on air quality as it occurs minimum once per day. Consequently, we decided to respect the cold start also in the evaluations for this paper. In addition, the tool EMROAD declares MAWs (see section “Introduction”) with an average positive engine power below 10 % as invalid and does not consider these emissions in the evaluation. In this paper, we show EMROAD results (clearly marked as such), which allow a comparison to the regulatory limit values, and additionally average values over total tests or single test phases including all emissions independent of EMROAD boundary conditions.

Although not all “ISC” trips fulfil the ISC boundary conditions completely, all were tested on an ISC like mission profile and consequently classified as ISC trips in this paper.

- Low load test: This cold started test represents a low load urban driving situation, which can include also stop&go traffic. Of course, this test profile is not very typical for vehicle categories like long haul trucks, but it gives a picture how such vehicles behave in worst case conditions. This test challenges the vehicles regarding heat up strategy after the cold start and checks if the exhaust aftertreatment system can be held in good operating conditions during long lasting low load phases. For comparison reasons all tests are shortened to exactly 1 hour duration.
- Chassis dyno
 - WHVC: The WHVC is measured in the form of a cold start test with two phases; the second phase is a repetition of the first phase after ten minutes soak time in between. For the final emission result the first phase is weighted by 14 % and the second phase by 86 %. This cycle allows an indicative comparison of the emission behaviour of the vehicle with the WHTC emission limits, which is driven on the engine test bed for the certification process.² This cycle sums up urban, rural and motorway driving in a 4200 seconds test and gives consequently a good picture about the emission behaviour of the test vehicle.

Measurement results

The first part gives an overview of all regulated and some important non-regulated emission components in type approval test cycles followed by sections which focus on NO_x, N₂O and particle emissions in tests, which exceed the regulatory boundary conditions.

² This method was developed while working on the Global Technical Regulation for the emission certification of hybrid HDVs [12]. To fit the engine load resulting from the WHVC to the WHTC, the vehicle mass and the driving resistance coefficients on the chassis dyno are calculated based on the rated engine power. Additionally, the gradient profile for the WHVC is calculated. This leads to an engine speed and power course, which is close to the one of the WHTC [13].

Type approval test conditions

Every vehicle has been tested in the WHVC on the chassis dyno and on-road in ISC tests. The WHVC results are weighted as already described in section “Test Cycles” and the ISC results are EMROAD results, consequently they allow an indicative comparison to the limit values³. The results are illustrated in Figure 2. The blue bar represents the average of all diesel vehicles and the black line shows the spread between the maximum and minimum value. The red bar illustrates the results of the LNG truck. Since there is only one LNG vehicle measured the average also represents the maximum and minimum in one value. All vehicles are below the limits for all different emission components with exception of NOx. A more detailed look on the single NOx results shows that there is only one diesel vehicle which exceeds the limit in both tests, the WHVC and the ISC test. All other vehicles are in all tests below the NOx limit. The LNG truck has higher CO and PN emissions compared to the average of the diesel trucks, but nevertheless the values are not higher than 50 % of the limit. The methane emissions of the LNG truck are also clearly below the limit.

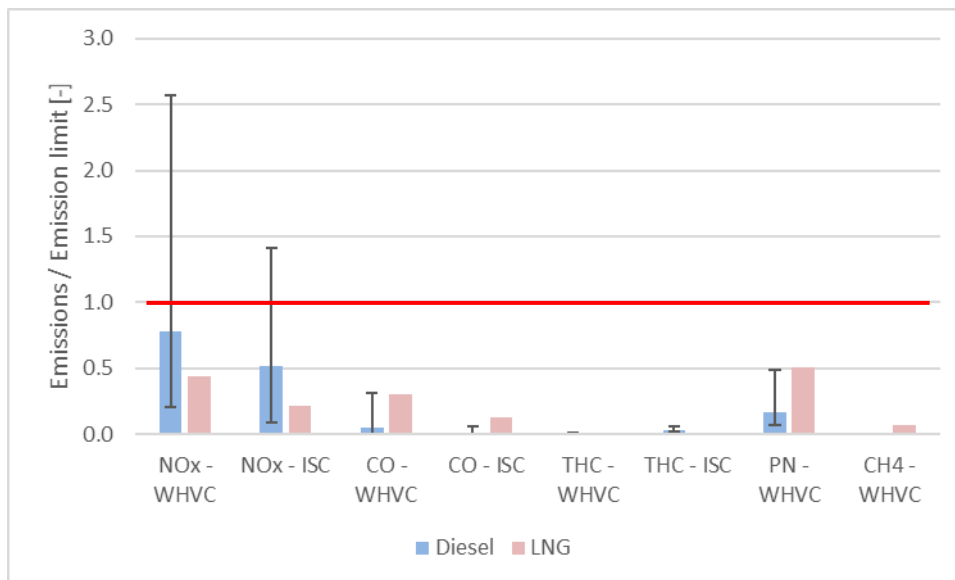


Figure 2: Measurement results in type approval test cycles for regulated emission components.

Figure 3 illustrates the results of non-regulated pollutants measured by FTIR on the chassis dyno in the WHVC. The diesel trucks come up with average N₂O emissions of nearly 80 mg/kWh. The maximum is even above 140 mg/kWh. Although N₂O has no significant impact on air quality, it effects the climate due to its global warming potential of 265 over 100 years [2]. Diesel vehicles can hold ammonia emissions low because of the ammonia slip catalyst (ASC), which is a standard equipment for diesel exhaust aftertreatment systems for Euro VI HGVs. Ammonia emissions of the LNG truck are higher because of its potential formation in the TWC, but the average level is still below the limit of 10 ppm. All trucks are on a very low level at formaldehyde, but the gas truck has noticeable methane emissions (already shown in Figure 2) in contrast to the diesel vehicles. Nevertheless, the total CO₂ equivalent emissions of the LNG truck are 10 % lower compared to ones of the average diesel truck. The diesel vehicles have H₂CO emissions on a low level. This is an unintentional by-product of the incomplete conversion of AdBlue in Ammonia, consequently the gas truck does not have any, because of its positive ignition concept with TWC.

³ Euro VI limits – WHVC: CO = 4000 mg/kWh, THC = 160 mg/kWh (only for compression ignition engines), NOx = 460 mg/kWh, PN = 6.0E+11 #/kWh, CH₄ = 500 mg/kWh (only for positive ignition engines); Euro VI limits – ISC = Euro VI limits – WHVC * 1.5 [9][14]

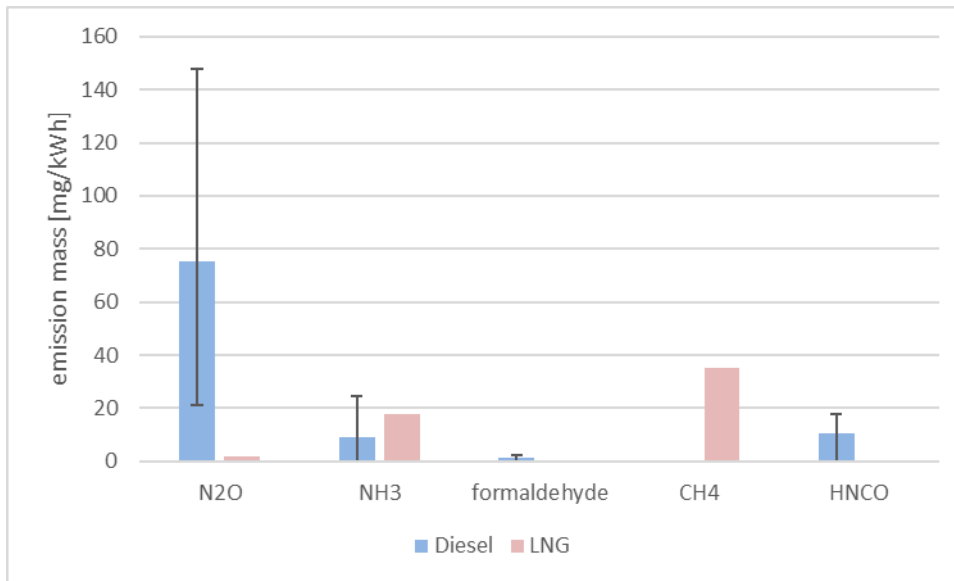


Figure 3: Measurement results in the WHVC for non-regulated emission components measured by FTIR.

The results show that only one Euro VI D vehicle is above the limits and all others are below the limits for all emission components. This illustrates that nearly all vehicles behave well inside of regulatory boundary conditions, which represent standard HGV mission profiles in the WHVC and especially in ISC trips. Especially the N₂O emissions show that non-regulated components can be an issue, e.g. N₂O contributes to up to 5 % of the CO₂ equivalent emissions. It has to be mentioned that N₂O was not a problem when initialising Euro VI, but the development to lower NO_x levels based on SCR catalysts increased the N₂O emissions in a noticeable way. Based on such measurement results it is quite possible that N₂O will be a topic for Euro 7.

Test conditions outside of regulatory boundaries

The tool EMROAD does not evaluate the cold start in ISC tests below an engine coolant temperature of 70°C and cuts off MAWs with an average power below 10 % of the rated engine power in Euro VI D, although these sections occur in real driving and thus have an impact on air quality. Of course, an urban only trip on such a low power level for a long haul truck is not very common, but similar driving conditions can happen in congestions in urban and motorway driving.

Figure 4 illustrates NO_x measurement results as average g/kWh. The red dots represent ISC tests inclusive cold start emissions and the blue dots show cold started urban only trips which were cut to a duration of exactly 1 hour for comparison reasons. In these urban tests, the vehicles drove with no extra payload in addition to the measurement equipment to generate very low load and consequently challenging conditions.

Regarding ISC trips, the NO_x emissions are in the same range as the EMROAD results shown in Figure 2, although the cold start is included in these tests. This can be explained by the test duration of 3 to 3.5 hours. This leads to a much higher weighting of the hot emissions compared to the cold start phase. This weighting represents also real world behavior in typical mission profiles, especially for long haul trucks. The results show also, that most of the ISC tests with lower average engine power due to lower payload come up with higher NO_x emissions compared to the tests at higher engine power. Lower engine loads, which occur especially in the urban parts of the test, lead to lower exhaust gas temperatures and consequently to problems to heat up the exhaust aftertreatment system to its optimal operation conditions and to keep it hot enough.

If we take a look at the urban trip results, we can see that the NO_x emissions increase clearly, even up to 7 g/kWh in one test. This test is from the same vehicle which was above the NO_x limits in the type approval test cycles. On the one hand, the cold start related extra emissions have a higher relevance for the test result due to the shorter trip duration compared to ISC trips, and on the other hand, the average engine power is lower in these tests. If the average power tends to zero, the g/kWh tend to infinite due to division of emissions [g/h] by low denominators [kW]. Nevertheless, it has to be mentioned that most vehicles seem to have special measures to maintain a working aftertreatment system also in such low load conditions. Only one vehicle is an outlier.

The LNG truck performed well in both tests. The concept of a positive ignition engine and a TWC shows even the best NO_x-performance in urban trips.

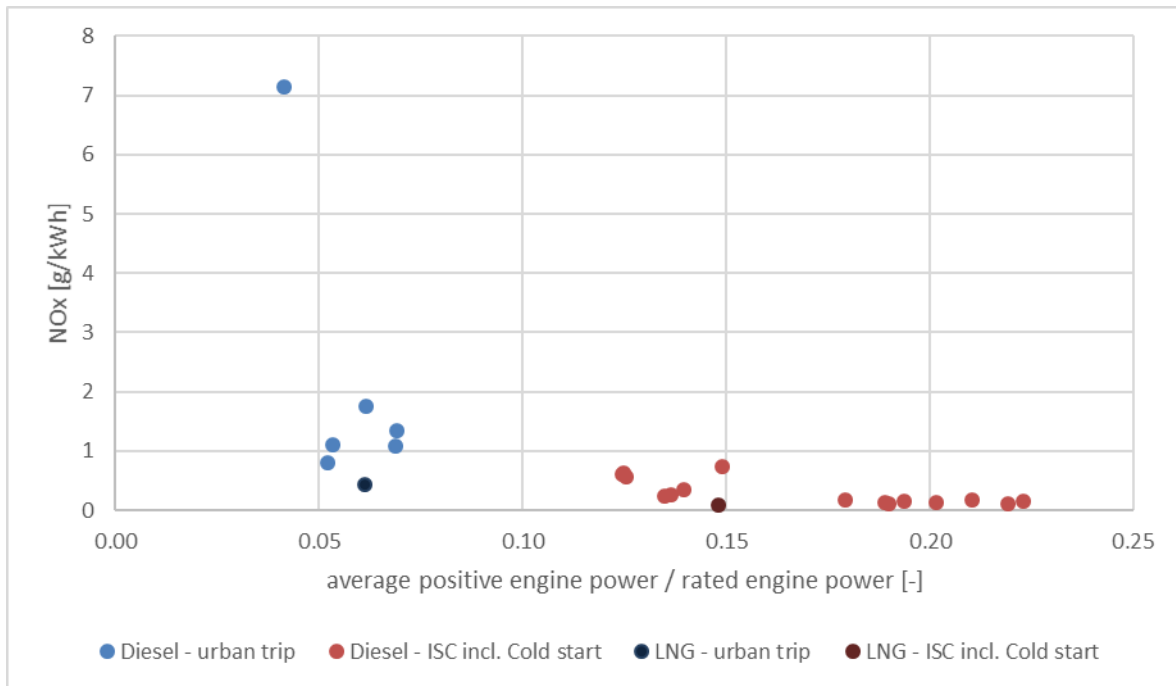


Figure 4: NOx measurement results for on-board tests outside of ISC boundary conditions.

Figure 5 gives a more detailed look on the relation between cold start emissions and emissions during hot engine operating phases for the best and worst performing diesel vehicle. Both are long haul trucks with comparable rated engine power and engine displacement. The cumulated emissions of the Euro VI D best performer show that nearly all emissions are generated during the cold start phase. In hot conditions it works more or less as at a zero emission level. That means, this vehicle can bring the exhaust aftertreatment system to its perfect working conditions by special heating strategies, even in the urban only test after a certain cold start phase. The worst performer diesel truck shows a much higher emission increase in the first part of the test due to the cold start and the cumulated emissions further increase even in the hot phase of the ISC test. It will be interesting to see the effect of Euro VI E on the cold start emissions, but it can be assumed that cold start will remain one of the main topics for future emission regulations.

It has to be mentioned, that the worst performer was measured at an ambient temperature of 2°C and the best performer at 15°C. Of course, this has an influence on the emission performance, but the chassis dyno results of the WHVC at 20°C for both vehicles show a similar relation between the NOx emission performances of these vehicles. Consequently, the different ambient conditions do not change the principal findings.

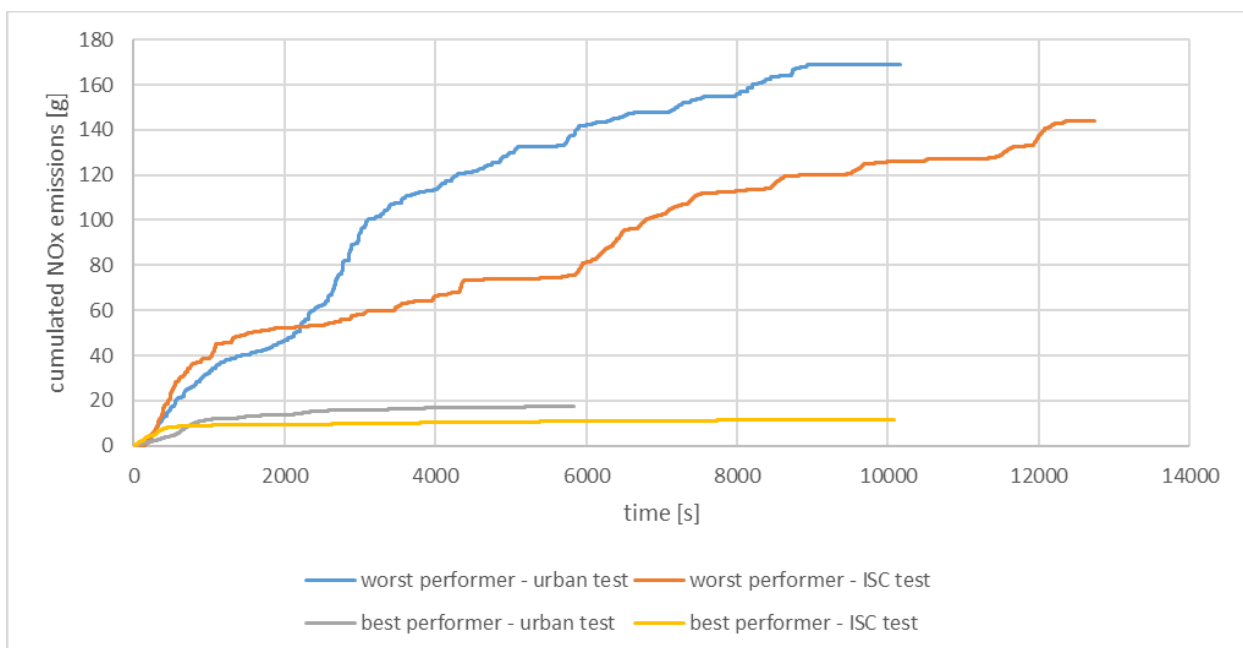


Figure 5: Cumulated NOx emissions for single tests of the best and worst performing diesel vehicle.

Section “type approval test conditions” showed also noticeable N₂O emissions of Euro VI D diesel trucks. In principal, N₂O is mainly created as an undesired by-product during the oxidation of NH₃ in the ASC [7]. Consequently, reducing the ammonia slip in the SCR would lead to lower N₂O emissions. Since lower NO_x limits or more challenging test boundary conditions (e.g. the introduction of Euro VI D) incentivise a more aggressive AdBlue dosing strategy with a higher NH₃/NO_x ratio than the stoichiometric one, further increases in N₂O emissions are expected in absence of N₂O limits. This relation is shown in Figure 6 on the left side for the WHVC for 7 diesel Euro VI D HGVs. Every dot represents the WHVC result of one vehicle.

The main issue regarding N₂O emissions is their global warming potential of 265 [2]. Consequently, CO₂ equivalent emissions can be increased up to 5 % by N₂O emissions in the WHVC of Euro VI D vehicles as the right graph of Figure 6 illustrates. The relation of these 2 graphs (every bar represents the WHVC result of one vehicle, colors fit together) shows that low NO_x emissions come along with a noticeable increase of CO₂ emissions for current vehicles. Based on these results N₂O should be discussed to be limited or accounted to CO₂ emissions in future regulations, because otherwise direct CO₂ saves are counterbalanced by CO₂ equivalent emissions and finally we do not have a positive effect on the climate.

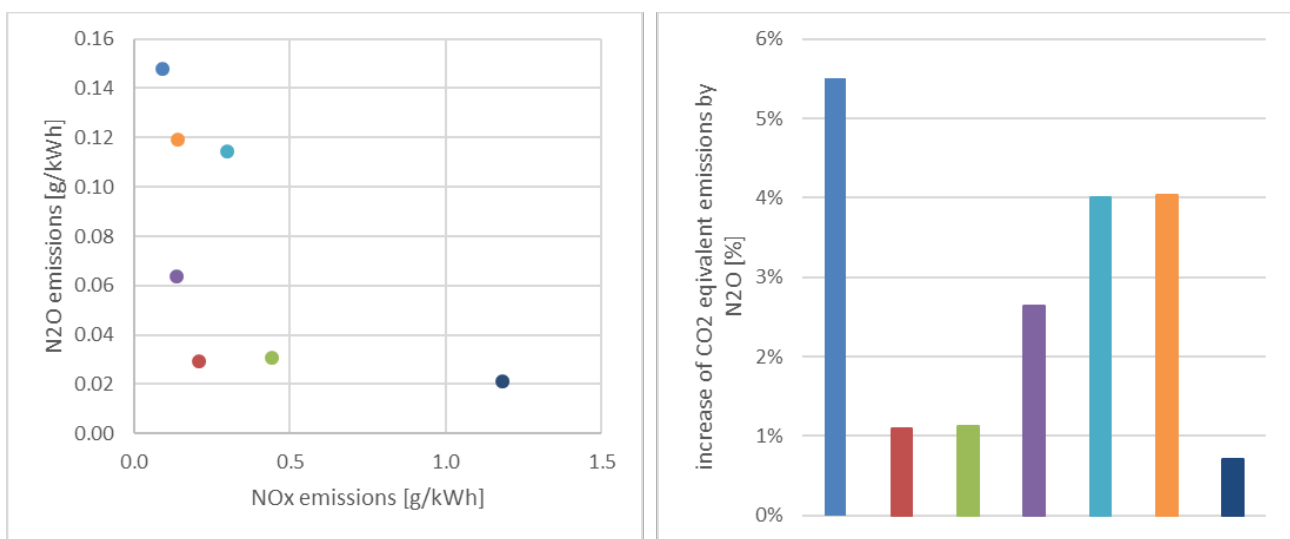


Figure 6: left: relation between N₂O and NO_x emissions for diesel HGVs in the WHVC, right: increase of CO₂ equivalent emissions due to N₂O for diesel HGVs in the WHVC.

If we take a look at the particle number emissions, it is noticeable that the PN₂₃ emissions in the WHVC and also in ISC RDE trips are well below the current limit value for all vehicles (see Figure 2 for the WHVC PN₂₃ average measurement results). Figure 7 shows the comparison of the cumulative PN₂₃ emissions of an LNG truck and a diesel truck. On-road driving (ISC and urban driving) is shown in solid lines, the dashed lines represent WHVC measurements on the chassis dyno. The very low PN₂₃ emission level of the diesel truck is clearly visible. In the case of the LNG vehicle, it is noticeable that the majority of the PN₂₃ emissions occur in steps which also occur at approximately the same time in the 3 measurements (see in Figure 7 at approximately second 1000). For these measurements, no lambda sensor data was available, so it is not possible to say exactly why these jumps in PN₂₃ emissions occur. Purely from the analysis of the engine coolant temperature, no statement can be made. This behaviour of LNG vehicles will have to be examined more closely in future measurements.

Comparing Figure 7 with Figure 5, the influence of the cold start phase on the total emission level for PN₂₃ is not so crucial for diesel trucks, in contrast to NO_x.

Table 1 gives an overview of the PN₁₀/PN₂₃ ratio of 2 diesel trucks and one LNG truck as well as the PN₂₃ and PN₁₀ emissions in #/kWh for an ISC trip. As mentioned before, the measured trucks are far below the PN₂₃ limit value, even the PN₁₀ emissions are far below this limit value.

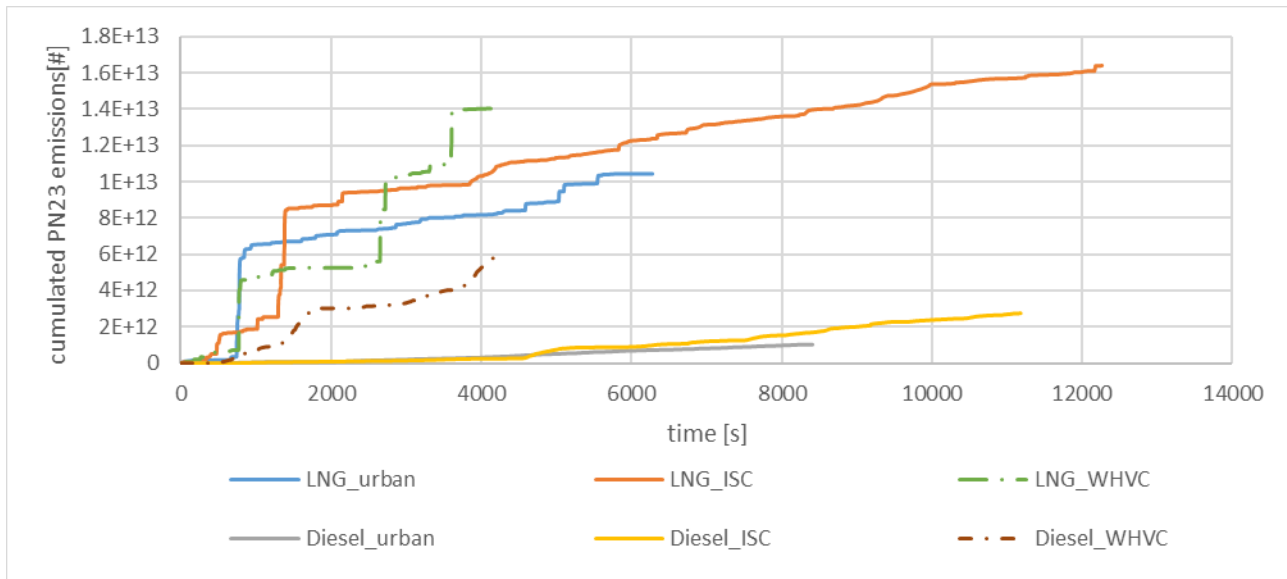


Figure 7: Comparison of cumulated PN23 of ISC and urban on road tests of a diesel and a LNG truck.

Table 1: PN10 to PN23 emission ratios

	Test	PN23 [#/kWh]	PN10 [#/kWh]	Ratio PN10/PN23
Diesel Truck A	ISC	2.56E+10	4.68E+10	1.8
Diesel Truck B	ISC	4.90E+10	1.12E+11	2.3
LNG Truck C	ISC	9.62E+10	1.27E+11	1.3

Classification of the emission levels

The results in section „Measurements results” compare different Euro VI D trucks to each other, but it is also important to benchmark the emission behaviour of these vehicles with other vehicles on the road. For this purpose, the following chapter compare the emission performance of Euro VI D trucks with trucks of emission standard Euro VI A, B and C and also with Euro 6d-temp and Euro 6d passenger cars.

Comparison to Euro VI A, B and C vehicles

The real world emission performance of Euro VI A, B and C vehicles was already elaborated in the HBEFA 4.1 [15]. The HBEFA provides real world emission factors for average vehicles divided in different size and vehicle categories, which mimic the total fleet in Europe’s average traffic situations. The results illustrate the emission performance in g/km, but for this exercise the results have been converted to g/kWh based on the kWh/km of the corresponding HBEFA traffic situations. Of course, also the mileage of the Euro VI D vehicle data set is taken in consideration regarding the correct application of mileage based deterioration effects to the HBEFA vehicles for this comparison. The HBEFA results in this paper are based on German traffic situations, as Germany can be seen as a good average for Europe. Since the HBEFA represents the emission performance in hot engine conditions, the cold start is also excluded of the Euro VI D measurement data, which is based on ISC tests, for this analysis. The average Euro VI D diesel truck is based on the already illustrated 2 rigid and 5 long haul trucks, which are all weighted in the same way. In this comparison, the HBEFA 4.1 average truck is based on the same share between the 14-20 tons rigid truck half loaded and the 34-40 tons tractor trailer combination half loaded.

Figure 8 shows that Euro VI D reduces the CO emissions compared to Euro VI A, B and C. The THC emissions decrease also, but the level of Euro VI A, B and C vehicles is already very low. The NOx emissions are also lower for EURO VI D in all parts, but especially in the urban part. This can be mainly attributed to the reduction of the power threshold in ISC tests from 20 to 10 % and consequently to the improved low load behaviour of Euro VI D vehicles. The PN emissions are a little bit higher, but they remain on the low level already reached by Euro VI A, B and C vehicles.

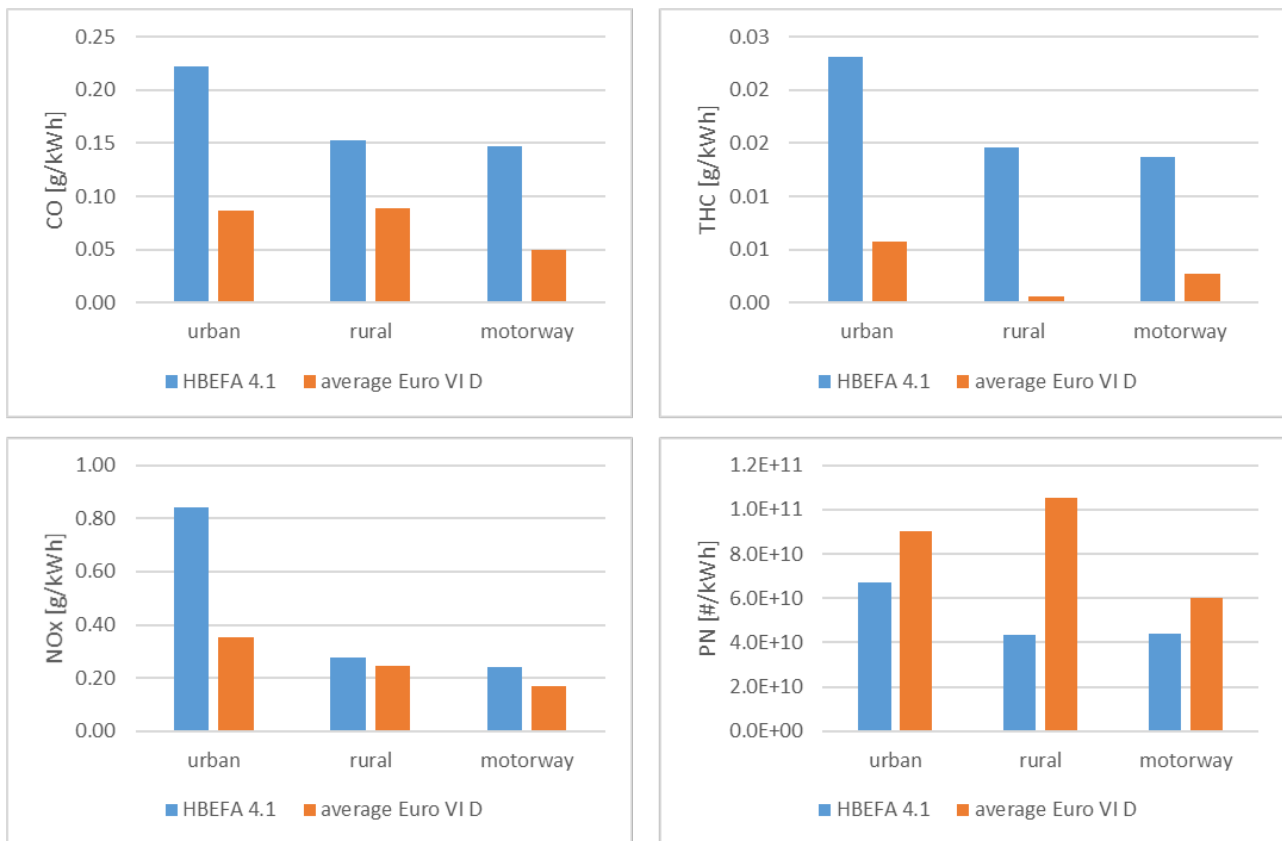


Figure 8: Comparison of HBEFA 4.1 (representing Euro VI A, B and C) and the average Euro VI D measurement results.

Comparison to passenger cars

It is also interesting to compare the real world emission performance of current HGVs with latest passenger cars (PC) with emission standard Euro 6d-temp and Euro 6d tested at TUG (see Figure 9). The following results are based on real world tests (HGV: WHVC, PC: IUFC with cold start and ERMES with hot start) measured on the chassis dyno because of the availability of non-regulated emission components by FTIR. To show HGV real world emissions with cold start for this paper, the cold started part of the WHVC was weighted by 67 % and the hot part by 33 %. For PC, the IUFC was weighted by 17 % and the ERMES by 83 %. The trips of PCs and HGVs have consequently both a distance of approximately 30 km for a reasonable comparison⁴ and represent standard driving (mix of urban rural and motorway parts). Normally, emissions of passenger cars are illustrated in g/km, but for comparison reasons the PC emissions are also shown in g/kWh in this analysis. The results show also the kWh/km for passenger cars, so the values can be converted to g/km, if needed. The coloured bar gives the average value for the specific category while the black bar shows the spread between the best and the worst performing vehicles.

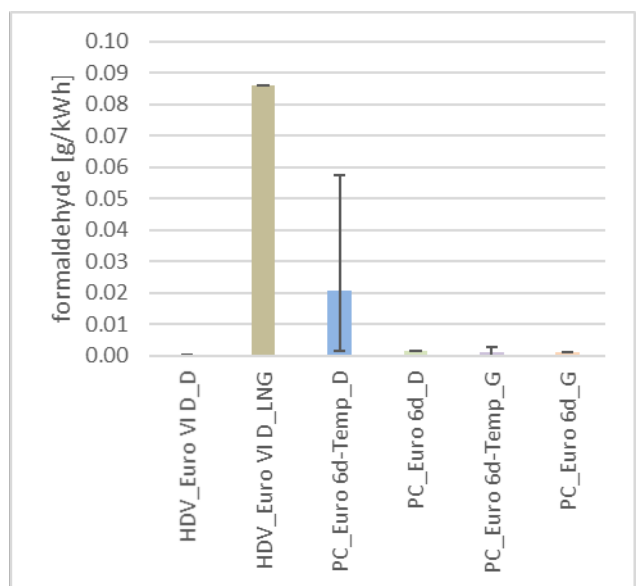
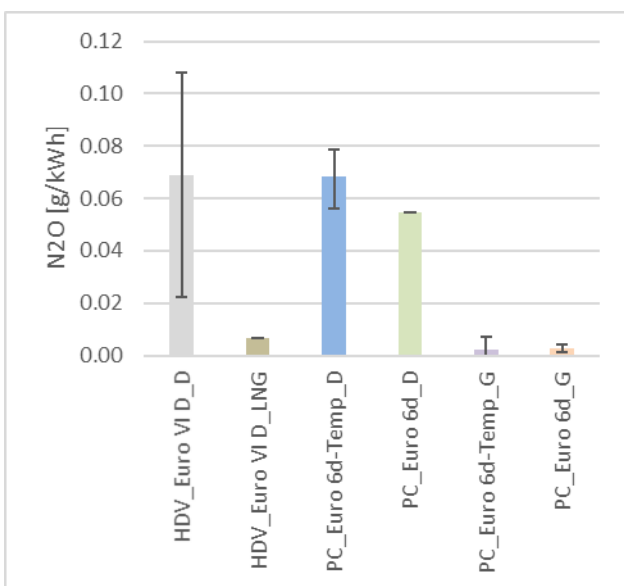
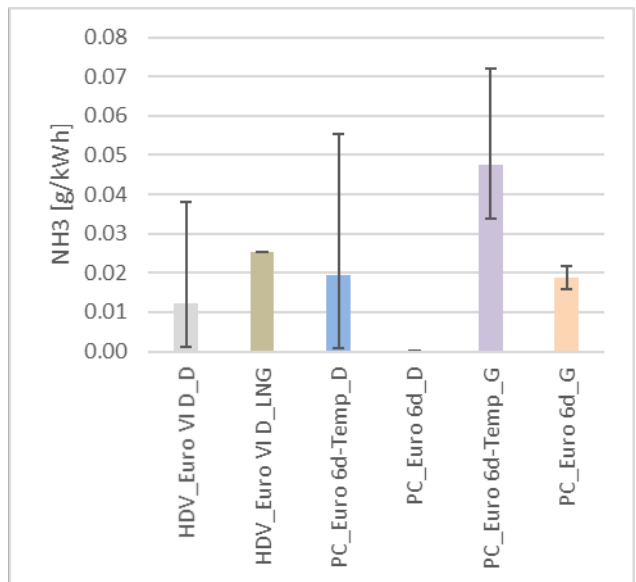
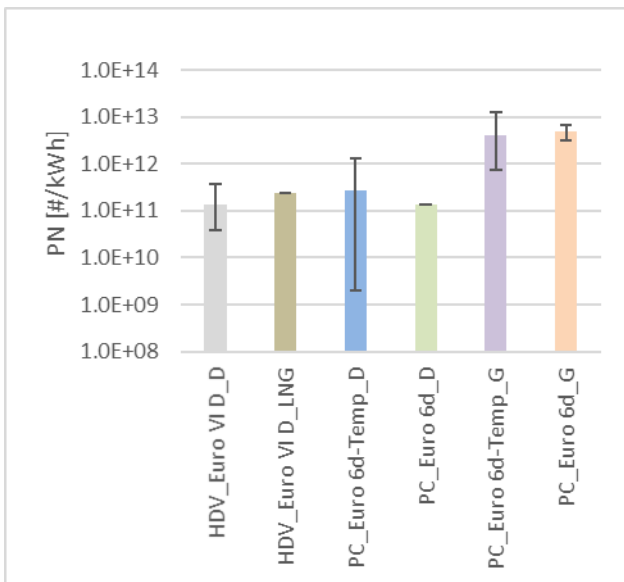
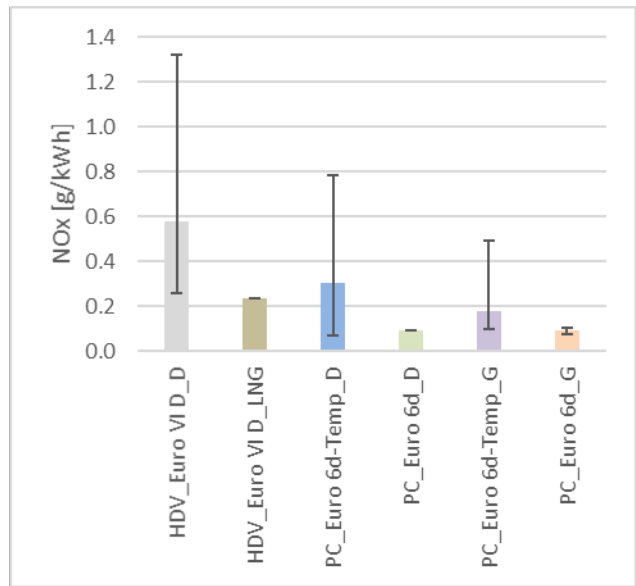
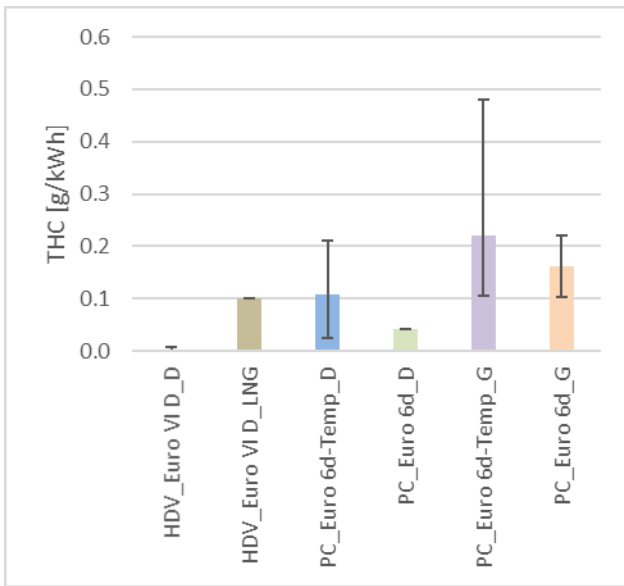
The measurement data contains 7 HGV Euro VI D diesel, 1 HGV Euro VI D LNG, 8 PC Euro 6d-Temp diesel, 1 PC Euro 6d diesel, 9 PC Euro 6d-Temp gasoline and 2 PC Euro 6d-Temp gasoline vehicles. Of course, a complete category is not well represented by only 1 or 2 measured vehicles, but the aim of this comparison is to give a first idea about the emission performance anyway.

Following trends can be seen in Figure 9.

The THC emissions of passenger cars are higher than the ones of trucks. Gasoline PCs are on a higher THC level than the LNG truck.

Regarding NO_x, the emissions of the diesel HGVs are above all PC categories. Although the spread in the tested Euro 6d-Temp PCs (diesel and gasoline) is large, the maximum of HGV diesel trucks is clearly higher than the highest PC. Euro 6d PCs tested so far are on a low level compared to the other categories. Note: compared to EURO 5 averages, all vehicles shown here are on a much lower level.

⁴ In real world operation HDVs have clearly longer average trip distances than cars. For the direct comparison however, a similar trip distance seemed to be more appropriate.



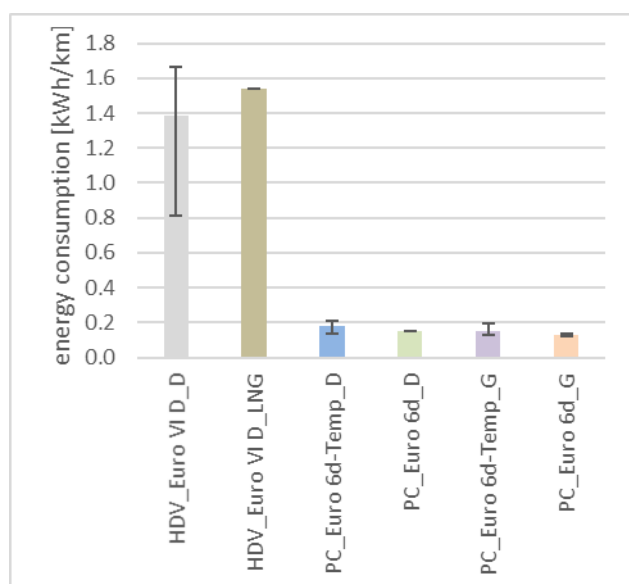


Figure 9: Comparison of recent PC and HGV measurement results.

PN is illustrated logarithmically. The gasoline PCs are on another level compared to all other vehicles.

The Higher NO_x but lower HC and PN emission levels of HDVs can partly be attributed to the lower engine speeds and larger cylinder volumes of the HD compared to LD engines which leads to higher lower wall heat losses and thus longer time at higher temperatures for NO_x formation but also for soot and HC burn-off in the later combustion phases. Certainly combustion control and aftertreatment technologies are becoming increasingly relevant for the tailpipe emissions and can outweigh these basic trends.

Ammonia emissions can more or less only be detected for gasoline Euro 6d-Temp PCs. All other vehicles categories are close to the detection limit.

N₂O seems to be mainly a problem of diesel vehicles, with PCs and HGVs on the same level in g/kWh. Section “Test conditions outside of regulatory boundaries” has already illustrated the problems according to the high greenhouse gas potential of laughing gas.

Formaldehyde is only visible for the HGV LNG truck and Euro 6d-Temp diesel vehicles.

Conclusions

The results in this paper show that the introduction of Euro VI step D for HGVs results in a better real world emission performance of current trucks for regulated emission components compared with vehicles of emission standard Euro VI A, B and C. The effect of lowering the power threshold in MAWs from 20 to 10 % can be especially highlighted. This leads to a better coverage of low load operations in type approval tests and consequently effects the real world emission behaviour.

Regarding the best performer vehicles, the NO_x emissions can be mainly assigned to the cold start. In hot engine operating phases the emissions are on a very low level. This results in NO_x emissions of less than 0.1 g/kWh in an ISC test while the worst performer exceeds the ISC limit by more than 50 % and has also noticeable NO_x emissions in best operating conditions on the motorway.

The results indicate also that low NO_x emissions come along with rather high N₂O emissions. The best performer in NO_x emissions increases its CO₂ equivalent emissions by more than 5 % due to laughing gas. Consequently, the next Euro legislation should take N₂O also in account in order not to undermine the ambitious CO₂ targets by side effects of possible ultra-low NO_x limits.

Each HGV was well below the current PN₂₃ limit in both the PN₂₃ and PN₁₀ measurement results. The measurement data set contains also one LNG truck. Although, this vehicle has higher methane emissions compared to the diesel trucks it can be ranked in total as one of the best performing trucks regarding real world pollutant emission behaviour and the total CO₂ equivalent emissions are also 10 % lower compared to the average of the diesel trucks.

The results illustrate the effectiveness of the emission standard Euro VI D compared to emission standard Euro VI A, B and C on the basis of the real world emission behaviour. Especially the performance in low load operation is

enhanced. The comparison to current passenger car real world emissions shows that the NO_x performance of PCs is a bit better compared to HGVs, even for diesel PCs. Similar to HDVs, also diesel PCs have the N₂O issue. Regarding particle and ammonia emissions, current diesel vehicles (PCs and HGVs) perform better than gasoline vehicles. With the beginning of 2021, the emission standard Euro VI step E was introduced for new models and in 2022 it will be valid for all new registered HGVs. The main topic is the inclusion of the cold start and PN measurements in ISC tests. It will be interesting when the first measurement results will be available for evaluating the real world emission behaviour.

Acknowledgement

All measurement data used in this paper was elaborated in the project “Projekt 91180: Realemissionen aus Fahrzeugen und Maschinen” funded by the Germany Environment Agency (UBA). We want to thank the UBA for the possibility to use these measurement data for this paper.

References

- [1] Regulation EU 2018_932
- [2] IPCC, 2014: Climate Change 2014: Synthesis Report. Contribution of Working Groups I, II and III to the Fifth Assessment Report of the Intergovernmental Panel on Climate Change [Core Writing Team, R.K. Pachauri and L.A. Meyer (eds.)]. IPCC, Geneva, Switzerland
- [3] VCÖ factsheet: Wachstum des Gütertransports in EU braucht Bahnausbau, Verkehr aktuell 2019-06, Wien, 2019
- [4] <https://de.statista.com/statistik/daten/studie/282282/umfrage/queteraufkommen-nach-verkehrstraegern-in-europa/>, last accessed: 01.03.2021
- [5] <https://www.umweltbundesamt.at/umweltthemen/mobilitaet/mobilitaetsdaten/stickoxide-verkehr>, last accessed: 01.03.2021
- [6] Regulation EU 2016_1718
- [7] Weller, K.: Emission Models for Heavy Duty Vehicles Based on On-road Measurements, Phd thesis, Graz University of Technology, 2020
- [8] Regulation EU 2019_1939
- [9] Regulation EU 2011_582
- [10] <https://www.iveco.com/germany/neufahrzeuge/pages/new-stralis-np-gas-truck.aspx>, last accessed: 25.01.2021
- [11] Regulation EU 2019_1242
- [12] Amendment 3 to UN GTR No. 4 - (ECE/TRANS/180/Add.4/Amend.3)
- [13] Six, C., Silberholz, G. et al.: Development of an exhaust emission and CO₂ measurement test procedure for heavy-duty hybrids (HDH), Vienna University of Technology, 2014
- [14] Regulation EU 2009_595
- [15] Matzer, C., Weller, K., Dippold, M., Lipp, S., Röck, M., Rexeis, M., Hausberger, S.: Update of Emission Factors for HBEFA Version 4.1, Graz University of Technology, 2019

2.5 Bus emissions measurement in operational conditions using PEMS: comparison between different Euro technologies and fuels

L. Deville Cavellin*, A. Arfire, F. Joly, A. Mahnaoui, C. Joly

¹Airparif (Association in charge of the air quality monitoring network of Île-de-France)

laure.deville-cavellin@airparif.fr

Abstract

Bus emissions in operational conditions are yet to be more deeply investigated, as buses have a very specific driving cycle compared to other heavy-duty vehicles. Aiming for better standards beyond Euro VI requires a precise knowledge of the current vehicle emissions in real conditions. A two-year experiment has been carried out by Airparif with the financial support of Île-de-France Mobilités to assess bus emissions in Île-de-France (Paris region), during operational conditions (i.e. carrying passengers) over various weather and traffic situations and over different types of bus lines (e.g., urban, suburban). Overall, 28 buses were tested along 16 two-week campaigns: the buses were Euro IV diesel, and Euro VI diesel, hybrid and CNG. The measured pollutants were: particle number (PN), nitrogen oxides (NO and NO₂), carbon monoxide CO and carbon dioxide CO₂, using a PEMS. More than 6,500,000 data points were collected per pollutant at a time resolution of 1 Hz, along with vehicle parameters, exhaust temperature, ambient temperature/humidity, and positioning. The uncontrolled driving conditions represented a challenge for data analysis but also a major opportunity for a first insight of real-world bus emissions at a massive scale.

This study found that a reduction in real-driving emissions, for all pollutants (PN, NO_x, CO) occurred from Euro IV diesel buses to Euro VI buses of all categories. On average, NO_x emissions were divided by 4 from Euro IV (around 13 g/km) to Euro VI diesel buses (around 3 g/km), and by 7 from Euro VI diesel to CNG buses (around 0.4 g/km). PN emissions were divided by more than 50 times from Euro IV (around 10¹³-10¹⁴ particles/km) to Euro VI buses of all categories (diesel, hybrid, CNG, around 10¹² particles/km). PN emissions from CNG buses tended to be higher than Euro VI diesel ones (depending on the bus considered) but overall remained within the same range. While CO concentrations are no longer a concern for the Paris region, the CO emissions were also observed to be reduced with diesel technology evolution (from around 7 to 0.5 g/km). For part of the CNG buses, CO emissions were higher than those of Euro VI and part of Euro IV diesel vehicles. CO₂ emissions ranges (from tank to wheel only) were also slightly shifted downwards, by 6% on average for Euro VI diesel (with an additional advantage of 17% for Euro VI hybrids). CO₂ emissions for Euro VI CNG were similar to Euro VI diesel ones. The COPERT 5 NO_x and CO emission factors for Euro IV and Euro VI diesel buses tend to underestimate the emission factors encountered in the conditions of this experiment, while remaining in the first quartiles of the measured emission ranges. Some factors and events influencing emissions were also analysed in this study: exhaust temperature, ambient temperature, cold-start, driving style, average velocity, and observed after-treatment systems failures.

Introduction

In Île-de-France (Paris region), around 500 000 people were still exposed to NO₂ levels beyond the European limit value in 2019 [1]. If the European standard for PM_{2.5} were met, the WHO recommendations were not and the whole agglomeration was concerned by higher levels [1]. In order to reduce population exposure by acting on the right levers, it is important to have a better understanding of the emission sources: passenger cars emissions, as a major source of NO_x and an important source of fine particles, are starting to be well-documented in real-driving conditions [2]. However, bus emissions are yet to be more deeply investigated, as buses have a very specific driving cycle compared to other heavy-duty vehicles, and large datasets of real-world bus emissions are lacking, especially since the start of the Euro VI standard [3]. Aiming for better standards beyond Euro VI requires a precise knowledge of the current vehicle emissions.

If the emissions of diesel buses and other heavy-duty vehicles have drastically decreased thanks to new technologies according to some studies [3], diesel still remains a fossil fuel at stake nowadays, and older vehicles, including diesel ones, are progressively getting banned from certain dense urban areas in France. Other engine technologies are available that might meet the demand for emissions decrease and for non-fossil fuel use, apart from electrical buses: CNG buses (with biogas), and the use of biodiesel in diesel engines. The former technology is assessed for Euro VI buses in this study; the latter will be tackled in another Airparif study.

ADEME, the French Agency for Ecological Transition, reported emissions in real-driving conditions without passengers (simulating an in-service conformity cycle, ISC) for Euro VI CNG buses [4]: for the urban conditions, NO_x emissions were 20 to 40% lower than Euro VI diesel buses, and up to 50% lower when taking cold start into account. PM emissions (in mass) were too low to be measured with a PEMS, for both technologies. CO₂ emissions from tank to wheel were

similar. Tests with an ADEME/RATP driving cycle on a test bench [4] showed, for CNG compared to diesel (Euro VI buses), higher CO emissions (0.52, against 0.02 g/km), CH₄ emissions (0.02 g/km) and higher total HC emissions (0.04, against 0.01 g/km), lower PM emissions (non-measurable, against 0.01 g/km), and lower NO_x emissions (0.24, against 4.17 g/km). Most studies agree on these results [5-8]: similar CO₂ emissions, higher CO and HC emissions (partly due to lower air/fuel ratio), negligible PM emissions, if not similar to Euro VI diesel buses [9] – for which PM emissions were considerably mitigated with Diesel Particulate Filter (DPF) – NO_x emissions 2 to 30 times lower, notably during harsh driving conditions [10]. PN emissions were less studied: a Danish study [5] tested Euro VI heavy-duty vehicles on a World-Harmonized Transient Cycle (WHVC) cycle, with PN emissions 4 times higher for CNG compared to diesel. Another publication [11] regrouped PN emissions of Euro VI heavy-duty vehicles (mostly trucks, but including two buses) from several studies using different methodologies: on-road testing with ISC cycles and laboratory testing with WHVC or ISC cycles. PN emissions ranges were around 2×10^{10} – 7×10^{11} particles/km for diesel, 8×10^{11} – 4.5×10^{12} particles/km for CNG. Those particles are assumed to come mostly from lubricant oil combustion [6, 11-13], in the range of 1-30 nm [8, 14], and could be less toxic than diesel particles in terms of lung-deposited surface area [15], which has to be confirmed by more studies on this matter.

In order to complement the current knowledge with the measurement of real-world bus emissions, with passengers, the objectives of the present study were: the comparison of the operational emissions of different bus technologies and fuels (Euro IV diesel, Euro VI diesel, hybrid and CNG) and the evolution of real-world emissions regarding the evolution of Euro standards; the analysis of certain emissions explanatory factors; a comparison to COPERT 5 emission factors.

As the regional observatory of air quality in Île-de-France, one of Airparif's missions is to support decisions makers in developing their action plans for better air quality, in particular for the transportation sector. The emission inventory used for prospective studies is based on emission factors with certain levels of uncertainties. Those uncertainties for bus emission factors could be mitigated with more field data.

Île-de-France Mobilités is the organization responsible for public transportation, including the bus fleet, in the Paris Region. Its efforts to improve air quality and reduce greenhouse gas emissions illustrates its commitment to ecological transition. Having a better knowledge of bus emissions in operational conditions is important to ensure that technological choices actually meet the expected performances.

Materials and methods

Instruments and set up

The measured pollutants were: particle number (PN, from 23nm to 2.5µm), nitrogen oxides (NO and NO₂), carbon monoxide CO and carbon dioxide CO₂, with the AVL M.O.V.E GAS PEMS 492 iS and the AVL M.O.V.E PN PEMS 496 iS. The devices were powered by a series of deep-cycle Absorbent Glass Mat (AGM) batteries providing a maximum autonomy of 8 hours.



Figure 1: Photo of the interior setup.

The batteries and the devices were fixed in two separate boxes, specifically made for the study, following a modular design in order to adapt to the different vehicle configurations. The boxes were fixed on the bus floor using already existing seat fixations and anchoring points.

The sampling probe was placed 20 cm upstream from the exhaust, where the flow is laminar. The exhaust temperature and flow rate were collected from the exhaust flow meter (AVL MOVE EFM, 31 cm upstream from the sampling probe). The diameters of the 5-meter long sampling lines were 4 mm for the PN PEMS, and 6 mm for the GAS PEMS. The sample lines were heated to prevent condensation, the dilution rate of the PN PEMS was set to 6:1. The passage through the engine trap was sealed with a fireproof paste.

To ensure the safety of the passengers, the design of the setup was verified by the manufacturers and the state authority to meet the requirements on load distribution, anchoring points, insulation and electrical conformity. Communication to the passengers was ensured by information panels and the presence of an agent answering potential questions.

A significant technical challenge of this project stemmed from the fact that the scope of our campaigns went beyond the typical use of PEMS instruments. Differently from certification tests which would typically last a few hours, our campaigns involved the deployment of the measurements systems for intensive operation over multiple weeks (typically two). More precisely, the PEMS were installed at the same time on the two buses and measurements would last up to 8 hours per day, 5 days per week, with one to two on-site interventions for device maintenance every week. In spite of this longer maintenance cycle, no significant drift was observed on the analyzers throughout the campaigns.

Having an operator on site for starting and stopping the measurement process was not practical as the various bus depots were spread out through the region, and assigned bus schedules could be modified to respond to demand. At the same time, keeping the devices measuring at all times would have been wasteful as it would significantly impact the lifespan of the sampling system subcomponents (e.g., pumps, valves, and filters). In order to optimize measurement system usage, an automatic software routine was designed and implemented to allow a safe and autonomous switching between the measurement and stand-by states of the PEMS. To this end a signal of the battery charging system that permitted to know when it was being supplied (i.e. plugged into a 220 V power socket) was leveraged. When the bus left the depot, the power cable would be disconnected, triggering our routine to switch the PEMS to the measurement state, without any additional human intervention. At the end of the day, or if the bus had to return to the depot during the day, the power cable supplying the battery charger would be plugged back in and the PEMS would switch to the stand-by state, and eventually time out into the pause state. This triggering mechanism also allowed to meet the objective of capturing cold-start emissions.

The communication link was ensured through a 4G data connection, enabling the automatic transfer of measurement log files to Airparif's servers for validation, database integration and analysis, but also remote inspection of the measurement system operation.

The measurement time resolution was of 1 Hz for the pollutants along with vehicle parameters collected from either the On-Board Diagnostics (OBD) interface, for most of the Euro IV vehicles, or from the Fleet Management System (FMS) interface, for Euro VI and retrofitted Euro IV vehicles. The list of accessible vehicle parameters varied for different vehicle models, but typically included velocity, engine speed, coolant temperature, throttle position, and fuel rate.

Other important measured parameters were ambient temperature and humidity collected from a sensor on the roof of the bus supplied with the AVL MOVE system, and positioning collected from an advanced Global Navigation Satellite System (GNSS) receiver from u-blox (NEO-M8U), which integrated Inertial Measurement Unit (IMU) and GNSS data. In order to protect the sensor equipment deployed on the roof of the buses, the operators were asked to exclude the roof from their regular vehicle wash routine.

Vehicles and routes

Buses

A panel of bus types from four different manufacturers were tested in order to study a representative panel of the Paris region bus fleet. 28 different buses were tested in total, divided in four main categories: four types of Euro IV diesel, four types of Euro VI diesel, three types of Euro VI hybrid (diesel/electric), and three types of Euro VI CNG, with two buses of each type in order to catch the emission variability within the same bus type as well. The fuel used in the CNG buses was taken from the natural gas network available at the bus depot, therefore composed of a mixed of fossil gas and biogas, depending on the biogas production in the area. The origin and composition of the gas was not analysed.

In terms of after-treatment systems, among the eight Euro IV diesel buses: two had an Exhaust Gas Recirculation (EGR) system, six had a Selective Catalyst Reduction (SCR) system and a Diesel Particulate Filter (DPF) – four of them being retrofitted DPF. Among the eight Euro VI diesel buses, all had a DPF, four had a SCR system, and four had a SCR system and an EGR system. Among the six Euro VI hybrid buses, all had a DPF, four had a SCR system, and two had a SCR system and an EGR system. The six Euro VI CNG buses had the three-way catalyst commonly used for this engine.

The mileage of the Euro IV diesel buses was between 500 000 and 600 000 km, the mileage for the Euro VI diesel and hybrid buses varied from 100 000 to 350 000 km.

Bus lines

The routes of the buses consisted of deadheading when the bus rides between two services, or from/to the bus depot, and of trips on defined bus lines. The periods of deadheading are important to assess cold start emissions. 11 different bus lines were considered: five bus lines in Paris, taken by buses of the four vehicle categories, two Euro IV diesel buses, four Euro VI diesel buses, two Euro VI hybrid buses, two Euro VI CNG buses; three bus lines in the inner suburbs, taken by six Euro IV diesel buses, three Euro VI diesel buses, four Euro VI hybrid buses; three bus lines in the outer suburbs, taken by one Euro VI diesel bus and four Euro VI CNG buses. Those bus lines have different configurations, in terms of bus stops frequency and medium speed over the whole bus line: the lines in Paris have a high bus stop frequency (2.5 to 3.5 per km) compared to the suburban lines (1.2 to 2.2 per km), and the average speed in Paris does not exceed 13 km/h compared to 14 to 22 km/h in the suburbs.

Variability of operating conditions

A total of 16 measurement campaigns were carried out. For each campaign, two buses were tested in parallel, on a different or on the same bus line, at different hours of the day thus different traffic and meteorological conditions, depending on the bus schedule. The two buses were running the normal routes, while carrying passengers. The buses were only riding from Monday to Friday, so that the batteries could recharge entirely during the weekend. Temperature conditions were diverse from winter to summer, with a medium temperature of 14°C for diesel and hybrid buses, but only 8 °C for CNG buses thus in harsher conditions overall. This bias is important to consider as it could have a certain influence on the emissions measured (see in the Results section).

One of the main characteristics of this study was to measure emissions in real operating conditions, with passengers. In this context, a single operator did not have vehicles from all the different bus categories. The different buses selected within the four bus categories were tested with their usual operator and on a selected bus line located in its operating area. Given the constraints, the study was designed so that we could cover as many different operating conditions as possible for each bus category, in terms of number of different buses, meteorology, traffic conditions and usage (e.g. driving styles, vehicle conditions in terms of state of maintenance), while ensuring to have enough data for each category to draw significant statistical conclusions. This design allowed to get a general overview of bus emission ranges in Île-de-France and to observe potential statistical differences from one bus category to the other.

Data analysis

The first step of analysis was data post-processing with the AVL Concerto software: synchronization of the signals, dry-to-wet correction, and humidity-temperature correction for NO_x (ISO16183 Diesel for diesel and hybrid buses, ISO16183 SI for CNG buses). Certain events, like regeneration attempts (which were very rarely observed, only three times) were tackled separately and not taken into account for the general analysis. Data at 1 Hz (g/s and particles/s) were analysed in three different ways: as is for time series, specific events analysis and the statistical model; transformed to g/km and particles/km for each km travelled, method used by O'Driscoll et al [16], for comparison to COPERT; or transformed to g/km and particles/km for each bus trip (from 3 to 20 km trips depending on the bus line) for global performance comparison. For COPERT comparison, it has to be noted that a segment of 1 km, with a certain average velocity, includes a number of accelerations and stops and is not a segment at a certain constant velocity. To assess the influence of driving style (smooth or irregular), the indicator called Relative Positive Acceleration [17] was used. Wilcoxon tests were performed to assess the significance of emission differences between two categories of buses.

Quantifying the influence of diverse explanatory variables on pollutant emissions

With the dataset obtained, we tried to quantify the influence of certain parameters on the emissions. This question was tackled as a regression problem: a gradient-boosting model was fitted, using classical methods (cross-validation, hyper-parameters optimization) to ensure the resulting model is accurate and not over-fitting. Thus, these gradient-boosting models were able to capture non-linear interactions between the input features and the output [18]. An explanatory analysis was then conducted using the SHAP approach [19]: it aims at interpreting any kind of statistical model, and provides individual feature responses. The SHAP approach takes into account how the model links each input feature to the output (the emission measurement), and how the input features covariate. Hence, these SHAP responses offered a better insight of how the emission measurement is determined by the engine parameters. In this work, the results for diesel and hybrid buses are presented, while the CNG campaigns, which were recently finalized, are still ongoing work.

Results

More than 6,500,000 data points were collected per pollutant, at a time resolution of 1 Hz, along with vehicle parameters, exhaust temperature, ambient temperature/humidity, and positioning. This dataset corresponds to more than 1600 trips: 528 trips for Euro IV diesel buses (87 in Paris, 441 in inner suburbs), 468 for Euro VI diesel buses (231 in Paris, 167 in inner suburbs, 70 in outer suburbs), 324 trips for Euro VI hybrid buses (67 in Paris, 257 in inner suburbs) and 298 trips for Euro VI CNG buses (66 in Paris, 232 in outer suburbs). For CNG buses, all the PN emissions from one campaign were considered invalid because of high humidity peaks (sometimes over 30% or 40%) noticeably impacting the measure.

Emissions of different bus technologies

This analysis regroups all the trips of the four bus categories, in all operating conditions. Statistically, the bus category has more impact than any other parameter (except after-treatment system failures, but this happens very rarely). The following boxplots show the results for PN (Figure 2), NO_x (Figure 3), CO (Figure 4) and CO₂ (Figure 5), for all bus trips taken together, in order to illustrate the emission ranges measured.

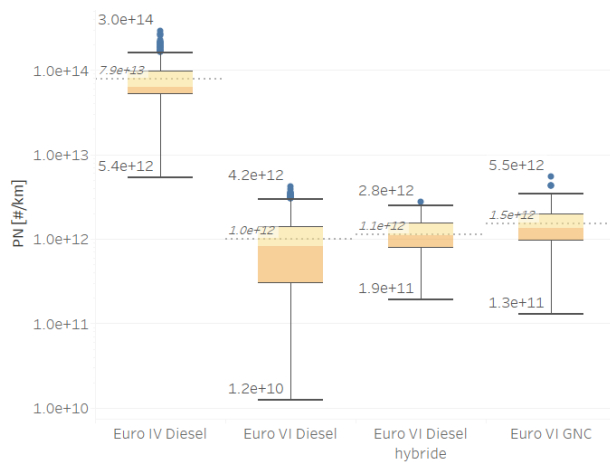


Figure 2: Boxplots of the PN emissions for all bus trips, by bus category (logarithmic scale); #/km = particles/km.

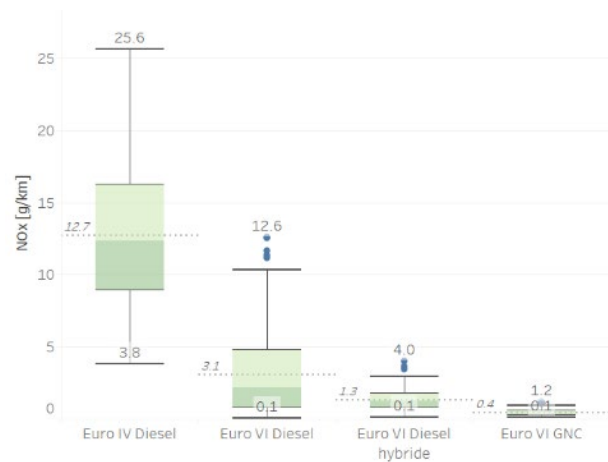


Figure 3: Boxplots of the NO_x emissions for all bus trips, by bus category.

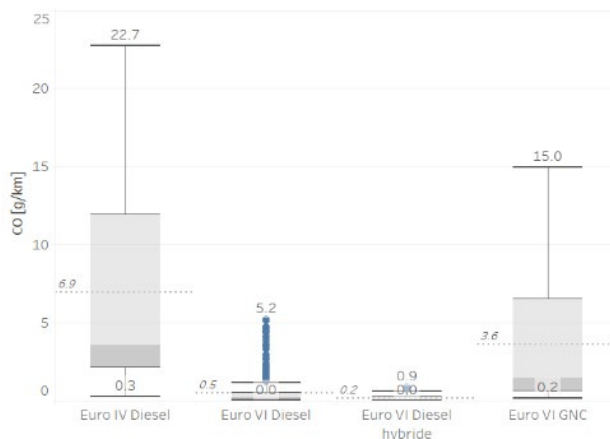


Figure 4: Boxplots of the CO emissions for all bus trips, by bus category.

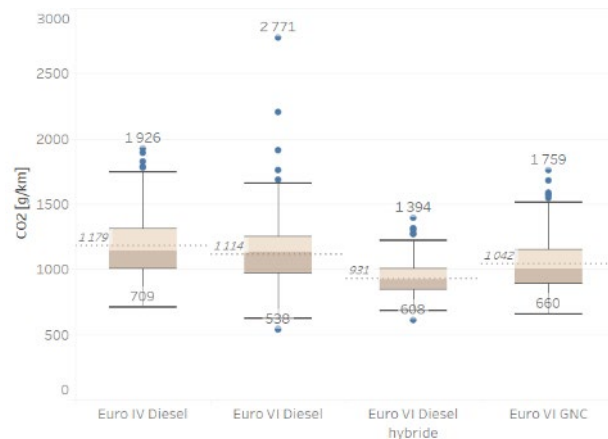


Figure 5: Boxplots of the CO₂ emissions for all bus trips, by bus category.

PN emissions

A great gap was measured between PN emissions of Euro IV buses and all the categories of Euro VI buses: on average, PN emissions for Euro VI buses were 50 to 80 times lower than those of Euro IV buses. Almost all Euro VI buses trips had lower PN emissions – except for one bus trip of a Euro VI CNG bus, which emitted the same PN rate as the minimum PN rate of all the trips recorded for Euro IV diesel buses. The range of Euro IV buses emissions was [5.4x10¹²; 3.0x10¹⁴] #/km (particles/km), the range of Euro VI diesel buses emissions was [1.2x10¹⁰; 4.2x10¹²] #/km, the range of

Euro VI hybrid buses emissions was $[1.9 \times 10^{11}; 2.8 \times 10^{12}]$ #/km and the range of Euro VI CNG buses emissions was $[1.3 \times 10^{11}; 5.5 \times 10^{12}]$ #/km. Emission ranges from one Euro VI technology to the other are very close. However, considering recent literature [11, 14], if PN<23nm were taken into account, PN emissions of Euro VI CNG buses could also reach higher levels than those of Euro VI diesel buses, as the fraction of sub-23nm in the total PN can be higher for CNG vehicles.

For a more precise analysis of the results, we also filtered the bus trips of Euro VI diesel buses and CNG buses by similar operating conditions: the two CNG buses tested on a Parisian bus line were compared to two diesel buses tested on Parisian bus lines, with average velocities ranging from 9 to 15 km/h and average ambient temperatures ranging from 1 to 13°C. The other four CNG buses tested on outer suburbs bus lines were compared to three diesel buses tested on inner and outer suburbs bus lines, with more variability than the previous group for average velocities and ambient temperature: the ranges between first and third quartiles were [15; 25] km/h and [5; 15] °C, except for two CNG buses operating during harsher temperature conditions (with negative temperatures, and an average of 4°C). Depending on the bus considered, PN emissions of CNG buses could be, on one hand, 1.5 to 7 times higher on average than those of four of the diesel buses considered, and on the other hand, lower than one diesel bus tested in similar operating conditions (as an indicative, at least twice lower on average). PN emissions of CNG buses were higher in most cases than those of diesel buses, but remain in the range of those of diesel buses because of a great variability in PN emissions within these diesel.

The ranges reported by Giechaskiel [11] for Euro VI heavy-duty vehicle were similar to the present study for CNG, but lower for diesel, hence a bigger difference between the two technologies than in the present study.

The difference in PN emissions might be linked to different engine and DPF settings. Regarding PN emissions for CNG buses, it is important to keep in mind that for the moment, this technology doesn't have any after-treatment system specific to PN and still shows good performances compared to diesel technology (CNG uses spark-ignited internal combustion engines like gasoline, instead of compression-ignition engines for diesel).

NO_x emissions

NO_x emissions were on average four times lower for Euro VI diesel buses compared to Euro IV diesel buses, and hybrid buses had even lower emissions, 10 times lower than Euro IV diesel buses. Euro VI CNG buses emitted 7 times less NO_x on average than Euro VI diesel buses. The range of Euro IV buses emissions was [3.8; 25.6] g/km, the range of Euro VI diesel buses emissions was [0.1; 12.6] g/km, the range of Euro VI hybrid buses emissions was [0.1; 4.0] g/km and the range of Euro VI CNG buses emissions was [0.1; 1.2] g/km, thus much less variable than diesel buses despite the harsh winter conditions encountered.

When filtering bus trips of Euro VI diesel buses and CNG buses by similar operating conditions (see the section on PN emissions for details), NO_x emissions were lower (1.2 to 89 times considering individual bus trips) and less variable for CNG compared to diesel (with a standard deviation 9 to 27 times higher for diesel buses). One diesel bus had similar NO_x emissions in terms of average and standard deviation, but this same bus also presented higher PN emissions than the CNG buses (see the PN emissions section).

An important difference in NO_x emissions was also visible among Euro VI diesel buses, even at similar ambient temperatures and average velocities: average NO_x emissions around 1 g/km for the four buses with DPF+SCR (DS buses), average NO_x emissions around 4 g/km for the four buses with DPF+SCR+EGR (DSE buses). An influence of another parameter not collected in this study cannot be ruled out, but from our analysis, the choice of NO_x after-treatment system (EGR+SCR or just SCR) and its optimization (see section 3.2 about exhaust temperature) might be a hypothesis to consider. This hypothesis however would have to be tested, which is beyond the scope of the present work. The Euro VI diesel buses for which the lowest NO_x emissions were measured, presented relatively higher PN emissions (NO_x/PN trade-off): average PN emissions around 1 to 3×10^{12} #/km for DS buses, against average PN emissions around 2 to 8×10^{11} #/km for DSE buses.

NO₂ emissions were generally lower for most of the Euro VI buses (diesel, hybrid and CNG, order of magnitude: <0.01-0.2 g/km) compared to most of the Euro IV buses (order of magnitude: 0.1-1 g/km). However, three Euro IV buses showed similar NO₂ emissions to those of the Euro VI buses, and two hybrid buses showed NO₂ emissions similar to some Euro IV buses, between 0.2 and 0.8 g/km. The Euro VI CNG buses emitted even lower NO₂ emissions (order of magnitude: 0.02 g/km) than the Euro VI diesel buses. In terms of NO₂/NO_x ratio, it very variable among Euro VI buses (not considering times when the SCR was obviously not working properly): while for Euro IV diesel buses the ratio did not exceed 5%, the other categories showed a number of statistically atypical trips with NO₂/NO_x ratios higher than 10% and up to 40% for Euro VI diesel and CNG buses. Apart from atypical trips, the two Euro VI hybrid buses with higher NO₂ emissions showed average ratios around 50% (from 28 to 77% precisely). These high NO₂/NO_x ratios are supposed to emerge from different engine and after-treatment system settings. However, it is of importance to reduce NO₂ as well as NO at the exhaust, which was already pointed out by Anses in 2009 [20].

CO emissions

A drastic mitigation of CO emissions was observed from Euro IV diesel buses to Euro VI diesel buses, 14 times lower on average. CO emissions varied widely from one Euro IV bus to another (standard deviation: 5.8 g/km). Hybrid buses encountered even lower CO emissions than diesel ones. For CNG buses, CO emissions were 7 times higher on average than Euro VI diesel buses, mostly because of two same buses emitting as much as some Euro IV buses (3 to 15 g/km). The four other CNG buses emitted less than 3 g/km (average: 0.5 to 1.5 g/km) The range of Euro IV buses emissions was [0.3; 22.7] g/km, the range of Euro VI diesel buses emissions was [<0.1 ; 5.2] g/km, the range of Euro VI hybrid buses emissions was [<0.1 ; 0.9] g/km and the range of Euro VI CNG buses emissions was [0.2; 15.0] g/km.

When filtering bus trips of Euro VI diesel buses and CNG buses by similar operating conditions (see the section on PN emissions for details), CO emissions were always higher for CNG compared to diesel (4 to 15 times on average), and way higher for two of them as pointed out previously.

CO₂ emissions

CO₂ emissions were slightly reduced with engine modernization: 5.5% reduction from Euro IV to Euro VI diesel buses, 16% reduction from Euro VI diesel to Euro VI hybrid buses on average. Euro IV CNG buses compared to Euro VI diesel buses had similar ranges. The range of Euro IV buses emissions was [709; 1926] g/km, the range of Euro VI diesel buses emissions was [538; 2771] g/km, the range of Euro VI hybrid buses emissions was [608; 1394] g/km and the range of Euro VI CNG buses emissions was [660; 1759] g/km.

Usage variability

Variability in emissions can also come from how the bus is “used” (e.g. driving style, load, state of maintenance), apart from meteorological/traffic conditions or technological differences. This variability can be called usage variability and is particularly observable when two similar buses (in terms of manufacture) run on the same bus line during the same time period. This situation was encountered for all the six CNG buses tested. These tests lead to significant discrepancies between buses of the same make: for example, PN emissions or CO emissions for one bus could be 2 times higher than for the other on average, up to 60% higher for NO_x emissions, up to 20% higher for CO₂ emissions.

Analysis of certain impact factors

After analysis, it was first concluded that the impact of the parameter “bus line” could not be isolated from the other parameters considered. Bus emissions varied consequently from one bus to another independently of the bus line, because of certain usage conditions, some that could not be monitored. The monitored parameters spotted as influential in the statistical model, as well as some observed events (exhaust temperature, ambient temperature, cold start, after-treatment system failures, velocity, driving style), were analysed to explain part of this variability.

Exhaust temperature

This parameter is important to assess whether the SCR is under its optimal functioning conditions or not. It is optimal when exhaust temperature is above 200°C. Between 150 and 200°C, urea injection cannot happen but reduction reaction can, only with the stored urea that was already injected, therefore it cannot last for a long time. Under 150°C, the SCR cannot function. This threshold is highlighted by the statistical model developed, Figure 6. NO_x emissions tend to increase by +0.01 g/s when exhaust temperature is below 200°C. That means, for a bus running with an average velocity of 12 km/h, an additional 3 g/km of NO_x emissions.

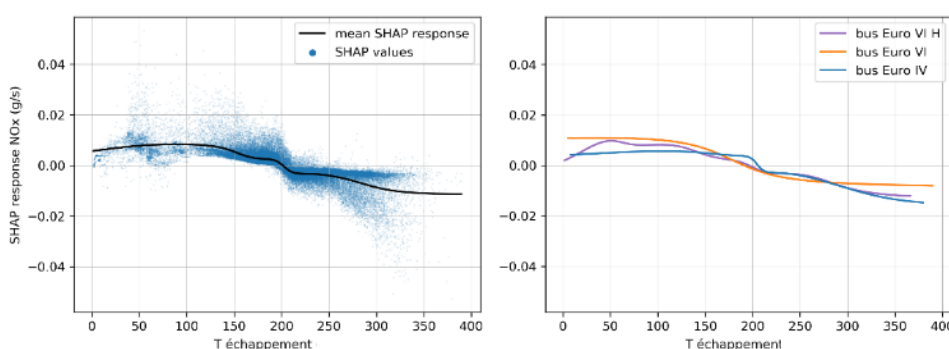


Figure 6: SHAP analysis over the whole set of diesel buses data - NO_x emissions vs. exhaust temperature.

At the scale of the bus trips, NO_x emissions of the Euro VI buses were the most impacted by exhaust temperature (see Figure 7). A group of different buses had most of the time an average exhaust temperature lower than 200°C, which potentially impacted NO_x emissions by preventing the SCR from working properly. Specific studies would be necessary to conclude on this point.

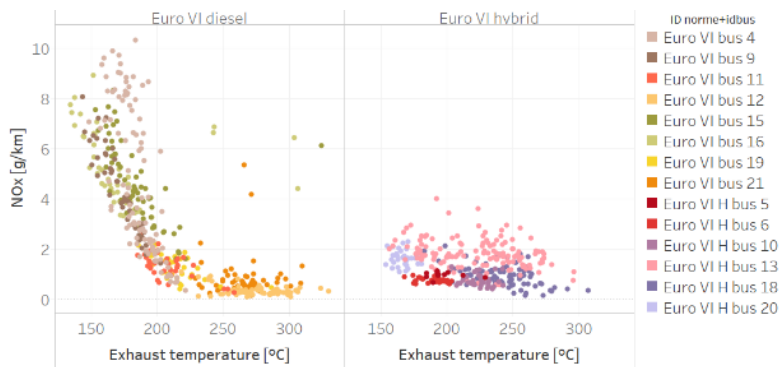


Figure 7: NO_x emissions vs. exhaust temperature for the Euro VI diesel and hybrid buses trips.

Ambient temperature

At low ambient temperatures, combustion conditions or after-treatment systems functioning conditions can be suboptimal: at hot engine and also during cold start (which can last longer at low temperatures).

For temperatures lower than 10°C, NO_x emissions could increase up to +0.01 g/s, especially for Euro IV buses (see Figure 8). After more detailed analysis at the scale of the bus trips, including comparisons of the emissions of four buses tested during winter and summer, the influence of ambient temperature highly depended on the bus considered. However, on average, from over 10°C to under 10°C, it was seen that NO_x emissions increased by 40% for Euro IV diesel buses, by 80% for Euro VI diesel buses, by 13% for Euro VI hybrid buses, while ambient temperature did not have observable effects on CNG buses (in the range of temperature encountered during the tests for these buses: -3 to 18°C).

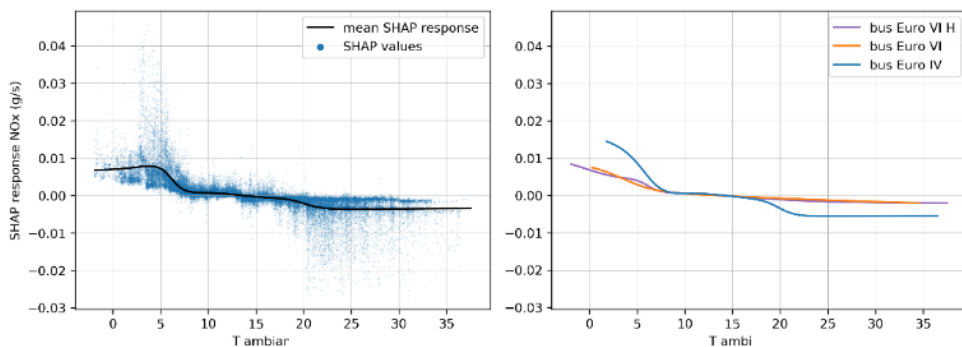


Figure 8: SHAP analysis over the whole set of diesel buses data - NO_x emissions vs. ambient temperature.

Cold-start

Cold-start is commonly linked to a coolant temperature under 70°C, indicator that was considered in this study. It was seen that cold-start duration was not depending on Euro standard. For all bus categories, considering data since engine start (sometimes a bus can stay a long time idling at the bus depot) cold-start was lasting between 14 and 35 minutes (or between 3 and 10 km), with a median around 20 minutes (or 6 km), with atypical trips when cold start would last a very long time, always at low temperatures below 10°C, for more than 1 hour (or more than 20 km). At cold-start conditions, NO_x emissions were on average 3 times higher than at hot engine for diesel and hybrid buses. However, CNG buses seldom experienced cold starts linked to high NO_x emissions, except for a few days when a bus was starting at an ambient temperature below 8°C: very short high NO_x spikes were observed, compensated afterwards by low NO_x emissions at hot engine.

Velocity

Average velocity for a bus trip during this study ranged from 8 to 25 km. Analysis showed that Euro VI buses (diesel, hybrid, CNG) emissions were not very sensitive to average velocity, contrary to Euro IV buses. For the latter, simple linear regressions were computed for each bus, resulting in an emission reduction from 8 to 20 km for each bus, which were then averaged over the Euro IV buses, resulting in: -42% of NO_x emissions, -38% for PN emissions and -27% for CO₂ emissions, from 8 to 20 km/h. There was no conclusive influence of average velocity on CO emissions.

Driving style

Driving style, through the RPA indicator, had a visible influence on CO₂ emissions (and on fuel consumption). It was considered that driving style was less smooth from a RPA > 0.2 m/s². For Euro IV diesel buses, +10 to +25% CO₂ emissions could be reached from RPA < 0.2 to RPA > 0.2 m/s², depending on the bus. For Euro VI diesel buses, it was +5 to +20% CO₂ emissions. PN emissions were also reaching higher values with higher RPA: +7 to 64% for Euro IV, +16 to 70% for Euro VI buses.

After-treatment systems failures

Four Euro VI diesel buses experienced visible (in terms of emissions) after-treatment systems defects during their service, showing the importance of maintenance and good settings to limit pollutant emissions.

One of them experiences urea injection defect during a winter campaign (average ambient temperature 6°C): ammonium salts deposited in the exhaust pipe, but no error signal was noticed on the dashboard. Compared to a summer campaign (average ambient temperature 25°C) when the same bus was tested, and isolating the effect of temperature, it is mostly NO₂ emissions that spiked because of the defect, on average almost 100 times higher than during the other campaign. This could be linked to excess NH₃ in the SCR exhaust, then oxidized as NO_x and mainly NO₂ in the Ammonia-Slip-Catalyst (ASC), then reacting with the leftover NH₃ in the ASC. A global NO_x conversion could be reached but with significant residual NO₂.

Another bus lacked some urea: it caused several NO_x and NO₂ spikes, on average 15 and 36 times higher respectively than under normal conditions. On the contrary, PN emissions collapsed to 40 times less than usual for this bus. A possible explanation is that soot might be oxidized by high residual NO₂ in the exhaust.

Two buses experienced what might have been an incomplete DPF regeneration because of a failed exhaust temperature increase: this should be higher than 550°C, or 350°C for a DPF with catalyst, but could not reach 350°C in this case. For one of them, it occurred twice, with one week interval. Instantaneous PN emissions (#/s) at this moment were on average 100 times higher than during normal conditions. No other regeneration event, which could have been observed through the exhaust temperature, was encountered during the whole study.

Comparison with COPERT 5

Overall, it was seen that COPERT 5.2 tends to underestimate the Euro IV and Euro VI diesel buses NO_x emissions and the Euro IV diesel buses CO emissions in the specific conditions of this experiment, while remaining within the encountered ranges (within the first quartile). To be more specific, considering only vehicle speed classes with more than 100 data and computing the difference between COPERT value and this experiment emissions median for each class: on average, for Euro IV diesel buses, measured NO_x emissions were about 1.6 times higher and measured CO emissions were 1.9 times higher than COPERT; for Euro VI diesel buses, measured NO_x emissions were about 2.8 times higher and measured CO emissions were 80% lower than COPERT.

NO₂/NO_x ratios in the EMEP/EEA [21] inventory are set to 14% for Euro IV heavy-duty vehicles, and to 10% for Euro VI heavy-duty vehicles. Therefore, the experimental results of this study showed an opposite evolution from Euro IV to Euro VI for buses, with the former quite stable around 2% on average, and the latter very variable from 2% to 66% on average depending on the bus.

Conclusions and perspectives

A large dataset of bus emissions, in real operating conditions while carrying passengers, was recorded, by implementing autonomous measurement process based on PEMS technology. This development is reproducible for any bus or coach.

Euro IV diesel buses, Euro VI diesel buses, Euro VI hybrid (diesel/electrical) buses and Euro VI CNG buses were tested on different bus lines (located in Paris, inner or outer suburbs), during various meteorological and traffic conditions, in order to investigate the emissions ranges encountered in the Parisian Region.

A reduction in real operating emissions was observed, for all pollutants (PN, NO_x, CO), from Euro IV diesel buses to Euro VI buses of all categories (diesel, hybrid, CNG). CO₂ emissions were also slightly shifted downwards but with close ranges. Factors and events influencing emissions were also analysed: exhaust temperature (suboptimal situations were observed for SCR functioning, leading to higher NO_x emissions), ambient temperature, cold start, driving style, average velocity (which notably influenced only Euro IV diesel buses, and not Euro VI buses).

The large amount of data generated by this campaign is a rich source of potential information which could yield further interesting findings. It will be proposed to the European Research for Mobile Emission Sources (ERMES).

For future work, there is an emerging demand for investigation of emitted particles smaller than 23 nm, and especially CNG buses, which needs to be addressed, as well as other pollutants like NH₃.

For more analysis on this dataset, please find the whole report (in French) on the Airparif website: <https://www.airparif.fr/>

Acknowledgement

We would like to thank Île-de-France Mobilités who financed this experimentation, and all the participants: Keolis, Transdev and RATP who made their buses available for the study, French Ministry of Environment, and bus manufacturers who helped us with the devices set up and security check.

References

- [1] Airparif, "Bilan de la qualité de l'air - Année 2019 - Surveillance et information en Île-de-France," 2020.
- [2] ICCT, "Road-tested: comparative overview of real-world versus type-approval NO_x and CO₂ emissions from diesel cars in Europe," 2017.
- [3] T. Grigoratos, G. Fontaras, B. Giechaskiel, and N. Zacharof, "Real world emissions performance of heavy-duty Euro VI diesel vehicles," *Atmospheric Environment*, vol. 201, pp. 348-359, 2019.
- [4] ADEME, D. Bénita, AJBD, and D. Fayolle, "Panorama et évaluation des différentes filières d'autobus urbains - Etat des lieux sur les technologies et les filières énergétiques existantes et en devenir pour le transport par autobus," 2018.
- [5] COMVEC, "Alternative Motor Fuels Technology Collaboration Programme Annex 49 : Fuel and Technology Alternatives for Commercial Vehicles," 2016.
- [6] ADEME, P. Coroller, and G. Plassat, "Comparative study on exhaust emissions from diesel and CNG-powered urban buses," presented at the DEER Conference, 2003.
- [7] J. Merkisz, P. Fuc, P. Lijewski, and J. Pielecha, "Actual emissions from urban buses powered with diesel and gas engines," *Transportation Research Procedia*, vol. 14, p. 3070:3078, 2016.
- [8] S. R. Opresnik, T. Seljak, R. Vihar, M. Gerbec, and T. Katrasnik, "Real-World Fuel Consumption, Fuel Cost and Exhaust Emissions of Different Bus Powertrain Technologies," *Energies*, vol. 11, p. 2160, 2018.
- [9] P. Söderena, N.-O. Nylund, and R. Mäkinen, "City bus performance evaluation, Customer Report, No. VTT-CR-00544-19," VTT Technical Research Centre of Finland, 2019.
- [10] IFSTTAR, B. Schnetzler, and F. Baouche, "Projet Équilibre : Analyse des consommation et émissions de véhicules Gaz et Diesel," 2019.
- [11] B. Giechaskiel, "Solid Particle Number Emission Factors of Euro VI Heavy-Duty Vehicles on the Road and in the Laboratory," *International Journal of Environmental Research and Public Health*, vol. 15, no. 2, p. 304, 2018.
- [12] A. Thiruvengadam et al., "Characterization of Particulate Matter Emissions from a Current Technology Natural Gas Engine," *Environmental Science and Technology*, vol. 48, no. 14, p. 8235:8242, 2014.
- [13] E. R. Jayaratne, N. K. Meyer, Z. D. Ristovski, and L. Morawska, "Volatile Properties of Particles Emitted by Compressed Natural Gas and Diesel Buses during Steady-State and Transient Driving Modes," *Environmental Science and Technology*, vol. 46, pp. 196-203, 2012.
- [14] Z. Toumasatos, A. Kontses, S. Doulgeris, Z. Samaras, and L. Ntziachristos, "Particle emissions measurements on CNG vehicle focusing on, sub-23nm," presented at the 23rd Transport and Air Pollution Conference, Thessaloniki, 2019.

- [15] H. Eisazadeh, M. A. Ehteram, and I. Khasaee, "Diffusion charging measurements on exhaust solid particle number and lung deposited surface area of compressed natural gas and diesel buses," *Environmental Science and Pollution Research*, vol. 27, p. 16929:16939, 2020.
- [16] R. O'Driscoll, H. M. ApSimon, T. Oxley, N. Molden, M. E. J. Stettler, and A. Thiyagarajah, "A Portable Emissions Measurement System (PEMS) study of NO_x and primary NO₂ emissions from Euro 6 passenger cars and comparison with COPERT emission factors," *Atmospheric Environment*, vol. 145, pp. 81-91, 2016.
- [17] Commission Regulation (EU) 2016/646 of 20 April 2016 amending Regulation (EC) No 692/2008 as regards emissions from light passenger and commercial vehicles (Euro 6) (Text with EEA relevance), European Commission, 2016.
- [18] T. Chen and C. Guestrin, "XGBoost: A Scalable Tree Boosting System," in *KDD '16: Proceedings of the 22nd ACM SIGKDD International Conference on Knowledge Discovery and Data Mining*, 2016. [Online]. Available: <https://arxiv.org/pdf/1603.02754.pdf>
- [19] S. M. Lundberg and S.-I. Lee, "A Unified Approach to Interpreting Model Predictions," presented at the 31st Conference on Neural Information Processing Systems, Long Beach, CA, USA, 2017.
- [20] afsset, "Impact des technologies de post-traitement sur les émissions de dioxyde d'azote de véhicules diesel, et aspects sanitaires associés," 2009.
- [21] EEA, "EMEP/EEA air pollutant emission inventory guidebook - Passenger cars, light commercial trucks, heavy-duty vehicles including buses and motor cycles," 2016 - Update Jul. 2018.

2.6 On-road emission measurements beyond type approval PEMS

N. Ligterink^{1*}, M. Vojtisek,² U. Stelwagen¹, S. van Goethem¹

¹ Sustainable Transport and Logistics, TNO, The Netherlands

²Center for Sustainable Mobility, Czech Technical University in Prague, Czech Republic

norbert.ligterink@tno.nl

Introduction

Exhaust emissions from internal combustion engines used in cars, trucks and various mobile machinery remain one of the most important sources of air pollution in metropolitan areas. The increasing discrepancy between legal emission limits and real-world emissions is partly due to engine design and calibration deficiencies, a manufacturing defect common to all vehicles of the same certification family, and partly due to the contribution of excess emitters, vehicles with high emission levels due to spontaneous defects and tampering. The new type-approval procedure, Real Driving Emissions (RDE) tests, are carried on the road, with portable emissions monitoring systems (PEMS) used to measure tailpipe emissions. These have been adopted in major legislations for automobiles (RDE) and heavy vehicles (PEMS ISC). Moreover, older vehicles may develop undetected malfunctions, which require emission measurements.

The currently applied PEMS have, however, some constraints and limitations. Firstly, contemporary PEMS measure only the “classic” pollutants, such as nitrogen oxides (NO_x). However, there appears to be a need to expand the on-road measurements to emerging pollutants of concern, such as ammonia (NH₃), e.g., relevant for eutrophication, and nitrous oxide (N₂O), a strong greenhouse gas. Secondly, the measurement of hot and pulsating exhaust gas flow with PEMS has been shown to have limitations. Within RDE emission legislation a 43% uncertainty margin is included based on the observed inaccuracies in PEMS measurements. This margin has been reduced to 32%, and a further reduction to 23% has been recently proposed by JRC. The European Commission aims to bring this margin down to zero, which is met with great opposition, from the collection of observed issues with the current PEMS equipment. In this paper other on-road emission measurement techniques are discussed that can help us to overcome these limitations of PEMS, via alternative approaches.

The PEMS designed for type approval testing currently include four gaseous pollutants: CO and CO₂, typically measured by a non-dispersive infra-red (NDIR) spectroscopy, and NO and NO₂, typically measured by non-dispersive ultra-violet (NDUV) spectroscopy or by chemiluminescence. On modern diesel engines, CO emissions are hardly an issue, and CO₂ concentrations can be inferred, albeit with an accuracy penalty, with a wide-band oxygen sensor mounted in the exhaust, if the fuel composition is known. In-situ NO_x sensors, frequently used on engines with selective catalytic reduction (SCR) devices, have been shown to provide a reasonably accurate determination of the concentrations of either NO_x, or NO_x plus some other reactive nitrogen species, in the exhaust. For practical purposes of identifying problematic vehicles and/or operating regimes, simple devices using in-situ NO_x and oxygen sensors, coupled with OBD-derived flow, can be used in lieu of PEMS.

With the deployment of NO_x aftertreatment technologies and advanced and alternative fuels, additional gaseous pollutants are worthy of consideration: potent greenhouse gases methane (CH₄, from methane based fuels) and N₂O (formed mainly in NO_x aftertreatment devices, like SCR); NH₃ and potentially other reactive nitrogen species, produced in three-way catalysts and SCR systems; aldehydes associated with ethanol addition in fuels. Most of the mentioned compounds, as well as all regulated compounds measured by type approval grade PEMS, can be measured with Fourier Transform Infra-Red (FTIR) analysers, already approved for laboratory measurements of NH₃ and N₂O measurements, with several instruments being also demonstrated and validated, at least for some pollutants, on the road.

The current legislative approach mandates a direct exhaust measurement with a device based on the difference between static and dynamic pressure. This technique provides a direct measurement right at the sampling point, eliminating errors associated with conversion and residence time of gases in the vehicle exhaust system, but it has downsides: It requires a reasonably laminar flow, achieved by a relatively considerable length of straight pipe. As the pressure difference is proportional to the square of the mean velocity of the measured gas, its useful range is about one order of magnitude, which is close to, or even less than, the ratio between exhaust flow at full load and that at idle.

In this paper alternative measurement approaches are discussed. This includes determination of the exhaust flow from measured or computed flow of intake air or fuel. For that purpose also separate flow sensors have been installed. In addition, using a trace gas, and a known dilution of the exhaust gas is discussed as a simple alternative. Attaching a pitot tube to the exhaust also allows to measure the exhaust gas flow. Retrieving intake air flow or fuel flow reported by the engine through on-board diagnostics (OBD) interface, when such data are available and reliable, is the simplest

and the least intrusive method. The quality of different OBD signals can be tested by simple calibration methods, for example, with a flow measurement system attached to the engine air inlet.

Analysis of NO_x sensor amplitude data

Sensor measurements can assist, possibly replace, the PEMS measurements. In the case of deviations of the PEMS system from a sensor reading, this can be reason to investigate the measurement accuracy further. Automotive sensors have been around for many years now, and are intended to assist or control the emission aftertreatment systems. Typically they last for 2000 to 5000 hours. To show the capabilities and limitations of such sensors, the in-line offset determination is discussed. In case of a suspected sensor failure, the sensors are re-calibrated at TNO in the laboratory.

Hypothesis

The amplitude distribution of NO_x sensor data may contain information on the functioning of the sensor. In particular, shifts in the distribution of the low NO_x amplitudes during motoring (O₂>19%, no fuel injection) might indicate sensor drift due to aging or damage over time and might be used as a sensor data quality indicator or a precursor of sensor failing.

Approach

The NO_x sensor data of three broken/failed NO_x sensors were analysed together with the data of two still functioning sensors. The five used sensors are same brand and type NO_x sensors as used in TNO SEMS monitoring of vehicle emissions. All five sensors for this analysis were used in NO_x emission monitoring in five same brand, similar type tractor-semi-trailer trucks during prolonged real-world driving use over many months.

Table 1: SEMS NO_x sensor overview from the sensor database.

Sensor Nr	Sensor ID	Data period	Current state	Valid NO _x samples (@1Hz)	Hours	Nr of graphs
1	1-06-190407-000002	2019-09-04 to 2020-02-13	broken	1210460	336.2	4
2	1-06-190329-000004	2020-04-07 to 2020-06-30	broken	1403048	389.7	5
3	1-06-190407-000007	2019-08-23 to 2020-07-24	broken	5068399	1407.9	17
4	1-06-190107-000018	2019-12-11 to 2020-10-22	functioning	2911792	808.8	10
5	1-06-190329-000002	2018-08-27 to 2021-03-03	functioning	22510597	6252.9	76

Method

Depict and visually analyse the time history of a sensors' amplitude distribution by plotting a series of amplitude distribution graphs for consecutive data sections of 300k valid (raw/uncalibrated) NO_x samples at 1Hz (in ppm). Each data section is thus equivalent to about 83 hours driving/engine runtime. Hence, for each sensor a series of four to 76 graphs resulted, giving a visual impression of developments over time for the amplitude distribution of the NO_x values acquired by the sensor.

In order to emphasize the low NO_x values during motoring, the analysis was repeated for valid NO_x samples for which the simultaneous O₂ values were above 19%. For these latter graph series, the first and last graph per series are shown in Figure 1 and Figure 2. Additionally for each graph series a video clip of the consecutive graphs was made in an attempt to better visualise developments over time in the NO_x amplitude distribution for each sensor. All sensors show a limited offset, or zero, value change over time.

Conclusion

Repeated visual analysis of all graph series as well as the corresponding video clips did not reveal any obvious changes in the NO_x sensor amplitude distributions, neither for those of the valid NO_x samples nor for those of the valid NO_x samples for which the simultaneous O₂ values were above 19%, that might be attributable to sensor drift, damage or aging. Though changes over time are observable, they are not consistently different for the three broken sensors from the two still functioning sensors. Also consistent drift of lower amplitudes was not observed.

TNO, 05-Mar-2021

SEMS NOx sensor 1-06-190107-000018

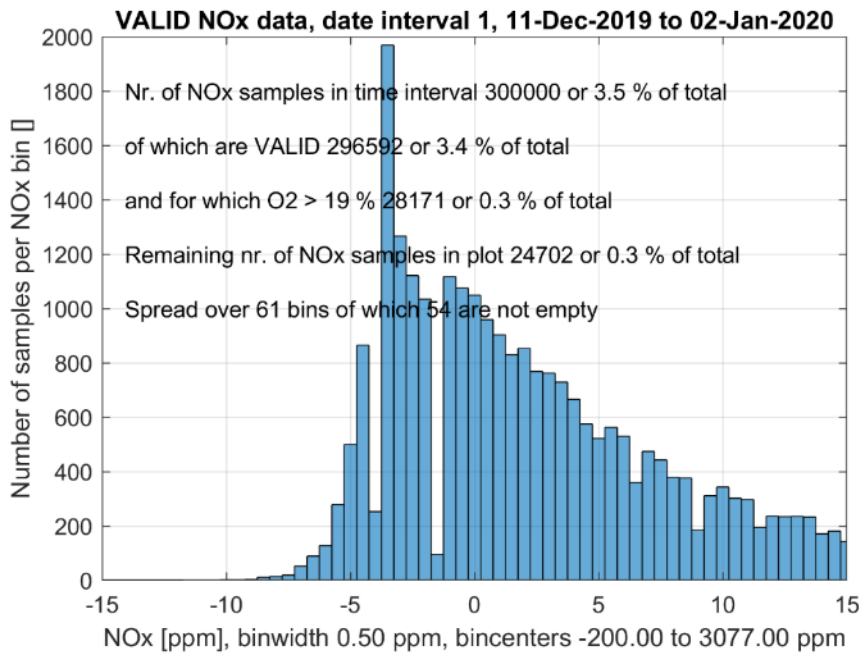


Figure 1: Sensor 4, NOx amplitude distribution of valid samples with O₂>19%, time section 1 of 10.

Sensor 4 is taken as an example. The offset seems about -3 ppm, with a measurement spread (based on the left flank) of about +/- 3 ppm. Since the left flank does not change over the 800 hours of operation, it is likely that spread in the right-hand side of the peak around 0 ppm NO_x is related to variation in engine operation and actual residual NO_x concentrations.

TNO, 05-Mar-2021

SEMS NOx sensor 1-06-190107-000018

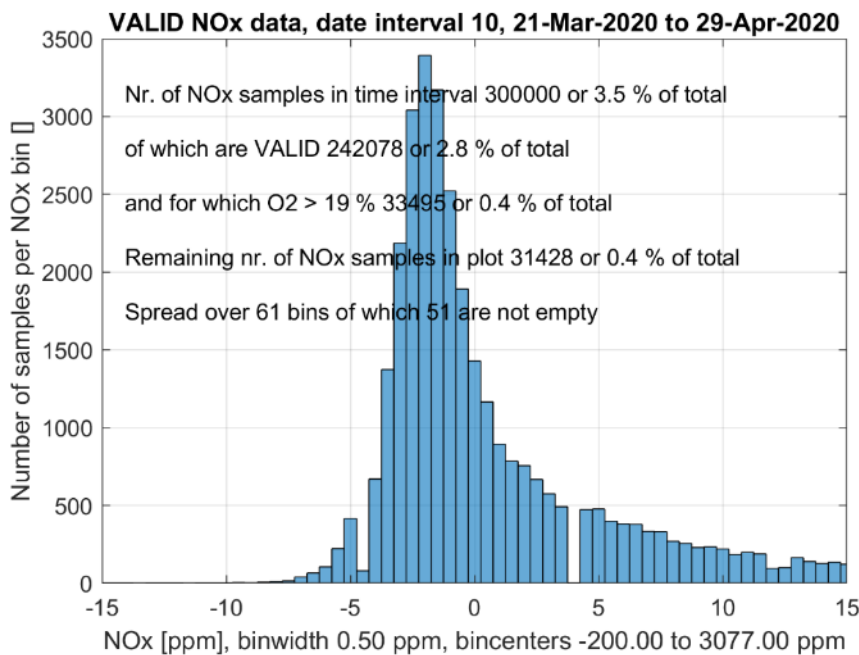


Figure 2: Sensor 4, NOx amplitude distribution of valid samples with O₂>19%, time section 10 of 10, after 800 hours.

It should be noted that a deviation of the NO_x concentration, as deduced from this magnitude of offsets, of 5 ppm is roughly 10-15 mg/km for a medium size passenger car. The current prescribed drift accuracy in the regulation is 5 ppm. Hence, sensors may help to ensure that a temporary drift is detected.

Using inlet mass airflow (MAF) to estimate NO_x exhaust emissions

Hypothesis

The mass airflow (MAF) and NO_x sensors in a modern vehicle can be used to estimate the exhaust flow rate and thus the NO_x emission mass flow rate in exhaust with an accuracy comparable to that of PEMS. The MAF sensor operates in the inlet at ambient conditions, and seems to react more quickly to the flow variations.

Approach

Show possibilities by combining the simultaneously measured PEMS and SEMS signals in a diesel, Euro 6 passenger car during a TNO RDE testing trip. The SEMS system is based on automotive sensors added to the exhaust line, in combination with the signals on the OBD. The sensors are calibrated independently. The OBD signals are sometimes validated in the workshop, by temporary adding a second calibrated MAF sensor. These MAF sensors use a thermo-resistive method, which works well in clean ambient air.

Method

Calculation of the exhaust flow rate (EFM_{OBD}) including the fuel burnt during the combustion can be done by combining the mass air flow (OBD_{MAF}) and the OBD O₂ concentration as follows.

$$EFM_{OBD}[g/s] = MAF_{OBD} * (1 + 0.067 * (20.8 - O_{2-OBD}[\%]) / 20.8)$$

The oxygen in ambient air is about 20.8%. The difference from the 20.8% is the oxygen used in combustion. The factor 0.067 is the reciprocal of the stoichiometric air fuel ratio (AFR), which is the maximum mass of fuel that can be added to air in stoichiometric combustion. This factor depends on the fuel composition; 0.067 is an approximate value for gasoline and diesel fuel. But in many of the legislation this composition is also assumed. Figure 3 shows the corresponding time signals (1 Hz) for the entire RDE trip with the diesel, Euro 6 passenger car, converted.

TNO, 15-Mar-2021

Combined SEMS & PEMS measurements on diesel Euro 6 PC

TNO innovation
for life

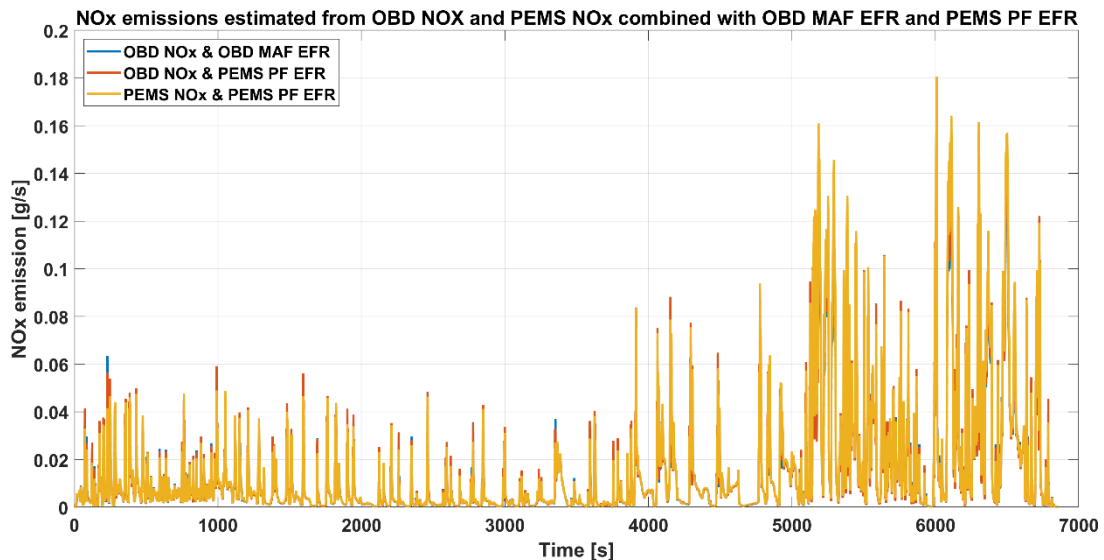


Figure 3: The three NO_x emission rates plotted together.

Next, by combining the NO_x concentration and the MAF-based exhaust flow rate the NO_x emission rate follows.

$$\text{NO}_{x\text{-OBD}}[\text{g/s}] = \left(\frac{\rho_{\text{NO}_x}}{\rho_{\text{exhaust gas}}}\right) * \text{NO}_x [\text{ppm}] * \text{MAF}_{\text{OBD}}[\text{g/s}] * (1 + 0.067 * (20.8 - \text{O}_{2\text{-OBD}}[\%]) / 20.8)$$

Where ρ_{NO_x} and $\rho_{\text{exhaust gas}}$ are the densities of NO₂ and diesel exhaust gas, respectively, in standard conditions. The density of exhaust gas is within 1% the same as the density of air. Similarly, the PEMS NO_x concentration and the PEMS PF exhaust flow rate (EFM_{PEMS}) can be combined to yield the PEMS NO_x emission rate (NO_{x-PEMS}).

$$\text{NO}_{x\text{-PEMS}}[\text{g/s}] = \left(\frac{\rho_{\text{NO}_x}}{\rho_{\text{exhaust gas}}}\right) * \text{NO}_x [\text{ppm}] * \text{EFM}_{\text{PEMS}}[\text{g/s}]$$

The aforementioned two estimates of the NO_x emission rates are plotted together, with a mixed OBD/PEMS variant as well, in Figure 4 which again shows the time signals for the entire RDE trip. The similarity between the three signals looks favourable. Because of the used scale, of almost two hours driving time, it is impossible to tell how good the similarity is and where and how large the differences are.

Therefore, in Figure 4 cumulative versions of the three signals, hence the estimated NO_x emissions in grams as functions of time, are given, which clearly show how the differences grow during the trip and also indicate that the differences grow faster at higher speeds. Figure 5 is a zoomed in version of Figure 3, showing five minutes of driving time on the motorway, which clearly illustrates that the differences mainly occur at higher speeds. This result is without the correction of the span and offset of the NO_x sensor.

TNO, 15-Mar-2021

Combined SEMS & PEMS measurements on diesel Euro 6 PC

TNO innovation for life

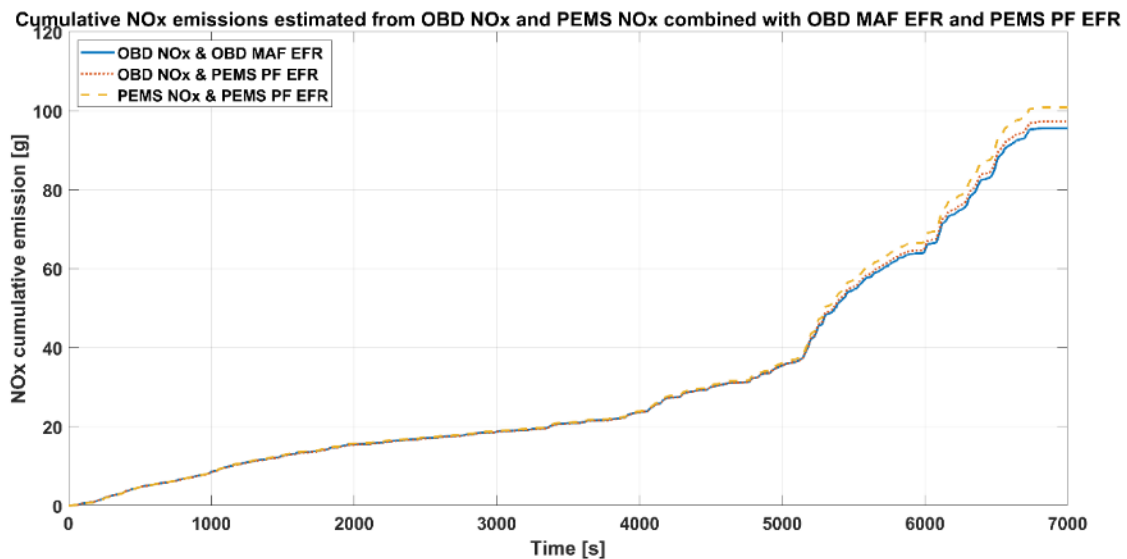


Figure 4: The three cumulative NO_x emissions plotted together. The concentration measurements give the largest deviation, the flow measurements deviate within 2%, over a long RDE test. But actual deviations occur at higher velocity and dynamics around 5000-6000 seconds.

Conclusion

The MAF airflow and NO_x sensors can be used to estimate the exhaust flow rate and thus the NO_x emission mass flow rate in exhaust with an accuracy comparable to that of PEMS. Zooming in on the sections in which the deviations occur (see Figure 5), it can be noted that the PEMS flow is somewhat higher in the peaks than the MAF, and the PEMS smoothens the variations observed in the MAF. The MAF is therefore a useful tool to ensure deviations in the flow measurements are detected. If the measurement principles are extended, the measurement of inlet airflow could be a suitable and robust alternative to measuring in the hot, wet and pulsating exhaust gas, with variable composition.

TNO, 15-Mar-2021

Combined SEMS & PEMS measurements on diesel Euro 6 PC

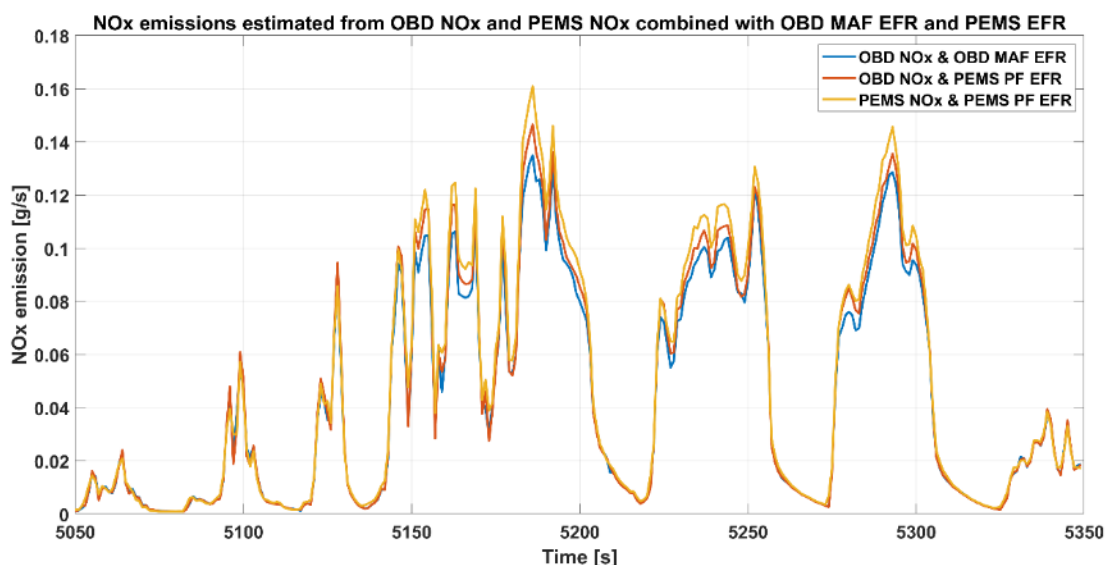



Figure 5: Zooming in to five minutes of the three NOx emission rates shows where the differences occur.

The use of FTIR

Likewise as the use of concentration sensors and MAF sensors, the FTIR (Fourier Transform Infrared spectrometer) allows for quality control beyond the current PEMS systems. Unlike instruments working at a specific wavelength, an FTIR can store the complete mid infra-red absorption spectra, which can be, at a later time, re-analysed for the concentrations of additional gases of interest. The measurement of all gases of interest simultaneously, with one instrument, simplifies both the measurement procedure and the post-processing. Several FTIR have been successfully used on the road, ranging from simple, compact instruments to laboratory instruments carefully installed in a test vehicle. The mass and power consumption of the smaller systems are comparable to those of type-approval grade PEMS. The relatively small amount of liquid nitrogen (tenths of a litre) for detector cooling is well contained and no process gases are required during the testing, making the FTIR a relatively safe instrument suitable for on-road measurements.

There are two major caveats with FTIR. One is the possible distortion of the spectra due to contamination of the optics, excessive vibrations and jolts, fluctuations in various temperatures (instrument case, optical cell, sample, etc.), and other reasons. The quality of the spectra can be checked by evaluating certain regions of the spectra and/or by comparing the concentrations of at least some gases for which reference measurement is available (CO₂ calculated from exhaust gas oxygen sensor, NO_x measured by a sensor in exhaust).

The second caveat is that the measured absorption spectra is the sum of the absorptions of all absorbing compounds, and that the contributions of each compound are calculated from often overlapping individual absorption spectra obtained by deconvolution of the measured spectra. Therefore, detection limits, uncertainties, or even the capability to obtain a meaningful reading for a given compound, are specific to the composition of the mixture. For example, the detection limit achieved with a mixture of calibration gas with dry nitrogen is unlikely to be achieved in the presence of several orders of magnitude higher concentrations of CO₂ and water vapor. This is, however, a known issue, common to both on-road and laboratory measurement, and is dealt with, to various degree of success, by spectroscopy specialists.

Since the FTIR is the preferred candidate instrument for Euro-7/VII legislation, to incorporate NH₃ and N₂O measurements, it is important to also ensure that the capabilities of FTIR are used to improve the measurement accuracy, and disqualify substandard measurements. Several N₂O measurements with FTIR indicate that this strong greenhouse gas contributes about 5% to the CO₂-eq emissions of diesel vehicles equipped with an SCR. If N₂O is only regulated in the laboratory, there is a risk that on-road N₂O emission levels are not curbed.

From the FTIR spectra themselves many aspects can be deduced. For example, misalignment, vibrations, noise, inlet gas composition, cross-correlations, light intensity fluctuations, temperature variations, fouling, etc. If such elements are taken into consideration, and possibly analysed in post-processing, it may reduce the risk of large measurement errors. In the best case, the actual measurement uncertainty can be deduced from the spectra themselves.

Conclusions

On-road emission measurements are, per definition, in an uncontrolled environment. Validating the measurement equipment in the laboratory, against laboratory equipment has its limitations, as often pointed out by the automotive industry, in the discussions on RDE legislation. This is not related to the average or general results, taken by JRC as the basis for the margin, but to the risk of a deviation results, possibly due to an undetected measurement problem. It is therefore essential to develop techniques to have real-time, on-board, quality control of the measurement systems.

Moreover, measurement alternatives, such as using inlet air flow, rather than exhaust gas flow, may improve the robustness of emission measurements and allow for a move towards lifetime monitoring. In the latter case, with sensor based measurements, the PEMS is only needed for validation.

The development of Euro-7 legislation, incorporating other emission components, is an opportunity to fundamentally improve the on-road measurement systems. It should no longer be bringing laboratory equipment instrument to on-road measurements. Instead, robustness should arise from real-time quality control, that can detect deviations in the results. Using two independent on-road measurement principles in conjunction, as shown here, can be at the basis of these improvements.

2.7 Insights for post-Euro 6, based on analysis of Euro 6d-TEMP PEMS data

J. Demuyne^{1*}, L. Sileghem², S. Verhelst², P. Mendoza Villafuerte¹, D. Bosteels¹

¹ Association for Emissions Control by Catalyst AISBL

² Ghent University

joachim.demuyne@aecc.eu

Abstract

Real-Driving Emissions (RDE) requirements were introduced in the European emission legislation to address the gap between lab and real-world emissions. The procedure focuses on on-road testing with a Portable Emissions Measurement System (PEMS) and defines a Not-to-Exceed limit for NO_x and PN emissions. This paper analyses a database of publicly available PEMS data of mostly Euro 6d-TEMP vehicles. Emissions data of 7 gasoline and 13 diesel vehicles are investigated. Different routes are included per vehicle to explore the emissions over a range of driving conditions. A standard analysis approach is to look at the average emissions per kilometre over the total test, but it has to become difficult to derive trends as overall emissions have reduced significantly compared to the pre-RDE era. This investigation therefore looks at smaller trips within the RDE tests. The intention is to explore remaining emission events to derive insights for Euro 7. The results firstly confirm a significant reduction in real-world emissions with the introduction of RDE requirements, both for PN and NO_x emissions. Secondly, the paper shows cold-start emissions are important for both gasoline and diesel vehicles. Once the emissions control technologies are at normal operation temperature, emissions are well controlled for most cases. Finally, it is shown that relatively high emission events are still happening and that this is not only limited during to the cold-start phase. As overall emission levels are indeed reducing, the relative contribution of the remaining emission events becomes significant. Effective legislation must ensure that the remaining emission peaks are properly controlled by designing the testing protocol to apply appropriate averaging of emissions over the emissions test, or part of it.

Introduction

Real-Driving Emissions (RDE) requirements were introduced in the European emission legislation to address the gap between lab and real-world emissions. The requirements are applied in 2 steps with Euro 6d-TEMP and Euro 6d type approvals. The procedure focuses on on-road testing with a Portable Emissions Measurement System (PEMS) and defines a Not-to-Exceed limit for NO_x and PN emissions. No compliance requirement is defined for the other regulated pollutants CO and THC, these are covered by the WLTC test in the lab. Data from type approval and independent third-party testing confirms Euro6d-TEMP and Euro 6d vehicles have low on-road NO_x and PN emissions. Most significant progress is made for gasoline PN and diesel NO_x. The positive trend from pre-RDE towards Euro 6d is shown in Figure 1, based on type-approval data in OEM RDE databases [1-2]. Pre-RDE emissions are based on emission factors [3] for gasoline PN and Euro 6b/c data in the OEM databases for diesel NO_x.

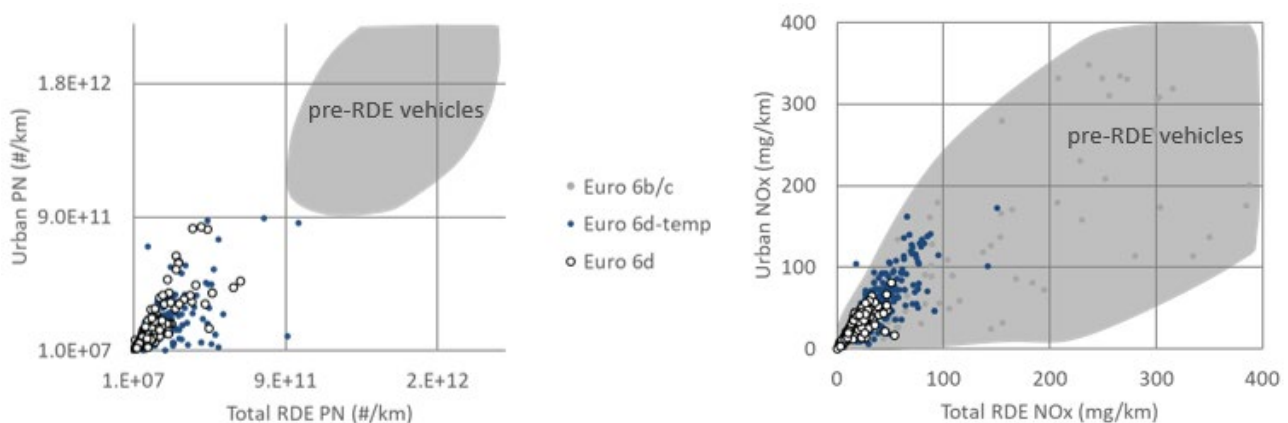


Figure 1: Reduction in gasoline PN and diesel NO_x emissions towards Euro 6d.

Emissions control technologies have evolved significantly towards vehicle RDE compliance, see some examples in Figure 2. For gasoline vehicles with direct injection, Gasoline Particulate Filters (GPF) are introduced to reduce PN emissions in addition to the existing Three-Way Catalysts (TWC) for conversion of gaseous emissions. For diesel vehicles, a combination of deNO_x technologies is integrated into the exhaust in addition to the Diesel Particulate Filter

(DPF). This can be a Diesel Oxidation Catalyst (DOC) or Lean NO_x Trap (LNT) in combination with one or more Selective Catalytic Reduction (SCR) volumes.

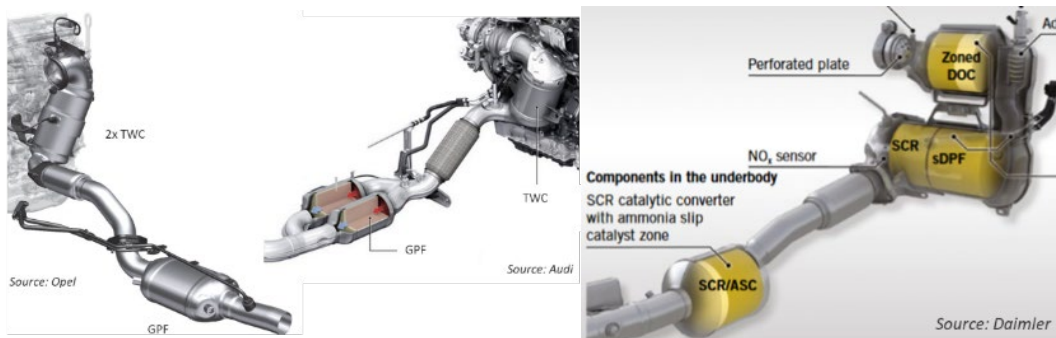


Figure 2: Example of Euro 6d(-TEMP) emission control systems for gasoline (left) and diesel (right).

The development process for a new Euro 7 emissions regulation for cars, vans, trucks and buses is ongoing. It continues to consider the stringency and testing measures to ensure low vehicle emissions. A European Commission proposal for Euro 7 is expected by the end of 2021. This paper analyses a PEMS database of mostly Euro 6d-TEMP vehicles. The intention is to investigate overall emissions performance of a range of gasoline and diesel vehicles and to identify remaining emission events. The data will be analysed to derive insights for the Euro 7 considerations. It is to be noted that the analysis presented in this paper does not allow to draw any conclusions about emissions compliance of the specific vehicles compared to their respective Euro 6 type approval requirements.

Research methodology

In this paper, RDE test results of several vehicles are investigated. The database consists of benchmark data obtained by AECC (vehicle 1), publicly available data from the global RDE database [4] and JRC publications [5-6]. Table 1 gives an overview of the vehicle specifications: fuel type, type-approval stage and engine and emission control technology. Vehicles 1-7 are gasoline, vehicles 8-20 are diesel.

A standard regulatory analysis approach is to look at the average emissions per kilometre over the total test. As overall vehicle emissions have reduced significantly compared to the pre-RDE era, it is difficult to derive trends when only looking at the total RDE test result. The RDE procedure introduced separate requirements for the urban part of the test because of specific attention to urban air quality. The investigation in this paper further looks at shorter trips anywhere within the RDE tests to screen for possible emission events.

The available PEMS data of these vehicles was measured according to the RDE procedure defined in Regulation (EU) 2017/1151. For this paper, the raw emission data is used, without applying some of the specific RDE data post-processing, to have a clear view on the emissions as measured at the tailpipe.

Results and discussions

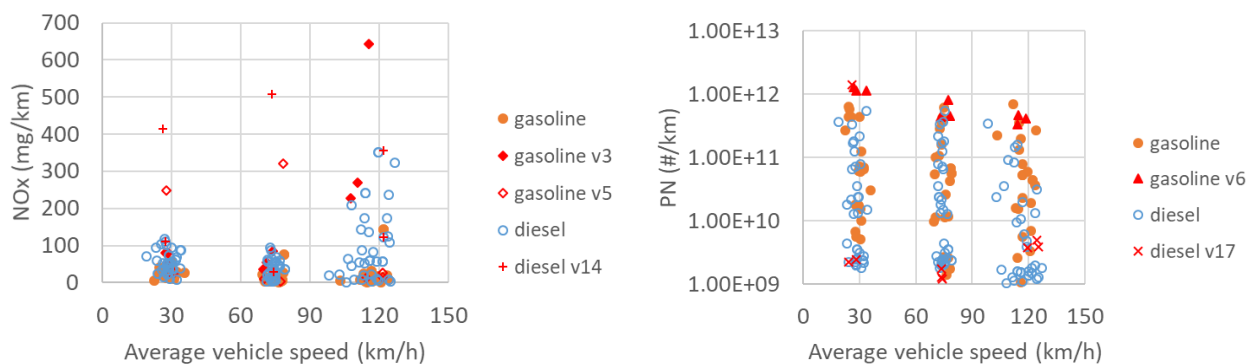
In a first step, the overall emissions performance of the vehicles is investigated. The data analysis focuses on those trips that are within current RDE boundary conditions for $v_{x_{a_{pos}}}$. As defined in the RDE procedure in Regulation (EU) 2017/1151, there is a limit for the 95th percentile of this parameter, which is the product of vehicle speed per positive acceleration greater than 0,1 m/s². It is an indication for the driving dynamics. In a second step, a more detailed analysis will be done for possible remaining emission events: the initial cold-start and any outlier result.

Figure 3 shows an overview of the NO_x and PN emissions of the different vehicles in the database. The emissions in mg/km or #/km of the urban (left), rural (middle) and motorway (right) part of the RDE trips are plotted vs. the average vehicle speed. An orange circle is used for the gasoline vehicles, an open blue one for the diesel vehicles. Outlier results are highlighted with a red marker for specific vehicle numbers. These will be discussed in more detail in the paper.

It can be seen that the emissions of the vehicles are generally very low for both NO_x and PN. The overall emissions of the diesel and gasoline vehicles are similar. For the motorway part, the graph indicates that the diesel NO_x emissions tend to be higher. Further reductions are possible through a combination of reduction in engine-out emissions and appropriate sizing of the emission control system, as demonstrated for a C-segment vehicle [6]. It is to be noted that the RDE legislation foresees a compliance requirement for the total test as well as for the urban part. There is no specific requirement for the motorway part. On the other hand, a majority of the motorway diesel PN emissions in Figure 3 are the lowest of the range observed.

Table 1: Overview of PEMS database.

VehicleID	Fuel_type	Type Approval	Technology
Vehicle 1	gasoline	Euro 6d-TEMP	GDI, TWC, GPF, 48V mild-hybrid
Vehicle 2	gasoline	Euro 6d-TEMP	GDI, TWC, GPF
Vehicle 3	gasoline	Euro 6d-TEMP	PFI, TWC
Vehicle 4	gasoline	Euro 6c	GDI, TWC
Vehicle 5	gasoline	Euro 6b	GDI, TWC, GPF
Vehicle 6	gasoline	Euro 6d-TEMP	PFI, TWC
Vehicle 7	gasoline	Euro 6d-TEMP	GDI, TWC, GPF
Vehicle 8	diesel	Euro 6c	DOC, EGR, DPF, SCR
Vehicle 9	diesel	Euro 6d-TEMP	DOC, EGR, DPF, SCR
Vehicle 10	diesel	Euro 6d-TEMP	DOC, EGR, DPF, LNT, SCR
Vehicle 11	diesel	Euro 6d-TEMP	DOC, EGR, LNT, DPF, LNT, pSCR
Vehicle 12	diesel	Euro 6d-TEMP	SCR, EGR, DPF
Vehicle 13	diesel	Euro 6d-TEMP	SCR, LNT, DPF
Vehicle 14	diesel	Euro 6d-TEMP	LNT, EGR, DPF
Vehicle 15	diesel	Euro 6d-TEMP	SCR, EGR, DPF
Vehicle 16	diesel	Euro 6c	SCR, EGR, DPF
Vehicle 17	diesel	Euro 6d-TEMP	SCR, EGR, DPF
Vehicle 18	diesel	Euro 6d-TEMP	SCR, EGR, DPF
Vehicle 19	diesel	Euro 6d-TEMP	SCR, EGR, DPF
Vehicle 20	diesel	Euro 6d-TEMP	SCR, EGR, DPF

**Figure 3:** NO_x and PN emissions vs. average vehicle speed of the urban/rural/motorway part of the PEMS tests.

NO_x outliers observed are gasoline vehicle 3 and 5 and diesel vehicle 14. These vehicles have test results that are within the range of other vehicles, but higher values are measured during specific parts of a certain test. For PN, diesel vehicle 17 will be analysed in more detail. 2 tests show PN results at the lowest range, whereas there is one test which shows an urban value at the higher end. Gasoline vehicle 6, a PFI with TWC, shows overall higher PN results for all tests.

Initial cold-start emissions

For both gasoline and diesel vehicles, the catalytic converters need to reach their operational temperature after an engine start. The operation temperature depends on the specific emission control technology. This leads to an initial cold-start peak of emissions. In the next sections, we will investigate the impact of the cold-start for gasoline and diesel vehicles.

Gasoline vehicles

The emissions for most of the RDE tests of the gasoline vehicles are very low, as explained in section 3.1. The main remaining emission event is expected to be the initial cold-start, which, relative to its duration, has an important impact on the emissions of the RDE test. This is certainly true for shorter trips, e.g. the urban part which includes the cold-start. The effect is less visible in the total RDE test result as it is averaged out over around 80-100 km. Once the emission control system is up to temperature, emissions are kept at a very low level, except for some remaining emission events which will be discussed in section 3.3.

In Figure 4, one can see the impact of the cold-start on the complete RDE tests of all the gasoline vehicles used in this study (except the outlier results). The horizontal axis represents the fraction (in distance) of the complete RDE test (if a test is 80 km, 1% = 0.8 km). On the vertical axis, the fraction of the NO_x emissions emitted for the complete RDE test up to the distance on the horizontal axis is shown. If the emissions would be constant per distance over the whole test, a straight line through the origin would occur on the figure, but this is clearly not the case.

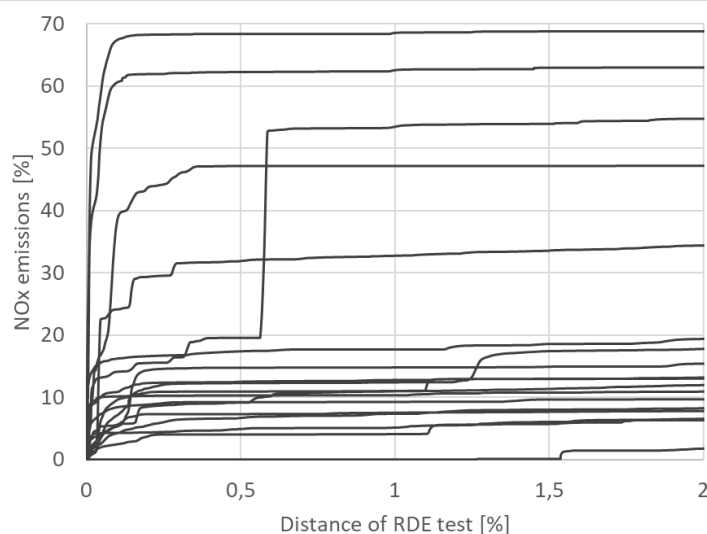


Figure 4: Impact of cold start on NO_x: Fraction of NO_x emissions as a function of the fraction of distance for RDE test of gasoline vehicles.

In the figure, only two percent of the complete distance of the RDE tests is shown. It can be seen that for some gasoline vehicles, more than 60% of all the NO_x emissions are already emitted in less than 0.5% of the distance of the test. This can mean two things: either a lot of NO_x is being emitted during the cold-start of those vehicles or the emission control system of those vehicles works very effectively once it is up to temperature, and very little NO_x is being emitted for the rest of the test. As it was already mentioned in section 3.1 that the emissions of these vehicles are, in general, very low over the complete RDE test, we can conclude that the latter is the dominant effect. Further emission reduction would need to come from the very initial seconds of the tests. For shorter trips, this impact would even be higher and it also means that the reported value in mg/km strongly depends on the minimum trip definition. On the other hand, Figure 4 also shows a majority of the vehicles emits less than 20% of the total emissions during the initial cold-start

phase. This means that the effectiveness of the emission control system still can be improved even once it is up to temperature.

Diesel vehicles

For diesel vehicles, as emissions are drastically reduced compared to pre-RDE vehicles, it is to be expected that the cold-start is also becoming more important. Especially if the emission control system of the diesel vehicles is working properly and the diesel vehicle has overall low emissions, the cold-start can have a significant contribution to the emissions which are still being emitted.

In Figure 5, a similar plot as for the gasoline vehicles (Figure 3) has been made for the tests of the diesel vehicles. The impact of the cold start on the emissions seems less strong compared to the gasoline vehicles. As diesel vehicles rely on a combination of deNO_x technologies, the cold-start effect is less pronounced as for gasoline, which relates to the light-off of the first TWC. But it is still significant for some of the best performing vehicles. The average NO_x emission of these vehicles for the complete RDE tests is 35.3 mg/km so these emissions are already at a low level, comparable to the gasoline vehicles. The same conclusions can be drawn as for the gasoline vehicles: to lower the emissions to extremely low values, the cold start can be further improved and for the vehicles for which the impact of the cold start was relatively limited, the effectiveness of the emission control system should also be further improved.

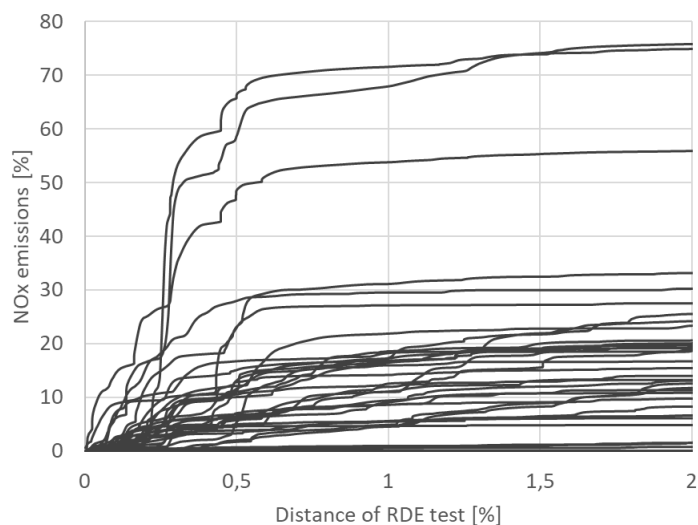


Figure 5: Impact of cold start on NO_x: Fraction of NO_x emissions as a function of the fraction of distance for RDE test of diesel vehicles.

Other emission events

In the next sections, we will look into remaining emission events during some of the RDE tests for both the gasoline and diesel vehicles. We will cover the vehicles that were highlighted in section 3.1 as outliers (vehicle 3, 5, 14 and 17), in addition, vehicles where a clear “event” was seen for a short period during the test despite overall low emission results will also be studied.

It needs to be noted upfront that not enough parameters were available to investigate the root cause for these emission events, but it will be clear that these can significantly impact the reported value of a certain vehicle. More detailed data about ambient conditions, exhaust temperature at different locations, etc. are needed to look into the root cause of these events and how to avoid them.

Gasoline vehicles

For the gasoline vehicles, only 4 of the 22 tests resulted in NO_x emissions that were higher than the lab limit of 60 mg/km. The tests of vehicle 3 and 5 were already mentioned in section 3.1. For vehicle 3, all three tests had higher NO_x emissions (122-267 mg/km for total RDE) and for vehicle 5, there was only 1 test (206 mg/km for total RDE) with high NO_x emissions.

All three tests of vehicle 3 show more or less the same behaviour. High emissions are mainly observed for the motorway part of the test. In Figure 6, the average NO_x emissions in mg/km for every kilometre of one RDE test of vehicle 3 are shown. Dividing the test in smaller trips of 1 km is used to screen for possible emission events instead

of only looking into the overall emission result. It is to be noted that this has a significant effect on the mg/km value for these short sections. On the right axis of the Figure, the average speed for each trip of 1 km can be seen. It is clear that the high NO_x emissions are located in the motorway part of the RDE test. The emissions calculated in this way are much higher on the motorway than for the initial cold-start, which is expected to be the main remaining emission event. A similar behaviour is seen for each test of vehicle 3.

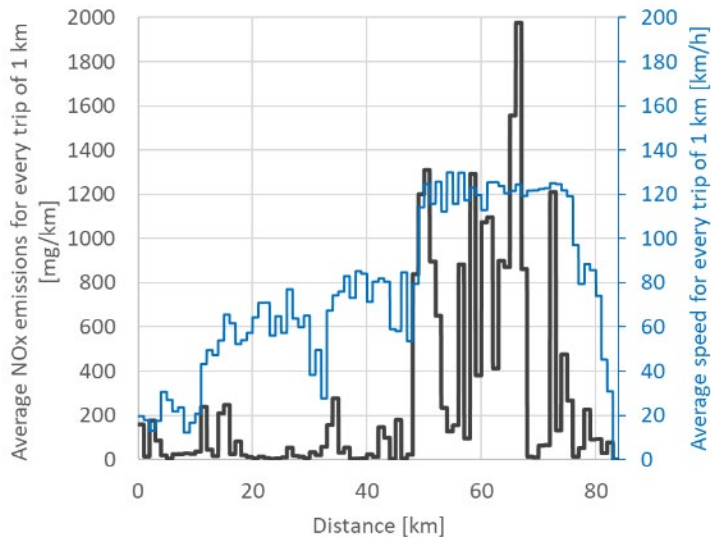


Figure 6: Average NO_x emissions for every trip of 1 km [mg/km] (left axis)
Average speed for every trip of 1 km [km/h] (right axis).

Up to km 45, the NO_x emissions for vehicle 3 are not abnormal. The average NO_x emissions over the three tests up to km 45 is 64.7 mg/km. This is still relatively high compared to the other vehicles, but within the RDE Not to Exceed limit for Euro 6d-TEMP. One of the reasons of the relatively high NO_x emissions in the urban and rural part of vehicle 3 and the very high NO_x emissions in the highway part of vehicle 3 might be that vehicle 3 is a small PFI car with 61 kW of engine power. Because of the limited power of the engine of this vehicle, this means that the load of this engine is always relatively high, combined with higher engine rpm at highway speeds. As CO emissions remained controlled, this could indicate that the total emission control system volume is not able to control the peak engine-out NO_x under these conditions. However, not enough parameters were available from the RDE tests to further examine this.

For vehicle 5, one test has considerably higher NO_x emissions than the other RDE tests. When the cumulative NO_x emissions are plotted as a function of distance for two very similar tests of vehicle 5 in Figure 7, it is very clear that for one test, after km 20 (more or less the beginning of the rural part), there is a sudden jump in NO_x emissions. The rest of that particular test seems to be similar to the other test. No clear hypothesis could be found for this sudden increase in NO_x emissions. Not enough parameters were available from the RDE tests to exactly explain this emission event. But it demonstrates that it is important to further eliminate single emission events as these could drastically impact the local air quality.

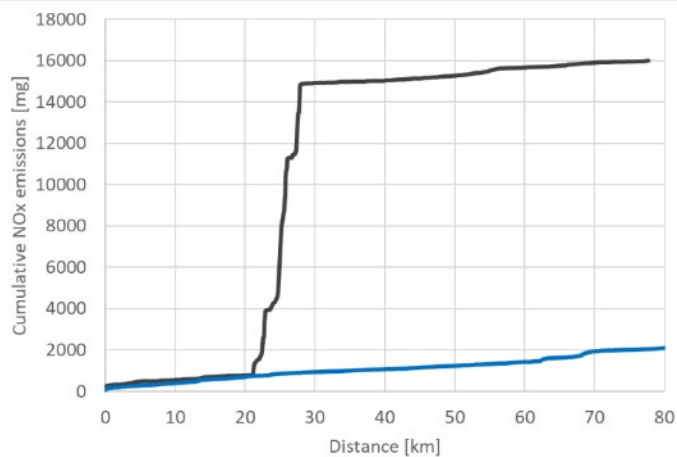


Figure 7: Cumulative NOx emissions of vehicle 5.

Diesel vehicles

For the diesel vehicles, vehicle 14 was mentioned in section 3.1 as an outlier. A closer look at the emission traces of this vehicle show there is a variation between the three tests available. The NOx emissions of the three tests can be seen in Figure 8. Total test results range from 86 up to 421 mg/km. It is clear that every test has completely different NOx emissions but it seems that it cannot only be attributed to a single unexpected emission event in this case. All three tests seem to have a couple of emission events during the test which cause an increase in the cumulative emissions. It is not caused by a continuously higher level of emissions. As a consequence, the initial cold-start is not the main remaining emission event of this vehicle. In different tests, this is occurring at a similar distance, but not to the same extent. It is to be noted that this vehicle relies on EGR and LNT only. The data indicates the emission control system hits some limitations under specific driving conditions. LNT can however well support SCR under urban driving conditions as demonstrated in [7]. Not enough parameters were unfortunately available, e.g. exhaust temperature or NOx emissions at different sampling points, to investigate the cause of this behavior in more detail.

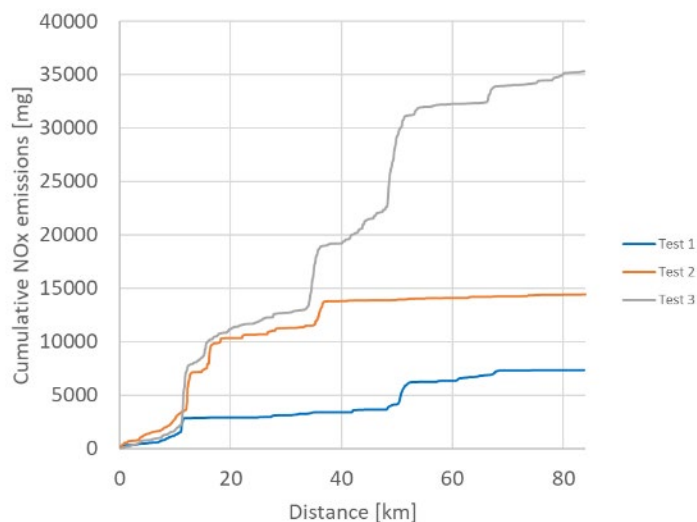


Figure 8: Cumulative NOx emissions of vehicle 14.

For the diesel vehicles, vehicle 18 is another interesting case because one of the three tests has higher NOx (134 mg/km vs. 21–22 mg/km) and PN ($2e11$ #/km vs. $2e8$ – $2e10$ #/km) emissions compared to the other two. For the first test, the high NOx emissions are due to a high emission event in the motorway part. This is clear from Figure 9. In Figure 10, the PN emissions have been plotted where a similar behavior can be seen.

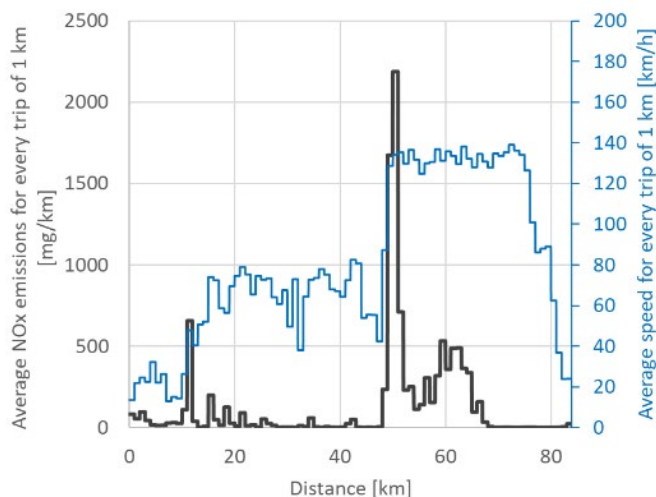


Figure 9: Vehicle 18: Average NO_x emissions for every trip of 1 km [mg/km]
Average speed for every trip of 1 km [km/h].

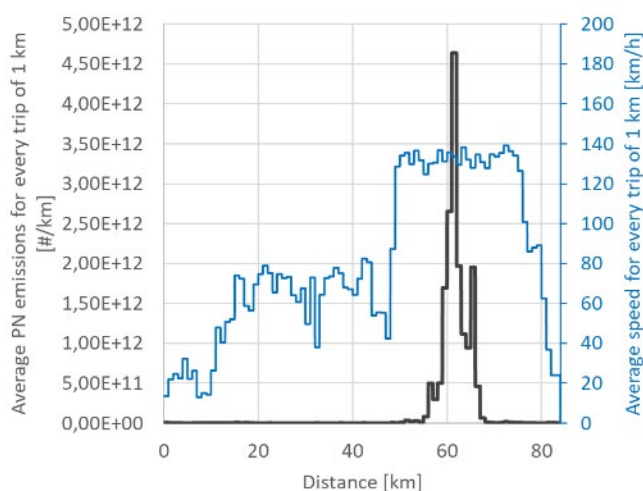


Figure 10: Vehicle 18: Average PN emissions for every trip of 1 km [# /km]
Average speed for every trip of 1 km [km/h].

As can be seen on the two Figures for NO_x and PN, first the NO_x emissions are peaking and after a few kilometres, the PN emissions start to peak as well. As there are few parameters from the engine and emission control system, nothing can be concluded with certainty, but this seems to be linked to a regeneration event of the filter. The increase in NO_x emissions could indicate the start of the DPF regeneration, the increase in PN the end. PN increase towards the end of the regeneration event is due to the complete burn-off of the soot cake layer which actually supports particle filtration. It is to be noted that the emissions (2e11 #/km) also remain within the Euro 6d-TEMP Not to Exceed limit for this particular test. There are some other tests in the database that could indicate DPF regeneration occurred. All the measured emissions remain within the Not to Exceed limit and unfortunately not enough parameters were available from the RDE tests to further investigate these emission events.

Conclusion

RDE regulation ensured that the on-road NO_x and PN emissions of gasoline and diesel vehicles significantly reduced. The data shown in this paper confirmed that Euro 6d-TEMP gasoline and diesel vehicles overall have very low emissions. The purpose of the analysis reported, was to look into remaining emission events and to derive potential insights for Euro 7. It was shown that still some outliers occur for both diesel and gasoline, which are to be tackled by Euro 7. Diesel NO_x emissions tend to be higher in the motorway section, whereas it is technically feasible to have consistent NO_x control with proper system volume and reductant injection strategy. Then it was shown that the initial cold-start becomes increasingly important when the overall emissions are reduced to Euro 6d-TEMP levels. Other outlier results can be linked to certain limitations of implemented emission control systems (no filter, no SCR) or certain emission events that only occur time to time (DPF regeneration). In summary, effective legislation must ensure that

the remaining emission peaks are properly controlled by designing the testing protocol to apply appropriate averaging of emissions over the emissions test, or part of it. Important aspects to consider for appropriate averaging are, for example, separate evaluation for specific driving conditions (especially urban) on top of the total test average and definition of the minimum evaluation distance. The effect of the initial cold-start on report value in mg/km and #/km needs to be considered. But challenging conditions should not be overcompensated by the rest of the test. The available dataset demonstrates such emission tests are a good way to judge overall emission performance on a total vehicle approach, but are too limited to investigate the specific root cause of observed emission events.

References

ACEA RDE monitoring database, <https://www.acea.be/publications/article/access-to-euro-6-rde-monitoring-data>

JAMA RDE monitoring database, <http://www.jama-english.jp/europe/publications/rde.html>

B. Giechaskiel; Solid Particle Number Emission Factors of Euro VI Heavy-Duty Vehicles on the Road and in the Laboratory, *Int. J. Environ. Res. Public Health*, 15 (2), 304, 2018

Terms of Reference and rules of procedure for the informal group on Real Driving Emissions (RDE-IWG), Informal document GRPE-78-24, 78th GRPE meeting, 8-11 January 2019

R. Suarez-Bertoa, et al.; On-road emissions of passenger cars beyond the boundary conditions of the real-driving emissions test, *Environmental Research*, Volume 176, 108572, 2019

V. Valverde, et al.; Joint Research Centre 2018 light-duty vehicles emissions testing, JRC report 117625, 2019

J. Demuyne, et al.; Integrated Diesel System Achieving Ultra-Low Urban and Motorway NO_x Emissions on the Road, 40th Vienna Motor Symposium, 2019

2.8 Validation of low cost sensors for gases and particulate matter in the city centre of Wuppertal, Germany

R. Kurtenbach¹, K. Ulianova², R. G. Gibilisco³, G. Villena¹ and P. Wiesen¹

¹Institute for Atmospheric and Environmental Research, University of Wuppertal, D-42097 Wuppertal, Germany

²National Aviation University, Lubomir Guzar Ave. 1, 03058 Kyiv, Ukraine

³Institut de Combustion, Aérothermique, Réactivité et Environnement (ICARE), CNRS - OSUC, 1C Avenue de la Recherche Scientifique, 45071 Orléans Cedex 2, France

kurtenba@uni-wuppertal.de

Abstract

Novel low-cost sensors could be the solution to the limitations we are facing when studying air quality in a city, a region or indoor environments. Novel low-cost sensors, however, could give us the possibility to develop novel monitoring networks to cover a large area of investigations and thus provide answers on the spatial and temporal distribution of key pollutants such as NO_x and particulate matter in a city.

In the present study, three commercially available low-cost sensor systems, one sensor system from the company *Oizom*, *Polludrone model*, two sensor systems from the company *Smart Sense*, *AirQ model* and six sensor systems from the company *AQMesh*, *AQmesh model* were tested and validated at the monitoring stations “Loher Kreuz” and “Gathe” of the national network and at five traffic hot spots in the city centre of Wuppertal from November 2019 to February 2021.

The sensor systems were equipped with electrochemical sensors from *alphasense* to measure NO, NO₂, O₃, depending on the sensor system also with a NDIR module to measure CO₂ and also with an optical particle counter (OPC) to measure particulate matter (PM_{2.5} and PM₁₀). Besides, they measure weather parameters (radiation, temperature, pressure and relative humidity).

The sensor systems were all calibrated (pre-scaled) before delivery by the companies. The pre-scaled data from the sensor system showed mostly the same time variation, e. g. NO and NO₂ peaks corresponding to the rush hours in the city can be clearly observed, but different mixing ratios in comparison with the reference data.

For the correction of pre-scaled data correlation plots between a reference system (RS) and the sensor system were made. Mostly a good linear correlation for the gaseous compounds NO, NO₂, O₃, and CO₂ were found. Exceptions were a) some NO sensors showed an offset effect that could be corrected by a rebasing of the sensor and b) PM data, because of the humidity effect, which could also be partly corrected by applying an approach based on the Köhler's theory.

Even though the linear correlation of the sensors were good they need to be rescaled by a scaling function. Taken into account the obtained scaling function (slope and intercept) pre-scaled data can be scaled very well to the reference data.

After the validation at the reference station Loher Kreuz four AQMesh units were moved to different traffic hot spots in Wuppertal where they were compared with NO₂ passive samplers. After one month of operation the monthly average NO₂ values obtained from the sensor systems showed a very good agreement with the NO₂ data obtained with passive samplers.

Two AQMesh units were also relocated to the monitoring station “Gathe” and the obtained scaled NO and NO₂ shows a very good agreement with the reference data.

The study shows that the tested sensor systems can be used for monitoring online NO, NO₂, O₃, CO₂ and PM emission in a city centre, e. g. traffic hot spots.

Due to the small-size and weight, these sensor systems provide the opportunity for more flexible measurements, e. g. mobile measurements and they could be installed at locations, which are currently difficult to access with standard devices.

Introduction

Despite a significant improvement of air quality observed in many European countries over the last decades, it still continues to have a significant impact on people's health, particularly in urban areas (EEA, 2020). Ambient air pollution is one of the main global health risks, causing significant excess mortality and loss of life expectancy (Lelieveld et al., 2020). The World Health Organization reported that in 2016, 4.2 million premature deaths worldwide could be attributed to outdoor air pollution (WHO, 2018). The classical view of urban air pollution monitoring is based on well-established and expensive reference methods installed in scarce and static monitoring stations. Wider geographical networks of passive diffusion samplers can alleviate restrictions on spatial coverage. However, this technique provides limited temporal information (Masey et al., 2018). The use of low-cost sensors (LCS) as a complementary tool for air quality monitoring could give us high spatial density and temporal resolution relevant for city scale measurements and more information related to air pollution exposure of the population. This potential is, however, associated with challenges, such as cross-sensitivity to other pollutants, the impact of environmental influences that require significant evaluation and calibration of the sensors to ensure data quality (Lewis and Edwards, 2016; Lewis et al., 2016).

Depending on the pollutant (gas or particle) there are several technologies available used with LCS. Gas pollutants can be detected using either metal oxide semiconductors (MOS), electrochemical sensors (EC), non-dispersive infrared (NDIR), or photo-ionization detectors (PID). Electrochemical sensors (EC) are the most widely used low-cost approaches for gaseous pollutant. Electrochemical sensors (EC) rely on oxidation-reduction reactions with the target gas generating an electrical signal which is proportional to the gas concentration (Masson et al., 2015). On the other hand, particulate matter (PM) is measured by light scattering or absorption, using algorithms to relate the attenuated signal to the particle size and/or particle mass (Castell et al., 2017). The most common low-cost PM sensors are based on the light scattering method where a light source illuminates the particles, and then the scattered light from particles is measured by a photometer (Rai et al., 2017 and references therein).

The European Union Air Quality Directive indicates that uncertainty should be the main indicator for the evaluation of the data quality objective of air pollution measurement methods (Directive 2008/50/EC). However, the evaluation of this metric is not included in most low-cost sensor systems studies (Karagulian, 2019). The most common metric informed either in field, laboratory or indoor intercomparisons against reference data is the coefficient of determination (R^2), which can be interpreted as an indicator of how well measurements obtained by means of a tested sensor fit with those obtained from the corresponding "reference" instrument. During the last ten years several intercomparisons have been carried out for gases and particulate matter, in the laboratory (Wang et al., 2015; Manikonda et al., 2016), in the field (Holstius et al., 2014; Borrego et al., 2016; Karagulian et al. 2019, Borghi et al., 2018; Malings et al., 2019; Collier-Oxandale et al., 2020), and also in indoor environments. (Kaliszewski et al., 2020; Demanega et al., 2021).

In the present study, three commercially available low-cost sensor systems were tested and validated at different locations in the city centre of Wuppertal from November 2019 to February 2021. One sensor system from the company *Oizom*, *Polludrone model*, (Oziom, 2021) named "A", two sensor system from the company *SmartSense*, *AirQ model* (SmartSense, 2021) named "B", and six sensor systems from the company *AQMesh*, *AQMesh model* (AQMesh, 2021) named "C".

Description of the experimental procedure

Measurement sites

The validation campaign was carried out in the city centre of Wuppertal, Germany at the monitoring stations "Loher Kreuz" and "Gathe" of the national network and at five traffic hot spots in city district Elberfeld, see figure 1 and 2. At the monitoring station "Loher Kreuz" all three sensor systems A, B and C were installed close to the sample point of the reference system RS.

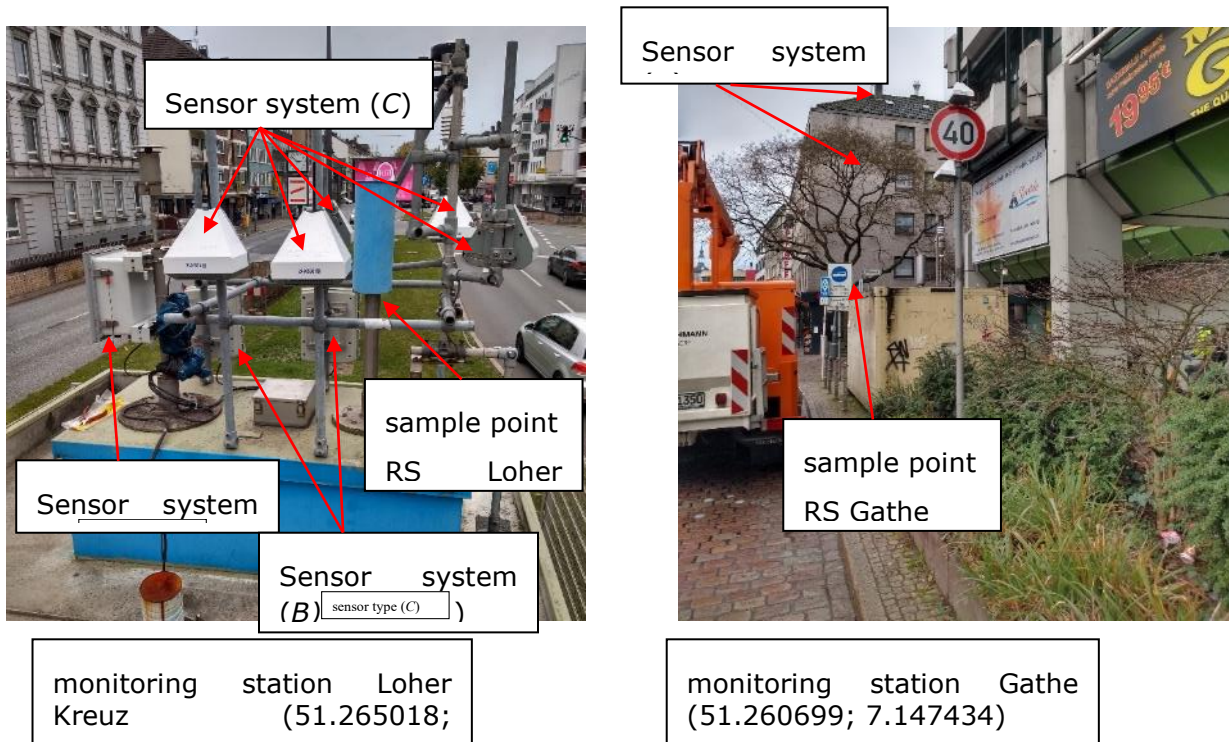


Figure 1: Monitoring stations close to main roads in Wuppertal: “Loher Kreuz” with all three sensor system (A, B and C) and Gathe with two sensor systems (C).

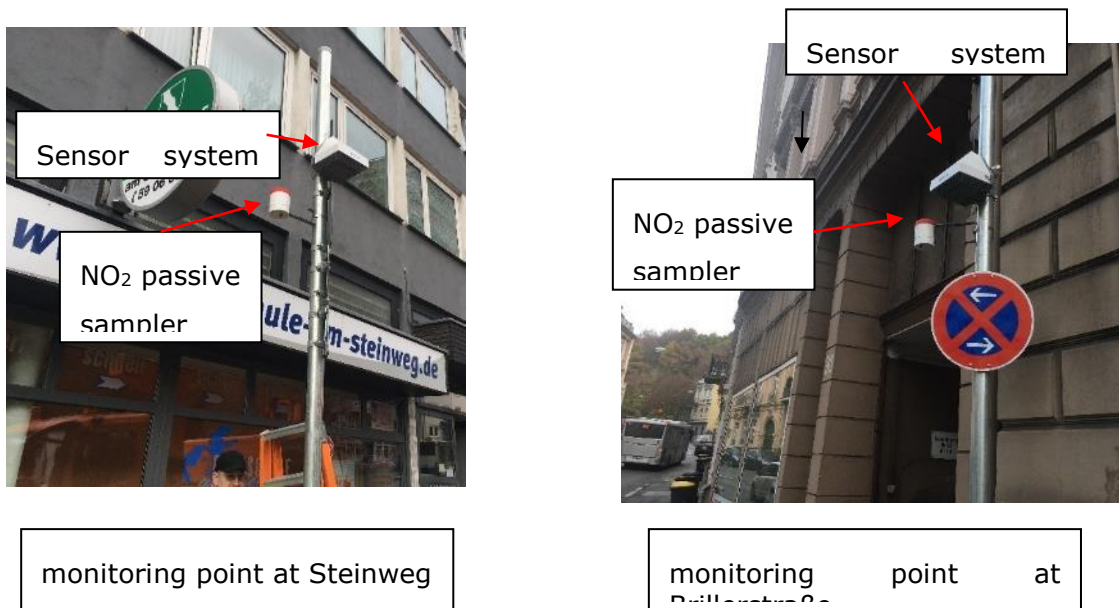


Figure 2: Two of the five traffic hot spots in Wuppertal: Steinweg and Brillerstraße; each equipped with one sensor system (C) and one NO₂ passive sampler.

Analytical Equipment

Reference equipment

The following reference systems (RS) were used at the roadside monitoring stations Loher Kreuz (a, b, c and d) and Gathe (a):

- a) Nitrogen monoxide (NO) and nitrogen dioxide (NO₂) were measured on-line with a commercial NO_x chemiluminescence analyzer (Environnemental, AC 31M / 32M with molybdenum converter). The time resolution was 10 s and the detection limit, which was calculated from the variation of the zero signal was 2 ppbV for NO and 3 ppbV for NO₂. The NO channel of instrument was directly calibrated by diluted standard NO calibration mixtures (Messer, stated accuracy 5 %). The NO₂ channel was calibrated by using a NO titration unit (Environnemental, GPT). NO₂ was produced by the reaction of NO with O₃ in a flow reactor leading to the quantitative conversion of the calibrated NO ($\Delta\text{NO} = \Delta\text{NO}_2$).
- b) Ozone (O₃) was measured on-line with a commercial O₃ monitor (Environnemental, O₃ 41M with UV absorption). The time resolution was 10 s and the detection limit, which was calculated from the variation of zero measurements, was 1 ppbV. O₃ was calibrated by using an O₃ calibration unit (Environnemental, K-O₃, accuracy 10 %). O₃ was produced by the photolysis of synthetic air in a flow reactor leading to the formation of O₃.
- c) Carbon dioxide (CO₂) was measured on-line with a commercial CO₂ monitor (Carbondio-1000 with IR absorption). The time resolution was 1 s and the detection limit, which was calculated from the variation of zero measurements, was 2 ppmV. CO₂ was directly calibrated by diluted standard CO₂ calibration mixtures (Messer, stated accuracy 2 %).
- d) Particulate matter was measured by an Optical Particle Counter (OPC) (Grimm Aerosol Technik GmbH, DustMonitor EDM 107). The OPC counts particles in a size range from 0.25-32 μm in 31 size-channels. The time resolution was 6 s and the detection limit 1 particle L⁻¹.
- e) In addition, NO₂ was measured off-line at all five traffic hot spots with commercial NO₂ passive samplers (Passam AG; Palmes-type DIN EN 16339). The time resolution was one month and the detection limit was 2 ppbV.

Sensor systems

The following sensor systems were tested:

- a) Sensor system A with micro sensors, which measure the concentrations of NO, NO₂, and O₃ using electrochemical sensors from *alphasense* (Alphasense, 2021). CO₂ is measured using a NDIR module and particulate matter (PM_{2.5} and PM₁₀) is measured with an OPC. Besides, it measures weather parameters (radiation, temperature, pressure and relative humidity). Electrical power supply: Mains operation 240 V AC. The detection limits as informed by the company was 20 ppbV for NO, NO₂ and O₃, 20 ppmV for CO₂ and 0.3 $\mu\text{g}/\text{m}^3$ for particulate matter.
- b) Sensor system "B" with micro sensors, which measure the concentrations of NO, NO₂, and O₃ using electrochemical sensors from *alphasense* (Alphasense, 2021). and particulate matter (PM_{2.5} and PM₁₀) is measured with an OPC. Besides, it measures weather parameters (temperature, relative humidity and pressure). Electrical power supply: Mains operation 240 V AC. The detection limit as informed by the company was 1 ppbV for NO, NO₂ and O₃ and 1 $\mu\text{g}/\text{m}^3$ for particulate matter.
- c) Sensor system "C" with micro sensors, which measure the concentrations of NO, NO₂, and O₃ using electrochemical sensors from *alphasense* (Alphasense, 2021). and CO₂ is measured using a NDIR module. Besides, it measures weather parameters (temperature, relative humidity and pressure). Electrical power supply: Internal Lithium battery pack 3.6 V DC. The detection limit as informed by the company was 1 ppbV for NO, NO₂ and O₃ and 1 ppmV for CO₂.

Results and Discussion

In the present study, data processing and validation was performed for all three sensor system units. However, for clarity, only a few examples were selected to show the data analysis of each pollutant measured during this study in a number of selected figures.

Particulate matter comparison

Optical sensors measure light scattering converted by computation to mass concentrations. Light scattering is expected to be strongly affected by parameters such as particle density, particle hygroscopicity, refractive index, and particle composition. All of these factors vary from site to site and with seasonality.

The relationship of the mass concentrations measured by the OPCs used in this study, relative to the reference instrument was plotted as a function of relative humidity (r.h.). A quasi-exponential increase was found when the humidity was above $\geq 85\%$ r.h. This finding suggests a behaviour similar to hygroscopic particle growth curves (Pöschl, 2005). As a result, we applied Köhler's theory (Petters and Kreidenweis, 2007), which describes the relationship between particle hygroscopicity and volume by a single hygroscopicity parameter, Köhler's K . This approach can be adapted to relate particle mass to hygroscopicity at a given relative humidity. In this study, following the assumptions given by Crilley, et al. (2018), a correction factor was derived to consider the hygroscopic particle growth effect. An example of this effect is shown in Fig. 3. A large overestimation of the readings of sensor system A with respect to the measurements of the reference monitor was observed, when the relative humidity exceeds a value of 85% (Fig. 3, A uncorrected). Hence, when the relative humidity was higher than 85%, shown by the dashed line in Fig. 3, the correction factor considering the hygroscopic growth of the particles was applied. As a result of this correction the values between sensor system A and the reference monitor showed much better agreement. (Fig. 3, A corrected).

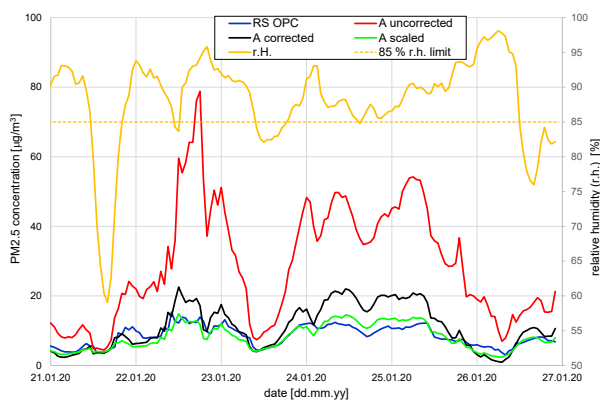


Figure 3: Diurnal variation of the PM_{2.5} concentration, uncorrected, corrected and scaled data from sensor system A in comparison with the reference and relative humidity data at the monitoring station “Loher Kreuz” in January 2020.

For the scaling of the corrected data to the reference data correlation plots were made. Figure 4 shows as an example the correlation of the PM_{2.5} values, Reference System (RS) vs sensor system A. Sensor system A shows a low correlation (uncorrected data) to the RS and a good linear correlation ($R^2 = 0.84$) between sensor A (corrected data) and RS when the humidity correction factors were applied. From the linear regression the following scaling function for the corrected concentration $X_{PM_{2.5}}^{corrected} [\mu g/m^3]$ were calculated. Figure 3 shows also, that the scaling function scaled the data (A scaled) very well to the reference data.

$$A: X_{PM_{2.5}}^{scaled} [\mu g/m^3] = (0.58 \pm 0.01) \cdot X_{PM_{2.5}}^{corrected} [\mu g/m^3] + (1.8 \pm 0.2) [\mu g/m^3], R^2 = 0.84$$

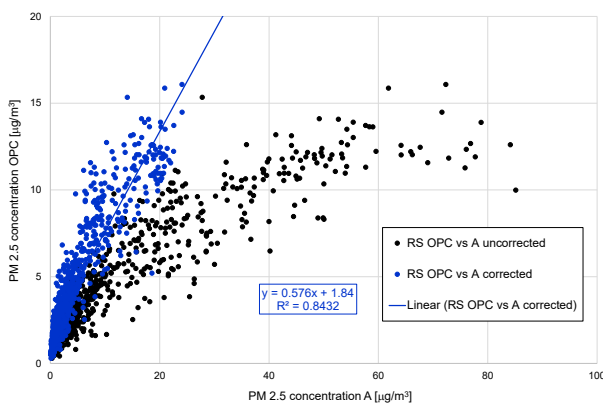


Figure 4: Correlation of the PM_{2.5} values, Reference System (RS) vs sensor system A.

Gas compound comparison

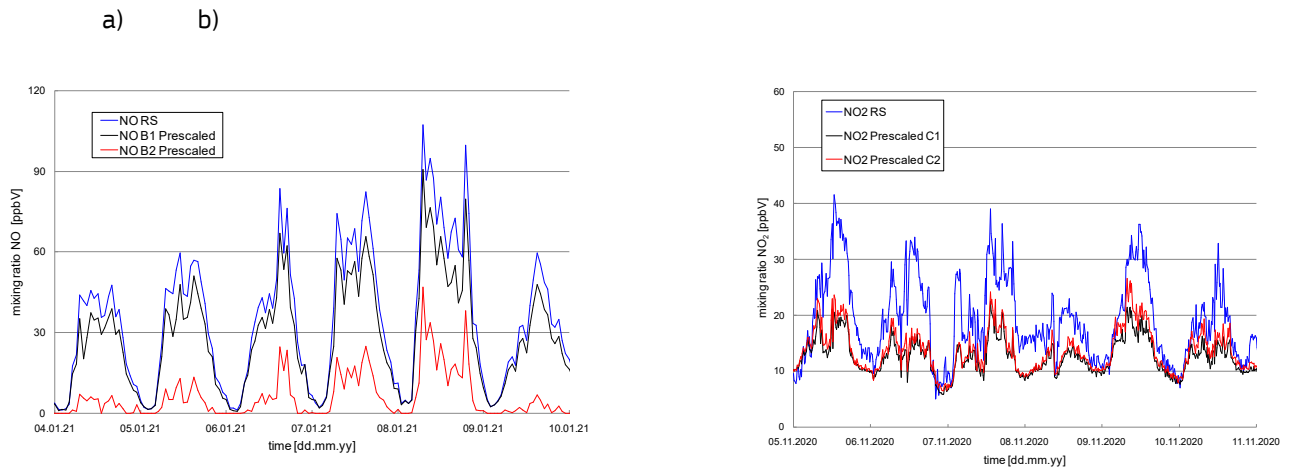


Figure 5: a) Diurnal variation of the NO mixing ratio, pre-scaled data from sensor systems B1 and B2 in comparison with the reference data at the monitoring station “Loher Kreuz” in January 2021. b) Diurnal variation of the NO₂ mixing ratio, pre-scaled data from sensor systems C1 and C2 in comparison with the reference data at the monitoring station “Loher Kreuz” in November 2020.

All three sensor systems were calibrated (pre-scaled) before delivery by the companies. Figure 5a shows as an example the diurnal variation of the NO mixing ratio, pre-scaled data from sensor system B1 and B2 in comparison with the reference data (RS) at the monitoring station “Loher Kreuz” in January 2021. The pre-scaled data from the sensor systems B1 and B2 show the same time variation, but different mixing ratios in comparison with the reference data. Figure 5b shows as an example the diurnal variation of the NO₂ mixing ratio, pre-scaled data from sensor systems C1 and C2 in comparison with the reference data (RS) at the monitoring station “Loher Kreuz” in November 2020. The pre-scaled data from the sensor systems C1 and C2 showed the same time variation, but different mixing ratios in comparison with the reference data.

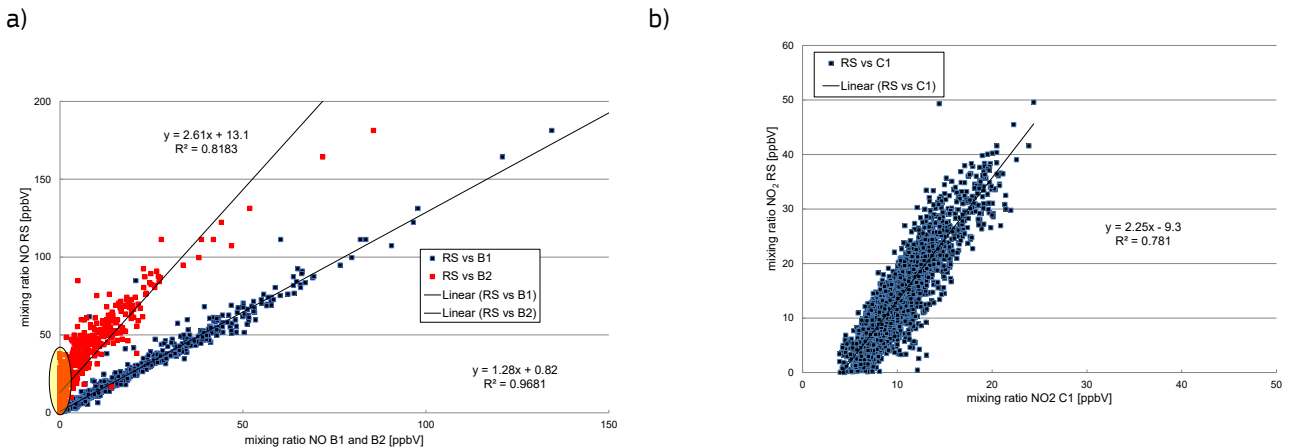


Figure 6: a) Correlation of the NO values, Reference System (RS) vs sensor systems B1 and B2. b) Correlation of the NO₂ values, Reference System (RS) vs sensor system C1.

Figure 6a shows as an example the correlation of the NO values, Reference System (RS) vs sensor systems B1 and B2. The sensor system B1 shows in comparison to B2 a very good correlation with the reference system. Sensor system B2 shows an offset (mark yellow in figure 6a) and, therefore, NO values below 13 ppbV could not be detected (see figure 7a). From the linear regression in figure 6a the following scaling functions for the B1 and B2 data $X_{NO}^{prescaled}$ [ppbV] were derived:

$$B1: X_{NO}^{scaled} [ppbV] = (1.28 \pm 0.01) \cdot X_{NO}^{prescaled} [ppbV] + (0.8 \pm 0.2) [ppbV], R^2 = 0.968$$

$$B2: X_{NO}^{scaled} [ppbV] = (2.61 \pm 0.04) \cdot X_{NO}^{prescaled} [ppbV] + (13.1 \pm 0.4) [ppbV], R^2 = 0.818.$$

Figure 6b shows as an example the correlation of the NO₂ data, Reference System (RS) vs sensor system C1. The sensor system C1 shows a good correlation to the reference system and the same correlation was found for sensor system C2. From the linear regression the following scaling functions for the C1 and C2 data $X_{NO_2}^{prescaled}$ [ppbV] were derived:

$$C1: X_{NO_2}^{scaled}[ppbV] = (2.25 \pm 0.02) \cdot X_{NO_2}^{prescaled}[ppbV] - (9.3 \pm 0.2)[ppbV], R^2=0.78$$

$$C2: X_{NO_2}^{scaled}[ppbV] = (2.00 \pm 0.02) \cdot X_{NO_2}^{prescaled}[ppbV] - (7.8 \pm 0.2)[ppbV], R^2 = 0.79.$$

From the scaling function scaled values for NO and NO₂ were calculated. In figure 7a the scaled NO values for sensor systems B1 and B2 are shown in comparison with the reference data. It can be recognised, that the scaling function for the sensor system B1 scaled the data very well to the reference data. However, for sensor system B2 it not possible to correct the data for mixing ratios < 13 ppbV, because of the offset mentioned above. This offset was also observed for two units of the sensor systems C. For sensor system C so called “rebasing” procedure by the company was possible. After this procedure the NO data correlated much better with the reference data and useful scaling functions were derived.

In figure 7b the scaled NO₂ values for sensor systems C1 and C2 are shown in comparison with the reference data. It can be observed, that the scaling function for both sensor systems scaled the data very well to the reference data.

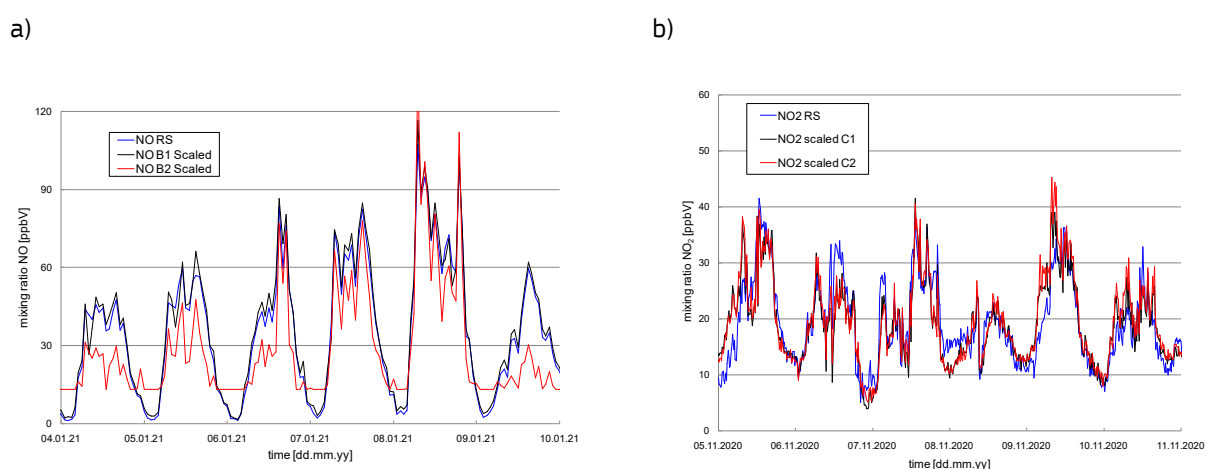


Figure 7: a) Diurnal variation of the NO mixing ratio, scaled data from sensor system B1 and B2 in comparison with the reference data at the monitoring station “Loher Kreuz” in January 2021.
b) Diurnal variation of the NO₂ mixing ratio, scaled data from sensor system C1 and C2 in comparison with the reference data at the monitoring station “Loher Kreuz” in November 2020.

In figure 8 the scaled NO₂ data for two different sensor systems B2 and C4 are shown in comparison with the reference data. The scaling function for sensor system B2 does not scaled the data well to the reference data in comparison to the sensor system C4. The difference between both sensor systems may be explained in terms of an aging effect. The sensor B could be less sensitive because it was running already for more than two years compared to system C4 that has been running only for the duration of this intercomparison study.

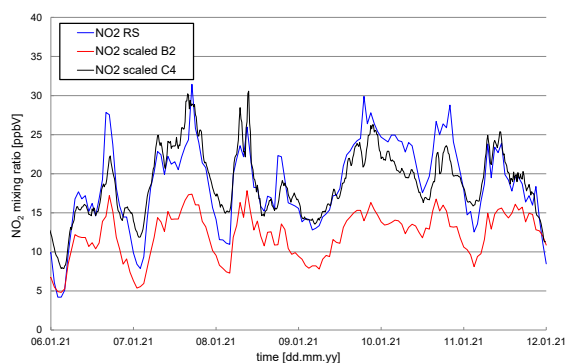


Figure 8: Diurnal variation of the NO₂ mixing ratio, scaled data from sensor system B2 and C4 in comparison with the reference data at the monitoring station “Loher Kreuz” in January 2021.

As an example the following scaling functions for all sensors of system C were derived. The comparison exhibited for all compounds a good linear correlation:

$$\text{NO: } X_{\text{NO}}^{\text{scaled}} [\text{ppbV}] = (1.39 \text{ to } 1.44) \cdot X_{\text{NO}}^{\text{prescaled}} [\text{ppbV}] + (-7.9 \text{ to } 2.3) [\text{ppbV}], R^2 \geq 0.90$$

$$\text{NO}_2: X_{\text{NO}_2}^{\text{scaled}} [\text{ppbV}] = (1.62 \text{ to } 2.25) \cdot X_{\text{NO}_2}^{\text{prescaled}} [\text{ppbV}] + (-9.3 \text{ to } -4.8) [\text{ppbV}]; R^2 \geq 0.78$$

$$\text{O}_3: X_{\text{O}_3}^{\text{scaled}} [\text{ppbV}] = (0.67 \text{ to } 0.85) \cdot X_{\text{O}_3}^{\text{prescaled}} [\text{ppbV}] + (0.3 \text{ to } 11.0) [\text{ppbV}], R^2 \geq 0.80$$

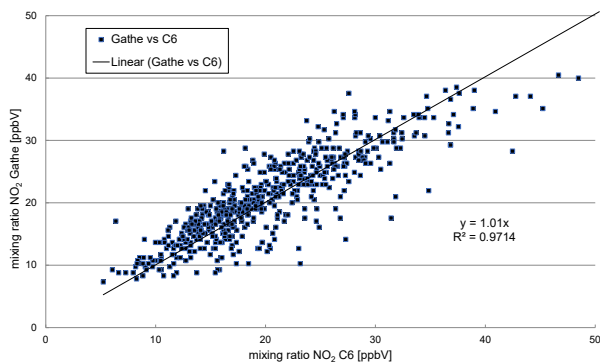
$$\text{CO}_2: X_{\text{CO}_2}^{\text{scaled}} [\text{ppmV}] = (1.06 \text{ to } 1.45) \cdot X_{\text{CO}_2}^{\text{prescaled}} [\text{ppmV}] + (-5 \text{ to } -125) [\text{ppmV}], R^2 \geq 0.81.$$

After the validation at the reference station Loher Kreuz four AQMesh units (C1, C2, C3 and C4) were shifted to four traffic hot spots in Wuppertal. After one month operation the monthly average NO₂ values obtained from the sensor systems were compared with NO₂ passive sampler measurements.

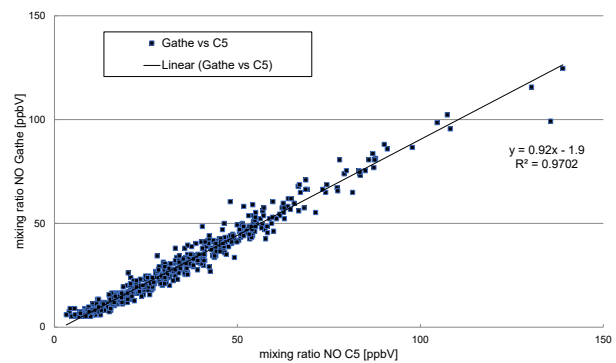
Table 1 shows the monthly average NO₂ values at the traffic hot spots measured with the sensor systems C (pre-scaled and scaled) in comparison with the result of the NO₂ passive sampler for time period 28.11.20 to 03.01.21.

Table 1: Monthly average NO₂ values at the traffic hot spots measured with the sensor systems C (pre-scaled and scaled) in comparison with the passive sampler for time period 28.11.20 to 03.01.21.

Measurement location	NO ₂ passive sampler [µg/m ³]	Sensor system C (pre-scaled) [µg/m ³]	Sensor system	Sensor system C (scaled) [µg/m ³]
Brillerstraße 28	35	24	C4	35 ± 4
Steinweg 25	33	25	C1	38 ± 4
Westkotterstraße 111	32	25	C2	35 ± 4
Haeselerstraße 94	27	23	C3	25 ± 3
LoherKreuz	28	22	C5	29 ± 3
LoherKreuz	28	24	C6	29 ± 3



a)



b)

Figure 9: a) Comparison of NO values, reference system Gathe vs C4, b) Comparison of NO₂ values, reference system Gathe vs C6.

Figure 9a shows as an example the comparison of the NO data from the monitoring station Gathe vs sensor system C5. A very good correlation was observed for system C5 and also for C6 (not shown) and from the linear regression correlation functions for the NO data $X_{NO}^{C5}[ppbV]$ and $X_{NO}^{C6}[ppbV]$ were derived:

$$X_{NO}^{Gathe}[ppbV] = (0.92 \pm 0.01) \cdot X_{NO}^{C5}[ppbV] - (1.9 \pm 0.3)[ppbV], R^2 = 0.97$$

$$X_{NO}^{Gathe}[ppbV] = (0.93 \pm 0.01) \cdot X_{NO}^{C6}[ppbV] - (0.5 \pm 0.3)[ppbV], R^2 = 0.95.$$

Within the standard deviation of 1 sigma the scaled NO₂ data from all sensor systems C were in a very good agreement with the data from the NO₂ passive samplers.

In order to re-check the sensor systems C5 and C6 they were moved from the reference station Loher Kreuz to the national network monitoring station "Gathe" for comparison of the NO and NO₂ data.

Figure 9b shows as an example the comparison of the NO₂ data from the monitoring station Gathe vs sensor system C6. A good correlation was observed for system C6 and also for C5 (not shown) and from the linear regression correlation functions for the NO₂ data $X_{NO_2}^{C6}[ppbV]$ were calculated:

$$X_{NO_2}^{Gathe}[ppbV] = (0.95 \pm 0.01) \cdot X_{NO_2}^{C5}[ppbV], R^2 = 0.96$$

$$X_{NO_2}^{Gathe}[ppbV] = (1.01 \pm 0.01) \cdot X_{NO_2}^{C6}[ppbV], R^2 = 0.97.$$

Within the standard deviation of 1 sigma the scaled NO and NO₂ values from the sensor systems C4 and C6 are in a very good agreement with the values from the monitoring station Gathe.

Summary and Conclusion

The validation of the sensor systems showed for most of them a linear correlation ($R^2 \geq 0.78$) between the pre-scaled and reference data.

Exceptions were

- a) some NO sensors showed an offset that could be corrected by a rebasing of the sensor,
- b) PM data, because of the humidity effect, which can also be partly corrected by applying an approach based on the Köhler theory.

Even though the linear correlation of the sensors were good they need to be re-scaled by individual scaling functions. Taken into account the obtained scaling functions (slope and intercept) pre-scaled data can be scaled very well to the reference data.

The scaled NO₂ data obtained at the traffic hot spots showed a very good agreement with the data of the NO₂ passive samplers.

Scaled NO and NO₂ data obtained at the traffic hot spot Gathe showed also a very good agreement with data of the network monitoring station Gathe.

The study shows that the tested sensor systems can be used to monitor online NO, NO₂, O₃, CO₂ and PM emission in the city centre, e. g. traffic hot spots.

Due to the small-size and weight, these sensor systems provides the opportunity for more flexible measurements, e. g. mobile measurements and they could be installed at locations, which are currently difficult to access with standard devices. However, long-term studies to analysing sensor aging, the effect of seasonality and other climatic factors that could influence the measurements over time will be necessary to further characterise the reliability of this technology.

Acknowledgement

R. Gibilisco acknowledges the Alexander von Humboldt foundation for providing a Georg Forster postdoctoral fellowship. The authors acknowledge financial support from the European grant EUROCHAMP-2020 and the Deutsche Forschungsgemeinschaft (DFG). K. Ulianova acknowledges Deutsche Bundesstiftung Umwelt for providing a DBU MOE scholarship.

References

Alphasense, 2021, <https://www.alphasense.com/>

AQMesh, 2021, <https://www.aqmesh.com/>

Borghgi, F., Spinazzè, A., Rovelli, S., Campagnolo, D., Del Buono, L., Cattaneo, A., & Cavallo, D. M. (2017). Miniaturized monitors for assessment of exposure to air pollutants: A review. *International journal of environmental research and public health*, 14(8), 909.

Borrego, C., Costa, A.M., Ginja, J., Amorim, M., Coutinho, M., Karatzas, K., Sioumis, Th., et al. (2016). Assessment of fair quality microsensors versus reference methods: The EuNetAir joint exercise, *Atmospheric Environment*, 147, 246-263.

Castell, N., Dauge, F. R., Schneider, P., Vogt, M., Lerner, U., Fishbain, B., Bartonova, A. (2017). Can commercial low-cost sensor platforms contribute to air quality monitoring and exposure estimates? *Environment international*, 99, 293-302.

Collier-Oxandale, A., Feenstra, B., Papapostolou, V., Zhang, H., Kuang, M., Der Boghossian, B., Polidori, A. (2020). Field and laboratory performance evaluations of 28 gas-phase air quality sensors by the AQ-SPEC program, *Atmospheric Environment*, 220, 117092.

Crilley, L. R., Shaw, M., Pound, R., Kramer, L. J., Price, R., Young, S., ... & Pope, F. D. (2018). Evaluation of a low-cost optical particle counter (Alphasense OPC-N2) for ambient air monitoring. *Atmospheric Measurement Techniques*, 11(2), 709-720.

Demanege, I., Mujan, I., Singer, B., Andelkovic, A.S., Babich, F., Licina, D. (2021). Performance assessment of low-cost environmental monitors and single sensors under variable indoor air quality and thermal conditions, *Building and Environment*, 187, 107415.

Directive 2008/50/EC of the European Parliament and of the Council of 21 May 2008 on ambient air quality and cleaner air for Europe.

EEA (European Environment Agency, 2020. Air Quality in Europe — 2020 Report, ISBN 978-92-9480-292-7. <https://doi:10.2800/786656>.

Holstius, D. M., Pillarisetti, A., Smith, K. R., & Seto, E. J. A. M. T. (2014). Field calibrations of a low-cost aerosol sensor at a regulatory monitoring site in California. *Atmospheric Measurement Techniques*, 7(4), 1121-1131.

Kaliszewski, M., Wlodarski, M., Mlynczak, J., Kopczynski, K., Comparison of low-cost particulate matter sensors for indoor air monitoring during COVID-19 lockdown (2020). *Sensors*, 20, 7290; doi:10.3390/s20247290.

Karagulian, F., Barbiere, M., Kotsev, A., Spinelle, L., Gerboles, M., Lagler, F., ... & Borowiak, A. (2019). Review of the performance of low-cost sensors for air quality monitoring. *Atmosphere*, 10(9), 506.

Lelieveld, J., Pozzer, A., Pöschl, U., Fnais, M., Haines, A., and Münzel, Th. (2020). Loss of life expectancy from air pollution compared to other risk factors: a worldwide perspective, *Cardiovascular Research*, 116, 1910-1917.

Lewis, A., Edwards, P., Validate personal air-pollution sensors, *Nature* 535 (2016), 29-31, <https://doi.org/10.1038/535029a>.

Lewis, A.C., Lee, J.D., Edwards, P.M., Shaw, M.D., Evans, M.J., Moller, S.J., Smith, K.R., Buckley, J. W., Ellis, M., Gillot, S.R., White, A., Evaluating the performance of low cost chemical sensors for air pollution research, *Faraday Discuss.* 189 (2016) 85-103, <https://doi.org/10.1039/C5FD00201J>.

Malings, C., Tanzer, R., Haurlyuk, A., Saha, P., Robinson, A., Presto, A., Subramanian, R. (2020). Fine particle mass monitoring with low-cost sensors: Corrections and long-term performance evaluation, *Aerosol Science and Technology*, 54, 2, 160-174.

Manikonda, A., Zikova, N., Hopke, Ph., Ferro, A. (2016). Laboratory assessment of low-cost PM monitors, *Journal of Aerosol Science*, 102, 29-40.

Masey, N., Gillespie, J., Ezani, E., Lin, C., Wu, H., Ferguson, N., Hamilton, S., Heal, M., Beverland, I., Temporal changes in field calibration relationships for Aeroqual S500 O₃ and NO₂ sensor-based monitors (2018). *Sensors & Actuators B. Chem.*, 273, 1800-1806.

Masson, N., Piedrahita, R., Hannigan, M. (2015). Quantification Method for Electrolytic Sensors in Long-Term Monitoring of Ambient Air Quality, *Sensors*, 15, 10, 27283-27302.

Oziom, (2021), <https://oizom.com/product/polludrone-air-pollution-monitoring>

Petters, M. D. and Kreidenweis, S. M. (2007). A single parameter representation of hygroscopic growth and cloud condensation nucleus activity, *Atmos. Chem. Phys.*, 7, 1961-1971, <https://doi.org/10.5194/acp-7-1961-2007>, 2007.

Pöschl, U.: Atmospheric aerosols: composition, transformation, climate and health effects (2005). *Angewandte Chemie Int. Ed.*, 44, 7520–7540.

Rai, A. C., Kumar, P., Pilla, F., Skouloudis, A. N., Di Sabatino, S., Ratti, C., & Rickerby, D. (2017). End-user perspective of low-cost sensors for outdoor air pollution monitoring. *Science of the Total Environment*, 607, 691-705.

SmartSense, (2021), http://smart-sense.hr/smart-city#first_page.

Wang, Y., Li, J., Jing, H., Zhang, Q., Jiang, J., Biswas, P. (2015). Laboratory evaluation and calibration of three low-cost particle sensors for particulate matter measurement, *Aerosol Science and Technology*, 49, 1063-1077.

WHO: Ambient (outdoor) air pollution (2018). WHO Fact Sheet, available at: [https://www.who.int/news-room/fact-sheets/detail/ambient-\(outdoor\)-air-quality-and-health](https://www.who.int/news-room/fact-sheets/detail/ambient-(outdoor)-air-quality-and-health) (last access: 08 March 2021).

2.9 Using modelling to improve air quality: The Concawe urban air quality studies

A. Megaritis*, and G. Valastro

Concawe, Environmental Science for European refining, Brussels, Belgium

athanasios.megaritis@concawe.eu

Introduction

Emission reduction measures have resulted in significant improvements in air quality in Europe. However, air quality remains an issue of concern in many urban areas. Road transport has been the primary focus for emission controls through several initiatives by the European Commission (EC) as it is often indicated as one of the main causes where pollutants such as nitrogen dioxide (NO₂) and particulate matter (PM) exceed the Air Quality Limit Values (AQLVs).

Air quality is also a multi-scale and multifactorial phenomenon with a strong spatial variability depending on the pollutant and location type. The attribution of the pollutant concentrations to different source categories should therefore be carefully evaluated when assessing local measures to improve air quality in hotspots to be sure to find the right solutions.

Under this context, air quality models have a significant role to play. Concawe performed two studies to highlight how air quality modelling can be used in supporting air quality assessments and for the development of effective air quality management plans.

The first study [1] aimed to assess whether existing regulations can be effective in reducing air pollutant emissions from road transport and eventually improving compliance over EU in the coming years. Using the results of an earlier Concawe study which determined the actual and expected real driving emissions (RDE) data for multiple classes of Euro 6 vehicles [2], several modelling scenarios were examined to determine the impact that fleet turnover to the latest stage of Euro 6 diesel passenger cars would have on NO₂ and PM compliance during 2020-2030 through EU.

One of the important findings derived from the first study was that the attribution of the pollutant concentrations to different source categories may be significantly variable in space and should carefully be evaluated when looking at local measures to improve air quality in hotspots.

The second Concawe study aimed to give more insights regarding the role of source apportionment in determining the effective solution for improving air quality. Common methodologies for air quality assessment at an EU-wide scale, typically use Chemical Transport Models (CTM) run at roughly, 7 x 7 to 10 x 10 km² grid resolution. The use of such typical coarse grid resolutions may provide reasonable information regarding the contribution of emissions sources to PM concentrations. However, due to the high spatial variability of sources such as traffic-related air pollution and the strong concentration gradients near the roads, these methodologies are inadequate to provide a detailed and robust information on the road-contributions in general. This is more evident to pollutants such as NO₂ where road transport emissions dominate its concentrations. To this end, a web-based EU-wide NO_x/NO₂ source apportionment tool was developed with a unique focus on road transport. The tool uses a high resolution of 125x125 m and provides explicit information on any location over Europe, regarding the contribution of different vehicle categories, the different EURO norms, as well as the different types of fuel used to NO_x emissions and NO₂ concentrations.

An overview of the two studies and the main findings derived are presented in the following Chapters.

Modelling the effectiveness of RDE of Euro 6 Diesel Passenger Cars in improving EU compliance

Methodology

In order to predict how the fleet turnover to the latest Euro 6 diesel passenger cars would impact the concentrations of NO₂ and PM into the future (i.e., 2020-2030) and eventually the compliance with air quality limit values (AQLVs), a modelling approach was taken using the model AQUIReS+ [3]. The model uses a gridded emission inventory and source-receptor relationships [4] that relate a change in emission to a change in concentration. These derive from regional chemical transport models (EMEP [5], CHIMERE [6]) used in air policy studies. The model takes into account the local environment, traffic, and topographical characteristics of each station. Model predictions were compared with the data from the EEA AQ e-Reporting dataset [7] to ensure that the model performs well to reproduce concentrations of pollutants over historic years.

For the purposes of this study, the results of an earlier Concawe study (in collaboration with Ricardo) [2] on Euro 6 diesel passenger cars performance under RDE conditions were used as input into the model. This study focused on determining the actual and expected RDE for multiple classes of Euro 6 vehicles (Euro 6b, Euro 6c, Euro 6d temp, Euro 6d). The study evaluated the test data for a number of diesel passenger cars tested using the newly developed on-road RDE test procedure and other real world driving cycles and provided a prediction for how different Euro 6 vehicles, included the most advanced (Euro 6d) would perform. The data included that taken from literature as well as based on test data generated by Ricardo. The results show that from existing data, real world NO_x emissions from diesel passenger cars are significantly reduced by successive improvements in Euro 6 legislation. In addition, the evidence suggests that the technical solutions currently being introduced when applied to Euro 6d cars will meet the future EU NO_x emission standard for Euro 6 passenger cars of 80 mg/km under real driving emissions test conditions.

The impact on air quality compliance was examined for numerous scenarios, and covered the whole Europe⁵. In addition, detailed analyses was performed for 10 European cities (i.e., Antwerp, Berlin, Bratislava, Brussels, London, Madrid, Munich, Paris, Vienna, and Warsaw). For brevity, results for the following two key scenarios will be used to illustrate the results for NO_x, while France, and Paris in particular, have been chosen as representative examples to demonstrate the outcome of this study.

- a) **Ricardo Median Scenario:** All Euro 6 diesel passenger cars introduced in a specific year are assumed to conform to the median level of the Concawe-Ricardo study results [2]. This scenario assumes that all new diesel passenger car registrations from 2020 onwards are Euro 6d, and uses the following conformity factors:

Table 1: Median Conformity factors for diesel passenger cars based on the Concawe – Ricardo study [2] – NO_x.

	Euro 6b Pre-2015	Euro 6b Post-2015	Euro 6c	Euro 6d (temp)
Median NO_x	5.41	1.90	1.21	0.76 ⁶

- b) **ZEV Scenario:** All new diesel passenger car registrations from 2020 onwards are replaced by a zero tailpipe emissions vehicle undertaking the same amount of kilometres driven.

A Base Case emissions scenario was used as a starting point for all diesel passenger car scenarios in the modelling. This Base Case is based on the January 2015 TSAP16 WPE (Working Party on Environment of the European Council) Current Legislation Baseline Scenario [8,9] associated with the EU Air Policy Review process [10] as generated by the IIASA GAINS model.

For PM_{2.5} emissions, two scenarios were considered. The first is the Base Case and the second models the elimination of all diesel exhaust emissions for new passenger cars registered from 2020. It is important to note that the activity generated, wear related PM emissions associated with tyre wear, brake wear and road abrasion remain unchanged between the scenarios, as only PM emissions related to combustion processes differ between the scenarios.

Overview of NO_x/PM emissions – (case study: France)

The Figures below show the projected national emissions of NO_x and PM_{2.5} split by sector used for the Base Case, using France as an example. The road transport NO_x contribution decreases into the future, largely as a result of significant reduction in heavy duty vehicle emissions, which are a result of Euro VI emissions regulations delivering successful on the road NO_x emissions reductions (Figure 1). The PM_{2.5} contribution from road transport stabilises from 2020 onwards as the non-exhaust fraction dominates the overall emissions of particulates. Residential combustion is by far the most significant source of PM_{2.5} emissions in all years shown (Figure 2).

⁵ EU-27 + UK

⁶ In any scenario where the conformity factor is measured as being less than 1 the modelling has assumed a conformity factor of 1 which serves to ensure that the model is reflecting the minimum effect that full compliance with the legislated emissions limits would have on air quality.

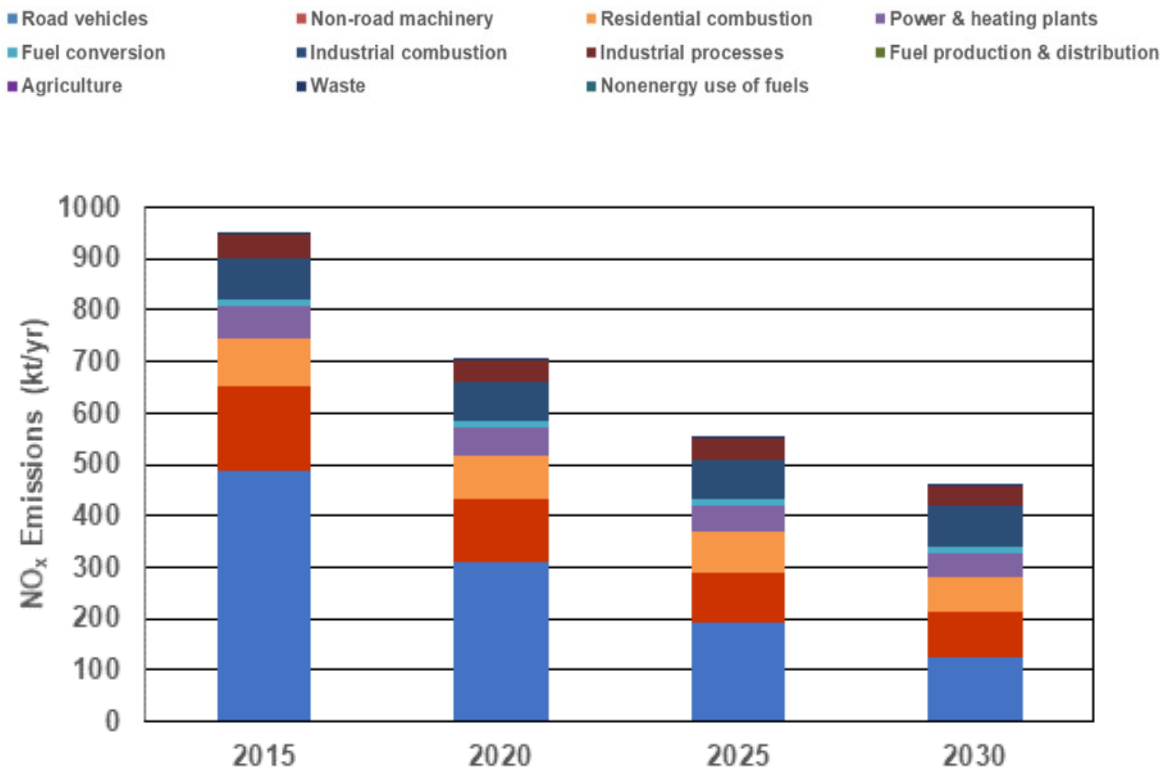


Figure 1: Sectoral NO_x Emissions for France with Road Transport at the bottom of the column.

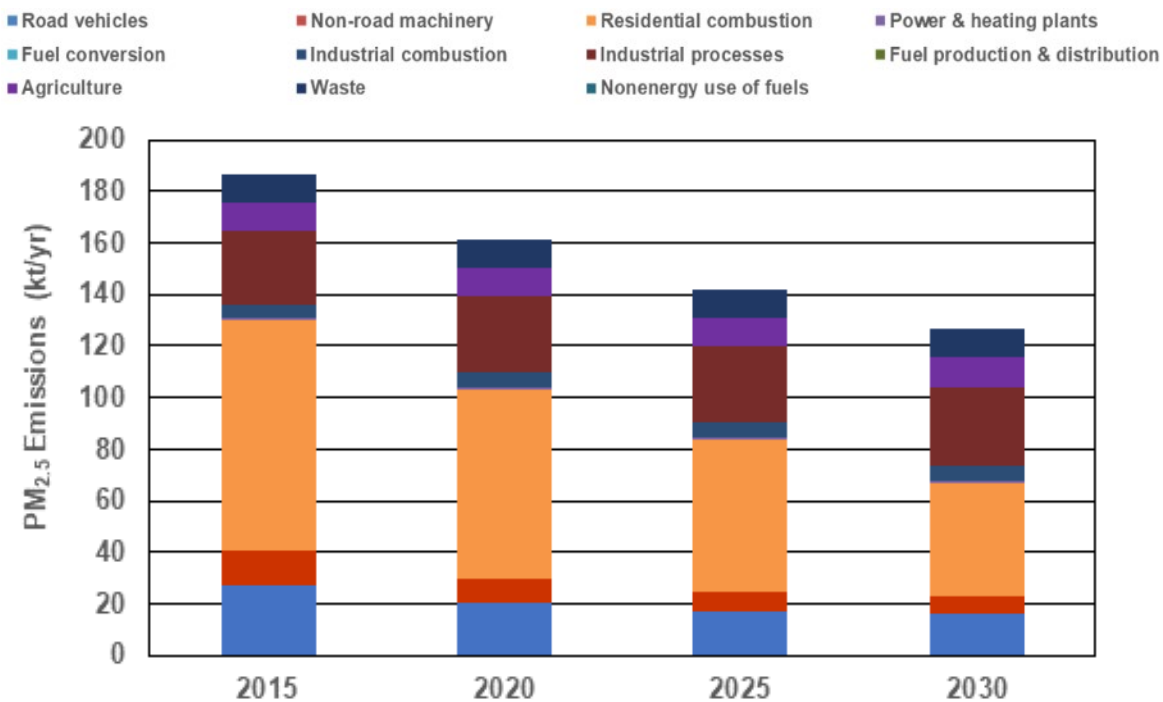


Figure 2: Sectoral PM_{2.5} Emissions for France with Road Transport at the bottom of the column.

Figure 3 shows NO_x emissions from diesel passenger cars in France with the Euro 6 diesel passenger car emissions modified to reflect the Ricardo Median scenario. The effect is a reduction in diesel passenger car emissions from 2015 onwards with an approximate 80% reduction by 2030 as a result of improved emissions from diesel car technologies. Figure 4 shows the diesel passenger car emissions in France modified to reflect the ZEV scenario. The ZEV scenario shows further reductions in 2025 and 2030.

■ PreEuro ■ Euro 1 ■ Euro 2 ■ Euro 3 ■ Euro 4 ■ Euro 5 ■ Euro 6

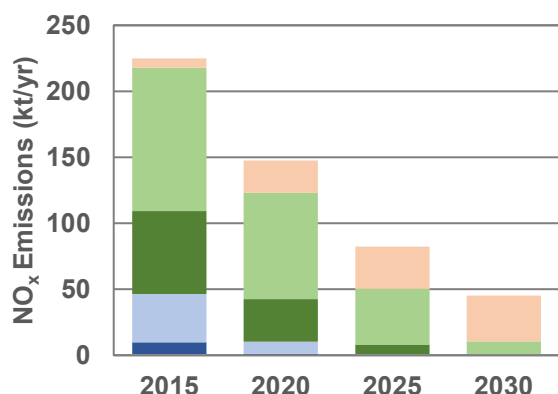


Figure 3: Diesel Passenger Car NOx Emissions in France for the Ricardo Median scenario.

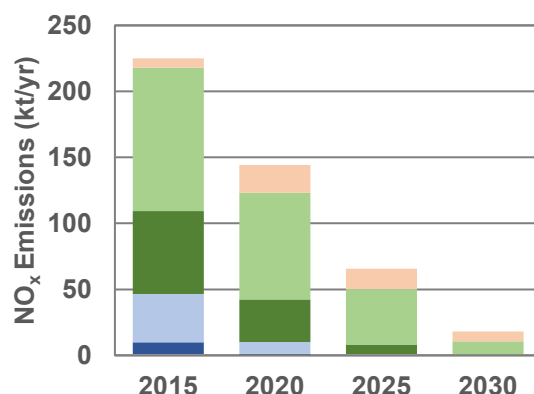


Figure 4: Diesel Passenger Car NOx Emissions in France for the ZEV scenario.

Figure 5 shows the Base Case emissions of PM_{2.5} from all diesel passenger cars split by Euro standard over time in France, while Figure 6 shows the PM_{2.5} emissions based on the ZEV scenario. Successful implementation of exhaust treatment systems removes nearly all PM exhaust emissions. The remainder of the PM emissions are abrasive emissions from road, brake and tyre wear which are related to activity rather than technology. This is clear on the figures which show that the non-exhaust PM emissions also persist in the ZEV scenario.

■ PreEuro ■ Euro 1 ■ Euro 2 ■ Euro 3 ■ Euro 4 ■ Euro 5 ■ Euro 6 ■ Non Exhaust

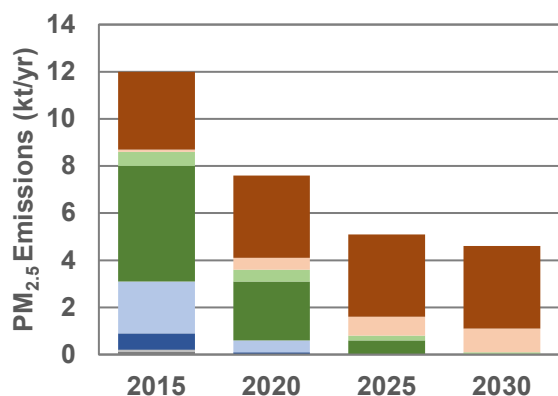


Figure 5: Diesel Passenger Car PM_{2.5} Emissions in France for the Base Case scenario.

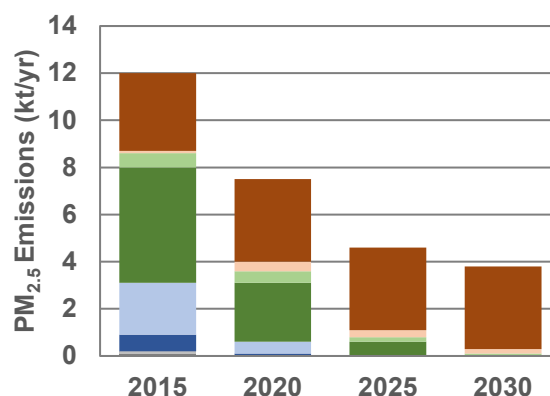


Figure 6: Diesel Passenger Car PM_{2.5} Emissions in France for the ZEV scenario.

Compliance Results – Country/City level

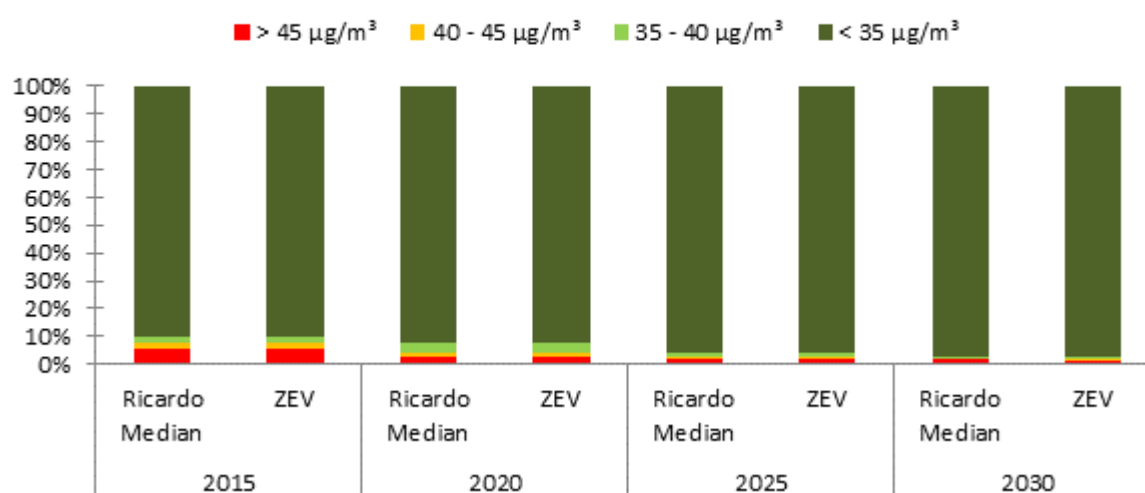
Table 2 and Figure 7 below show the modelled compliance of NO₂ monitoring stations throughout France for the Ricardo Median and ZEV scenarios.

The results show that both the Ricardo Median and the ZEV scenarios exhibit a similar evolution of compliance over time. The difference in the overall number of stations achieving compliance between the two scenarios is 0% in 2020 and 2025, and less than 0.5% in 2030, while in both scenarios NO₂ non-compliance will remain an issue in France. These strongly suggest that the progressive replacement of older diesel passenger cars by Euro 6d diesel cars will show a similar improvement in urban air quality compliance compared to a replacement with zero exhaust emission cars as the ZEV scenario is unlikely to deliver any significant improvement compared to the Ricardo Median scenario.

Table 2: NO₂ Air Quality Monitoring Station Compliance in France for the Ricardo Median and ZEV scenarios (AQLV = 40 µg/m³).

France	Ricardo Median (NO ₂)				ZEV Scenario (NO ₂)				
Year	Compliant ⁷	Likely Compliant	Likely Non-Compliant	Non-Compliant	Compliant	Likely Compliant	Likely Non-Compliant	Non-Compliant	
2015	206	6	4	13	206	6	4	13	
2020	212	7	3	7	212	7	3	7	
2025	219	4	2	4	219	4	2	4	
2030	222	3	0	4	223	2	1	3	

NO₂ Station Compliance in France (% compliant out of 229)

**Figure 7:** NO₂ station compliance in France for the Ricardo Median and ZEV scenarios.**Table 3:** PM_{2.5} Air Quality Monitoring Station Compliance in France for the GAINS Base Case and ZEV scenarios (AQLV = 25µg/m³).

France	Base Case (PM _{2.5})				ZEV Scenario (PM _{2.5})				
Year	Compliant ⁸	Likely Compliant	Likely Non-Compliant	Non-Compliant	Compliant	Likely Compliant	Likely Non-Compliant	Non-Compliant	
2015	347	23	1	1	347	23	1	1	
2020	362	9	1	0	362	9	1	0	
2025	367	4	1	0	367	4	1	0	
2030	368	4	0	0	368	4	0	0	

⁷ "Compliant": < 35 µg/m³, "Likely Compliant": 35-40 µg/m³, "Likely Non-compliant": 40-45 µg/m³, "Non-Compliant": > 45 µg/m³.

⁸ "Compliant": < 20 µg/m³, "Likely Compliant": 20-25 µg/m³, "Likely Non-compliant": 25-30 µg/m³, "Non-Compliant": > 30 µg/m³.

Noting that PM emissions are unaffected by choice of NO_x conformity factor, the table below shows the modelled compliance of PM_{2.5} monitoring station numbers for the Base Case and ZEV scenarios:

Unsurprisingly, given the negligible difference in PM_{2.5} emissions between the two scenarios, there is no difference in the compliance outlook between the Base Case and ZEV scenarios. This strongly suggests that Euro 6d passenger cars will result in the same PM_{2.5} compliance improvement as zero emission vehicles.

The analysis at a city level shows that Paris follows a similar compliance progression to the whole of France as discussed above, with just a small difference between the Ricardo Median and the ZEV scenarios in 2030 (Table 4, Figure 8).

Table 4: Paris NO₂ Air Quality Monitoring Station Compliance for the Ricardo Median and ZEV scenarios (AQLV = 40 µg/m³).

Paris	Ricardo Median (NO ₂)				ZEV Scenario (NO ₂)				
	Compliant ⁹	Likely Compliant	Likely Non-Compliant	Non-Compliant	Compliant	Likely Compliant	Likely Non-Compliant	Non-Compliant	
2015	10	3	0	5	10	3	0	5	
2020	13	1	0	4	13	1	0	4	
2025	14	1	0	3	14	1	0	3	
2030	14	1	0	3	15	0	1	2	

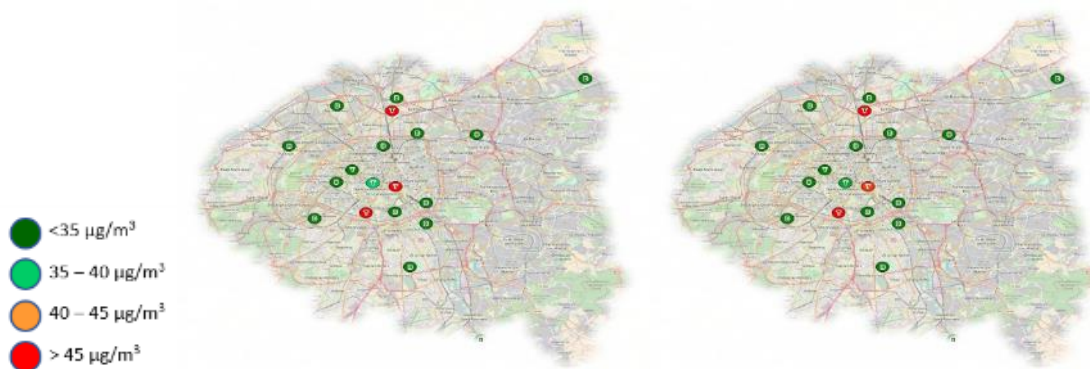


Figure 8: Paris NO₂ Air Quality station compliance in 2030 for the Ricardo Median (left) and ZEV (right) scenarios.

The fact that there is no appreciable effect on air quality compliance between the Ricardo Median and ZEV scenarios can also be seen when looking at the highest and second highest NO₂ monitoring stations in Paris. The figure below shows that the two highest stations in Paris never reach compliance even in the ZEV scenario. This suggests that a localised targeting of the issues in those areas will be needed to resolve the residual non-compliance.

⁹ "Compliant": < 35 µg/m³, "Likely Compliant": 35-40 µg/m³, "Likely Non-compliant": 40-45 µg/m³, "Non-Compliant": > 45 µg/m³.

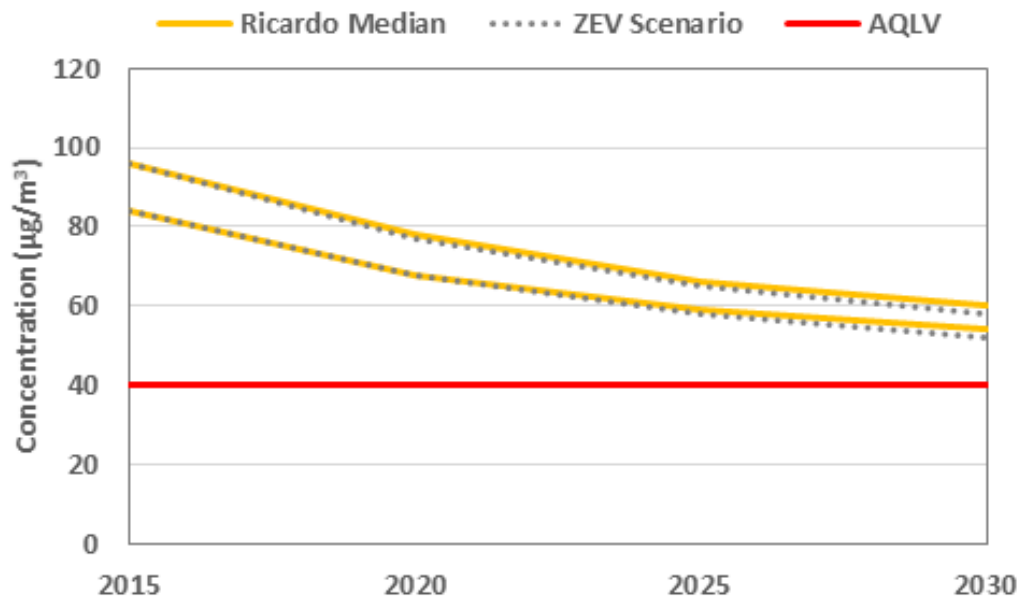


Figure 9: NO₂ modelled concentrations at the two highest stations in Paris10 - Ricardo Median and ZEV scenarios.

Concawe NO_x/NO₂ Source Apportionment Viewer

The Concawe NO_x/NO₂ source apportionment viewer was built based on a recent methodology called QUARK (Quick Urban Air Quality using Kernels) [11]. The methodology has been developed by VITO to estimate the annual NO₂ concentrations in Europe at a high resolution (~ 100m) and has recently been used in a similar project funded by the European Commission aiming to find well suited tools for EU-wide NO₂ assessment.

The tool uses a dispersion kernel based air quality modelling approach [12] to account for the local contribution of the different vehicle categories combined with a breakdown of the background NO_x concentrations in SNAP sectors via the SHERPA tool [13]. The EU-wide background concentrations for NO_x, NO₂ and O₃ needed in the approach were sourced from the CAMS reanalysis data. The dispersion kernels were calculated using the IFDM Gaussian dispersion model [14], generating annual averaged patterns using a unit emission source under different orientations and local meteorology. The emissions of each of the vehicle categories and for each of the years that info is available in the tool (i.e., 2015-2020-2025-2030) are generated using the vehicle stock baseline as generated by Sibyl linked to country specific COPERT 5.3 emission factors to calculate the emissions per country and FASTRACE to distribute them geographically in the line segments.

¹⁰ Both stations are characterised as traffic.

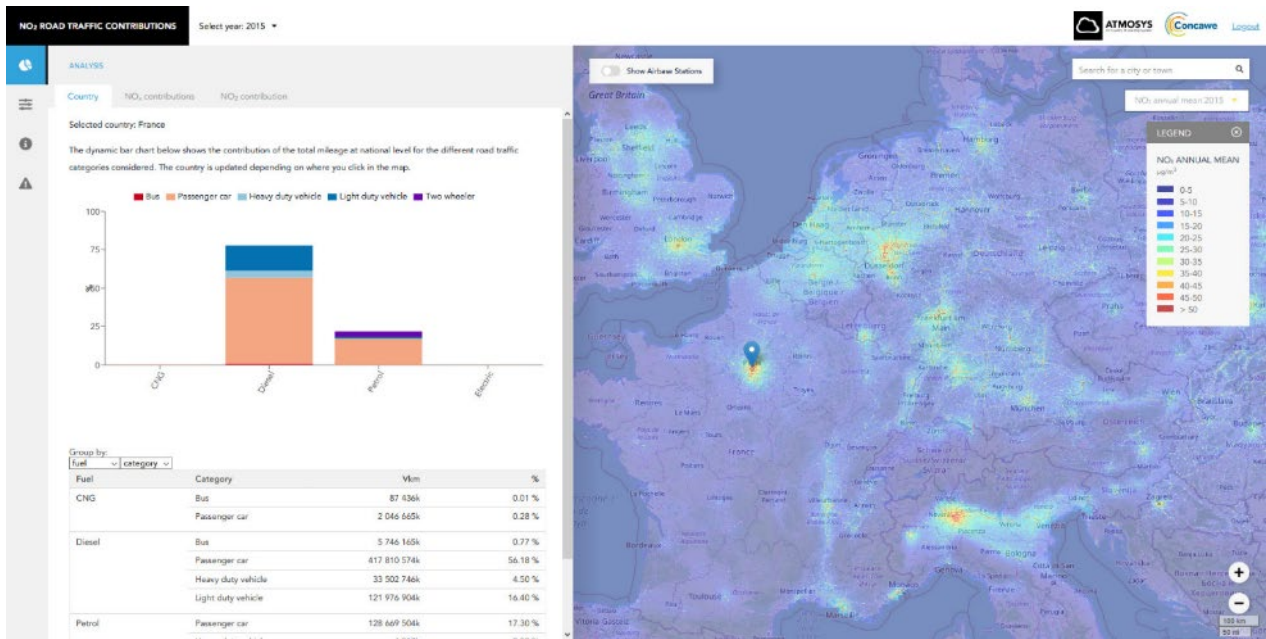


Figure 10: The Concaawe NO_x/NO₂ source apportionment viewer.

The tool allows the user to select any location in Europe and get explicit information regarding the predicted NO₂ concentrations (Figure 11) as well as the contribution of different vehicle categories, the different EURO norms, as well as the different types of fuel to NO_x emissions and NO₂ concentrations for current and projected years (Figure 12). Information regarding national fleet composition (Figure 13) as well as the contribution of other sectors to NO_x emissions is also available.

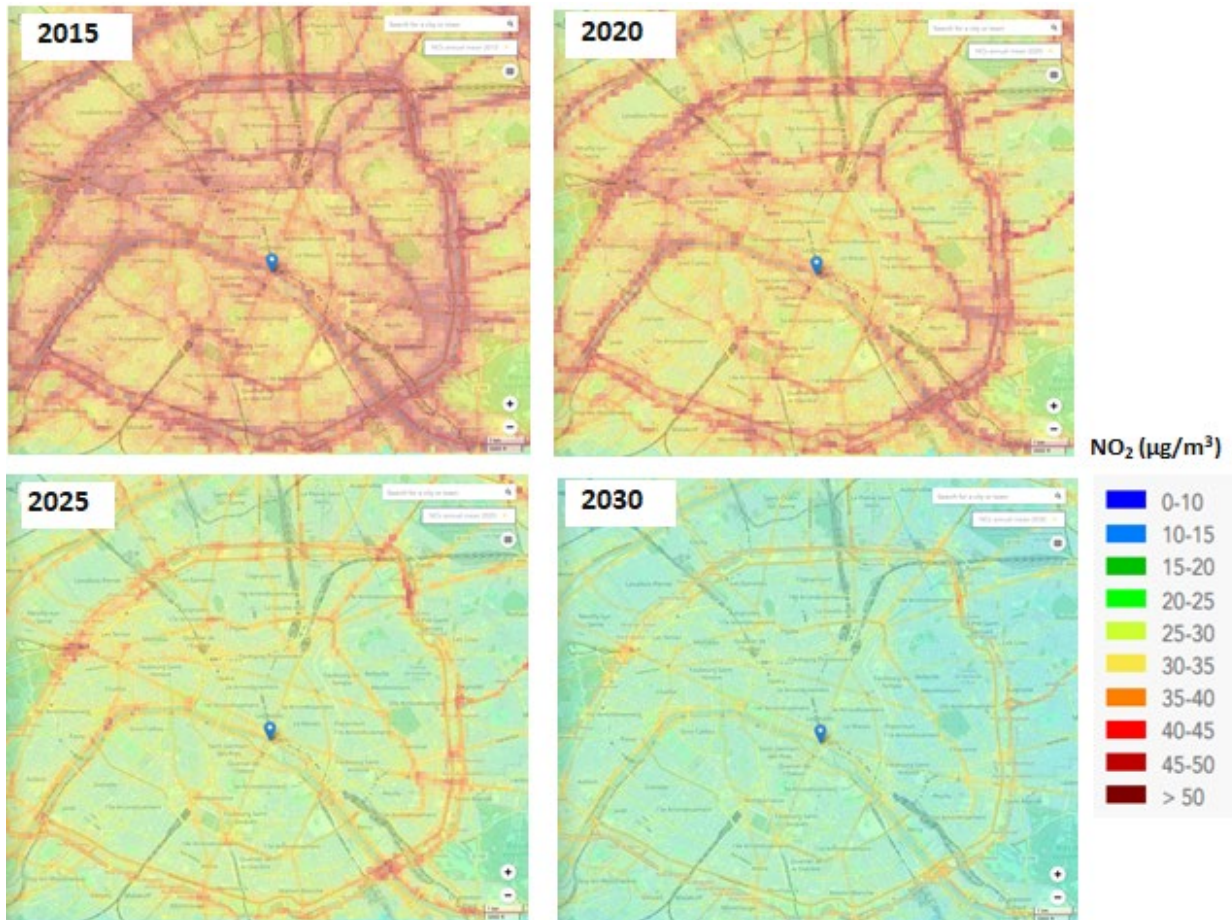


Figure 11: Predicted annual mean NO₂ concentrations (µg/m³) in 2015-2030 in Paris as a result of the turnover of the vehicle fleet from older vehicles to new vehicles.

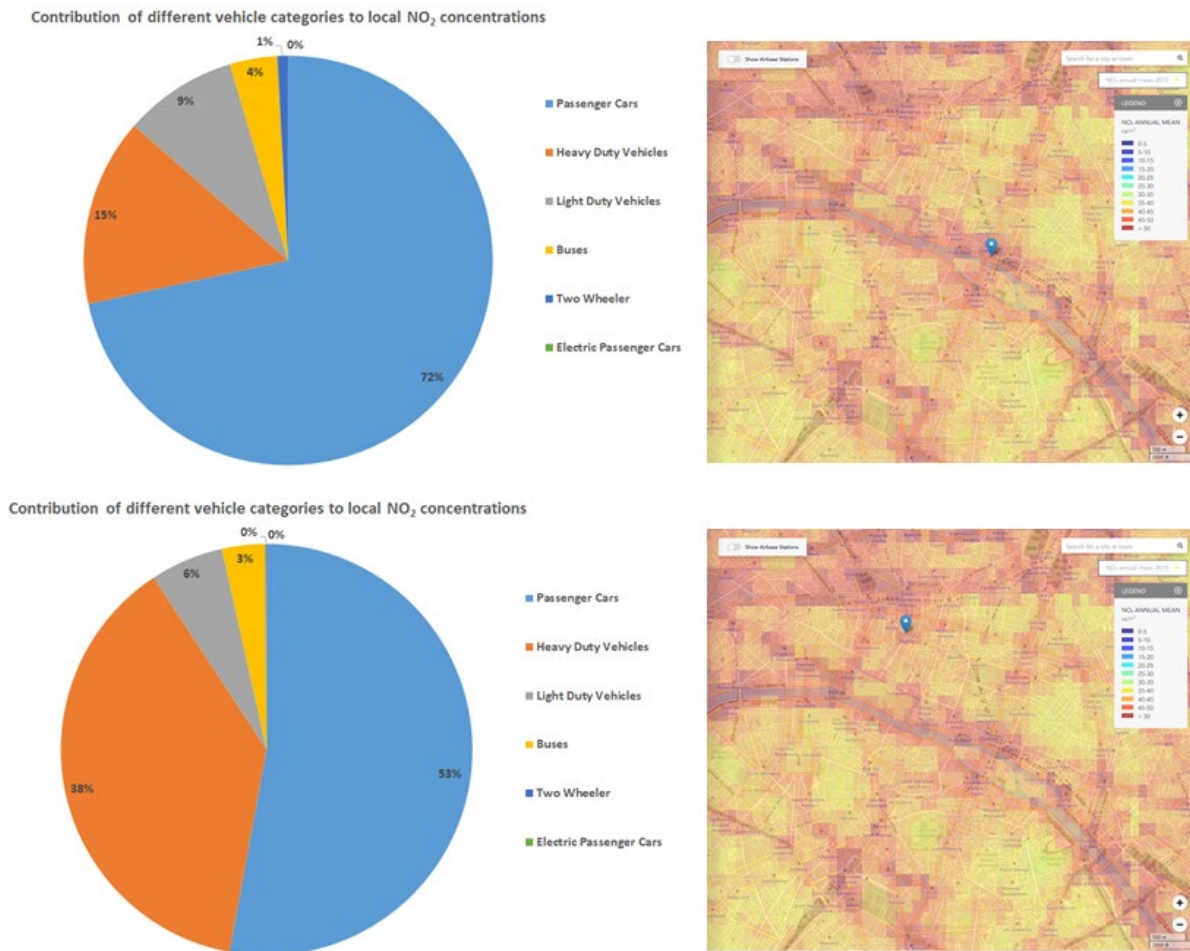


Figure 12: Predicted contribution of the different vehicle categories to local NO₂ concentrations in two busy roads in Paris.

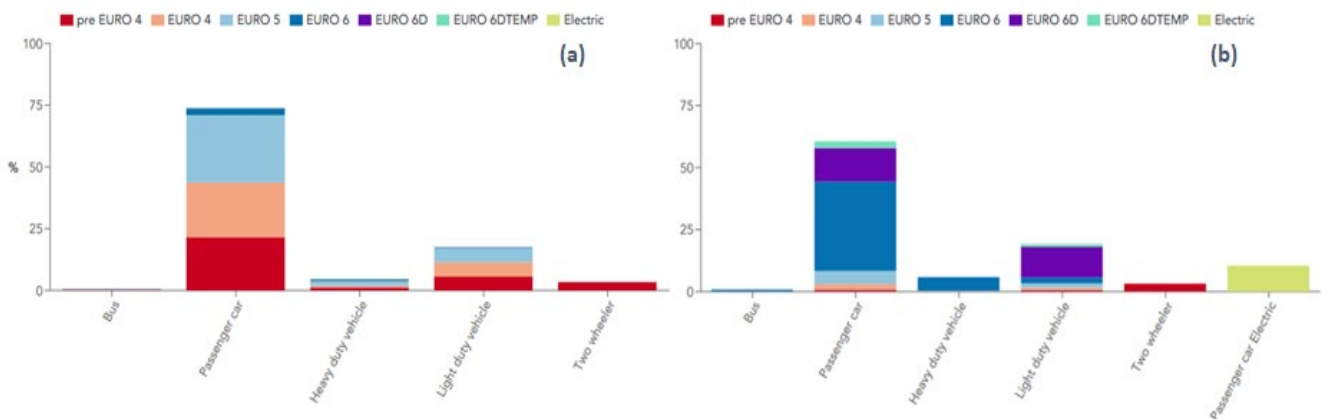


Figure 13: National fleet composition in France in 2015 (a) and 2030 (b).

Conclusions

Two recent studies conducted by Concaave have shown how air quality modelling can offer a means of robust, evidence based approach in supporting air quality assessment and assessing how air quality can be further improved. The main findings from these can be summarised as follows:

- The modelling work to assess air quality compliance under the scenario of Euro 6d compliant vehicles in comparison of a zero emission vehicle scenario have shown that the existing regulation can be effective in reducing air pollutant emissions from road transport and eventually improving compliance over EU in the coming years.

- In the turnover of the vehicle fleet from older vehicles to new vehicles, the latest Euro 6d diesel vehicles will be as effective as zero emission vehicles in helping cities become compliant with Air Quality Limit Values.
- Further developments on new vehicle emission standards is unlikely to deliver earlier compliance or a reduction in population exposure to non-compliant levels.
- When hot spots, would remain, those will require a detailed analysis to define which are the most effective measures that need to be taken to improve the urban air quality. Therefore, understanding the source attribution is important to address remaining exceedances.
- To this end, high resolution and EU-wide modelling tools will be essential to provide a detailed view of the contribution of emissions sources with high spatial variability, such as road transport, and eventually determine the most effective solutions for improving air quality.

Acknowledgement

We would like to acknowledge Aeris Europe for their work in the modelling study to assess the effectiveness of RDE of Euro 6 Diesel Passenger Cars in improving EU compliance and VITO for their work in the development of the NO_x/NO₂ source apportionment viewer.

References

Concawe: A comparison of real driving emissions from Euro 6 diesel passenger cars with zero emission vehicles and their impact on urban air quality compliance, Concawe Report 4/18, 2018.

Concawe and Ricardo: Expectations for Actual Euro 6 Vehicle Emissions, Concawe Report 2018.

Concawe: Urban Air Quality Study – Sections 5.2-5.4: Description of AQUIRES+, Concawe Report 11/16, 2016.

Norwegian Meteorological Institute: Transboundary acidification, eutrophication and ground level ozone in Europe, EMEP Status Report 1/2004, 2004.

Simpson, D., Benedictow, A., Berge, H., Bergström, R., Emberson, L.D., Fagerli, H., Flechard, C.R., Hayman, G.D., Gauss, M., Jonson, J. E., Jenkin, M.E., Nyíri, A., Richter, C., Semeena, V.S., Tsyro, S., Tuovinen, J-P., Valdebenito, A., and Wind, P.: The EMEP MSC-W chemical transport model – technical description, *Atmos. Chem. Phys.*, 12, 7825–7865, doi:10.5194/acp-12-7825-2012, 2012.

Ecole Polytechnique: CHIMERE: Documentation of the chemistry-transport model CHIMERE. CNRS, IPSL, INERIS Report, available at: <http://www.lmd.polytechnique.fr/chimere/docs/CHIMEREdoc2017.pdf>, 2017.

European Environment Agency: Air Quality e-Reporting Dataset, <https://www.eea.europa.eu/data-and-maps/data/raqereporting-8>. Created 23 March 2018, 2018.

Amann, M., Bertok, I., Borcen-Kleefeld, J., Cofala, J., Heyes, C., Höglund-Isaksson, L., Kiesewetter, G., Klimont, Z., Schöpp, W., Vellinga, N., and Winiwarter, W.: Adjusted historic emission data, projections, and optimized emission reduction targets for 2030 – A comparison with COM data 2013. Part A: Results for EU-28, IIASA, 2015.

Amann, M., Imrich, B., Borcen-Kleefeld, J., Cofala, J., Heyes, C., Höglund-Isaksson, L., Kiesewetter, G., Klimont, Z., Schöpp, W., Vellinga, N., Winiwarter, W., 2015. Adjusted Historic Emission Data, Projections, and Optimized Emission Reduction Targets for 2030 – A comparison with COM Data 2013 Part B : Results for Member States, IIASA, 2015.

Review of EU Air Quality Policy – Commission Staff Working Document (SEC(2011)342). European Commission, 2011.

Lefebvre, W., and Maiheu, B.: QUARK –Quick Urban Air quality model using Kernels Version 1.1, <https://ec.europa.eu/environment/air/publications/models.htm>, 2017.

Maiheu B., Lefebvre W., Walton H., Dajnak D., Janssen S., Williams M., Blyth L and Beevers S.: Improved methodologies for NO₂ exposure Assessment in the EU, Study accomplished under the authority of the European Commission under service contract 070201/2015/SER/717473/C.3, Report no.: 2017/RMA/R/1250, 2017.

Pisoni, E., Clappier, A., Degraeuwe, B., and Thunis, P.: Adding spatial flexibility to source-receptor relationships for air quality modeling, *Environ. Model. Softw.* 90, 68–77, 2017.

Lefebvre, W., Van Poppel, M., Maiheu, B., Janssen, S., and Dons, E.: Evaluation of the RIO-IFDM-street canyon model chain. *Atmos. Environ.* 77, 325–337, 2013.

2.10 Operational GRAL urban street-canyon air quality forecast: Model assessment and COVID-19 restrictions impact in air quality

J.A. Gonzalez^{1*}, D. Cartelle^{1,2}, J.M. Vellon², S. Piñeiro², X. Diz¹, J.R.R. Viqueira³, D. Martinez³

¹ CRETUS Institute, Dept. Chemical Engineering, University of Santiago de Compostela, Spain

² Labaqua, S.A.U. Air Quality Department, Ferrol, Spain

³ Centro Singular de Investigación en Tecnoloxías Intelixentes (CITIUS), University of Santiago de Compostela, Spain

ja.souto@@usc.es

Abstract

Nowaday urban air quality is a significant air pollution problem, both because of its large pollutant emissions and high population density. Road traffic is a relevant emission source in urban environments. In order to prevent urban air pollution episodes, typically operational Eulerian Chemical Transport Models, with extremely high horizontal resolution grids (hundreds of meters) are applied. However, because of the urban domain complexity, their results are usually far from street canyon simulations using either CFD/RANS or, even, LES.

Focused in NO_x as primary pollutants, Lagrangian models are usually applied to the simulation of single air pollutants plumes, because of their ability to represent microscale atmospheric diffusion phenomena. In urban environments, with large number and variety of urban emission sources (vehicles, domestic heating), last generation GRAL Lagrangian particle model is able to manage them, and to calculate fast street canyon level simulations in parallel supercomputers.

As TRAFair Project application, an operational air quality forecast based on GRAL model is applied over the city of Santiago de Compostela, Spain. Main operational GRAL model inputs are: detailed streets and buildings digital terrain models; operational WRF model regional forecast; NO_x emissions inventory based on hourly road traffic intensities at 815 streets segments, and domestic fossil fuel consumption, both using standard EEA/EMEP emissions factors.

Assessment of this operational air quality forecast is performed with a complete set of statistics and, also, following FAIRMODE criteria, against both background urban stations and low-cost air quality sensors located at street level along this city. Modelling performance shows good agreement to observations at background stations and most of the street level locations.

Finally, COVID-19 mobility restrictions impacts over NO_x and O₃ levels are analysed over both background and street level locations. Different and, even, opposite behaviour in both pollutants levels are observed, depending on the location considered and surrounding NO_x sources.

Introduction

Air pollution associated with road transport is one of the major environmental issues in urban areas (Murena et al., 2009). The deterioration of urban air quality occurs due to the combined effects of emissions source from road traffic and other urban sources, dynamical processes (reduced dispersion caused by buildings) and chemical processes (evolution of reactive pollutants; formation of secondary pollutants) (Li et al., 2008). However, focused in primary gas pollutants with main road traffic contribution, as NO_x, mainly atmospheric dispersion at the urban boundary layer (UBL) is involved; with minor influence of chemical reactions at urban scale periods.

In the urban boundary layer (UBL), particular analysis of the urban canopy layer (UCL) is required; including the main UCL generic geometry unit in urban areas, i.e. street canyon. Therefore, atmospheric dispersion at UCL requires very high resolution modelling approaches, in order to take into account dynamical processes at street canyon. Focused in primary pollutants urban dispersion, in the last 20 years different studies have examined several aspects of numerical simulation of urban street canyon dynamics/pollution. Ahmad et al. (2005) reviewed wind tunnel experiments on wind flow and pollutant dispersion patterns in street canyons; such experiments do not however examine chemical processes, i.e., only inert tracer gas is considered. Vardoulakis et al. (2003) covered a wide range of approaches of the air quality in street canyons focussing upon measurement and parametric modelling approaches, with little discussion on computational fluid dynamics (CFD) modelling. Subsequently, Li et al. (2006) conducted a separate review on CFD modelling of wind flow and pollutant transport in street canyons. Their study focused mainly on the dynamic processes of pollutant dispersion within street canyons, rather than on the chemical processes. Yazid et al. (2014) reviewed a variety of studies on the flow structure and pollutant dispersion to provide guidelines of urban planning strategies for urban developer. Particularly, CFD technique (Chang, 2006) has become a powerful numerical tool mainly including Reynolds-averaged Navier–Stokes (RANS) and Large-Eddy Simulation (LES). RANS models are, by nature, a steady-

state methodology, while LES models can handle the unsteadiness and intermittency of the flow and retrieve the transient structure of turbulence flow within street canyons. The choice between them depends on the computational cost, the accuracy required, and hence the application. While both are highly intensive in computational effort required, LES usually requires more, as the atmospheric turbulent flow involves in and above street canyons turbulent eddies on a variety of scales (McNabola et al., 2009). Also, the performance in modelling turbulence diffusion by LES or RANS played an important role in the accuracy of pollutant dispersion predictions (Tominaga and Stathopoulos, 2010).

Nowaday, operational air quality modelling forecast (Baklanov and Zhang, 2020) is widely extended, both in rural and urban environments, including both primary and secondary pollutants; in order to prevent and manage air quality episodes considering both human health risks and natural environment damages. However, these air quality modelling forecasts are limited by their environments complexities, their required computational cost, and the time response required by a feasible forecast; considering the computational resources available.

When an operational air quality forecast at street canyon is considered, because of their high computational effort requirements usually both LES and RANS modelling approaches are not feasible; even though only flow dynamics in primary pollutants atmospheric dispersion is considered. Therefore, usually different approaches based on simplified parameterisations of street canyon dynamic are applied (Murena et al., 2009). These approaches are usually based on numerical modelling street canyon idealised results. Detailed applications of the parametric modelling are reviewed by Vardoulakis et al. (2007) and Kakosimos et al. (2010). These simplified parameterisations of turbulent exchange between the street canyon and the overlying atmospheric boundary layer can represent the overall performance of the dynamics in street canyons, but necessarily fails to reproduce the flow field within street canyons.

An alternative approach, only valid for primary pollutants, takes advantage of last generation Lagrangian particle models, as in microSWIFT-SPRAY (Oldrini et al., 2017) and GRAL (Oettl, 2016) modelling systems. Because Lagrangian approach is not limited by a computational grid resolution, while these last generation models optimize the number of particles required to represent the dispersion of a large number of sources, as in urban environments. In this work, a new operational air quality forecast street canyon modelling system, based on GRAL Lagrangian particle model, is presented and compared to standard and street level NO_x observations. This approach does not require any specific domain modelling parameterisation, as it is based on the direct application of: (a) meteorological diagnostic, using a very high resolution grid with a urban digital terrain model at street canyon scale; and (b) GRAL Lagrangian dispersion model solution, which is independent on any numerical domain grid. Also, the impact of restrictions during over Spanish COVID-19 2020 lockout in 2020 over urban background and street level air quality NO_x is analysed.

Operational air quality forecast

Operational air quality forecast over Santiago de Compostela urban domain is based on GRAL v. 20.01Beta2 Lagrangian particle model, running every day to simulate NO_x emission dispersion along 48-hr. GRAL transient mode is applied, as meteorological input changes every hour and it is assumed no steady state conditions are achieved in less than 1 hour. Road traffic and domestic sources are considered to estimate typical hourly NO_x emissions every day of the week, as no other relevant NO_x sources are located inside this urban domain. GRAL meteorological input is based on its meteorological diagnostic model, which includes buildings effects over the wind flow at this urban domain, using a detailed urban digital terrain model (including buildings area and height) provided by the Santiago de Compostela Municipality. Neither dry nor wet depositions are considered.

Simulation domain and urban air quality network

Although GRAL Lagrangian model simulates pollutants dispersion as particles plumes, both for its meteorological input and concentrations computation spatial grids are required. Santiago de Compostela simulation domain covers 5.5x5.3 km², and the same spatial grid is defined over it with an horizontal resolution of 4x4 m² and 8 vertical levels at 3, 6, 10, 14, 18, 24, 28 and 31 m above ground level; with a total of 1388x1326x8 cells. For ground level concentration, only 3 m level computation is considered.

Figure 1 shows the domain limits, roads/streets (line sources) and buildings. Also, an urban air quality network is shown, including 2 reference air quality stations (namely, AQMs) and 10 low cost air quality sensors units, as follows,

- a) Standard air quality stations, Campus and San Caetano, installed at green areas inside the city domain: These stations provide high quality and validated standard pollutants concentrations, as their equipment follows the standard EN ISO/IEC 1702. However, they are not always affected by the traffic emissions, as their locations followed European recommendations for air quality stations representativeness (Larsen et al., 1999).

- b) Low-cost air quality sensors installed close to city streets/roads, from medium to high traffic intensity, with different and complex buildings setups around them. In order to assure the quality of low-cost sensors measurements, sensors were calibrated against 10-min. observations from one AQM (Campus station) during at least 3-weeks using Random Forest based calibration method (Bigi et al., 2018). Also, two of them are located at the Campus AQM station for continuous checking of their calibrated concentrations.

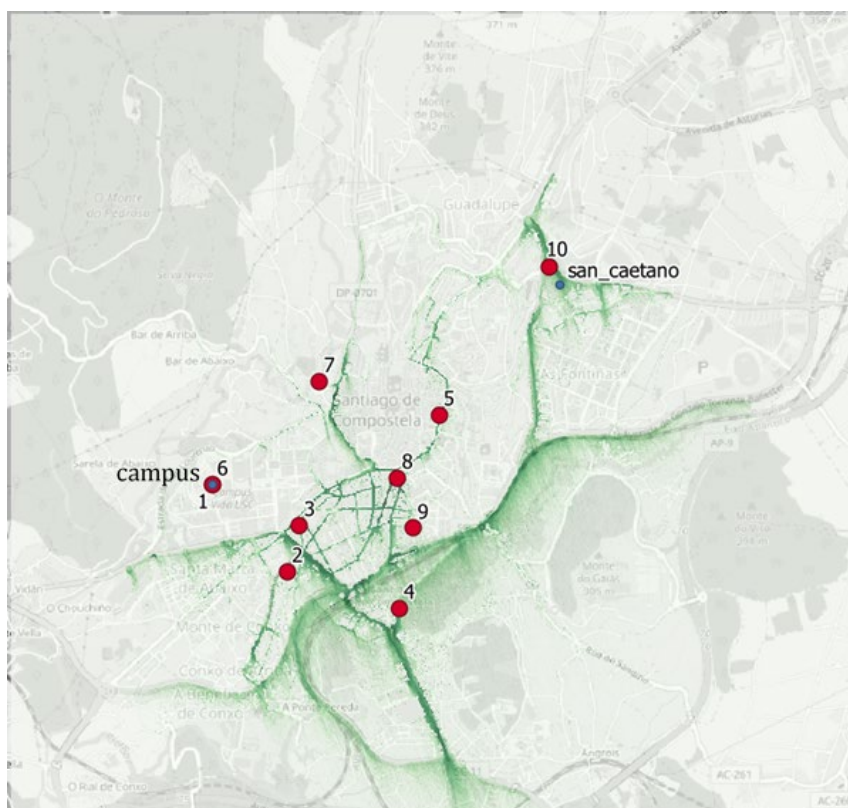


Figure 1: GRAL model simulation domain at Santiago de Compostela. Limits are: S-W Border, 534680 m – 4744944m to N-E border, 540232 m – 4750248 (UTM WGS-84, 29N). Also, the location of current urban air quality network sites is shown: Two air quality standard sites, AQMs (MeteoGalicia, Xunta de Galicia), and ten numbered low-cost air quality sensors.

Emissions input

NO_x emissions in the simulation domain come from both road traffic and domestic sources. Also, there are no other relevant sources around the simulation domain.

About traffic NO_x emissions, typical hourly emissions per day of the week were estimated, based on,

- DISIT Lab traffic reconstruction model results along 4 months (Sep-Dec 2019): At Santiago de Compostela, this model (Bellini et al., 2018) applies measurements from 80 traffic sensors and the streets network topology to estimate hourly traffic densities at 815 street segments. From the statistical analysis of this dataset, an average daily traffic intensity value at each street segment per day of the week was derived; also, it was observed that the same relative traffic intensity hourly profile per day of the week can be applied at any segment.
- Daily traffic intensity values and vehicles fleet composition were used as input to estimate typical NO_x road traffic emissions per day of the week at each street segment, following EEA Emissions Inventory Guidebook (2016), with 2018 emission factors update.
- Daily NO_x emissions at each segment and day of the week were distributed using relative traffic intensity hourly profiles previously obtained.
- Additionally, AP-9 motorway crosses along the domain southeast corner, and their NO_x daily emissions were separately estimated using official traffic intensity data from the Ministry of Transport, as this road is not included in DISIT model.

NO_x domestic emissions were estimated from fossil fuel and biomass (for heating) annual consumption, also following EEA Emissions Inventory Guidebook (EEA, 2016). Fossil fuel combustion emissions are segregated according to population, while biomass burning emissions take into account single family homes, as common domestic heating fuel.

Meteorological input

GRAL system meteorological diagnostic model can provide high resolution 3-D wind and fields (saved as GFFs files) using as input only three meteorological parameters at one location (wind speed, wind direction, and Pasquill stability class), and an urban buildings digital terrain model. In this operational air quality forecast system, meteorological input is obtained from WRF model regional forecast (4x4 km² resolution) daily supplied by the Galician Regional Weather Service (MeteoGalicia), namely: Hourly surface wind, temperature (at the 2 lowest levels), and shortwave surface solar radiation at one domain location. From these dataset, Pasquill stability class is estimated following solar radiation/delta-T method (US EPA, 2000), to complete the GRAL system diagnostic model input. Then, hourly GFFs files with a horizontal resolution of 4x4 m² are obtained, to supply the meteorological input to GRAL along the 2-days forecast period.

Table 1: Short names, locations, sensors type/manufacturer and location type for air quality observations sites at Santiago de Compostela air quality network.

Short name	Location	Sensors Type / Manufacturer	Location type
San Caetano	San Caetano	AQM	Green area, close to urban traffic
Campus	Campus Vida	AQM	Urban background
1	Campus Vida	Libelium low-cost	Urban background
2	Ferrol Av.	Libelium low-cost	Residential, close to urban traffic
3	Vigo Square	Libelium low-cost	Residential, close to urban traffic
4	Brañas de Sar	Decentlab low-cost	Green area, close to urban traffic
5	Virxe da Cerca St.	Decentlab low-cost	Urban traffic
6	Campus Vida	Decentlab low-cost	Urban background
7	Galeras Park	Kunak low-cost	Green area, close to urban traffic
8	Galicia Square	Libelium low-cost	Urban traffic
9	Constitution Square	Libelium low-cost	Green area, close to urban traffic
10	Berlin St.	Libelium low-cost	Urban traffic

Air quality forecast assessment

The main goal of this operational air quality forecast approach is providing useful information about air quality (NO_x concentrations) at street canyon scale to the Public Administrations; in order to support their short and long-term decisions about urban air quality, i.e., road traffic management, domestic heating policy, Therefore, as main air quality modelling assessment criteria, standard FAIRMODE methodology (Janssen et al., 2017) was adopted. In

addition, several statistics, Taylor Diagrams and scatter plots are analysed, in order to better understanding this modelling system performance.

With these goals, GRAL-based operational air quality forecast results were compared against NO+NO₂ (NO_x) available observations from the TRAFAIR urban air quality network installed in the simulation domain. All hourly datasets, both model results and observations, were processed using Openair (Carslaw and Ropkins, 2012), and Dartle (Bonafè, 2017) R packages; following Delta tool (Thunis et al., 2012) statistics and diagrams, and including FAIRMODE assessment criteria. As daily operational forecast provides results for two days (48 hours) everyday, model performance is separately evaluated for the first and the second day of forecast. Evaluation period is May/23/2020 – Feb/28/2021, as the operational period currently available.

Table 1 includes the main characteristics of the air quality stations shown in Figure 1. While low-cost sensors units from three different manufacturers are installed all of them are equipped with Alphasense electrochemical cells for NO, NO₂ and O_x. When possible, low-cost sensors units are located at the surroundings of medium/high traffic intensity streets, but not close to the vehicles. However, FAIRMODE methodology is mainly oriented to regional modelling, so it will be more difficult to achieve its modelling acceptance criteria at street canyon scale, as usually the pollutants concentrations variations are larger at smaller scales. While it is possible at AQM stations, as background reference stations, model performance at some low-cost sensors locations pretty close to the vehicles should be worse.

Table 2: Statistical metrics for predicted NO_x hourly concentrations for the first day of forecast (see Table 1 for station short name). MB is reported as ($\mu\text{g m}^{-3}$).

AQM/Low Cost Station	FAC2	MB	MGE	NMB	NMGE	RMSE	r	COE	IOA
San Caetano	0.315	-12.418	15.175	-0.620	0.758	30.541	0.338	0.108	0.554
Campus	0.137	-9.251	9.748	-0.816	0.860	17.935	0.240	-0.067	0.466
2	0.423	-1.124	11.609	-0.084	0.863	18.327	0.035	-0.802	0.099
3	0.510	2.791	19.351	0.115	0.795	30.701	0.266	-0.315	0.342
4	0.390	-11.167	17.542	-0.518	0.813	70.387	0.019	-0.130	0.435
5	0.299	-7.388	13.346	-0.416	0.751	18.489	0.269	-0.246	0.377
7	0.111	-9.442	10.182	-0.796	0.859	12.019	0.131	-1.183	-0.084
8	0.474	25.621	39.653	0.913	1.412	81.234	0.232	-1.104	-0.049
9	0.369	-3.150	7.453	-0.297	0.704	10.488	0.215	-1.247	-0.110

Tables 2 and 3 summarize above mentioned metrics at air quality stations, for the first and the second day of forecast, respectively. There is a wide variety of values for each statistic depending on the station; however, in most of them model underestimates the observations, except in sensors 3 and 8, which are located very close to the vehicles circulation.

All AQM available stations and most of low-cost sensors datasets are applied in this GRAL model assessment, only low-cost sensors 1, 6 and 10 were excluded: Sensors 1 and 6 are located at Campus AQM station, so only this AQM observations dataset were considered at this location; and, sensor 10 dataset has less than 10% of data available.

The following statistics between modelled and observed concentrations were done: Fraction of predicted values within a factor of two of observations (FAC2), Mean Bias (MB), Mean Gross Error (MGE), Normalized Mean Bias (NMB), Normalized Mean Gross Error (NMGE), Root Mean Square Error (RMSE), Pearson correlation coefficient (r), Coefficient of Efficiency (COE), and Index Of Agreement (IOA).

Table 3: Statistical metrics for predicted NO_x hourly concentrations for the second day of forecast (see Table 1 for station short name). MB is reported as (µg m⁻³).

AQM/Low Cost Station	FAC2	MB	MGE	NMB	NMGE	RMSE	r	COE	IOA
San Caetano	0.295	-12.533	15.207	-0.638	0.775	29.843	0.325	0.087	0.543
Campus	0.133	-9.345	9.770	-0.826	0.863	18.075	0.251	-0.064	0.468
2	0.409	-1.466	11.757	-0.109	0.875	18.130	0.023	-0.820	0.090
3	0.500	2.880	19.832	0.118	0.810	31.458	0.271	-0.341	0.330
4	0.391	-10.777	17.438	-0.506	0.819	69.678	0.020	-0.146	0.427
5	0.302	-7.680	13.317	-0.431	0.748	18.411	0.270	-0.242	0.379
7	0.105	-9.532	10.206	-0.800	0.857	12.012	0.157	-1.203	-0.092
8	0.476	26.071	40.111	0.934	1.437	84.282	0.262	-1.127	-0.060
9	0.378	-2.902	7.632	-0.275	0.722	11.068	0.155	-1.315	-0.136

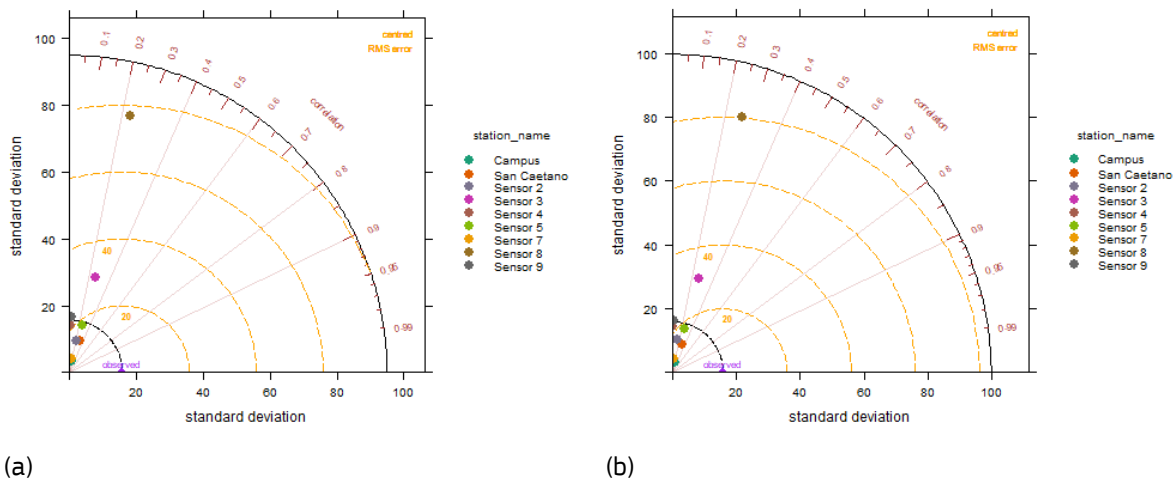


Figure 2: Taylor Diagrams displaying the performance of GRAL in reproducing observed concentrations at air quality stations locations, both AQM and low-cost sensors, for (a) first day of forecast, and (b) second day of forecast.

In order to better understanding these statistics analysis, different statistical plots are considered. First, Taylor Diagrams for first and second day of forecast are shown in Figure 2, for all available air quality stations. According to the location of each station statistics at Taylor Diagrams, model performance between first and second day of forecast is quite similar. Also, correlation between modelled and observed concentrations is quite good at the majority of stations, except at sensors 4 and 8.

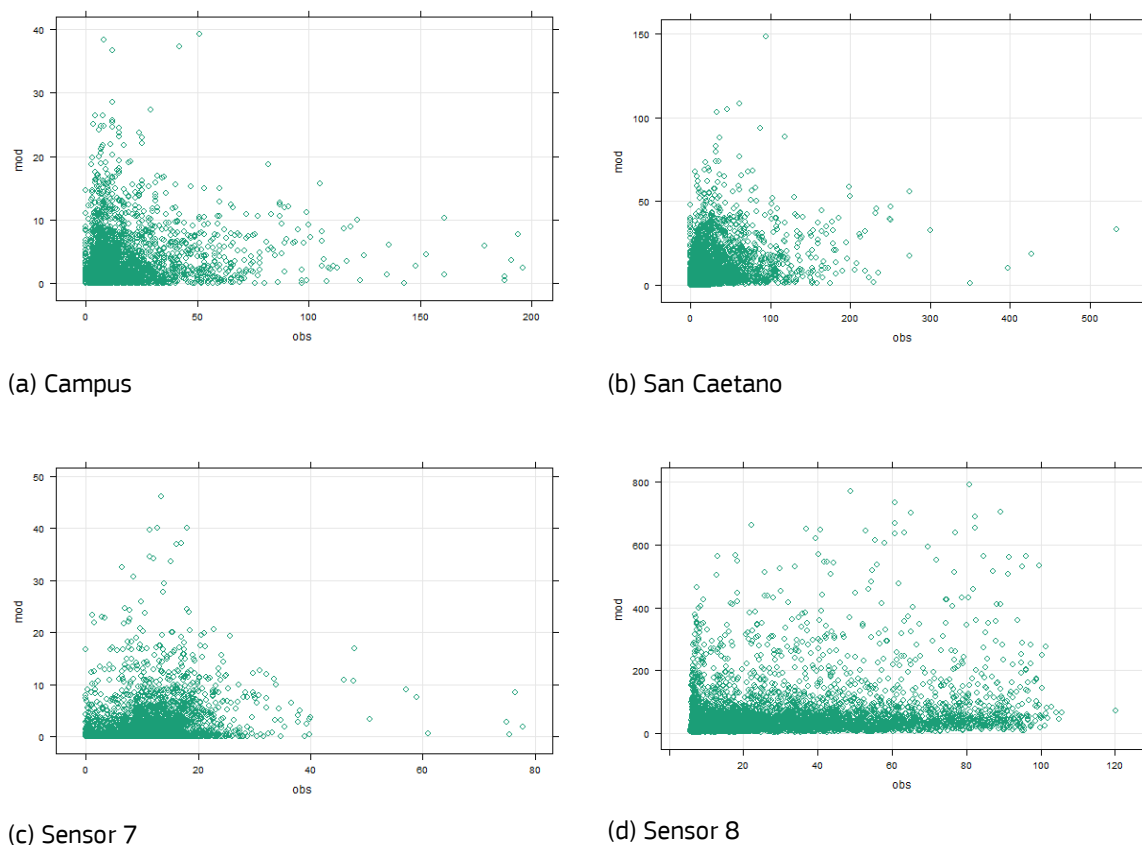


Figure 3: Scatter plots of modelled (mod) vs. observed (obs) NO_x concentrations for the first day of forecast at: (a)-(b) the two AQM stations, and (c)-(d) two low-cost sensors locations, in Santiago de Compostela, for the assessment period May/23/2020 – Feb/28/2021. Concentration in $\mu\text{g}\cdot\text{m}^{-3}$.

In Figure 3 scatter plots of these hourly NO_x concentrations predicted vs. observed along the 1st day of forecast are shown, at four different sites: The two AQM stations, and two selected low-cost sensor sites as the best (sensor 7, model underestimation) and the worst (sensor 8, model overestimation) modelling performance. Most of observed vs. modelled concentrations at the same station cover similar ranges, except at sensor 8, where model strongly overestimate observations. Even though very high horizontal grid resolution ($4\times 4\text{ m}^2$) is applied to compute ground level concentrations at this GRAL operational forecast, it is not enough to get a good estimation very close to vehicles circulation.

In order to decide if an air quality modelling simulation is acceptable FAIRMODE defined MQO criterion (Janssen et al., 2017), based on the model quality indicator (MQI). This is a statistical indicator based on a combination of different statistics from observations vs. model results, that is, the ratio between modelled-observed bias and a quantity proportional to the observations uncertainty. MQO is considered fulfilled when $\text{MQI} \leq 1$. Also, FAIRMODE defined Target Plot, which graphically displays not only MPI but also different statistics to obtain MPI. It is important to notice that, although MQO criteria for model assessment should be applied to 1-year simulation period, in this work it is limited to the available operational forecast period.

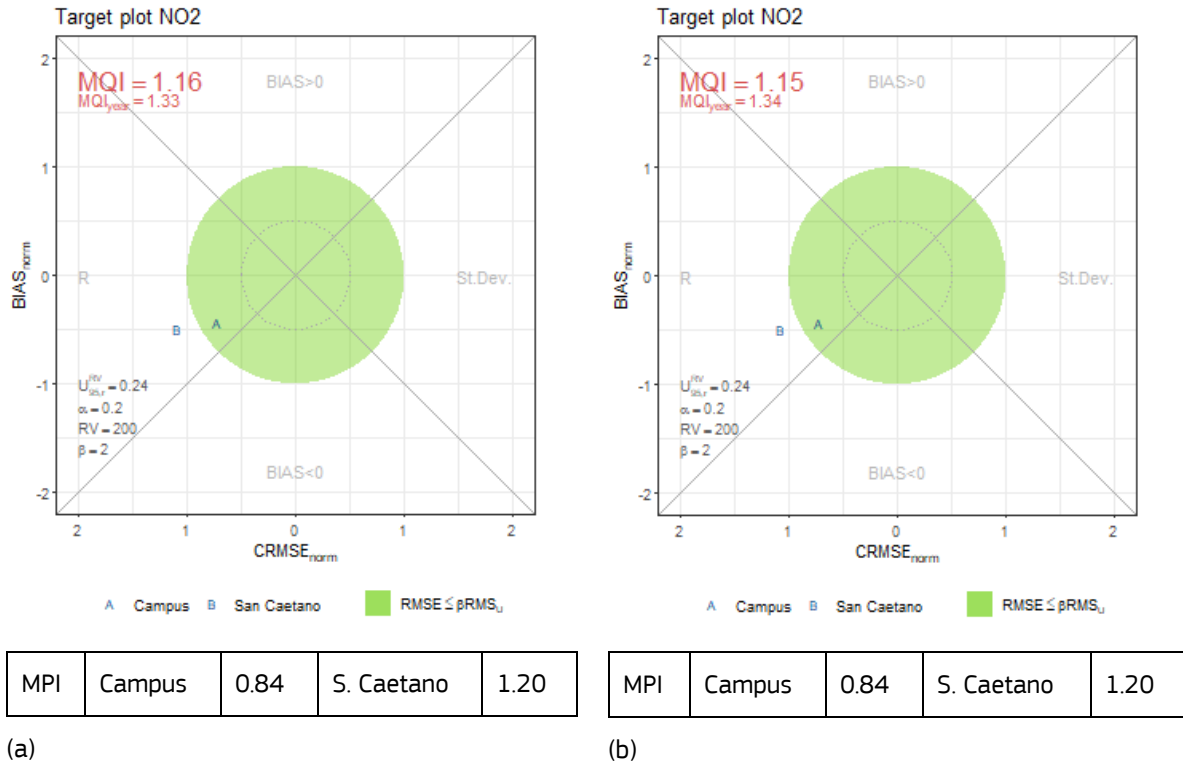


Figure 4: NO_x Target plot for modelled and observed concentrations during the assessment period May/23/2020 – Feb/28/2021 at the AQM stations, for (a) the first day of forecast and (b) the second day of forecast. Also, MPI values per station location are shown.

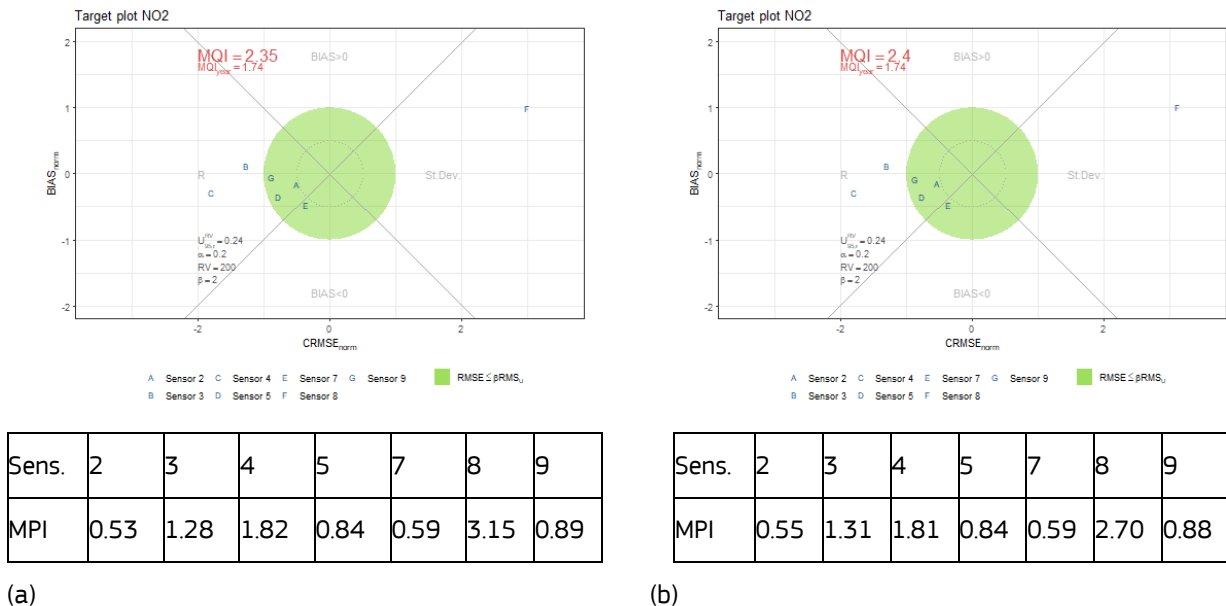


Figure 5: NO_x Target plot for modelled and observed concentrations during the assessment May/23/2020 – Feb/28/2021 at the low-cost sensors stations, for the first day of forecast (a) and the second day of forecast (b). Also, MPI values per sensor location are shown.

According to FAIRMODE, MQO criteria must be accomplished at AQM sites in order to consider that air quality modelling performance is acceptable. Therefore, Figure 4 shows separately Target Plots for modelled and observed NO_x concentrations at the two urban AQM stations in Santiago de Compostela, referred to the first and the second day of

forecast, respectively; including global MPI values. Below each Target Plot, also MPI values for every AQM station are shown. Global MPI values are very similar in both forecast days (1.16 and 1.15), and just a bit higher than 1.0. MQO criterion is fulfilled at Campus station, and also San Caetano station is pretty close to achieve it.

Also MPI values are calculated for low-cost sensors stations, although their locations correspond to street level environments. Figure 5 shows similar Target Plots at the low-cost sensor unit locations in Santiago de Compostela, and their corresponding MPI values. In both forecast days, MPI values at sensors 2, 5, 7 and 9 are pretty good (much below 1.0), while they are poor at sensors 4 and 8, and sensor 3 MPI values are better, but over 1.0 (1.28 and 1.31). About sensors 3 and 8, they are located very close to medium/high traffic intensity streets, so it seems this GRAL operational forecast overestimates NO_x close to vehicles circulation. On the other hand, GRAL model underestimation at sensor 4 could be derived from changes in the road traffic and other activities (including current building of a new Central Bus Station close to it) during the assessment period respect to the typical conditions (Sep-Dec 2019 road traffic patterns) applied in this operational system.

COVID-19 lockdown impact over urban air quality

During the Spanish COVID-19 2020 lockdown started on May 14th 2020 road traffic intensity go dramatically down, as population was closed in their own homes, and only circulation for urgent and first necessities (medicines, food) were allowed. Therefore, it was expected a significant impact in road traffic emissions, with effect in urban air quality.

Figure 6 shows hourly average and peak NO_x concentrations profiles before (Jan/01/2020 – May/13/2020) and during the COVID-19 lockdown period (May/14/2020 – May/31/2020) at two Santiago de Compostela air quality stations: Campus station (urban background station) and low-cost sensors unit 8 located at Galicia Square (urban station in a residential neighbourhood, also with high traffic intensity in normal conditions).

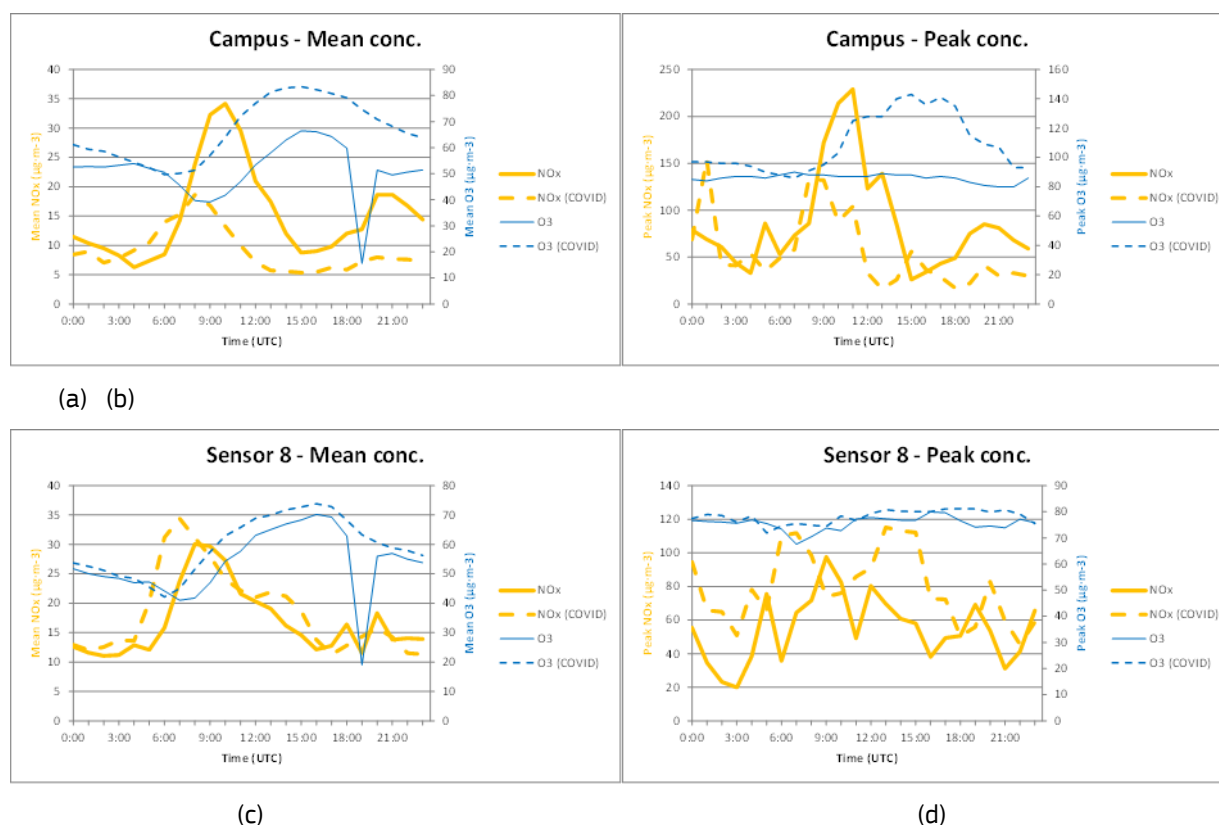


Figure 6: NO_x and O_3 hourly mean and peak concentrations profiles before and during the COVID-19 lockdown period at two different Santiago de Compostela air quality stations: (a)-(b) Campus station (urban background station) and (c)-(d) Galicia Square station (low-cost sensor 8, urban residential with usual high traffic intensity station).

Considering Campus urban background station hourly profiles, as expected both NO_x mean and peak values are reduced during lockdown, but not so far as expected, showing that other urban sources contributions (i.e., domestic heating) are as much important as road traffic in NO_x levels at this background location; about O_3 , a significant increase of

daytime levels is observed during lockdown, especially in hourly O_3 peaks; even though spring weather is dominant during lockdown period, with low to moderate solar radiation. At the opposite, at sensor 8 residential area NO_x increases during lockdown (both mean and peak values), even though road traffic dramatically go down due to restrictions; while O_3 levels are very similar during both periods. As a consequence, it seems domestic heating in this residential area is the most important NO_x source, also increasing NO_x levels during lockdown due to higher domestic activity; while its NO emissions effect in decreasing O_3 ground level concentration is very low, as domestic heating emissions are emitted aloft, so most of NO is converted to NO_2 in the air before achieving sensor 8 at ground level.

Conclusions

Street canyon scales air quality modelling is one of the great challenges, as it requires high spatial resolution over very complex environments with a large variety of different sources. Eulerian-based CFD approaches, including RANS and LES models, are very powerful air quality modelling techniques which also allow including detailed chemistry, but both require a very high resolution grid to achieve meaningful results at street canyon scale. As a consequence, their large computing time requirements are a significant drawback for their application to operational air quality forecast. On the other hand, last generation Lagrangian approaches, as GRAL model, can compute very high spatial resolution primary pollutants concentrations in reasonable time, also at urban environments with a large number of sources; being a feasible candidate to street canyon scale primary pollutants operational air quality forecast.

In this work, an operational air quality forecast based on GRAL Lagrangian Particle Model is tested against NO_x observations from urban background standard stations and street level low-cost air quality sensors, at Santiago de Compostela city downtown. Model performance statistics show quite good agreement between model and observations at urban background stations, and also at most of street level locations; even though applying FAIRMODE assessment criteria designed for regional air quality modelling. However, model deviations strongly depend on the observations location and their surroundings, as usually model underestimates NO_x observations, except at some low-cost sensors located close to vehicle circulation, where model results can suffer strongly overestimation.

In addition, from the comparative analysis of air quality observations before and during COVID-19 2020 lockdown with severe mobility restrictions it is observed that lockdown effects over NO_x and O_3 levels are very different depending on each specific location: During lockdown, at a background urban location station NO_x decreases and O_3 increases (due to lower NO levels) as expected, because road traffic emissions are dramatically reduced. Otherwise, at a residential urban location with high traffic intensity in normal conditions, NO_x increases during lockdown due to the increment of domestic heating emissions around the location, over the road traffic emissions depletion; also O_3 level is a bit higher during lockdown at this location, perhaps because of its lower consumption due to less NO contribution from domestic heating at ground level, respect to the NO contribution from road traffic out of lockdown period.

Although model performance statistics are significant, this first release of GRAL-based operational urban air quality forecast at street canyon level required some approaches to simplify both urban emissions and meteorological inputs. About emissions, significant improvements in traffic modelling reconstruction could be done, in order to get better estimations of road traffic NO_x emissions at every street segment; some DISIT Lab model limited tests shown differences between its results and traffic intensity observations. Other traffic models, as SUMO open source code (Alvarez Lopez et al., 2018), can be a more flexible alternative. Moreover, GRAL meteorological input improvements can be done using GRAMM model (Berchet et al., 2017), including not only buildings topology, but also topographic features in unsteady state conditions; although additional computing time will be required.

This modelling system can be applied not only to provide operational air quality forecast, but also to study different urban emissions scenarios impacts over NO_x levels, i.e., to understand COVID-19 2020 lockdown effects, and to evaluate possible changes in the vehicle fleet at the cities according to the last EU traffic emissions regulations and future road traffic vehicle trends.

Acknowledgement

We thank Environmental Department (Xunta de Galicia) and Santiago de Compostela Municipality for datasets access and support, Technische Universität Graz and M. Kuntner for GRAL model access and support, and O. Zivan (Unimore) for low-cost sensors calibration support. This work is developed in TRAFair Project, co-financed by the Connecting Europe Facility of the European Union, Agreement No INEA/CEF/ICT/A2017/1566782.

References

Ahmad, K. et al. Wind tunnel simulation studies on dispersion at urban street canyons and intersections - a review. *Journal of Wind Engineering and Industrial Aerodynamics*, 93, 697-717, 2005.

- Alvarez Lopez, P. et al. Microscopic Traffic Simulation using SUMO. IEEE Intelligent Transportation Systems Conference (ITSC), 2018.
- Baklanov, A. and Zhang, Y. Advances in air quality modeling and forecasting. *Global Transitions*, 2, 261-270, 2020.
- Bellini, P. et al. WiP: Traffic Flow Reconstruction from Scattered Data. IEEE International Conference on Smart Computing (SMARTCOMP), Taormina, pp. 264-266, 2018. doi: 10.1109/SMARTCOMP.2018.00052.
- Berchet, A. et al. Evaluation of high-resolution GRAMM–GRAL (v15.12/v14.8) NO_x simulations over the city of Zürich, Switzerland. *Geoscientific Model Development*, 10, 3441-3459, 2017. doi: 10.5194/gmd-10-3441-2017
- Bigi, A. et al. Performance of NO, NO₂ low cost sensors and three calibration approaches within a real world application. *Atmospheric Measurement Techniques Discussion*, 11(6), 3717-3735, 2018. doi: 10.5194/amt-2018-26
- Carslaw, D.C. and Ropkins, K. Openair – An R package for air quality data analysis. *Environmental Modelling and Software*, 27-28, pp. 52-61, 2012. <https://CRAN.R-project.org/package=openair>
- Chang, C.H. Computational fluid dynamics simulation of concentration distributions from a point source in the urban street canyons. *Journal of Aerospace Engineering*, 19, 80-86, 2006.
- Bonafè, G. Dartle: A toolkit of R functions for air quality model benchmarking, inspired by the DELTA tool (JRC-IES) and the work of the FAIRMODE WP1. Github, 2017. <https://rdrr.io/github/jobonaf/dartle/>
- European Environment Agency. EMEP/EEA air pollutant emission inventory guidebook 2016. doi:10.2800/247535
- Janssen, S. et al. Guidance Document on Modelling Quality Objectives and Benchmarking. FAIRMODE, Forum for Air Quality Modelling in Europe, 2017.
- Kakosimos, K.E. et al. Operational Street Pollution Model (OSPM) - a review of performed application and validation studies, and future prospects. *Environmental Chemistry*, 7, 485-503, 2010.
- Larssen, S. et al. Criteria for EUROAIRNET: The EEA Air Quality Monitoring. Technical Report No. 12, 1999.
- Li, X.-X. et al. Recent progress in CFD modelling of wind field and pollutant transport in street canyons. *Atmospheric Environment*, 40, 5640-5658, 2006.
- Li, X.-X. et al. Large-eddy simulation of flow and pollutant dispersion in high-aspect-ratio urban street canyons with wall model. *Boundary-Layer Meteorology*, 129, 249-268, 2008.
- McNabola, A., et al. A numerical investigation of the impact of low boundary walls on pedestrian exposure to air pollutants in urban street canyons. *Science of the Total Environment*, 407, 760-769, 2009.
- Murena, F., et al. Modelling dispersion of traffic pollution in a deep street canyon: Application of CFD and operational models. *Atmospheric Environment*, 43, 2303-2311, 2009.
- Oettl, D. Documentation of the Lagrangian Particle Model GRAL 16.8. Technical report, 2016. doi: 10.13140/RG.2.2.16031.76967GRAL
- Oldrini, O. et al. Description and preliminary validation of the PMSS fast response parallel atmospheric flow and dispersion solver in complex built-up areas. *Environmental Fluid Mechanics*, 5, 997-1014, 2017. doi:10.1007/s10652-017-9532-1
- Thunis, P, et al. A tool to evaluate air quality model performances in regulatory applications. *Environmental Modelling & Software*, 38, pp. 220-230, 2012.
- Tominaga, Y. and Stathopoulos, T. Numerical simulation of dispersion around an isolated cubic building: Model evaluation of RANS and LES. *Building and Environment*, 45, 2231-2239, 2010.
- U.S. Environmental Protection Agency. Meteorological Monitoring Guidance for Regulatory Modeling Applications. EPA-454/R-99-005, 2000.
- Vardoulakis, S. et al. Modelling air quality in street canyons: a review. *Atmospheric Environment*, 37, 155-182, 2003.
- Vardoulakis, S. et al. Operational air pollution modelling in the UK - Street canyon applications and challenges. *Atmospheric Environment*, 41, 4622-4637, 2007.
- Yazid, A.W.M. et al. A review on the flow structure and pollutant dispersion in urban street canyons for urban planning strategies. *Simulation-Transactions of the Society for Modeling and Simulation International*, 90, 892-916, 2014.

2.11 Design of a program for the identification and correction of high emitting vehicles in Europe using remote sensing devices

J. Buhigas¹, M. Fleire¹, M. Pujadas²

¹ Opus Remote Sensing Europe, Madrid, 28015, Spain

² CIEMAT - Centro Investigaciones Energéticas, Medioambientales y Tecnológicas, Madrid, Spain

javier.buhigas@opusrse.com

Abstract

The impact from High Emitting vehicles (HE) has been estimated in the past to be from 19% to 60% of the total on-road traffic emissions, depending on the pollutant¹¹. Different studies have estimated that these vehicles represent between 3% to 5% of the circulating fleet [1]. Most of these HEs are faulty vehicles that could be detected, inspected and repaired. That action could reduce their emissions to normal vehicle emission levels and thus significantly decrease the total road transport emissions and consequently the health-related issues that air pollution causes. Remote sensing (RS) technology makes it possible to identify vehicles on public roads that emit high concentrations of pollutants in real-world driving conditions. This technology is used in the USA, China, Hong Kong and South Korea to identify HEs, but it has not been implemented in Europe yet for this purpose. To facilitate this application in Europe, this study explores how the identification of these vehicles on the road could be implemented.

- The first step is to conduct a remote sensing campaign using remote sensing devices (RSD) to screen and characterize the road transport emissions of the circulating fleet. The estimation of the minimum data needed for one of these campaigns consists in at least 100.000 valid measurements. This data should be collected in two different seasonal periods and with a mix of sites that guarantees a homogeneous vehicle specific power (VSP) distribution.
- By analyzing the data from the remote sensing campaign, a limit can be established to define what emission level is so high that a vehicle surpassing the limit is to be considered a HE.
- We propose a methodology that consists of establishing two different emission limits and that requires a minimum of two valid emission measurements per vehicle for a categorization. The first limit, called On-Road High-Emitter limit (ORHE), would represent the top 2% of emissions in the remote sensing campaign (P_{98}). The second limit would be the 20th upper percentile of the dataset (P_{80}). Taking into account these limits, there would be two options to label vehicles as HE: 1) Vehicles that exceed P_{98} once and at least P_{80} another time and 2) vehicles whose emissions are over P_{80} more than 70% of N , being N the number of times the vehicle is measured (with $N > 3$), should also be labeled as HE.
- If an on-road detection of a HE happens, the competent authority will demand the vehicle owner to perform an extraordinary test of the vehicle in a Periodical Inspection Station (PTI), to confirm the faulty function of the vehicle, with tests performed under a controlled environment. However, actual European PTIs lack of competent equipment to correctly assess some of the most harmful pollutants, as NO_x. Our proposed methodology would require that at least a few stations on a given territory (i.e., only two stations per large city) should be equipped with new testing equipment to verify vehicles' emissions more correctly, as current procedures are not adequate.

To evaluate our proposed methodology, the Opus RSD has been compared to different modern vehicle emission testing equipment facilitated by different suppliers. The results indicate that using different measurement techniques (RSD and PTI tests) high NO_x and CO emitting vehicles can be detected both on the road (by the RSD) and during in-situ inspections with new testing equipment. We have also studied the distribution of emissions of vehicles identified as HE by our methodology versus the rest of the vehicles. The results indicate that by applying this high emitter detection methodology, HE vehicles could reliably be identified without producing false positives, that is, without attributing high emitter characteristics to vehicles emitting normal pollution levels.

Introduction

The harmful impact of transportation on the population is one of the most important health problems in the world, especially on cities, where most population concentrates and most vehicles circulate. Urban traffic is the main cause of air pollution. Exposure to air pollution causes direct health problems, such as asthma, hypertension, heart related diseases and cancer. More than 4 million people die each year from environmental pollution [2], resulting deadlier than AIDS, malaria and traffic accidents combined.

¹¹ According to CORETRA project (see ref. [1]), 19% for NO, 40% for HC, 39% for CO and 60% for PM_{2.5}.

Cities main source of air pollution is road traffic. According to data from the inventory of polluting emissions to the atmosphere in the municipality of Madrid [3], road traffic is responsible, in average, of 55% PM_{2.5} air pollution and 48% NO_x pollution in all the region, while in some areas of the city the road traffic is responsible for more than 80% of all NO_x pollution (especially in areas with heavy traffic). This is also a growing problem, since actual demographic trends suggest that by 2050 around 70% of the world's population will live in cities.

Part of this problem is caused by broken, misaligned or tampered vehicles. These vehicles circulate among us emitting very high amounts of polluting substances practically without any control. Various studies (CORETRA 2016, Barcelona 2017, GYSTRA 2018-2021) have identified that high-emitting vehicles (or simply High-Emitters, hereinafter HE) are only around 3 or 5% of the circulating fleet (depending on the study), while they are responsible for around 20% and 60% of the total emissions of NO_x and PM_{2.5}, respectively. This means that it should be possible to decrease up to a 60% of the road transport pollution by identifying only 5% of the worst polluters and taking corrective measures on them. This would also be a minimal impact policy, as air quality could be improved with the least possible sanctioning policies.

The identification of HEs cannot currently be carried out by Periodical Technical Inspections (PTI) in Europe. This is because pollutant emissions from motor vehicles are mainly produced when the vehicle's engine is under load. In European PTIs, only CO emissions or opacity are measured, and they are tested with the engine at idle state, so its emissions in this state may not be realistic. On the other hand, NO_x is one of the most worrying pollutants in cities, mainly produced by road transport, but it is not controlled in the PTI, as it can only be evaluated when the vehicle is under load. Moreover, PTI testing should be traceable to the rest of the vehicle controls, such as the one done in the Type-Approval process, that is with the vehicle loaded or even tested on the road in most recent Euro Standards (RDE test).

To measure remotely the real-driving emissions of circulating vehicles is perfectly possible through optical techniques - and deploying them on the public roads will allow to identify the HEs in an automated and cost-effective way. Although this technique has been used in numerous research projects in Europe there is currently no operational remote sensing program for the identification of high-emitting vehicles in Europe. This experience has been implemented successfully in other countries such as USA, China, Hong Kong and South Korea [4].

State of the art

The first remote technique applied to the vehicle exhaust emissions detection was developed at the University of Denver (USA) and patented in the 1980s. This technique has been verified and validated by numerous research papers, independent testing agencies and accreditation bodies, with extensive literature on the subject [5]. In this study, Opus RS technology has been used, specifically the RSD+ version of the Opus Remote Sensing Device (RSD). A single RSD can measure thousands of vehicles per day. Each measurement is carried out in half a second, through which the device quantifies the pollutant concentrations in the exhaust plume (it evaluates the following regulated pollutants according to the Euro Standard directives: HC, CO, NO, NO₂ and opacity). The RSD also measures the speed and acceleration of the vehicle, the environmental conditions at the time of the measurement (humidity, temperature and pressure) and it automatically takes a picture of the vehicle's license plate.

The Opus RSD has a practical application in the USA, which is the identification of the most polluting vehicles in real-world conditions. For decades, different programs in various states of the country (like Colorado, Indiana, Texas and Virginia) have used RSDs to monitor the circulating fleet on the road, thus identifying the high-emitters [6]. Once identified, their owners are officially notified to undergo a confirmation test at an emissions inspection facility, using ASM or IM240 cycles and dedicated inspection equipment. The results of the application of RS in the USA for this purpose have also been widely published. Moreover, the fact that these programs are still in operation in several territories is proof of their effectiveness in state control of the vehicles' emissions. The use of RS to identify high-emitters on the road has also been used in other Asian countries, such as China, but the available information on the effectiveness of these programs has not been found to be solid. However, this again indicates that this is an application that could be replicated in Europe.

The experience in the USA and Asia shows that the identification of HEs on the road through remote sensing techniques implies the establishment of certain emission limits for each pollutant that mark from which emission value a vehicle is identified as a High Emitter by the RSD. These limits are called ORHE limits: On-Road High-Emitters limits. However, these limits are not universal values. As the fleet circulating in each city or territory is different, as are the urban characteristics, driving behaviours, vehicle maintenance, etc., the distribution of the real-world emissions from road transport is different in every part of the world. In addition, in European regulation there is no specific emission limit for which a vehicle is or is not a HE, since there is no control on real-driving emissions after type-approval. While it is understood that limits should be set to identify extraordinarily high emissions, the specific values are not defined, and it is probably not possible to set single limits for the whole of Europe.

In Europe there have been some initiatives in the past to implement a high-emitter program. In Spain, the Spanish Center for Energy, Environmental and Technological Research (CIEMAT) led the CORETRA project in the years 2014 and 2015 [1], in which the circulating fleet in the Madrid region was extensively monitored for two years with Opus RSDs. As a result, CIEMAT proposed specific emission limits for detecting high emitters, but that proposal was not finally implemented in the Spanish traffic emissions legislation.

Proposed high-emitter control methodology for Europe

One of the regulatory barriers that are holding back in Europe the use of remote sensing for emission control purposes is lack of a legal support for sanctioning or regulating a vehicle solely on the basis of its remote emissions measurement. To solve this issue, a methodology combining an initial identification of a HE with remote techniques and a final verification of the vehicle in an official Technical Inspection centre is proposed. This strategy can be implemented under current European legislation. The high-emitter methodology we propose for Europe consists of the following steps:

- **Set High-Emitter limits:** In order to define the HE limits statistically representative for the circulating fleet of interest; the first step is to develop an extensive remote sensing campaign to get information about the current emitting behaviour of the fleet of interest that will be confronted with these limits. The measurements should be carried out in as many different locations as possible and in at least two different seasonal periods, in order to evaluate a significant sample of the fleet and guaranteeing a homogeneous VSP distribution (0-10, 10-20 and 20-30). It is very important to avoid measuring locations where the possibility of detecting engine cold emissions is not negligible. The number of remote sensing devices, measuring locations and sensors reallocation intervals should be customized for each territory to be screened, as the urban, fleet and socio-economic characteristics of each territory can be very different. The emission data collected should be analysed in order to define the representative HE limits according to the local fleet emissions distribution and the regulatory claims of the competent administration. Another important issue is whether the emission limits should be particularized for each type of vehicle according to fuel type, Euro standard and age, but this should be agreed with the competent authorities in each place.

As predetermined ORHE limits values for the fleet of interest, the 98th (P_{98}) and 80th (P_{80}) percentiles obtained for each pollutant from the monitoring campaign database could be taken. Consequently, a vehicle could be considered HE if it at least exceeds the P_{98} and P_{80} once each or exceeds the P_{80} 70% of its measurements.

- **On-road High-Emitter identification:** The systematic control of traffic emissions by remote sensing monitoring in different places of a given territory will provide the information to identify continuously High Emitters on the road.
- **Notification for verification:** After a positive HE identification occurs, an instant notice can be sent to the vehicle owner by the traffic authority, to require the vehicle to be checked at a PTI in a short period of time. This notification procedure is already envisaged in current legislations in most of Europe. The shorter the time frame the vehicle is inspected, the better the chance of a correct vehicle verification. At the same time, a certain time margin may be considered necessary to provide legal certainty to the owner.
- **Confirmation test at a technical inspection:** The extraordinary inspection would be carried out in an inspection centre equipped with adequate instruments for a complete and dedicated test of polluting exhaust emissions. Some of these possible systems are evaluated in section 4.
- **Correction:** If the vehicle is confirmed as High-Emitter in the verification test, it could lose its circulating permit. To avoid this, the vehicle should be repaired in a workshop in a short period.

Obviously, this methodology of HE detection can be more sophisticated and, for instance, different criteria could be considered for each pollutant. Also, rules to combine two or more pollutants could be defined, but the protocol proposed here is considered to be sufficiently robust. This methodology has been designed to give the least possible number of false positives, ensuring that the vehicles called to extraordinary inspections (as identified as HE on the road) have extreme emissions in at least one of the monitored pollutants. Vehicles that do not exceed the ORHE limit but present frequent emissions between the two limits, strongly contribute also to increase the pollutant emission balance of the fleet and their correction is very important. National or regional authorities should determine the necessity for establishing in each case a specific protocol to adapt the general procedure here proposed to the necessities of each HE control program and the region characteristics.

Example case: High emitter detection applied to Madrid circulating fleet

This section describes the studies, experiments and analyses that have been carried out in Madrid, Spain, to evaluate the suitability of the proposed high-emitter control methodology described before.

Madrid fleet emissions remote sensing screening

The first part of the study concerns the collection of measurements with the Opus RSD+ in real circulating conditions. We have compiled 758352 measurements collected at 22 different locations in the metropolitan area of Madrid between the years 2018 and 2021. These measurements have been carried out under the EU-funded project LIFE GySTRA. From the license plate number identified for each vehicle, the Spanish General Traffic Authority (DGT) provides technical characteristics of these vehicles. The data sample used for this study (see section 5.1) has only passenger cars with sufficient technical information for analysis. This data sample ($n=382180$) has a mean VSP of 10.20 kW/Ton ($s=6.20$), mean ambient temperature of 21.62 °C ($s=7.85$), mean vehicle speed of 37.8 km/h ($s=9.6$ km/h) and mean road slope of 2.32 ° ($s=0.73$). This data sample includes vehicles with an average age of 9.61 years ($s=5.75$). 68.3% of the vehicles analysed in this study are pure diesel-fuelled, 29.9% are pure petrol-fuelled and the rest have another type of propulsion system. The sample is formed by 25.2% Euro 3 and older cars, 25.1% Euro 4, 15.9% Euro 5, 30.3% Euro 6-b, 1.5% Euro 6-c and 1.8% Euro 6-dTemp.

HE identification protocol

The highest measurement values in a remote sensing monitoring campaign represent the highest emission cases of the entire fleet, but they do not necessarily represent the most polluting vehicles in all cases, as the emissions of a vehicle are variable. This means, a vehicle can have a one-time emission level within 2% of the highest values of an entire campaign but have other lower measurements as well. This variability, intrinsic to the vehicle emissions, makes identifying the most polluting vehicles quite complex. However, the pollutant emissions behavior of a High Emitter is typically highly variable too, but with high individual emissions throughout most of its operating cycle [10, 11]. In contrast, a perfectly good-maintained vehicle has relatively low emissions and it is extremely rare for it to have an extremely high emission episode.

Considering the general methodology proposed in section 3 for HE detection, in this study we have defined a procedure adapted to as best as possible to the characteristics of Madrid region. These conditions refer to the fact that a vehicle will be considered a HE on the road (and therefore will be sent for a verification test) if and only if:

- The VSP (kW/Ton) to consider a measurement as valid is between 0 to 30. This range has been established as a normal operating range in an urban environment.
- The minimum number of measurements of the same vehicle above the ORHE limit on a given pollutant is 1.
- The minimum number of measurements of the same vehicle above the 80th percentile (20% most polluting) on the same pollutant is 2.
- The 70% of N, being N the number of times a vehicle was measured (with $N > 3$), are in the 80th Percentile of all the values in a remote sensing monitoring campaign for a given pollutant.

With the above conditions a vehicle could be a HE in one pollutant or in several, but in this study it is proposed to start with a simple protocol that evaluates each pollutant individually with the same logic. It should be noted that the different ORHE limits (for each pollutant) do not depend on the type of fuel.

Once a confirmatory test is established at the PTI, equipped with enough tools to analyze these potentially defective vehicles, the proposed protocol could be tested and improved if necessary. Confirmation tests would show whether the protocol is too rigorous or too lax, based on the results of the confirmatory tests at the inspection station. Likewise, the result of the entire protocol depends on the final tests carried in the inspection stations and the results of these through tests to finally confirm that a vehicle is a HE.

Tests

To further evaluate the capabilities of the Opus RSD system to identify high-emitting vehicles, a series of specific experiments have been conducted in the year 2020. These experiments were carried out at the facilities of the PTI center: ITV Pinto Applus+ (Parcela M-1 3^a, Calle Carpinteros, 13, 28320 Pinto, Madrid, Spain). The study carried out is intended to cover two objectives:

1. To evaluate if a vehicle identified as a high-emitter on the road (in NO_x or CO) with an RSD is also identified as a high-emitter with new testing equipment and new inspection methods at the PTI.
2. To evaluate if a high-emitter can be detected on the road consistently against vehicles that are not so much polluting, despite the variability of vehicles' emissions.

For objective 1, some vehicles measured with the RSD were also measured with new equipment from CAP-ASM and MAHA-MET, testing vehicles on a dynamometer, simulating different loads and measuring NO_x and CO with a probe into the tailpipe. The measurements were done simulating the vehicle in two different regimes: (a) 50% of the vehicle power, speed at 15 mph and in 2nd gear; (b) 25% of the vehicle power at 25 mph and in 3rd gear.

For objective 2, we analyzed the data from the Madrid remote sensing campaign (LIFE GySTRA, see section 4.1).

Measurements with the RSD were done with the OPUS Accuscan™ RSD5000 (to remotely measure CO, NO, NO₂, HC and opacity at 230nm, hereinafter PM) with the vehicle in free circulation on the roadway, in the PTI parking facilities.

For this purpose, 35 different vehicles have been evaluated, which have been subjected to numerous measurements with the RSD at different driving conditions and to different tests carried out by the PTI equipment listed above. Most of these vehicles were provided by customers who voluntarily agreed to participate in the tests. Ten of the vehicles are petrol and the rest are diesel. Table 1 shows the tests that have been performed on each vehicle. The "✓" symbol indicates which tests have been successfully performed for each vehicle.



Figure 1: Pictures of the tests performed at the PTI. Left: tests with dynamometer; Middle and right: tests with the RSD.

Table 1: Tests performed on each vehicle.

Vehicle ID	Fuel type (P= petrol; D= diesel)	OPUS RSD (CO, NO _x , PM)	CAP ASM. 50/15 - 2 ^a		MAHA. 50/15 - 2 ^a		CAP NO _x . 50/15 - 2 ^a	CAP ASM. 25/25 - 3 ^a		MAHA. 25/25 - 3 ^a		CAP NO _x . 25/25 - 3 ^a	
			CO	NO _x	CO	NO _x		NO _x	CO	NO _x	CO	NO _x	CO
1	P	✓	✓	✓				✓	✓	✓	✓		
2	P	✓	✓	✓				✓	✓	✓	✓		
3	D	✓				✓							
4	D	✓				✓							
5	D	✓				✓							
6	D					✓							
7	D	✓				✓							
8	D	✓				✓							
9	P	✓	✓	✓	✓	✓		✓	✓				
10	P	✓		✓	✓			✓	✓				
11	D	✓		✓		✓			✓				
12	D	✓		✓		✓			✓				
13	P	✓	✓	✓	✓	✓		✓	✓	✓	✓		
14	D	✓	✓	✓	✓	✓		✓	✓	✓	✓		
15	D	✓		✓	✓	✓	✓		✓		✓		✓

Vehicle ID	Fuel type (P= petrol; D= diesel)	OPUS RSD (CO, NOx, PM)	CAP ASM. 50/15 - 2 ^a		MAHA. 50/15 - 2 ^a		CAP NOx. 50/15 - 2 ^a	CAP ASM. 25/25 - 3 ^a		MAHA. 25/25 - 3 ^a		CAP NOx. 25/25 - 3 ^a	
			CO	NOx	CO	NOx	NOx	CO	NOx	CO	NOx	CO	NOx
16	D	✓	✓	✓	✓		✓		✓				✓
17	D	✓	✓	✓	✓	✓		✓	✓	✓	✓		
18	P	✓		✓	✓	✓		✓		✓			
19	P	✓			✓			✓		✓			
20	D	✓	✓	✓	✓	✓		✓	✓	✓	✓		
21	D			✓		✓	✓		✓		✓		✓
22	P	✓	✓	✓	✓	✓	✓	✓	✓	✓	✓		✓
23	D	✓	✓	✓	✓	✓		✓	✓	✓	✓		
24	D	✓	✓	✓	✓	✓	✓	✓	✓	✓	✓		✓
25	D	✓	✓	✓	✓	✓	✓	✓	✓	✓	✓		✓
26	P		✓	✓	✓	✓				✓	✓		
27	D		✓	✓	✓	✓		✓	✓	✓	✓		
28	D		✓	✓	✓	✓		✓	✓		✓		
29	D			✓		✓			✓		✓		
30	D	✓		✓		✓	✓		✓		✓		✓
31	D			✓		✓			✓		✓		
32	D			✓	✓	✓			✓		✓		
33	P	✓	✓	✓	✓	✓		✓	✓	✓	✓		
34	D	✓	✓	✓	✓	✓			✓	✓	✓		
35	D	✓		✓	✓	✓			✓	✓	✓		

Results

Remote sensing screening results and proposed on-road high-emitter limits for Madrid

From the remote sensing screening in Madrid (see section 4.1), the data is analysed. Considering that an RSD directly reports emission in ratios of pollutants with respect to CO₂ (in the case of particulate matter, it simply reports opacity at 230 nm), emission limits should be set at the same magnitudes that the system provides, in order not to introduce further transformations. Table 2 shows the results obtained in Madrid with the data sample explained in section 4.1 and the ORHE limit calculation procedure as defined in section 4.2. The methodology results in a share of high-emitters between 3.67% and 5.28% of the whole fleet, depending on the pollutant. The last column shows the estimated share of total emissions these vehicles are responsible for, assuming that their respective emitting behaviours are always similar in all conditions. As we are evaluating only passenger cars, this refers to the share of total emissions caused by this type of vehicles. For instance, the table shows that 5.28% of the most polluting cars in NO are responsible for 17.81% of all NO emissions emitted by all passenger cars.

Table 2: Average passenger cars emissions and ORHE limits for Madrid, Spain.

Pollutant	Magnitude (units)	Average fleet value	ORHE limit (P ₉₈)	Lower limit (P ₈₀)	Vehicles that are categorized as HE (number and percentage of the fleet)	Share of total cars emissions emitted by the HEs
Nitrogen oxide	NO/CO ₂ (ppm/%)	19.7	101.2	42.3	n=4701; 5.28%	17.81%
Nitrogen dioxide	NO ₂ /CO ₂ (ppm/%)	5.8	58.4	13.1	n=4203; 4.9%	26.29%
Particulate matter	Opacity in UV at 230nm (%)	0.16	2.6	0.3	n=3493; 4.01%	41.04%
Carbon monoxide	CO/CO ₂ (%/%)	0.005	0.05	0.006	n=4117; 4.32%	23.04%
Hydrocarbons	HC/CO ₂ (ppm/%)	2.0	15.1	5.0	n=3061; 3.67%	18.83%

Note that these limits would apply generically to any passenger car (and could possibly include vans and other light vehicles), regardless of the type of fuel used by the vehicle, its age, engine size or any other technical characteristics. Also, the percentages on the previous table refer to the vehicles that could potentially be considered as HE (in the range of VSP 0-30, with at least two correct measurements per pollutant and being passenger cars).

To evaluate if a common ORHE limit can be set to all vehicles, regardless of their technical characteristics, Figure 2 shows the average emissions of HE and non-HE vehicles per fuel and euro standard for nitrogen oxide. The graphs show that the mean emissions of the non-High Emitters differ abruptly from petrol to diesel cars, while the mean emissions of High Emitters are similar regardless of the fuel type. Also, even if there are differences by Euro Standard, the lowest mean emission of a HE group (8.2 g/kg) is higher than maximum mean value of any non-HE groups (7.0 g/kg), indicating that these limits can be established as common for all the fleet, independent to the fuel type and Euro Standard. This is further explored in section 5.3.

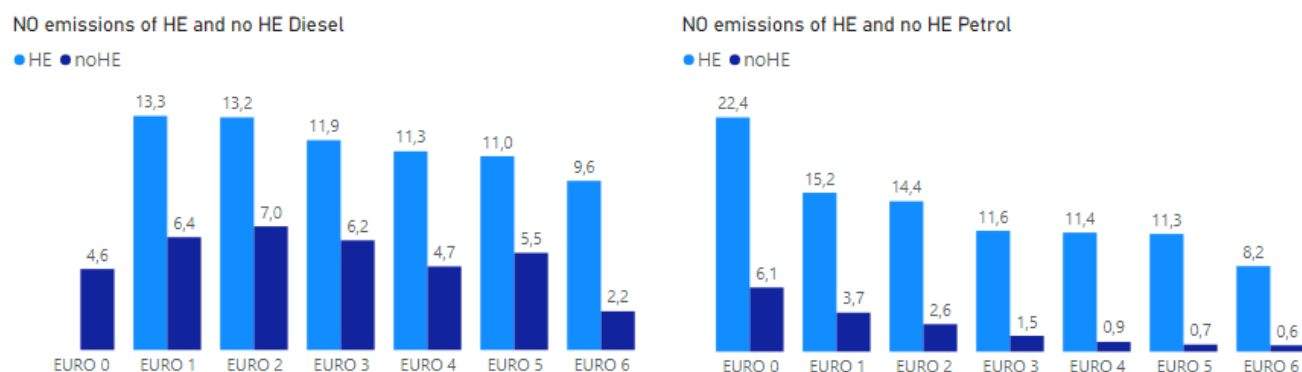


Figure 2: NO fuel-specific emissions (g per kg-fuel) of HE (light blue) and non-HE (dark blue) passenger cars by fuel and Euro Standard (x-axis). Left chart, diesel cars; right chart, petrol cars.

Comparison of remote sensing with new inspection testing equipment

From the experiments listed in Table 1, comparative measurements of carbon monoxide (CO) and nitrogen oxides (NOx) are made (RSD vs CAP and RSD vs MAHA). The measuring methods and measurement magnitudes of each equipment are completely different, so a direct and quantitative comparison of the measurements provided by each system cannot be made. Furthermore, the measurements of each vehicle with the different methods and equipment have not been made at the same time (the vehicle was tested with one equipment and then moved to conduct a test with another equipment). As the emissions of a vehicle are variable, there may not necessarily be a relationship between the measurement of a vehicle with one method or another. However, the objective of these tests is to simply assess whether the qualitative identification of the emission status of a vehicle with one measurement method is similar to the qualitative identification of another method. In other words, it is of interest to know whether when one

measurement method indicates that a vehicle has relatively high emissions, a different method shows a similar indication. Similarly, if an equipment shows a low level of emissions, the other equipment should indicate the same.

To make this qualitative comparison, the 35 vehicles on Table 1 have been taken as control fleet and the average values for all the measurements of each pollutant obtained with each method have been taken as reference values to analyze the behavior of the individual vehicles checked with the same measurement system. Afterwards, the individual values given by the correspondent equipment for a specific vehicle and the average reference values are calculated. This comparison is shown in Figure 3 and Figure 4. The results show that both measurement methods can identify when a vehicle has much higher emissions than other vehicles, for CO and NOx.

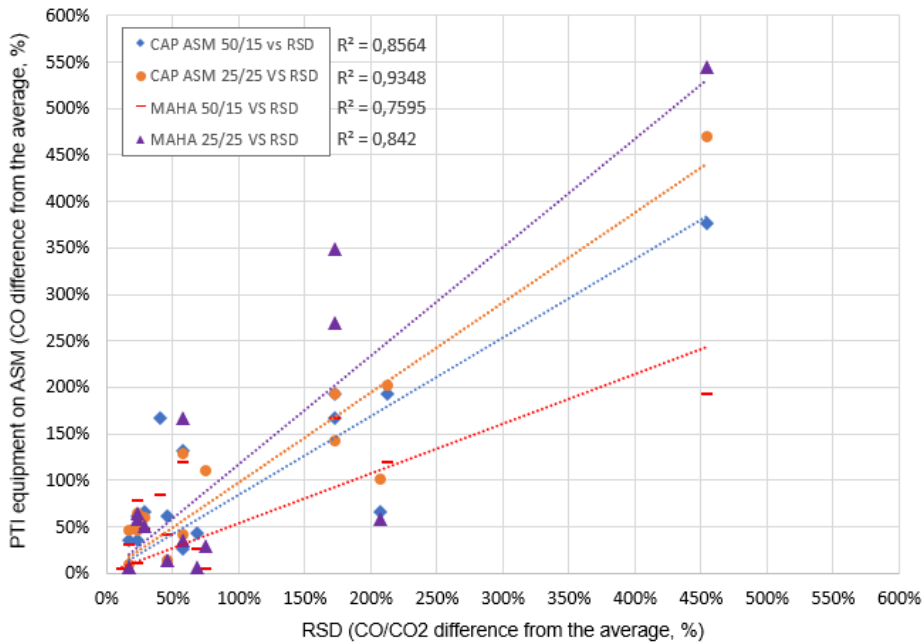


Figure 3: CO comparison between the RSD to CAP and MAHA systems. The X-axis shows the percentage difference of each vehicle's CO/CO₂ measurement done with the RSD compared to the average of all other RSD measurements. The Y-axis shows the percentage difference of each vehicle's CO measurement with the CAP and MAHA systems compared to the average of all CO measurements of these systems.

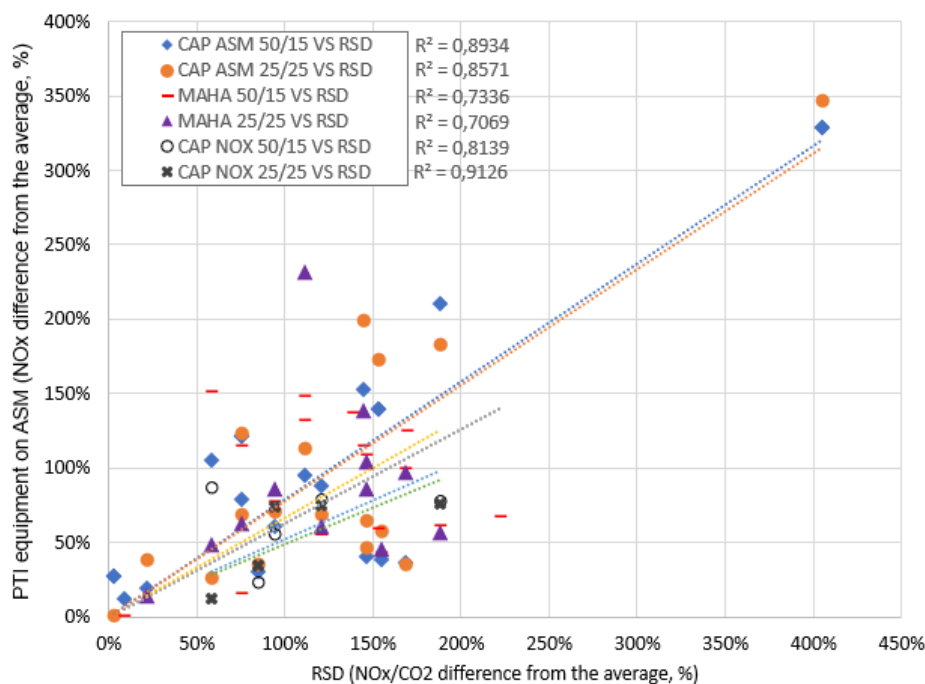


Figure 4: NOx comparison between the RSD to CAP and MAHA systems. The X-axis shows the percentage difference of each vehicle's NOx/CO₂ measurement done with the RSD compared to the average of all

other RSD measurements. The Y-axis shows the percentage difference of each vehicle's NO_x measurement with the CAP and MAHA systems compared to the average of all NO_x measurements of these systems.

Emissions assessment of a high-emitting vehicle

To assess the effectivity of the proposed high-emitter methodology, we evaluate the real-world behavior of high-emitters and non-high-emitters. Five of the vehicles that were measured most times in the Madrid remote sensing campaign are selected and plotted on Figure 5. Three of these vehicles are classified by the high-emitter protocol as non-HE and two other vehicles are classified by the high-emitter protocol as HE in nitrogen monoxide (NO). As NO emissions are typically higher in diesel-fueled cars, only this fuel has been selected for a proper comparison. A summary of the main characteristics of these vehicles is shown in Table 3.

Table 3: Technical characteristics of five random vehicles measured more than 40 times by the RSD.

Vehicle ID	Fuel type	Euro Standard	Manufacturer	Model	Engine power (kW)	HE (Yes/No)
228700	Diesel	EURO 4	MERCEDES	CLASS E	140	No
246907	Diesel	EURO 6b	MERCEDES	CLASS E	143	No
257376	Diesel	EURO 5b	RENAULT	MEGANE	81	Yes
267939	Diesel	EURO 4	RENAULT	MEGANE	63	Yes
273741	Diesel	EURO 6b	RENAULT	CLIO	66	No

All these vehicles had more than 40 valid measurements with VSP between 0-30 kW/Ton. They are examples of typical vehicles that can be found in any European city. Each point in the graph represents an individual measurement of NO to CO₂ ratio. As it is known that NO emissions have an increasing tendency dependence on vehicle specific power, this analysis also allows to observe the sensitivity of finding a high emitter over a wide range of VSP.

The graph shows the higher variability of HEs and their tendency to high emission levels at any VSP. It can be seen that individual emission events of a high-emitter are most of the time above the lower limit (P_{80}) and even sometimes above the upper limit (ORHE, P_{98}). On the contrary, non-HEs have variable emissions, but consistently below the two limits, regardless of the VSP and other real-world factors. Even if the non-high emitting vehicles sometimes overpass the lower limit, this is a rare event, so it would be extremely unlikely that these vehicles could be classified as a HE with the proposed protocol. Also, if a vehicle does not overpass the ORHE limit but stays in the zone between both limits, it is safe to say that it can be classified as a high-emitter, as it would be showing the same behavior of a HE even without any individual emission was above the ORHE limit.

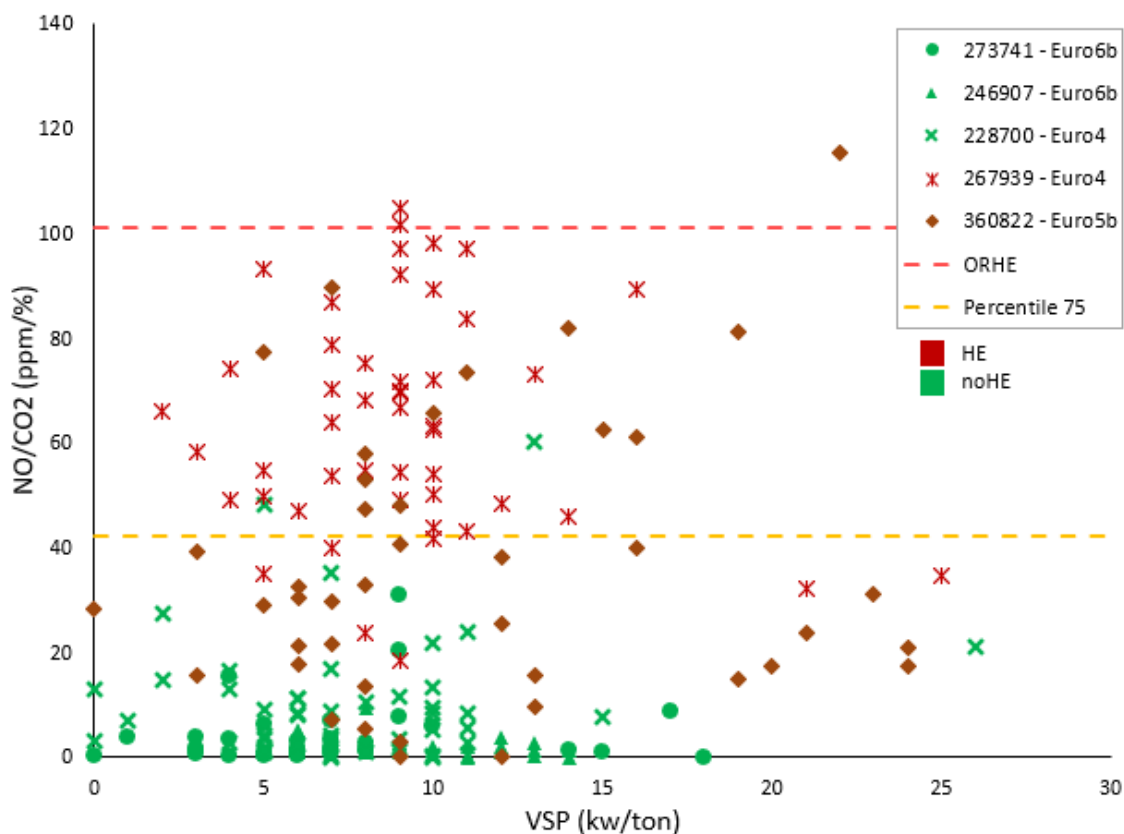


Figure 5: NO emission ratios (NO/CO₂) of five vehicles measured at least 40 times by the RSD in Madrid's roads. VSP is represented in the X axis. Red markers: individual measurements of vehicles classified as HE. Green markers: individual measurements of vehicles classified as non-HE. Upper horizontal dash line: ORHE limit of NO (101.2). Lower horizontal dash line: Lower limit of NO (42.3).

Conclusions

The results show that the Opus RSD can be used in Europe to identify high-emitting vehicles and that a methodology can be defined to identify high-emitters on the road by the RSD and be inspected for verification in a well-equipped inspection station, providing full traceability and legal safety on the driver. Other relevant conclusions of the study are:

- We estimate that the sample needed to define ORHE limits on a given territory should be at least 100.000 valid measurements of the vehicles to be subject to the program (i.e., passenger cars) measured with RSDs. To consider ambient and driving-style variability, this data should be collected in two different seasonal periods and with a site mix that guarantees a homogeneous and wide VSP distribution.
- The proposed methodology consists of defining two limits (for each pollutant) based on the collected remote sensing data. The first limit (ORHE) is the Percentile 98 of emissions from the remote sensing campaign. The second limit is the Percentile 80. Vehicles that exceed each limit at least once with at least two different observations or vehicles that have a continuous high-emitting behavior (70% of their measurements exceeding the top 20% of the fleet emission records) would be classified as HE. Our assessment indicates that this criterion clearly identifies in a safety way whether or not a vehicle is a HE despite the variability of its emissions. The results suggest that the emission performance of a HE has a distinguishable pattern on the road.
- The results indicate that it could be possible to set a single ORHE limit (per pollutant) irrespective of the type of vehicle measured by the RSD. Figure 5 shows that a HE can be an old or a modern vehicle (i.e. Euro 6b), of any fuel type and of any brand, model or engine power. This limit simplification would greatly facilitate the implementation of a HE program for two reasons. First, because otherwise individual limits would have to be designed for each vehicle type (which would require estimating and testing the suitability of dozens of different limits). Second, because otherwise the emissions of each vehicle would have to be checked against its technical characteristics, which would be too technically complex and would require a level of harmonization of technical data in traffic databases that does not exist today.

- The results indicate that there is a good correlation between the identification of a heavily polluting vehicle with the criteria established from the remote on-road measurements with RSD and the dynamometer measurements and direct exhaust measurements. In particular, CO and NO_x measurements made with the Opus RSD adequately correlate with CAP and MAHA results.
- Our estimations show that a few high-emitting vehicles (between 4.3% and 5.6% of the circulating fleet) are responsible for a significant portion of the total emissions generated by all road urban traffic. Specifically: 18.9% of NO, 29.5% of NO₂, 44.4% of PM_{2.5}, 25.7% of CO and 22.2% of HC. These figures are consistent with other studies [1]. The large contribution of HEs on particulate matter emissions is noteworthy, possibly due to vehicles circulating without a particulate filter or with a broken particulate filter.
- High-emitters are most likely to be found by RSDs in cities, as this is where most vehicles circulate and where the air quality problem is severe. As the number of HEs found in cities will be very small (around 5%, as mentioned before), there would only need to be one or two properly equipped stations per every large European city to properly verify these vehicles. This will reduce the investments needed to improve vehicle monitoring in Europe, as not all stations would need to be modernized.
- As far as we know, there is currently no industry consensus or scientific clarity as to what new equipment or inspection methods should be implemented in Europe to improve the control of vehicles' emissions in the PTIs, especially for assessing NO_x emissions. According to all the studies performed during our research, we believe it is feasible to consider that the RSD could become an inspection system to be installed inside the PTI. It is known that this system can assess with sufficient accuracy whether a vehicle is a high emitter on the road and that this categorization is in line with that of other sensors (CAP and MAHA). Since the RSD can evaluate all pollutants currently regulated by the EU (NO_x, CO, PM and HC) at the same time, it could be a low-cost equipment to be installed permanently in the PTI to check vehicles previously identified on the road. This approach, in turn, would increase the traceability of the entire program, since a vehicle identified on the road as a HE would be verified with the same technology, but in a controlled environment, in an inspection center.

Acknowledgements

This project was funded by the European Commission within the LIFE programme in the GySTRA project: <https://lifegystra.eu>. The authors thank Applus+ for their excellent and professional collaboration and for facilitating a site and equipment to conduct the tests.

References

- Pujadas M. et al, Real-driving emissions of circulating Spanish car fleet in 2015 using RSD Technology, *Science of The Total Environment* 576, 2017.
- Jens Borcken-Kleefeld and Tim Dallmann "Remote Sensing of motor vehicle exhaust emissions", ICCT 2018
- Landrigan P. J., Air pollution and health, *The Lancet*, 2017.
- Estudio para la cuantificación de la contribución de fuentes a los niveles de calidad del aire en el municipio de Madrid, Universidad Politécnica de Madrid, 2017.
- Carsten G. et al. Potential of Remote Sensing Devices (RSDs) to screen vehicle emissions, Publications Office of the European Union, 2019.
- McClintock, P., The Colorado Remote Sensing Program January–December 2011, Colorado Department of Public Health and Environment, 2012.
- Dallmann T. et al., Remote sensing of motor vehicle emissions in London, *The ICCT*, 2018.
- Feng A. et al. Development of Comprehensive Modal Emissions Model, Contractor's Final Report for NCHRP Project 25-11, 2000.
- Bernard Y. et al. Worldwide use of remote sensing to measure motor vehicle emissions, *The ICCT*, 2019.
- Yuhan H. et al. Remote sensing of on-road vehicle emissions: Mechanism, applications and a case study from Hong Kong. *Atmospheric Environment*, 2018.
- Bishop, G.A et al., Multispecies remote sensing measurements of vehicle emissions on Sherman Way in Van Nuys, California. *Journal of the Air & Waste Management Association*, 2012.

2.12 Environmental assessment of different transport modes for all lifecycle stages

K. Biemann^{1*}, W. Knörr¹, M. Allekotte¹, H.-J. Althaus², D. Sutter², T. Bergmann³

¹ Institut für Energie- und Umweltforschung Heidelberg gGmbH, D

² INFRAS Zürich, CH

³ formerly at Öko Institut

kirsten.biemann@ifeu.de

Introduction

There is great demand for ecological comparisons of different types of transport in the environmental policy debate. So far, the focus of most existing analysis are on the well-to-wheel emissions (use phase and energy provision). We expanded the scope by including the other relevant lifecycle stages: vehicle and infrastructure supply. Furthermore, we included a wide range of impact categories (GHG emissions, air pollution, cumulative energy demand, cumulative raw material demand, traffic areas) in our analysis. In addition to these classic impact indicators, traffic accidents and external costs were also assessed.

Methodology and data

To be able to compare different types of transport the entire life cycle of the vehicles, from manufacture to use phase and disposal, as well as the required transport infrastructure was included into the assessment.

The following life cycle stages were described:

- Use phase (vehicle operation including energy consumption and exhaust gas emissions)
- Energy supply of fuels and electricity
- Production, maintenance and disposal of vehicles
- Construction, maintenance and operation of the required transport infrastructure

All relevant modes of transport (road, rail, water and air) as well as the associated means of transport were analysed.

Table 1: Transport types.

Term	Content
Mode of transport	Road, rail, water, air
Transportation mode	Passenger transport, freight transport
Means of transport	foot, bicycle, pedelec, car, motorcycle, moped, local and regional bus, long-distance bus, coach, tram, city railway, metro, long-distance train, local train, cargo bike, light commercial vehicle, lorry, truck train, articulated truck, freight train, inland waterway vessel, aircraft

Transport is associated with a range of environmental impacts. The most important impact categories were investigated in a comparison of types of transport:

- Greenhouse gas emissions
- Air pollutants: nitrogen oxides (NO_x), particulate matter (PM_{2.5} and PM₁₀) and carbon monoxide, non-methane hydrocarbons and sulphur dioxide
- Resource consumption based on cumulative energy demand (CED), cumulative raw material demand (CRD) and land use

In addition to these classic impact indicators, noise pollution, traffic accidents and external costs were also included in the transport type comparison.

The focus of this paper will be on greenhouse gas emissions and nitrogen oxides as well as particulate matter (PM₁₀). All results describe the situation in Germany in 2017.

Main results and discussion

Passenger transport

One of the main indicators used was the climate impact.

In Figure 1, the distribution of transport modes according to the number of trips, transport performance (passenger kilometres) and climate impact (in CO₂ equivalents) is compared. Outbound international air traffic is included in this representation.

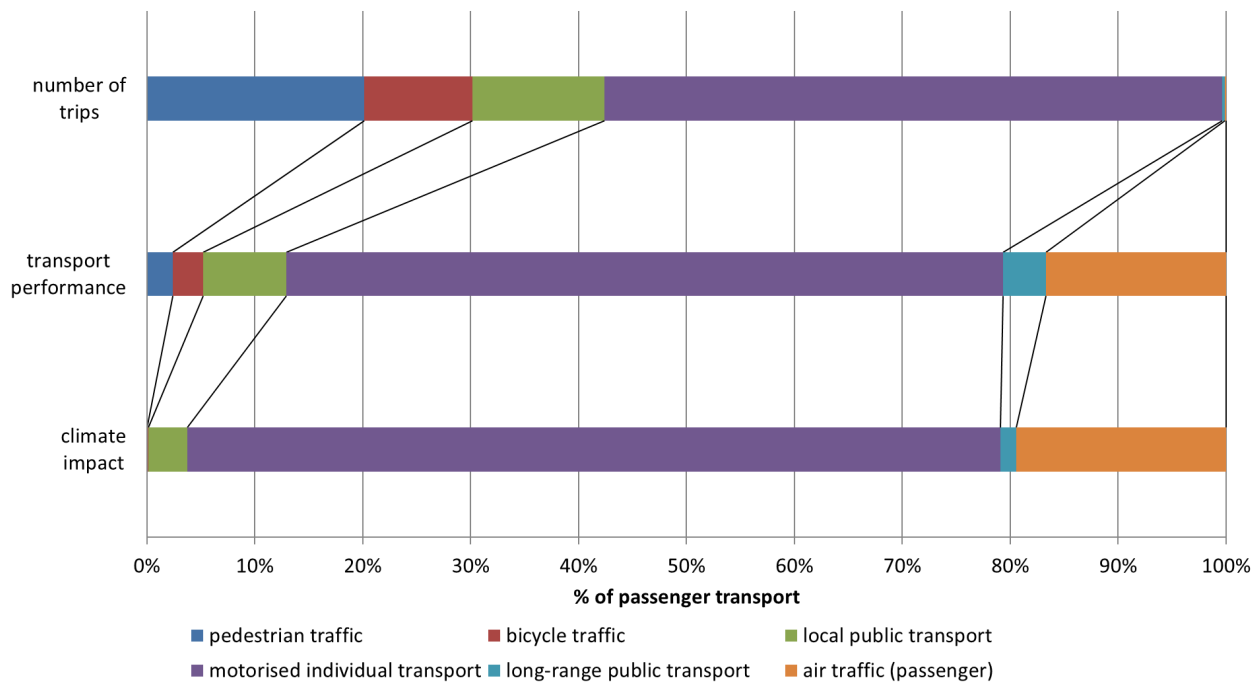


Figure 1: Importance of different transport modes and climate impacts.

The most climate-friendly modes of transport are walking and cycling. Almost every third trip is made on foot or by bicycle in Germany. However, since the distances travelled are relatively short, walking and cycling account for only 5% of transport performance. The resulting climate impact is almost zero. Local public transport is also an environmentally and climate-friendly way of being mobile. It provides 8% of the transport performance, but causes only 4% of the greenhouse gas emissions of passenger transport.

Car and motorcycle travel show the greatest climate and environmental impact in comparison: they account for 57 % of trips, 66 % of transport performance, but 75 % of greenhouse gas emissions. Flying also has a comparatively high impact on the climate: Air traffic originating in Germany accounts for only 0.1 % of trips and 17 % of transport performance. However, its share of the climate impact is 19 %.

Some detailed results for local transport (see Figure 2) are:

- Pedestrian and bicycle traffic cause very low GHG emissions, which result primarily from vehicle provision. For pedelecs, the electric drive using electricity causes a relevant, but comparatively small amount of emissions.
- Buses and trains have around six to nine times higher GHG emissions than bicycles and pedelecs. The importance of the individual life cycle stages differs: In the case of rail transport, the contribution of infrastructure is significantly higher than for regular buses. For electric-powered railroads, a large part of the GHG emissions comes from energy provision, while for internal combustion vehicles it comes from direct use. The contribution of vehicle provision is relatively low for all these systems because of the high mileage over the life of the vehicle.
- Passenger cars, on the other hand, have on average two to three times higher specific GHG emissions per passenger kilometre than buses and trains. In addition to vehicle use, climate impacts are also significantly determined by vehicle production.

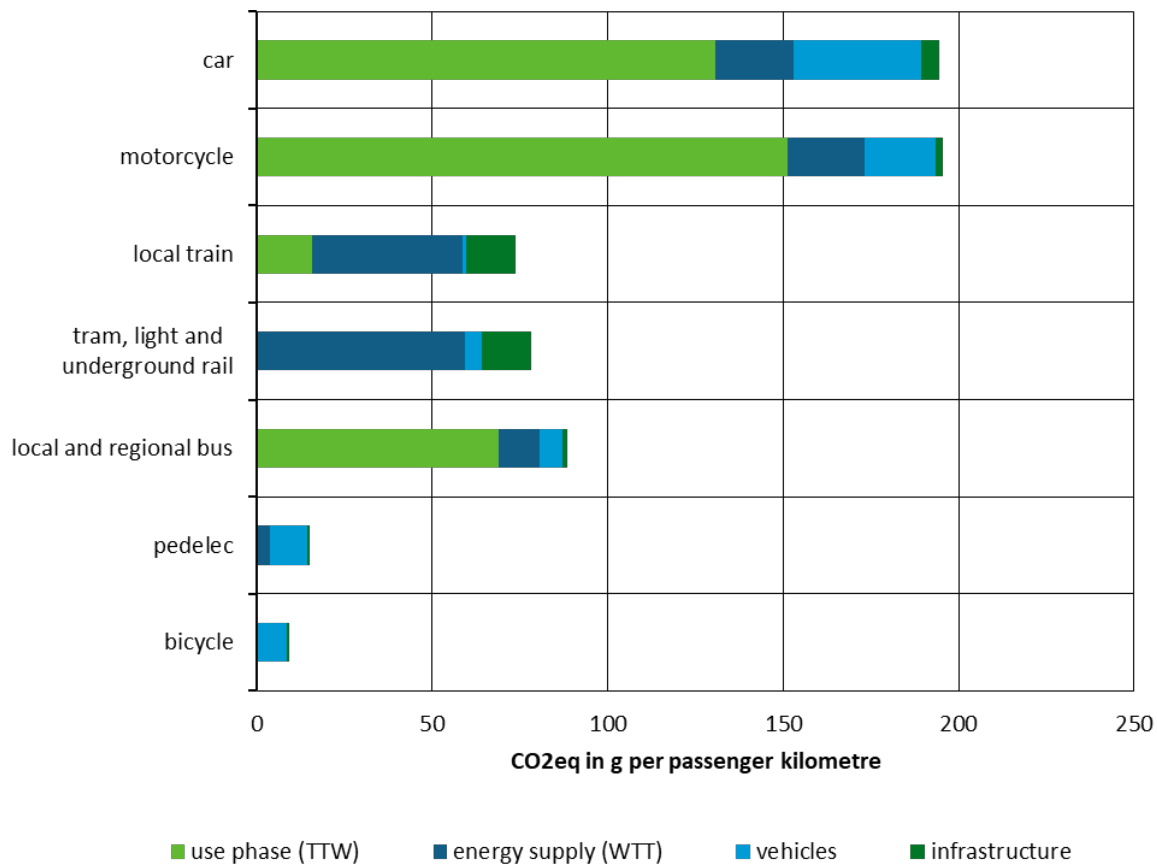


Figure 2: Climate impact of passenger transport (short distance).

For long-distance traffic (see Figure 3):

- Bus and rail perform best. In the case of buses, vehicle operation dominates by far, while for railroads, the provision of electricity has the greatest impact on the climate. For rail the construction of the infrastructure has a relevant share.
- On average, passenger cars have four to five times higher specific GHG emissions per passenger kilometre than buses and trains. This is due to vehicle operation and by a lesser extent due to vehicle provision. For passenger cars, vehicle provision play a bigger role than for all other modes of transport.
- The climate impact of air travel is the highest. Here, with increasing travel distance, it is primarily the additional climate impact of aircraft emissions at high altitude (NO_x , particulates, water vapour) as well as direct greenhouse gas emissions from fuel usage that have an high share, while aircraft production and infrastructure construction have a relatively low impact due to the high mileage of an aircraft.

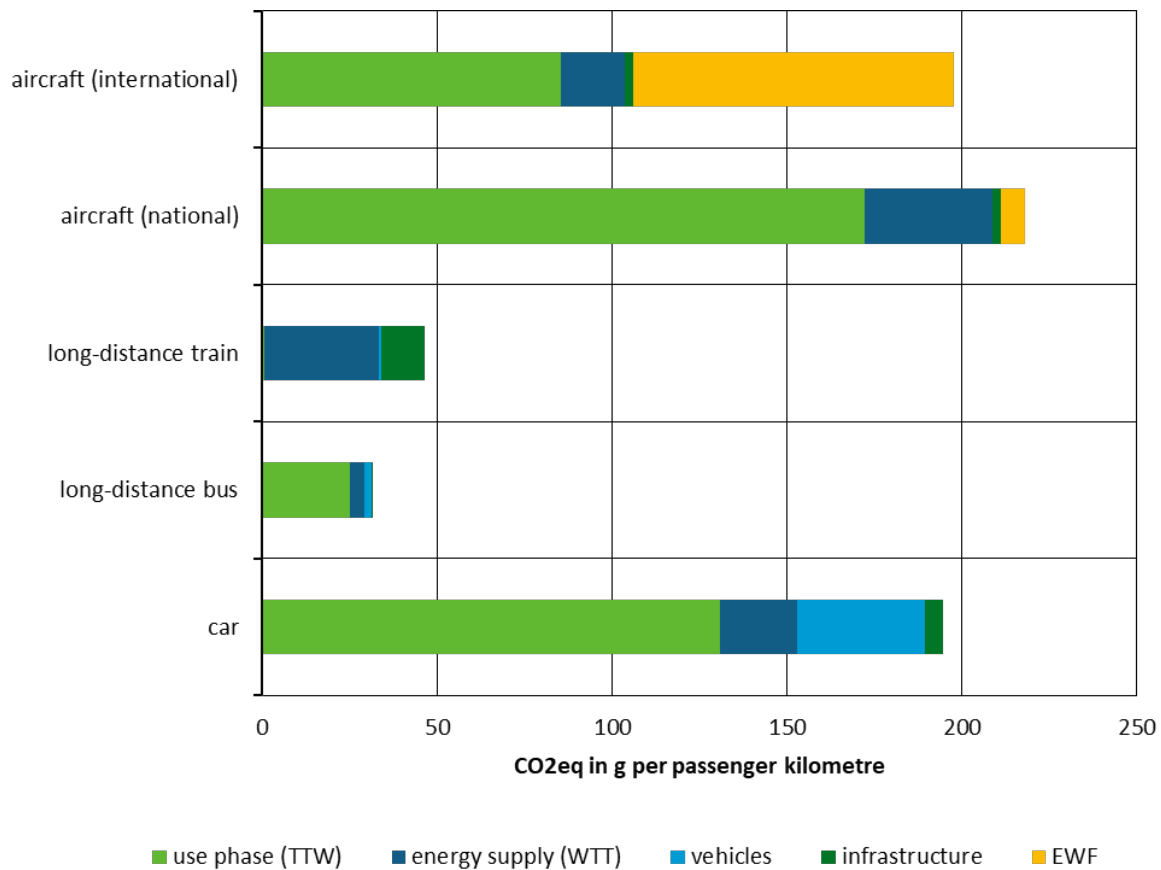


Figure 3: Climate impact of passenger transport (long-distance).

Unlike greenhouse gases, air pollutants are mostly relevant for local air quality. Therefore, direct tailpipe emissions emitted near settlements are assessed differently than emissions from energy, vehicle and infrastructure provision and emissions from air traffic at cruising altitude.

In recent years, tailpipe emissions have been greatly reduced by emissions legislation. However, there are still numerous locations where the applicable air pollution limits, especially for NO_2 and PM_{10} , are not met. In most cases, road traffic contributes relevant amounts to air pollution in these areas.

Other life cycle stages contribute to background pollution, such as power plants close to cities, refineries and production facilities, or construction work on the transport network. These emissions always occur temporally before vehicle use.

The following figures show the specific NO_x and particulate emissions of the means of transport in local and long-distance passenger traffic. The high proportion of NO_x emissions from the use of cars as well as trains and buses with combustion engines in local transport is clearly visible.

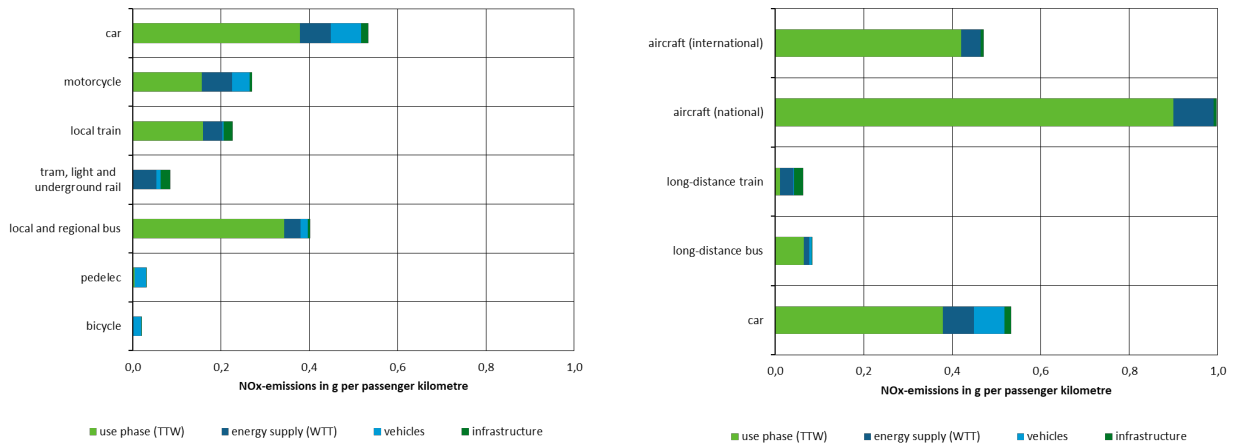


Figure 4: Air pollutant emissions of passenger transport (NO_x).

PM₁₀ emissions from cars and buses have been significantly reduced in the past by particulate filters. Nevertheless, coaches and long-distance buses cause significantly lower PM₁₀ emissions per passenger kilometer than passenger cars. Air traffic causes high direct emissions, but only a small part of these emissions is emitted near the ground at airfields. At cruising altitude, these additionally affect the climate. A large proportion of particulate emissions do not come from combustion in the vehicle, but are generated during the processes of the other life cycle stages.

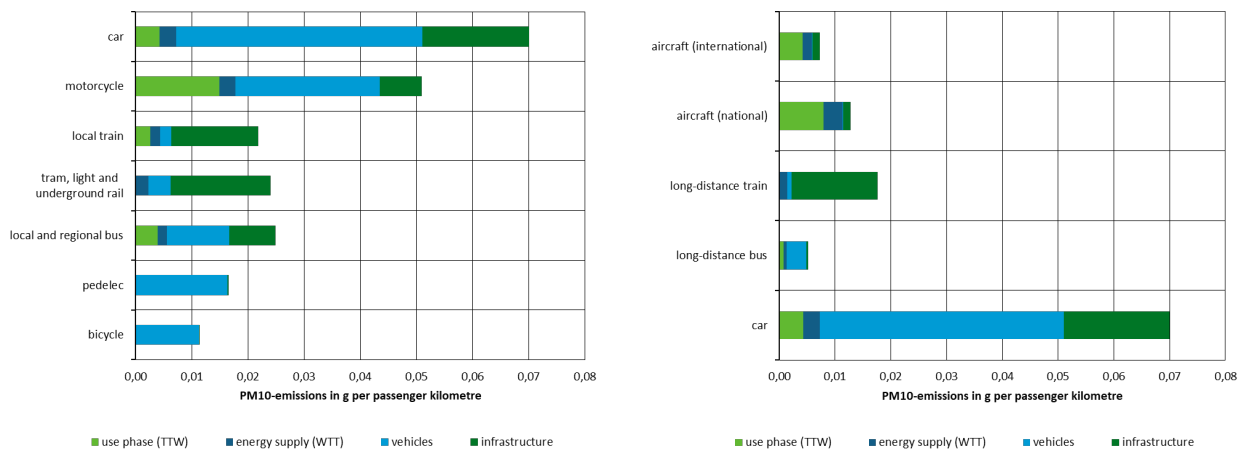


Figure 5: Air pollutant emissions of passenger transport (PM₁₀).

Freight transport

The Figure 6 compares the distribution of transport modes for freight transport by number of trips, transport performance (ton kilometres) and climate impact (in CO₂ equivalents), including outbound international air traffic. The comparison does not include cargo bikes, as no basic transport data is yet available for them in Germany and therefore no - certainly still very low - total emissions can be determined. For light commercial vehicles, GHG emissions can be calculated on the basis of mileage.

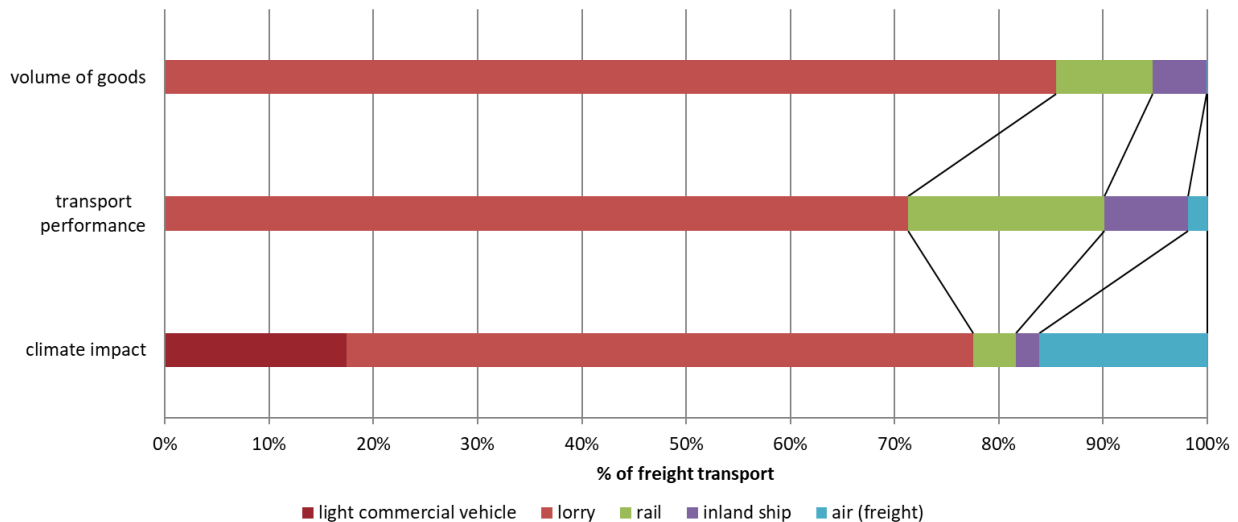


Figure 6: Importance of different transport modes and climate impacts.

85 % of all goods are transported by truck. Since many of the goods are transported in the local area, the share of trucks in the transport performance is lower at 71 %. 60 % of GHG emissions are caused by trucks, 17 % by light commercial vehicles. Rail transport, with a 9% share of freight volume, thus provides 19% of the transport performance, but causes only 4% of the GHG emissions of freight transport. Inland waterway vessels, with a share of 5% of the volume, 8% of the transport performance and 2% of the GHG emissions, are about half that of rail. In terms of freight volume, air traffic originating in Germany is rather negligible: only 0.06 % of goods are transported by air, but these flights account for 16 % of the climate impact.

For local and distribution traffic (see Figure 7), the following applies:

Similar to passenger transport, climate impacts in freight transport are also strongly determined by vehicle operation and energy supply.

- Freight transport with small vehicles causes high specific GHG emissions. The larger the truck and the more goods transported in a vehicle, the better the GHG balance. For large trucks and tractor-trailers with medium loads, they are higher than for rail transport by a factor of three; for smaller vehicles, the factor even rises to 7 to 18.
- In freight distribution with small vehicles, the cargo bike has a major climate advantage over a delivery truck (light commercial vehicle).

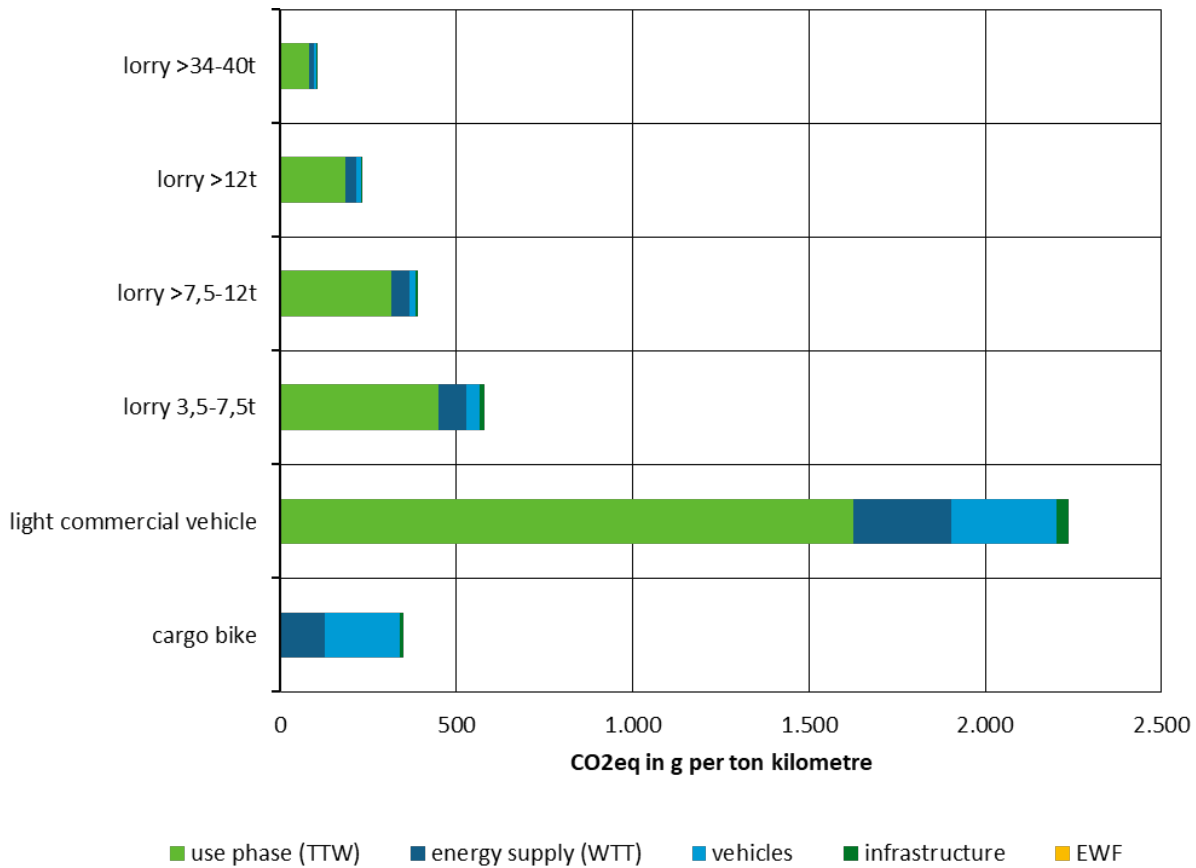


Figure 7: Climate impact of freight transport (short range).

The following applies to long-distance transport (see Figure 8):

- Rail freight transport causes the lowest specific GHG emissions, followed by inland shipping.
- In long-distance freight transport, truck size and capacity utilization are decisive. Here, the large vehicles dominate, so that the mean value of GHG emissions across all trucks is only one-fifth higher than the value for the large trucks and tractor-trailers.
- Freight transport by aircraft (air freight) causes high specific GHG emissions. They are higher by a factor of 45 to 62 than for transport by rail

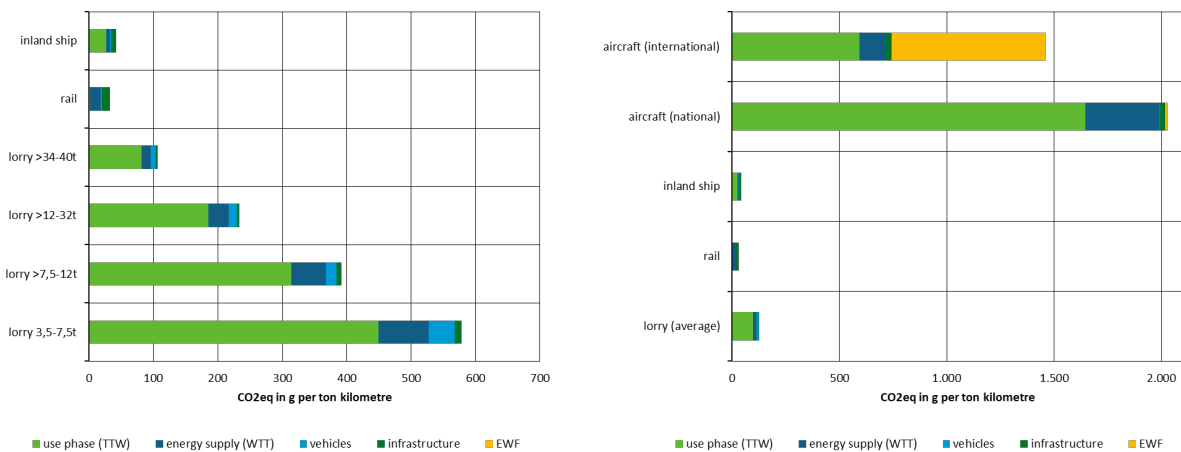


Figure 8: Climate impact of freight transport (long range).

For freight transports, the local impact of air pollutants show a similar trend than for passenger transport. The high proportion of locally effective NO_x emissions from the use of vehicles with internal combustion engines (trucks, inland waterway vessels, and aircraft) is clearly visible. In contrast, exhaust-related PM₁₀ emissions from vehicle use have already been significantly reduced by the use of particulate filters, so that the majority of PM₁₀ emissions result from the remaining life cycle stages.

Final remarks

The comparison of the various modes of transport shows clear differences in their environmental and climate impact. At the same time, the different modes of transport fulfil very different transport tasks for which there are often only limited alternatives. Strategies for reducing impacts must therefore include various aspects from the areas of avoidance, shifting and improvement.

The average metrics presented in this paper provide a valuable basis for the environmental assessment of transportation. The average values provide a good starting point for balancing. However, actual use can differ significantly from the average use of a mode of transport. Different utilization of vehicles or increased environmental impacts due to detours or changes in the means of transport may occur. In addition specific drive train concepts or the usage of different (renewable) energy carriers may offer benefits.

Therefore, it is necessary to take into account the specific conditions for certain questions. This can only be done in a case-by-case assessment.

Acknowledgement

All facts and figures are taken from the brochure "Umweltfreundlich mobil! - Ein ökologischer Verkehrsartenvergleich für den Personen- und Güterverkehr in Deutschland" from 2020 and are based on the study "Ökologische Bewertung von Verkehrsarten" done by ifeu/ INFRAS/ Öko Institut for the German Environment Agency (Umweltbundesamt).

2.13 Effect of auxiliary usage on bus CO₂ emissions through vehicle simulation

N. Zacharof¹, O. Özener², M. Özkan², O. Gezer², S. Broekaert³, G. Fontaras³, Z. Samaras¹

¹ Laboratory of Applied Thermodynamics, Aristotle University of Thessaloniki, Thessaloniki, Greece

² Department of Mechanical Engineering, Yildiz Technical University, İstanbul, Beşiktaş, 34349, Turkey

³ Joint Research Centre of European Commission, Ispra, 21027, Italy

zacharof@auth.gr

Abstract

Road passenger transportation needs are estimated at 3000 billion p-km in the EU annually. Passenger vehicles include cars and motorbikes for personal transportation and buses for collective transportation. There have already been regulations (Regulation (EC) 443/2009) to reduce the fuel consumption and CO₂ emissions from passenger cars as they comprise the highest share of vehicles in terms of absolute numbers. Although heavy-duty vehicles, namely trucks and buses, comprise a relatively low share of about 4% of the vehicle fleet, they are responsible for about 25% of the road emissions, out of which about 7.5% is attributed to buses. Respective measures to reduce CO₂ emissions for buses are to be evaluated by 2022, while measures are already being implemented for rigid and tractor-trailer trucks that transfer goods (Regulation (EU) 2019/1242).

Under the heavy-duty certification scheme, CO₂ emissions from trucks are calculated from vehicle simulations through the Vehicle Energy Consumption Calculation Tool (VECTO), capable also of simulating buses. Buses as heavy-duty vehicles share similar technical characteristics with trucks such as engine and gearbox models and could be highly customizable. However, there are several differences as buses need to accommodate people and create a pleasant cabin atmosphere during the trip. This leads to increased use of auxiliaries that has been found to be at ~16% of the total energy use compared to the 5% of the trucks.

This difference highlights the need to assess the usage of auxiliaries under different operating conditions properly. The current study investigated the auxiliary usage by making use of the VECTO advanced auxiliaries module. The development of the model was based on on-road measurements that were performed with a city bus over a real-world route in Istanbul. Subsequently, the effect of the auxiliaries on fuel consumption was investigated by creating scenarios with varying environmental conditions over one year. The results were compared with the reference environmental conditions in Europe and it was found that they diverge between 2% and 7%. The investigation showed that VECTO has potential beyond the type-approval procedure. It could be utilized to simulate vehicles for future fleets in public transportation by considering the local environmental characteristics.

Introduction

The road passenger transport needs in the European Union are estimated to be in the range of 3000 billion p-km annually (Eurostat, 2020). Passenger vehicles include cars and motorbikes, mostly for personal transportation and buses and coaches for collective transportation. According to the Eurostat data, bus and coach use comprise about 12% of the total passenger-km in 2018, while passenger cars are the most popular means of road transportation (ICCT, 2020). For this reason, passenger cars have been the target of regulations to reduce fuel consumption (Regulation (EC) No 443/2009) and ensure real-world compliance (Regulation (EU) 2017/1154). Heavy-duty vehicles that include buses and trucks have a relatively low share of 4% of the vehicle fleet (Muncrief and Sharpe, 2015), but they are collectively responsible for about 25% of the road emissions. Out of the heavy-duty road emissions share, 7.5% is attributed to buses (European Commission, 2020a). CO₂ emissions for trucks and vehicles that transfer goods have already been the target of relative regulating actions (Regulation (EU) 2019/1242), while the respective measures for buses will be evaluated by 2022 (European Commission, 2020a). Under the Clean Vehicles Directive (Directive (EU) 2019/1161) there is a driving force for 2026 towards zero emissions light-duty vehicles and heavy-duty vehicles that deploy alternative fuels such as hydrogen, natural gas and synthetic fuels.

The certification of the fuel consumption and CO₂ emissions of heavy-duty vehicles is realized through a simulation approach due to the high vehicle customizability, whereas a laboratory vehicle measurement approach as in the case of light-duty vehicles, would pose a high financial cost, technical difficulty and increased certification times (Savvidis, 2014). For this reason, the European Commission has developed the Vehicle Energy Consumption Calculation Tool (VECTO), which is capable of taking into account this degree of customization and perform vehicle simulations. VECTO covers buses, and their simulation is to a high degree pretty straight forward as they share many similarities with trucks. However, there are some differences in energy consumption usage as buses need to accommodate their passenger in a pleasant travelling environment. Such accommodations lead to increased auxiliary usage compared to

trucks, which could be ~16% of the break power output for buses (Zacharof *et al.*, 2019) and 5% for trucks (Tansini *et al.*, 2019) as shown in Figure 1.

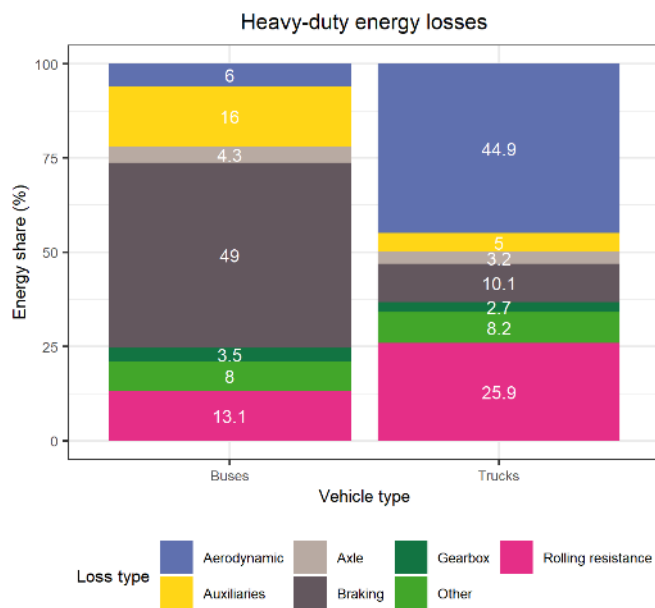


Figure 1: Heavy-duty vehicles energy losses by vehicle type.

This difference highlights the need to properly assess the usage of auxiliaries in VECTO which include the air compressor, steering pump, engine fan, the heating/air-condition system and the electric system. These components could present varying energy usage under different ambient conditions that could have daily, weekly and monthly fluctuations. For this reason, it is not easy to pinpoint specific ambient values that would be representative for year-round at the local and European level. To address the needs of the certification process, it was agreed to set a series of representative environmental conditions in Europe and attribute a weighting factor to them. However, VECTO is equipped with an advanced auxiliary module for buses, which enables the user to adjust ambient parameters and experiment with different scenarios.

The current study investigated the effect of auxiliary usage under different ambient conditions using the VECTO advanced auxiliary module. In this way, it is attempted to offer insight into their effect on CO₂ emissions and ways and technologies that could reduce them. Utilizing a vehicle simulation tool such as VECTO could be a useful approach for public transport organizations, policymakers and research institutes to propose and plan more energy-efficient vehicle fleets.

Methodology

Approach overview

The basis for this investigation was on-road measurements of a city bus in Istanbul that were used for developing a vehicle model in VECTO. The vehicle model was validated with the advanced auxiliary module, which facilitated introducing a series of different ambient parameters. In the next step, the investigation retrieved regional environmental data and subsequently generated the respective simulation scenarios. The approach is described in detail based on the following structure:

- Travel route and vehicle model
- Environmental parameters
- Simulation scenarios

VECTO offers two modes that can be used in running simulations. The vehicle certification process uses the Declaration mode that utilizes a series of pre-set parameters. In this way, it is ensured that all vehicles are certified within a common operational framework. In addition to the Declaration mode, VECTO also deploys an Engineering mode, where the users are free to adjust to a high degree the simulation parameters and experiment with their vehicles. For the current study's needs, all the runs were performed in engineering mode and the utilized version was VECTO 3.3.9.2175.

Travel route and vehicle model

The simulation model was structured by utilizing on-road measurements with the use of Portable Emissions Measurement System (PEMS) that were performed on a city bus in Istanbul and it was developed within the context of a previous study (Zacharof *et al.*, 2019). Detailed information regarding the vehicle can be found in the respective publication, but some information is presented in the current study to understand the applied simulation scenarios better.

The test route is part of the Istanbul Metrobus Line and the selected part was the Avcılar-Beylikdüzü with 12 stops, as shown in Figure 2, where the number labels indicate the bus stops. The developed model included – simulated with the use of sandbags – two different payloads, 6,500 kg and 13,000 kg, over both directions of the Metropolitan line. However, the current study focused only on the 13,000 kg payload. The route had a high road grade, which affected fuel consumption, respectively, with an overall altitude difference of 173 m.



Figure 2: Avcılar-Beylikdüzü (AB) Test route (Google Earth image).

The vehicle was a Euro V city bus with Automatic Transmission-Serial (AT-S) that circulates in Istanbul's Bus Rapid Transport (BRT) system. It was an articulated vehicle with a gross vehicle mass rating of 32 t and an axle configuration of 8 x 2. Since the investigation focused on the use of the Heating Ventilation Air Conditioning (HVAC) systems, it was important to also retrieve vehicle dimensions to enable cabin volume calculation by the tool. Table 1 provides engine technical characteristics, along with the vehicle dimensions.

Table 1: Vehicle characteristics.

Field	Parameter	Value
Engine	Engine capacity (L)	11.9
	Engine power (kW)	260 @ 2000 RPM
	Engine torque (Nm)	600 @ 1100 RPM
Dimensions	Length (m)	18
	Width (m)	3.155
	Height (m)	2.37

The main adjustments of the vehicle model for the purpose of the current study took place within the VECTO advanced auxiliary module. There are several options that the user can adjust to simulate auxiliary usage due to ambient conditions. Initially, it is required to set up the vehicle electricals, pneumatic and HVAC system's technical characteristics.

The electric and pneumatic system was considered to be not affected significantly by the fluctuations of the ambient conditions, and the focus was on the HVAC system, which also has its own dedicated sub-module.

The HVAC module primarily contains the technical parameters of the HVAC system such as compressor type and capacity, technologies that affect energy consumption such as window insulation, fan control strategy, and boundary conditions that indicate when and how the system functions, providing minimum and maximum comfort temperature and other relative data. Table 2 provides more detailed information regarding the HVAC setup.

Table 2: HVAC setup data.

Field	Parameter	Value
Boundary conditions	Passenger boundary temperature (°C)	12
	Heating boundary temperature (°C)	18
	Cooling boundary temperature (°C)	23
	Specific ventilation power (Wh/m ³)	0.56
	Aux heater efficiency	0.84
A/C system	AC – compressor capacity (kW)	32.5
Aux heater	Fuel fired heater (kW)	30
Ventilation	Ventilation on during heating	High
	Ventilation on when both heating and A/C inactive	High
	Ventilation during A/C	High

The introduction of the environmental conditions is done by providing the environmental conditions in terms of ambient temperature and solar radiation which are described in detail in section 0.

Environmental conditions

The HVAC setup parameters assists VECTO to predict the behaviour of the auxiliary systems, which is translated into a mechanical and electrical load. The main inputs are the ambient temperature (°C) and solar radiation (W/m²), which can be provided as single values or in a table for batch mode. The batch mode table contains temperature and solar radiation values along with the weighting factor and it is useful when the environmental conditions need to be averaged over a specific period of times e.g. in a year. Although not accessible to the user, the Declaration mode uses this functionality to assess average environmental conditions in Europe.

The current study generated cases for every month of the year by retrieving the relative data for Istanbul through the tool of the Prediction of Worldwide Energy Resources (POWER) project (NASA, 2021). POWER tool provided minimum, average and maximum temperature values and solar radiation at 9.00 GMT for each month. The tool also provided solar radiation values for other times of the day, but the 9.00 GMT was chosen as it corresponds closer to the highest values expected in the respective time zone. The data were averaged over a period of 30 years, from January 1984 to December 2013. Figure 3 presents the average midday solar radiation and the average temperature values in Istanbul.

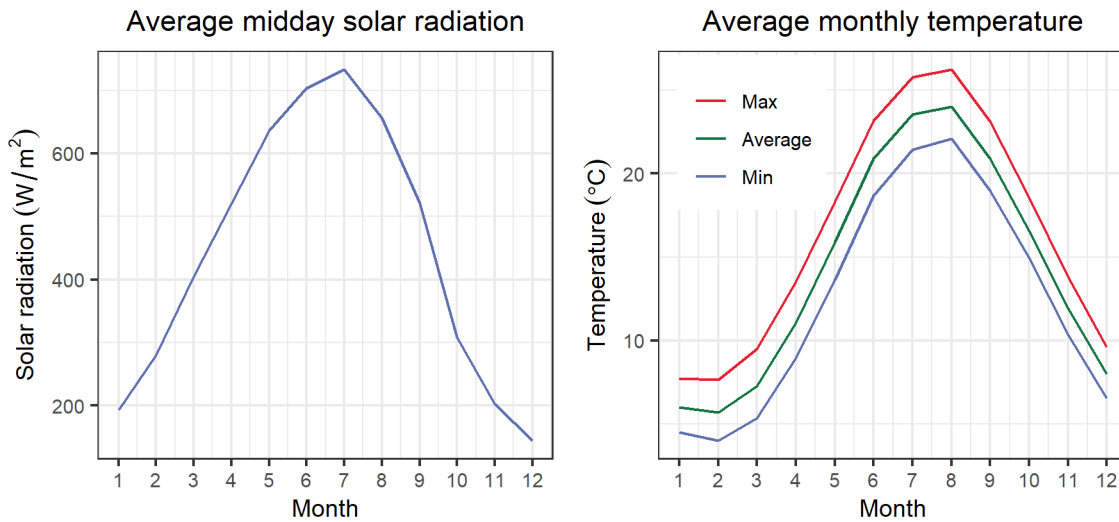


Figure 3: Average midday solar radiation in Istanbul by month.

VECTO also allows introducing a table of batch environmental conditions, where the user enters temperature, solar radiation and a weighting factor. This functionality could give average energy consumption over a specific period, area, or both. In the Declaration mode, the underlying environmental batch conditions table contains information on how much these conditions are met in Europe over the year. Investigating the software's code reveals the underlying environmental parameters, the reference environmental conditions, currently used in the Declaration mode, as shown in Table 3 (European Commission, 2020b). It should be highlighted that the term batch does not mean that several simulation results are produced, but a single value, which uses as power demand of the HVAC system, the weighted average of the HVAC power over a series of environmental conditions. In addition, it should be considered that these parameters are to be confirmed as conclusive with the finalization of the relative bus regulation.

Table 3: Environmental conditions batch mode parameters in declaration mode.

ID	Temperature (°C)	Solar Radiance (W/m ²)	Weighting
1	-20	10	0.53%
2	-5	30	8.26%
3	2	30	8.26%
4	8	20	16.63%
5	8	155	8.26%
6	14	30	8.26%
7	14	175	12.45%
8	20.5	30	12.45%
9	20.5	200	12.45%
10	26	150	8.26%
11	33	150	4.19%

Simulation scenarios

The simulation scenarios were structured to investigate the effect of different environmental conditions on HVAC use and compared them to the reference case. The reference case was based on the batch environmental conditions as they are foreseen in declaration mode. In this way, it is possible to provide a proxy of the vehicle's energy and fuel consumption values under type approval conditions.

In the next step, the reference environmental conditions run value was compared to the simulated actual environmental conditions to identify a possible divergence. The need to use the simulated measured values, instead of the measurements directly was to remove any simulation bias. As an indication, the divergence between the measured data and the simulation was found to be -1.2% for the AB direction and 3.4% for the BA (Zacharof *et al.*, 2019).

In the next step, a series of simulations was formulated to compensate for every month by combining temperature values to solar radiation resulting in 36 cases.

Results and Discussion

The environmental batch conditions, which are the reference environmental conditions for certification purposes, present a divergence of ~5.6% compared to the actual conditions of the simulated measured data, as shown in Figure 4. Of course, the actual conditions represent a snapshot of the environmental conditions at a specific time period, but the comparison presents an indication of the divergence under real-world conditions.

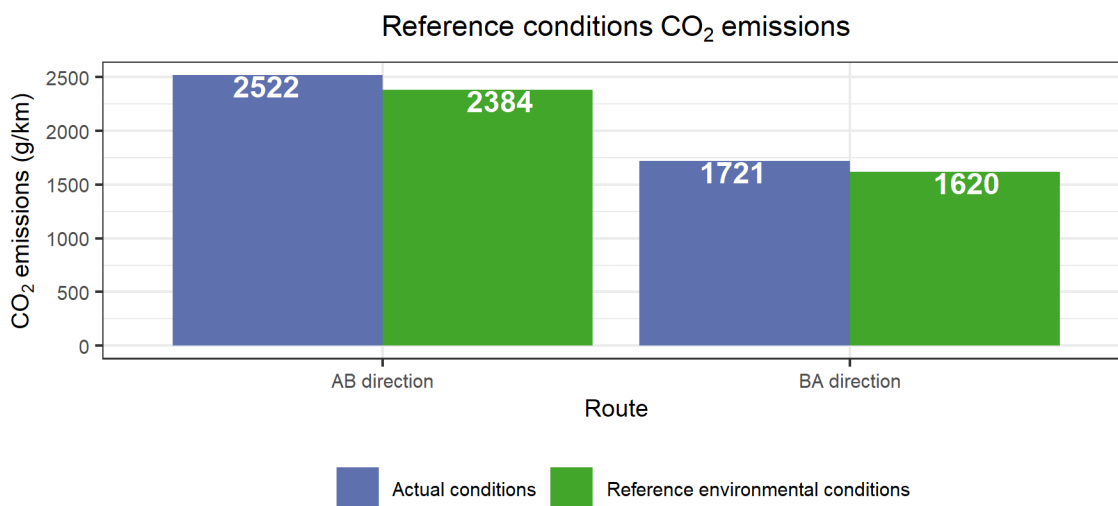


Figure 4: Measurement and environmental batch CO₂ emissions comparison by route.

Figure 5 presents the effect of temperature due to HVAC usage, where as expected, the CO₂ emissions are higher between May and October when the temperatures are higher. From November to April the trend is a bit different, with higher CO₂ emissions for the lowest temperatures due to the use of the fuel-fired heater. Additionally, the difference between AB and BA directions could be attributed to the difference in speed profile due to road grade.

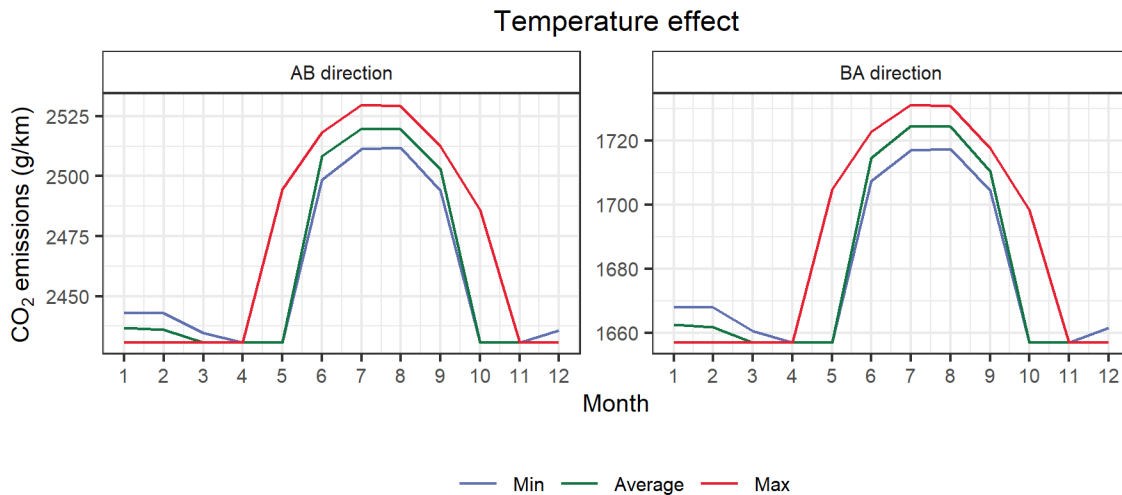


Figure 5: Average annual CO₂ emissions by month.

The mean divergence between the reference conditions and the monthly fluctuation is about 3.5%, with the reported range being 2% - 6.1% for the AB direction and from 2.3% to 6.9% for the BA direction. These values indicate that auxiliary usage has quite a significant effect on CO₂ emissions. Figure 6 presents the auxiliary power requirements by month, but it should be highlighted that the auxiliary values contain the power demand of all auxiliaries and not only the HVAC. However, it is easily observed that there is a similar trend between May and October and from January to April with the maximum difference in the peak of the curve being at 6.3 kW.

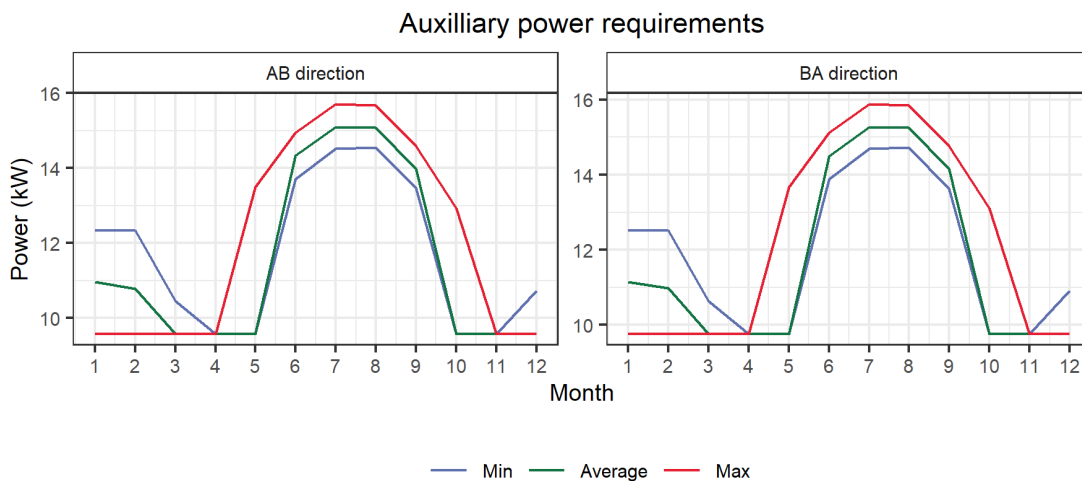


Figure 6: Auxiliary power requirements by month.

In order to identify the contribution of the HVAC, VECTO offers a breakdown of the energy required to utilize the components to operate the system. Figure 7 presents the average annual power needs of electric ventilation, fuelled fired heater and mechanical load that are used for cooling, heating and ventilation by function. The electric ventilation needs are relatively constant throughout the year and are independent of cooling / heating application. The mechanical load demands increase through the May - October period for cooling, while the fuel-fired heater covers the heating needs. The error bars indicate the minimum and maximum values that have been calculated. According to a study, the lowest energy consumption from HVAC is between 15 - 20 °C, while it increases significantly the more it diverges from these values (Basma *et al.*, 2020).

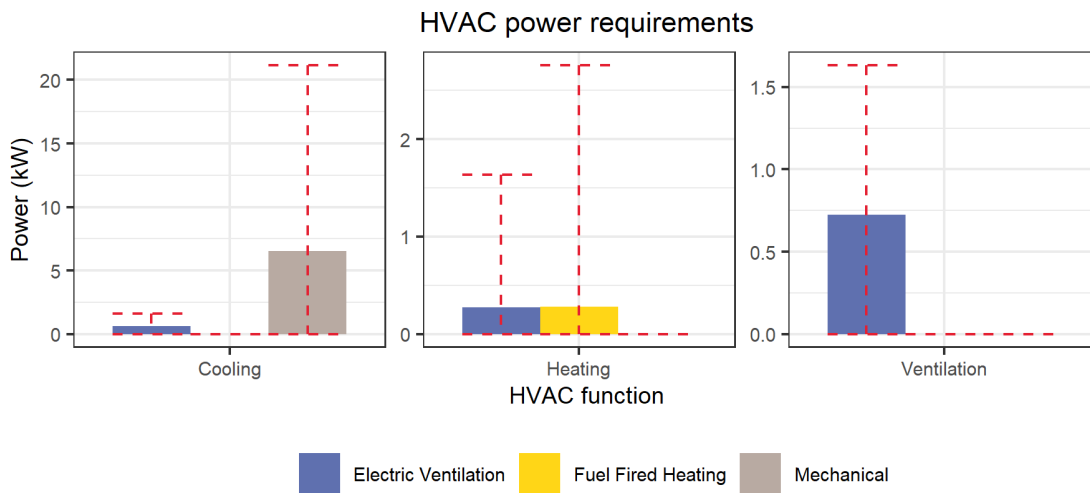


Figure 7: HVAC average annual power needs by function.

VECTO takes into consideration also the number of passengers, which in this case based on the payload it was calculated to be 173. Every person radiates a certain amount of heat that contributes to the cabin's heating and affects therefore the HVAC needs. At the current stage, VECTO is not able to have an adjustable payload and/or number of passengers and these values are considered to be stable throughout the run. The use of HVAC on the passenger thermal comfort has been an object of extensive studies (Pala and Oz, 2015; Velt and Daanen, 2017) and it is a field for potential improvements to reduce CO₂ emissions and energy consumption (Tozzi *et al.*, 2020). Heat pumps and waste heat recovery systems have been the focus of various studies to improve HVAC efficiency (Yilmaz, 2015; Hsieh *et al.*, 2018; Han *et al.*, 2020).

The possibility of introducing a series of parameters as time-series would better assess the effect of energy consumption due to HVAC use. It could be recommended to enable the addition of time-series for a variable mass / passenger number and different environmental conditions in order to capture local features, such as buildings and treelines that could affect auxiliary usage. Perhaps such improvements could be beyond the scope of the type approval procedure, but there seems to be a potential for using VECTO in other uses such as in planning future bus fleets.

Conclusion

The investigation focused on evaluating the effect of auxiliary usage on the CO₂ emissions of a city bus. The difference between the reference environmental conditions and monthly fluctuation ranged from 2% to 6.9%, which significantly contributed to the HVAC system's power demand. The use of VECTO showed that there is a potential to use the tool for simulating vehicles that could be deployed in future fleets with one of the main strong points would be the possibility to adjust the vehicle usage to specific regions. Although VECTO was built with the vehicle type-approval process as a focal point, it has the potential to gain widespread use in several fields. For this reason, it could be facilitated by developing a more flexible Engineering mode.

Acknowledgement

The experimental part of this work is supported by the Istanbul Development Agency – ISTKA, under information focused Economic Development Programme, project No. BIL-86 with the partnership of Istanbul Public Transportation Company (IETT).

References

Basma, H. *et al.* (2020) 'Comprehensive energy modeling methodology for battery electric buses', *Energy*, 207, p. 118241. doi: 10.1016/j.energy.2020.118241.

Directive (EU) 2019/1161 (2019) DIRECTIVE (EU) 2019/1161 OF THE EUROPEAN PARLIAMENT AND OF THE COUNCIL of 20 June 2019 amending Directive 2009/33/EC on the promotion of clean and energy-efficient road transport vehicles. Available at: <https://eur-lex.europa.eu/eli/dir/2019/1161/oj> (Accessed: 12 March 2021).

- European Commission (2020a) *Reducing CO₂ emissions from heavy-duty vehicles, Climate Action - European Commission*. Available at: https://ec.europa.eu/clima/policies/transport/vehicles/heavy_en (Accessed: 22 April 2020).
- European Commission (2020b) Vehicle Energy Consumption Tool (VECTO).
- Eurostat (2020) *Passenger road transport on national territory, by type of vehicles registered in the reporting country*. Available at: https://appsso.eurostat.ec.europa.eu/nui/show.do?dataset=road_pa_mov&lang=en (Accessed: 22 April 2020).
- Han, X. *et al.* (2020) 'Investigation on the heating performance of the heat pump with waste heat recovery for the electric bus', *Renewable Energy*, 152, pp. 835–848. doi: 10.1016/j.renene.2020.01.075.
- Hsieh, Y.-Y. *et al.* (2018) 'A study of heat-pump fresh air exchanger', *Applied Thermal Engineering*, 132, pp. 708–718. doi: 10.1016/j.applthermaleng.2017.12.122.
- ICCT (2020) *European vehicle market statistics 2020/21*. The International Council on Clean Transportation. Available at: <https://theicct.org/publications/european-vehicle-market-statistics-202021> (Accessed: 4 March 2021).
- Muncrief, R. and Sharpe, B. (2015) *Overview of the heavy-duty vehicle market and CO₂ emissions in the European Union*. Washington, D.C.: International Council on Clean Transportation. Available at: <https://theicct.org/publications/overview-heavy-duty-vehicle-market-and-co2-emissions-european-union>.
- NASA (2021) *Prediction of Worldwide Energy Resources (POWER) Data Access Viewer*. Available at: <https://power.larc.nasa.gov/data-access-viewer/> (Accessed: 5 March 2021).
- Pala, U. and Oz, H. R. (2015) 'An investigation of thermal comfort inside a bus during heating period within a climatic chamber', *Applied Ergonomics*, 48, pp. 164–176. doi: 10.1016/j.apergo.2014.11.014.
- Regulation (EC) No 443/2009 (2009) Regulation (EC) No 443/2009 of the European Parliament and of the Council setting emission performance standards for new passenger cars as part of the Community's integrated approach to reduce CO₂ emissions from light-duty vehicles. Available at: <http://eur-lex.europa.eu/legal-content/EN/TXT/PDF/?uri=CELEX:32009R0443&from=EN>.
- Regulation (EU) 2017/1154 (2017) Commission Regulation (EU) 2017/1154 of 7 June 2017 amending Regulation (EU) 2017/1151 supplementing Regulation (EC) No 715/2007 of the European Parliament and of the Council on type-approval of motor vehicles with respect to emissions from light passenger and commercial vehicles (Euro 5 and Euro 6) and on access to vehicle repair and maintenance information, amending Directive 2007/46/EC of the European Parliament and of the Council, Commission Regulation (EC) No 692/2008 and Commission Regulation (EU) No 1230/2012 and repealing Regulation (EC) No 692/2008 and Directive 2007/46/EC of the European Parliament and of the Council as regards real-driving emissions from light passenger and commercial vehicles (Euro 6) (Text with EEA relevance), OJ L. Available at: <http://data.europa.eu/eli/reg/2017/1154/oj/eng> (Accessed: 6 February 2020).
- Regulation (EU) 2019/1242 (2019) Regulation (EU) 2019/1242 of the European Parliament and of the Council of 20 June 2019 setting CO₂ emission performance standards for new heavy-duty vehicles and amending Regulations (EC) No 595/2009 and (EU) 2018/956 of the European Parliament and of the Council and Council Directive 96/53/EC, OJ L. Available at: <http://data.europa.eu/eli/reg/2019/1242/oj/eng> (Accessed: 10 December 2019).
- Savvidis, D. (2014) 'Preparing for the implementation of the simulation based test procedure VECTO'. *Meeting of the Expert Group on policy development and implementation of CO₂ from road vehicles*, Brussels, 22 May.
- Tansini, A. *et al.* (2019) 'A method for calculating Heavy-Duty Trucks energy and fuel consumption with the use of correlation formulas derived from VECTO simulations', in *SAE Technical Paper*. SAE International. Available at: <https://saemobilus.sae.org/content/2019-01-1278>.
- Tozzi, M. *et al.* (2020) 'Testing innovations for increased energy efficiency of electric buses: evidence from the EBSF_2 project', *Transportation Research Procedia*, 48, pp. 2166–2175. doi: 10.1016/j.trpro.2020.08.273.
- Velt, K. B. and Daanen, H. A. M. (2017) 'Optimal bus temperature for thermal comfort during a cool day', *Applied Ergonomics*, 62, pp. 72–76. doi: 10.1016/j.apergo.2017.02.014.
- Yilmaz, A. (2015) 'Transcritical organic Rankine vapor compression refrigeration system for intercity bus air-conditioning using engine exhaust heat', *Energy*, 82, pp. 1047–1056. doi: 10.1016/j.energy.2015.02.004.
- Zacharof, N. *et al.* (2019) 'Simulating City-Bus On-Road Operation With VECTO', *Frontiers in Mechanical Engineering*, 5, p. 58. doi: 10.3389/fmech.2019.00058.

2.14 Understanding the fuel consumption gap using self-reported user and smartphone application datasets

M.A. Ktistakis^{1*}, J. Pavlovic^{1*}, G. Fontaras^{1,2*}, P. Michel², S.S. Rodriguez², A. Chasse²

¹ European Commission, Joint Research Centre, Ispra 21027, Italy

² IFP Energies Nouvelles, 1 et 4 avenue de Bois-Préau, 92852 Rueil-Malmaison, France

markos.ktistakis@ext.ec.europa.eu

Abstract

Regulation (EU) 2019/631 requires the set up of a mechanism for monitoring the gap between the fuel consumption (FC) determined during type-approval tests and in real-world operation. To this end, understanding the FC gap and its variability would be helpful, particularly if a sampling approach is employed. This study uses data from two user-based datasets (Geco air and Spritmonitor.de) to quantify the FC gap, its variability and to find factors contributing to it. Data gathered by the European Environment Agency were utilised to examine the representativeness of the two datasets. Both datasets provide fairly good representations of their respective countries' sub-fleets. According to both user datasets the average FC gap decreased by 4% between 2018 and 2019. The standard deviation of the FC gap was 20-22%. 20-28% of the FC gap's variability was explained using multiple regression models by factors based on macroscopic vehicle data. The results indicate that the vehicle manufacturer and the type-approval CO₂ explain a significant part of the variability of the FC gap. The contributions of the engine rated power and the total distance driven to the FC gap's variability were not negligible.

Introduction

To monitor carbon dioxide (CO₂) emissions and fuel consumption (FC) from light-duty vehicles (LDV) the European Commission's (EC) Regulations foresee official type-approval figures resulting from controlled laboratory tests. This resulted in the average official CO₂ emissions of new passenger cars reducing from 170 g/km in 2001 to 119 g/km in 2017 while rebounding to 122g/km in 2019 (EEA, 2020). However, the reduction trends observed in the actual real-world operation did not follow at the same pace, an observation that is generally known as FC-CO₂ emissions gap. The problem has been documented using analyses of real-world trends that relied on statistical evaluations of voluntarily self-reported consumer or fleet operator FC data and experimental testing. Studies suggest that the gap widened substantially, from about 8% in 2001 to about 40% in 2017 (Fontaras et al., 2017; Tietge et al., 2018).

A major reason for this gap was that up to 2017 official type-approval FC figures were based on the New European Driving Cycle (NEDC), which was developed in the seventies and did not reflect state of the art in testing and vehicle technologies. The EC, acknowledging the issue, introduced the Worldwide harmonised Light vehicles Test cycle and Procedure (WLTP) in the type-approval procedure from September 2017. The WLTP phased-in and by 2021 is the only cycle used for vehicle CO₂ certification in EU. This new certification procedure is expected to decrease the gap by more than half, to an order of about 20% when compared with the certification average CO₂ value (Pavlovic et al., 2018; Tsiakmakis et al., 2016). Dornoff et al., 2020 confirm these estimates, suggesting that WLTP closes the gap by 22% to 24% compared to the NEDC.

To monitor the FC gap and avoid a gradual recurrence of the gap's increase Regulation (EU) 2019/631 for LDV requires setting up a mechanism to monitor the real-world representativeness of the FC determined during the type-approval tests. To this end, a good understanding of the FC gap and its variability would be very useful, especially in the case of applying a sampling scheme. Having a-priori estimates of the variabilities per strata enables optimisation. The impact of environmental, traffic, and driving factors have been studied before (Pavlovic et al., 2020). Ntziachristos et al., 2014 and Tietge et al., 2017 have utilised regression models to explain the variability of the FC gap. The analysis was performed on data before the FC gap peaked. Under the current conditions, analysing the FC gap and decomposing its variability appears to be of interest.

This research work uses 2018 and 2019 data from two user-based datasets (Geco Air and Spritmonitor.de) to understand better the FC gap and factors affecting it. Data gathered by the European Environment Agency (EEA) for all new passenger cars registered in the Member States in 2018 and 2019 were also utilised to examine the representativeness of the two datasets and the sub-fleets of their respective countries in respect to fuel type, type approval CO₂ emissions, vehicle manufacturer and engine rated power. First, the FC gap was analysed as a stand-alone variable, then in relation to other variables (fuel type, transmission type, vehicle manufacturer, type approval

* Corresponding authors jelica.pavlovic@ec.europa.eu; georgios.fontaras@ec.europa.eu

CO₂ emissions, engine rated power and total distance driven). Multiple regression models were utilised to quantify the importance of various factors in the variability of the FC gap.

Methodology

Data sources – data cleaning

Geco air is a mobile application designed by IFP Energies Nouvelles to help individual users to become aware and master the environmental footprint of their mobility, including the impact of driving personal vehicles by estimating their pollutant (NO_x and CO) and CO₂ emissions and evaluating their driving behaviour (Thibault et al., 2017). Upon detection of the use of a personal vehicle, the real-world CO₂ emissions are calculated using a physical model of the vehicle (Michel et al., 2021) that uses the real-world data profiles of speed and altitude, which are calculated using the GPS measurements recorded at 1 Hz by the mobile phones, and the vehicle technical specifications inferred from vehicle registration data.

IFP Energies Nouvelles provided JRC anonymised data of approximately 4,200 vehicles, driven on real-world conditions, registered from 1988 to 2020 (approximately 342 and 173 were registered in 2018 and 2019, respectively). For each vehicle the FC gap was calculated using the provided aggregated data of the real-world and the type approval CO₂ emissions. The FC gap is calculated as $FC_{gap} = \frac{FC_{RW} - FC_{TA}}{FC_{TA}} * 100$, where FC_{TA} is the type-approval fuel consumption and FC_{RW} the real-world fuel consumption in L/100 km. Additionally, the dataset included the fuel type, manufacturer, registration year, engine rated power, transmission type and distance recorded. Non-conventional vehicles, outliers and vehicles with a recorded mileage less than 1,000 km were removed. The criterion of 1,000 km was chosen because it was found that there is no statistically significant difference ($pvalue \leq 0.05$) between the subpopulations of vehicles driven for at least 1,000 km and at least 1,500 km. Applying the above criteria 141 and 63 vehicles from 2018 and 2019 remained for further analysis.

Spritmonitor.de is a free web service where vehicles' owners report real-world FC. It was launched as a website in Germany in 2001, to provide users with a simple tool to monitor their FC. To start making use of the service users are requested to fill the fuel tank, and the first event provides the reference for calculations of FC. In every fuelling entry, the user is requested to record the mileage, and the litres fuelled.

The Spritmonitor.de dataset had anonymised data on approximately 122,000 vehicles registered from 2014 to 2019 (approximately 20,270 and 12,220 were registered in 2018 and 2019, respectively). For every vehicle, the FC gap was computed using the type-approval FC, the total fuel consumed and the total mileage driven. This dataset also contained the fuel type, manufacturer, registration year, engine rated power and transmission type. Using the same methodology as for Geco air, it was calculated that the minimum mileage that would not produce statistically significant differences was 1,250 km. After applying the criteria 7,218 and 3,642 vehicles registered in 2018 and 2019 respectively, were left for the analysis.

Regulation (EU) 2019/631 requires Member States to record information for each new passenger car registered in their territory. EEA collects this information and provides public datasets with anonymised data. The annual datasets include the type-approval CO₂ emission, fuel type, manufacturer, engine rated power, country of registration and more information not used in this report. The EEA datasets do not include real-world CO₂ emissions and FC. In this article the 2018 and 2019 final datasets were used. They consist of approximately 15,273,000 and 15,452,000 vehicles, respectively; after removing electric and hybrid vehicles 14,623,747 and 14,703,831 remained. No other entries were removed because it was of interest to use this dataset to better understand the census, hence removing vehicles because one variable was missing was not the suitable approach.

Dataset Representativeness

To evaluate if the two user-datasets could be utilised to support the determination of the FC gap of vehicles registered in the EU, it was investigated whether:

- The two datasets were representative of the fleet of EU vehicles registered in 2018 and 2019;
- The two datasets were representative of the sub-fleets of their respective countries (Geco air for France and Spritmonitor.de for Germany);
- Vehicles from these two countries could represent the 2018 and 2019 population of passenger vehicles in the EU.

Representativeness was determined with respect to fuel type, type approval CO₂ emissions, vehicle manufacturer and engine rated power. The distribution of the whole fleet of vehicles introduced in the EU market in 2018 and 2019 was calculated from the EEA dataset, the country-wise sub-fleets and Geco air and Spritmonitor.de for the manufacturer, type-approval CO₂ emissions (g/km), fuel type and engine power (kW). The distributions of the country - wise sub-

fleets were collected for the above four variables. For the same variables, the distribution was calculated of the Geco air and Spritmonitor.de datasets.

For each of these four variables, density plots were drawn and used to compare the Geco Air and Spritmonitor.de datasets to the French and German sub-fleets, respectively, as well as to the whole European fleet. It should be noted that a limited number of vehicles were used from each dataset. The main purpose of this section was not to evaluate the datasets but to check whether, and to what degree, it is justified to use them for getting a valid indication of the FC gap across the EU. The datasets cannot be used in the context of Regulation (EU) 2019/631 as they are not relying on OBFCM data. All the hypothesis tests performed in this article, to examine if there were statistically significant differences, are done with a confidence level of 95%.

Fuel Consumption gap analysis

Descriptive statistics were used to get an understanding of the FC gap. Firstly as a stand-alone variable, then in relation to the other used variables (fuel type, transmission type, vehicle manufacturer, type approval CO₂ emissions, engine rated power and total distance driven).

Multiple regression models were utilised to quantify the importance of various factors (independent variables) to the FC gap (dependent variable). There are many definitions of importance, however, dispersion importance metrics are the most widely accepted and were used in this study. Dispersion importance refers to the amount of the dependent's variance, explained by the regression equation, attributable to each independent variable. The metric proposed by Lindeman et al., 1980, which satisfies the most important requirements, according to Grömping, 2015, was used for quantifying the dispersion importance. By calculating and decomposing the R-squared coefficient (R^2) it was possible to examine how much of the variability of the FC gap can be explained by each model and each factor.

Results and discussion

Dataset representativeness results

In respect to the ratios of diesel and petrol vehicles for both user datasets, there were statistically significant differences between 2018 and 2019. The share of newly registered diesel and petrol vehicles in 2018 and 2019 for the German and French market is close to the share of the whole EU (Figure 1). In the Geco Air dataset approximately 50% of the vehicles were diesel-powered. This is a substantial difference compared to EEA (35%) and EEA France (40%). 20% of Spritmonitor.de vehicles were diesel-powered, which is a statistically significant difference compared to the German sub-fleet's share (32%).

Figure 2 presents all manufacturers that have a share of a least 2% on the respective dataset. There are no large differences from year to year, especially on the EEA fleet and sub-fleets. In both years, the French sub-fleet is not representative of the whole European fleet, because Renault, Peugeot and Citroen share almost 50% of the French market, while their portion of the whole EU fleet is less than 20%. In Germany there is a similar situation, e.g. Volkswagen has a significantly higher share of the German market (19%) in comparison to its share in the European fleet (11%). The Geco Air dataset is representative of the French market in respect to most manufacturers. The major exceptions, which are overrepresented in Geco air, are Peugeot in 2018 and Citroen in 2019. Spritmonitor.de is representing with greater success the whole European fleet than the German sub-fleet. The more significant divergence is Renault, which has around 4% less share in Spritmonitor.de than the whole EEA.

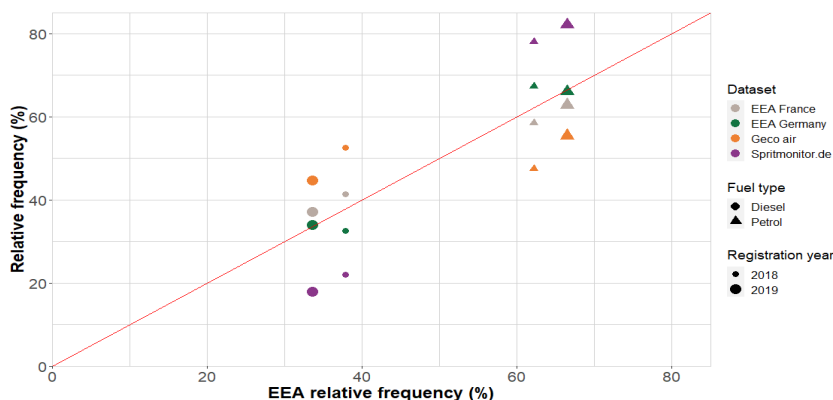


Figure 1: Representativeness of datasets per fuel type.

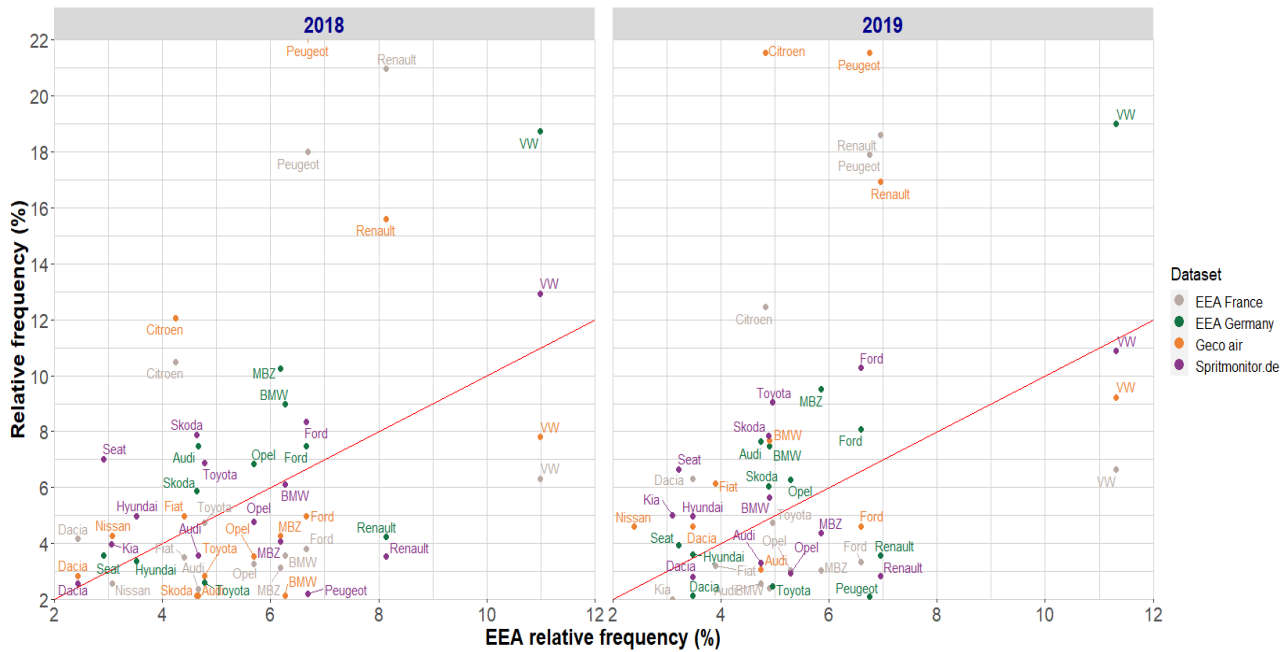


Figure 2: Representativeness of datasets per manufacturer.

As far as type-approval CO₂ emissions is concerned, both years Geco Air and French sub-fleet have more vehicles with low type-approval CO₂ emissions in comparison to the whole fleet (Figure 3). On the other hand, Spritmonitor.de and the German sub-fleet have a higher percentage of vehicles with high type-approval CO₂ emissions registered in both years compared to the whole EU market. Geco air represents satisfactory, in respect to type-approval CO₂ emissions, both the EEA and the French EEA datasets. Spritmonitor.de is closer to the German sub-fleet, but vehicles with type-approval CO₂ emissions around 110g/km are underrepresented, while vehicles with higher than 160g/km are overrepresented.

For both years, vehicles sold in France had on average lower engine rated power than the average across the EU. The same parameter in Germany was higher (Figure 3). Geco air represents France’s situation in all aspects, except for vehicles with low engine rated power (<70kW). Spritmonitor.de is representative of the German sub-fleet.

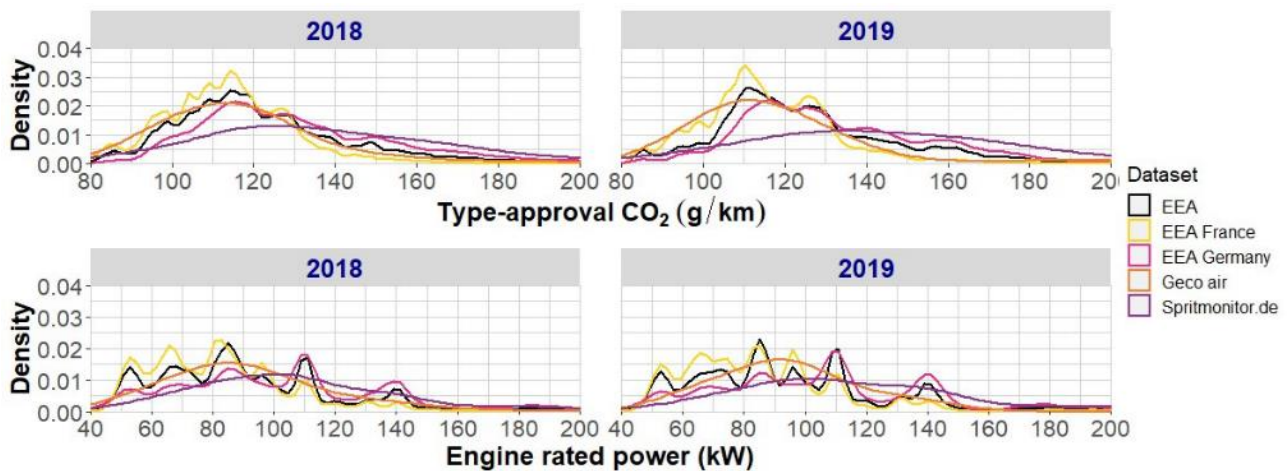


Figure 3: Representativeness of datasets per type approval CO₂ emissions and per engine power.

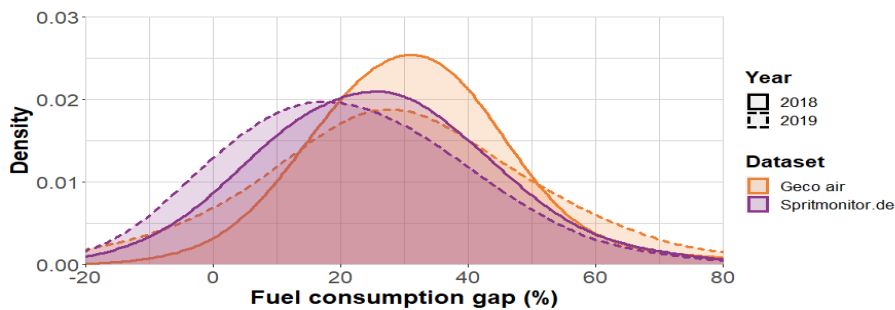
The current assessment is seen from a purely scientific perspective, in fact, both datasets provide fairly good representations of their respective countries’ sub-fleets and to a lesser extend the EU fleet, particularly considering the uncertainty of other datasets and calculations. The main conclusions concerning the representativeness of the datasets can be summarised as:

- The French sub-fleet represents the EU fleet satisfactorily with respect to fuel type, type-approval CO₂ emissions and engine rated power;
- The German sub-fleet represents the EU fleet satisfactorily with respect to fuel type, type-approval CO₂ emissions and engine rated power;

- The Geco Air dataset can represent the vehicles registered in France satisfactorily with respect to type-approval CO₂ emissions and engine rated power;
- The Spritmonitor.de dataset can represent the vehicles registered in Germany satisfactorily concerning type-approval CO₂ emissions and engine rated power and the whole EU fleet with respect to the manufacturers.

Fuel consumption gap results

Spritmonitor.de for both years and Geco air in 2019 are approximately symmetrical, while Geco air in 2018 was right-skewed (skewedness=2.5) (Figure 4). In both datasets the average FC gap decreased by around 4%. This decrease can be attributed to the increase of WLTP type approval values in the datasets. The International Council on Clean Transportation (ICCT) reported for Spritmonitor.de in 2018 an average FC gap of 39% (Dornoff et al. 2020). This difference of 13.7% could be attributed to the exclusion in the present analysis of hybrid vehicles that reportedly exhibit higher gap values and to the use of different type-approval FC values. The ICCT research team used in their analysis an ICCT maintained dataset for linking it to Spritmonitor.de vehicles. In this analysis, the vehicle owners' self-reported values in Spritmonitor.de were utilised without any correction. Another possible factor could be the differences in criteria used to remove vehicles during the data pre-analysis. An interesting observation, because of its importance in understanding the FC gap and making the regression models in section 0, is that the standard deviations of the FC gap of Geco air and Spritmonitor.de are around 20-22% for both years.



Dataset	Registration year	Number of Vehicles	Mean	Median	Standard Deviation
Geco air	2018	141	33.4	31.9	19.6
Geco air	2019	63	29.3	27.8	21.6
Spritmonitor.de	2018	7218	25.3	25.1	19.7
Spritmonitor.de	2019	3642	21.3	20.0	19.9

Figure 4: Density plots and statistics of the fuel consumption gap.

The correlation between the gap and the fuel type presents similar patterns in both datasets and years (Figure 5). Diesel vehicles had on average a higher FC gap, however, there was no statistically significant difference. The variability of the FC gap also did not present a statistically significant difference between diesel and petrol vehicles.

No statistically significant difference was observed between the mean values and the variabilities of vehicles with manual and automatic transmission per year (Figure 5).

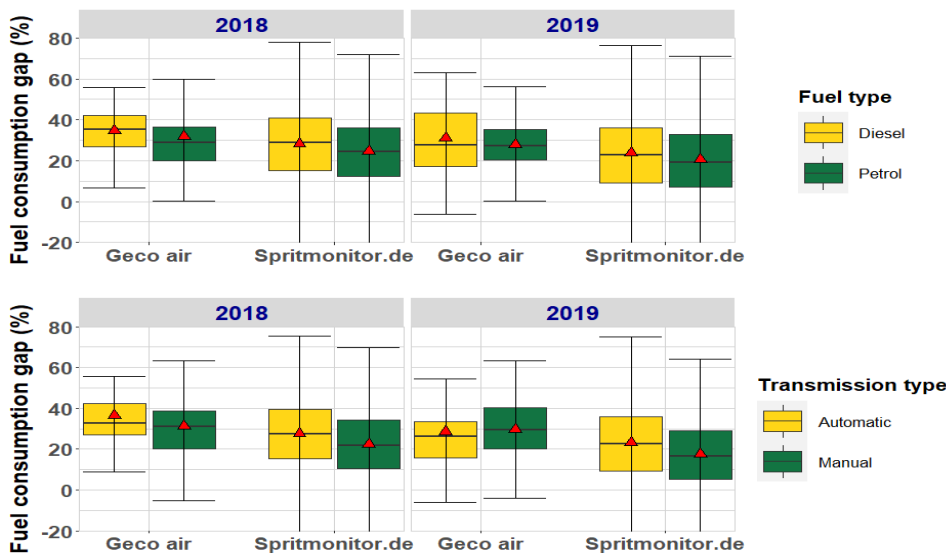


Figure 5: Fuel consumption gap by fuel type and by transmission type. Red triangles depict the mean values. The upper/lower whiskers extend from the hinge to the largest/smallest value no further than 1.5*(inter-quartile range) from the hinge.

Figure 6 presents the boxplots of the FC gap of the manufacturers that had at least a 4% share in one dataset-year. The boxplots are presented in ascending order of the average FC gap. It can be seen that in Geco air both the averages and the variables per manufacturer vary a lot, while for Spritmonitor.de the variations are much smaller. The two datasets do not agree between them and big variations are presented for some manufacturers on the same dataset from 2018 to 2019.

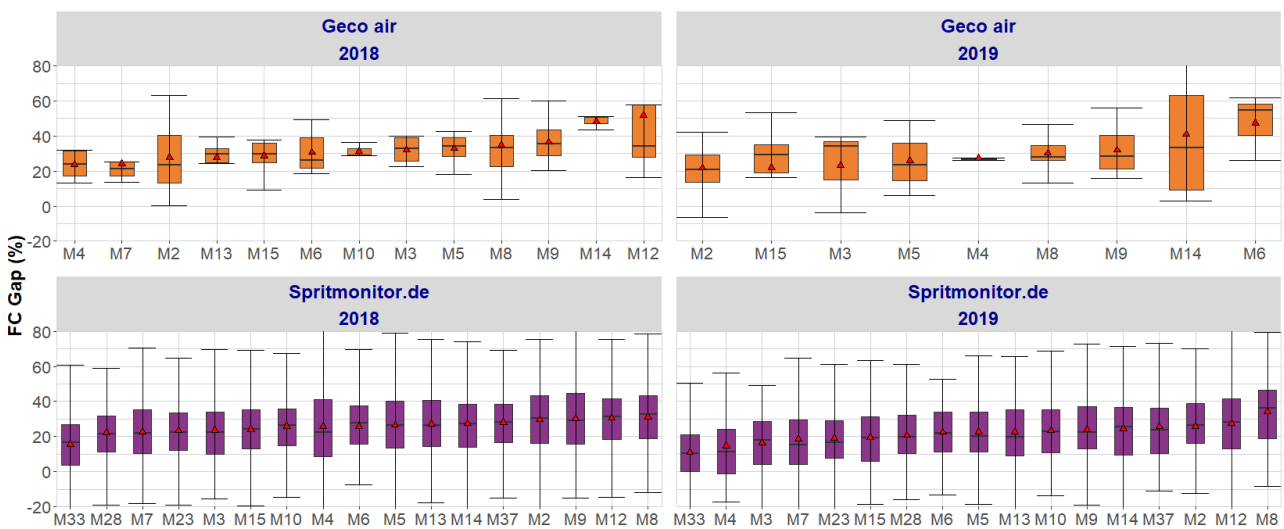


Figure 6: Fuel consumption gap by manufacturer. Red triangles depict the mean values. The upper/lower whiskers extend from the hinge to the largest/smallest value no further than 1.5 * (inter-quartile range) from the hinge.

In Figure 7 the relation between the FC gap and the type-approval CO₂ emission, the engine rated power and the total distance driven are presented for each dataset and each year. The curves are an estimate of the conditional median function, i.e. an estimate of the median FC gap conditional on the variable shown on the x-axis. For Spritmonitor.de results from 2018 and 2019 show similar trends for all three variables. For Geco air 2018 and 2019 vehicles trends are similar in respect to the total distance driven and in some areas of the type-approval CO₂ emission and the engine rated power.

In Spritmonitor.de vehicles the FC gap reduces as the type approval CO₂ emissions increase (Figure 7). The FC gap has the biggest variability in respect to the type approval CO₂, starting from around 40% for low type-approval CO₂ emissions and reaching an average of less than 15% for the vehicles with the highest type-approval CO₂ emissions. In Geco air vehicles with higher type approval CO₂ emissions have a higher FC gap, with the exception of 2018 vehicles with type approval CO₂ emissions around 130g/km.

Spritmonitor.de vehicles with low engine rated power have a lower FC gap in average, while the largest is found for vehicles with engine rated power around 170kW (Figure 7). Geco air 2019 vehicles exhibit a different trend with an almost constantly decreasing FC gap as the engine power increases.

Vehicles from both datasets show small variations in FC in relation to the total distance driven (Figure 7). Also for both datasets and years the FC gap converges as the distance driven gets above 15 thousand kms.

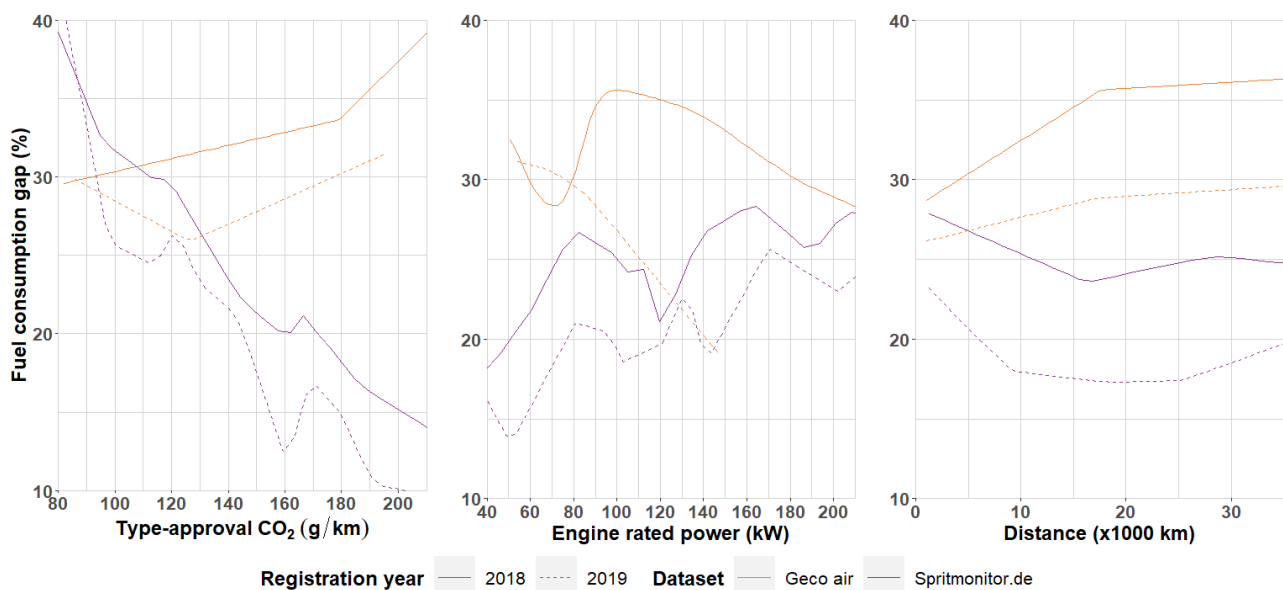


Figure 7: Fuel consumption gap by type approval CO₂, by engine power and by driven distance.

Regression model results

The models constructed explained 20.2% and 26.3% of the FC gap's variability, for Geco air and Spritmonitor.de, respectively (Table 1). This low percentage can be attributed to the lack of environmental and driver factors. In the models five technical characteristics of the vehicles have been used, plus the total driven distance and the registration year. In spite of the low R^2 , the models can explain adequately the variability attributed to the vehicles' technical characteristics. In Geco air dataset almost 77% of the FC gap's variability explained by this multiple regression model can be attributed to the manufacturers (Table 1). This high percent comes from the high variability between manufacturers (Figure 6). However, it should be taken into account, that when stratifying Geco air vehicles by year and manufacturer many strata had very few vehicles and they were not enough for the strata average and variability to converge to the "true" values. Also, that the manufacturer information is not an input used for the Geco air model parametrization, therefore, even if the CO₂ score is correlated there is no causal link. The causal link is rather to the vehicle dimensions (empty weight, height, wheelbase etc.) that are used to parametrize the vehicle model and in themselves can be correlated to the OEM. The second higher contributor is the total distance driven.

For Spritmonitor.de the type approval CO₂ contributed 62.6% of the explained variability. An indication of this high percentage can be found in Figure 7, where it is shown that the average FC varies a lot as the type-approval CO₂ changes. Following the type approval CO₂ it is the manufacturer (17.1%) and the engine rated power (12.3%) that contribute the most.

A combined dataset was prepared to test the regression model. All vehicles from Geco air were used, from Spritmonitor.de a sample analogous to the vehicles registered each year in Germany and France was sampled. For this dataset the variability of the FC gap explained by the model was 27.8%. The most significant contributors were the manufacturer (39.6%) and type-approval CO₂ emissions (43.4%). The engine rated power (10.1%) followed.

Table 1: Results of the multiple regression models that quantify contribution on fuel consumption gap.

Variable	IMPORTANCE (RELATIVE IMPORTANCE (%))		
	Geco air	Spritmonitor.de	Combined
Fuel type	0.3 (1.4)	0.3 (1.0)	0.5 (1.7)
Manufacturer	15.5 (76.9)	4.5 (17.1)	11.0 (39.6)
TA CO ₂	0.1 (0.7)	16.4 (62.6)	12.1 (43.4)
Engine power	0.2 (1.0)	3.2 (12.3)	2.8 (10.1)
Transmission	0.5 (2.5)	1.4 (5.3)	0.3 (1.1)
Distance	2.8 (13.7)	0.1 (0.3)	0.0 (0.2)
Year	0.8 (3.8)	0.4 (1.4)	1.1 (3.9)
Total R ²	20.2 (100)	26.3 (100)	27.8 (100)

Conclusions

The main conclusions drawn from the analysis can be summarized as follows.

- Vehicles of Geco air and Spritmonitor.de represent satisfactorily their respective countries' fleets of LDVs vehicles when it comes to type-approval CO₂ emissions and engine rated power.
- The mean FC gap of conventional petrol and diesel vehicles according to both user datasets has reduced by around 4% between 2018 and 2019. The standard deviation was consistently found to be around 20-22%.
- 20-28% of the FC gap's variability can be explained with multiple regression models using the fuel type, the transmission type, the vehicle manufacturer, the type approval CO₂ emissions, the engine rated power, the total distance driven and the registration year.
- There were no statistically significant differences of the FC gap between manual and automatic vehicles, neither between petrol and diesel fuelled ones. The fuel type and the transmission type did not contribute significantly to the variability of the FC gap.
- From the factors examined, the vehicle manufacturer and the type-approval CO₂ contribute the most to the variability of the FC gap. The contributions of the total distance driven and the engine rated power are not negligible.
- While this study does not offer a conclusive answer to the relative importance of all the parameters contributing to the variability of the FC gap, it does provide indications of its true value and which vehicle characteristics contribute to it.
- Available factors based on macroscopic vehicle data can only partially describe the FC gap, but have the merit of being readily available. In order to enhance understanding of the FC gap, deriving descriptors of real life vehicle use (e.g. average vehicle speed, acceleration, driving dynamicity, charging frequency in case of plug-in vehicles, etc.) can complete the existing set of vehicle descriptors and be monitored in the future. While these are intrinsically more difficult to capture and characterize, the analysis of anonymized crowd-sensed speed and GPS data provide the opportunity of obtaining meaningful descriptors for use patterns and their spatial (infrastructure) and temporal (traffic) dependence.
- Combining these data with vehicle simulation further expands the potential for understanding the real-world FC, and consequently the FC gap, as the product of the interaction between vehicle size and technology, user driving behaviour and traffic, and finally spatial coverage of personal vehicle mobility and associated infrastructure.

Acknowledgement

The authors gratefully acknowledge Ilias Cheimariotis from the Institut Français du Pétrole Energies Nouvelles (IFP Energies Nouvelles) for his valuable and constructive comments and the revision of the manuscript.

References

- Dornoff, J., Tietge, U., Mock, P., On the way to “real-world” CO₂ values: The European passenger car market in its first year after introducing the WLTP. 2020.
- EEA, Average CO₂ emissions from newly registered motor vehicles in Europe — European Environment Agency [WWW Document]. URL <https://www.eea.europa.eu/data-and-maps/indicators/average-co2-emissions-from-motor-vehicles/assessment-2> (accessed 3.3.21).
- Fontaras, G., Zacharof, N.-G., Ciuffo, B., Fuel consumption and CO₂ emissions from passenger cars in Europe - Laboratory versus real-world emissions. *Progress in Energy and Combustion Science* 60, 97–131. 2017.
- Grömping, U., Variable importance in regression models. *WIREs Computational Statistics* 7, 137–152. 2015.
- Lindeman, R.H., Merenda, P.F., Gold, R.Z., Introduction to bivariate and multivariate analysis. *Vereniging voor Statistiek Bulletin* 14, 11. 1980.
- Michel, P., Rodriguez, S.S., Chasse, A., Fontaras, G., Pavlovic, J., Ktistakis, M.A., Komnos, D., Conventional Engine Vehicles Model Parametrization for Real-World Fuel Consumption Estimation. Presented at the International Transport and Air Pollution Conference TAP, Graz, Austria. 2021.
- Ntziachristos, L., Mellios, G., Tsokolis, D., Keller, M., Hausberger, S., Ligterink, N.E., Dilara, P., In-use vs. type-approval fuel consumption of current passenger cars in Europe. *Energy Policy* 67, 403–411. 2014.
- Pavlovic, J., Ciuffo, B., Fontaras, G., Valverde, V., Marotta, A., How much difference in type-approval CO₂ emissions from passenger cars in Europe can be expected from changing to the new test procedure (NEDC vs. WLTP)? *Transportation Research Part A: Policy and Practice* 111, 136–147. 2018.
- Pavlovic, J., Fontaras, G., Ktistakis, M., Anagnostopoulos, K., Komnos, D., Ciuffo, B., Clairotte, M., Valverde, V., Understanding the origins and variability of the fuel consumption gap: lessons learned from laboratory tests and a real-driving campaign. *Environmental Sciences Europe* 32, 53. 2020.
- Regulation (EU) 2019/631 of the European Parliament and of the Council of 17 April 2019 setting CO₂ emission performance standards for new passenger cars and for new light commercial vehicles, and repealing Regulations (EC) No 443/2009 and (EU) No 510/2011, 2019.
- Thibault, L., Dégeilh, P., Sabiron, G., Voise, L., Thanabalasingam, K., Corde, G., GNSS data-based approach to monitor real-world exhaust emissions at microscopic resolution. Presented at the International Transport and Air Pollution Conference TAP, Zürich. 2017.
- Tietge, U., Díaz, S., Mock, P., Bandivadekar, A., Dornoff, J., Ligterink, N., A 2018 update of official and “real-world” fuel consumption and CO₂ values for passenger cars in Europe. 2018.
- Tietge, U., Mock, P., Franco, V., Zacharof, N., From laboratory to road: Modeling the divergence between official and real-world fuel consumption and CO₂ emission values in the German passenger car market for the years 2001–2014. *Energy Policy* 103, 212–222. 2017.
- Tsiakmakis, S., Ciuffo, B., Fontaras, G., Anagnostopoulos, K., Arcidiacono, V., Praksova, R., Marotta, A., Introducing a New Emissions Certification Procedure for European Light-Duty Vehicles: Monte Carlo Simulation of the Potential Effect on Fleet Carbon Dioxide Emissions. *Transp Res Rec J Transp Res Board* 2572, 66–77. 2016.

2.15 VECTO meets real world: A comparison of fuel consumption as determined by the official European method with data from fleet management systems

M. Röck¹, M. Rexeis¹, S. Hausberger¹, H. Wentzel²

¹Graz University of Technology, Institute of Internal Combustion Engines and Thermodynamics, Austria

²Scania CV AB, Sweden

röck@ivt.tugraz.at

Abstract

Since January 2019, in the European Union for each newly produced long-haul truck individual figures for fuel consumption and CO₂ emissions have to be determined according to the method as laid down in Commission Regulation (EU) 2017/2400. This approach is based on the measurement of the energy demand and/or the efficiencies of the individual vehicle components and the simulation of fuel consumption and CO₂ emissions of the complete vehicle using the "VECTO" software (Vehicle Energy Consumption Calculation Tool). The related vehicle-specific CO₂ values also form the basis for the CO₂ standards that manufacturers will have to comply with in the coming years compared to the 2019 baseline (2025: minus 15%, 2030: minus 30%).

The paper gives an overview on the VECTO approach and its underlying boundary conditions like considered mission profiles, applied payloads and reference conditions for determination of vehicle parameters like air drag and rolling resistance.

For comparison of VECTO results with real world fuel consumption data as recorded by fleet management systems on approximately 3500 long haul vehicles is analysed. The vehicles have been produced in Q1 2019 and been operative over the entire year 2019. The paper examines the consistency between VECTO and fleet data in terms of overall fuel consumption level and analyses possible causes of observed differences.

Introduction

Road freight transport accounts for the largest share of the total inland freight transport performance in the EU-27 [1]. The HDV vehicle fleet contributes with about 25% to a significant share of the resulting greenhouse gas emissions of road transport [2], [3] (Figure 1). Looking at trends, a further increase of the freight transport demand in the future can be expected [4]. Hence, this sector provides a significant contribution to GHG emissions and global warming.

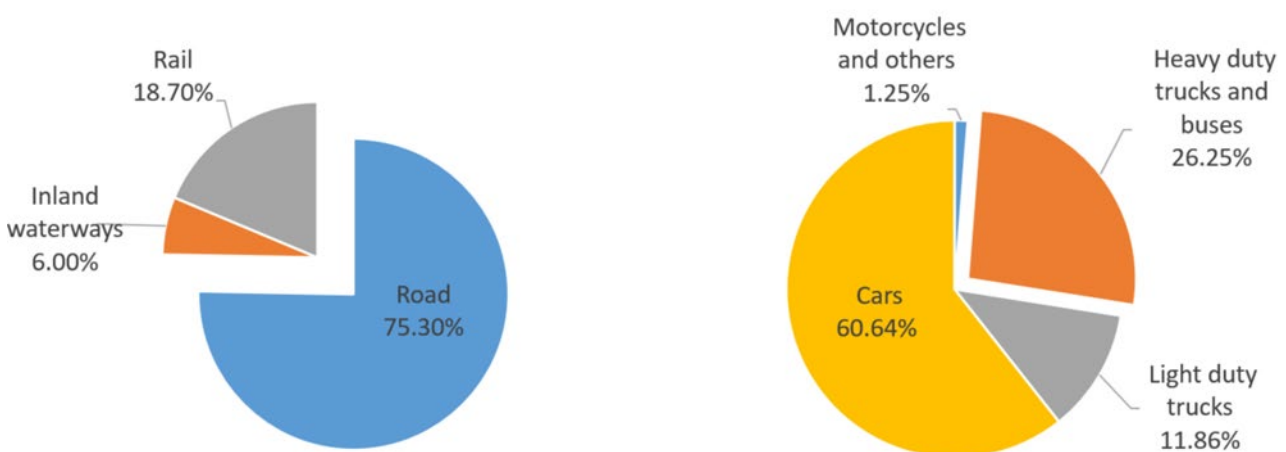


Figure 1: Modal split of inland freight transport, EU-27, 2018 [1] (left); Ghg emissions of road transport, EU-28, 2018 [3] (right).

In order to reduce the global warming, the EU Commission aims to be climate-neutral by 2050 [5]. To achieve this goal, among many other measures, CO₂ standards were introduced for heavy duty vehicles (HDV) to cut down their CO₂ fleet emissions. The legislative provisions of these CO₂ standards are described in Regulation (EU) 2019/1242 [6]. The aim is a CO₂ reduction of 15% by 2025 and 30% until 2030 compared to a reference which is based on new vehicles registered between 01.07.2019 and 30.06.2020. The HDV CO₂ standards currently in force cover rigid trucks and tractors with axle configurations of 6x2 and 4x2, which are predominantly used for the delivery of goods in long-haul and regional delivery missions.

The HDV CO₂ standards are based on official CO₂ values, which are determined individually for each vehicle in accordance with Regulation (EU) 2017/2400 [7]. This CO₂ determination is based on the certified measurement of the energy demand and/or the efficiencies of the individual vehicle components and the simulation of fuel consumption and CO₂ emissions of the complete vehicle using the "VECTO" software (Vehicle Energy Consumption Calculation Tool).

This paper gives an overview on the VECTO approach and its underlying boundary conditions like considered mission profiles, applied payloads and reference conditions for determination of vehicle parameters like air drag and rolling resistance. Furthermore, this study analyses the consistency between VECTO and fleet data in terms of the VECTO boundary conditions up to the overall fuel consumption level. Finally, possible causes of the observed differences are described.

VECTO

The simulation tool VECTO was developed on behalf of the European Commission DG CLIMA and is in a constant process of further development. The Institute of Internal Combustion Engines at Graz University of Technology (TUG) plays a leading role in the development of the tool and the associated legislation. Since January 2019, VECTO is applicable for the official CO₂ determination procedure of new trucks in the EU [7]. The following section gives a brief explanation of why VECTO is the preferred CO₂ determination method and how the VECTO approach works in principle.

A CO₂ determination of HDVs on the chassis dynamometer with reasonable effort was not considered possible due to the large number of different HDV models/types (e.g. variation of axle and transmission configurations) and diverse areas of application. Furthermore, since the incidents of recent years ("Dieselgate"), chassis dynamometer measurements have generally fallen into disrepute as a certification method. The disadvantages of other possible methods such as engine tests (no assessment of vehicle efficiency) and on-road tests (costly and poorly reproducible) also outweigh the advantages. A combination of certification tests on component level and simulation methods for the vehicle was found to be the most suitable determination method. This approach is implemented in Regulation (EU) 2017/2400 and the associated simulation tool VECTO. The approach is characterised by the following pro's (+) and cons's (-):

- + Cost efficient, due to comparable low certification effort
- + High reproducibility of results
- + Consideration of the interaction of all vehicle components and vehicle characteristics
- Ongoing updates of Regulation (EU) 2017/2400 and VECTO necessary to cover new technologies
- Certain manufacturer-specific controls (i.e. gear shifting, ADAS) can only be covered by generic approaches

VECTO uses input data on the main fuel consumption relevant components like engine, transmission, axle, tyres and air drag from certified component tests. The model is based on a time resolved vehicle longitudinal dynamics simulation to determine the required vehicle propulsion power as well as internal combustion engine torque and speed to interpolate from a fuel consumption map (Figure 1). A driver model operates the simulated HDV in a realistic way over predefined target speed over distance cycles ("mission profiles"). VECTO offers two simulation modes, one is the so-called "declaration mode" which is relevant for the official CO₂ determination. In the "declaration mode" all parameters like driver model settings, mission profiles, vehicle payloads and data on power consumption from auxiliary units are predefined as generic datasets. The second mode is the so-called "engineering mode" which it provides any kind of flexibility in model parameter settings. A more detailed description of the generic data as used in the current official VECTO version can be found in [8].

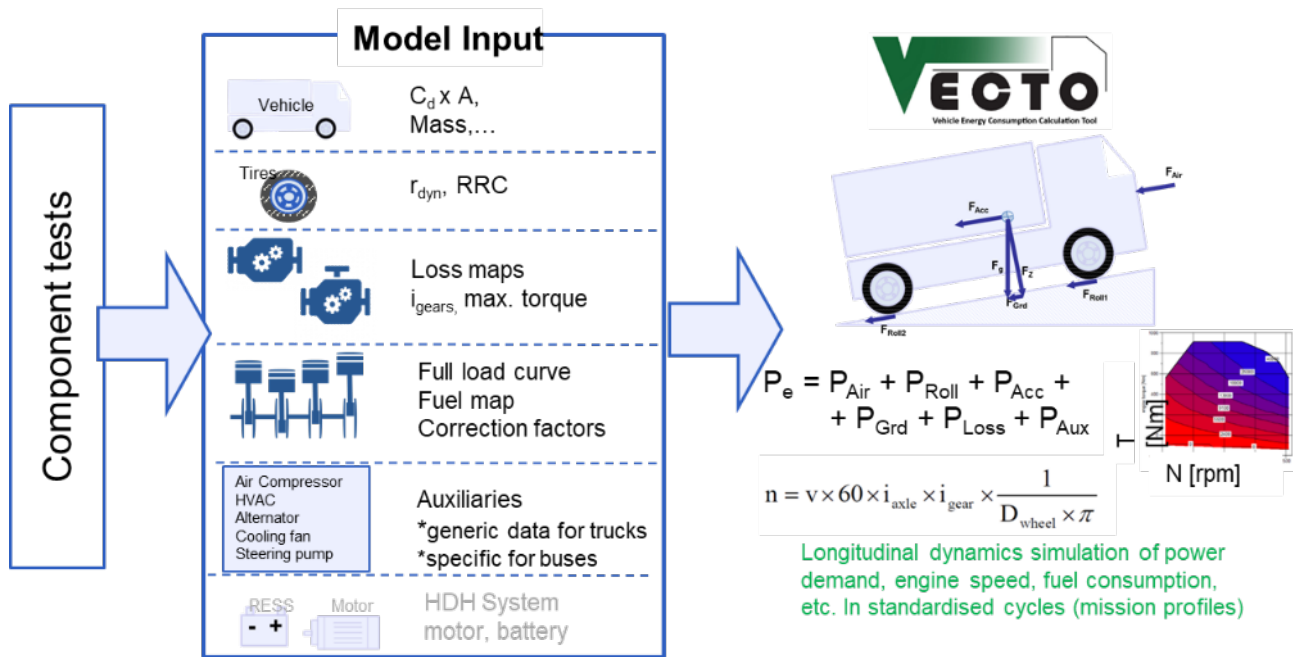


Figure 2: VECTO calculation scheme.

In the “declaration mode”, which is relevant for the official CO₂ determination, VECTO simulates two CO₂ values for each allocated mission profile (long haul, regional delivery, urban delivery etc.), one for “low payload” and one for “representative payload”. In order to give each vehicle a single CO₂ value (e.g. for application in the CO₂ standards and for putting a single CO₂ value into the vehicle papers), the individual simulation results for mission profiles and payloads have to be aggregated to a single CO₂ result. Allocated mission profiles, payload values and weighting factors are defined as a function of the vehicle sub-group, i.e. depending on the number of axles, chassis configuration (rigid or tractor) and other technical parameters. The general weighting formula is shown in Equation 1.

$$V_{wt} = V_{RDL} * RDL + V_{RDR} * RDR + V_{LHL} * LHL + V_{LHR} * LHR + V_{UDL} * UDL + V_{UDR} * UDR \quad \text{Equation 1}$$

With:

V_{wt} : Weighted simulation value for CO₂, FC (can be applied also to speeds, gradients in a distance based consideration)

$V_{RDL,RDR,LHL,LHR,UDL,UDR}$: Mission profile and payload specific simulation result

$RDL, RDR, LHL, LHR, UDL, UDR$: Mission profile and payload specific weighting factors

The corresponding weighting factors are shown in Table 1.

Available data

This chapter describes the data that has been available to analyse the correlation of real world fuel consumption data with the values determined by VECTO.¹³

Fleet data

Modern HDVs provide the option for connection with fleet management systems (FMS) to monitor operations. For customers who choose this option sensor- and actuator signals in the vehicle are recorded during operations and processed in different control units on-board and at regular intervals the processed data is transmitted to an off-board server for access by the FMS. For different reasons not all customers choose to have their operational data transmitted to an off-board server.

The foundation for the analysis carried out in this paper is formed by FMS operational data made available by Scania CV AB. The data comes from approximately 5000 vehicles produced in Q1 2019 and in operation in Europe during the year 2019. All vehicles are 4x2 tractors with over 16 tons gross vehicle weight and over 265 kW rated engine power and a sleeper cab and therefore belong to the vehicle subgroup “5-LH” according to [6]. Only vehicles for which

¹³ Fuel consumption and CO₂ emissions of a vehicle correlate almost completely linearly for a given fuel. In the following sections, therefore, only fuel consumption will be discussed. All conclusions can also be applied to CO₂ emissions.

meaningful operational data is available are included; they have more than 30 000 km mileage and the operational variables have been processed with reasonable results. Thus, the 5000 vehicles in the study is a sub-set of approximately 7000 vehicles produced in the time period for which VECTO data exists but no meaningful operational data is available. It is possible that this pre-selection has a minor impacts on the fuel consumption of the assessed fleet but it is not evident that the pre-selection has an impact on the correlation between VECTO and the fuel consumption of the same fleet. Table 2 gives an overview on the available operational dataset for each vehicle.

Table 1: Mission profile weights [6].

Vehicle group	Mission profile					
	RDL*	RDR	LHL	LHR	UDL	UDR
4-UD	0	0	0	0	0,5	0,5
4-RD	0,45	0,45	0,05	0,05	0	0
4-LH	0,05	0,05	0,45	0,45	0	0
9-RD	0,27	0,63	0,03	0,07	0	0
9-LH	0,03	0,07	0,27	0,63	0	0
5-RD	0,27	0,63	0,03	0,07	0	0
5-LH	0,03	0,07	0,27	0,63	0	0
10-RD	0,27	0,63	0,03	0,07	0	0
10-LH	0,03	0,07	0,27	0,63	0	0

* The first two characters describe the mission profile: long haul (LH), regional delivery (RD), urban delivery (UD); The last character describes the payload condition: representative (R), low (L)

Table 2: Available operational data for each vehicle.

Data
Annual distance (km/year), annual operation time (h/year)
Altitude (m) - share of time per bin
Ambient temperature(°C) - median and share of time per bin
Stop frequency (stops/100km)
Slope (%) – share of distance per bin
Gross train weight (kg) – average, highest 10th percentile and share of distance per bin
Speed (km/h) - Average speed and share of distance per bin
Idling share (%) with and without power take off
Cruise control usage (%)
Fuel consumption (l/100 km, l/h)

In the further analysis all kind of data provided per bin (e.g. distance shares driven in the speed range from 3 to 10 km/h) were always allocated to the mean value of the respective bin. To clean the data from outliers as well as incomplete data sets, the following vehicles were removed from the original dataset:

- 1) Vehicles without a provided GTW value and curb mass
- 2) Vehicles without information about the annual distance travelled

Subsequently, a further selection of the vehicles was carried out in order to generate a data set that can be directly compared with the simulations on the basis of the available VECTO models and results, the following vehicles were also removed from the original dataset:

- 3) Vehicles with an average altitude of above 1000 m
- 4) Vehicles with an idling power take off share of higher than 1%
- 5) Vehicles with an average distance based speed of lower than 74 km/h.¹⁴

After this selection process, a dataset of 3449 vehicles ("FMS - reduced") remain for further in-depth analysis. For the entire dataset of approximately 5000 vehicles ("FMS - all") also a comparison of "raw" fuel consumption of operational conditions is performed.

Official VECTO results

In addition to the data from the FMS, the official VECTO results shown in Table 3 were also provided for the respective vehicles. These data were available separately for the mission profiles long-haul and regional delivery and the two VECTO payload conditions.

Table 3: Provided VECTO data.

Data	Unit(s)
Average speed	km/h
Rated Power	kW
Fuel consumption	g/km, g/t-km, l/100km, g/m ³ -km, l/m ³ -km
CO ₂ emissions	g/km, g/t-km, g/m ³ -km
Actual curb mass	kg

VECTO average vehicle model

For the in-depth analyses done on the correlations between FMS data and VECTO results, also own simulations were carried out at TUG. For this purpose, a simulation model was compiled that shall represent the average vehicle in the FMS data as well as possible. This simulation model was compiled based on the few available vehicle specifications in the FMS data, generic data as used in VECTO and TUG assessments on the remaining set of parameters typical for such vehicles. The main vehicle specifications as represented in this simulation model are shown in Table 4.

¹⁴ For lower average speeds the operating conditions cannot be recreated for correlation using the submitted official VECTO results (see section 3.2).

Table 4: Vehicle specifications “average vehicle model”.

VECTO input data average vehicle		Source
Curb mass [kg]	8372	FMS data
Curb mass trailer [kg]	7500	VECTO generic data
P _{rated} [kW]	340	FMS data
cdxA [m ²]	5.390	TUG assumption
RRC Trailer [N/kN]	5.500	VECTO generic data
RRC steered [N/kN]	5.000	TUG assumption
RRC driven [N/kN]	5.500	TUG assumption
Air density [kg/m ³]	1.188	VECTO generic data
Transmission type	AMT	TUG assumption
Efficiency direct gear	98%	TUG assumption
Efficiency indirect gear	96%	TUG assumption
Axle ratio	2.64	TUG assumption
Axle efficiency	96%	TUG assumption
ADAS	---	TUG assumption

Comparison of FMS data and VECTO

Raw comparison of fuel consumption (lit./100 km)

Figure 3 gives a comparison of the fuel consumption (“FC”) data from FMS and the official VECTO results. Average FC from FMS in the entire dataset is found to be at 27.3 l/100km, in the reduced dataset at 26.4 l/100km. The fact that FC in “FMS - all” is higher than in “FMS - red” seems plausible, as vehicles with lower average speeds and significant proportions with PTO operation in idling were sorted out in “FMS - red”. The average official VECTO FC for the “FMS - red” vehicles is at 28.3 l/100km, which is an overestimation of about 7 percent. All further FC comparisons with VECTO are only carried out with regard to “FMS - red”, because - as already mentioned above - this data set provides a better basis for comparison.

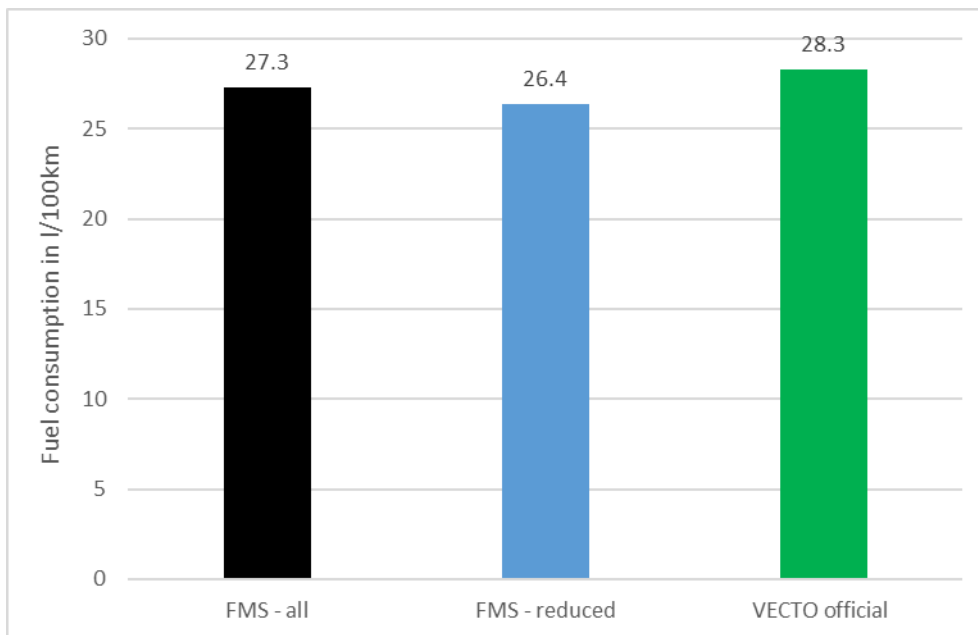


Figure 3: Comparison of fuel consumption from FMS and official VECTO results.

Comparison of operational conditions

Figure 4 gives a comparison of vehicle speed data between FMS and VECTO. The left diagram gives the distribution of instantaneous vehicle speeds, consolidated by weighting of data from each vehicle using the annual driven mileage. This picture thus can be considered as the speed distribution of all driven kilometres. The right diagram shows the data on average speed per vehicle, again consolidated by weighting per annual mileage. The speed data in both diagrams refer to a distance-based consideration, i.e. the time shares are weighted with the speed in the calculation. This applies to the determination of the shares of the individual speed bins in the left image and to the calculation of the average speed of the individual vehicles in the right image. As before “VECTO official” refers to the weighted results according to Equation 1 and Table 1.

The speed distribution of all driven kilometres (left picture) is found to be less broadly spread in the official VECTO results than in FMS. VECTO has lower top speeds and lower distance shares in the medium speed range (40 km/h to 80 km/h). Looking at the average speed per vehicle (right picture) VECTO only produces a single value in the speed bin of 75 to 80 km/h, since the average speeds in the simulated VECTO cycles vary only slightly between the individual vehicle configurations (e.g. influence of motorisation and mass). The FMS data naturally show a relatively broad distribution with average speeds in the entire range from 70 km/h to 90 km/h. Overall the average VECTO speed is found to be some 2% higher than in FMS (79,7 km/h vs 81.3 km/h).

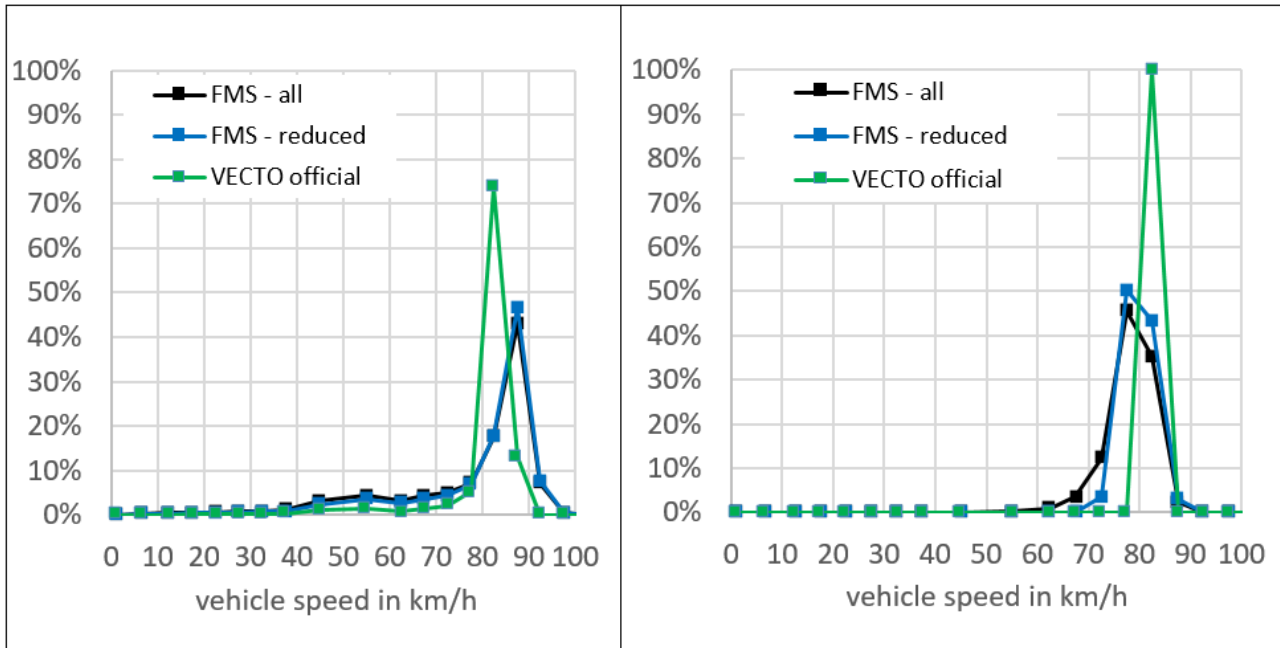


Figure 4: Comparison of vehicle speed data: distribution of instantaneous speeds (left) and vehicle average speeds (right).

Analogous analyses were also carried out for gross tone weight (GTW) which reflects the total vehicle mass incl. trailer and current payload (see Figure 5). The distribution of the total vehicle mass in VECTO is less continuous as in the fleet as only three different payload conditions¹⁵ are simulated (left picture). The average vehicle masses in VECTO however correspond very well with the FMS data (right picture). In the overall average, the vehicle masses in VECTO are 4% higher than in the FMS data.

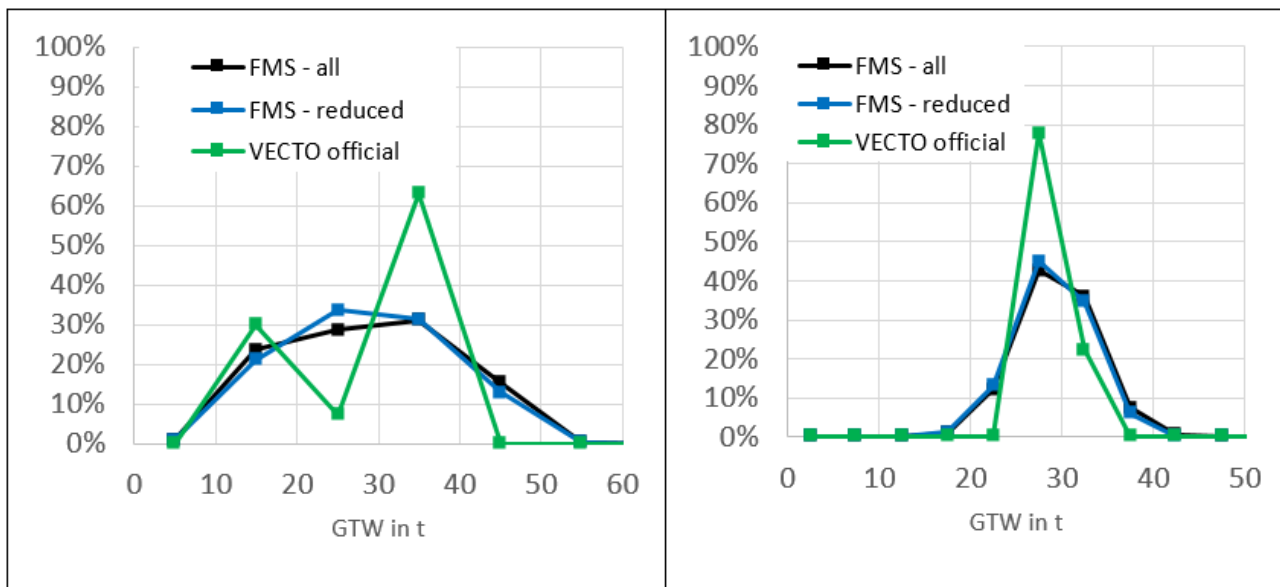


Figure 5: Comparison of gross tone weight (GTW): distribution of instantaneous data (left) and average vehicle masses (right).

¹⁵ For group 5 vehicles: Long haul: 2 600 kg low payload, 19 300 kg representative payload; Regional delivery: 2 600 kg low payload, 12 900 kg representative payload

A further and in particular for HDV important influence on fuel consumption comes from road gradients. Figure 6 shows the kilometre shares according to gradient bins, whereby positive (uphill) and negative (downhill) gradient values were combined in the bins. It turns out that the distribution from VECTO matches the FMS data considerably well. However, this analysis is not able to include all parameters relevant to slope influence. In addition, the sequence of the longitudinal slopes (hilliness) is also relevant for fuel consumption. In this respect, it is assumed that the gradient profile of the current long haul mission profile is less hilly (and thus contains longer continuous uphill and downhill sections). This is particularly relevant for the evaluation of vehicle technologies that work with efficient use of potential and kinetic energy (e.g. predictive cruise control, hybridised drives, etc.). Work on a possible update of the long haul mission profile for a future version of the official VECTO is already underway.

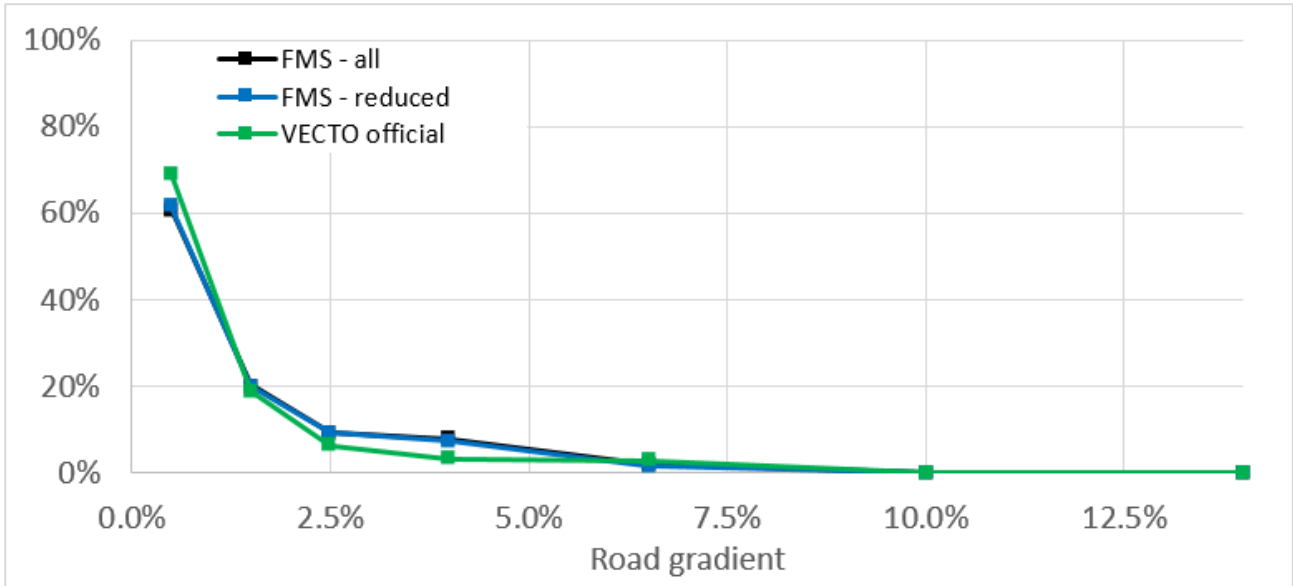


Figure 6: Distribution of gradient (share of distance).

Finally, the number of stops and the idling timeshares were analysed (Figure 7). Regarding number of stops, the official VECTO results contain with 3.7 stops per 100 km a significantly lower number of stopping and drive-off operation than the FMS distribution, which peaks at 10 stops per 100 km (left picture). Also the time shares of idling on the total vehicle operation time is underestimated by VECTO (right picture). In this regard FMS data also contains idling timeshares occurring during driving (e.g. eco-roll) but this proportion is estimated to be low compared to idling at standstill.

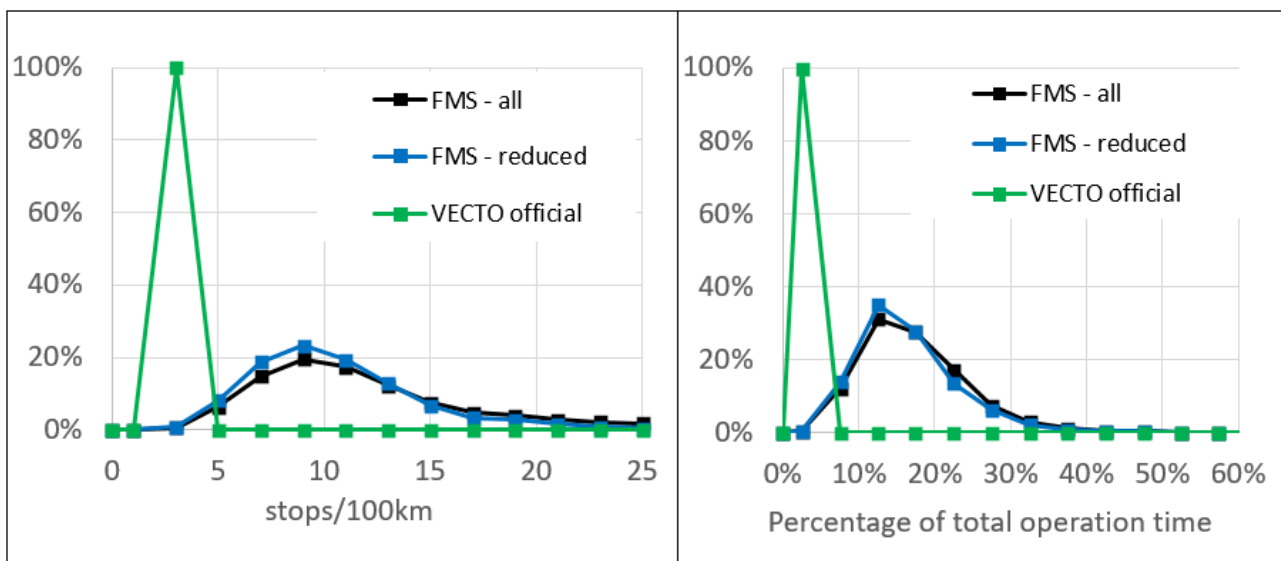


Figure 7: Comparison of number of stops (left) and idling time shares (right).

Adjustment of operational conditions in VECTO to FMS data

As discussed above the comparison of operational data in VECTO and from FMS shows some differences. This raises the obvious question of the extent to which the differences in fuel consumption between VECTO and FMS are due to the differences in operating conditions. Therefore, in this work the exercise was undertaken to adjust the VECTO results for the individual vehicles of the "FMS - reduced" data set to their actual operating conditions.

First step of the adjustment was the correction of the VECTO top speed. For this purpose, the speed profile of the long haul (LH) mission profile has been increased by 2.5 km/h. For this modified cycle the ratios of fuel consumption and average vehicle speed - each compared to the values from the original LH mission profile - was determined in the VECTO "engineering mode" using the average vehicle model as described in section 3.3. Based on these ratios the official VECTO results for each particular vehicle in the "FMS - red" dataset have been corrected.

In the next step, for each vehicle a new set of individual weighting factors for the four combinations of mission profiles and payloads RDL, RDR, LHL and LHR (acc. to Equation 1) have been determined to adjust VECTO vehicle speed and total mass distributions. This was done based on a non linear solving function with the following criteria:

- Requirement: sum of weighting factors = 1
- Constraints:
 - $v_{wt, adjusted} = v_{avg, FMS}$
 - $GTW_{wt, adjusted} = GTW_{FMS}$

With:

$v_{wt, adjusted}$: Weighted average speed of the VECTO mission profile – after top speed correction - for the particular vehicle

$v_{avg, FMS}$: Average speed from FMS data for the particular vehicle

$GTW_{wt, adjusted}$: Weighted gross ton value from VECTO (acc. to Equation 1) for the particular vehicle

GTW_{fleet} : Average GTW from FMS data for the particular vehicle

The resulting weighting factors were then consolidated based on the annual mileage of each particular vehicle to obtain new average weighting factors (see Table 5) which represent the analysed fleet data in terms of average speed and average GTW. As already indicated for the comparison of the operating data, the regional delivery cycle has a significantly higher share in the new calculated weighting factors.

Table 5: Adjusted weighting factors for the FMS – reduced dataset.

	Mission profile					
	RDL	RDR	LHL	LHR	UDL	UDR
Adjusted	0.14	0.31	0.15	0.40	0	0
Official	0.03	0.07	0.27	0.63	0	0

Since in the official VECTO the payload is limited to 19 300 kg to the upper end and 2 600 kg to the lower end, a few vehicles in FMS – red were found to be heavier or lighter than the approach as described above is able to cover. For such cases an additional GTW correction was applied. This additional correction is based on the observation that, in a good approximation, a linear dependency between vehicle mass and fuel consumption can be applied.

Figure 8 (vehicle speed) and Figure 9 (gross ton weight) show the comparison of the operational data after above-mentioned adjustments. A high level of correlation could be achieved between the adjusted VECTO and the FMS data.

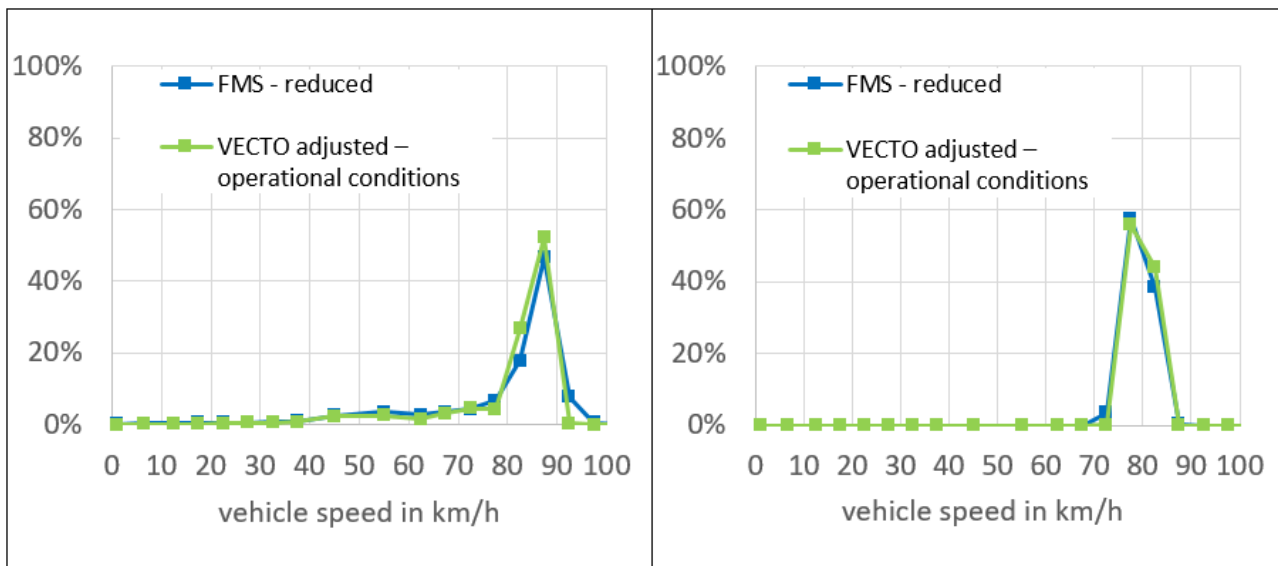


Figure 8: Comparison of adjusted vehicle speed data: distribution of instantaneous speeds (left) and vehicle average speeds (right).

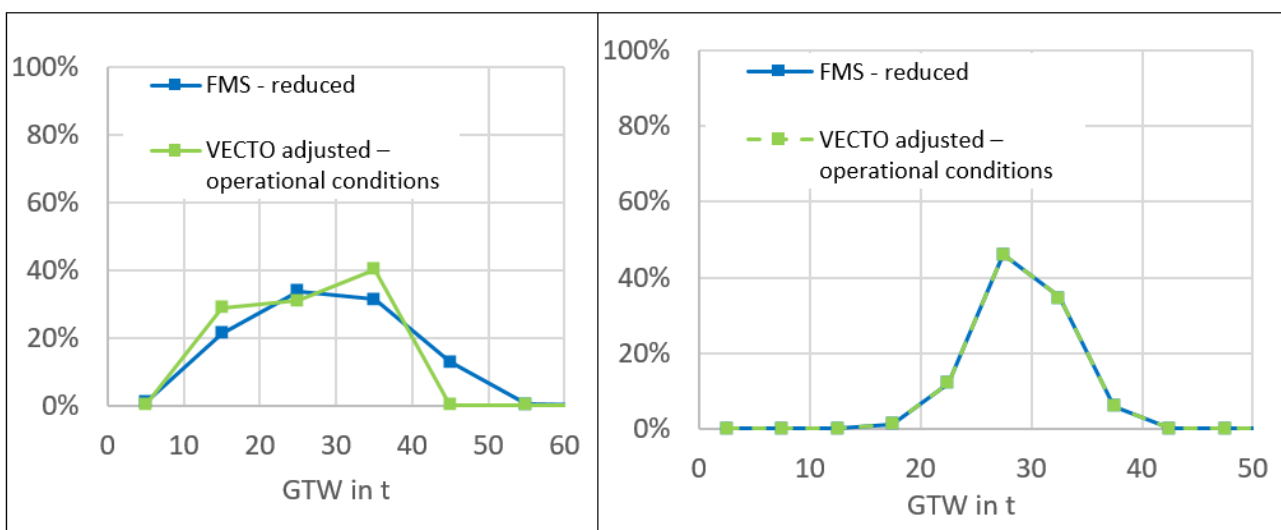


Figure 9: Comparison of adjusted gross tone weight (GTW) data: distribution of instantaneous data (left) and average vehicle masses (right).

In a final correction step, the operating conditions were adjusted with regard to the number of stops per 100 kilometres and the idling time at standstills. The number of stops influences the braking energy occurring in the cycle, idle times with the engine-on add additional fuel consumption with engine idle. To determine the first influence, the VECTO mission profiles were simulated once with and once without stops. This allows for calculation of the weighted fuel consumption for each vehicle stop-start off procedure and thus a vehicle individual adjustment of the fuel consumption caused by different stop counts could be performed. The correction of fuel consumption due to different standstill times is based on the determination of the idling fuel consumption in g/s of the average vehicle. This value is then multiplied by the difference of idling time between VECTO and fleet data and added as a correction.

Based on the above mentioned steps VECTO results have been corrected for all operational information available from FMS. The only exception is the gradient distribution, as already a good correlation was observed for the official VECTO (see Figure 6). These corrections made cannot, of course, represent exact adjustments, but should tend to reflect well the trend in the fuel consumption due to the different operating conditions.

Figure 10 shows the comparison of the fuel consumption values including VECTO results with the adjusted operating conditions. As expected, the simulated FC value increases to 29.6 l/100km due to the adjustments (higher top speed, higher proportion of regional delivery mission profiles, more stops per kilometre). This also increases the discrepancy of the VECTO results with the direct comparison value "FMS - reduced" to 12%.

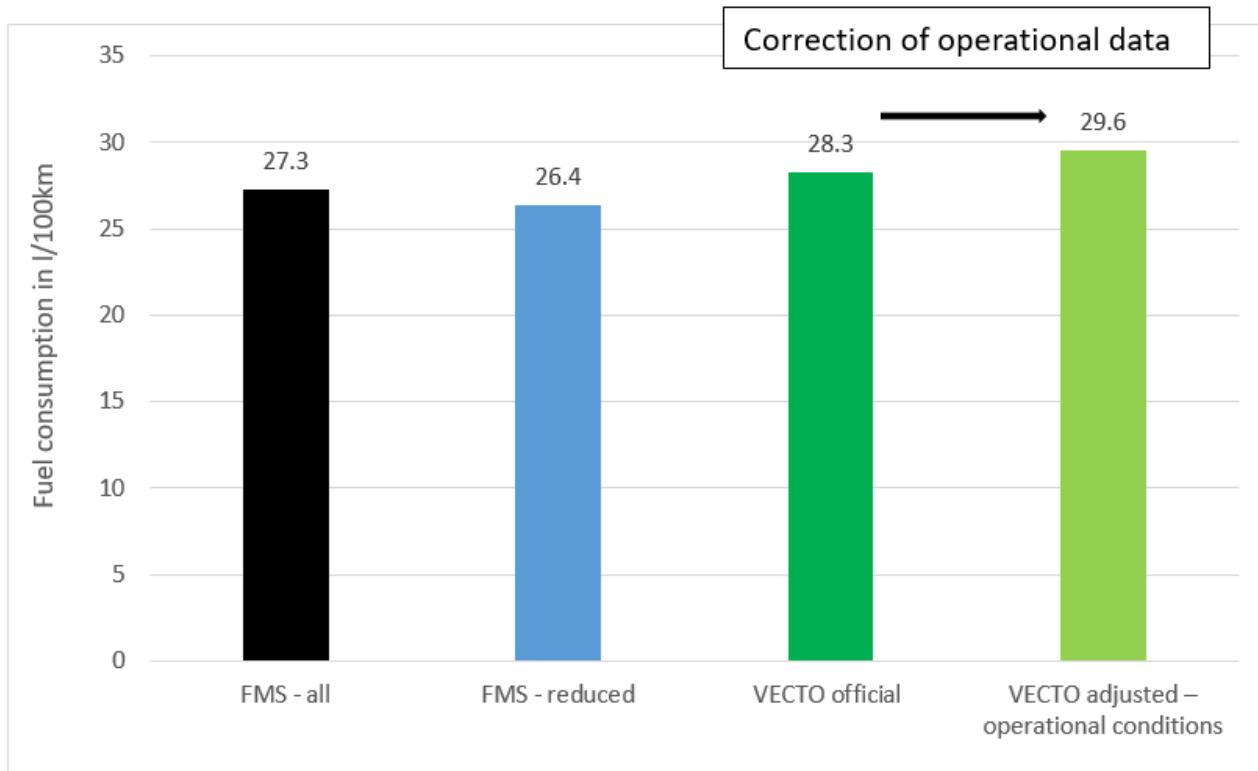


Figure 10: Comparison of fuel consumption from FMS and VECTO including results adjusted for operational conditions.

Analysis of the possible causes of the remaining deviations in fuel consumption

In this chapter, the remaining deviations in fuel consumption between the VECTO results adjusted for operating conditions and the values from the "FMS - reduced" data set are further analysed. Reasons for deviations can naturally lie on both sides of the comparison, i.e. on the side of the consumption determination by FMS and at VECTO.

Possible causes from the FMS fuel consumption determination

In order to determine the consumption value as analysed in this paper in the unit of l/100km, both the fuel volume flow and the distance driven must be determined on-board the vehicle.

Fuel volume flow is usually determined by an ECU model which calculates the amount of fuel injected via the opening times of the diesel injectors. A rough expert estimate for the uncertainty of this method for a single vehicle gives a range of about +/- 5%. For an exact comparison with the standardised VECTO consumption values of a vehicle, furthermore the variation of the fuel density (ca. +/- 1.5%) and of the lower heating value of the fuel used in real operation (estimate ca. +/- 1.5%) would also have to be taken into account.

For determining the speed and travelled distance HDV use the system required by Regulation (EU) 165/2014 (Smart Tachograph). This Regulation stipulates that the deviation of the distance actually travelled from the measured value must be less than +/- 4% in real operation.

In order to conclude from these uncertainties for tolerances at individual vehicle level towards the overall effect on the accuracy of a fleet consumption value, it would have to be statistically examined whether individual effects are normally distributed or have a systematic bias. These analyses clearly go beyond the scope of this work, but are currently being determined in a study commissioned by the European Commission on OBFCM provisions (On Board Fuel Consumption Monitoring).

Possible causes from the VECTO fuel consumption determination

As a matter of principle, simplifications and generalisations must be made when depicting real world fuel consumption by a system of component tests and overall vehicle simulation. This is especially the case if, as for the VECTO approach, it is a method within the framework of an official legislative procedure that is to be designed in a deliberately robust manner and applicable to all vehicles in the EU. In the following, such simplifications or generalisations are listed and, if possible, indicatively quantified with regard to possible effects on the comparison with FMS data.

Air drag – Overestimation of C_dxA by Constant Speed Test (CST)

The test procedure for the determination of the C_dxA value for VECTO is the CST which consists of measurement of total driving resistances in a high speed part (ca. 90 km/h) and in a low speed part (ca. 15 km/h). In the evaluation of the measurement data, it is assumed for simplification that the rolling resistance is constant over the entire speed range. In reality, however, the rolling resistance at 15 km/h is approximately 15% less than at 90 km/h. This simplification results in an overestimation of the C_dxA value by 5% to 10% for a group 5 vehicle as analysed in this study [8]. If the VECTO fuel consumption value is corrected for this influence, the result decreases by approx. 2%.

Air drag – Influence of real semi-trailer geometry

The C_dxA value applied by VECTO for a group 5 vehicle is related to a standard semi-trailer geometry as defined in Annex VIII of Regulation (EU) 2017/2400. This standard semitrailer is defined as a 3-axle drybox-body in a typical configuration and without any extra features like pallet box or any dedicated aero features. The real semi-trailer geometries used in the fleet of course differ from this configuration. It can however be assumed that box bodies (e.g. besides drybox also curtain siders and reefers) will be used for the most part with group 5-LH vehicles. In any case, the deviation of the real trailer geometry from the standard trailer geometry results in an uncertainty in C_dxA and thus also can be a source for the deviation of the VECTO consumption from FMS. This uncertainty cannot be seriously quantified here. Both (slightly) lower and worse real C_dxA values are conceivable.

Air drag – Influence of the air density

The generic air density in VECTO (1.188 kg/m³) refers to an average ambient temperature of 12°C and an average altitude of 200 meters. The average temperature of the FMS data was at 18°C, for the average altitude no detailed information is available (only that the average altitude was below 1000 m). If just the air density applied in VECTO is corrected to 18°C, the simulated fuel consumption decreases by 0.7%.

Rolling resistance – influence of flat road surface, warm-up, pressure and ambient temperature

Certification of tyre rolling resistance (RR) is performed in repeatable laboratory conditions with correct pressure, warmed-up tyres and on a large steel drum. Real world RR differs from the certified conditions due to several influences, where the most important are influence of flat road surface, warm-up conditions, tyre pressure and ambient temperature. A study performed by FAT indicated that new tyres at 10°C ambient temperature and in fully warmed up conditions have about 20% higher RR than in the laboratory [12]. For ambient temperatures it is known that warm conditions correlate with lower RR (e.g. +1°C corresponds to -0,6 %RR in a range from 10°C to 40° [13]). The above information applies to tyres at operating temperature, whereby it takes approximately one hour of driving time for the tyre to reach a steady-state temperature and pressure level. Especially at the beginning of the warm-up period, the rolling resistance is significantly increased (e.g. +25% in the first 30 minutes, according to [12]).

If the above-mentioned influencing factors are added together in an indicative estimate, a cumulative effect of approx. +18% on RR emerges. If this were taken into account in the VECTO calculations, there would be an increase in fuel consumption of about 6%. In any case, this figure should be treated with caution, but based on the analysis it can be assumed that the RR tends to be higher than the certified RR with regard to the influencing factors listed in this section.

Rolling resistance – Influence of trailer tyres

In the official VECTO calculations a generic RRC (Rolling Resistance Coefficient) value for the tyres of the trailers of 5.5 kg/ton (mean value of the efficiency class “C”) is used. Current and reliable figures on the actual rolling resistance of current trailer tyres are not available. In an optimistic scenario, it could be assumed that a large part of the trailer tyres already belong to efficiency class B (4.5 kg/ton). If this were actually the case, the VECTO fuel consumption for group 5 vehicles would be reduced by some 3.0%. The actual tyres used could of course also have worse RRC values, but a plausible maximum range in this direction is estimated to be smaller (indicatively half the tolerance).

Rolling resistance – Influence of tyre wear

In the course of a tyre's life tyre wear causes a decrease in rolling resistance of up to 35% (referring to minimum tread depth reached after approx. 150,000 to 300,000 kilometres, depending on the tyre type) [10]. For the vehicles

in the FMS data set, the average mileage is known (approx. 65 000 km). For the tyres on the semi-trailers the mileage is not known as they have different life-cycles and tyre change patterns than the towing vehicles. It is thus assumed that half worn tyres do represent the average semi-trailer conditions in the FMS dataset. Applying these figures to the VECTO fuel consumption value results in a reduction of approx. 3.5%.

Advance Driver Assistance Systems (ADAS) – Influence of simplified VECTO approach

The absolute majority of the vehicles in the study are equipped with predictive cruise control (PCC) but the system does not qualify as ADAS in the certification requirements of the VECTO Regulation (EU) 2017/2400, notably the system is not always switched on at key-on. As a consequence VECTO over-estimates the energy losses due engine- and service-braking. Where the vehicles in the study do qualify for PCC with eco-roll but without engine off this would lower the VECTO results with 1.5 % in the latest VECTO version.

Advance Driver Assistance Systems (ADAS) – Influence of hilliness

As already briefly discussed in section 0 the gradient profile of the LH cycle is assessed as not hilly enough compared to representative European road conditions. This has a particular impact on the effect of ADAS systems such as PCC. The possible effects on the simulated consumption value were discussed in expert groups in the course of further development of VECTO and are currently being estimated at a reduction of approximately 1%.

Regarding reflection of ADAS in VECTO it needs to be mentioned that in the actual vehicles different systems with partly very OEM specific control algorithms are installed and these are not fully captured by the generic implementation. The associated uncertainties also relate to the driving style of the actual drivers (or in the context of ADAS, how much the fuel saving cruise control is used) and the representativeness of the VECTO driving cycles in general. Considering the relatively large share of energy that is wasted on braking it may be worthwhile to develop even more advanced systems for speed optimization.

Wheel bearings

Losses from wheel bearings are not covered in the current VECTO approach. Only the measurement of axle losses includes a part of the friction losses of the wheel bearings of the driven axle. For future extensions of the procedure, methods are currently being discussed to also certify the wheel bearings as components and thus to be able to explicitly map their losses on all axles of the vehicle in VECTO. From the discussions in the expert group dealing with this issue, it can be concluded that at the moment about 2kW of losses are not mapped in VECTO. If the effect were reflected in VECTO, fuel consumption would increase by about 2%.

Gear shifting

Gear shifting is a significant parameter influencing fuel consumption. Generic gearshift programmes are implemented in VECTO for this purpose. In the VECTO version used to determine the official values of the FMS data set, a relatively simple gearshift programme is applied based on fixed gearshift lines defined by engine speed and load. Current HDV generations use much more sophisticated shift strategies that take into account the individual engine and drive train efficiencies at the various operating points. In order to take the influence of such algorithms into account in VECTO, improved generic models have already been developed for VECTO, which will presumably also be used in the official version from 2022 on [9]. For the comparison between FMS and VECTO in the LH and RD cycles as performed in this paper, the influence is however to be assumed to have a considerably lower uncertainty as other influence factors.

Certification worst case principles

All components in the VECTO regulation are certified according to the “worst case” principle. This means that the test setup used to generate VECTO input data corresponds to the worst installation of all installations covered by the certificate, for example the worst air ducts for engine breathing. The majority of the 4x2 tractors in the study are rather on the good side in all that relates to fuel consumption and the effect of the worst case principle on this collective is estimated to be 1-2 %.

The above-mentioned parameters influencing simulated fuel consumption by VECTO are summarised in Table 6. This table also contains some other influencing variables that are known but cannot be quantified.

If all the influencing factors quantified in Table 6 are combined (range of ca. +/-0% to -12%), averaged (-6%) and applied to the VECTO result adjusted for operational conditions as determined in section 0, a “final adjusted” VECTO result of 27.5 l/100km is obtained. This leaves an overestimation of the consumption value from the “FMS - reduced” data set (26.4 l/100km) by VECTO of approximately 4%. Such a remaining non-attributable deviation can be well explained by the above analysed and non-quantifiable causes, the main ones coming from the real world driving resistances and also including the uncertainties from the FMS side.

Table 6: Possible causes for VECTO deviations to FMS data.

Influence factor		Indicative change of VECTO fuel consumption if considered
Air drag	Overestimation of CdxA by Constant Speed Test	- 2%
Air drag	Air density influence (18° as in FMS - reduced instead of 12°)	- 0.7%
Air drag	Real semi-trailer geometry vs. standard semitrailer geometry	n.q. but significant (↑↓)
Rolling resistance	Influence of road surface, warm-up and pressure	+6% with significant uncertainty
Rolling resistance	Uncertainty regarding trailer tyres	- 3% to +1.5%
Rolling resistance	Influence of tyre wear	- 3.5%
ADAS	Influence of simplified VECTO approach	- 1.5%
ADAS	Influence of hilliness	- 1%
Wheel bearings	Losses not considered	+ 2%
All tested data	Worst case certification	-2%
Gear selection	Representativeness of VECTO generic gear shift model	n.q. (low)
Driving resistance	Bad weather conditions (rain, snow etc.)	n.q. (↑)
Driving resistance	Influence of cornering neglected	n.q. (↑)
Auxiliaries	Representativeness of generic data in VECTO	n.q. (?)
VECTO driver behaviour (and ADAS parameters)	Influence of driving style and applied ADAS settings	n.q. (?)
...
n.q. ... not quantifiable		

With regard to the simplifications or generalisations in VECTO, the question naturally arises as to whether these represent a problem for the quality or the application of the official CO₂ values. Simplifications regarding effects that have a similar influence on all vehicles or technologies and that offer little or no potential for technological improvement do not pose a problem. From the list above, this clearly applies e.g. the overestimation of CdxA values from the constant speed test or the influence of bad weather. As mentioned above, improved methods are already being developed for some topics (ADAS, gearshifting, wheel bearings). Furthermore, a separate official CO₂ and energy efficiency assessment procedure for trailers is currently being developed. Some topics could be taken up additionally in the future, e.g. the influence of cornering, which plays a central role in the evaluation of steered axles.

Summary and final conclusions

In this paper, the operational data and fuel consumption recorded by means of Fleet Management Systems (FMS) in real operation of a fleet of approx. 5000 vehicles is compared with the official fuel consumption data determined with VECTO, the official certification tool of the European Commission. For more in-depth analyses, the vehicle sample was reduced to approx. 3500 vehicles. The vehicles have been produced in Q1 2019 and been operative over the entire year 2019. All vehicles belong to the HDV CO₂ standards subgroup “5-LH” i.e. are tractors usually operated with semitrailers predominantly in long haul and partly in regional delivery missions.

From the comparison of operational conditions between VECTO and FMS it is concluded:

- Vehicle speed distribution in VECTO is slightly less broad with lower top-speeds and slightly lower proportions in the 40 km/h to 80 km range. Overall the average VECTO speed was found to be some 2% higher than in FMS (79.7 km/h vs 81.3 km/h, where the averaging of the velocities was carried out distance-based and not time-based). VECTO applies less stops/100km and less idling times than found in the FMS data.
- The distribution of the total vehicle mass in VECTO is less continuous as in the fleet. The average vehicle masses in VECTO however correspond very well with the FMS data. In the overall average, the vehicle masses in VECTO are 4% higher than in the FMS data.
- Regarding distribution of road gradients the distribution from VECTO matches the FMS data very well. A comparison of the hilliness of the VECTO cycles, as currently discussed in the VECTO working groups, cannot be investigated on the basis of the FMS data used here.

A comparison of fuel consumption values shows a deviation of the official VECTO values (28.3 l/100km) of +3.5% compared to the complete FMS dataset (27.3 l/100km) and of +7% compared to the more closely analysed” FMS – reduced” data set (26.4 l/100km). If for the latter the VECTO results are corrected for the different operational conditions the deviation of VECTO compared to FMS increases to +12%.

Finally, the paper analyses possible causes for the remaining deviations. Possible inaccuracies from the determination of the FMS consumption value cannot be quantified here. With regard to simplifications and generalisations in VECTO, a number of influencing factors could be determined and quantified, which, when included in the VECTO results, tend to correct the simulated FC value downwards by some 7%, i.e. leaving a remaining gap of +4% to the FMS data. The identified simplifications and generalisations are assessed either to be not critical to the quality of the official VECTO result (e.g. the simplifications to be made regarding driving resistances) or are already subject for revision in future steps of the Regulation (EU) 2017/2400 and the VECTO Tool (e.g. improved generic models for ADAS and gear shifting, certification of wheel bearing losses).

Finally, based on this first systematic comparison of real consumption data from the fleet with the official values from VECTO, it can be concluded that the VECTO consumption values provide a very good and slightly conservative estimate of the real fuel consumption of long-haul trucks.

References

- [1] Freight transport statistics -modal split, Eurostat,
https://ec.europa.eu/eurostat/databrowser/view/tran_hv_frmod/default/table?lang=en
- [2] Muncrief, R. and Sharpe, B., “Overview of the Heavy-Duty Vehicle Market and CO₂ Emissions in the European Union,” 2015..
- [3] European Environment Agency (EEA), Share of transport greenhouse gas emissions, 2019,
https://www.eea.europa.eu/data-and-maps/daviz/share-of-transport-ghg-emissions-2#tab-googlechartid_chart_12
- [4] Schade, Wolfgang & Krail, Michael. (2010). iTREN-2030: Experiences and results for integrated technology, energy and transport policy assessment. 10.13140/2.1.2035.4887.
- [5] European Commission, “2050 low-carbon economy|Climate Action,” 2017,
https://ec.europa.eu/clima/policies/strategies/2050_en

- [6] Regulation (EU) 2019/1242 of the European Parliament and of the Council of 20 June 2019 setting CO₂ emission performance standards for new heavy-duty vehicles and amending Regulations (EC) No 595/2009 and (EU) 2018/956 of the European Parliament and of the Council and Council Directive 96/53/EC, 2019.
- [7] Regulation (EU) 2017/2400 of 12 December 2017 implementing Regulation (EC) No 595/2009 of the European Parliament and of the Council as regards the determination of the CO₂ emissions and fuel consumption of heavy-duty vehicles and amending Directive 2007/46/EC of the European Parliament and of the Council and Commission Regulation (EU) No 582/2011, 2017.
- [8] Rexeis M., Quaritsch M., Hausberger S., Silberholz G., Steven H., Goschütz M., Vermeulen R.: VECTO tool development: Completion of methodology to simulate Heavy Duty Vehicles' fuel consumption and CO₂ emissions. Final Report By order of EUROPEAN COMMISSION DG CLIMA Report No. I 15/17/Rex EM-I 2013/08 1670 from 07.08.2017
https://ec.europa.eu/clima/sites/clima/files/transport/vehicles/docs/sr7_lot4_final_report_en.pdf
- [9] Martin Rexeis, Martin Röck, Markus Quaritsch, Stefan Hausberger, Gérard Silberholz: Further development of VECTO. Final Report By order of EUROPEAN COMMISSION DG CLIMA Report No. I 16/19/Rex EM-I 17/24 5670 from 29.11.2019
- [10] Kurt Bergmüller, Robert Dworzak, Kraftstoffsparen mit Lkw-Reifen, Semperit Reifen GmbH, 27.03.2015
- [11] Georgios Fontaras et al: Development of a CO₂ certification and monitoring methodology for Heavy Duty Vehicles – Proof of Concept report, 2014. JRC87799. ISBN 978-92-79-32146-4
- [12] Bode M.: Der Rollwiderstand von Nutzfahrzeugreifen unter zeitvarianten Betriebsbedingungen, Forschungsvereinigung Automobiltechnik e.V. (FAT) 2018. ISSN 2192-7863
- [13] Michelin. Der Reifen – Rollwiderstand und Kraftstoffersparnis. 2005. ISBN 2-06-711658-4

2.16 Using a simulation approach to reconstruct the lab values with real-world driving data

D. Komnos^{1,2*}, J. Suarez-Corujo³, J. Pavlovic³, L. Ntziachristos², G. Fontaras³

¹ FINCONS Group, 20871 Vimercate, Italy

² Mechanical Engineering, Aristotle University of Thessaloniki, 54124 Thessaloniki, Greece

³ European Commission, Joint Research Centre (JRC), Ispra, Italy

Dimitrios.Komnos@ext.ec.europa.eu

Abstract

Recent EU regulations introduce mandatory monitoring of in-use fuel and energy consumption through On-Board Fuel Consumption Meters (OBFCM) in order to limit the divergence between officially reported and real-world CO₂ emissions. Still, a reference value per vehicle, as the one produced in well-defined lab conditions, is essential to compare vehicle efficiency among different vehicles, since the OBFCM is likely to give a wide dispersion of fuel consumption (FC) per vehicle model. In the present study, with the use of data of a 4-wheel drive mini-Sport Utility vehicle (SUV) collected over one year under real-world driving conditions, driven by 19 different drivers, and an accurate vehicle simulator, we assess the possibility to reconstruct the lab FC value. The results of the calculations show an adequate accuracy, with an unbiased error distribution when comparing to the reference lab value. The error distribution replicates a normal function, with 76% of the values falling inside the 20% range of fuel consumption error. The simulated FC gap is calculated, showing sufficient alignment to the measured with a bias of 2%. As a final step, an analysis of the trip characteristics needed for better capturing the laboratory value is performed.

Introduction

A discrepancy exists between official, laboratory-based, vehicle fuel consumption (FC) values and the ones reported by real world emissions; the discrepancy, also known as the FC gap, is reported both by scientific testing and by real users (Ligterink and Eijk, 2014; Tietge et al., 2015; Triantafyllopoulos et al., 2019). Passenger and light-duty vehicles (LDV) come first in the share of EU greenhouse gas emissions in road transport, comprising together 15.3% (European Automobile Manufacturers Association, 2020). Between the years 1990 and 2014, the CO₂ emissions from road transport increased by 17%, and this evolution is assigned to both personal and freight transport (Hoofman et al., 2018). This growth is estimated to reach 40% by 2050 (European Environment Agency, 2016; Hoofman et al., 2018). These figures point out the importance of monitoring the gap to ensure it is low and does not artificially grow.

The main factor explaining the FC gap was the test procedure used in the past for the fuel consumption and CO₂ emissions certification (Pavlovic et al., 2018; Tietge et al., 2015). The New European Driving Cycle (NEDC) has been reported to poorly represent real driving styles and vehicle operation (Weiss et al., 2011). More interestingly, studies show that the gap increased up to 40% in 2017 (Duarte et al., 2016; Fontaras et al., 2017b; Tietge et al., 2015). In the same year, the EU introduced a new test protocol to replace the NEDC also to limit this problem. The Worldwide harmonised Light-duty vehicle Test Protocol (WLTP) (European Commission, 2017a) includes a more detailed test procedure, making it more robust than its predecessor (Pavlovic et al., 2018; Tietge et al., 2019). Studies show that the new protocol increases the reported CO₂ emissions by 15-20% (Fontaras et al., 2017a; Pavlovic et al., 2018). Still, the difference in FC between laboratory test and real-world driving (RWD), although likely to have reduced, remains significant (Dornoff et al., 2020).

In an attempt to identify the origins of this divergence, a study by Fontaras et al. (2017b), including a comprehensive literature review, categorised the factors into three main groups. The first includes the vehicle characteristics and state; the second is related to the environmental and traffic conditions, while the third covers the vehicle driver. In an experimental campaign, where twenty different drivers were asked to drive a specific vehicle for their day to day needs, many recorded parameters falling under the environmental, traffic, and driver factors, were subsequently assessed in a holistic approach (Pavlovic et al., 2020). The average speed (falling under the driver factor), the road grade and the distance driven (falling under the environmental factors) seem to explain already a significant portion of the gap. An essential outcome of that study was that one should consider the vehicle characteristics, the driver style, the environmental and traffic factors, and the driver's needs to explain the FC gap.

A new regulation was recently adopted by the European Commission, in which new cars and vans are required to collect FC information through On-Board FC Monitoring devices (OBFCM) (European Commission, 2019a, p. 631). Similar provisions are set also for Heavy Duty Vehicles (HDVs) (European Commission, 2019b). For LDVs the accuracy of these devices is prescribed to be within $\pm 5\%$ compared to the fuel consumption reported in the laboratory during WLTP type-

approval test. A study on both LDV and HDV OBFCMs confirmed that this accuracy can be achieved in most vehicles registered in the EU market already before the new OBFCM regulation (Pavlovic et al., 2021).

The gap will need to be monitored and explained in the years to come. Respective tools need to be developed for this purpose. A simulation approach can serve in this direction because the impact of different factors can be analysed to reach the real cause of the gap. It is essential to assess the data at a higher level with statistical approaches and to understand the trip specificities with physical models following a simple but comprehensive analysis. Testing energy and fuel consumption in the lab is vital for benchmarking purposes, especially for the customers. To this end, this study assesses the possibility to use laboratory test data to confirm the RWD figures. Similar studies exist in the literature (Doulgeris et al., 2020; Mogno et al., 2020; Tsiakmakis et al., 2019; Zacharof et al., 2020), but to the authors' knowledge, not using extended RWD datasets and not described in detail.

Methodology

Vehicle measurements

The vehicle studied is a Euro 6b, mini-Sport Utility vehicle (SUV) from 2016. Technical specifications are presented in Table 1, while more details can be found in (Pavlovic et al., 2020), where the same experimental campaign was used to analyse the factors impacting the FC gap (compared to manufacturer declared NEDC values).

Table 1: Vehicle technical characteristics.

Engine capacity [cc]	1956
Engine Type [-]	Turbo Diesel
Engine Power [kW]	103
Gear box [-]	Automatic, 9 speed
Mass in running order [kg]	1562

The vehicle has been tested both in the laboratory and on-road. In the laboratory, WLTP, and NEDC tests were performed. Since the vehicle was Euro 6b, the official Road Load (RL) coefficients used during the Type Approval (TA) procedure were not readily available. For this reason, two different approaches were used to calculate them. In the first one, the JRC in-house formulas calculated the NEDC RLs from representative values of the rolling resistance coefficient (RRC) and the drag coefficient (Cd) for the specific vehicle category. The WLTP RL values are then calculated based on the NEDC RLs, considering all the factors differentiating the two testing protocols. More details can be found in (Tsiakmakis et al., 2017). In the second option, default RL values have been applied in WLTP tests, and the present study focused mainly on them. The formula used to derive the resistive forces from the RL coefficients is explained in regulation (European Commission, 2017a) and also presented in equation (1). In addition, the WLTP TA RLs for the vehicle's Euro 6d successor were retrieved. It should be noted that the TA RL coefficients obtained for the Euro 6d follow the well-defined WLTP regulation (European Commission, 2017a), where coast down tests are performed in test tracks for both High and Low vehicle configurations.

$$Fr(t) = F0 + F1 \cdot v(t) + F2 \cdot v(t)^2 \quad (1)$$

Where:

Fr	Deceleration Force [N]
$F0$	constant resistance [N]
$F1$	resistance proportional to vehicle speed [N/(km/h)]
$F2$	resistance proportional to speed squared [N/(km/h) ²]
v	Vehicle speed [km/h]

On the road, 5 Portable Emissions Measurement System (PEMS) tests were performed in two different routes during autumn and winter times. More information about these is presented in Table 2. During these tests, a driver and a co-driver are inside the vehicle, where also the PEMS instrumentation is placed.

Table 2: PEMS route characteristics.

	Route 1	Route 2
Total distance driven [km]	79	94
Altitude gain [m]	101	210
Average trip temperature [C°]	14.5-21	17.5-19
Number of repetitions	3	2

Further to the above testing, 20 different drivers were asked to drive the vehicle for their day-to-day needs, as they would do with their own. This project lasted for 11 months, and a total of 13990 km were driven. Together with other signals, the fuel consumption was measured with an On-Board Diagnostics (OBD) logger. Further details on the trip characteristics, the data manipulation and the assessment of the accuracy of the FC measurements can be found in (Pavlovic et al., 2020). For the present study, the 458 resulting trips were filtered, and the ones that the slope signal was not updating for more than 20% of the trip were excluded, resulting to 245 trips, from 19 drivers. Most of the recordings were performed in North and central Italy, but also other areas and countries were visited in that period.

Fuel consumption data

In Table 3, the measured FC values during laboratory testing (WLTP with the calculated RLs, and the tabulated ones), the average PEMS on-road testing, and the average RWD of the 245 trips used in the present study.

Table 3: Measured fuel consumptions during the different types of tests.

Test	Combined Fuel consumption (l/100km)
WLTP cold - tabulated RLs	7.3
PEMS - Route 1	7.4*
PEMS - Route 2	7.4*
RWD	7.85*

*Average value

The average RWD value is by 6% higher compared to the average PEMS values. Still, one should consider that this value was calculated considering the driving characteristics of different people in a period of almost one year. This means that different needs, and driving styles, can result in averaging and smoothing any outlier resulting from specific driving patterns. This is analysed in more detail by Pavlovic et al. (2020), where, in driver level, the average consumption could differ as much as 50% from the PEMS values. In trip level, this discrepancy can reach values up to 200%. The factors of the variability assessed by Pavlovic et al. (2020) can be considered generic, and thus apply for a typical vehicle use. The vehicle adopted in the specific assessment, was selected to be automatic to exclude the gear shifting pattern from the factors impacting the fuel gap. Still, a closer look to the data reveals that, except of the influence of the stops in the trip the FC gap, instances where excessive engine load while standing still are observed. This fact can be attributed to excessive auxiliary usage, warm up operation, but also to the instances when the Start

Stop (SS) functionality either is not performing, or it is disabled. The engine is running, and ready to move the vehicle, the brake pedal keeps the vehicle standing. This behaviour, not present in a manual vehicle, can be frequently found in an automatic vehicle in RWD operation, and sometimes holds a not negligible share of the trip (Figure 1a). Comparing the FC including versus excluding these parts, a considerable increase is observed (Figure 1b).

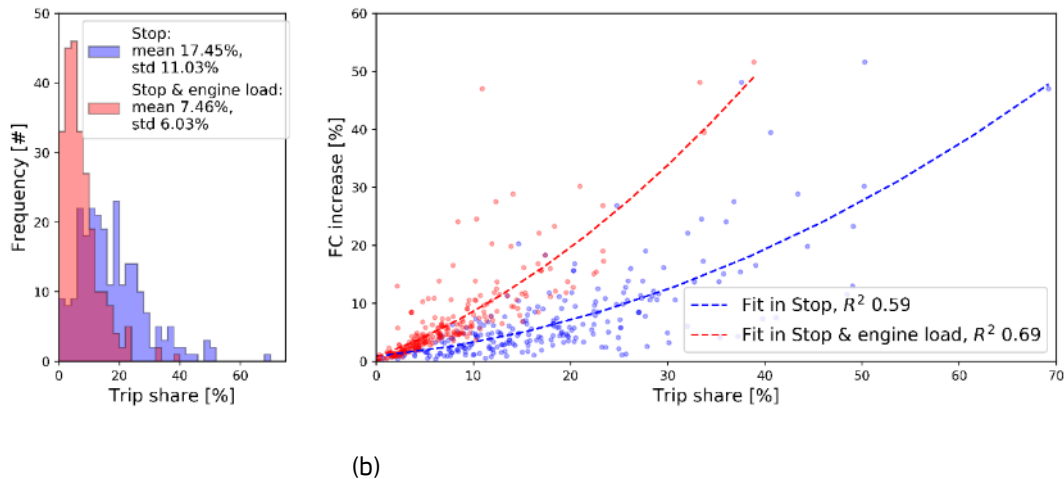


Figure 1: (a) Distribution of the shares of stops and stops with engine load in the RWD trips; (b) Stop (blue points) and stop & engine load (red points) shares are projected versus the percentage increase of the FC due to the stops. The dashed lines correspond to second order regression fitting in the points, and the coefficient of determination (R^2) is presented for the fittings. The value of engine load during the stop considered as a limit was 1.5 kW.

In the specific PEMS trips used for the present study the share of the stops is close to the average values appearing in the RWD. For Route 1 the average share is 18%, while for the Route 2, the share is 11%. Nevertheless, the SS was performing correctly, resulting to a limited increase of FC when the stop periods were considered. In detail, the average increase was 1.95% and 0.75% for Route 1 and Route 2, respectively.

Vehicle simulator

The simulator used in the present study is CO2MPAS in the latest public release. The tool was built by the Joint Research Centre (JRC) of EU Commission to support on a progressive, and smooth transition from the NEDC to WLTP, and entered the TA procedure regulation for passenger and light-duty vehicles for the period 2017 to 2020 included (European Commission, 2017b, p. 2017). More details on the model, testing with laboratory data, and the influence of the model in the European CO₂ schema of passenger and light-duty vehicles are described by Fontaras et al. (2018). Various studies used the tool, either for replicating RWD (Komnos et al., 2020; Tsiakmakis et al., 2019), or for performing sensitivity analysis (Komnos et al., 2020; Pavlovic et al., 2018). CO2MPAS needs few experimental data to work and counts on its self-calibrated models to reproduce the operation of a vehicle.

Model calibration with laboratory data

WLTP cold test data with the use of the default RLs were used for model calibration. For validation purposes, a simulation of the same cycle is then performed to ensure that the model effectively reproduces the FC values during the test. Once the prediction results are satisfactory (from datasets in different sources, this can be set to $\pm 1-2\%$), the next step is to predict tests performed on the road.

For the resistive forces occurring during the driving on the road, the equation (1) for the road loads is used by default in the tool, combined with the various inertia and the force to overcome road inclination (Fontaras et al., 2018). The RLs used are the TA High (from WLTP procedure) because they are more realistic, and model variant specific. Yet, the coefficients F₀, and F₂ need to be corrected for the specifications of each trip. In more detail the F₀, that is mainly associated to the rolling resistance due to tyre deformation, is related to the vehicle mass. The F₂ accounts mostly for the aerodynamic resistance (Komnos et al., 2020; Robert Bosch GmbH, 2018), and it is related to the air density during the trip. These relations result to the correction formulas (2) and (3). The coefficient F₁ counts mostly for drivetrain losses, and no correction was applied.

$$F0_{corrected} = Mass_{RWD Trip} \cdot \frac{F0_{WLTP}}{Mass_{WLTP}} \quad (2)$$

$$F2_{corrected} = \rho_{RWD Trip} \cdot \frac{F2_{WLTP}}{\rho_{WLTP}} \quad (3)$$

$Mass_{RWD Trip}$ is the vehicle mass during the trip [kg], while $Mass_{WLTP}$ is the test mass calculated according to the WLTP procedure (European Commission, 2017b, p. 115). $\rho_{RWD Trip}$ [kg/m³] is the density of the ambient air during the RWD test, while ρ_{WLTP} is the density of air at 20 °C, the mean ambient temperature prescribed for the WLTP procedure.

On-road driving introduces further auxiliary demands (both electrical and mechanical) compared to the laboratory tests. The engine demand due to electrical consumption is estimated to be on average 0.75 kW (Hill et al., 2018). For the tested vehicle, extra mechanical auxiliary losses were added to account for losses due to the drivetrain, and alternator power demand for the battery recharge. From simulations in the PEMS data, these were estimated to 1.5 kW, resulting to a satisfying FC agreement compared to the measured by the PEMS, throughout the trip. With the above adjustments, the 245 RWD trips were predicted, and this is considered as the 'base case'.

Correction methodology

Further adjustments are needed because the extra auxiliary losses, and the extra mass due to extra passengers, and equipment are unknown. Still, the engine reference torque was recorded from the Controller Area Network (CAN). Together with the engine speed, the reference engine power is produced. The engine power output was calculated applying a correction to exclude the motoring power and friction losses. The correction is a function of the engine speed as described in equation (4), which is a simplified procedure derived by Knauder et al. (2019), where simulations were performed in similar engine characteristics.

$$Engine\ losses(t) = 0.7 + \frac{Engine\ Speed(t) - Idle(t)}{28 \cdot 10^5} \cdot Engine\ Speed(t) \quad (4)$$

The engine losses are calculated in [kW], and the engine speed and idle (engine idle speed at hot conditions) in [RPM]. Then, the calculated engine power output is used to derive the missing information. The procedure followed is:

1. Prediction of the RWD tests with a first guess of mass (1765 kg), and the base auxiliary losses (1.5 kW). The input RLs are adjusted according to the equations (2) and (3). The gear box efficiencies and the alternator power calculated by the simulator are collected. This is considered the 'base case' describe in the previous chapter.
2. Calculation of the extra auxiliaries by comparing the measured with the simulated power output of the tool in the 'base case' during the stop phases of the trip.
3. Loop in a set of vehicle masses and:
 - 3.1. Calculation of the motive power using the new mass and adjusting the F0 coefficient as described in equation (2).
 - 3.2. Reconstruction of the simulated engine power with the new motive power, the extra auxiliaries, and the data from the 'base case'.
 - 3.3. Comparison of the simulated power output with the measured in the acceleration events of the trip.

An illustration of the process during one iteration is shown in Figure 2. The vehicle mass, connected to the simulated engine power that gives the lowest error compared to the measured engine power (target), is attributed to the trip.

Model calibration with road data

After deriving the auxiliary losses and the vehicle mass per trip with the above method, these data are fed as inputs to CO2MPAS for calibration. The WLTP velocity profile is used for prediction that initially was used for calibration. For the calibration of the simulator with the RWD trips, there were two possibilities for the inputs needed to construct the fuel map. Either directly passing as input to the simulator the measured FC signal or modifying the regular CO2MPAS procedure (WLTP to NEDC). In the latter way, the phase distances of the WLTP are modified, and the overall consumption is assigned as the first phase value of the WLTP test, putting the rest of the phases as 0 consumption, and 0 km driven. Although it can result to lower accuracy, since the optimisation is performed to 1, rather to 4 cycle phases, this way was used to assess the performance for future tests, where only one value per trip will be retrieved. The loop described in the step 3 is performed inside loop in a range of vehicle masses:

$$Vehicle\ Mass = [1565|2060\ kg, step\ of\ 5\ kg] \quad (5)$$

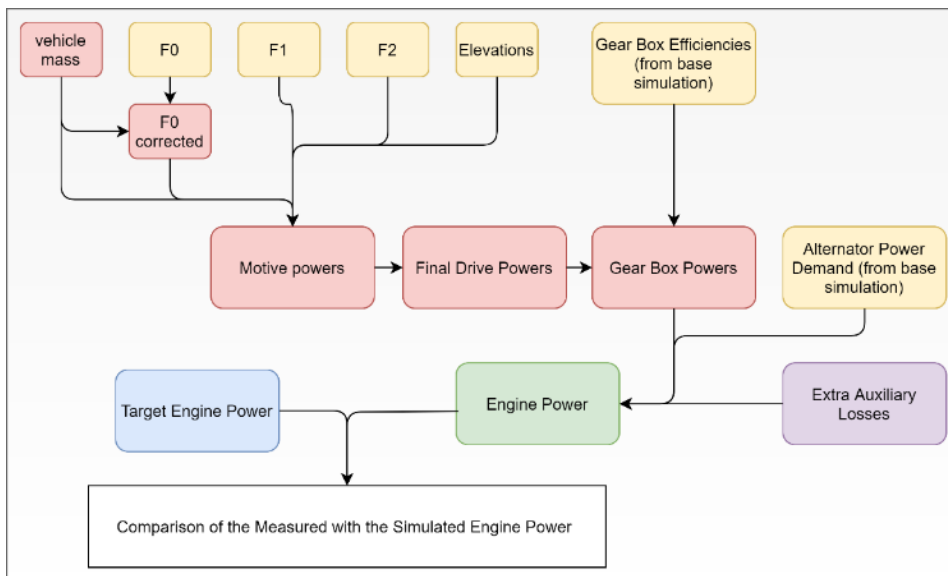


Figure 2: Schematic presentation of the methodology followed to derive the auxiliary losses and the mass during the trip.

Results

Correction for mass and auxiliaries

In Figure 3, the results of the correction methodology are presented. In Figure 3a, it is observed that starting from an initial guess vehicle mass of 1765 kg, the procedure resulted to a wide range of mass values. Most of them are close to the 1565 kg, which is the lowest possible. This means that the vehicle did not contain further equipment, or passengers. Still, there were cases that the model calculated masses that are close to the maximum permissible laden mass of the vehicle. Regarding the auxiliary losses (Figure 3b), in most of the trips further auxiliaries were added to the initial 1.5 kW. There were cases where the method calculated up to 3.5 kW additional auxiliaries.

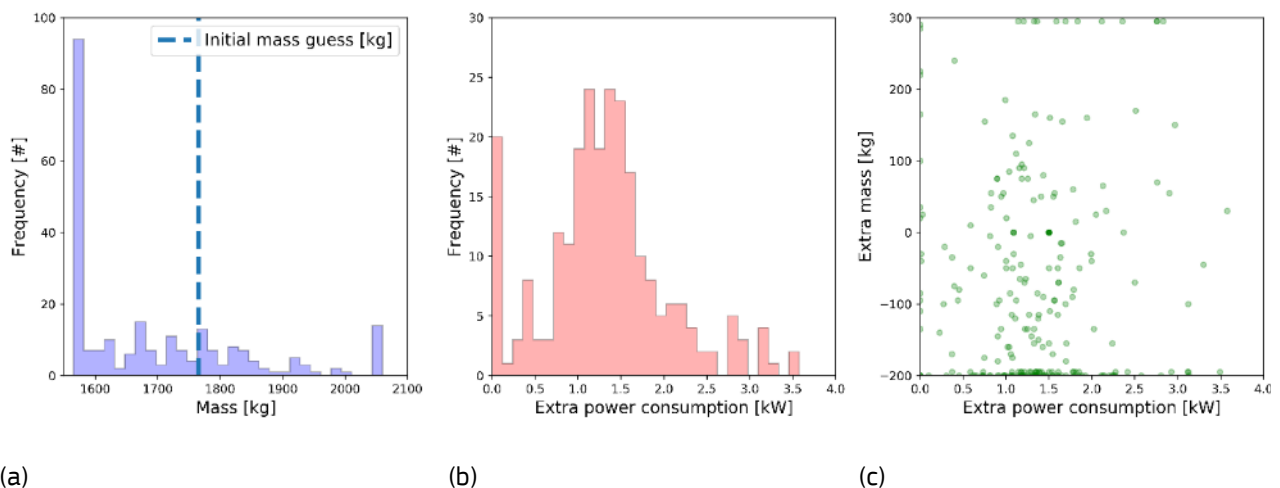


Figure 3: Results of the methodology for each RWD trip. (a) Distribution of the vehicle masses; (b) Auxiliary power consumption; (c) Vehicle mass versus auxiliary power consumption.

These extra auxiliaries can be attributed to many factors, either vehicle operation, or environmental conditions related. Moreover, losses in the drivetrain in case it did not reach hot conditions could originate the divergence. To explain this behaviour, fittings of the extra auxiliary median values per clusters of ambient temperature and trip distance were carried out. As shown in Figure 4a, more auxiliaries were needed in very high and low ambient temperatures which could be justified by the use of heating, ventilation, and air conditioning (HVAC) in the cabin. Similar patterns have been reported in literature regarding the energy consumption of HVAC versus the ambient temperature (Lajunen, 2017).

A weak correlation appears between the need for extra engine power and the distance of the trip can be observed in Figure 4b, with less power dispersion at longer distances. At the same time, the extra power decreases with increasing distance, which can be explained by the engine operating in warmer -and thus more efficient- conditions. On the contrary, higher friction losses appear during the warmup operation for the first kilometres driven. The mean trip time is 17 minutes (median 13 minutes, 3rd quartile 20 minutes), meaning that a big share falls inside a thermal engine efficiency significantly lower (Roberts et al., 2014). As the trip gets longer (in distance and time), the methodology calculates fewer extra auxiliaries because it averages more instances between the measured and the initially simulated engine power output. Similar pattern appears also projecting the extra losses to the mean transmission temperature of each trip (Figure 4c), which can be considered an indication of the thermal state also of the liquids and the lubricants of the vehicle.

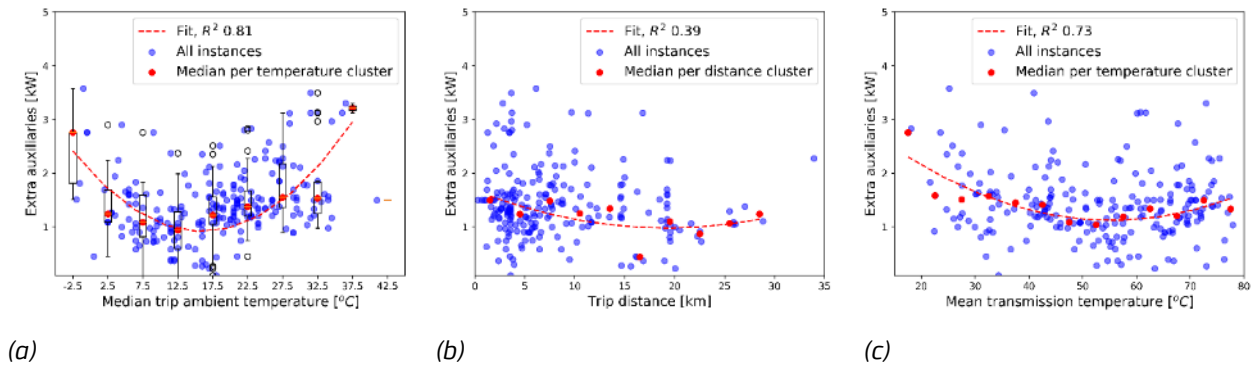


Figure 4: Blue dots represent the extra auxiliaries calculated versus median ambient temperature of the trip (a), trip distance (b), (c) mean transmission temperature. Red dots represent the median extra auxiliary values calculated versus the middle point of (a) ambient temperatures in clusters of 4 °C, (b) trip distances in clusters of 3 km, (c) clusters of 5 °C. The dashed lines correspond to second order regression fitting in the red points, and the R² is presented for the fittings.

Figure 5 shows an example of this correction. In the base CO2MPAS run, the simulated engine power is visibly lower than the measured throughout the trip. After the correction, the simulated and the measured engine power are very close throughout the whole trip, with the only exception of some short-time high-power demands.

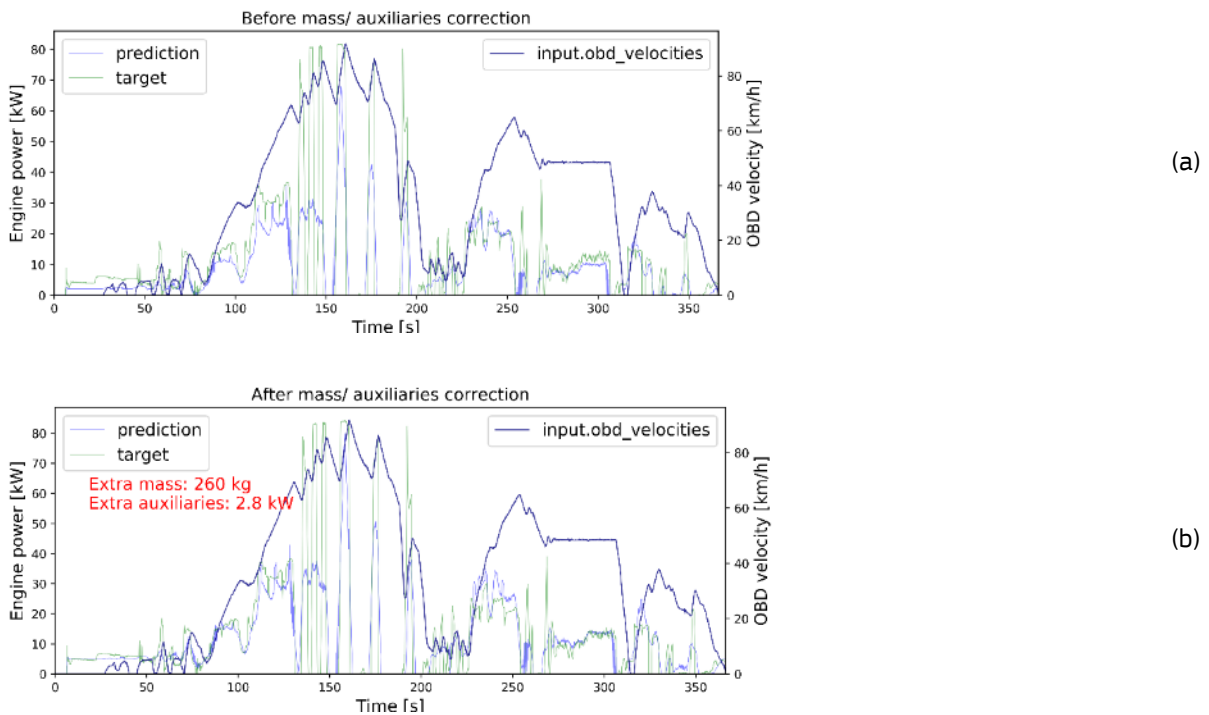


Figure 5: Example of simulated and measured engine power output before (a), and after (b) correction for an RWD trip.

Estimating the fuel consumption gap

By using the above procedure, we derived key missing inputs for each of the RWD trips, such as the extra auxiliaries, losses, and vehicle mass. In this chapter, we further assess the possibility to use the CO2MPAS simulation tool in a reverse way, calculating the WLTP FC value from a calibration procedure that is based on each single RWD trip.

Figure 6 presents the FC error values calculated as the deviation of the RWD trip-based co2mpas predictions -including the calculated missing inputs- from the reference lab WLTP value. The statistics are presented in several layers, in order to assess the representativeness of the outlier data points. The error distribution replicates a normal function with its centre close to the origin, indicating a non-biased distribution. The standard deviation (STD) of 14.5 to 8.5%, for 90 to 76% sample coverage, respectively, is satisfying considering all the uncertainties regarding vehicle operation, driving styles, and trip specificities. For example, the median value for trip distance is 6 km, which is a relatively low value where the dispersion of the extra auxiliaries' power is still high (Figure 4b), and 75% of the trips cover less than the NEDC distance (11 km). Despite of it, a more than fair agreement between the measured and the simulated values is achieved, with 76% of the simulation results falling inside an error of $\pm 20\%$.

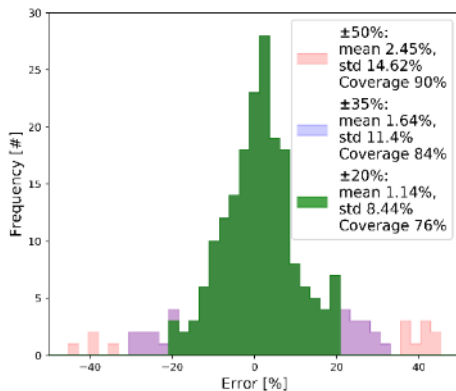


Figure 6: FC error distribution of WLTP test using as input the corrected RWD data.

For the simulations that fall inside the $\pm 20\%$ error range, the simulated FC gap, defined as $FC_{RWD\ Trip, Simulated} - FC_{WLTP, Simulated}$, is compared to the measured FC gap (WLTP based), defined as $FC_{RWD\ Trip, Measured} - FC_{WLTP, Measured}$. In Figure 7a, the distribution of the gap for both Simulated and Measured cases is pictured. The simulated gap averages in 18.5%, while the measured one in 20.5%, both having similar dispersions throughout the trips. Comparing the Simulated versus Measured gaps in the individual trips, the average discrepancy is 2%. More details are presented in Figure 7b.

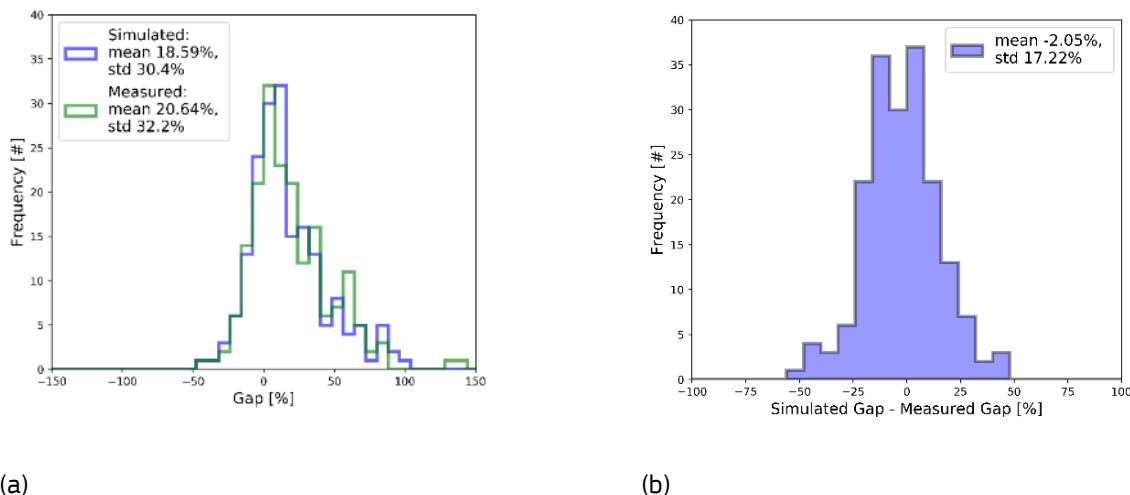


Figure 7: (a) WLTP based FC gap [%] calculated by the simulations (blue), and the measurements (green); (b) Difference between the simulated and the measured gap [%].

Finally, an assessment to explain the dispersion of the simulated WLTP error values follows. For this purpose, a multi-linear regression model has been used. The adjusted R-squared coefficient (R^2) is used to explain the variability of the error, while the standardized coefficients of each parameter represent the mean change in the response given a one standard deviation change in the predictor. The standardized values for the fitting were constructed by subtracting the mean, and dividing by the standard deviation, and they were used to identify the most important predictor variables.

According to the results of the Figure 8, the most important parameters are the trip distance, the energy consumed per trip distance, and the initial engine temperature. The trip distance factor is related to the different operations of the engine. Similarly, the energy consumed in a specific distance is an indicator of how much of the power potential of the vehicle was explored. These two can help to reconstruct the engine operation and calculate an accurate engine fuel map. Regarding the initial engine temperature, using as calibration data recordings in warm conditions, results to a poorly calibrated thermal model. Overall, the parameters explain 22.3% of the error dispersion.

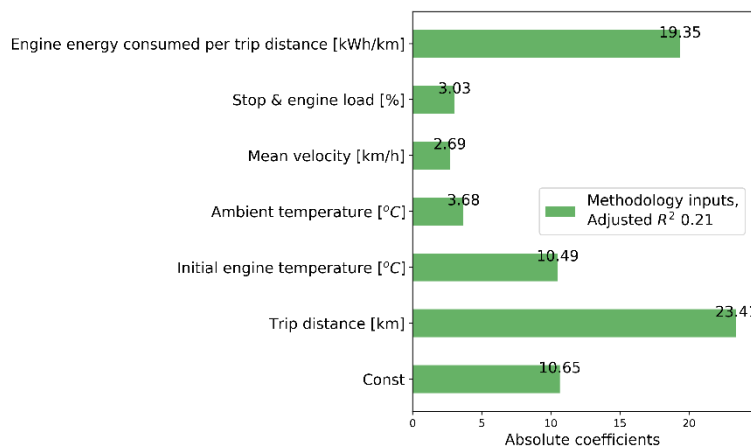


Figure 8: Absolute coefficients of the standardized parameters used to explain the FC simulated error dispersion.

Conclusions

A compact methodology for exploring the possibility to reproduce the reference laboratory FC value from on-road trip simulations is carried out. The work also included the analysis of the impact that different factors have on the divergence of the FC simulations from the reference value.

The first step concerns the calibration of the simulator with laboratory test data, and the subsequent prediction of the RWD trips. At a second stage, we derived the auxiliaries' power and the vehicle mass of the trip by comparing the base case simulated engine power to the measured one. Once the missing information about the on-road trips has been obtained, the simulator is re-calibrated, using this time the RWD data to predict the WLTP laboratory FC values.

Considering that most of the trips are short in time and distance, and the engine operation area is limited, the fact that 76% of the trips fall inside an un-biased error of $\pm 20\%$ with a STD of 8.5%, confirm the consistency and stability of the employed simulation tool and the methodology followed. Additionally, based on the simulated results, the FC gap (WLTP based) was calculated and compared to the measured FC gap. The simulated distribution of the gap has an average value of 18.5%, and it is satisfactorily aligned with the measured gap with an average difference of 2%.

Overall, this activity targets to support in linking the WLTP CO₂ laboratory testing with the new OBFCEM data monitoring foreseen by recent EU regulation. The eventual limitations have been identified. In particular, the calculated extra auxiliaries' power needs to be clarified and attributed correctly to the exact sources. Nevertheless, this is a first pioneering step that can serve as a possible base for future improvement.

References

- Dornoff, J., Tietge, U., Mock, P., 2020. On the way to “real-world” CO₂ values: The European passenger car market in its first year after introducing the WLTP 30.
- Doulgeris, S., Dimaratos, A., Zacharof, N., Toumasatos, Z., Kolokotronis, D., Samaras, Z., 2020. Real world fuel consumption prediction via a combined experimental and modeling technique. *Science of The Total Environment* 734, 139254. <https://doi.org/10.1016/j.scitotenv.2020.139254>
- Duarte, G.O., Gonçalves, G.A., Farias, T.L., 2016. Analysis of fuel consumption and pollutant emissions of regulated and alternative driving cycles based on real-world measurements. *Transportation Research Part D: Transport and Environment* 44, 43–54. <https://doi.org/10.1016/j.trd.2016.02.009>
- European Automobile Manufacturers Association, 2020. CO₂ emissions from heavy-duty vehicles Preliminary CO₂ baseline (Q3-Q4 2019) estimate.

European Commission, 2019a. Regulation (EU) 2019/631 of the European Parliament and of the Council of 17 April 2019 setting CO₂ emission performance standards for new passenger cars and for new light commercial vehicles, and repealing Regulations (EC) No 443/2009 and (EU) No 510/2011 (Text with EEA relevance.) (No. 32019R0631).

European Commission, 2019b. Regulation (EU) 2019/1242 of the European Parliament and of the Council of 20 June 2019 setting CO₂ emission performance standards for new heavy-duty vehicles and amending Regulations (EC) No 595/2009 and (EU) 2018/956 of the European Parliament and of the Council and Council Directive 96/53/EC.

European Commission, 2017a. Commission Regulation (EU) 2017/1151 of 1 June 2017 supplementing Regulation (EC) No 715/2007 of the European Parliament and of the Council on type-approval of motor vehicles with respect to emissions from light passenger and commercial vehicles (Euro 5 and Euro 6) and on access to vehicle repair and maintenance information, amending Directive 2007/46/EC of the European Parliament and of the Council, Commission Regulation (EC) No 692/2008 and Commission Regulation (EU) No 1230/2012 and repealing Commission Regulation (EC) No 692/2008 (Text with EEA relevance) (No. 32017R1151).

European Commission, 2017b. Commission Implementing Regulation (EU) 2017/1152 of 2 June 2017 setting out a methodology for determining the correlation parameters necessary for reflecting the change in the regulatory test procedure with regard to light commercial vehicles and amending Implementing Regulation (EU) No 293/2012 (Text with EEA relevance) (No. 32017R1152).

European Environment Agency, 2016. Transitions towards a more sustainable mobility system - TERM 2016 (Publication No. 34/2016).

Fontaras, G., Ciuffo, B., Zacharof, N., Tsiakmakis, S., Marotta, A., Pavlovic, J., Anagnostopoulos, K., 2017a. The difference between reported and real-world CO₂ emissions: How much improvement can be expected by WLTP introduction? *Transportation Research Procedia*, World Conference on Transport Research - WCTR 2016 Shanghai. 10-15 July 2016 25, 3933–3943. <https://doi.org/10.1016/j.trpro.2017.05.333>

Fontaras, G., Valverde, V., Arcidiacono, V., Tsiakmakis, S., Anagnostopoulos, K., Komnos, D., Pavlovic, J., Ciuffo, B., 2018. The development and validation of a vehicle simulator for the introduction of Worldwide Harmonized test protocol in the European light duty vehicle CO₂ certification process. *Applied Energy* 226, 784–796. <https://doi.org/10.1016/j.apenergy.2018.06.009>

Fontaras, G., Zacharof, N.-G., Ciuffo, B., 2017b. Fuel consumption and CO₂ emissions from passenger cars in Europe – Laboratory versus real-world emissions. *Progress in Energy and Combustion Science* 60, 97–131. <https://doi.org/10.1016/j.pecs.2016.12.004>

Hill, N., Skinner, I., Zazias, G., Siskos, P., Petropoulos, A., Fragkiadakis, K., Paroussos, L., 2018. Assessing the impacts of selected options for regulating CO₂ emissions from new passenger cars and vans after 2020 219.

Hoofman, N., Messagie, M., Van Mierlo, J., Coosemans, T., 2018. A review of the European passenger car regulations – Real driving emissions vs local air quality. *Renewable and Sustainable Energy Reviews* 86, 1–21. <https://doi.org/10.1016/j.rser.2018.01.012>

Knauder, C., Allmaier, H., Sander, D.E., Sams, T., 2019. Investigations of the Friction Losses of Different Engine Concepts. Part 1: A Combined Approach for Applying Subassembly-Resolved Friction Loss Analysis on a Modern Passenger-Car Diesel Engine. *Lubricants* 7, 39. <https://doi.org/10.3390/lubricants7050039>

Komnos, D., Fontaras, G., Ntziachristos, L., Pavlovic, J., Ciuffo, B., 2020. An Experimental Methodology for Measuring Resistance Forces of Light-Duty Vehicles under Real-World Conditions and the Impact on Fuel Consumption (SAE Technical Paper No. 2020- 01–0383). SAE International, Warrendale, PA. <https://doi.org/10.4271/2020-01-0383>

Lajunen, A., 2017. Energy Efficiency and Performance of Cabin Thermal Management in Electric Vehicles (SAE Technical Paper No. 2017- 01–0192). SAE International, Warrendale, PA. <https://doi.org/10.4271/2017-01-0192>

Ligterink, N., Eijk, A., 2014. Real-World Fuel Consumption of Passenger Cars. <https://doi.org/10.13140/2.1.1252.3527>

Mogno, C., Fontaras, G., Arcidiacono, V., Komnos, D., Pavlovic, J., Ciuffo, B., Makridis, M., Valverde, V., 2020. The application of the CO₂MPAS model for vehicle CO₂ emissions estimation over real traffic conditions. *Transport Policy*. <https://doi.org/10.1016/j.tranpol.2020.01.005>

Pavlovic, J., Ciuffo, B., Fontaras, G., Valverde, V., Marotta, A., 2018. How much difference in type-approval CO₂ emissions from passenger cars in Europe can be expected from changing to the new test procedure (NEDC vs. WLTP)? *Transportation Research Part A: Policy and Practice* 111, 136–147. <https://doi.org/10.1016/j.tra.2018.02.002>

Pavlovic, J., Fontaras, G., Broekaert, S., Ciuffo, B., Ktistakis, M.A., Grigoratos, T., 2021. How accurately can we measure vehicle fuel consumption in real world operation? *Transportation Research Part D: Transport and Environment* 90, 102666. <https://doi.org/10.1016/j.trd.2020.102666>

- Pavlovic, J., Fontaras, G., Ktistakis, M., Anagnostopoulos, K., Komnos, D., Ciuffo, B., Clairotte, M., Valverde, V., 2020. Understanding the origins and variability of the fuel consumption gap: lessons learned from laboratory tests and a real-driving campaign. *Environmental Sciences Europe* 32, 53. <https://doi.org/10.1186/s12302-020-00338-1>
- Robert Bosch GmbH, 2018. *Bosch Automotive Handbook*, 10th Edition. John Wiley & Sons, West Sussex, England.
- Roberts, A., Brooks, R., Shipway, P., 2014. Internal combustion engine cold-start efficiency: A review of the problem, causes and potential solutions. *Energy Conversion and Management* 82, 327–350. <https://doi.org/10.1016/j.enconman.2014.03.002>
- Tietge, U., Díaz, S., Mock, P., Bandivadekar, A., Dornoff, J., Ligterink, N., 2019. From laboratory to road: A 2018 update | International Council on Clean Transportation [WWW Document]. URL <https://theicct.org/publications/laboratory-road-2018-update> (accessed 2.22.21).
- Tietge, U., Zacharof, N., Mock, P., Franco, V., German, J., Bandivadekar, A., Ligterink, N., Lambrecht, U., 2015. A 2015 update of official and “real-world” fuel consumption and CO₂ values for passenger cars in Europe 56.
- Triantafyllopoulos, G., Dimaratos, A., Ntziachristos, L., Bernard, Y., Dornoff, J., Samaras, Z., 2019. A study on the CO₂ and NO_x emissions performance of Euro 6 diesel vehicles under various chassis dynamometer and on-road conditions including latest regulatory provisions. *Science of The Total Environment* 666, 337–346. <https://doi.org/10.1016/j.scitotenv.2019.02.144>
- Tsiakmakis, S., Fontaras, G., Ciuffo, B., Samaras, Z., 2017. A simulation-based methodology for quantifying European passenger car fleet CO₂ emissions. *Applied Energy* 199, 447–465. <https://doi.org/10.1016/j.apenergy.2017.04.045>
- Tsiakmakis, S., Fontaras, G., Dornoff, J., Valverde, V., Komnos, D., Ciuffo, B., Mock, P., Samaras, Z., 2019. From lab-to-road & vice-versa: Using a simulation-based approach for predicting real-world CO₂ emissions. *Energy* 169, 1153–1165. <https://doi.org/10.1016/j.energy.2018.12.063>
- Weiss, M., Bonnel, P., Hummel, R., Provenza, A., Manfredi, U., 2011. On-Road Emissions of Light-Duty Vehicles in Europe. *Environ. Sci. Technol.* 45, 8575–8581. <https://doi.org/10.1021/es2008424>
- Zacharof, N., Doulgeris, S., Myrsinias, I., Dornoff, J., Fontaras, G., Toumasatos, Z., Kolokotronis, D., Dimaratos, A., Mock, P., Samaras, Z., 2020. A Methodology for Monitoring On-Road CO₂ Emissions Compliance in Passenger Vehicles (SAE Technical Paper No. 2020-37- 0034). SAE International, Warrendale, PA. <https://doi.org/10.4271/2020-37-0034>

2.17 Conventional engine vehicles model parametrization for real-world fuel consumption estimation

Pierre Michel¹, Sol Selene Rodriguez¹, Alexandre Chasse¹, Georgios Fontaras², Jelica Pavlovic², Markos Alexandros Ktistakis², Dimitrios Komnos²

¹ IFP Energies nouvelles, 1 et 4 avenue de Bois-Préau, 92852 Rueil-Malmaison, France

² European Commission, Joint Research Centre, Ispra 21027, Italy

pierre.michel@ifpen.fr

Abstract

Environmental issues and an increasing gap between homologated fuel consumption and Real-World Fuel Consumption (RWFC) implies for decision makers to monitor accurately this fuel consumption gap. Smartphone applications propose a very promising way to crowdsense RWFC once trips data are aggregated and simulated provided that a precise fuel consumption model is available. In this perspective, this paper focuses on such a conventional car model parameterization. Thanks to real-world tests campaigns a method is presented to tune accurately €6 conventional vehicle. The model parameterization is validated on tests campaigns and achieved a good level of results with a good accuracy and represents a promising approach to estimate the gap between homologated fuel consumption and RWFC.

Introduction

Well-known environmental issues promote a more and more stringent fuel consumption legislation [1]. On one hand homologated CO₂ emissions decreased quickly during the last twenty years but on the other hand real-world CO₂ emissions decreased much slower. As a result the gap between homologated fuel consumption and Real-World Fuel Consumption (RWFC) is increasing starting from 10% in 2000 to more than 30% in 2020 [2]. To control and monitor the gap, On-Board Fuel Consumption Meter (OBFCM) is introduced in all new vehicles from 2021 to monitor real-world CO₂ [3].

In this context of CO₂ reduction, monitoring the CO₂ gap represents a central issue. Smartphone applications propose a very promising way to crowdsense RWFC. For example Geco air [4, 5] is an application ensuring users to become aware of their mobility environmental footprint by estimating their pollutant and CO₂ emissions during a trip with a personal vehicle. A trip refers to a GNSS (global navigation satellite system) speed and slope measured by the phone. The RWFC is influenced by three main factors [6]: the use case, the driving behavior and the vehicle. Use case and driving behavior are directly imposed by trip measurements i.e. a GNSS speed trace. Then estimating the RWFC associated to the trip implies to model accurately the vehicle.

Our work in this paper presents a quasi-static conventional vehicle model aiming to estimate precisely the fuel consumption along a speed driving cycle. The paper is organized as follows:

- a generic model able to model real-world fuel consumption from Euro 6 conventional vehicles,
- a methodology to parameterize such a vehicle model, this method is the main contribution,
- a validation of the vehicle model based on more than 200 real world driving tests.

A first section presents tests campaigns performed by OEM, IFPEN and JRC. Tests are performed in real-world driving conditions: open road with different traffic conditions, ambient temperature, auxiliaries electrical consumption...

A second section describes the longitudinal quasi-static model. Classically, the energy demand at the wheel is first estimated thanks to a resistive forces balance applied on the vehicle modeled by a weight and a resistive road load. Then the energy demand at the engine is calculated by modeling the powertrain ratios and efficiency. Finally the fuel consumption map is generated by modeling the engine fuel efficiency from the engine parameters: fuel type (gasoline or diesel), maximum power, displacement.

A third section presents a methodology to parameterize accurately the vehicle model from vehicles test measurements (speed, engine speed and torques). Parameterization is performed by different steps to set physical parameters with the largest impacts on the fuel consumption: first the engine thermal behavior, second the vehicle weight and the resistive forces, third the gearshift strategy and fourth engine efficiency.

A fourth section proposes a vehicle model validation on tests campaigns. Model results and dispersion are discussed and a conclusion proposes some explanations on dispersion resulting mostly from the non-modeled physical phenomena.

Real-world test campaigns

A campaign is composed of several real-world tests performed on an open road with CO₂ emissions measured with a Portable Emissions Measurement System (PEMS). From the CO₂ measurement the fuel consumption can be deduced by assuming that the CO₂ emissions are directly proportional to the fuel consumption.

3 main tests campaigns are used in next sections and details on the tested vehicle are given in Table 1.

- OEM RDE campaign: this tests set is composed of Real Drive Emissions (RDE) compliant tests performed by different OEM. Euro 6d Temp regulation introduces RDE procedure and defines conditions on road typology repartition and driving behavior dynamism limits. This dataset includes 92 tests all performed on a different vehicle.
 - Engine torque measurements subset: A subset can be defined with 65 tests with an engine torque estimation available and coming from the Engine Control Unit (ECU). The engine torque is a crucial information to understand the vehicle operation, see Section 4.2.
- JRC campaign: most of the tests were real-world driving (RWD) tests carried out to assess the FC from normal vehicle use [7] without specific testing boundaries and not compliant with the official RDE requirements.
- MTES campaign: this campaign requested by the French Ministry of the Ecological Transition [8] concerns an experimental campaign on 22 vehicles (16 conventional vehicles): for each vehicle, several RDE tests are performed to measure fuel consumption, regulated and non-regulated pollutant emissions under various driving and climatic conditions. The perimeter of this study also includes sensitivity analysis of hybridization and impact of use case.

Table 1: tests campaign details.

	Standard	Vehicles	Tests number	tests type
OEM RDE campaign	€6	92 vehicles	92	RDE
		Incl. 65 vehicles with an engine torque measur.	65	
JRC campaign	€6b	5 vehicles 3 diesel and 2 gasoline	65	RWD
MTES campaign	€6d temp	16 vehicles 8 diesel and 8 gasoline	85	RDE

Vehicle model description

This section describes a quasi-static conventional engine vehicle model [9], [10]. The vehicle model is developed in discrete time t with a discretization time step Δt . The main modeling assumption is that the vehicle, at each time t , is moving exactly at the speed $v(t)$ defined by a driving cycle. This assumption means that the vehicle sizing (mainly the engine maximum power and the gearbox range) ensures to track the driving cycle speed. In this paper, driving cycles correspond to real-world trips measurements according time: the vehicle speed $v(t)$ and the road slope $\alpha(t)$. An example of a driving cycle is presented in Figure 1.

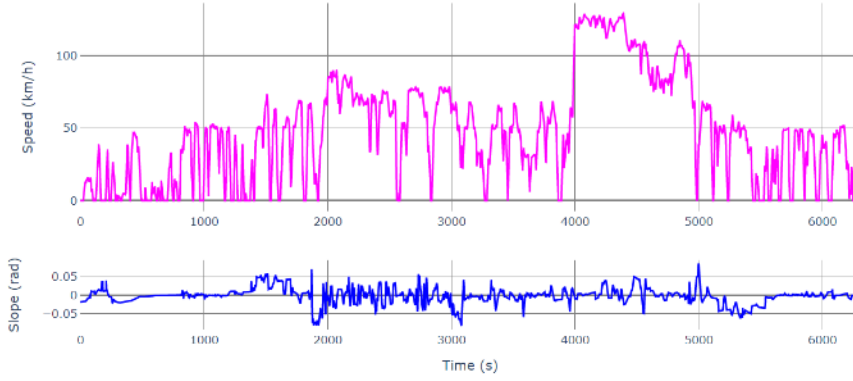


Figure 1: RDE driving cycle example with vehicle speed and road slope.

From the driving cycle speed, the vehicle acceleration $a(t)$ can be deduced simply by:

$$a(t) = \frac{v(t) - v(t-1)}{\Delta t} \quad (1)$$

Then the Newton's second law is applied to the vehicle:

$$ma(t) = F_{wheel}(t) - (F_{aero}(t) + F_{roll}(t) + F_{slope}(t)) \quad (2)$$

where m is the vehicle mass, $F_{wheel}(t)$ the requested force at the wheel, $F_{aero}(t)$ the aerodynamic drag defined by:

$$F_{aero}(t) = \frac{1}{2} \rho_{air} S C_x \quad (3)$$

with ρ_{air} the air density, S the vehicle frontal surface and C_x the drag coefficient;

$F_{roll}(t)$ the rolling resistance force defined by

$$F_{roll}(t) = c_{RR} mg \quad (4)$$

with c_{RR} the rolling resistance coefficient and g the standard gravity;

$F_{slope}(t)$ the slope resistance force

$$F_{slope}(t) = mg \sin(\alpha(t)) \quad (5)$$

By using (2), (3), (4) and (5), $F_{wheel}(t)$ can be deduced and the requested torque at the wheel

$$T_{wheel}(t) = F_{wheel}(t) r_w \quad (6)$$

with r_w the wheel radius.

Then the torque requested by the engine T_{eng} can be deduced from:

$$T_{eng} = \frac{T_{wheel}(t)}{\eta_{GB} k_{GB}(t)} + T_{aux} \quad (7)$$

where η_{GB} is the gearbox efficiency, T_{aux} the torque corresponding to electrical auxiliaries taken via the alternator, assumed constant for the entire trip, and $k_{GB}(t)$ is the gear engaged determined by the gearshift strategy GS :

$$k_{BV}(t+1) = GS(k_{BV}(t), \omega_{eng}(t)) \quad (8)$$

with the engine speed ω_{eng} deduced from the vehicle speed $v(t)$ by

$$\omega_{eng} = \frac{60k_{GB}(t)v(t)}{2\pi r_w} \quad (9)$$

Next the fuel consumption $\dot{m}_{fuel}(t)$ can be deduced from a fuel consumption map M_{fuel} by

$$\dot{m}_{fuel}(t) = M_{fuel}(T_{eng}(t), \omega_{eng}(t)) f_{corr}(T_{water}(t)) \quad (10)$$

with $T_{water}(t)$ the engine water temperature determined by a one-state thermal model depending on the engine displacement and f_{corr} a correction function modeling the impact of engine temperature on fuel consumption and defined according to:

$$f_{corr}(t) = c_{corr} \frac{T_{amb} - T_{water}(t)}{T_{amb} - T_{sp}} \quad (11)$$

where c_{corr} the fuel correction constant equals to 1,5, T_{amb} the ambient temperature and T_{sp} the engine water setpoint temperature equal to 85°C. The one-state engine thermal model is not presented in this document, see [11] and [12] for further details. Finally the simulated fuel consumption fc over the entire driving cycle is simply obtain by summing \dot{m}_{fuel} over time from 0 to the time end of the trip t_{end} :

$$fc = \sum_0^{t_{end}} \dot{m}_{fuel}(t) \quad (12)$$

and the engine efficiency η_{fuel} can be deduced by:

$$\eta_{fuel} = \frac{fc \text{ LHV}}{P_{eng}} \quad (13)$$

where LHV is the Lower Heating Value of the fuel and $P_{eng}(t)$ is the engine power:

$$P_{eng}(t) = T_{eng}(t) \omega_{eng}(t) \quad (14)$$

Vehicle model parameterization method

The vehicle model parametrization is performed in two steps:

1. In a first step the vehicle license plate is used to retrieve some initial vehicle characteristics from a database. These characteristics are general information concerning the vehicle. They are not sufficient to parameterize directly the vehicle model but they are used as inputs of the second step.
2. A second step is required to represent a real-world vehicle behavior i.e. to ensure real-world representative power flows and fuel consumption model. Section 4.2 presents a methodology to tune correctly some key vehicles parameters thanks to vehicle tests. This methodology is derived from feedbacks learnt by analyzing and modeling tests campaigns vehicles.

Initial parameterization

Some general vehicle characteristics available on the registration card can be obtained by using the vehicle license plate. For a particular vehicle the following characteristics can be found:

- Vehicle empty mass m_{init}
- Vehicle frontal surface S
- Vehicle body type: sedan, SUV or break
- Vehicle segment: A,B,C,D,E or F
- Gear ratio number
- Engine maximum power
- Engine displacement

Initial $C_{x\ init}$ and $c_{RR\ init}$ parameters are tabulated according vehicle body type and segment. Section 4.2.2. presents how these characteristics are used as inputs to parameterize real-world vehicle model parameters.

Real-world vehicle model parametrization

This subsection defines different methods in next sections to set vehicles model parameters with different measurements derived from vehicles tests, see Figure 2.

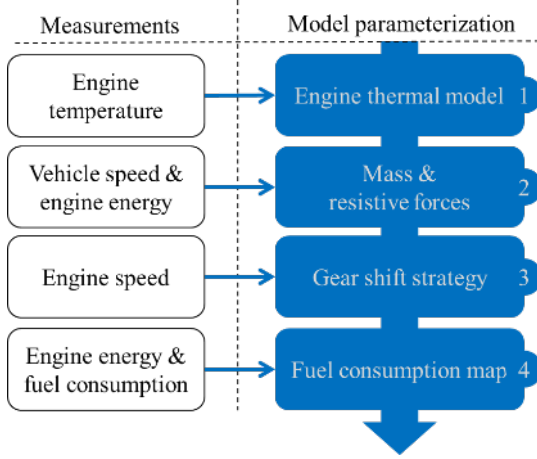


Figure 2: Real-world vehicle model parametrization methods with measurements inputs.

Engine thermal model parameterization

A first step to represent real-world condition is to verify that the engine thermal is appropriate to represent the engine temperature dynamic. As explained in Section 3 engine thermal model parameters depends on engine displacement, i.e. the engine volume. To validate this model and its parameterization, a qualitative validation is performed. Figure 3 compares measured and simulated engine water temperature. The model is adequate for the rest of the work mainly because engine temperature impact on fuel consumption can be considered as a second order impact.

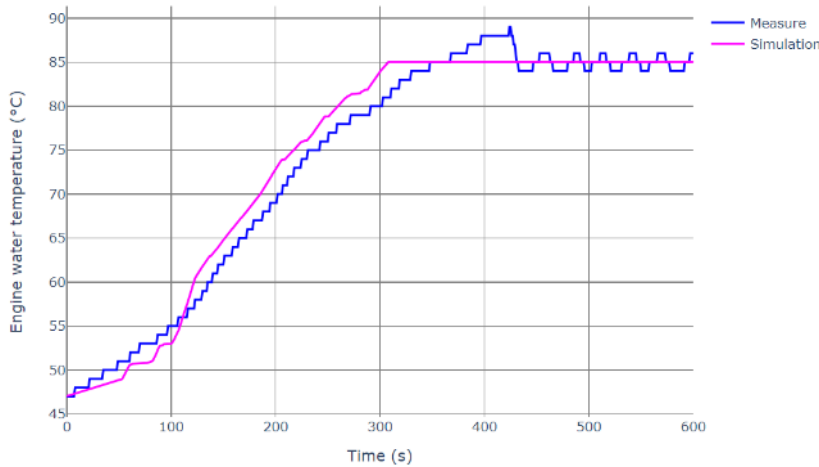


Figure 3: Measured and modeled engine water temperature.

Mass and resistive forces parameterization

When considering a conventional vehicle, all the positive force requested at the wheel $F_{wheel}^{pos}(t)$ is fulfilled by the engine through the gearbox. The modeled energy demand is directly proportional to the $F_{wheel}^{pos}(t)$ and can be studied by analyzing the modeled engine power error $\varepsilon_{eng}(t)$ defined as:

$$\varepsilon_{eng}(t) = P_{eng}^{meas}(t) - P_{eng}(t) \quad (15)$$

where $P_{eng}(t)$ is the modeled engine power defined by (14) and $P_{eng}^{meas}(t)$ the measured engine power:

$$P_{eng}^{meas}(t) = T_{eng}^{meas}(t)\omega_{eng}^{meas}(t) \quad (16)$$

with the engine torque $T_{eng}^{meas}(t)$ and speed $\omega_{eng}^{meas}(t)$ estimated by the ECU. $\varepsilon_{eng}(t)$ is a key indicator to analyze the representativeness of the vehicle parameters: $\varepsilon_{eng}(t)$ tending to zero means that the vehicle parameters related to the vehicle body (m , C_x and c_{RR}) and gearbox (gear box efficiency) are well completed i.e. the forces balance at the wheel (2) fairly represents the real-world energy demand at the wheel.

Starting from (15) 2 criteria can be defined. For each criterion the goal is to minimize ε_{eng} to ensure that the forces balance at the wheel is correct.

- **Mass parametrization.** When acceleration is important, a threshold of 0.5 ms^{-2} being considered in this work, then the majority of force $F_{wheel}(t)$ supplied by the engine to the wheel ensures the vehicle to accelerate. The vehicle mass m is empirically tuned by analysing ε_{eng}^{meas} depending on acceleration $a(t)$ according to:

$$\varepsilon_{eng}(a(t)) \forall a(t) \in [0.5; \Delta a; 1] \quad (17)$$

where $\Delta a = 0.1 \text{ ms}^{-2}$.

- **C_x and c_{RR} parametrization.** When acceleration is close to zero, then the majority of force $F_{wheel}(t)$ supplied by the engine to the wheel ensures to counter the resistive forces. The rolling resistance coefficient c_{RR} the drag coefficient C_x are empirically tuned by analysing ε_{eng} depending on low speed $v(t)$ according to:

$$\varepsilon_{eng}(v(t)) \forall v(t) \in [10; \Delta v; 110] \quad (18)$$

where $\Delta v = 10 \text{ km/h}$.

Simulations are performed for the 65 tests of OEM RDE campaign with ECU engine torque measurements, see Section 2 and ε_{eng} is calculated. $\varepsilon_{eng}(a(t))$ and $\varepsilon_{eng}(v(t))$ are deduced from the criteria (17) and (18) and are aggregated in acceleration and speed bins for all the tests. Figure 4 presents ε_{eng} results with the initial vehicle parametrization and after m , and c_{RR} and C_x tuning. $\varepsilon_{eng}(a(t))$ and $\varepsilon_{eng}(v(t))$ are represented in pink box plots for different acceleration and speed bins.

In order to facilitate the parameterization and the associated results high level criteria ε_m , $\varepsilon_{c_{RR}}$ and ε_{C_x} are defined: first ε_{eng} median values are fitted with a first degree polynomial equation and next high level criteria are obtained by doing the fitted line average over $[0.5; \Delta a; 1]$, $[10; \Delta v; 40]$ and $[80; \Delta v; 110]$ respectively for ε_m , $\varepsilon_{c_{RR}}$ and ε_{C_x} . c_{RR} and C_x are tuned with the same criteria with different speed range because they are predominant respectively at low and high speed in the deduction of $F_{wheel}^{pos}(t)$. The best parameterization is obtained by parameterizing m , C_x and c_{RR} as:

$$\begin{aligned} m &= 1.15 m_{init} + m_{passenger} + m_{fluid} + m_{extra} \\ c_{RR} &= 1.1 c_{RR \text{ init}} \\ C_x &= 0.85 C_x \text{ init} \end{aligned} \quad (19)$$

where $m_{passenger} = 80 \text{ kg}$, $m_{fluid} = 40 \text{ kg}$ and $m_{extra} = 100 \text{ kg}$ representing a vehicle mass in real world conditions. c_{RR} and C_x parameterization represent adjustments compared to the initial model presented in Section 4.1. Finally $\varepsilon_{c_{RR}}$ and ε_{C_x} are reduced respectively from 26.9%, 18.9%, 30.7% to -0.2% , 0.5% and -0.2% . As a conclusion of this subsection, by defining criteria on the engine power error, a simple parameterization is achieved to represent physically resistive forces applied to the vehicle.

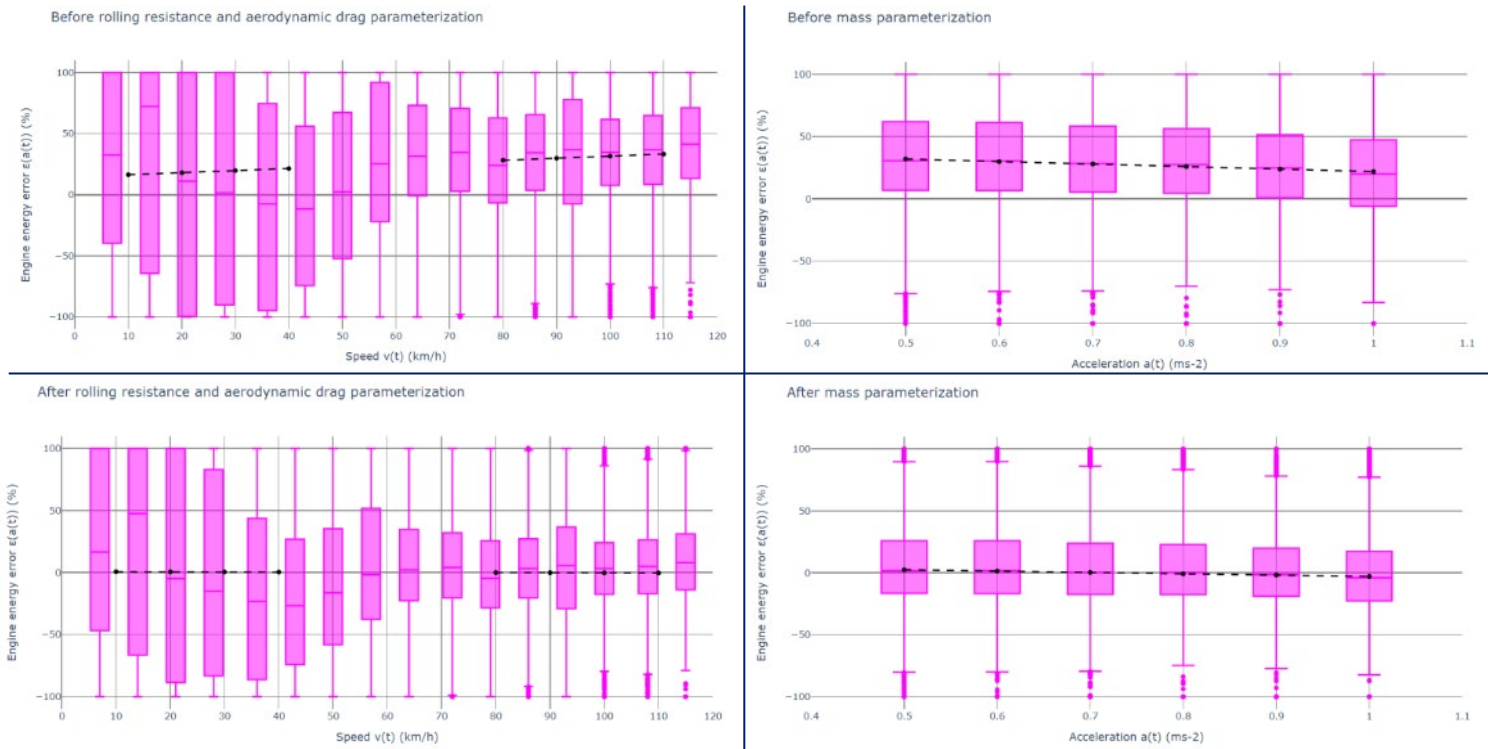


Figure 4: Engine power error ϵ_{eng} aggregated before (top figures) and after (down figures) m (right figure), C_{RR} and C_x (left figures) tuning.

Gear shift strategy parameterization

To model gear shift a gearshift strategy is required, see (8). This strategy is parameterized from all tests with an engine speed measurement: engine speeds when upshift and downshift occur are aggregated for all vehicles with the same gear ratio number. For all vehicles with the same gear ratio number upshift and downshifts engine speeds can be aggregated as shown for the 5 gears gearboxes example in Figure 5. Then a simple gearshift strategy can be deduced:

- a constant upshift engine speed threshold,
- and a downshift first degree polynomial function of the engine speed.

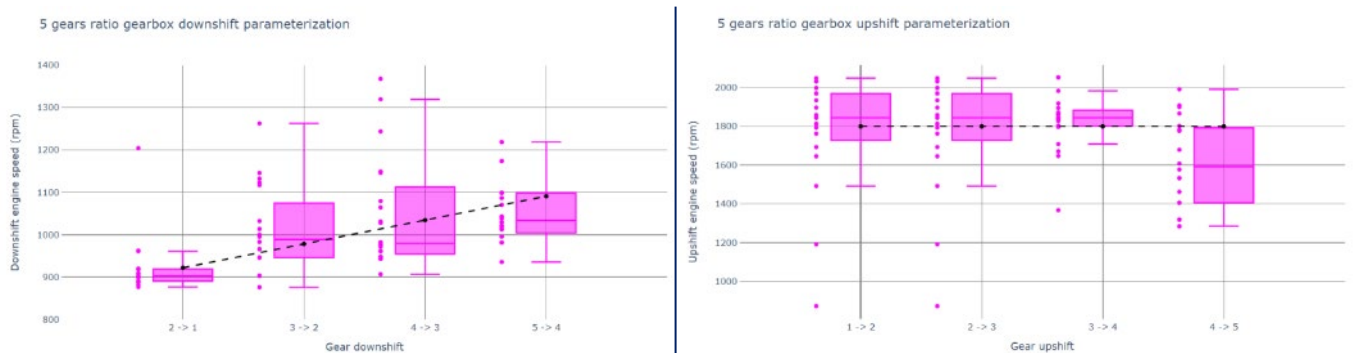


Figure 5: Downshift (left) and upshift (right) depending on engine speed for vehicle tests with a five gear ratio gearbox with dots as engine gearshift, boxplots as aggregated engine speed gearshift and black line the parameterized gearshift strategy.

This method is applied to 5, 6 and 7 gears ratio gearboxes and ensures to model representative gearshift. Then the resulting engine speed is representative of real-world driving.

Engine fuel consumption parameterization

As presented in Section 2 the engine fuel consumption is modeled by a map M_{fuel} . This map is generated by a tool presented in [13] and validated with engine test bench experimental measurements. Engine fuel consumption map is modeled from an energy losses balance: heat losses, friction losses and pumping losses. 2 main high level parameters: friction and indicated efficiency are modeled from engine displacement, fuel type and maximum power, obtained with the initial vehicle parameterization. The engine fuel consumption map tool is parameterized by tuning the friction losses and pumping losses. Parametrizations are validated by comparing η_{fuel}^{meas} the measured efficiency defined from f_c^{meas} and P_{eng}^{meas} as η_{fuel} in (13) with the modeled engine efficiency η_{fuel} .

Figure 6 shows η_{fuel}^{meas} and η_{fuel} before and after engine fuel consumption parameterization reducing average error from 3,2% to 0,3%. The parameterization mainly consists on reducing the engine efficiency η_{fuel} which was initially too optimistic: indicated efficiency parameters are reduces to 38% for gasoline and 38,5% for diesel engine and frictions are slightly increased. This engine efficiency reduction represents a more “constrained” environment in real-world vehicle compared to an engine test bench environment: extra losses due for example to gearbox oil pump losses, more friction losses due to older engine design, fuel with a lower energy density. In these conditions, a model parameterization ensures to represent correctly €6 engines functioning in real-world conditions.

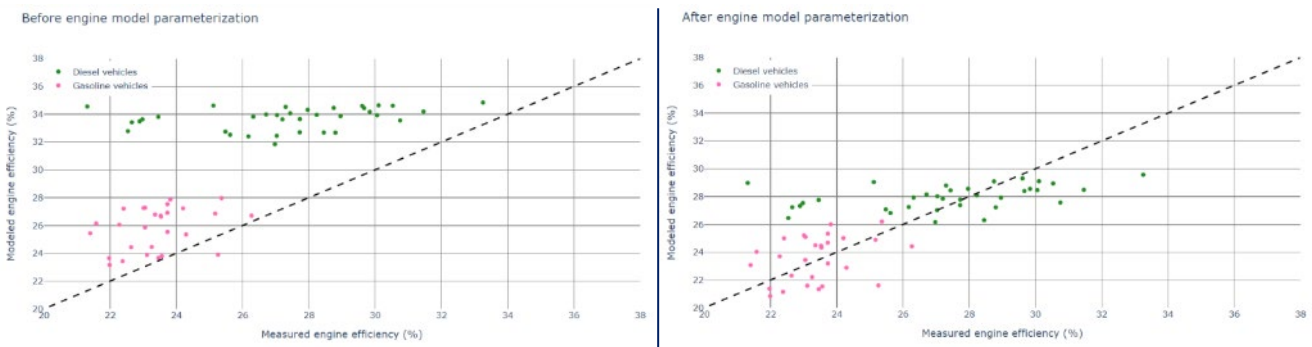


Figure 6: η_{fuel}^{meas} and η_{fuel} before (left figure) and after (right figure) engine fuel consumption parameterization, a dot corresponds to a unique test.

Vehicle model parameterization validation

As a validation of the method presented in Section 4, simulations are performed on all the tests presented in Section 2. The fuel consumption model relative error ϵ_{fc} (expressed in %) is introduced as:

$$\epsilon_{fc} = 100(f_{c_{sim}} - f_{c_{meas}})/f_{c_{meas}} \tag{20}$$

where $f_{c_{meas}}$ is the test measured fuel consumption.



Figure 7: Fuel consumption model relative error ϵ_{fc} dispersion for campaign tests, a dot corresponds to a unique test and boxplot to diesel or gasoline vehicles test of the same campaign.

Figure 7 presents results as box plots dispersions, with dot representing single test error and gasoline and diesel are separated. ε_{fc} results are presented in the table 2. The model ensures to simulate RWFC with a good precision: respectively 69% and 96% of real-world tests can be simulated with an error below 10% and 15%. The average error is -1.9% meaning that the model parametrization ensures to represent averagely RWFC.

Table 2: mean and standard deviation in % fuel consumption relative error ε_{fc} results and test percentage with an error below 5, 10 and 15%.

	Tests number	ε_{fc}		Test percentage with $ \varepsilon_{fc} $ below		
		Mean	Standard deviation	5%	10%	15%
OEM RDE campaign	92	-1.9	10.5	41	64	93
JRC campaign	36	2.8	7.6	47	86	97
MTES campaign	85	-4.0	13.7	36	67	98
Total	213	-1.9	11.7	40	69	96

The total standard deviation of the fuel consumption error is 11.7% and is mainly due to [4]:

- some vehicle model parameters that may differ from the model presented in Section 4: vehicle mass higher or lower than mass parameterized as (19), auxiliaries electrical consumption, fuel quality with a lower or an higher power density impacting engine efficiency, more aggressive or more economic gearshift strategy than the strategy presented in subsection 4.2.3
- or some vehicle model parameters that aren't modelled with a second order impact on RWFC: under-inflated or used tires, ambient conditions: temperature, slippery road, wind..., different vehicle modes (sport mode for example...

Conclusion

The main contribution of this work is to propose a method to obtain a generic parameterization of the model ensuring to represent different vehicles with different physical characteristics in different test conditions with a good level of accuracy. The main advantage of the resulting model is its simplicity versus accuracy trade-off.

In this work a simple quasi-static vehicle model has been presented. The model is based on physical equations and takes into account the first order parameters impacting RWFC. Next an original method to parameterize the model from vehicle measurements has been presented. This method results from tests campaigns analysis feedbacks and ensures to represent a vehicle operating in real world conditions. The approach proposes to estimate the energy delivered by the engine and to split the problem: in one hand criteria for mass and resistive forces parameterization and in the other hand the engine efficiency. Once parameterized, the model is validated on a 200 test database with good level of results ensuring to model RWFC.

Perspectives of this work are numerous:

- Firstly as explained in introduction the gap between homologated fuel consumption and RWFC is a worrying problematic [3]. A very promising way to measure this gap could be achieved from trips data obtained via an application like Geco air [4], [5]. As explained briefly in the introduction, the model parameterization presented here is used to predict CO₂ emissions of Geco air users based on their trips and individual vehicle. The RWFC is in this case very sensitive because the RWFC estimation is directly related to the vehicle model accuracy.
- Secondly the gap between homologated fuel consumption and RWFC can be estimated from crowdsensing trips data, see for example [14] for a gap representativeness analysis with RWFC estimated with the vehicle model presented in this paper.
- Thirdly analysing the gap and understanding gap causes is also a big challenge: in [15] elements are given to analyse data representativeness and which vehicle parameters contribute the most to the gap.

Finally the model presented in this paper and its accuracy represents a promising approach to estimate the gap between homologated fuel consumption and RWFC. With the On-Board Fuel Consumption Meter introduction as a regulatory technology to monitor the real-world CO₂, needs in gap analysis will increase. Therefore the RWFC representative vehicle model approach is a prerequisite to understand the main reason of the gap related to vehicle, use case and driving behavior and also to predict future evolution of the gap.

References

- [1] Regulation (eu) 2019/631 of the European parliament and of the council of 17 april 2019 Setting co2 emission performance standards for new passenger cars and for new light commercial vehicles, and repealing regulations (ec) no 443/2009 and (eu) no 510/2011. 2019.
- [2] Commission Regulation (EU) 2018/1832 of 5 November 2018 amending Directive 2007/46/EC of the European Parliament and of the Council, Commission Regulation (EC) No 692/2008 and Commission Regulation (EU) 2017/1151 for the purpose of improving the emission type approval tests and procedures for light passenger and commercial vehicles, including those for in-service conformity and real-driving emissions and introducing devices for monitoring the consumption of fuel and electric energy. 2018.
- [3] Uwe Tietge, S. Díaz, P. Mock, A. Bandivadekar, J. Dornoff, and N. Ligterink, "From laboratory to road a 2018 update of official and 'real-world' fuel consumption and CO₂ values for passenger cars in europe," TNO, ICCT, Jan. 2019.
- [4] L. Thibault, P. Degeilh, O. Lepreux, L. Voise, G. Alix, and G. Corde, "A new GPS-based method to estimate real driving emissions," in *2016 IEEE 19th International Conference on Intelligent Transportation Systems (ITSC)*, Rio de Janeiro, Brazil, Nov. 2016, pp. 1628–1633.
- [5] L. Thibault, P. Degeilh, G. Sabiron, L. Voise, K. Thanabalasingam, and G. Corde, "GNSS data-based approach to monitor real-world exhaust emissions at microscopic resolution," in *International Transport and Air Pollution Conference TAP*, Zurich, Switzerland, 2017, pp. 1–14.
- [6] G. Fontaras, N.-G. Zacharof, and B. Ciuffo, "Fuel consumption and CO₂ emissions from passenger cars in Europe – Laboratory versus real-world emissions," *Progress in Energy and Combustion Science*, vol. 60, pp. 97–131, May 2017.
- [7] J. Pavlovic *et al.*, "Understanding the origins and variability of the fuel consumption gap: lessons learned from laboratory tests and a real-driving campaign," *Environ Sci Eur*, vol. 32, no. 1, p. 53, Dec. 2020.
- [8] IFP Energies Nouvelles, "Study of Euro 6d-TEMP emissions – IFPEN for DGEC, Summary report," Dec. 2020. [Online].
Available: https://www.ifpenergiesnouvelles.fr/sites/ifpen.fr/files/inline-images/Innovation%20et%20industrie/Motorisations%20thermiques/Study-of-Euro-6d-TEMP-emissions_IFPEN-DGEC_SynthesisReport_Dec2020.pdf.
- [9] L. Guzzella and A. Sciarretta, *Vehicle Propulsion Systems*. Berlin, Heidelberg: Springer Berlin Heidelberg, 2013.
- [10] R. Rajamani, *Vehicle Dynamics and Control*. Boston, MA: Springer US, 2012.
- [11] L. Serrao *et al.*, "Open Issues in Supervisory Control of Hybrid Electric Vehicles: A Unified Approach Using Optimal Control Methods," *Oil Gas Sci. Technol. – Rev. IFP Energies nouvelles*, vol. 68, no. 1, pp. 23–33, Jan. 2013.
- [12] J. Lescot, A. Sciarretta, Y. Chamailard, and A. Charlet, "On the integration of optimal energy management and thermal management of hybrid electric vehicles," in *2010 IEEE Vehicle Power and Propulsion Conference*, Lille, France, Sep. 2010, pp. 1–6.
- [13] G. Alix, J.-C. Dabadie, and G. Font, "An ICE Map Generation Tool Applied to the Evaluation of the Impact of Downsizing on Hybrid Vehicle Consumption," in *12th International Conference on Engines & Vehicles*, Sep. 2015, pp. 2015-24–2385.
- [14] P. Michel, A. Pirayre, S. S. Rodriguez, and A. Chasse, "From trips database to real-world fuel consumption. model and large-scale simulation framework," in *2020 IEEE 23rd International Conference on Intelligent Transportation Systems (ITSC)*, Rhodes, Greece, Sep. 2020, pp. 1–6.
- [15] M. Ktistakis, J. Pavlovic, G. Fontaras, P. Michel, S. S. Rodriguez, and A. Chasse, "Understanding the Fuel Consumption Gap Using Self-Reported User and Smartphone Application Datasets," in *International Transport and Air Pollution Conference TAP*, Graz, Austria, 2021, pp. 1–9.

2.18 RDE of NRMM – Comparing portable and stationary measurement methods

Johannes Ettl*, Klaus Thuneke, Peter Emberger, Edgar Remmele

Technology and Support Centre (TFZ), Straubing, Germany

johannes.ettl@tfz.bayern.de

Abstract

Exhaust gas emission limits from non-road mobile machinery (NRMM) such as tractors, excavators or loaders have been increasingly tightened during recent years. In addition to steady state and transient test cycles for the application at test stands, a monitoring of real driving emissions (RDE) in the field by using portable emission measurement systems (PEMS) has been introduced. Portable emission measurements, however, are associated with considerable technical, temporal, and economic expenses as well as poor repeatability. Thus, a new method would be beneficial, to evaluate real-world emissions more easily under reproducible conditions. It is the purpose of this work to develop a simplified tool for determining real-world exhaust gas emissions of tractors at a PTO test stand. For this purpose, CAN bus signals of engine speed (n_{CAN}) and torque (M_{CAN}) from in-field RDE measurements during ploughing will be transferred to a tractor test stand in full length. Additionally, a short practical tractor driving cycle (PTFZ) is being developed, which is based on representative speed and torque segments from the in-field measurement. For evaluation the exhaust gas emission values measured at the test stand are compared with those assessed in the field. As a result, a high congruency in emission behaviour between in-field recorded values and values replicated at the test stand can be observed. Furthermore, no significant differences between PEMS and stationary gas analysers are recognized. The generated practical tractor driving cycles (PTFZ) allow time-saving, work specific fuel consumption and emission measurements as well as optimisation processes in terms of emission reduction, efficiency increase and the usage of alternative fuels. Further investigations should clarify whether the method is applicable to different tractors and tractor works and useful to collect data for emission inventories.

Introduction

Exhaust gas emission limits for non-road mobile machinery (NRMM), like tractors, excavators or loaders have been increasingly tightened in the European Union (EU) during recent years. Emission testing for type-approval is performed on dismantled engines on engine test benches by applying both the non-road steady-state test cycle (NRSC) as well as the non-road transient test cycle (NRTC). Besides legally determined test methods, stationary emission measurements on the entire tractor, using eddy current brakes connected to the tractor's power take-off (PTO) shaft have become a practicable alternative [3][4][7].

Since both test cycles NRSC and NRTC do not represent actual conditions in real-world applications properly, the monitoring of real driving emissions (RDE) by using portable emission measurement systems (PEMS) has been introduced with emission stage V in the year 2019. Portable emission measurements, however, are associated with considerable technical and economic expenses as well as poor repeatability in contrast to the test stand. Additionally, previous investigations show large fluctuations of RDE values produced with varying tractors, agricultural implements, work types and fuels [1][2][5][8][6].

Thus, a new method would be beneficial, to evaluate real-world emissions and fuel consumption more easily and under reproducible conditions. Such a method could help assessing data of single tractors and tractor fleets for emission inventories and simplifying optimization processes in terms of emission reduction, efficiency increase and the usage of alternative fuels.

Purpose

The purpose of this work is to develop a convenient tool to determine real-world exhaust emissions of tractors at a PTO test stand. As a first step gaseous emissions, such as nitrogen oxides (NO_x), carbon monoxide (CO), hydrocarbons (HC), carbon dioxide (CO_2) and the exhaust gas mass flow (Q_M) of a tractor should be recorded during field work (ploughing) with a portable emission measurement system (PEMS). In a second step, the Controller Area Network (CAN) bus signals engine speed (n_{CAN}) and torque (M_{CAN}) from the in-field RDE measurements should be transferred to a tractor test stand, where the same tractor is connected to an eddy current brake via the PTO shaft. The exhaust gas emissions should be measured on the tractor test stand, simultaneously with PEMS and stationary gas analysers (GA). In addition to the full time ploughing cycle, the measuring time on the test stand should be significantly reduced by generating a short practical driving cycle (PTFZ) based on representative speed and torque segments from the in-field measurement [3]. Finally, the emissions measured in the field should be compared with the test stand results for evaluation of this method.

Approach

Figure 1 shows the in-field RDE emission measurements with a Fendt Vario 724 S4 tractor connected to a 5-furrow Pöttinger Servo 45 Plus plough. The tractor is equipped with a Deutz TCD 6.1 L6 engine (exhaust gas emission stage IV), which is compatible for rapeseed oil fuel operation. It features an exhaust gas recirculation (EGR) as well as an exhaust gas after-treatment system (EAT) comprising a diesel oxidation catalyst (DOC), a diesel particle filter (DPF) and a selective catalytic reduction (SCR). The in-field exhaust gas emissions are measured with a Semtech Ecostar PEMS of the company Sensors Inc. The PEMS combines the analysers NDUV, NDIR, FID as well as an exhaust gas mass flow meter. All analysers are mounted in a dust- and water-resistant housing on the front linkage of the tractor. The ECU parameters engine speed (n_{CAN}) in min^{-1} and engine torque (M_{CAN}) in % are monitored from the CAN bus interface according to SAE J1939. The total measurement time was 8.5 h. It was carried out in three parts, lasting 2.9 h, 3.2 h and 2.4 h at an average ambient temperature of 8 °C.



Figure 1: Rapeseed oil fuelled Fendt 724 S4 with a PEMS mounted in the front during ploughing.

At the tractor test stand (Figure 2) the limited exhaust gas emission components nitrogen oxides (NO_x), carbon monoxide (CO), carbon dioxide (CO_2) and hydrocarbons (HC) are recorded by both, the Semtech Ecostar PEMS and the AVL SESAM 4 stationary gas analysis system (including FTIR, FID and PMD). The exhaust gas mass flow (Q_M) is calculated according to ISO 8178 on basis of fuel consumption, which was measured by continuous weighing of an external fuel tank using a Mettler-Toledo KB60.2 platform scale. Measurements of the emission behaviour were conducted with rapeseed oil fuel (fuel standard DIN 51605).

The emission measurements at the tractor test stand are firstly performed with the same engine speed (n_{CAN}) and torque (M_{CAN}) profile as recorded during the in-field RDE measurements over the full operation time of 8.5 h. In order to transfer the recorded CAN bus data from ploughing into target values for the gas pedal regulator and the eddy current brake (EGGERS PT 301 MES) on the test stand, 130 different levels of engine speed (n_{CAN}) and torque (M_{CAN}) in the engine operation map are determined [3]. On basis of these data, fit curves for engine speed and torque are computed. By doing so, the emission measurements at the tractor test stand can be performed with the same engine speed (n_{CAN}) and torque (M_{CAN}) profile as the previous in-field measurements [3]. The ploughing test cycle is started after the tractor was conditioned to the same coolant temperature (of 41 °C, 67 °C and 66 °C) as at the beginning of the in-field emission measurements. The average ambient temperature at the tractor test stand (16 °C) was higher compared to the measurements on the field, because there was no active cooling system available.

By applying the practical tractor driving cycle (PTFZ) method [3], the necessary measuring time on the test stand can be reduced from 8.5 h to 0.55 h. This is possible, because for developing the PTFZ the full ploughing operation time is divided into single segments, as there are working, turning and residual time. Then, the frequency distribution of each time segment is compared with the frequency distribution of all the time segments of the corresponding category using the least squares method. Segments with the highest average coefficient of determination (R^2) are rated as being representative and therefore used for cycle creation. The proportion of working time, turning time and residual

time should vary by less than two percentage points between ploughing in the field and the generated test cycle. [3] The average ambient temperature during the performance of the PTFZ at the tractor test stand was 15 °C.

The exhaust gas emission results measured in the field are compared with those from the test stand for both full and reduced (PTFZ) measurement time by using a t-test. The following presentation of results focuses on the particularly relevant emission components NO_x and CO₂.

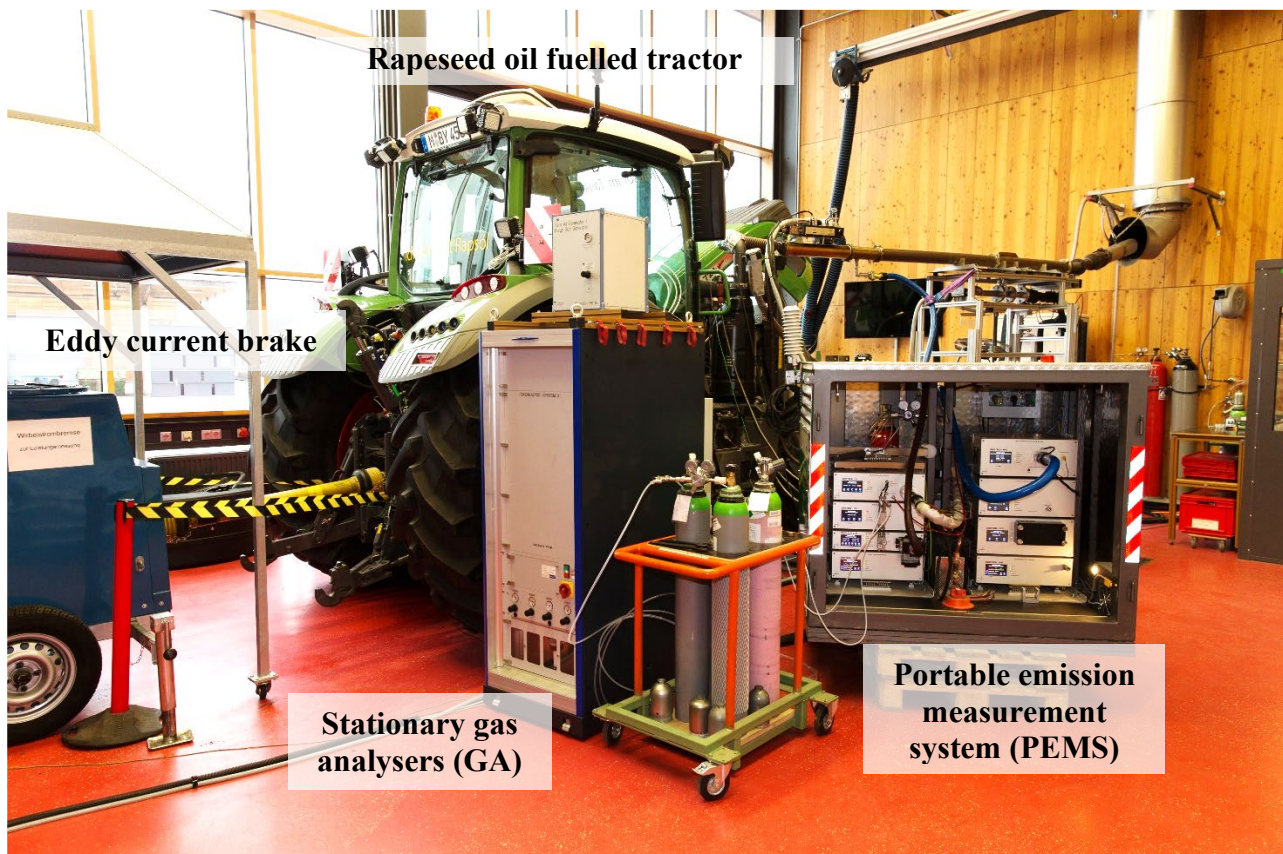


Figure 2: Setup for emission measurements at the tractor test stand with stationary gas analysers (GA) and a portable emission measurement system (PEMS).

Results

Engine and emission data from measurements over 8.5 h ploughing in the field were evaluated and resulting field-work profiles were transferred to the tractor test stand. Figure 3 shows engine speed, torque, NO_x, CO₂, and the exhaust gas flow rate over a 1200 seconds long segment of ploughing, recorded in-field and replicated at the tractor test stand, using the PEMS. The widely congruent courses of the curves for n_{CAN} and M_{CAN} demonstrate the high degree of accordance between in-field recorded and on the test stand replicated values with regression coefficients (R^2) over 98 %. Deviations, if any, mainly occur in transient phases corresponding to the turning on the headland as an effect of the inertia of the tractor system.

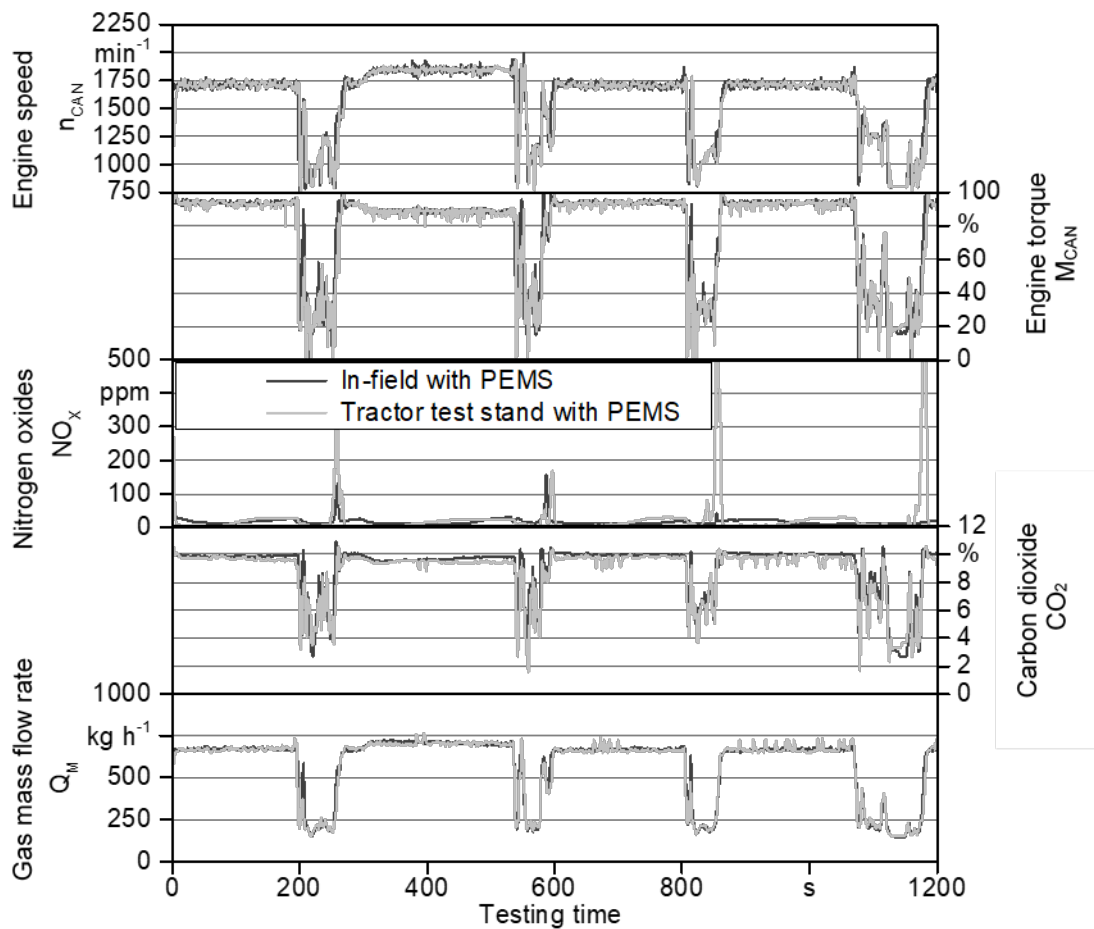


Figure 3: Engine speed, torque, NO_x , CO_2 and Q_M values during a 1200 seconds long segment of ploughing, recorded in-field and replicated at the tractor test stand with PEMS.

The NO_x and CO_2 emissions as well as the exhaust gas mass flow rate Q_M of the tractor were well reproducible with a high conformity at the tractor test stand. Both, during the original in-field and the replicated test stand measurements the NO_x emissions are mostly far below 50 ppm. Some higher peaks of NO_x emissions, however, occur shortly after the turning segments during the insertion of the plough into the soil. These NO_x peaks arise more frequently at the tractor test stand than in the field. The reason therefore might be that the gas pedal regulation for the value n_{CAN} responses around a second slower than during the field work (for example at 240, 820 or 1180 s testing time). In this situation, the engine is throttled back for a short time, getting into an emergency mode, where the NO_x reduction of the SCR system as well as the exhaust gas recirculation rate are reduced. By increasing the control frequency on the test stand from 1 to 10 Hz, this effect can most likely be avoided.

When looking at the medians and the average values between in-field recorded and on the test stand replicated values for NO_x , CO_2 and Q_M they differ only slightly over the entire measuring period of 8.5 h. This can be seen in the box plots of Figure 4. The boxes include the upper and lower quartiles, the whiskers indicate the 95th and the 5th percentile, the medians are marked as horizontal lines and the arithmetic means are displayed as honeycomb-shaped dots.

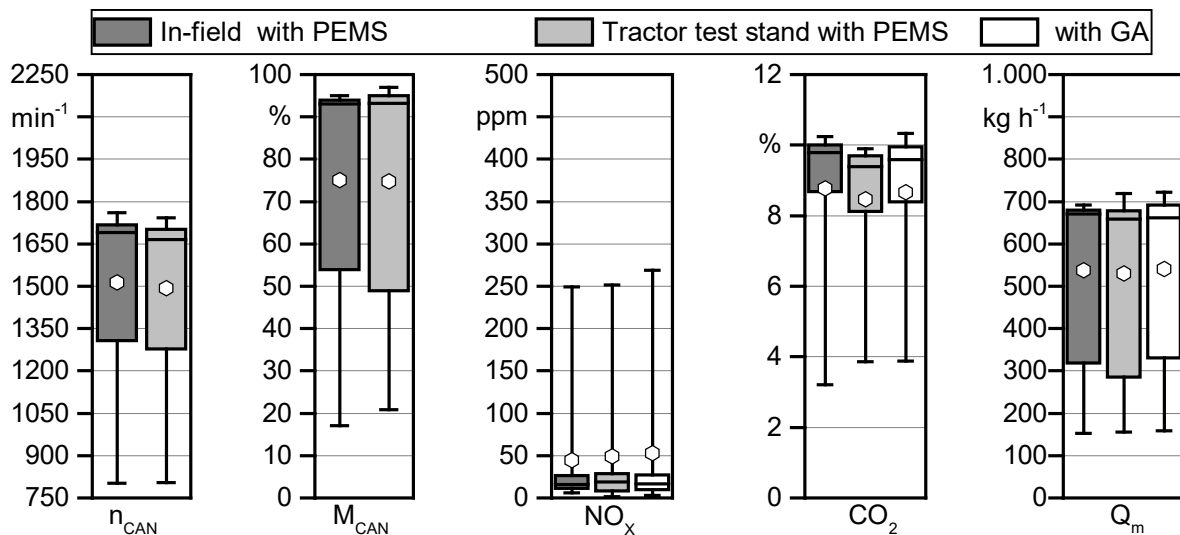


Figure 4: Medians and arithmetic means, quartiles and percentiles of engine speed, torque as well as exhaust emission concentrations measured in-field and at the tractor test stand with PEMS and stationary gas analysers (GA) over the full operation time of 8.5 h.

Overall, the arithmetic mean and median values vary only slightly between in-field and test stand runs. With PEMS in the field, the average NO_x concentration is 6.3 ppm lower, the average CO_2 concentration 0.3 vol.-% higher and the average exhaust gas mass flow 7.0 kg/h higher compared to the test stand measurement.

Comparing the measured arithmetic mean values of the PEMS with the GA, deviations of max. 3.0 ppm NO_x , 0.19 vol.-% CO_2 and 10 kg/h exhaust gas mass flow are observed. Thus, despite different measurement principles and accuracies of the analysers, the results with the used portable and stationary gas analysers are well congruously.

The deviations of the measured values between the test environments (field and test stand) as well as between the exhaust gas analysis systems (PEMS and stationary exhaust gas analysers) are not statistically significant. The mean comparison with the t-test showed no significant difference for NO_x , CO_2 and Q_m at a significance level of $\alpha = 0.05$ between measured values with PEMS in the field ($n=3$) and PEMS ($n=3$) or the stationary GA ($n=3$) at the test stand.

Figure 5 shows the mean specific NO_x emissions during ploughing in the field and at the tractor test stand for full length as well as for the shorter practical tractor driving cycle (PTFZ) using rapeseed oil fuel. The specific NO_x emission values of all measurements are generally on a low level, under the limit value of 0.4 g/kWh, which applies to the legal test cycles according to the EU regulation 2016/1628.

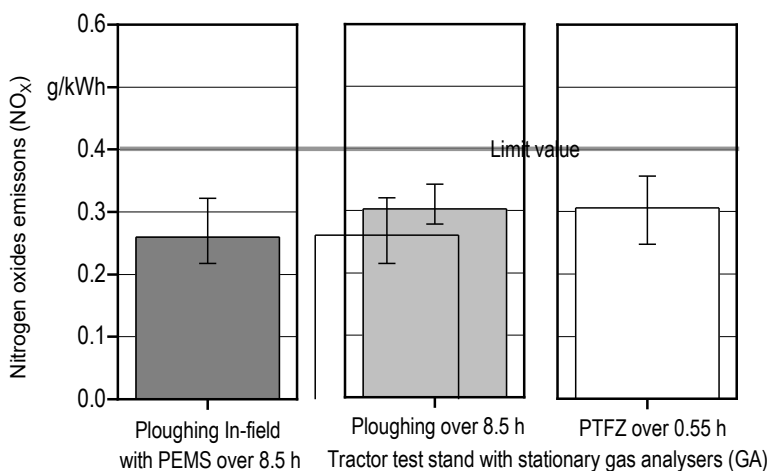


Figure 5: Specific NO_x emissions during ploughing in the field and replicated at the tractor test stand over 8.5 h as well as during the practical tractor driving cycle (PTFZ) over 0.55 h with rapeseed oil fuel ($n = 3$).

The test stand trials show little higher NO_x emissions (0.05 g/kWh) with stationary gas analysers (GA) compared to the in-field measurement with PEMS, as also explained in Figure 4. The mean NO_x emissions in the practical tractor driving

cycle (PTFZ) over 0.55 h at the tractor test stand differ by less than 0.01 g/kWh compared with the test over the full operation time of 8.5 h. In comparison to the RDE during ploughing in the field, the mean value of the NO_x emissions of the PTFZ over 0.55 h is 0.06 g/kWh higher but does not vary significantly (significance level $\alpha = 0.05$).

Practical tractor driving cycles (PTFZ) allow to determine real world exhaust emissions of tractors in a simplified way on a tractor test stand. This enables time-saving measurements of fuel consumption and exhaust gas emissions.

Conclusions and Outlook

Tractor engine data, derived from RDE measurements during ploughing could be transferred successfully to the tractor PTO test stand, where they serve as target values for equally replicated or shortened driving cycles. By comparing emission results between ploughing in the field and the replicated ploughing at the tractor test stand, a high congruency in emission behaviour could be observed. This shows that the application of practical tractor driving cycles (PTFZ) can complement the rather complex RDE measurements with PEMS. Thus, work specific real-world emissions and emission factors of agricultural mobile machinery can be determined effectively and reproducibly. Further advantages of the PTFZ compared to RDE measurement with PEMS are the possibility to vary influencing factors (fuel, temperature etc.) systematically and to use non-mobile measurement technology. Applying this method, the development and optimisation of propulsion systems that are compatible with alternative fuels can be supported. Further investigations should clarify whether the method is applicable to different tractors and other tractor works and also for collecting data for emission inventories.

Acknowledgements

The authors would like to thank the Bavarian State Ministry of Food, Agriculture and Forestry, the Bavarian State Ministry of Economic Affairs, Regional Development and Energy and the German Federal Ministry of Food and Agriculture (BMEL) through the Agency for Renewable Resources (FNR) for financial support.

References

- [1] BONNEL, P., PERUJO, A., PROVENZA, A., & VILLAFUERTE, M. (2013). *Non Road Engines Conformity Testing Based on PEMS: Lessons Learned from the European Pilot Program (JRC Scientific and Policy Reports No. EUR 26438 EN)*.
- [2] CAO, T., DURBIN, T. D., RUSSELL, R. L., COCKER, D. R., SCORA, G., MALDONADO, H., & JOHNSON, K. C. (2016). Evaluations of in-use emission factors from off-road construction equipment. *Atmospheric Environment*, 147, 234–245.
- [3] Ettl, J.; BERNHARDT, H.; PICKEL, P.; REMMELE, E.; THUNEKE, K.; EMBERGER, P. (2018): *Transfer of agricultural work operation profiles to a tractor test stand for exhaust emission evaluation. Biosystems Engineering, Jg. 176, S. 185–197*
- [4] Ettl, J.; BERNHARDT, H.; HUBER, G.; THUNEKE, K.; REMMELE, E.; EMBERGER, P. (2020): *Evaluation of pure rapeseed oil as a renewable fuel for agricultural machinery based on emission characteristics and long-term operation behaviour of a fleet of 18 tractors. SN Applied Sciences, Jg. 2, Nr. 10, 82, 1-16*
- [5] Ettl, J., Huber, G., Bernhardt, H., & Thuneke, K. (2016). *Real Emissions of a Plant Oil Compatible Tractor: Measured by PEMS and on the Tractor Test Stand. ATZ offhighway, 9(11), 46–51.*
- [6] EMBERGER, P.; HINRICHS, M.; HUBER, G.; EMBERGER-KLEIN, A.; THUNEKE, K.; PICKEL, P.; REMMELE, E. (2021): *Field tests and real-world exhaust gas emissions of a pure rapeseed oil-fuelled harvester in forestry. Testing a solution for combined water, soil, and climate protection. Journal of Cleaner Production, Jg. 280, 124360, 1-10*
- [7] EMBERGER P, LANDIS M, KRAMMER K, PRANKL H, SCHAUFLE H, SCHIESS I ET AL. (2011): *Measurement of emissions of a tractor — round robin test of ART, FJ-BLT and TFZ. Landtechnik 2011;66(1):56–9.*
- [8] GIETZELT, C., DEGRELL, O., & MATHIES, K. (2012). *In-use emission measurements on combustion engines used in mobile machinery. Landtechnik, 67(5), 366–369.*

2.19 Emissions of passenger cars in special driving situations

Danilo Engelmann ^{1*}, Andreas Hüsey ¹, Pierre Comte ¹, C Jan zerwinski ², Peter Bonsack³

¹ University of Applied Sciences, Biel-Bienne, AFHB¹, CH

² CJ Consulting, Port, CH

³ Federal Office for the Environment (FOEN), Air Pollution Control and Chemicals Division, Bern, CH

danilo.engelmann@bfh.ch

Abstract

Testing of real driving emissions (RDE), as an element of a type approval of passenger cars (since September 2017), offers the opportunity to collect the data about the emissions in special driving, or non-driving situations. These situations are: cold start, warm-up of the engine, stop & go and idling.

In the present work of the Laboratory for Exhaust Emissions Control (AFHB) of the Berne University of Applied Sciences (BFH), the definitions of the special driving situations were proposed and the emissions of 7 passenger cars (gasoline & Diesel) were extracted from the present RDE data.

Furthermore, some special driving situations, particularly the stop & go operation with varying share of idling were reproduced on chassis dynamometer.

As expected, the emissions of CO, NO_x and PN are in the cold start and in the first part of the warm-up phase (c.a. 25s) considerably higher than in the rest of the investigated urban phase.

The singular emitting situations like “stop & go” or idling occur frequently in the warm-up phase, i.e. in the city operation when the engine and the exhaust system are still not warm enough.

The emissions in the investigated particular driving situations scatter considerably for the different vehicles due to varying efficiencies and warm-up of the exhaust aftertreatment systems.

Introduction

Emission factors and emission inventories are an important source of data for compiling and modelling the emissions of traffic in different situations. There is in EU a continuous work and development of emission data inventories, [1-5].

Since the introduction (in 2017) of the road-testing (RDE...real driving emissions) as an obligatory element of the legal testing procedures, the increased amount of RDE-data can be used for different objectives, such as: further development of emission inventories, compliance with “In-Service Conformity” (ISC, EU regulation 2018/1832) and market surveillance activities (EU regulation 2018/858). Extensive activities of testing RDE by means of PEMS (portable emissions measuring systems) have been performed in the last years, aiming not only the emissions but also the improvements of instrumentation, of testing procedures and of evaluation [4-12].

A well-known fact is that the emissions at cold start, during the warm-up and at the low speed phases of urban operation, both in the laboratory and on the road, tend to be higher for all pollutants, [9, 13-15]. This fact supports even the idea for future introduction of urban emission limits for the short trips, which are very frequent in Europe, [4].

In order to enable an automatic co-evaluation of emissions from the special (non)driving situations, the necessary definitions were proposed in the present work. With these definitions, the RDE data of 7 vehicles were processed and the emissions in special driving situations were obtained (part 1). Additionally, some special situations like cold start, warm-up and stop&go were reproduced on the chassis dynamometer with cars of different ages and different technology.

This paper gives some new insights in the topic of emissions from special driving situations.

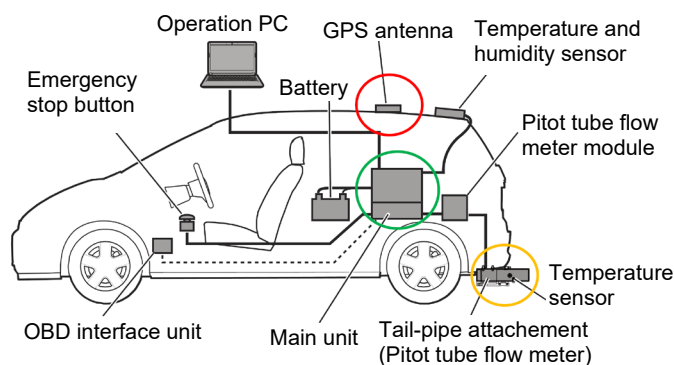
Analysis of present RDE data

Data origin & processing

The emissions data originate from testing of different vehicles with Horiba PEMS (Portable Emission Measuring Systems for gaseous emissions) and with PN-PEMS (for particle number PN) at AFHB.

The Horiba OBS-ONE-PN PEMS uses two-step dilution, a catalytic volatile particle remover (350°C) and an Isopropanol-based CPC as a main measuring unit.

Figure 1 represents the PEMS installation on a vehicle.



Concentrations, Mass Flow, Distance ⇒ g/km

Figure 1: Set-up of PEMS on a vehicle.

The results of exhaust gas measuring devices are given as volume concentrations. Nevertheless, the legal limits are expressed in [g/km] for LDV, or in [g/kWh] for HDV. Therefore, it is necessary to install a flowmeter at the tailpipe of the vehicle and to estimate the instantaneous exhaust gas mass flow in the transient operation.

In the data processing, the vehicle positions and speeds are required. They are usually registered from the GPS (Global Positioning System), which is installed on the vehicle. If this signal is not available, e.g. in the tunnel, the speed can be obtained from the OBD-interface (on Board Diagnose) of the vehicle. Additionally, the parameters such as the engine coolant temperature and the engine speed are registered by the OBD.

The pollutant components measured by both PEMS (Gas & PN) are carbon dioxide CO₂, carbon monoxide CO, nitric oxides NO_x (consisting of NO and NO₂) and particle number PN (considering the invisible nanoaerosol).

For the choice of data (vehicles previously measured in other projects) following criteria were taken into consideration:

- Version of the RDE route
- The same measuring system
- Engine cold start measured
- Engine start measured
- Emission components measured (CO₂, CO, NO_x, PN, HC)
- Start-stop-system (switched off).

Seven vehicles (three gasoline and four Diesel) could be chosen for the data evaluation. Table 1 summarizes the most important data of these vehicles.

Some criteria could not be completely fulfilled:

- Start-stop-system of LDV 07 was switched on
- PN was not measured for some vehicles
- HC was not measured for all vehicles

Table 1: List of vehicles chosen for the data evaluation (LDV ... light duty vehicle).

Nr.	Fuel	Displacement	Exhaust Aftertreatment System	Injection
LDV01	Gasoline	1.6	TWC	PFI
LDV02	Gasoline	4.0	TWC, GPF	DI
LDV03	Gasoline	6.2	TWC	PFI
LDV04	Diesel	2.0	DOC, DPF	DI
LDV05	Diesel	2.1	DOC, DPF, SCR	DI
LDV06	Diesel	3.0	DOC, DPF, SCR	DI
LDV07	Diesel	3.0	DOC, DPF, SCR	DI

Definitions of non-driving situations

Distance driven and urban part

In the legal RDE-evaluation of LDV's the parts of driving, which were performed with the speed lower than 60 km/h, are considered as "urban", even if they were performed outside of the city. In opposition, the urban part in this work is defined as the first 13.7 km of the distance driven. This was decided after investigating the speeds, distances and emission traces of the chosen vehicles. 13.7 km is the shortest distance before one of the vehicles reached the speed of 60 km/h.

With this definition of urban part, it is fixed that all investigated vehicles were driven below this speed limit value (60 km/h). Furthermore, it was observed that during this 13.7 km, there were the specific driving-and emissions-situations, which are the subject of this research: cold start, warm-up, stop&go, idling.

The investigation of the high-speed driving parts – rural and highway – showed no noticeable emission events.

Cold start

The cold start is defined with the engine coolant temperature (ECT) as: $(ECT + 2^{\circ}C) < t_{amb}$, or $ECT < 30^{\circ}C$. This means that ECT can be up to 2°C higher than the ambient temperature or it must be lower than 30°C. This definition originating from the HDV-legislation is applied in this work because it is stricter than the definition from the LDV-legislation (+7°C, 35°C).

Engine warm-up

The warm-up time is defined in two ways:

- from the engine start ($n > 500$ rpm) to the instant of $ECT = 70^{\circ}C$ – this is named: "ECT 70" and
- from the engine start ($n > 500$ rpm) to the duration of 5 minutes – this is named: "5 minutes".

These definitions and examples of the warm-up for two vehicles (gasoline & Diesel) are represented in Figure 2. It can be clearly remarked that the Diesel vehicle needs a longer time to attain the ECT 70.

Figure 5 summarizes the time-traces of ECT for all investigated vehicles. For LDV1 and LDV5, there are some irregular increases of ECT. ECT of LDV1 reaches 70°C in approximately 4 minutes after start. However, it falls again below 70°C for approximately 1 minute. This 1 minute is accounted to the warm-up according to the definition.

For more detailed analyses it is useful to consider both warm-up definitions and the time-courses of the increasing ECT.

Stop&go

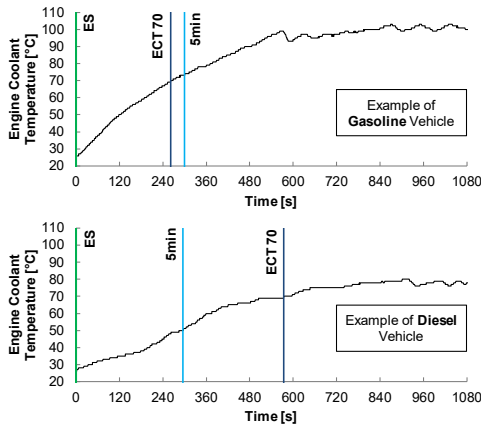
According to ASTRA, the definitions of traffic congestion which are used for the public traffic information are:

- the traffic jam on the extra-urban route is given when the speed is below 10 km/h during at least 1 minute and frequent standstill occurs,
- in the city circulation, the traffic jam is considered when the loss of summary time is over 5 minutes.

These definitions are close to the stop&go operation and they gave the basis for the definition which is easy to understand and which depicts well this driving situation.

The operation of the vehicle with the driving speeds between 1km/h and 10 km/h is considered as a "stop&go" phase. In this way, the vehicle standstill (stop) and the short acceleration by moving (go) are included in this operation mode.

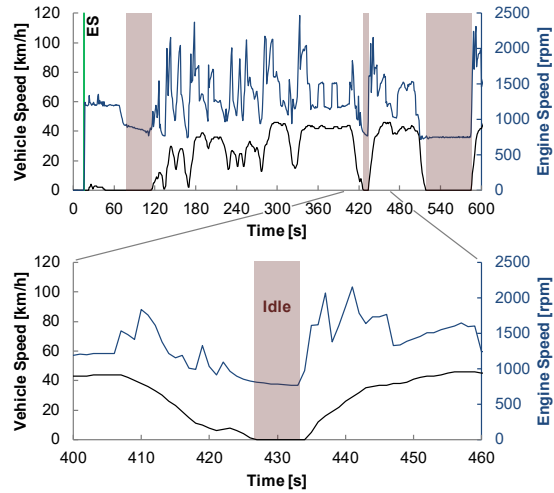
Figure 3 shows the definition and example of stop&go in the urban part (13.7 km). Figure 5 summarizes the shares of stop&go in the urban part for all investigated vehicles. These shares are in the range of 13% to 19%.



ES: Engine Start (Start of "Engine In Operation")
 ECT 70: Engine Coolant Temperature (ECT) reaches 70°C
 5min: 5min after Engine Cold Start

Definitions	start	end
Cold Start	state ECT < T _{ambient} +2°C OR ECT < 30°C	-
Engine in Operation	state Engine Speed > 500 rpm	-
Warm-Up ECT 70	phase Cold Start AND Engine in Operation	ECT > 70°C
Warm-Up 5min	phase Cold Start AND Engine in Operation	Phase Time > 5min

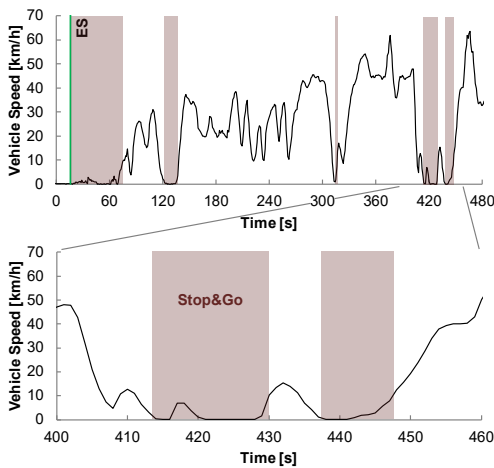
Figure 2: Definition of warm-up in RDE-test.



ES: Engine Start (Start of "Engine In Operation")

Definition	start	end
Idling	state 500 rpm < Engine Speed < 900 rpm	-
Idle	phase Vehicle Speed < 1 km/h AND Idling	Idle Start Cond. False

Figure 4: Definition of idling in RDE-test.



ES: Engine Start (Start of "Engine In Operation")

Definition	start	end
Stop&Go	phase Vehicle Speed < 1 km/h	Vehicle Speed > 10 km/h

Figure 3: Definition of stop&go in RDE-test.

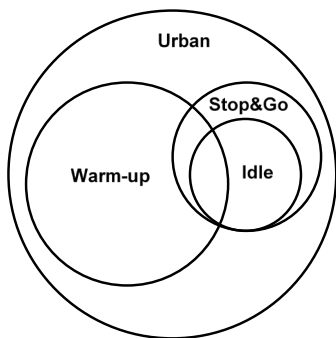


Figure 6: Qualitative overlapping of the analyzed data in the RDE-tests.

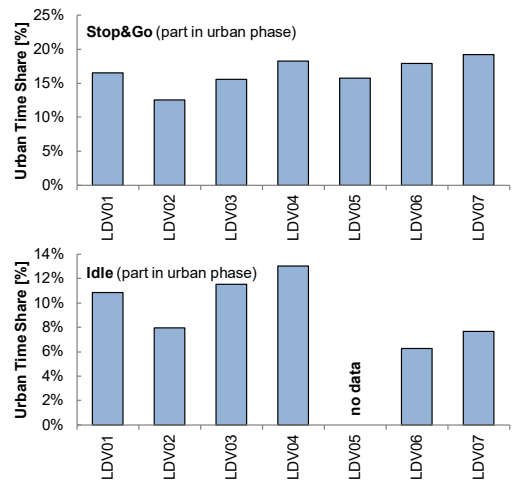
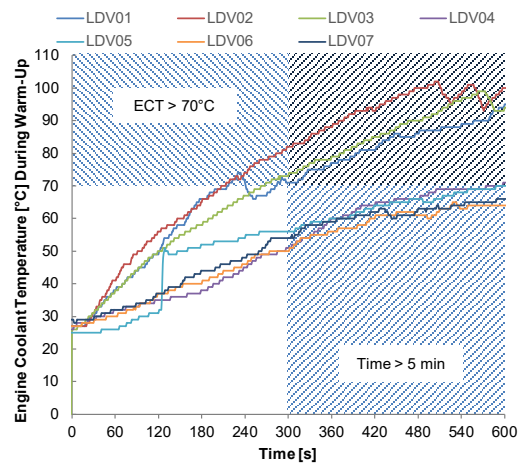


Figure 5: Time courses of the engine coolant temperature during warm-up and time shares of stop&go and idling

The idling phase is given, when the engine speed is between 500 rpm and 900 rpm and the vehicle speed is below 1 km/h.

Figure 4 shows the definition and example of idling in the urban part and Figure 5 summarizes the shares of idling in the urban part for all investigated vehicles. These shares are in the range of 6% to 13%.

According to these definitions, there is a certain overlapping of the data of the considered non-driving situations, see Figure 6.

Results

The evaluated emissions data are expressed as total cumulated values in [g], [#], as emissions per time in [g/min], [#]/min or as specific emissions per distance [g/km], [#]/km. The specific emissions (per km) respond to the legal view, they are comparable with legal limit values, but they are not applicable for the non-driving situations, where the distance driven is zero (like idling or stop&go). These facts are considered in the data representation.

Warm-up

Figure 7 represents the cumulative emissions over time during the urban phase (13.7 km) for the gasoline vehicles. Figure 8 shows the analogous results for Diesel vehicles. It can be remarked that for the gasoline vehicles (LDV1 - LDV3), the ECT 70-warm-up happens earlier or simultaneously with the 5 minutes-point. For the Diesel vehicles (LDV4 - LDV7) inversely, the ECT 70-warm-up takes generally a longer time and it arrives after the 5 minutes-point.

From the comparison of vehicles, it can be stated, that:

- vehicles with smaller engine displacement produce lower CO₂-emissions,
- most emissions of CO and NO_x, especially in the “gasoline” group are produced during and shortly after cold start,
- in both vehicles’ groups: “gasoline” and “Diesel”, there are quite considerable emissions differences between the vehicles, resulting mostly from different efficiencies of the exhaust aftertreatment systems,
- the urban phase (13.7 km) is driven by different vehicles at different time, due to different average speeds resulting from the traffic situations.

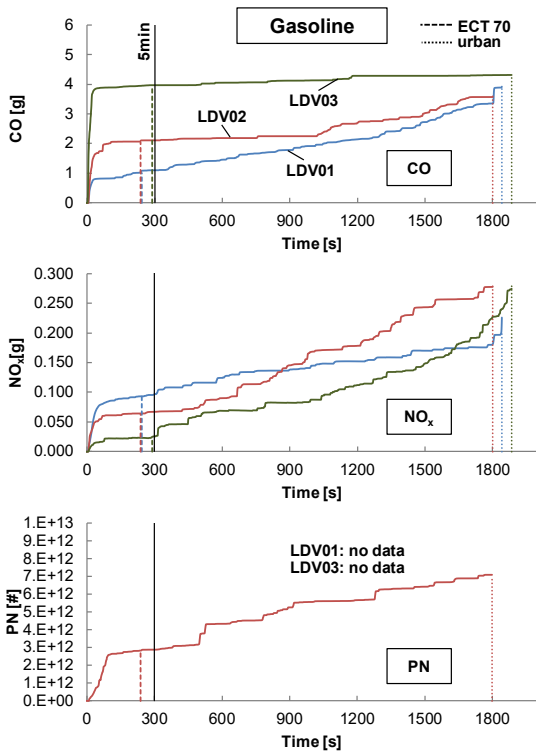
Specific emissions (per km) and their increase factors in the warm-up phase are compared for all vehicles in the Figure 9.

The CO [g/km] in warm-up are generally higher than in the entire urban phase (13.7 km). The “warm-up increase factor” varies between 2 & 11 for gasoline and 1 & 4 for Diesel vehicles. CO-values of LDV4 are particularly high indicating most probably some problems of engine, or of inactive DOC.

The NO_x [g/km] values of two Diesel vehicles (LDV4 & LDV5) are very high, which particularly signals a malfunction of the SCR-system of LDV5 (LDV4 is not equipped with SCR). The specific emissions in warm-up are sometimes higher than in the urban phase with the “increase factor” ranging between 0.9 & 7.5 for gasoline and 0.9 & 5 for Diesel vehicles.

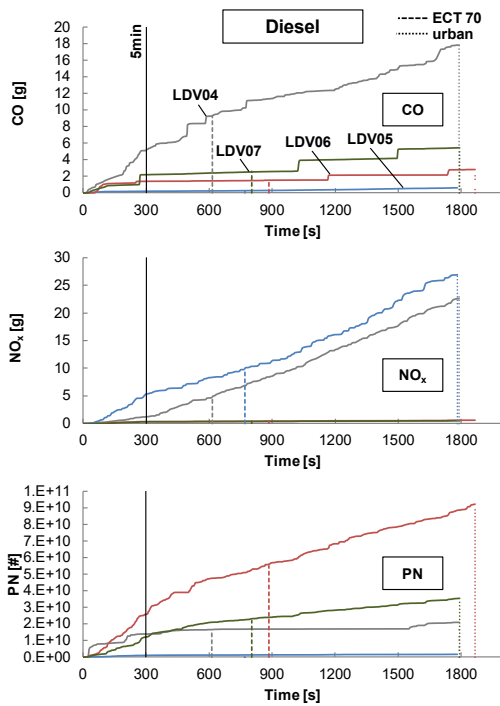
The nanoparticle emissions PN are efficiently eliminated by the DPF’s – all investigated Diesel vehicles were equipped with a filter. In the “gasoline” group, the PN-data were available only for the LDV2, which was equipped with GPF. This GPF enables the urban PN-emission to be reduced below the limit value ($6 \cdot 10^{11}$ #/km). For the shorter warm-up phases, the emission peak of the cold start gets more weight and the distance driven is shorter. The filtration quality of this GPF, comparing to the DPF’s is quite weak and the high specific PN-emission over the warm-up gets high above the limit value. Similar experiences exist at AFHB from the previous research on GPF’s, [16, 17]: the PN-emissions of a gasoline car (sometimes also with PFI) can reach 10^{13} #/km in WLTC_{cold}. The particle count filtration efficiency of the investigated GPF’s could be as low as 70%-80% in WLTC, in opposition to DPF’s. With this knowledge the authors suggest that the non-measured PN-values of the other two gasoline vehicles could be in average of this “urban” phase at least in the range of [10^{13} #/km].

The PN warm-up increase factors for gasoline vehicle are between 2 & 4 (regarding both definitions of warm-up) and for Diesel vehicles these increase factors are between 1.5 & 10. This means that even the DPF’s with the best filtration quality allow a certain penetration of the cold start PN-emission peak, of course at an absolute very low emission level.



ECT 70: engine coolant temperature reaches 70°C
 5min: 5 min after engine cold start
 urban: part of RDE-Route (geographically defined distance: 13.7 km)

Figure 7: vehicles during the warm-up phase.



ECT 70: engine coolant temperature reaches 70°C
 5min: 5 min after engine cold start
 urban: part of RDE-Route (geographically defined distance: 13.7 km)

Figure 8: Cumulated emissions of Diesel vehicles during the warm-up phase.

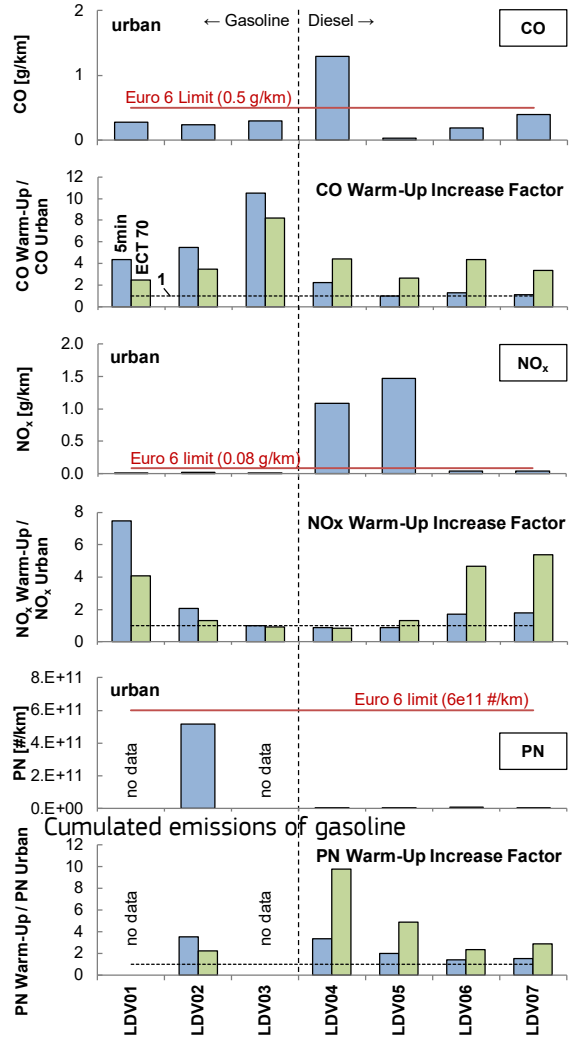


Figure 9: Specific emissions and their increase factors in the warm-up phase

Stop&go

The cumulated emissions in stop&go phases are summarized for all vehicles in Figure 10.

The comparison of emissions of the single vehicles offers a similar picture, as in the previous Figure 9:

- in the “gasoline” group: CO₂-emission is higher for bigger engines (engine swept volume increases from LDV1 to LDV3); CO-value is the highest for LDV3, which shows the slowest warm-up (see Figure 5); the PN-values are only given for LDV2 (equipped with GPF) and they confirm the mediocre filtration quality comparing to DPF’s.

in the “Diesel” group: high CO for LDV4 (insufficiency of engine, or of DOC); high NO_x for LDV4 (no SCR) and for LDV5 (inadequacy of SCR); near-to-zero PN-emissions, thanks to right-quality DPF’s. An interesting finding is given by the higher CO- and NO_x-emissions of LDV7 relatively to LDV6. Both vehicles have the same engine displacement volume and nearly identical exhaust aftertreatment systems (DOC, DPF, SCR). LDV7 was driven with its start-stop-control switched on.

This means that during the stop&go operation, the engine was stopped and started independently on the drivers wish.

By engine stop, there are no emissions produced, but by engine start, there is always an emission peak. The balance between the emission saving and emission over-producing depends on how long is the stop-time and how intense is the start-peak. The last one depends strongly on the thermal condition of the engine and of the exhaust system. In the present urban part (first 13.7 km) several start-stops must have been performed with not entirely warm exhaust aftertreatment system and the higher emission peaks at engine restart overweighed the emissions results of LDV7.

Relatively to the urban part (13.7 km) the cumulated emissions in stop&go are increased / decreased by the following factors:

	for gasoline vehicles:	for Diesel vehicles:
CO	2 - 6	0.2 - 2.2
NO _x	0.7 - 2.5	0.1 - 0.4
PN	1.7 (1 vehicle)	0.4 - 2.3
CO ₂	0.5 - 0.7	0.3 - 0.6

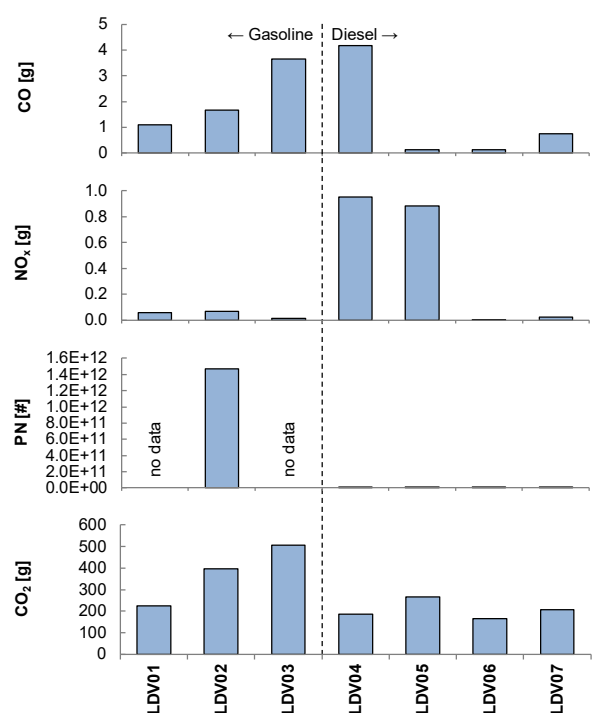


Figure 10: Cumulated emissions in stop&go.

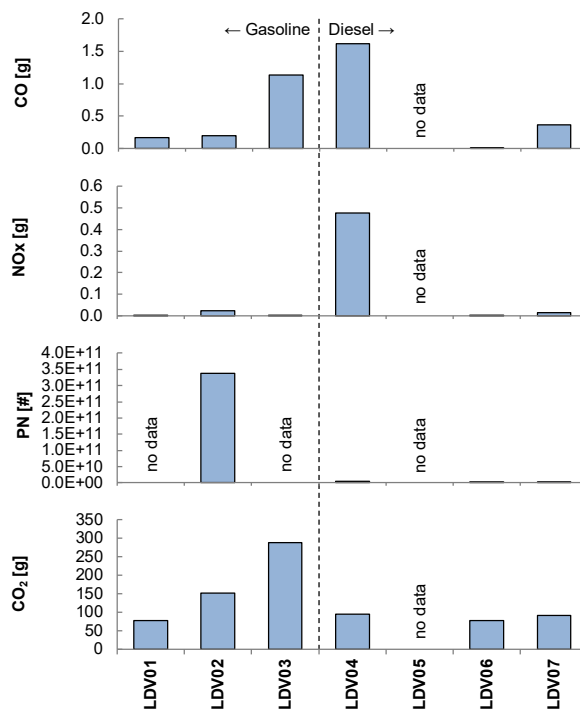


Figure 11: Cumulated emissions at idling

Idling

Figure 11 represents the cumulated emissions at idling for all investigated vehicles. The relationships between the vehicles and the technical explanations are similar as in the previous section for “stop&go”.

Relatively to the urban part (13.7 km) the cumulated emissions at idling are mostly decreased with the following factors:

	for gasoline vehicles:		for Diesel vehicles:
CO	0.5 - 2.5	CO	0.1 - 0.9
NO _x	0.3 - 1.1	NO _x	0.1 - 0.4
PN	0.7 (1 vehicle)	PN	0.5 - 1.8
CO ₂	0.3 - 0.6	CO ₂	0.3 - 0.4

Reproduction of non-driving situations

The tests were performed on chassis dynamometer with two gasoline and two Diesel passenger cars. The simulated driving situations were:

- Cold start (at 20-25°C) and warm-up phase with different load after start (15 km/h and 80 km/h).
- Stop&go operation with different portions of idling.

The vehicles of each group represented a newer and an older technology.

In the gasoline group, the newer (modern) vehicle is equipped with the engine and exhaust aftertreatment technology Euro 5 (with GDI, TWC) and the older vehicle (dated) responds to the emission class Euro 3 (with MPI, TWC).

As the most interesting findings can be mentioned:

- the emissions of CO, HC, NO_x and PN are generally higher for the older vehicle and, for both vehicles, these emissions are higher with higher load in the warm-up phase,
- the majority of these emissions is cumulated in the first 0.5 km of distance approximately,
- the PN-emissions of the dated vehicle (MPI) at high load are identical with the emissions of the modern vehicle (GDI); this confirms the high PN-emissions potential of the MPI fleet as well.

In the Diesel group, the modern vehicle means Euro 6 (DOC, DPF, SCR) and the older (dated) means Euro 2 (DOC).

Some remarkable findings are:

- the emissions of CO, HC, NO_x and PN are generally higher for the older vehicle, the emissions of CO, HC, and for the older vehicle, also NO_x, are higher with lower load (inversely to gasoline vehicles),
- the emissions of CO, HC and NO_x for the older vehicle, and particularly at low load, are cumulated not only at cold start but also in the entire represented time slot until 4 km distance driven,
- the PN-emissions of both vehicles are cumulated mainly during the cold start; for the older vehicle they are significantly higher than for the newer one (up to 6 orders of magnitude) and are independent of the load.

The tests of the stop&go operation with varying portion of idling were performed with warm engine and warm exhaust aftertreatment system. As a consequence, the measured emission values were very low. The exception is the older Diesel vehicle, which was equipped with a quite aged DOC only. The higher emissions which result from this vehicle allow to remark much better the effects of the idling rate.

The answer to the question: how does the share of idling influence the emissions in the stop&go operation? – finally depends on the representation (consideration) over the distance or over the time. With increasing portion of idling the distance-specific emissions (per km) increase and the time-specific emissions (per min) decrease.

Conclusions

Analysis of present data

For research of emissions from non-driving or special driving situations the RDE data of 7 vehicles (3 gasoline and 4 Diesel) were analyzed.

The first 13.7 km of distance after cold start were defined as “urban” part and definitions of: warm-up (including start), “stop&go” and idling, were established in order to enable the automatic evaluation.

The most important conclusions from this research are:

- the emissions of CO, NO_x and PN are in the cold start and in the first part of the warm-up phase (c.a. 25s) considerably higher, than in the rest of the investigated urban phase, (HC-data were not available),
- the special emitting situations: “stop&go” and idling are frequently given during the warm-up phase, i.e. with engine and exhaust treatment system not warm enough,
- vehicles with smaller engine displacement have lower cumulated CO₂-emissions (lower fuel consumption), they are tendentially quicker to be warmed-up,
- in both vehicles’ groups: “gasoline” and “Diesel” there are quite considerable emissions differences between the vehicles, resulting mostly from different efficiencies of the exhaust aftertreatment systems,
- the specific emissions [in g/km] are in the warm-up generally significantly higher than in the investigated urban phase (13.7 km); the respective “increase factors” are in average: for CO 6; for NO_x 4; for PN 6,
- the GPF, which was applied on one of the investigated gasoline vehicles showed a weak filtration quality comparing to the DPF’s which were used on the Diesel vehicles,
- the start-stop-system switched on during the warm-up is tendentially disadvantageous because the cold exhaust aftertreatment system cannot eliminate sufficiently the emissions peaks produced by restarting the engine.

Reproduction of non-driving situations

The non-driving (or special driving) situations – warm-up with different engine load and stop&go with different portions of idling – were reproduced on a chassis dynamometer with two gasoline vehicles and two Diesel vehicles. Both vehicles types were represented by a newer and an older technology.

During the cold start and warm-up in the first 2.5 km, the emissions of older type vehicles are generally higher than for the newer technology. The majority of emissions are accumulated in the first 0.5 km of the distance driven.

The PN-level of older technology gasoline vehicle (MPI) at higher load (80 km/h) is equal to the PN-level of the newer technology (GDI) – both vehicles without GPF.

The advantages and the efficiency of the modern Diesel aftertreatment (DPF) are confirmed by a significant reduction of PN.

In the stop&go operation, there are several tendencies of increasing the specific emissions [mg/km] with the higher share of idling (except of: HC for gasoline vehicles and PN for all vehicles). One of the factors taken into consideration is the shorter distance driven with the higher portion of idling in the tested time interval. The consideration of emissions per time [mg/min] results in lowering most of the emissions with higher portion of idling.

Acknowledgement

The authors express gratitude to the Swiss Federal Offices for Environment (BAFU) for the financial support of these activities.

References

- [1] European Environment Agency. EMEP/EEA Air Pollutant Emission Inventory Guidebook 2016. EEA Report. No 21/2016. 2016. Available online: <https://www.eea.europa.eu/publications/emep-eea-guidebook-2016> (accessed on 29 March 2019).
- [2] Franco V., Kousoulidou M., Muntean M., Ntziachristos L., Hausberger S., Dilara P. Road vehicle emission factors development: A review. Atmosphere Environment, 2013, 70, 84–97.

- [3] Ntziachristos L., Gkatzoflias D., Kouridis C., Samaras Z. COPERT: A European road transport emission inventory model. In *Information Technologies in Environmental Engineering*; Athanasiadis P.A., Mitkas A.E., Rizzoli J., Gómez M., Eds., Springer: New York, NY, USA, 2009. pp. 491–504.
- [4] Valverde V., Mora B. A., Clairotte M., Pavlovic J., Suarez-Bertoa R., Giechaskiel B., Astorga-Llorens C. and Fontaras G. Emission Factors Derived from 13 Euro 6b Light-Duty Vehicles Based on Laboratory and On-Road Measurements, *Atmosphere*, 2019, 10, 243; doi:10.3390/atmos10050243
- [5] Giechaskiel B., Giora R., Carriero M., Lähde T., Forloni F., Perujo A., Martini G., Bissi L. M., Terenghi R. Emission Factors of a Euro VI Heavy-Duty Diesel Refuse Collection Vehicle. *Sustainability*, 2019, 11, 1067; doi:10.3390/su11041067
- [6] May J., Bosteels D., Favre C. An Assessment of Emissions from Light-Duty Vehicles using PEMS and Chassis Dynamometer Testing. *SAE Int. J. Engines*, 2014, 7, 1326–1335.
- [7] Clairotte M., Valverde V., Bonnel P., Giechaskiel B., Carriero M., Otura M., Fontaras G., Pavlovic J., Martini G., Krasenbrink A., et al. Joint Research Centre, Light-Duty Vehicles Emissions Testing; Publications Office of the European Union: Luxembourg, 2018.
- [8] Czerwinski J., Zimmerli Y., Comte P., Cachon L., Riccobono F. Potentials of the portable emission measuring systems (PN PEMS) to control real driving emissions (RDE). 38. International Vienna Motor Symposium, 27-28 April 2017, VDI Fortschritt- Bericht, Reihe 12, Nr. 802, Vol. 2.
- [9] Czerwinski J., Comte P., Zimmerli Y., Cachon L., Remmele, E., Huber, G. Research of Emissions with Gas PEMS and PN PEMS. TAP Paper, International Transport and Air Pollution Conference, 15th -16th November 2017, EMPA, Zürich, Switzerland.
- [10] Giechaskiel B., Rocobono F., Bonnel P. Feasibility study on the extension of the Real Driving Emissions (RDE) procedure to Particle Number (PN). European Commission, Joint Research Centre, ISBN: 978-92-79-51003-8, ISSN: 1831-9424, DOI: 10.2790/74218
- [11] Suarez-Bertoa R., Valverde V., Clairotte M., Pavlovic J., Giechaskiel B., Franco V., Kregar Z., Astorga C. On-road emissions of passenger cars beyond the boundary conditions of the real-driving emissions test. *Environmental Research* 176 (2019) 108572
- [12] O'Driscoll R., Stettler M.E.J., Molden N., Oxley T., ApSimon H.M. Real world CO₂ and NO_x emissions from 149 Euro 5 and 6 diesel, gasoline and hybrid passenger cars. *Sci. Total Environ.*, 2018, 621, 282–290.
- [13] Ko J., Myung C.L., Park S. Impacts of ambient temperature, DPF regeneration, and traffic congestion on NO_x emissions from a Euro 6-compliant diesel vehicle equipped with an LNT under real-world driving conditions. *Atmos. Environ.*, 2019, 200, 1–14.
- [14] Czerwinski J., Comte P., Engelmann D., Bonsack P. Non-legislated emissions and PN of two passenger cars with gasoline-butanol blends. *PTNSS Journal Combustion Engines*, 2018, 172(1), 64-72. DOI:10.19206/CE-2018-108.
- [15] Stepien Z., Czerwinski J. Cold Start with Ethanol-Blend Fuels and Influences on Non-Legislated Emissions of a GDI Flex Fuel Vehicle. *Pol. J. Environ. Stud. (INIG)*. Vol. 26, No. 5, 2223-2229, 2017. DOI: 10.15244/pjoes/69282.
- [16] Czerwinski J., Comte P., Heeb N., Mayer A., Hensel V. Nanoparticle Emissions of DI Gasoline Cars with/without GPF. SAE Technical Paper 2017-01-1004, Detroit, April 2017.
- [17] Czerwinski J., Comte P., Engelmann D., Heeb N., Muñoz M., Bonsack P., Hensel V., Mayer, A. PN-Emissions of Gasoline Cars MPI and Potentials of GPF. SAE Technical Paper 2018-01-0363, Detroit, April 2018. DOI:10.4271/2018-01-0363.

Abbreviations

AFHB	Abgasprüfstelle FH Biel, CH
ASTRA	Federal Office of Roads
CF	Conformity Factor
CLD	Chemoluminescence Detector
DI	Direct Injection
DOC	Diesel Oxidation Catalyst
DPF	Diesel Particle Filter
ECT	engine coolant temperature
EFM	Exhaust Flow Meter
EMPA	Eidgenössische Material-Prüfanstalt
EMROAD	Data processing reference software

EOT	engine oil temperature
ES	engine start
EU	European Union
FID	Flame Ionization Detector
FOEN	Federal Office of Environment, CH
GPF	Gasoline particulate filter
GPS	Global Positioning System
HD	Heavy Duty
HDV	Heavy Duty Vehicles
ISC	In-Service Conformity
LD	Light Duty
LDV	Light Duty Vehicles
NDIR	Non-Dispersive Infrared
OBD	On Board Diagnosis
OCE	Off-Cycle Emissions
PEMS	Portable Emissions measurement system
PFI	port fuel injection
PN	Particle Number
RDE	Real Driving Emission
ResRDE	research of RDE
SCR	Selective Catalytic Reduction
TA	Type Approval
TPA	Tailpipe Attachment
TWC	Three-way catalyst
V	vehicle
WHTC	World Heavy-Duty Transient Cycle
WLTC	World Light-Duty Transient Cycle

2.20 Particulate matter emissions in railway operation – in-situ measurements in an Austrian railway tunnel

Daniel Fruhwirt¹, Peter Sturm¹, Helmut Steiner²

¹ Graz University of Technology

² ÖBB Infrastruktur AG

fruhwirt@ivt.tugraz.at

Abstract

Quite little information is available concerning PM emissions from electrified rail traffic. However, in special locations such as in or near railways stations, rail tunnel portals or similar locations, PM resulting from rail traffic can make a significant contribution to local air pollution. The few existing measurements show remarkably high dust loads (FVT-LUA 2015, INFRAS 2007).

In order to improve the data base a research project was set up, with the aim of generating non-exhaust particle emission factors for rail vehicles. For this reason the Austrian railway corporation initiated a pilot-project at Unterwalder tunnel on the Schoberpass-track in Styria. The focus of this project was on testing electrical components under in-situ conditions, dust concentrations inside the tunnel were measured as a by-product, so to say. Dynamic measurements of particle concentrations, using a gravimetric and a hybrid (nephelometer/radiometer) measurement system as well as dust composition analysis of PM samples were performed.

On the basis of these investigations, emission-factors for railway operations were calculated and assigned to different train types. Usually wear effects on catenary system, breaks and rails are the main sources of particle emissions. The main particle size range is PM₁₀, which accounts for 75% of the total measured particles.

Next to wear effects, the type of load on railways is essential for particle emissions. Since the Schoberpass track is heavily used by freight trains, this influence is definitely given. For being able to differentiate between various loads, a video-monitoring system was installed next to the tunnel portal. Although container transport dominated, there were also open wagons transporting bulk freight (e.g. iron ore, gravel) which caused very high PM concentrations in the tunnel air. It can be noted that the measured concentrations also varied depending on the train type, train speed and on weather conditions. The type of train was monitored via the installed video cameras at portal site, train speed was not directly recorded, but the influence was given due to the recorded tunnel air velocity. In addition, a meteorological station for recording precipitation was installed near the tunnel.

In total, emission factors for more than four thousand train movements were derived from the measurements. This includes passenger and freight trains, which were further split into several sub-categories. It can be concluded, that freight trains cause PM emissions roughly 4 times higher than passenger trains. Finally, chemical analysis of the dust composition was made. It was found that iron particles are responsible for about 50 % of the total emitted particle mass.

Introduction

In Austria there are currently three long (> 27 km) railway tunnels in construction. All of them are part of the Trans-European Network – Transport (TENT-T) (see ÖBB Infrastruktur AG, 2012). While the Semmering Base Tunnel (SBT) and the Koralmtunnel (KAT) are core sections of the Baltic-Adriatic corridor, the Brenner Base Tunnel (BBT) belongs to the Scandinavian-Mediterranean axis. Figure 1 shows a scheme of the European railway network passing Austria. The newly built tunnels are constructed as twin tube single track tunnels and contain a slab track, which is a decisive aspect in terms of PM loads inside the tunnel. The tunnel tubes are connected via cross-passages in distances of roughly 500 m (SBT & KAT) or less (350 m at BBT). These cross-passages mainly serve as escape routes in an incident situation, but additionally host technical facilities for railway operation purposes. In the case of KAT and SBT there are separated utility-rooms for various systems (e.g. telecommunication, power supply, etc.), which have certain requirements on the room climate as well as on PM concentrations.



Figure 1: Left – Trans-European railway network; Right - Parent railway corridors in Austria (Fruhwirt, 2018).

Experience from Switzerland, where long railway tunnels have already been in operation for some years (e.g. Lötschberg tunnel, Gotthard basetunnel, etc.), shows that dust pollution in the tunnel cause malfunctions of various systems and is a major reason for the massive maintenance effort. In addition to an unfavourable atmosphere due to high PM concentrations, some dust components have a high potential for damage to sensitive components of telecommunication and power supply equipment. In this context, metals have to be mentioned that are characterized by high conductivity (e.g. iron, copper, etc.).

In general, PM emissions of railways are mainly related to non-exhaust emissions as the electrification of European railway routes is well developed, although there are some local differences. In Austria, the share of electrified railway lines is about 75 %, but a high number of regional railway lines are still diesel-powered. Nevertheless, the focus of current investigations is clearly on the non-exhaust PM emissions. Although the sources for PM emissions are well known, there is quite little information about quantitative aspects available. (INFRAS, 2007) and (BUWAL, 2002) are well-known documents in this area, as they represent the benchmark for the derivation of emission factors, the assignment to certain emission sources as well as for the quantification of the total annual emissions due to the railway-traffic (see Table 1).

Table 1: Annual PM10 emissions related to emission sources according to (BUWAL, 2002).

Source	t/a	%
Breaks	2066	73
Rails	546	19
Wheels	124	4
Contact wire	36	1
Exhaust emisisions	45	2
Total	2816	100

Investigation targets

In order to deepen the knowledge about PM emissions from railways a research-project was commissioned by the Austrian railway corporation (ÖBB Infrastruktur AG). The overall aim of this project was to test sensitive components of telecommunication and medium-voltage units that are exposed to unfavourable thermal conditions and high dust loads. For this purpose, test conditions with different temperatures, humidity and high dust loads had to be created. A total of 12 test-scenarios for various target room air temperatures, from ambient temperature level up to 50°C, as well as another scenario with the aim of generating condensation in the utility room, were defined. The total project duration was 2.5 years during which the PM monitoring was permanently active. For further information on the thermal

aspects, reference (Institut für Verbrennungskraftmaschinen und Thermodynamik, 2019) is recommended. This paper focuses on the investigations related to PM monitoring and the emission factors derived from these measurements.

Test and Measurement Set-Up

A suitable test location was found at the Unterwalder tunnel. This tunnel is located in Upper Styria and is part of the Schoberpass line. It is characterized as a single tube double-track tunnel with a total length of 1'075 m. The tunnel has an orientation from east to west with a constant grade of 1.52 %. Generally, it consists of the railway tunnel and an adjacent escape tunnel, which is about 200 m long. This escape tunnel provided the possibility to set-up a dedicated utility-room, which served for housing of the test facilities. The railway tunnel and the escape tunnel are separated by a 15 m long sluice. This sluice consists of two massive concrete walls and escape doors, which have to fulfil strict fire safety requirements. In order to achieve high PM concentrations, tunnel air was injected into the utility room. For this reason, a mechanical ventilation system was implemented in the test installation. This system consisted of supply air ducts and a standard supply air fan, which was designed to generate a supply air volume-flow of 0.25 m³/s. In addition, a PM filter was installed at the exhaust air outlet of the test room. This filter was used to observe the filter lifetime in a real-world railway tunnel application. Figure 2 shows the location of the project area as well as the general tunnel layout.

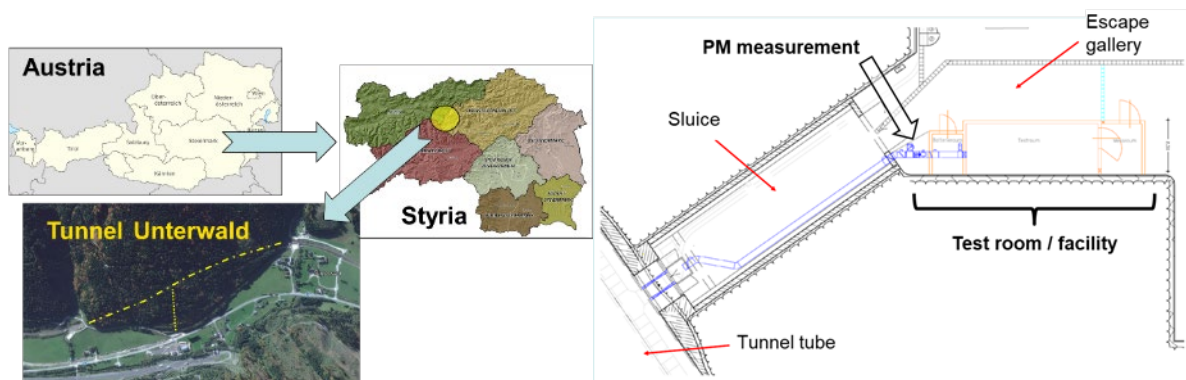


Figure 2: Left -Location of the project area; Right – General test configuration.

PM monitoring was carried out using three different PM monitors. These monitors also use different measurement principles. The first monitor was a Tapered Element Oscillating Microbalance (TEOM 1400a) monitor. TEOM is a gravimetric instrument that draws a sample air flow (16.7 l/min) through a Teflon coated glass filter. This filter is situated on a tapered element that vibrates at its natural frequency. This frequency decreases with increasing particle mass on the filter plate. By sensing the change of frequency, the particle mass growth can be determined. Compared to that, the second PM monitor (SHARP 5030 monitor) uses a hybrid system. A nephelometer gives information about the short-term signal for PM concentration, a long-term correction is performed using the signal from a radiometer. The third monitor was a high-volume particle sampler (PARTISOL Plus 2025), which was used for taking samples for the analysis of dust composition. It has to be mentioned that this system was not permanently in operation, but was equipped with three different filters. While quartz filters were used for the analysis of salts and ions, cellulose filters provided the possibility of analyzing heavy metals. The third filter category applied was glass, which only can be used to determine average values of PM concentration over the entire sampling period (24 h). Figure 3 shows the utility room including the supply air ventilation duct as well as the applied PM monitors. It has to be noted that TEOM was situated directly in front of the utility room and its sample pipe tube entered the supply air duct. Contrary to that, the SHARP monitor was installed inside the utility room, and the sample tube ended directly at the supply air entrance. This definitely does not represent the optimum for the extraction of the sample air flow and for a comparison of results, but was due to the available space and the local fire safety requirements. During the periods in which the PARTISOL monitor was activated, it replaced SHARP in its position in the test room.



Figure 3: Left - Impression of the test room, Center - Position of the TEOM and SHARP monitors, Right - Image of the PARTISOL monitor.

Since railway tunnels are not permanent workspaces, the effects of PM on the human health is of minor interest. The most important aspect, however, is the service life of the tunnel equipment and thus the availability of the railway track. Since there is no defined PM fraction that is mainly responsible for the damage potential for electro-mechanical components, the quantity to be assessed was Total Suspended Particles (TSP). This is one more aspect to be considered when comparing the results of the monitors being used.

To be able to derive PM emission factors, the tunnel air volume flow had to be monitored permanently. Therefore an air velocity sensor (WS500) was mounted directly in front of the sluice on the tunnel lining. The illustration on the left side of Figure 4 shows the applied sensor for tunnel-air flow monitoring.



Figure 4: Left – Air flow measurement within the railway tunnel; Right – PM filter application at the top of top of the utility room.

At the right side of Figure 4 the installed PM filter housing at the exhaust air side of the test room is shown. This application included a single stage standard F7 filter, according to ÖNORM EN ISO 16890-1: 2017 06 15. This filter is characterized by an average efficiency of 80 % up to 90 %.

Results

In general, there were two different processes analysed during the Unterwalder tunnel tests. On the one hand, this was the PM concentration curve that occurred during a single train pass. This investigation also included the analysis of the effects of certain parameters such as train-related quantities (mass, length, etc.) as well as precipitation. On the other hand, long-term processes related to the filter service lifewere assessed with the purpose of giving a forecast on the filter lifetime at the KAT.

Non-exhaust PM emission factors

Based on detailed analyses of the results of the pre-tests of the two PM monitors, one was selected for the further investigations. Left side of Figure 5 shows the comparison of TEOM and SHARP monitor during a single train passing the test location. Qualitatively both recorded curves fit quite well, but when assessing the peak values quantitatively, there is a difference of $200 \mu\text{g}/\text{m}^3$ (~ 28 %). This is remarkable at first glance if one thinks about the applied mean value formation (TEOM - 10 minutes average, SHARP – 1 minute average). However, this seems to be an effect of the SHARP system configuration. According to the SHARP manual, the nephelometer has a cut-off at particles $> 14 \mu\text{m}$. Hence, lower peak values in the SHARP PM concentration curve for TSP seem plausible.

When comparing 24 h mean values derived from the TEOM and SHARP measurements, the ratio of SHARP/TEOM is in the range of 33 % (24 h mean value < 5 µg/m³) and 122 % with an average of 86 %. This comparison is illustrated in Figure 5. Both showed different quantities of the PM mass concentrations, but with no clear tendency. For operational and data processing reasons, however, it turned out that the SHARP monitor (one-minute running average) met the needs of short-term measurements better than the TEOM monitors (10 minutes running average).

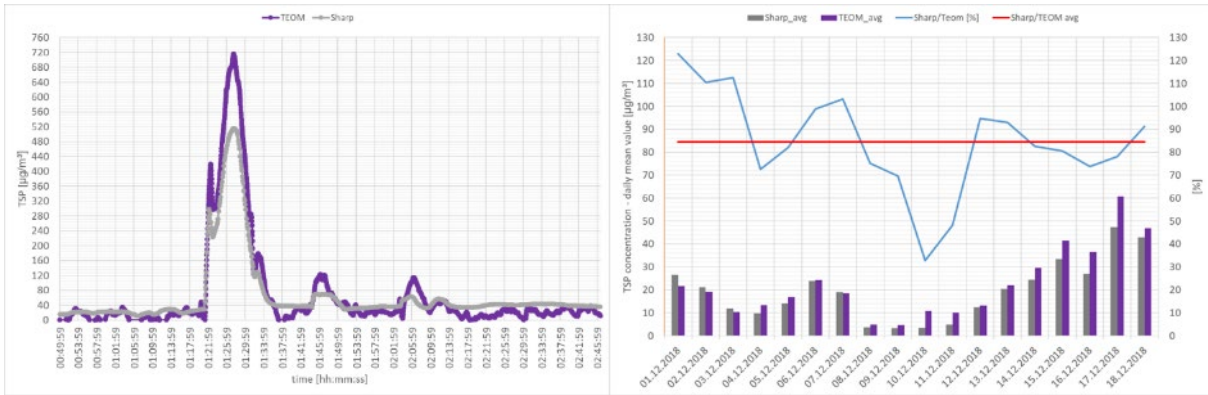


Figure 5: Left - Example of PM concentration curves during a single train pass; Right - Comparison of 24 h mean values of SHARP and TEOM monitor (Steiner, 2020).

Generally, the determination of PM emission factors was done using the correlation shown in equation (1). There Δm_{conc} is defined by the difference of the PM peak concentration due to a train pass and the background level right before the train pass. $\Delta \tau$ is the time interval from the first increase of PM concentration until the maximum PM concentration occurs. v_{tunnel_avg} is the average air velocity inside the railway tunnel within this time interval. This quantity multiplied by the tunnel cross section A_{tunnel} defines the average air volume flow. l_{char} defines a characteristic length to relate the emitted PM mass to a certain distance. In the situation of the Unterwalder tunnel tests l_{char} is 0.535 m which is equivalent to the distance from the entrance portal to the monitoring position. Figure 6 shows graphically the determination of the quantities Δm_{conc} and $\Delta \tau$.

$$EMF_{peak} = \frac{\Delta m_{conc} * A_{tunnel} * v_{tunnel_avg} * \Delta \tau}{l_{char}} \left[\frac{\mu g}{km} \right] \quad (1)$$

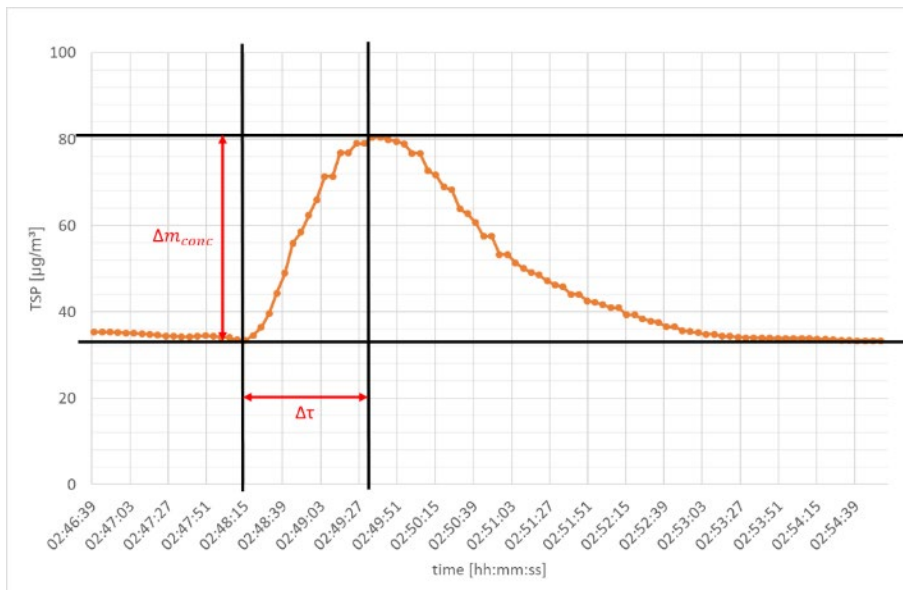


Figure 6: Graphical illustration of the applied methodology on the determination of PM emission factors (Steiner, 2020).

Several options were discussed for the determination of Δm_{conc} . It was found that the increase of PM mass concentration up to the occurrence of the maximum value is most representative for the derivation of emission factors and has the additional benefit since it can be easily triggered.

Independent on the applied method, derived PM emission factors include emissions due to wear effects and abrasions caused by the emission sources listed in Table 1 and their resuspension as a consequence of a train passage. At this point it has to be noted that the slab track of the Unterwalder tunnel represents a case in which resuspension is definitely less compared to a gravel bed. Another information that must be noted is the speed limit of 100 km/h which is valid for the Unterwalder tunnel.

Under the boundary conditions explained, an average non-exhaust emission factor of 1.87 g/km was derived on bases of the 4'100 analyzed train passes. Compared to that the median value is 0.63 g/km. A breakdown into categories for passenger and freight trains shows that according to median values, freight trains (1.62 g/km) cause about four times higher PM emissions than passenger trains (0.37 g/km). separated categories for passenger- and freight trains it can be observed that based on median values freight trains (1.62 g/km) cause about 4 times higher PM emissions compared to passenger trains (0.37 g/km). Table 2 shows the emission factors and percentile values derived from all analyzed train movements and for both train categories.

Table 2: Non exhaust PM emission factors for passenger- and freight trains.

	Number of trains [#]	EMF_avg [g/km]	EMF_median [g/km]	EMF_25 percentile [g/km]	EMF_75 percentile [g/km]
Total	4'100	1.87	0.63	0.162	1.433
Passenger trains	2'126	0.66	0.37	0.103	0.651
Freight trains	1'974	3.24	1.62	0.425	2.771

Table 3: PM emission factors for various train categories.

Freight trains	Transported good	Number of trains [#]	EMF_avg [g/km]	EMF_median [g/km]
	Running highways	105	3.91	1.91
	Cars	25	3.07	1.28
	Wooden goods	43	3.02	1.55
	Bulk materials	159	5.08	2.57
	Containers	106	2.59	2.04
	No assignment	652	3.48	2.04
Passenger trains	Train-type	Number of trains [#]	EMF_avg [g/km]	EMF_median [g/km]
	Local traffic	925	0.24	0.11
	Long-distance traffic	1'049	0.73	0.47

These emission factors do not consider any variations of parameters than train type. To have an idea of the influence of selected parameters, some of them were assessed in detail. This mainly includes train related parameters, such as a further classification depending on the train type. While freight trains are classified in terms of the transported goods and the configuration of the freight cars, passenger trains are categorized by trains for regional traffic and long-distance traffic. Table 3 shows determined PM emission factors for freight trains with focus on the transported goods. This analysis shows that trains for the transport of cars cause the lowest (1.28 g/km) and trains transporting bulk

material cause two times higher PM emissions (2.57 g/km). The categorization according to freight cars did not show significant differences in PM emission factors. The categorization of passenger trains for regional and long-distance traffic lead to emission factors as shown in Table 3. The final outcome is that trains which are assigned to the local traffic are responsible for the lowest PM emissions of all trains. Compared to that, long distance trains (Inter City, Euro City, Night Jet) show four times higher emissions. The observation of precipitation lead to the outcome that precipitation with an intensity above 0.5 mm/h had a significant influence on the PM emissions.

Chemical analysis of dust composition

In addition to the PM concentration, the dust composition is decisive for the damaging potential of dust loads in railway tunnels. Conductive metals are mainly responsible for malfunctions of electro-mechanical systems and cause an intensive maintenance effort or even were the reason for tunnel closures. In total 46 filter samples were analysed in the course of the Unterwalder tunnel tests.

The left side of Figure 7 shows the result of the chemical analysis of selected quartz filter samples. The mass-fraction of mineral substances and salts was roughly 40 % during the test period. Total carbon (27 %) was the decisive substance within this category. It has to be noted that the recorded mass of organic carbon is expected to be the results of an enhanced activation of biomass usage, which is the common heating system in the region of the tunnel. Hence, organic carbon definitely cannot be assigned to the railway traffic. This expectation is additionally based on the observation of only two diesel powered trains passing Unterwalder tunnel during the entire test duration.

The most important information about the dust composition was derived from the chemical analysis of the cellulose filters. Figure 7 (right side) shows the determined mass-fractions of metals for selected cellulose filter samples. These results show that metals account for roughly 60% of the mass, having iron particles accounting for 45%. An average mass-fraction of 9 % is related to Aluminium, but they could be identified to result from the background air (Amt der Steiermärkischen Landesregierung, 2007). Some small amounts of Copper and Manganese were also identified. These substances are mainly used in the catenary wire of railways. Mass-fractions lower than 5% assigned to Titanium, Chrome and Zirconia were identified only in some days. Usually, those substances can be found in alloys of various break-systems. It has to be noted that grey-cast iron breaks represent the most common system currently in use.

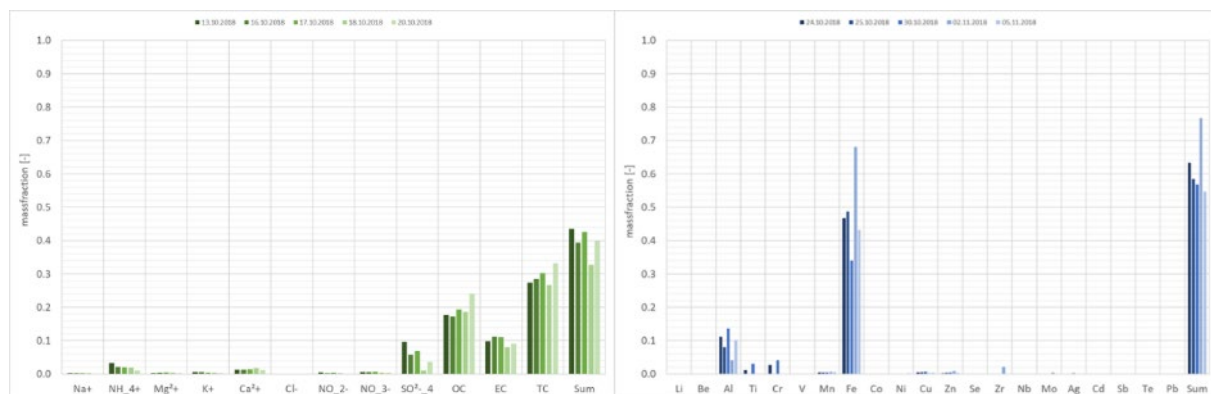


Figure 7: Left - Results of chemical analysis of quartz filters;
Right - Results of chemical analysis of cellulose filters.

PM filter lifetime monitoring

The pressure drop over a filter is usually a measure for its service life. This pressure loss is a function of the air volume flow and the particle load on the filter material. While the initial pressure drop at nominal air flow (1 m³/s) over a F7 filter is below 50 Pa, the pressure drop at the end of service life (given by the producer) is 500 Pa. The recorded curve of pressure drop over the applied F7 filter as a function of the particle mass is shown in Figure 8. The initial pressure loss was about 30 Pa, which was the result of a four times lower air volume flow at Unterwalder tunnel compared to the nominal air flow. The derived quadratic correlation of total pressure loss and the total particle mass is shown in equation (2).

$$y = 2.398 * 10^{-3} * x^2 + 0.22807 * x + 30.636 \quad (2)$$

This correlation can be used as the base for the forecast on filter lifetime in the application of the KAT cross-passage ventilation system. There, the supply air flow is equivalent to the nominal air flow for the filter. One decisive assumption has to be made when transferring this Unterwalder tunnel correlation to KAT. This assumption relates on the PM concentrations due to the local background air quality as well as to the train schedule. Although the Unterwalder tunnel

and KAT have different characteristics, the methodology applied is regarded as an indicative approach. When using equation (2) for KAT, the constant term on the right side of the equal sign has to be modified due to the higher air volume flow. Based on the measurements at the Unterwalder tunnel, a pressure-loss coefficient of 2.515 was determined for the clean filter. Using this factor results in an expected initial pressure loss of 39.25 Pa for the KAT application and an expected filter lifetime of roughly 5 months when considering a permanent operation of the cross-passage ventilation system.

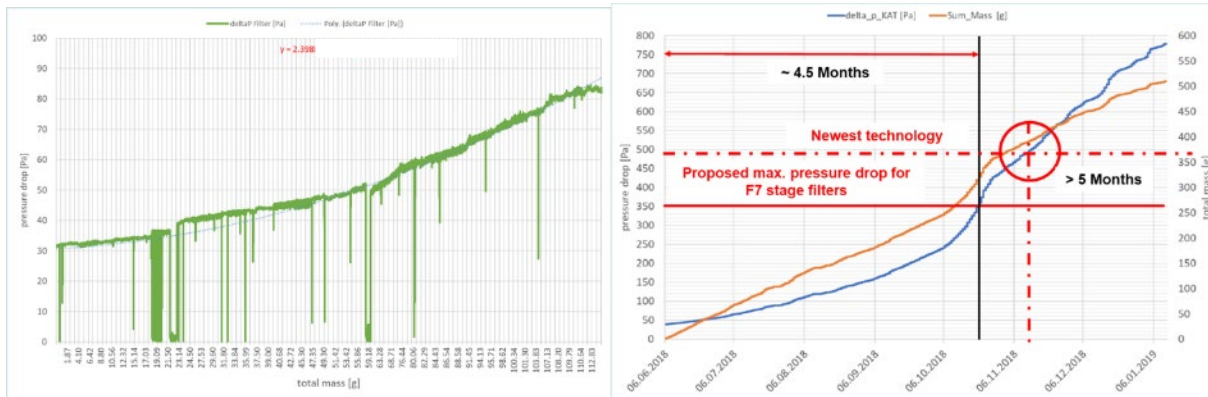


Figure 8: Left - Recorded pressure drop curve over a single stage F7 filter stage;
Right - Forecast on filter lifetime in the cross passage ventilation system at KAT.

Conclusion

Railways in general have the reputation of being a “green” transport system, although little information of their contribution to PM air quality is available. Results of measurements published in Switzerland represent the benchmark for all further attempts to quantify the total PM emissions of railways. Generally, the mechanical processes which lead to PM emissions are well known. These mechanisms are mainly related to wear effects and abrasions in contact areas of fixed and moving railway components as there are rails-wheels, pantograph-contact wire and breaks. The latter one is expected to be the main source for non-exhaust particle emissions. Exhaust emissions in general have no major influence anymore, since most European railway lines are electrified.

Dust loads are a concern for the operation of railway tunnels. Experiences made in Switzerland, where several long railway tunnels are in operation for some years, demonstrate that the required maintenance effort in these tunnels is enormous.

In Austria there are three long railway tunnels in construction. Due to lack of valid information on the dust loads, the Austrian railway corporation (ÖBB Infrastruktur AG) initiated a research project with the aim of investigating the effect of high dust concentrations on sensitive components in a railway tunnel. In the course of this research project extensive PM measurements were carried out. Results from these investigations gave information about non-exhaust PM emission for different train categories. The final outcome is that freight trains cause four times higher PM emissions compared to passenger trains and trains transporting bulk material represent the worst case.

Conductive materials have the highest damaging potential for electronic equipment within a railway tunnel. To gain further information about the dust composition filter samples were taken and analysed. This analysis showed that iron particles are responsible for roughly half of the total recorded particle mass. Small amounts of Copper and Manganese, which usually are used in alloys of breaks, were also identified. Since the test tunnel only had a length of about 1 km, there was also a remarkable influence of secondary sources such as biomass burning for heating purposes, which are common in the project area.

In general, it should be noted that there are further parameters (train speed, driving mode, etc.) should be assessed in future projects, as these are likely to have an impact on the PM emissions.

Acknowledgement

The project was funded by the Austrian railway corporation (ÖBB Infrastruktur AG). Special thanks to Mr. Hermann Riedl and his team for the on-site support at the Unterwalder tunnel.

References

- Amt der Steiermärkischen Landesregierung, Final report from „AQUELLA“ project, Steiermark Bestimmung von Immissionsbeiträgen in Feinstaubproben, August 2007, [available: <http://www.umwelt.steiermark.at/cms/beitrag/11023498/19222537/>] [access: April 14th 2020]
- BUWAL, PM10 Emissionen des Verkehrs – Statusbericht Teil Schiene, Bern 2002
- Fruhwirt, D.; CHANGE IN THERMAL CONDITIONS DURING CONSTRUCTION AND OPERATION OF A LONG RAILWAY TUNNEL – TAKING THE KORALMTUNNEL AS AN EXAMPLE; Conference Paper, 9th International conference on tunnel safety and ventilation, Graz, 2018
- FVT-LUA, 2015: Ermittlung von aktuellen Emissionsfaktoren für limitierte und nicht limitierte Schadstoffkomponenten des Straßen- und Schienenverkehrs, Final Report, 2015
- INFRAS; PM10 Emissionen Verkehr, Teil Schienenverkehr; Final report; Bern; 2007
- Institut für Verbrennungskraftmaschinen und Thermodynamik; In Situ Tunnelklimaversuche Unterwaldertunnel – Zwischenbericht, Final report; Graz; 2019
- ÖBB-Infrastruktur AG; The Koralm Railway, A part of the new Southern Railway Line; technical report; Vienna; 2012
- Rausch J., Jaramillo D., Zünd T., Bestimmung des PM10 Anteils aus dem Schienen- und Straßenverkehr im Urner Reustal, Bundesamt für Umwelt, Freiburg, 2016
- Steiner, H.; Sturm, P.; Fruhwirt, D.; DUST LOADS IN RAILWAY TUNNELS – RESULTS FROM IN-SITU MEASUREMENTS AND CONSEQUENCES FOR TUNNEL FACILITIES AND RAILWAY OPERATION; Conference Paper, Virtual conference on tunnel safety and ventilation, 2020 (<https://www.tunnel-graz.at/archive/tunnel-2020.html>)

2.21 Monitoring of ship emissions to enforce environmental regulations. The SCIPPER project.

S. Mamarikas¹, V. Matthias², M. Karl², L. Fink², P. Simonen³, J. Keskinen³, M. Dal Maso³, E. Fridell⁴, H. Winnes⁴, J. Moldanova⁴, Å. M. Hallquist⁴, J. Mellqvist⁵, V. Conde⁵, R. Verbeek⁶, J. Duyzer⁶, D. van Dinther⁶, H. Timonen⁷, J.-P. Jalkanen⁷, A.-M. Sundström⁷, E. Majamäki⁷, A. Stylogiannis⁸, V. Ntziachristos⁸, T. Smyth⁹, M.i Yang⁹, A. Deakin¹⁰, R. Proud¹⁰, J. Oeffner¹¹, V.E. Schneider¹¹, J. Beecken¹², A. Weigelt¹², S. Griesel¹², H. Schoppmann¹², S. Oppo¹³, A. Armengaud¹³, B. D'Anna¹⁴, B. Temime-Roussel¹⁴, B. Knudsen¹⁵, J. Knudsen¹⁵, M. Kuosa¹⁶, M. Irjala¹⁶, L. Buckers¹⁷, J. van Vliet¹⁷, L. Ntziachristos¹⁷

¹AUTH, ²HZG, ³TAU, ⁴IVL, ⁵CHALMERS, ⁶TNO, ⁷FMI, ⁸HMGU, ⁹PML, ¹⁰eEE, ¹¹CML, ¹²BSH, ¹³ATMOSUD, ¹⁴AMU, ¹⁵EXPLICIT, ¹⁶AEROMON, ¹⁷ILT

leon@auth.gr

Abstract

The present paper presents the methodological framework that has been adopted by the EU-funded project SCIPPER in order mainly to assess the potential of various shipping emission measurement techniques in monitoring the emission performance of vessels under real-world operation, as well as to provide evidence on the capacity of these techniques to be used by enforcement authorities to check the compliance of ships to emissions' regulations and limits. Furthermore, SCIPPER intends to assess the impact of shipping emissions on air quality (AQ) under regulatory enforcement scenarios. The overall methodology is mainly concentrated around five real-world measurement campaigns at major seas and ports of Europe, where the different techniques are being tested under various operating conditions and compared regarding their accuracy, ease of implementation and cost. The techniques include on-board sensors (high-end systems and prototypes), remote techniques including sniffers and aerial means (drones). In addition, the possibility of monitoring emissions from satellites is examined. Real-world measurements also provide evidence on the AQ aspects that are being examined by the project, mainly related to the understanding of plume ageing, pollutants' atmospheric transformation mechanisms and dispersion. The measurements are supplemented by other methodological tools as in-lab tests mainly for testing the developed methodology for plume ageing, desktop reviews for recognizing state-of-art technologies of on-board and remote sensors, as well as the development of emission factors for ships. Finally, AQ modelling activities for evaluating the impact of shipping emissions' regulations on harbour and city scale levels are conducted.

Introduction

The maritime transport sector is characterized by particularly high emissions of harmful pollutants, such as Sulfur Oxides (SO_x) and Nitrogen Oxides (NO_x) and particulate matter (PM), thus causing a significant deterioration of AQ, particularly in coastal areas (Corbett et al., 2007), (Matthias et al, 2010). In recent years, regulations and emission limits have gradually begun to be implemented in the sector and applied to ships, with the aim of significantly reducing emissions.

In 1997, the International Maritime Organization (IMO) adopted the MARPOL Annex VI Regulation to address such AQ issues. This regulation required that, from 1 January 2015, the equivalent Fuel Sulphur Content (FSC) in Sulphur Emission Control Areas (SECAs) dropped from 1.0% m/m down to 0.1% m/m. On 1 January 2020 a maximum FSC of 0.5% was globally entered into force outside SECAs. In the EU, additional requirements for ferries and ships at berth go beyond the IMO regulations. This framework creates requirements to monitor the compliance of ships with sulphur regulations separately in port areas and in the open-seas. Further to SO_x, vessels built after 1 January 2016 sailing in the North American ECA and after 1 January 2021 sailing in the North and Baltic Seas ECA, need to comply with Tier III NO_x standards. Ships also emit primary PM, in the form of Black Carbon (BC), Organic Carbon (OC), ash and metallic aerosol, that largely resides in the ultrafine particle (UFP<100 nm) range (Ntziachristos et. al. 2016). PM from vessels is currently not regulated but BC control is under discussion within the IMO, due to its potent impacts on climate. Secondary aerosol, through the photooxidation of SO_x, NO_x and gaseous OC, also has consequences to coastal AQ.

However, a fundamental prerequisite for the effective implementation of regulations and limits is the systematic monitoring of ships' compliance, which is achieved by measuring shipping emissions at various phases of their normal operation (Verbeek, et al. 2021). The purpose of this paper is to present and analyse the methodology of the EU-H2020 project SCIPPER - "Shipping Contributions to Inland Pollution Push for the Enforcement of Regulations", that evaluates the suitability of various emission measurement techniques for checking ships' compliance with regulations, as well as to assess the impacts of shipping emissions on AQ, under different regulatory enforcement scenarios. Furthermore, the paper presents initial project results, which have been derived by some of the so far implemented activities.

Theoretical framework

The SCIPPER project implements available and innovative techniques for monitoring the compliance of individual ships to existing sulphur and future NO_x and PM air pollution regulations. The overall objective of SCIPPER is to provide authorities with: (i) fundamental technical information in developing their enforcement approaches and (ii) modelling tools and monitoring techniques, to quantify the environmental benefits of successful enforcement. In this context SCIPPER mainly intends to provide evidence on the performance and capacity of different techniques for shipping emission monitoring and to assess the impacts of shipping emissions on AQ, under different regulatory enforcement scenarios

To address the many and largely unexplored problems related to vessels emissions monitoring, SCIPPER aims at deploying state-of-art and next-generation measurement techniques to monitor emissions of vessels under their normal operation, such as on-board sensors, sniffers, optical remote techniques, Unmanned Aerial Systems (UAS) and Vehicles (UAVs) and satellite systems. The overall SCIPPER concept, along with the techniques that are being deployed is provided in Figure 1.

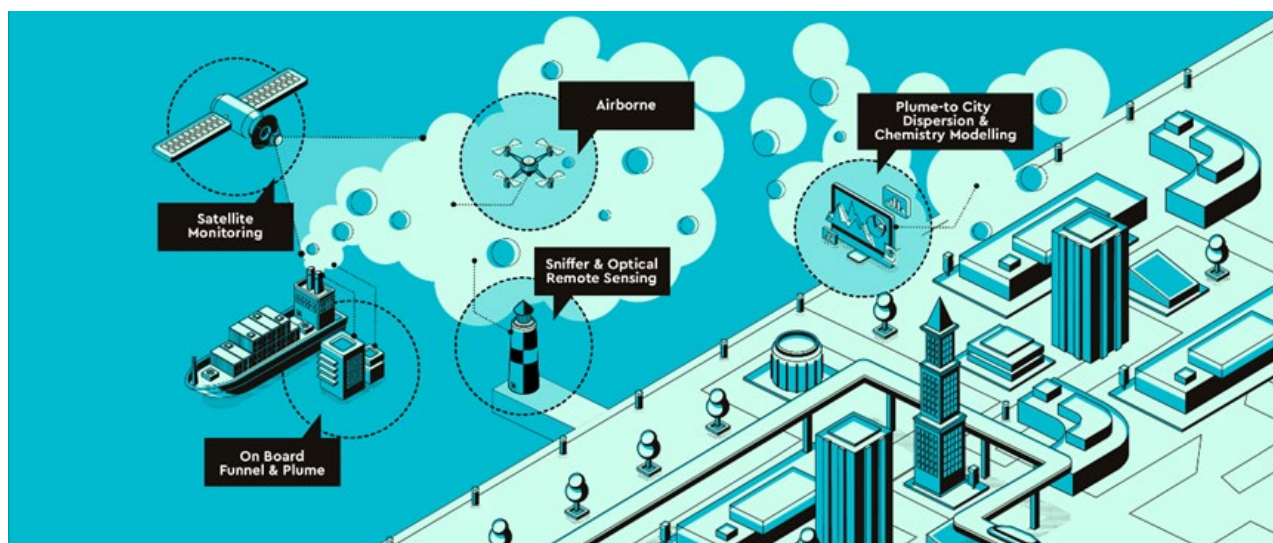


Figure 1: Representation of the SCIPPER concept.

Different measurement techniques are being tested in five real-world campaigns over the main shipping areas in the EU. Together with SO_x and NO_x, which are the current regulatory priority, techniques to characterize PM, including Ultrafine Particles (UFP) and BC are being used. Experimental information in the campaigns are combined with advanced plume dispersion and Chemical Transport Models (CTMs) to estimate current ship-induced air pollution and predict the impact of various degrees of compliance to major port areas in the EU. Using five field measurement campaigns and long-term monitoring data SCIPPER will assess the suitability, operational capacity, and cost-effectiveness of various monitoring methods.

The techniques identified include on-board, onshore in situ and optical remote, airborne, and satellite systems. Assessment of these will be performed in ports (Gothenburg, Hamburg) and in the shipping lanes of the North and Baltic Seas, the English Channel and the Mediterranean (specifically the port of Marseille). Where available these assessments will be carried out in parallel with established official monitoring methodologies. The conceptual flow diagram of SCIPPER is shown in Figure 2 and comprises three technical pillars:

- Pillar 1: In-parallel demonstration of the potential of several monitoring techniques over five EU experimental campaigns. This feasibility study is necessary to demonstrate sensitivity to low sulphur limits, monitoring of new pollutants and the performance specificities of the various techniques. Data collection across several methods in each campaign, together with reference and scientific instruments, allows the comparative assessment of the different methods.
- Pillar 2: Data collected from the range of techniques, sensors and instruments provides new experimental information. This includes performance of the different techniques, pollutants concentration for emissions factor determination, plume characterization, and air pollution levels in harbors, cities, and shipping routes. Although this also supports new science, it is mostly necessary to fulfil the key objectives of SCIPPER, i.e. assessing the monitoring potential of the different techniques.
- Pillar 3: The experimental information collected in Pillar 2 is used to advance current AQ simulation models to allow for the assessment of shipping's contribution to air pollution in port locations, urban areas, and

coastal regions. Such models are used to assess current contributions, as well as to estimate future AQ impacts of shipping in a variety of regulatory and compliance scenarios.

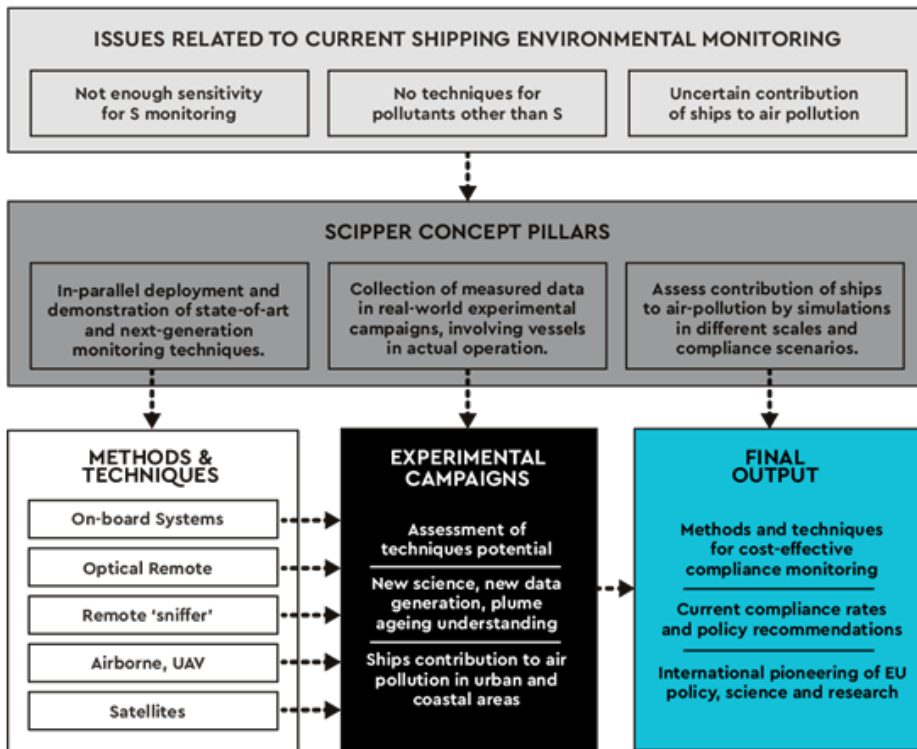


Figure 2: Project overview.

Therefore, the main methodological tool to assess the potential of the different techniques is their real-world implementation and comparison in five field campaigns to be executed within the project. Results from long-term shipping compliance monitoring are also being collected and assessed. The experimental campaigns are horizontal activities on which different tasks on monitoring techniques and emission and AQ modelling will be anchored to. The methodology of the project is schematically represented in Figure 3.

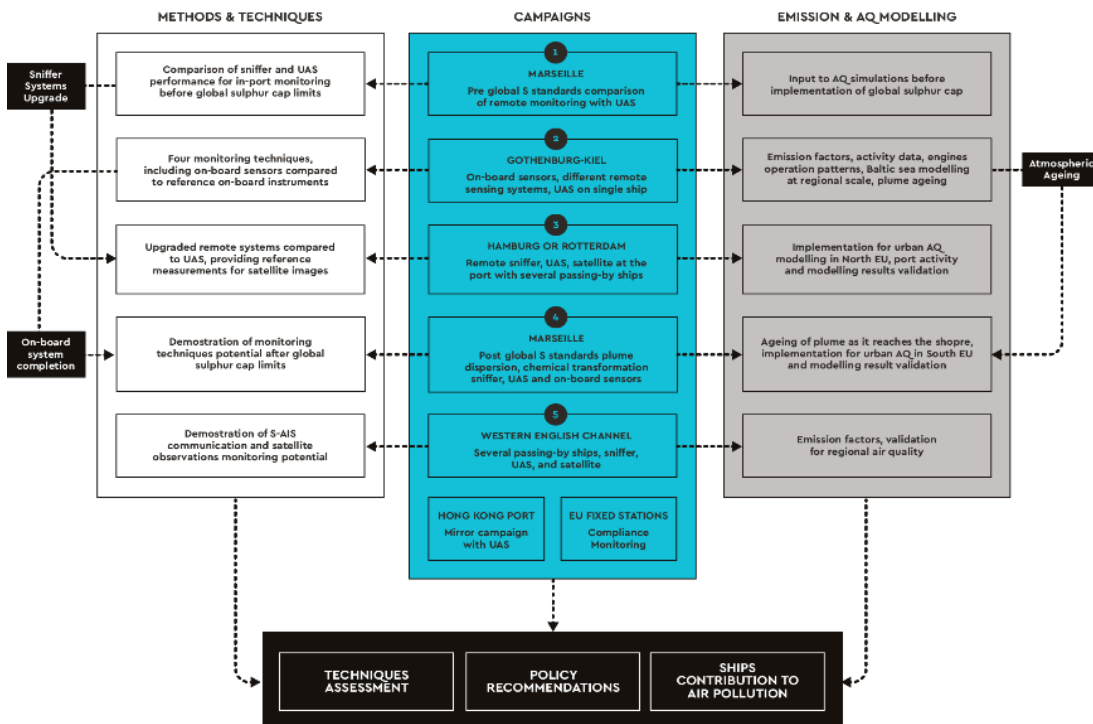


Figure 3: SCIPPER Methodology.

In more details, the five experimental Campaigns of SCIPPER will be the following:

- C1 in Marseille (FR): Pre-global sulphur standards comparison of remote monitoring and UAS.
- C2 from Gothenburg (SE) to Kiel (DE): Use of on-board sensors, various remote sensing systems, UAS on a single ship in actual service.
- C3 in Hamburg (DE): Use of sniffers, UAS, and satellite at the port observing several passing-by ships, and intercomparison of the sniffer and the optical measurements on the locally used stationary and airborne platforms.
- C4 in Marseille (FR): Post-global sulphur standards, plume dispersion and chemical transformation, use of sniffers, UAS and on-board sensors.
- C5 in the Western English Channel (UK): Use of sniffers, UAS, and satellite imaging on several passing-by ships.

Measurement results are also being used, along with desktop literature review, for developing up-to-date emission factors, which are required for emissions inventories construction and AQ simulation models' application. AQ models are being enhanced to better simulate secondary aerosol formation as the emission plume ages in the atmosphere. Using these advanced simulation tools, SCIPPER quantifies the environmental and health impacts of varying degrees of regulatory compliance for selected test cases. The project will synthesize outputs from all methodological steps to draft guidelines and recommendations for the enforcement of shipping emission limits and the impact of regulations on AQ.

Table 1: SCIPPER expected outputs.

Outputs	Description
Sensors	They will be developed and/or tested for conducting on-board emissions monitoring.
Measurement Techniques	They will be deployed for the remote monitoring of shipping emissions, including sniffers, optical remote sensors and satellites. Harmonization of QA/QC standards and reporting procedures will be addressed.
Environmental sensing UAS	It will be developed and demonstrated, using latest sensor packages to measure an enhanced range of pollutants.
Communication protocols	They will be demonstrated between ship and shore for signal transmission involving satellite communications.
Environmental shipping monitoring center	It will be established, utilizing the new communication protocols, and demonstrate real-time environmental information delivery from working ships, based on robust parameters.
Advanced algorithms	They will be elaborated for the detection from space of emissions from single ships or groups of ships.
Emission factors	They will be developed for estimating in-port ship emissions and advanced emission inventory tools that will be used for quantifying pan-EU and global contributions of ships to air pollution.
Ship plume ageing module	It will be developed and integrated into urban and regional dispersion air quality models for better prediction of atmospheric pollutants transformations
New dispersion models	They will be created based on computational fluid dynamics to simulate in detail ship plume dispersion over port and neighboring urban areas.
Guidelines and policy recommendations	They will be drafted to support improved policy and regulations addressing the environmental consequences of shipping, innovative guidelines and policy recommendations.

Therefore, through the combination of the experimental work with the modelling activities, new technology (i.e. sensors, demonstration of new techniques), new environmental tools (emission factors, AQ models) and policy recommendations (efficient enforcement, internationally pioneering, EU policy outreach) are the three directions of the project main outcomes. All the main expected outputs are listed and described in Table 1. The following chapter highlights some of these outputs, as these have been delivered during the first period of the SCIPPER implementation.

Achieved outputs

Regulatory and enforcement gaps in shipping emissions' regulatory framework

The first step in the overall SCIPPER approach was the review of the existing international and national regulatory framework on shipping emissions, with emphasis on highlighting the provisions related to the enforcement of the established emissions' limits. Existing gaps in the regulatory framework were identified, such as the absence of PM emission limits and the fact that the negative side effects of abatement technologies are currently not addressed. Enforcement gaps, such as the lack of regulatory prescribed approaches to the use of remote sensing technology, all raise topics where the project will focus while studying the emission enforcement techniques (Winnes et al. 2019). The main regulatory and enforcement gaps that have been identified per pollutant type are presented in Table 2.

Emission measurement results

The research around the emission enforcement techniques, such as on-board sensors, sniffers, optical remote techniques, UAS and satellite systems is being accomplished, as already mentioned, in five field campaigns at major sea areas in the EU. These campaigns are the main methodological tool to assess the potential of the different techniques in their real-world operation and comparison.

In the context of the 1st experimental campaign of SCIPPER, ship emission measurements were carried out at the port of Marseille, France, during a 5-day period in September 2019. A measurement vessel, which was stationed in the northern part of Marseille was equipped with a suite of sniffer instruments for gas and particles (SO₂, CO₂, NO_x, BC, PN, PM_{2.5}) and an optical sensor (sky-DOAS), measuring columns of SO₂ and NO₂. The instruments were all operated by Chalmers University. The measurement vessel tracked ships that were in-, or out-bound to the two ports of Marseille and Fos-sur-Mer. In the map of Figure 4, results for the % FSC are shown for individual ships, indicating the existing condition in terms of the sulphur content of the fuel used before the enforcement of the global sulphur cap of 0.5% on January 2020. Similar measurements are planned for the upcoming measurement campaign at the same port, in order to compare the conditions before and after the global sulphur cap. In addition, the detections of NO_x emissions are also presented in Figure 4(b).

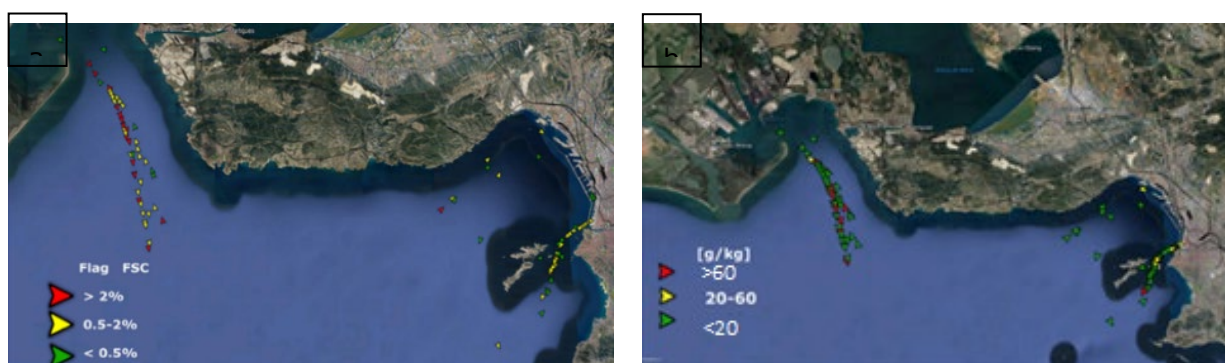


Figure 4: FSC (a) and NO_x (b) measured using the sniffer technology from a measurement vessel prior to the global cap of 0.5 %.

Also, a drone-based sniffer (BH-12) measurement was carried out from the measurement vessel, by the project partner Aeromon. The drone was used in order to chase shipping plumes and measure the emitted quantities of pollutants. Measurements of 15 vessels were carried out simultaneously with the drone and the sniffer system for comparison purposes. Indicative results of this comparison of the two methods are provided in Figure 5, for an indicative single ship, showing a good agreement of the two methods. Figure 6 also displays the timeseries of the measurements as derived by the two methods' application.

Table 2: Regulatory and enforcement gaps per examined pollutant.

Type	Pollutant	Identified gap
Regulatory	Sulphur and PM	Regulations on other fuel characteristics than S-content are lacking
		Regulated limits on PM are lacking
		Regulated limits of emission of the non-volatile particulate fraction BC are lacking.
		Regulations on negative side effects of Exhaust Gas Cleaning Systems are lacking
		PM emission measurement standards of emissions to air are insufficient
	NO _x and other emissions	NECA geographical scopes are possibly not enough to accomplish the technology demand from the industry that would be needed to have efficient NO _x -regulations
		Simple legislative test procedure allows for a substantial difference between test cycle emissions and real sailing emissions, especially using modern engine technology
		Control procedures to discover Selective catalytic reduction (SCR) deactivation are missing
		Regulation on ammonia slip over time after SCRs are lacking
		SCR function in port areas and other close to shore locations are not well covered by the regulation
		Knowledge of NO _x sensor performance over time
		Side effects on the marine environment from the use of Exhaust Gas Recirculation (EGR) scrubbers are not regulated
		EGR function in port areas and other close to shore locations are not well covered by the regulation
		No regulation limits the methane slip from Liquefied natural gas (LNG) engines.
Enforcement	Sulphur and PM	Regulatory prescribed approaches to the use of remote sensing technology is lacking
		Cost efficient technologies for certifying compliance at sea are lacking
	NO _x and other emissions	Emissions of NO _x from the operational phase are not monitored
		Time intervals for parameter checks are not specified
		The applicability of the not-to-exceed limit for international shipping is small
		Regulatory prescribed approaches to the use of remote sensing technology for NO _x emissions is lacking
		Sufficient monitoring procedures at the use of NO _x abatement equipment for Tier III is lacking

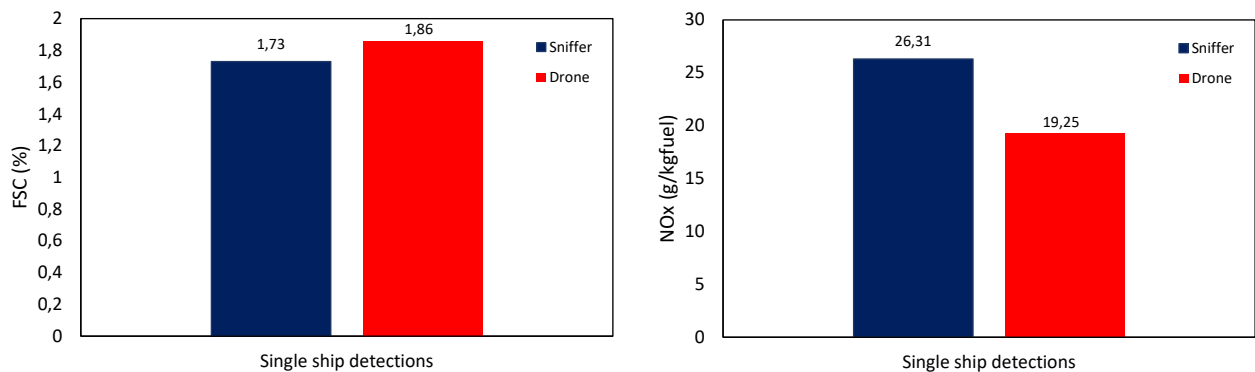


Figure 5: FSC (%) and NOx (g/kg fuel) derived by sniffer and drone measurements for an indicative ship.

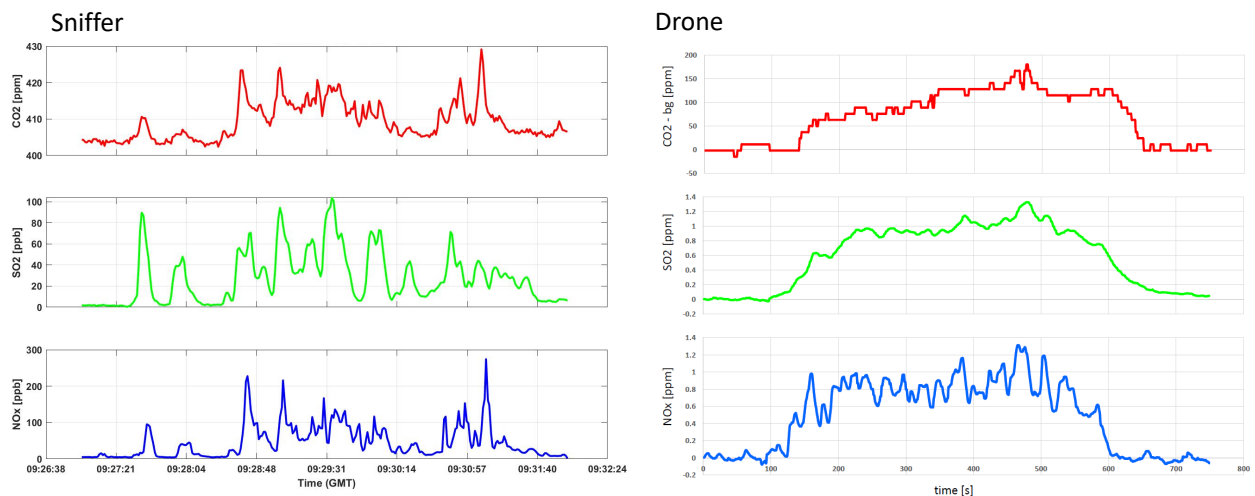


Figure 6: Timeseries of sniffer and drone emission measurements for an indicative ship.

A side-by-side assessment of state of the art and next-generation remote sensing techniques took also place in campaign 3 (C3) in Wedel near Hamburg between September – October 2020 in Hamburg. In total, 6 different land-based sniffer systems were operated whereof one laser spectrometer for SO₂ and CO₂ measurements was operated for the first time as a new method for remote compliance monitoring. The land-based measurements were complemented by measurements from two UAV-borne systems. Also, regional satellite data is available for further comparison. More than 520 ship plumes from more than 250 different vessels were analysed by land-based systems and around 65 plumes from more than 50 different vessels by UAS. Fifty-five fuel samples onboard 32 selected vessels were taken for later intercomparison with the results of the remote measurements.

Emission factors development & air quality simulations

In order to provide a realistic description of ship emissions, modelling of instantaneous power needs of ships is required, but it needs to be combined with up to date information of emission factors. In parallel, the experimental information collected is being used to produce shipping emission factors and to advance current air quality simulation models to allow for the assessment of shipping contribution to air pollution in port locations, urban areas and coastal regions. Such models will be used in air quality simulations to assess current contributions, as well as to estimate future air quality impacts of shipping in a variety of regulatory and compliance scenarios.

Emission factors are often expressed as a function of engine and fuel type, as well as engine load. Additional contributions may be needed, because some pollutant species require the description of engine age, crankshaft revolutions per minute or fuel sulphur content to provide a relevant description of contributing factors to emission factor development.

The methodology for developing EFs is primarily based on a Literature Review (LR), which resulted in the collection of 76 papers, with more than 182 reported results of emission test configurations of various methods, mainly derived by on-board measurements and marine engine test-beds. For each test configuration various emission rates, including

gaseous pollutants (NO_x, CO, SO₂, THC, etc.), greenhouse gases (CO₂), BC and PM, as well as energy consumption rates have been collected. Therefore, all these reported EFs found in LR (expressed in g/kWh or g/kg fuel) have been organized in a unique database and divided into category groups, relevant to the ones of the AEIG (fuel type, engine type, ship category etc.).

Therefore, applying a statistical analysis on the reported emission factors, a dimensionless dependence of the emission rate with the engine load occurred, in order to understand the overall trends of this variance of EFs with the load. This normalization is performed per pollutant by dividing all the measured emission values collected at the various loads of each test found in literature, with the respective value within the same dataset obtained at a reference engine load point. This reference load point was selected to be the one most frequently observed in the available literature. For the different engine types and pollutants this was found to be in the range of 40-50%. The normalization provides the link of emission differentiation with load point for the different pollutants.

Mean values for each pollutant (Base EFs) for this reference load point have been calculated for the three categories of marine engine (slow speed, medium speed and high speed) and fuel types. Indicative examples of this statistical process outputs are provided in Figure 7, where the dimensionless emissions rates' dependence with the engine load for various emissions (NO_x, CO, HC) are provided. This variance is depicted by the formed best-fit trend line formed over all the dimensionless points, which have occurred from the normalization process of the emission rates.

Respective dependence is also depicted in Figure 7 for the Specific Fuel Oil Consumption (SFOC). The normalization reference value for all of these pollutants is found at the 50% engine load. Each panel of Figure 7 also contains the calculated mean absolute value and the standard deviation at the reference point per engine type as an inset.

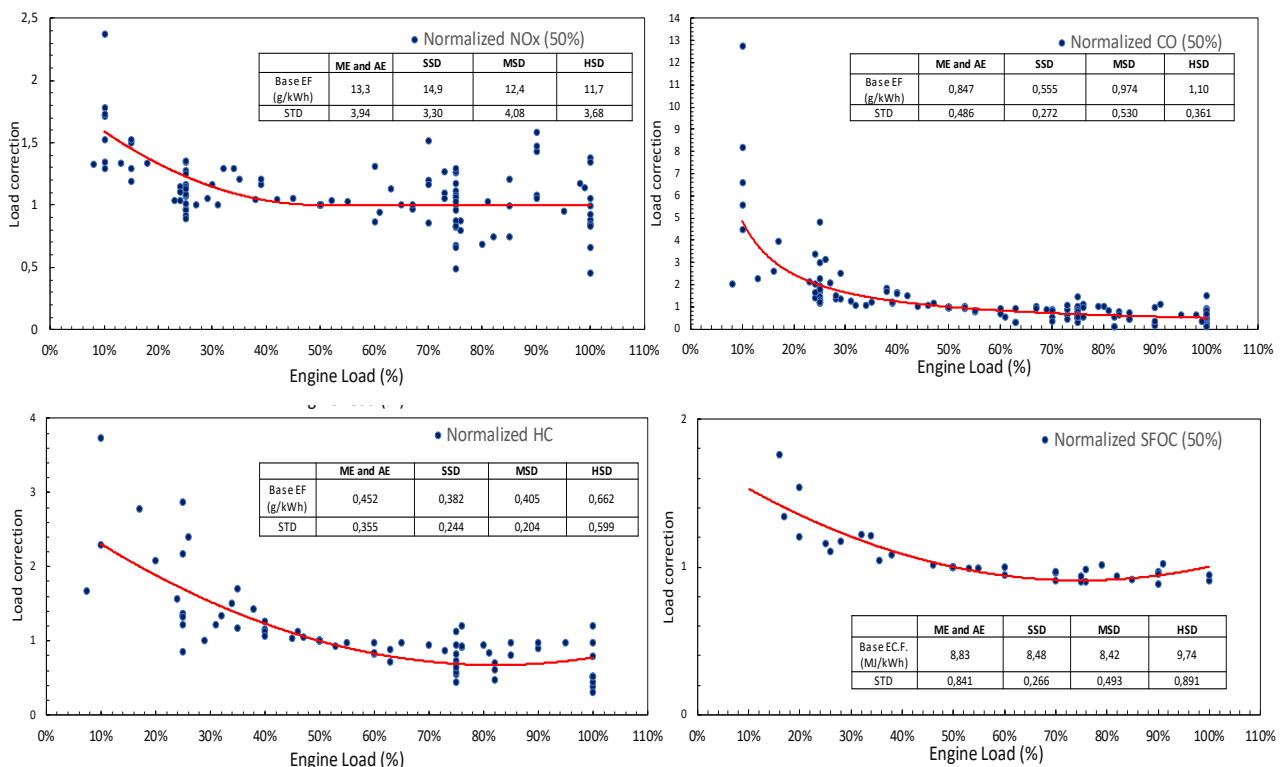


Figure 7: Gaseous pollutants and Fuel consumption dimensionless trend line, as a function of the engine load, derived by LR measurements.

Similar EF graphs to those presented in Figure 7 have been also produced for SO₂, Black Carbon (BC) and Organic Carbon (OC). The developed EFs will be supplemented and validated with the results of the measurement campaigns and will enhance those already included in the STEAM model. In addition, EFs expressed as a function of the operating mode will also be developed.

The general trend of the LR findings shows that EF in g/kWh are high for lower engine loads and is decreased or stabilized with increasing load. For some pollutants (i.e. HC) and the fuel consumption, EFs are again increased at

tending full load. In absolute values, EFs for NO_x are higher in slow speed engines and lower at high speed. In contrast CO EFs are higher for high speed engines.

The impact of shipping on the concentration of air pollutants in the Mediterranean Sea area was investigated by Chemistry Transport Model (CTM) simulations. Results for NO₂ concentrations in June 2015 are indicatively presented in Figure 8. The result shown here is based on STEAM shipping emissions for 2015 and a CMAQ model simulation on a 12 x 12 km² grid for the Mediterranean Sea. Shipping lanes and important port areas are clearly visible.

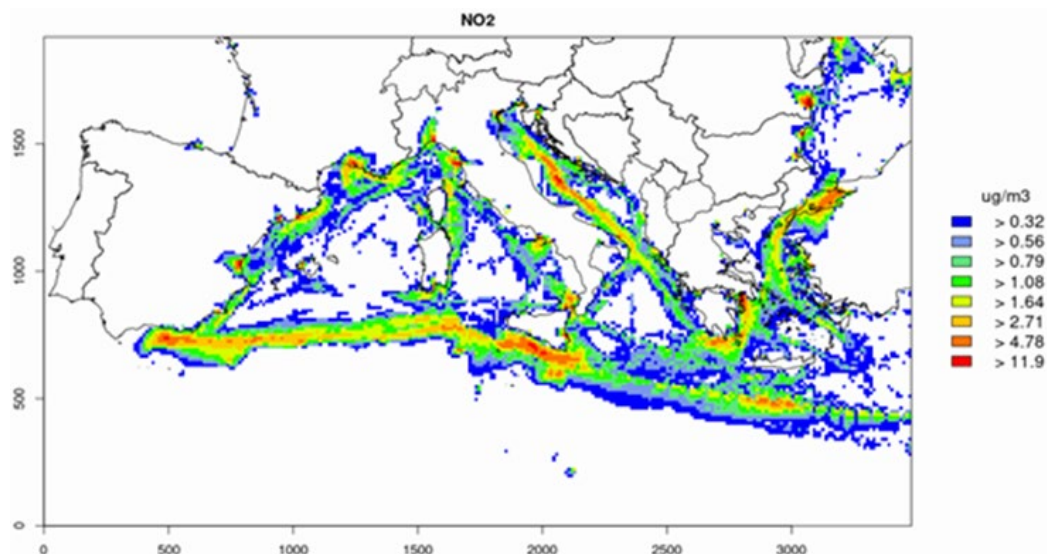


Figure 8: NO₂ concentrations caused by shipping in the Mediterranean Sea area, June 2015.

Conclusions

The SCIPPER project, through its integrated approach, assesses the potential of various techniques in the enforcement of the new emissions limits that are being applied to the sector in recent years. In parallel, it evaluates the impact of the established emission limits on the air quality of harbors and of wider areas that are located close to the sea. The methodology combines actual field measurements at ships and ports, in-lab tests, modeling activities and desktop reviews. During the field measurement campaigns on-board and remote techniques are deployed and compared on the basis of ease of application, accuracy and cost. The monitoring of emissions via satellites is also explored. Initial results from the comparison of sniffers with sensors carried by drones at the port of Marseille show a good agreement between these two methods in identifying the FSC of ships and in measuring NO_x emissions. Future publication will provide in detail the comparison outputs. Desktop reviews led to the development of a new set of emission factors for ships, which are compatible with the STEAM model. These new sets reveal the dependency of emissions with the engine load, while the characteristics of this dependency are affected by the nature of each pollutant. In addition, the absolute values of the developed emission factors depict the effect of the engine type and the fuel used on various pollutants. The load dependent EFs along with the emissions from other sources are used as input in the air quality simulations, which reveal the contribution of shipping activity to the concentration of harmful pollutants. So far results quantify the impact of shipping in the NO₂ concentrations in the Mediterranean Sea for the year 2015. Desktop reviews also provided a valuable tool on identifying regulatory and enforcement gaps in national and international regulatory framework for shipping emissions. Through the overall work carried out by the project, SCIPPER will try to address these gaps drafting policy proposals, guidelines and recommendations.

Acknowledgement

The SCIPPER project has received funding from the European Union's Horizon 2020 research and innovation programme under grant agreement Nr.814893

References

- Corbett, J. J., Winebrake, J. J., Green, E. H., Kasibhatla, P., Eyring, V., & Lauer, A. (2007). Mortality from ship emissions: a global assessment. *Environmental science & technology*, 41(24), 8512-8518.
- Matthias, V., Bewersdorff, I., Aulinger, A., & Quante, M. (2010). The contribution of ship emissions to air pollution in the North Sea regions. *Environmental Pollution*, 158(6), 2241-2250.

Ntziachristos, L., Saukko, E., Lehtoranta, K., Rönkkö, T., Timonen, H., Simonen, P., ... & Keskinen, J. (2016). Particle emissions characterization from a medium-speed marine diesel engine with two fuels at different sampling conditions. *Fuel*, 186, 456-465.

Jalkanen, J.-P., Brink, A., Kalli, J., Pettersson, H., Kukkonen, J., and Stipa, T., "A modelling system for the exhaust emissions of marine traffic and its application in the Baltic Sea area", *Atmospheric Chemistry and Physics* 9 (2009) 9209-9223

J.-P. Jalkanen, L. Johansson, A. Brink, J. Kalli, J. Kukkonen and T. Stipa, "Extension of an assessment model of ship traffic exhaust emissions for particulate matter and carbon monoxide", *Atmos. Chem. Phys.*, 12 (2012) 2641-2659.

R. Verbeek, et.al. 'Real Sailing Emissions' for maritime vessels using sensors and satellite data transmission. 24th TAP conference, online, <https://www.tapconference.org/>. 30 March – 1 April 2021

Winnes, H., Fridell, E., Verbeek, R., Duyzer, J., Weigelt, A., Mamarikas, S., and Ntziachristos L., "Gaps in current emission enforcement regulations and impacts to real-world emissions", SCIPPER project Deliverable 5.1, (2019)

Aristeidis K Georgoulas, K Folkert Boersma, Jasper van Vliet, Xiumei Zhang, Ronald van der A, Prodromos Zanis and Jos de Laat: Detection of NO₂ pollution plumes from individual ships with the TROPOMI/SSP satellite sensor. *Environmental Research Letters* 15 (2020) 124037

2.22 ‘Real Sailing Emissions’ for maritime vessels using sensors and satellite data transmission

Ruud Verbeek¹, Tim Smyth², Anthony Deakin³, Richard Proud³, Nikos Kousias⁴, Matti Irjala⁵, Jonathan Weisheit⁶, Johannes Oeffner⁶, Vincent Schneider⁶, Darren Snee², Declan van Heesen¹, Vincent Verhagen¹, Jana Moldanova⁷, Erik Fridell⁷, Antti Rostedt⁸, Jorma Keskinen⁸, Panu Karjalainen⁸, Antonios Stylogiannis⁹, Linda Haedrich⁹ and Vasilis Ntziachristos⁹, Leonidas Ntziachristos⁴

¹TNO, ²PML, ³exactEarth Europe, ⁴AUTH, ⁵Aeromon Oy, ⁶CML, ⁷IVL, ⁸TAU, ⁹HMGU

ruud.verbeek@tno.nl

Abstract

Exhaust emissions of maritime vessels are becoming increasingly important due to their contribution to air pollutant concentration on land, especially in port areas. For this reason, Emission Control Areas (ECA) were introduced in Europe to reduce SO_x emissions. This has been expanded to more stringent NO_x regulations for new vessels in 2021.

The EU H2020 SCIPPER project was set-up to study various possibilities for monitoring and enforcement of pollutant emissions from vessels, and how this would contribute to the air quality in port areas. This paper reports on onboard monitoring options, data formats and metrics and continuous data transmission via satellite. Several onboard emissions monitoring systems, built around low costs sensors, have been constructed for this purpose. The sensors include NO_x, NO₂, SO₂, NH₃, PM and BC, so have a broader scope than just supporting legislative requirements. Regarding the monitoring strategy, it is proposed to monitor ‘Real Sailing Emission’ (RSE) rather than mimicking the formal E3 cycle. It is also proposed to use as few as possible parameters for this monitoring. Basically exhaust gas concentrations (ratio of pollutant with CO₂) in combination with a pre-set break-specific fuel consumption (BSFC) is sufficient for good monitoring. For NO_x, the Not To Exceed (NTE) limit (max 150% of E3 cycle average) is seen as the most practical requirement for this monitoring.

A simple and robust data format has been defined which is suitable for satellite data transmission. By transmitting ratios of pollutants with CO₂ (in exhaust gas), the transmission can handle different type of sensor signals with a good accuracy. For example, raw and diluted concentrations can be handed with the same accuracy.

Introduction

Exhaust emissions of maritime vessels are becoming increasingly important due to their contribution to air pollutant concentrations on land, especially in coastal and port areas. For this reason, Emission Control Areas (ECA) were introduced in Europe and other parts of the world to reduce SO₂ and NO_x emissions. In Europe, the ECA includes the Baltic sea and the North Sea. To reduce SO₂ emissions, the latest low Fuel Sulphur Content (FSC) requirement entered into force in 2015. In 2021 more stringent NO_x regulations have entered into force for new vessels, the IMO MARPOL Tier III regulation.

The EU Horizon 2020 project SCIPPER¹⁶ stands for: “Shipping Contributions to Inland Pollution Push for the Enforcement of Regulations”. The project was set-up to study the various possibilities for monitoring and enforcement of pollutant emissions from vessels, and how this would contribute to the air quality in coastal and port areas. Within SCIPPER, different kinds of monitoring will be studied and developed, including continuous monitoring on vessels (in the exhaust stack and in the plume) and several types of remote sensing options (onshore, via drones and satellite). Monitoring onshore and via drones are focussed in port areas, while monitoring onboard and via satellite can capture the entire voyage. Pollutants emitted along the coast and further offshore are also a large contributor to the background levels of air pollutants on land. Refer also to the overview paper in this conference (Ntziachristos, 2021).

SCIPPER Deliverable D5.1 (Wines, 2019) identifies a broad range of regulatory and Enforcement gaps. Important gaps in this context include:

- Lack of limits regulating emissions for PM and EC, also PM measurement standards are insufficient.
- Tier III NO_x limits have limited geographical scope and are only applicable to new vessels.
- Simple legislative test cycle (E2, E3, etc.) allows for substantial difference between test cycle emissions and Real Sailing Emissions, RSE, Equivalent to Real Driving Emissions, RDE for road transport.
- Selective catalytic reduction (SCR) equipment functioning in Port areas and close to shore areas (low engine load), are not well covered by the regulation.
- Control procedures to discover SCR deactivation and excessive NH₃ slip over time are missing.

¹⁶ EU H2020 project No. 814893. <https://www.scipper-project.eu>

- Sufficient monitoring procedures at the use of NO_x abatement equipment for Tier III is lacking.

Many of these gaps are addressed in this paper, which focusses on continuous onboard monitoring of SO₂, NO_x, NO₂, NH₃, BC, PM and PN (both in the exhaust stack and in the plume). Within SCIPPER several sensors and sensor systems, developed by the partners, will be brought together to be tested. This publication will present the sensor systems and a proposal for the monitoring parameters and calculation method for comparison with legislative requirements. This will also include automatic data transmission via satellite (figure 1).

Apart from the legislative argument, continuous emissions monitoring can also be used to show the environmental performance to customers and to secure a level playing field. Furthermore, it can generate data for air quality calculations and emission factors.

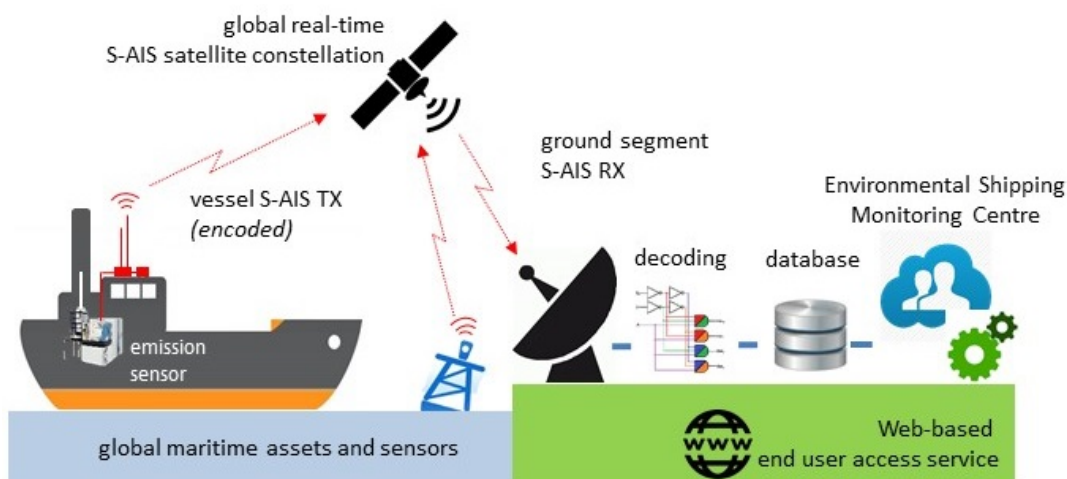


Figure 1: A schematic showing the end-to-end emissions reporting service from ship-to-shore and then to the cloud-based user access services.

Onboard monitoring options

The SCIPPER strategy for onboard monitoring includes:

- Reducing the number of parameters to the bare minimum. If possible, exhaust gas only (which makes simple validation, and third party checks possible).
- Increase transparency by continuous monitoring and by publishing average performance.
- Monitoring of 'Real Sailing Emissions' (RSE), rather than mimicking the formal test cycles (E3, E2, D2).
- Accept somewhat lower accuracy if needed.

Monitoring for legal limits

Only ships equipped with SO_x scrubbers Scheme B must be equipped with SO_x monitoring. Fuel Sulphur Content (FSC) monitoring in the exhaust gas is relatively simple, because it is not dependent on engine load. The legal requirements and calculation method is clearly described within MEPC 259(68) (MEPC, 2015): it requires simultaneous monitoring of SO₂ and CO₂ in the exhaust gas, and FSC is calculated as follows:

$$\text{Fuel S content: } \text{FSC (m/m)} = \frac{SO_x^{\text{ppm}}}{CO_2^{\text{ppm}} \cdot 0.86} \cdot \frac{M_S}{M_C}$$

In this equation: M_S : molecular mass Sulphur is: 32 g/Mol. M_C : molecular mass carbon is: 12 g/Mol and 0.86 is the carbon content of the fuel.

The (continuous) onboard monitoring of NO_x is possible, but not required by international regulations. Many SCR systems are simply open-loop. The amount of reagent, urea-water solution, is then only dosed based on the engine load map. The simplest method to show NO_x compliance is an engine parameter check method, that verifies that the engine's components, setting and operating values do not deviate from the specifications in the engine's technical file. Direct NO_x monitoring is however possible and promoted in SCIPPER, including continuous transmissions of the emissions performance to an 'Environmental Shipping Monitoring Centre'.

There are several options for comparing NO_x monitoring data against the legal limits. The Tier III NO_x requirements include two parts:

- Weighted average emissions during the applicable test cycle: E2, E3 (refer to Figure 2A-2B) or D2.
- Not To Exceed (NTE) requirement of 1.5 times the cycle average. This is a requirement to each point in a substantial part of the engine map (roughly above 35% load). Refer to figure 2C below.

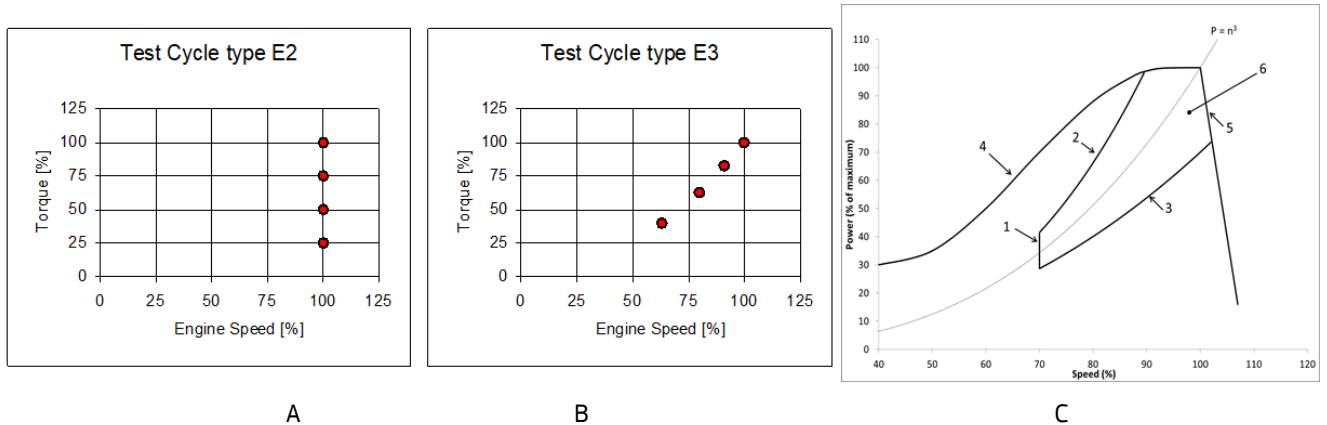


Figure 2: A+B) ISO test cycles E2 and E3 for NO_x emissions.
B) Not to Exceed, NTE, emissions area in the engine map.

For continuous monitoring of emissions the E3 cycle is not very practical, since the E3 cycle consists of four fixed points within the engine map. The IMO onboard measurement is based on this E3 cycle, but this is meant for a single measurement and not for continuous monitoring. The NTE is a much more practical requirement to handle in practice, since it is a requirement applicable to each point of the applicable part of the engine operating map (figure 2C).

The NTE NO_x emissions in g/kWh can be calculated in a very simple way, using just the NO_x and CO₂ concentrations in the exhaust gas in combination with a reference BSFC. The final equation (3) is derived in a few simple steps:

$$\text{Calculation gram NO}_x \text{ per gram CO}_2: \quad \frac{NO_x}{CO_2} = \frac{NO_x^{ppm}}{CO_2\% \cdot 10000} \cdot \frac{M_{NO_x}}{M_{CO_2}} \quad (1)$$

$$\text{Calculation gram NO}_x \text{ per gram fuel:} \quad \frac{NO_x}{m_{fuel}} = \frac{3,15 \cdot NO_x^{ppm}}{CO_2\% \cdot 10000} \cdot \frac{M_{NO_x}}{M_{CO_2}} \quad (2)$$

$$\text{Calculation NO}_x \text{ in g/kWh:} \quad NO_x = BSFC \cdot \frac{3,15 \cdot NO_x^{ppm}}{CO_2\% \cdot 10000} \cdot \frac{M_{NO_x}}{M_{CO_2}} \quad (3)$$

In which 3.15 is the mass ratio between CO₂ and fuel, and M_{xyz} is the molecular mass. Parameter options for onboard monitoring on inland vessels are extensively described in Deliverable D5.8 of the H2020 PROMINENT project (Verbeek, 2017). Similar equations as for NO_x can be derived for BC, PM and PN if desired.

It is recommended to use a fixed BSFC per engine type, also independent of the load point. There are several reasons to use very few parameters and also a fixed BSFC per engine type:

- It is transparent and avoids calculation errors.
- It makes independent, third party checks very simple. Just the measurement of concentrations in the exhaust is sufficient to check the NO_x calculation and the proper functioning of the monitoring system.
- It makes economic and independent monitoring systems feasible. The monitoring system can measure the NO_x-CO₂ ratio in raw exhaust, in diluted exhaust or even in a plume. Dilution does not change the ratio and the dilution factor is not needed.
- With a constant nominal BSFC, there is no penalty on the NO_x due the increased internal engine friction at low load. In that way the NTE can be extended down to 25% load without making it too severe for the SCR aftertreatment system. It would also be important to further extend the load range down to 10% load in the future, because of the importance of low NO_x in port areas during low-speed sailing and manoeuvring.

Regarding the limit value for the real-world NO_x in the applicable part of the engine map, the NTE value of 1.5 times the E3 cycle limit value can be used. It is also possible to use an additional factor for real world NO_x since the 1.5 is

specified for the laboratory measurement. In that case, an additional margin of 10% or 20% could be used resulting in an overall factor of 1.65 to 1.80 compared to the E3 cycle requirement. With road transport, such a factor is referred to as CF, Conformity Factor.

Comparison with road transport and NRMM

Measurements of real-world emissions in road transport are part of the emissions type approval. For road vehicles, this is referred to as RDE (Real Driving Emissions for cars) and ISC (In Service Conformity for HD vehicles). ISC for HD vehicles became obligatory with the start of Euro VI in 2013. For cars RDE first entered into force in 2017. For these RDE/ISC tests a so called PEMS, Portable Emissions Monitoring System, is used. This system consists of compact analysers and an exhaust flow measurement.

The operational practice of road vehicles is entirely different to maritime shipping. Road vehicles are characterized by very dynamic engine behaviour, while load is quite stationary on ships. However, in terms of calculation procedure and limit setting, it is interesting to look at road transport. In this respect it is also interesting to take a look at land based NRMM for which a monitoring requirement is in place. This has a more flexible definition with respect to the operational profile than for road vehicles.

For road transport a standard trip composition is used consisting of three equivalent time parts of city driving, rural driving and motorway driving. During this trip, the emissions are calculated during a 'work based' or 'CO₂ based' Moving Averaging Window (MAW). In practice this is approximately a 20 minute moving average. The limit value for the real-world test is higher than for the laboratory type approval test. The so-called Conformity Factor, CF is used for that. The CF is defined as 1 plus a margin, which is based on the PEMS accuracy. For HD vehicles, this margin is 0.5. For cars it started with 1.1, but this is in steps reduced to 0.32 (CF from 2.1 to 1.32).

Monitoring for air quality

For calculating mass flow emissions rather than specific emissions (g/kWh, g/kg fuel), an additional parameter is needed. This calculation can be based on exhaust flow¹⁷ or on fuel or CO₂ mass flow or on engine power. With real-time fuel flow, pollutant mass emission can be calculated over an entire trip or during certain parts of the trip (e.g. near ports).

For example, NO_x mass flow in kg/h and kg//km can be based on the NO_x/CO₂ ratio and the fuel flow as shown below:

$$\left. \begin{array}{l} \text{NO}_x/\text{CO}_2 \text{ ratio in exhaust gas} \\ \text{Fuel flow} \rightarrow \text{CO}_2 \text{ mass flow} \end{array} \right\} \longrightarrow \text{NO}_x \text{ mass flow (CO}_2 \text{ based calculation)}$$

Obtaining reliable real-time fuel flow is however difficult, also time alignment and difference in averaging leads to errors in practice. Instead of fuel flow it is recommended to use engine speed or engine power.

$$\left. \begin{array}{l} \text{NO}_x \text{ in g/kWh} \\ \text{Power or } \int (\text{engine speed})^3 \end{array} \right\} \longrightarrow \text{NO}_x \text{ mass flow (work based calculation)}$$

In SCIPPER the impact of shipping on air quality is assessed utilizing a chain of emission and atmospheric chemistry models. The shipping emissions are calculated with the STEAM model (Jalkanen et al., 2009, 2012) which combines shipping activities derived from AIS signals with emission factors for air pollutants. The mass flow emissions can be used for validation of STEAM on voyage level. Also, the observed emission factors will be used to improve emission factors in STEAM, especially their load dependence.

Sensors and measurement practices

SCIPPER focusses on low-costs sensors, although the monitoring strategy described in section 2 works as well for high-end monitoring systems. The low-cost sensors may need periodic replacement (e.g. every one or two years), but then the costs should be lower than maintenance and depreciation costs of high-end monitoring devices. SCIPPER also evaluates sensing in the plume of the exhaust stack. Advantage of such an option is easy installation and fewer sensors needed since usually the exhaust of several engines is combined in one funnel so in one plume. Several monitoring systems are built-up around commercially available sensors for NO, NO₂, NO_x, SO, SO₂, NH₃, PM and CO₂,

¹⁷ Not practical for ship size engines

either measuring directly in the exhaust pipe or in the plume. These are BH-12 system from AEROMON, the MESU system from CML and the SEMS system from TNO.

Black Carbon sensor

One of the sensors that will be tested on a vessel is a miniaturized optoacoustic sensor for Black Carbon particles measurements (Figure 3). The miniaturized optoacoustic BC sensor for BC comprises of an ellipsoid chamber which offers good sound behavior while additionally minimizing the contact of sensitive components with the polluted sample. Moreover, the sensor uses low-cost components, specifically a Laser Diode (LD) as a light source and a QTF as a sensitive sound transducer. The LD is driven by a custom-made electronic circuit which provides very short pulses (~ 10 ns) with large peak-power and thus increases its energy output. The final scope of the sensor is to function as a monitoring device for exhaust applications (cars, ships, etc.) but also for air pollution measurements.

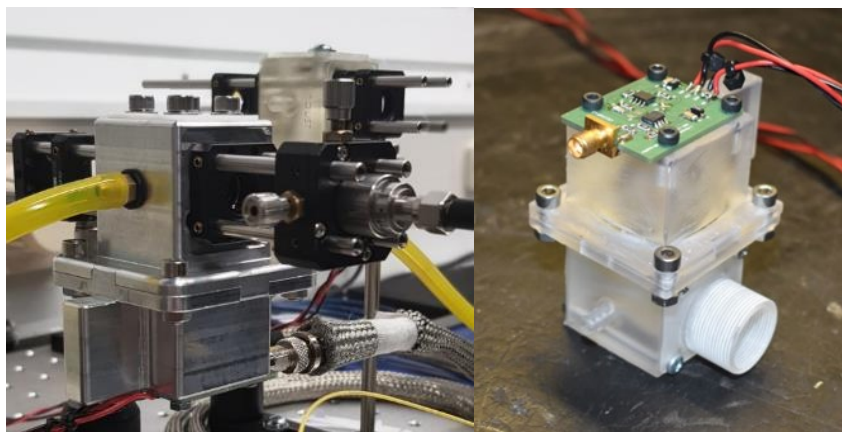


Figure 3: Photoacoustic Black Carbon sensor: prototype in with metal (left), and 3D-printed polymer housing (right).

A 3D-printed polymer prototype of the sensor has been manufactured and tested against a gold-standard reference instrument (Pegasor PPS) and showed great performance in real-time measurements of BC particles. Thus, the sensor currently has a Technology Readiness Level (TRL) equal to 4. During Project SCIPPER the potential of the sensor for monitoring BC emissions from ships will be investigated and any possible disadvantages or required improvements will be identified.

At the SCIPPER campaign two metal prototypes will be used, instead of the initial polymer prototype, in order to withstand the conditions of ship measurements. The sensors will be located at the exhaust stack, downstream of a dilution tunnel which will frequently flush clean air in the system to better protect the sensitive components. In addition, to the custom-made LD driver, a second laser system will be available which can provide sinusoidal and rectangular pulses of larger duration but smaller peak power. The second laser system will be used as a backup in case of any unforeseen malfunctions of the custom driver. The two prototypes will have different light modulation, in order to check the influence of modulation parameters (light beam size, pulse type, pulse duration) in the output signal of the sensor under simultaneous real-world measurements. The modulation of both prototypes can be controlled by a single arbitrary function generator. Finally, a portable oscilloscope (PicoScope 3000 Series) will be used for data acquisition and transfer of data to a laptop for signal processing and data storage. Both prototypes can be connected to the same oscilloscope, thus the total size of the setup will not be affected by the extra prototype.

Monitoring in exhaust stack

Monitoring in diluted as well as in raw exhaust gas will be addressed in SCIPPER. The campaign structure of the project is planned to enable on-board verification of the monitoring instruments with simultaneous measurement with high-end instruments.

Monitoring in the raw exhaust gas will be done with automotive NO_x and NH₃ sensors. Measures will be taken to reduce the exposure time to the exhaust gases, because exhaust gases of maritime engines contain much more impurities like metal traces, heavy hydrocarbons, tar and sulphate, than automotive diesel fuel. Impurities will affect the life time of these sensors.

As many of the monitoring instruments are not suitable for measuring the raw exhaust gas directly, sample dilution and preconditioning needs to be used. The purpose of the dilution is to lower the concentration of the emission components and water in the sample and to cool down the sample. A commercial dilution system (eDiluter Pro, Dekati Ltd, Finland) was chosen as the dilution system for the monitoring instruments. The rationale behind this choice is

twofold: a desired effect on the aerosol particle population and the straightforward controllability of operation. The system is based on a two-stage ejector diluter, where the first dilution stage is heated. Therefore, it provides a representative sample of the non-volatile fraction of the particles, enabling the measurement of the Solid Particle Number (SPN) emission (see Giechaskiel et al., 2017). The solid particle sample is also expected to minimize the interferences of the black carbon measurement. In the system, both primary and secondary dilution ratios as well as the first stage dilution air temperature can be separately controlled. Furthermore, the system can be set to a flush-mode, in which only clean dilution air is provided to the instruments. The ability to vary the dilution parameters provided the possibility for setting up a periodic measurement, where the system is set to the flush mode for most of the time and short samples with varying dilution ratios are provided to the instruments periodically. This greatly reduces the fouling of the dilution system and the instruments, allowing the monitoring system to operate extended times without maintenance. Furthermore, the zero levels of the instruments are recorded repeatedly and can be corrected from the measured data. The periodic operation of the dilution system is accomplished by a customized control software.

The Sensors used to measure the diluted sample include Electro-Chemical (EC), Non-Dispersive Infrared (NDIR), Micro Electro Mechanical System (MEMS) and Optical Particle Counter (OPC) sensor technologies. The sensor data will be compared with reference methods. This will also include commercial diffusion charging PN/PM sensors from Dekati Ltd and Pegasor Oy.

Monitoring in diluted exhaust will be done with the AEROMON BH-12 emission measuring device. This is a modular and portable piece of equipment intended for simultaneous detecting, measuring and mapping of multiple airborne gaseous compounds and particulate matter.

Aeromon has developed and tested BH-12 as a fixed vessel installation onboard Finnish Environment Institutes R/V Aranda between 2016 - 2020. The main challenge has been to find a low-cost and reliable solution for sample dilution needed for measuring exhaust gases with sensor technology directly from stack. This has been found to be a design issue as raw exhaust gas will easily ruin the low-cost components in case of dilution malfunction and raw exhaust introduction into device. The generic sensor technology seems to tolerate moderate dilution of exhaust gases within their optimal measurement range even up to 6-12 months when sensor specific measurement ranges are not exceeded. This lifetime is achieved with intelligent sampling where system is flushed with “clean” ambient air regularly. However, condensation control, sample line filtering and robust material selections in high-risk parts of dilution system require careful design in order for the system to be both low-cost and low maintenance.

In addition, BH-12 has been used as a fixed installation to study potential methane slip and NO_x emissions from an LNG cargo vessel (ESL, 2019).



Figure 4: BH-12 with combined dilution system fitted inside a case.

Plume monitoring on board

Fraunhofer CML has developed a sensor box that is composed of two identically constructed measuring units. Each Mobile Environmental Measurement Unit (MESU) can be applied as independent unit but within SCIPPER they are designed to work together. The sensor box is equipped with electrochemical gas-sensors by Membrapor. Detectable gases are NO, NO₂, SO₂, and CO₂. Additionally, it has sensors for temperature, humidity, as well as PM_{2.5} and PM₁₀. The only difference between the two MESUs is the measurement range of gas sensors.

MESU is located on deck and with its compact dimensions of 280 mm height, 300 mm width and 192 mm depth and can be easily fixated at a pipe, pole or up against a wall. One unit is positioned in preferably close vicinity of the plume, while the other one is positioned as distant as possible. In that manner ship emissions can be determined by differential measurement. The gas sensors are mounted on a base plate that allows sensors to get in contact with ambient air.

Electronic components like PCBs, RaspberryPi, and power transformers are fixed at mounts within a box that can be screwed down to the baseplate. The MESU and its components are sheltered against splash water and harsh offshore environment.

During a SCIPPER campaign MESU can easily be applied. Supplied with electrical power the RaspberryPi boots and starts collecting sensor data. The RaspberryPi initiates the software developed by CML and addresses the gas sensors individually. Data collection begins as soon as functionality is confirmed and the system's real-time clock (RTC) is synchronized with the system.

Remote telemetering of individual ship data

The overall set-up of data-collection onboard and transmission to shore via satellite is presented in Figure 1.

The VHF data transmission of sensor data is being done in the form of a specially encoded two-slot AIS Message 26 (multiple slot binary message with communications state) transmitted on the ASM-1 maritime VHF frequency. The encoding is designed to enhance satellite detection in noisy RF areas of the world. The transmitted messages are collected via the new Iridium NEXT satellite constellation, which carries AIS/ASM VHF receivers on 58 of its satellites. A proof-of-concept system from PML and exactEarth Europe has been installed on the RV Plymouth Quest. The data pipeline has recently passed through its proof-of-concept stage and extends from ship-to-shore and on to an Amazon Web Service (AWS) for collection by data consumer systems. From there the data are decoded and then visualised using a Web Feature Server (WFS); first results of this are shown in Figure 5.

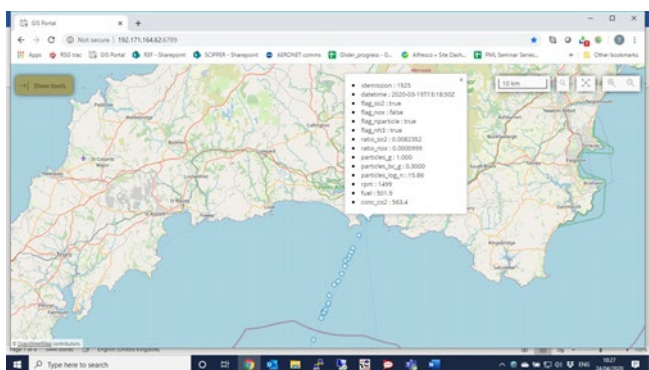


Figure 5: Test emissions data for the RV Plymouth Quest (dark blue circles) with pop-up data shown for an individual point. Data transmitted from ship using satellite VHF data communications and displayed via a Web Feature Server.

Standardized data format

Standard formats are very important in order to have clear interfaces between the different parts in the data chain from the sensors to the satellite VHF transmitter and to a central database. From there certain processed emission parameters can be send to an 'Environmental Shipping Monitoring Centre', which is also being developed within SCIPPER.

The data format is optimized in such a way that maximum accuracy and flexibility is maintained within the data bandwidth of the data transmission was restricted to 113 bits. The data-format defined within SCIPPER is shown in Table 1. This format includes emissions, engine parameters, GPS and meteorological data. By defining ratios of emissions with CO₂, this format maintains the same accuracy for raw and diluted emission signals. So, it is suitable for both sensors in the exhaust stack, for diluted samples as well as for samples from plume measurements. The format also includes all parameters necessary to check emissions against legal limits (NO_x in g/kWh, SO_x in g/kg fuel) and also for air quality modelling to calculate emissions in kg/km and kg/h.

Table 1: Data format for satellite VHF data transmission of onboard monitoring.

#2 bit identifier (e.g. for engine #)
#21 bits Latitude
#22 bits Longitude
#1 bit Flag SO ₂ /CO ₂ threshold exceeded
#1 bit Flag NO _x /CO ₂ threshold exceeded
#1 bit Flag Particles/CO ₂ threshold exceeded
#1 bit Flag NH ₃ /CO ₂ threshold exceeded
#8 bit SO ₂ ppm/CO ₂ ppm (range 0 -> 0.05; precision 0.000196)
#8 bit NO _x ppm/CO ₂ ppm (range 0 -> 0.255; precision 0.001)
#8 bit Particles/CO ₂ g/kg (range 0 -> 1; precision 0.0039)
#8 bit BC/CO ₂ g/kg (range 0 -> 0.3; precision 1.176e-03)
#4 bit Number of particles N/kg(CO ₂) (range 10 ² - 10 ¹⁸ ; precision - order of magnitude)
#9 bit engine speed rpm (range 0 -> 2000; precision 3.91)
#8 bit Fuel consumption kg/hr (0 -> 2000; precision 7.81)
#11 bit CO ₂ concentration (400 ppm -> 100000 ppm; log ₁₀ transform; precision 1.0 ppm)

Actual data transmission was successfully tested on the Plymouth Quest research vessel of PML, using dummy data from a road vehicle. This test period ran from January till late 2020. Figure 6 shows the daily average number of data transmission per hour in the very busy English Channel. The overall average number of transmission messages is six per hour, with a minimum of about two per hour. In October this was increased to just over 13 transmission messages per hour on average. In other areas with less intensive ship movements, the transmission rate will be much higher.

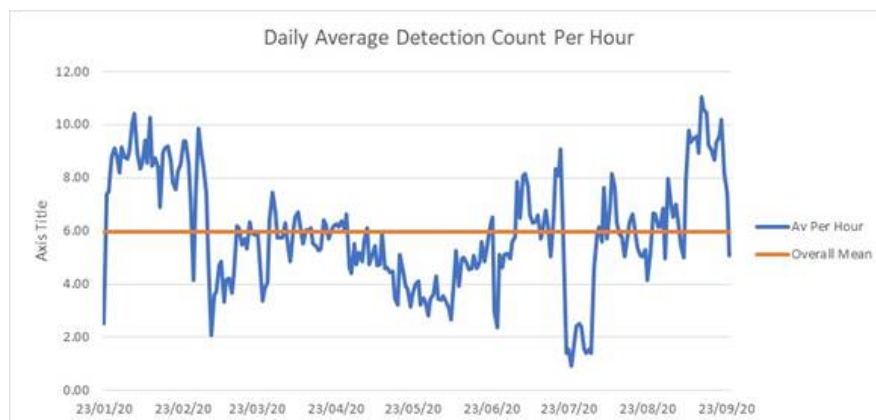


Figure 6: Daily average of hourly data transmission from Plymouth Quest research vessel to shore via satellite VHF detections from the PML/exactEarth deployment from January 2020 to September 2020.

Apart from the satellite data transmission with rather small bandwidth, per second data for all sensor systems will be stored on board of the vessel. This data will be sent to a cloud service, when in port areas broadband LTE connection (cellular) becomes available. From the cloud services, it is available for more in depth analysis and comparison with high-end reference measurements.

Discussion

In this paper we aimed to show options for continuous real time monitoring of the environmental performance of ships. This is important because on ship there is a broad range of fuel and technology options and the legal requirements vary on the sailing location, and may even vary within trips. Due to this, emission control equipment may be switched on and off along the trip, which makes continuous monitoring of key importance. In this paper options are shown on the sensor side, as well as on parameter options. The aim of the latter is to minimise the number of parameters, yet achieving good values to compare with the legal requirements such as for NO_x and SO_x. It appeared that NO_x can be compared with legal limit, just by measuring NO_x and CO₂ concentration in the exhaust gas. The NTE limit (individual points within the engine map need to be lower than 150% of the E3 cycle average) is a practical requirement to monitor. There is no immediate need or high value in calculating E3 cycle emissions. Instead, weighted average emissions along each (type of) trip would be much more interesting. We refer to this as Real Sailing Emissions (RSE). This has also been the direction of legal requirement developments for road vehicles during the past decade. This is referred to as Real Driving Emissions (RDE) for cars, LD and In Service Conformity (ISC) for HD vehicles. It would be good to expand MARPOL requirements with Real Sailing Emissions, requirements. This requirement could for example be 150% of the E3 cycle requirement, very similar to this requirement for road vehicles and also consistent with the NTE. Real Sailing Emissions requirement can secure correct sizing and operation of engines in ships.

A universal data format has been proposed for satellite VHF data transmission. This format would work for in-stack emissions monitoring as well as for 'plume' monitoring, in which one sensor system can monitor several engines. With satellite VHF data transmission of ~six measuring points per hour can be transmitted to a central database. This would be sufficient to provide a good daily environmental performance indicator of ships. How to present this to the shipping stakeholders, legal authorities and possibly to the public, is still a subject of further investigation. Ultimately this is a decision to be made by the main stakeholders; the ship owners and the authorities.

Conclusions

The EU H2020 SCIPPER project focusses on simple and robust monitoring options for Real Sailing Emissions and Enforcement options. This paper reports on onboard monitoring options, data formats and metrics and continuous data transmission via satellite.

The following conclusions are made based on the first work done up till now.

- The (e.g. Tier III) NO_x emissions can be compared with the legal limits based on just exhaust NO_x and CO₂ concentrations in exhaust and a representative BSFC. Cumbersome signals like exhaust flow or real-time fuel flow, with risks of deterioration, instability and misalignment, are not needed. The NTE limit (max 150% of E3 cycle average) is the most practical requirement for this monitoring.
- Monitoring on E3 cycle performance does not add much value, since it is often not very representative for Real Sailing Emissions (RSE). Instead it is recommended to monitor weighted average trip emissions, in line with procedures developed over the past decade for road vehicles. The requirements for RSE could be less stringent than for the E3 cycle, for example 150% of E3 cycle limit. This percentage is also used for road transport and does include measurement uncertainty.
- Several onboard emissions monitoring systems, build around low costs sensors, have been prepared and will be tested in SCIPPER campaigns. These sensor systems include monitoring of BC, NO_x, NO₂, SO₂, NH₃ and PM. Monitoring will take place in raw exhaust, diluted exhaust and also in the exhaust plume onboard.
- A simple and robust data format has been defined which is suitable for satellite data transmission. By transmitting ratios of pollutants with CO₂ (in exhaust gas), the transmission can handle different type of sensor signals with a good accuracy. For example, raw and diluted concentrations can be handed with the same accuracy.

Acknowledgement

The SCIPPER project has received funding from the European Union's Horizon 2020 research and innovation programme under grant agreement Nr.814893

References

ESL, 2019: ESL Shipping. Sustainability report 2019. Page 16. <https://view.24mags.com/eslshipping/sustainability-report-2019>

Gieschaskiel, 2017: B. Gieschaskiel, J. Vanhanen, M. Väkevä & G. Martini (2017) Investigation of vehicle exhaust sub-23 nm particle emissions, *Aerosol Science and Technology*, 51:5, 626-641, DOI: 10.1080/02786826.2017.1286291

Jalkanen, 2009: J.-P. Jalkanen, A. Brink, J. Kalli, H. Pettersson, J. Kukkonen and T. Stipa, "A modelling system for the exhaust emissions of marine traffic and its application in the Baltic Sea area", *Atmospheric Chemistry and Physics* 9 (2009) 9209-9223

Jalkanen, 2012: J.-P. Jalkanen, L. Johansson, A. Brink, J. Kalli, J. Kukkonen and T. Stipa, "Extension of an assessment model of ship traffic exhaust emissions for particulate matter and carbon monoxide", *Atmos. Chem. Phys.*, 12 (2012) 2641-2659.

MEPC, 2008: IMO Resolution MEPC 177(58), Amendments to the technological code on control of emission of nitrogen oxides from marine diesel engines, NOx Technical Code 2008, 10 October 2008.

MEPC, 2015: IMO Resolution MEPC 259(68), 2015 Guidelines for exhaust gas cleaning systems. Annex 1. 15 May 2015.

Ntziachristos, 2021: L. Ntziachristos et.al.: Monitoring of ship emissions to enforce environmental regulations. The SCIPPER project. 24th TAP conference, online, <https://www.tapconference.org/>. 30 March – 1 April 2021

Verbeek, 2017: Verbeek, Ruud, et.al.: Technical recommendations on options for specifications of monitoring equipment and database set-up: description of (high level): on board systems, data transmission, database set up, data aggregation for specific stakeholders. TNO et.al. PROMINENT WPS report, Deliverable 5.8. grand agreement 633929, June, 2017.

Winnes, 2019: Hulda Winnes, Erik Fridell, Ruud Verbeek, Jan Duyzer, Andreas Weigelt, Sokratis Mamarikas, Leonidas Ntziachristos: Gaps in current emission enforcement regulations and impacts to real-world emissions. SCIPPER deliverable D5.1, October 2019. EU Horizon 2020 project No. 814893. <https://www.scipper-project.eu/library/>.

2.23 Emission estimation and uncertainty analysis of nonroad construction machinery

Ran Tu¹, Tiezhu Li (corresponding author)¹, Chunsheng Meng¹, Jinyi Chen¹, Zhen Sheng², Yisong Xie³, Fangjian Xie³, Feng Yang³, Haibo Chen⁴, Ying Li⁵, Jianbing Gao⁴, Ye Liu⁴

¹ School of Transportation, Southeast University, Nanjing, China;

² School of Medicine, Southeast University, Nanjing, China;

³ Nanjing Institute of Ecological Environmental Protection, Nanjing, China;

⁴ Institute for Transport Studies, University of Leeds, UK;

⁵ Dynnoteq, Kington UK

turancoolgal@seu.edu.cn

Abstract

Nonroad construction machinery has become one of the major contributors to air pollution in cities, such as Particulate Matter (PM) and Nitrogen Oxides (NO_x). Current models for the nonroad machine emission estimation are usually derived from the dynamometer test, while due to varied fuel quality, engine attributes, machine maintenance, and the management of machine operation, emissions of nonroad machinery in the real-world have a huge uncertainty, and they are significantly different from those estimated by emission models. In this study, a real-time emission measurement experiment is conducted and the city-wide emissions from construction machines are explored in Nanjing, China. The operational emission factors (EFs), including Carbon Monoxide (CO), Hydrocarbon (HC), NO_x, and PM, from ten construction machines with six machine types, are measured in three activity modes (idling, moving, and working) by a Portable Emission Measurement System. The idling mode shows the least variation and the highest average CO EFs, while the working mode leads to the highest HC and PM emissions with a high variability. Variations are also identified among different machine types given similar engine attributes, possibly due to different working conditions. The model suggested EFs are in general lower than the measured EFs, leading to the underestimation of total emissions by 10% to 69%. Moreover, the uncertainty of the city-wide construction machinery emissions is illustrated from the perspective of data availability and model complexity. The coefficient of variation of the emission estimation from these two aspects ranges from 0.38 to 0.65.

Introduction

The construction industry is a great contributor to the energy consumption as well as the air pollution, especially in urban areas of developing countries due to their high population density and rapid urbanization development (Devi and Palaniappan, 2017). A strongly positive relationship between total emissions and the level of urbanization has been demonstrated in previous studies (Fan et al., 2018; Guo et al., 2020). In the Pearl River Delta Region, one of the most urbanized regions in China, nonroad machines with diesel engines are the third largest contributor of the total Nitrogen Oxides (NO_x) emissions (Zhang et al., 2019). Over 37% contributions from construction machinery to the nonroad emissions were also identified in Tianjin, another metropolitan city in the northern China (Y. Zhang et al., 2020). Most of the nonroad equipment are diesel-fueled, which are proved to be a key source for NO_x and PM emissions (Zhao et al., 2015). In 2017, the total NO_x and PM emissions from construction and agricultural machines reached 3.65 million tonnes and 320,000 million tonnes respectively in China, which were comparable to the total emissions from on-road diesel vehicles (Huanxing et al., 2020). Similarly, in 2014 of the United States, nonroad diesel machinery contributed over 35% and 44% of total mobile source NO_x and particulate matter (PM) emissions, respectively (U.S. Environmental Protection Agency, 2014).

The estimation of construction machinery emissions in previous studies depends on three major factors, the number of machines, machine activity, and the emission factor (EF) of machines. The EFs can be obtained from nonroad vehicle emission models such as NONROAD developed by the US Environmental Protection Agency (USEPA) (Marshall et al., 2012; Rasdorf et al., 2012; U.S. Environmental Protection Agency, 2005), the OFFROAD model developed by the California Air Resources Board (CARB) (Lewis et al., 2012; Rasdorf et al., 2010; Shao, 2016), and The Compilation Guide for Non-road Mobile Source Emission Inventory (the Guide) developed by the Ministry of Environmental Protection of China (Fan et al., 2018; Guo et al., 2020; Ministry of Environmental Protection of China, 2014). The model suggested EFs are usually derived from engine dynamometer tests through lab tests with the assistance of real-world measurements, where various test conditions with different engine parameters as well as after-treatment equipment can be conveniently implemented (Pirjola et al., 2017; Zhang et al., 2019). Rated power, machine types, and the emission standard the machine is obligated to, are commonly used as parameters in nonroad emission models. Particularly, EF values reported in the Guide were determined by a Portable Emission Measurement System (PEMS) on 50 typical construction machines (Guo et al., 2020).

However, due to heavy workload, excessive year of usage, and lack of maintenance, the model suggested EFs cannot represent the real-world emission of the nonroad machinery. Moreover, the uncertainty of emissions due to different machinery activity modes, varied operations, machinery types, as well as fuel types, cannot be captured by a single value provided by the model (Cao et al., 2018; Lewis et al., 2019, 2009; Sepasgozar and Blair, 2019). Previous studies have identified significant differences between the real-time measurements and the EFs from models (Abolhasani and Frey, 2013; Wang et al., 2016; Q. Zhang et al., 2020). In the study of Frey et al. (2010), the emission rate and fuel consumption of nine machinery types with various engine load and three activity modes (idling, working, and moving) were measured using a Portable Emission Measurement System (PEMS). The results showed a strong positive relationship between the time-based emission rate and engine attributes, such as engine load, power and displacement (Frey et al., 2010). Time-based emission rates of construction machinery in the working mode and the moving mode are found to be significantly higher than those from the idling mode (Abolhasani et al., 2008; Fu et al., 2012), while in terms of the fuel-based emission factor, decreasing the idling mode ratio in the machine operation can effectively reduce the additional fuel use and excess CO₂ emissions (Hu et al., 2019; Lewis et al., 2012). Due to lower combustion efficiency, worse engine wear, and less stringent emission limits, construction machines with older engines lead to higher emission rates in the real-world operation (Desouza et al., 2020; Fu et al., 2012).

Despite the breadth of emission modelling and measurements of construction machines, the uncertainty of the emission estimation, especially the variation of EFs, have seldom been investigated with real-world measurements. In addition, due to the data availability, appropriate models to estimate the emissions are varied, while the uncertainty from the model perspective has rarely been discussed in previous studies. In this paper, the construction machinery emissions are estimated based on the real-world measurement from a PEMS. The uncertainty of the EFs is captured from the measured data by differentiating activity modes and machine types. Besides the measured EFs, three sets of EFs reported in the Guide (Ministry of Environmental Protection of China, 2014), which correspond to three levels of data availability, are applied to illustrate the uncertainty from various data resolution and emission models.

Methodology

Emission measurements of nonroad construction machines were conducted in the winter of 2018 in Nanjing, China. The type and the number of construction machinery that are in use in the city, as well as their annual operating hours (when the engine is on, including both idle and operating states), were first collected through on-site interview and questionnaire. Second, machinery emissions in different activity modes were measured by a Portable Emission Measurement System (PEMS). Annual construction machinery emissions were then estimated using the EF derived from the measurement with the consideration of uncertainties on machinery type, activity mode, and operation. The results were compared with those from the Guide EFs.

Data collection

The emission estimation of construction machinery primarily depends on three factors: the number and the type of machines used, operating hour of each machine, and operational emission factors. In this study, the data for these three factors were collected from 20 representative construction sites selected in the city. In addition, total area of all construction sites in the city was also surveyed in order to estimate city-wide emissions. Questionnaires, phone calls, and individual interview were implemented to collect the information of different types of machinery, including their type of use (such as excavating and loading), model, manufacturer, age, operating hour, fuel type, fuel rate, engine type, and emission standard. In total, 126 construction machines with 8 categories and 10 sub-categories were surveyed in 20 sites. Table 1 shows the annual operating hour and the annual total fuel consumption of machines in each category. Note the working time listed in the table means the duration when the machine engine is on, which includes operating, moving, and idling time. The survey shows that the rated power of more than 90% of the construction machines is higher than 75kW with emission standards equivalent to or higher than Stage II. About 30% of machines are equal to or less than one-year-old, while more than 30% of machines have been used for seven years or longer.

Given the distribution of machinery types in Table 1, ten construction machines, including 3 cranes, 2 loaders, 2 excavators, 1 forklift, 1 concrete pump truck, and 1 sprinkler, representing 104 machines with the same machinery types at 20 construction sites, were selected for the operational emission measurement. Table 2 presents the proportion of time spent in each activity mode summarized from the survey. The specifications as well as the measurement equipment of these 10 machines are listed in Table 3. The measurement was implemented in three operational activity modes (idling, moving, and working), each lasting for 5 to 15 minutes. Noted that the moving cycle was excluded from cranes and the concrete pump truck. Second-based Carbon Monoxide (CO), Hydrocarbon (HC), Nitrogen Oxides (NO_x), and Particulate Matter (PM) emission factors (g/second) were measured by the PEMS. The fuel use rate (kg/hour) was estimated based on the carbon balance of emissions, and the fuel-based emission factors (g/kg)

can be further generated. Two types of PEMS (HPC501 and SEMTECH-DS developed by Sensors, Inc.) were utilized to measure emissions from the real-world operation. Note that Dekati eFilter was added onto SEMTECH-DS for the PM measurement. The frequency of the data record was 1Hz, except for the PM measurement from HPC501, by which only the total value of PM emissions per test was given. In this study, the fuel-based EFs (in g/kg) were adopted due to their less variability compared to the time-based results (in g/second) (Frey et al., 2010).

Table 1: Category and operating hour of construction machinery at 20 sample sites.

Type of machinery		Number	annual operating hour (excluding holidays)	
Category	Sub-category		Working time (hour)	Fuel consumption (litre)
Transport	Muck	5	2125	18875
	Loader	10	3225	33212.5
	Bulldozer	7	2350	36100
Concrete	Concrete pump truck	7	2535.7	11160.7
Excavator	excavator	64	2578.1	35207
Lifting	Crane	13	2317.3	17740.4
Industrial	Forklift	1	2250	14625
Piling	Rotary excavator	3	2750	56250
Sanitation	Sprinkler	9	2416.7	9305.6
Compaction	Roller	9	1613	19080.1

Table 2: Proportion of time spent in each activity mode for each type of machinery.

Machinery type	Activity mode	Time proportion
Crane	Idling:Working	0.1:0.9
Excavator	Idling:Moving:Working	0.1:0.2:0.7
Loader	Idling:Moving:Working	0.1:0.2:0.7
Forklift	Idling:Moving:Working	0.1:0.2:0.7
Concrete pump truck	Idling:Working	0.1:0.9
Sprinkler	Idling:Moving:Working	0.1:0.2:0.7

Table 3: Specifications of machines for the emission measurement.

ID	Machinery type	Model	Engine model	Registration	Emission standard	PEMS type	Rated power (kW)
1	Crane	Xugong	SC7H260Q5	2017.5	Stage V	HPC	192
2	Crane	XugongXCT50L5	SC9DF300.2Q5	2018.5	Stage V	SEMTECH + Efilter	219
3	Crane	Liugong5301JQZ25	ISD28550	2017.9	Stage V	SEMTECH + Efilter	204
4	Excavator	Xiagong822LG	6BG1TABFD08C2	2010.11	Stage II	HPC	120
5	Excavator	Doushan DX150W0-9C	DL06B-C3	2018.1	Stage V	SEMTECH + eFilter	103
6	Loader	Longgong	WD10G220E11	2010.4	Stage II	HPC	162
7	Loader	W156 Wheel Loader	WD10G220E21	2009	Stage II	SEMTECH + eFilter	162
8	Forklift	Longgong FD35	QC490GP	-	Stage III	SEMTECH + eFilter	36.8
9	Concrete pump truck	ACTROS5041	OM501LA.IV/3	2017.6	Stage IV	SEMTECH + eFilter	300
10	Sprinkler	5106GSS	YC4E140-30	2011.05	Stage III	SEMTECH + eFilter	105

Emission estimation

The emission estimation approach adopted in this study is provided by the Compilation Guide for Non-road Mobile Source Emission Inventory (the Guide) released by the Ministry of Environmental Protection of China (Ministry of Environmental Protection of China, 2014). In the Guide, three approaches varied by the data availability and calculation complexity are provided. When the rated power, emission standard, total number, and annual operating hour of each construction machine are available, a complex approach (M3) is suggested in the Guide, as *Equation 2*. If the rated power and the annual operating hour are not available, M2, which is less complicated than M3, is recommended as *Equation 3*. Otherwise, when only fuel usage of a specific type of machinery are collected, M1 is applied as *Equation 4*. Note in the Guide, the type of the construction machine (such as crane, excavator, and forklift) cannot be distinguished. Instead, one identical EF of each pollutant is provided to all types of construction machines given the rated power and the emission standard. In this study, M1, M2 and M3 approaches were applied respectively to calculate the total emissions from selected sites, and the value was proportionally scaled by the area to estimate total emissions from construction machines in the whole city.

$$E = \sum_j \sum_k \sum_n (P_{j,k,n} \times G_{j,k,n} \times LF_{j,k,n} \times hr_{j,k,n} \times EF_{j,k,n}) \times 10^{-6} \quad \text{Equation 2}$$

$$E = \sum_j \sum_k (Y_{j,k} \times EF_{j,k}) \times 10^{-6} \quad \text{Equation 3}$$

$$E = \sum_j (Y_j \times EF_j) \times 10^{-6} \quad \text{Equation 4}$$

Where:

E is the total amount of CO, HC, NO_x, PM_{2.5}, or PM₁₀ emissions in tonnes;

P is total number of the machine;

G is the rated power in kW/vehicle;

LF is the loading factor which is set as 0.65 based on the Guide;

hr is annual operating hour;

Y is annual fuel usage in kg (the density of diesel is adopted as 0.86 kg/L);

EF in Equation 1 and 2 is the power-based emission factor in g/kWh; in Equation 3, it is the fuel-based emission factor in g/kg;

j is the category of the nonroad machinery; k is emission standard; n is the level of the rated power that is defined in the Guide.

Due to limited onboard measurements implemented in this study, the EF (in g/kg) measured by PEMS cannot be disaggregated into a specific level of the rated power or an emission standard. Therefore, measured EFs are not applicable for M2 and M3. A modified M1, which identifies specific types of construction machines, such as crane, forklift, and excavator, was applied to estimate emissions from PEMS-based EFs. For each machinery type, the EF was the weighted average of different activity modes, the weight being the proportion of time spent in the corresponding mode. The mean value and the variation of the measured EFs from 10 selected machines were compared with the Guide-suggested EFs, which were determined by the rated power and the emission standard of each machine.

Besides, the uncertainty of PEMS-based EFs from different machinery types and activity modes was analyzed using Monte-Carlo random process. In one random iteration, for each machinery type, the EF of each activity mode was randomly selected, and the weighted average EF was calculated. The iteration was repeated for n times to generate a distribution of EFs for each machinery type. The iteration number should be large enough to reach the convergence that the mean of random sample falls into the 95% confidence interval of the population mean. In this study, n was determined as 1000. The distribution of total emissions of sampled machines was then generated using the modified M1 with the use of the EF distribution. The emission estimation from the Monte-Carlo random process was implemented in the surveyed construction sites, and the result was compared to the estimation using Guide suggested EFs. To make a fair comparison, the modified M1 is also adopted for the estimation using the Guide EFs, and the EF of each type of machine is the average value of corresponding selected machines.

Results and Analysis

Time-based emission rate and fuel-based emission factor from the measurement

Emission rates of CO, NO_x, HC, and PM were measured as time-based by the PEMS. The result shows that during the idling activity mode, the instantaneous emission rate is more stable than the other two modes, possibly due to stable engine RPM (revolution per minute). The trend of time-elapsing emission rate (black line) is consistent with existing literature (Fu et al., 2012).

Figure 1 shows the average EF for four pollutants grouped by machine types. The colored bars indicate the average value of EFs, and error bars indicate the standard deviation. Similar to the time-based emission rate, due to stable engine RPM and consequently stable fuel consumption rate, fuel-based EFs during idling generally have lower variations compared to the other two modes, especially for CO, HC, and PM. Due to varied workloads, the working mode shows a large variation on fuel-based EFs. The average fuel-based EFs in the idling activity mode, however, are not necessarily lower than other activity modes: it has the highest average CO EFs except for the forklift. However, for HC and PM, the working mode generally leads to the highest average EFs.

For each activity mode, EFs also show significant differences among machine types given similar engine attributes, which is possibly due to different working conditions. The concrete pump truck and the sprinkler have the lowest level of EFs for CO, HC, and PM. Cranes also have relatively lower CO and PM EFs. Forklifts and loaders have significantly higher HC and PM EFs. Figure 2 shows the average EF of each tested machine in three activity modes, error bars indicating the standard deviation. Comparing crane #2 and #3, with the same measurement system, rated power, and emission standard, these two machines lead to significantly different EFs especially for CO and NO_x. Similarly, although both loader #6 and loader #7 have the same rated power and emission standards, average EFs of loader #6 exceed loader #7 by 103%, 287%, and 78% for CO, NO_x, and PM, respectively. Same manufacturers but different engine types can also result in different levels of EFs. With the same manufacturer as crane #2, the average CO EF of crane #1 reaches over 90 g/kg, which is higher than crane #2 by 277% with a much larger standard deviation. With similar rated

power but less stringent emission standard, average EFs of excavator #4 can be 113%, 398%, and 69% higher than excavator #5 for CO, HC and PM EFs, respectively. This trend is consistent with the Guide, which suggests lower EFs for higher rated power or more stringent emission standards. NO_x EFs, however, present different trend: NO_x EFs of crane #1, excavator #4, and loader #6 are lower than those from the same machine types.

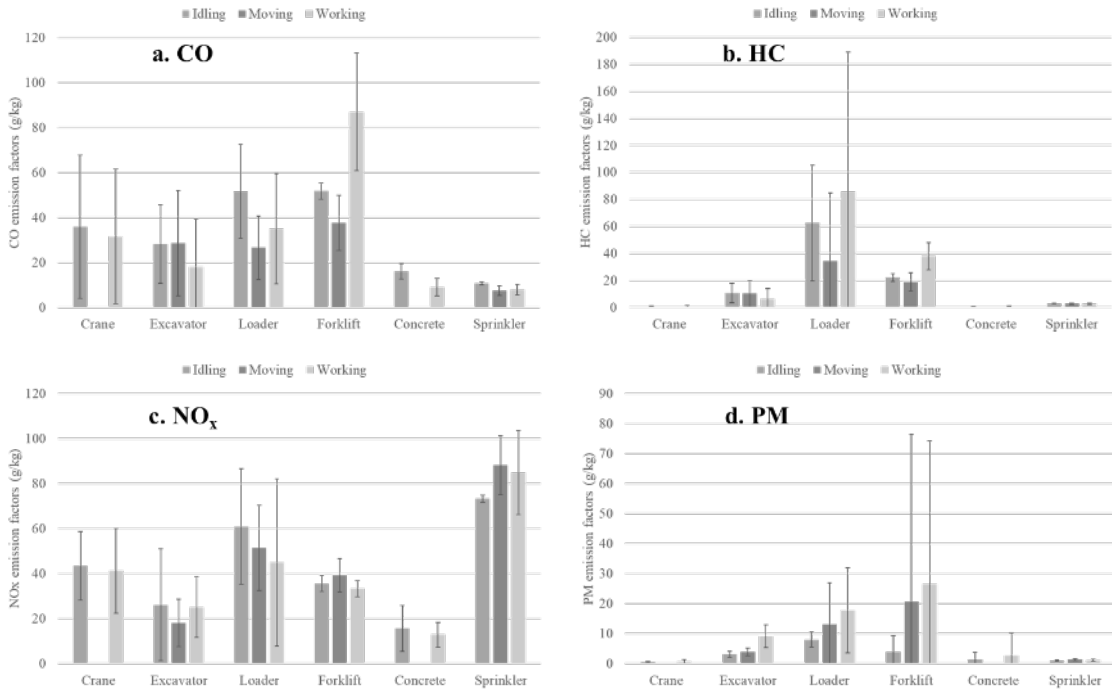


Figure 1: Fuel-based emission factors (in g/kg) of CO, NO_x, HC, and PM, for 6 types of machinery in three activity modes.

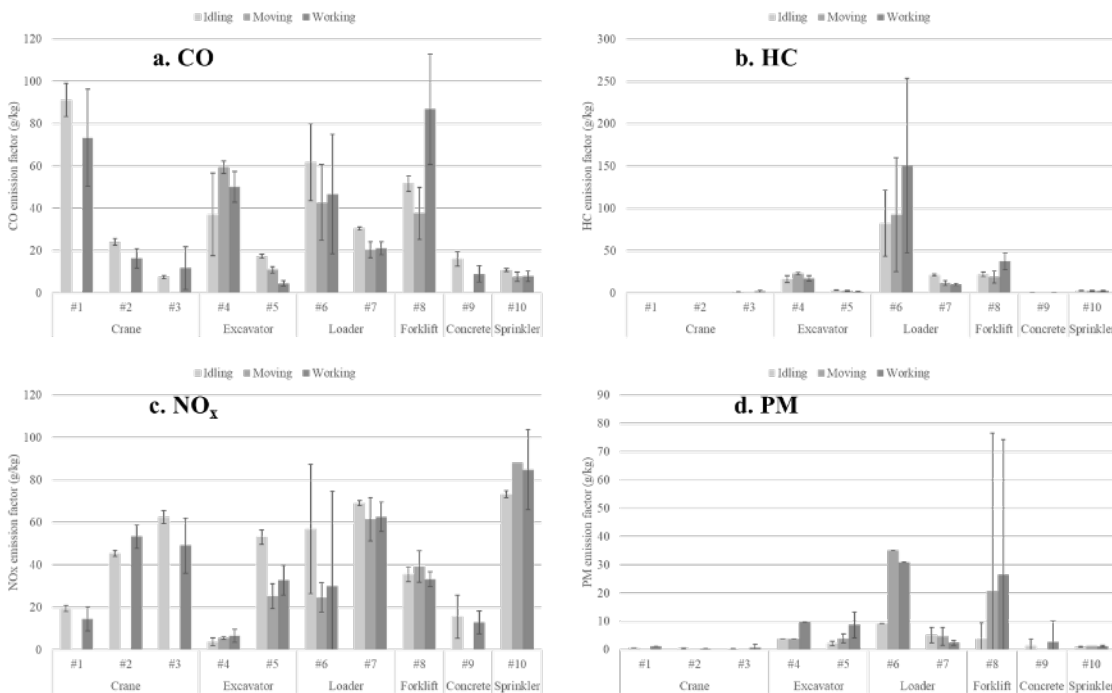


Figure 2: Mean and standard deviation of CO, NO_x, HC, and PM EFs (g/kg) for 10 measured machines.

Comparison between measured results and the Guide

A weighted average EF is calculated for each tested machine based on the activity mode proportion listed in Table 2. For each type of machine, the EF is the average value of all measured machines with the same type. The comparison between the PEMS-based weighted average EFs and the Guide-based EFs is illustrated in Figure 3. Note that PM₁₀ and PM_{2.5} which are distinguished in the Guide, cannot be differentiated by the measurement. Therefore, PM EFs from the Guide refer to PM₁₀, which includes both PM₁₀ and PM_{2.5}. All EFs of the loaders exceed the Guide suggested values. Especially for HC and PM, measured EFs of two loaders are 14 and 8 times of the suggested EFs, respectively. These two tested loaders have been used for around 10 years, with Stage II emission standard. The deterioration may be the major contribution to the extremely high measured EFs, compared to the Guide suggested values. Similar issues can also be noticed for the tested forklift. For the forklift, which was made in 2011 with Stage III standard, the measured EFs are 182%, 523%, and 196% higher than those of the Guide for CO, HC, and PM, respectively. For CO, HC, and PM, the measured EFs of excavators are higher than the Guide by 26%, 134%, and 196%, respectively. From the comparison, significant differences between the Guide EFs and measured results can be identified. EFs from the Guide, in most of the time, underestimate emissions of different machinery types. This may result from extremely high operating hours of construction machines in the city. Although the age of machine is in a reasonable range, overloaded work and a lack of maintenance may deteriorate the engine and after-treatment equipment, consequently leading to much higher EFs. Lower Guide-based EFs may further underestimate total emissions of construction sites.

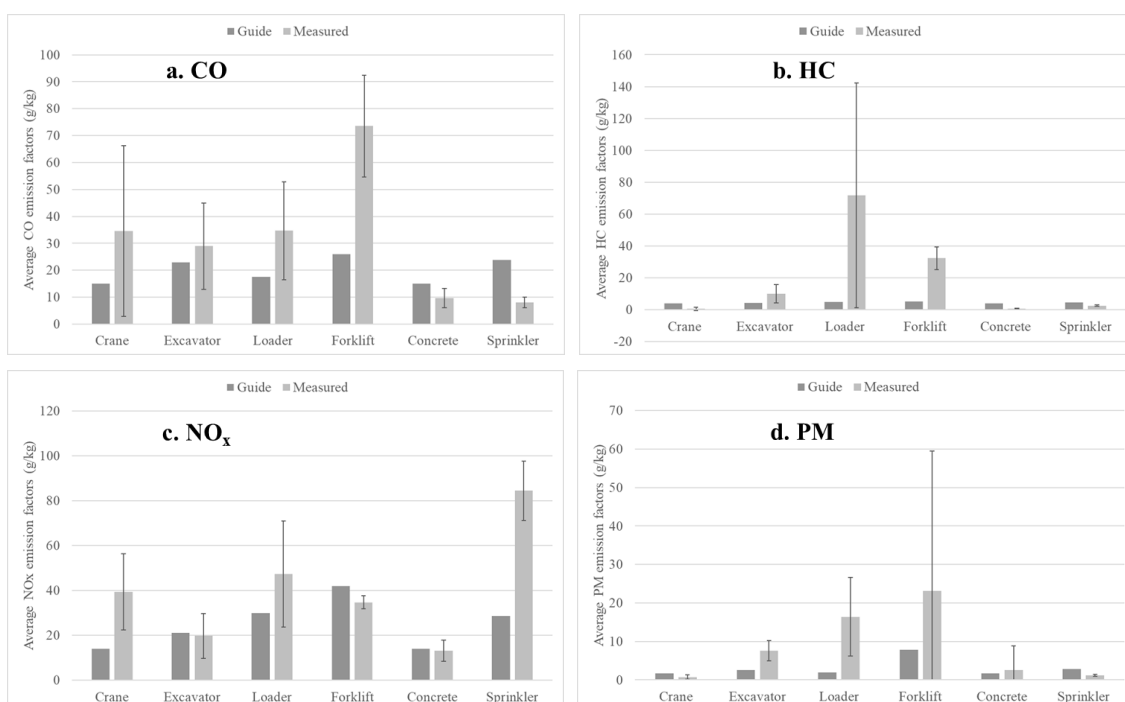


Figure 3: Average EFs of the Guide and measured results for 6 machinery types. The error bar represents the standard deviation of measured EFs.

Annual total emissions of 104 surveyed machines, which have the same machinery type as 10 measured machines at 20 construction sites, are estimated. Total emissions from both the Guide and the PEMS measurement are calculated. Figure 4 illustrates the difference of the emission estimation results between the Guide and the PEMS. Excess HC and PM emissions of loaders estimated from the PEMS EFs are demonstrated in the figure, which results from extremely high HC and PM EFs measured from the loaders as well as the large population of loaders at construction sites. Although gaps between the measured EFs and the Guide EFs of the excavators are not as large as the loaders, due to their highest population (64 in total), total CO, HC, and PM emissions from excavators using the measured EFs present significant differences to the Guide-based result. Figure 5 shows the comparison between two sets of results as well as the standard deviation of the emission estimation using the measured EFs. The relative difference is calculated using the result from the Guide-based EFs and the average measured EFs. Average total annual emissions of 104 machines estimated from the measured EFs are 60.21, 73.38, 35.19, and 19.55 tonnes for CO, NO_x, HC, and PM, respectively. The estimated CO emissions have the highest variation, followed by HC. PM emissions, however, shows the least variation. Although EFs of some machinery types are higher in the Guide than the measurement as shown in Figure 3, due to the large share of excavators and loaders as well as their high measured EFs, emissions estimated with the measured EFs are higher than those with the Guide EFs for all types of pollutants, especially for HC and PM. The Guide-based EFs underestimate the amount of CO, NO_x, HC, and PM by 10%, 26%, 69%, and 69%, respectively.

The result supports the findings in the EF comparison, that HC and PM EFs suggested by the Guide highly underestimate the real-world condition, and this consequently leads to an unignorable underestimation of total emissions.

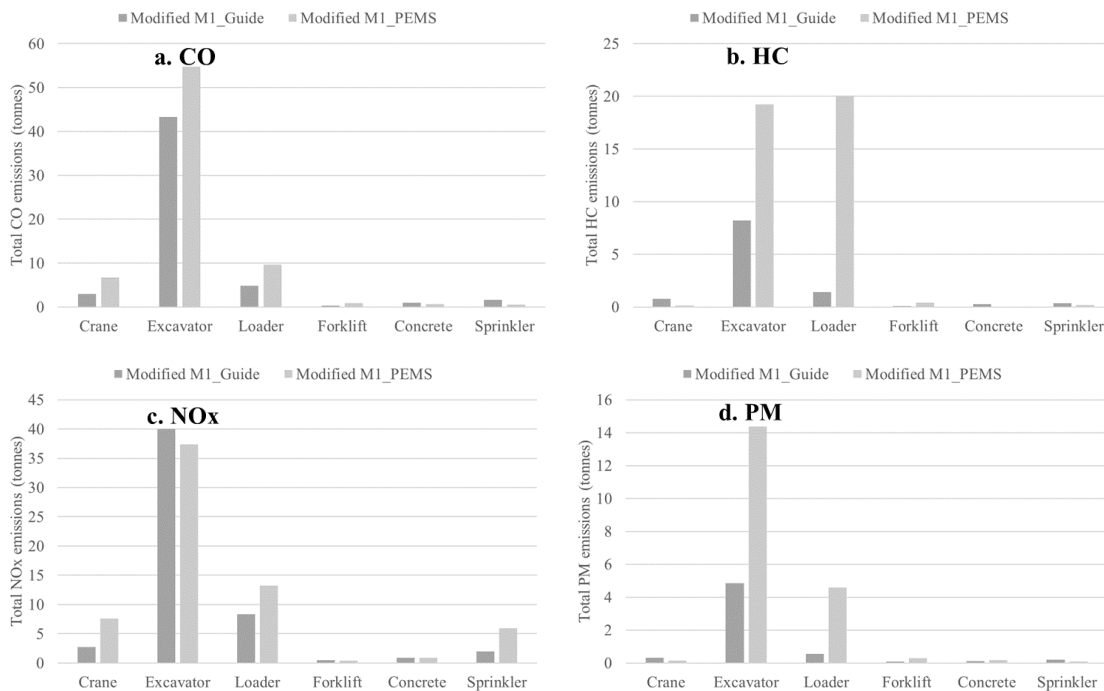


Figure 4: Total CO (a), HC (b), NO_x (c), PM (d) emissions of all construction machines with the same type as the surveyed machines in 20 construction sites. The emissions are estimated using the modified M1 method with the measured EFs and the Guide EFs, respectively.

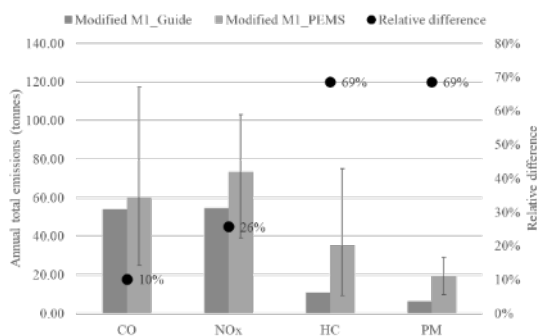


Figure 5: Total emissions of 104 machines at 20 construction sites calculated from measured EFs and Guide suggested EFs. The relative difference equals the difference between the PEMS-based result and the Guide-based result divided by the PEMS-based result.

The measured EFs of this study are compared with those from published research on the real-world non-road machinery emission measurement in the same country. Yu et al. (2020) found PM EFs are higher during working and moving conditions, which is consistent with the findings presented in this paper. The value of PM EFs for Stage I and Stage II machines measured in this paper is much higher than those in Yu et al. (2020); while for Stage III, the value of EFs shows little difference between Yu et al. (2020) and the study in this paper. The working hour presented in Hou et al. (2019) is further reviewed, which are 500 and 150 for machines with 37-75kW and 75-135kW rated power, respectively, while the annual working hours in this study are over 2000. Overworking conditions of the surveyed machines in this study may be one of the significant factors for the exceeding EFs measured. The comparison illustrates the influence of machine deterioration on EFs, suggesting a more rigorous management on the machine replacement as well as a more organized working plan of construction machines.

Comparison of different emission models with varied data availability

Emissions of all 126 surveyed machines at 20 selected construction sites are estimated by M1, M2 and M3, respectively. For M3, power-based EFs (in g/kWh) are applied. EFs used in M2 are fuel-based (in g/kg). For each pollutant, the fuel-based EF used in M1 is identical for all construction machines. The city-wide emissions of construction machines are scaled from the results of the surveyed sites by the ratio of area. In total, city-wide annual

emissions of CO, NO_x, HC, PM₁₀, and PM_{2.5} from construction machines are estimated as 1590.54, 4865.09, 502.98, 310.1, and 310.10 tonnes respectively by M1; 3185.32, 3994.65, 719.25, 240.38, and 225.96 tonnes respectively by M2. By M3, the estimation is 6353.60, 8669.73, 1516.57, 504.96, and 476.49 tonnes, respectively. The comparison shows that emissions estimated by different approaches with various data resolution can show a significant difference. The coefficient of variation for five emission types ranges from 0.38 to 0.65 as depicted in Figure 6c. The estimation of CO has the highest CV (0.65), followed by the HC (0.58). Due to more specific information on the emission standards and the level of rated power, the result of M2 can be more accurate than M1, which only applies a flat EF for all machine types. By specifying the value of rated power, emissions estimated by M3 are twice of those from M2. However, because of different calculation methods and units of EFs, it is hard to determine which one is closer to the real-world condition.

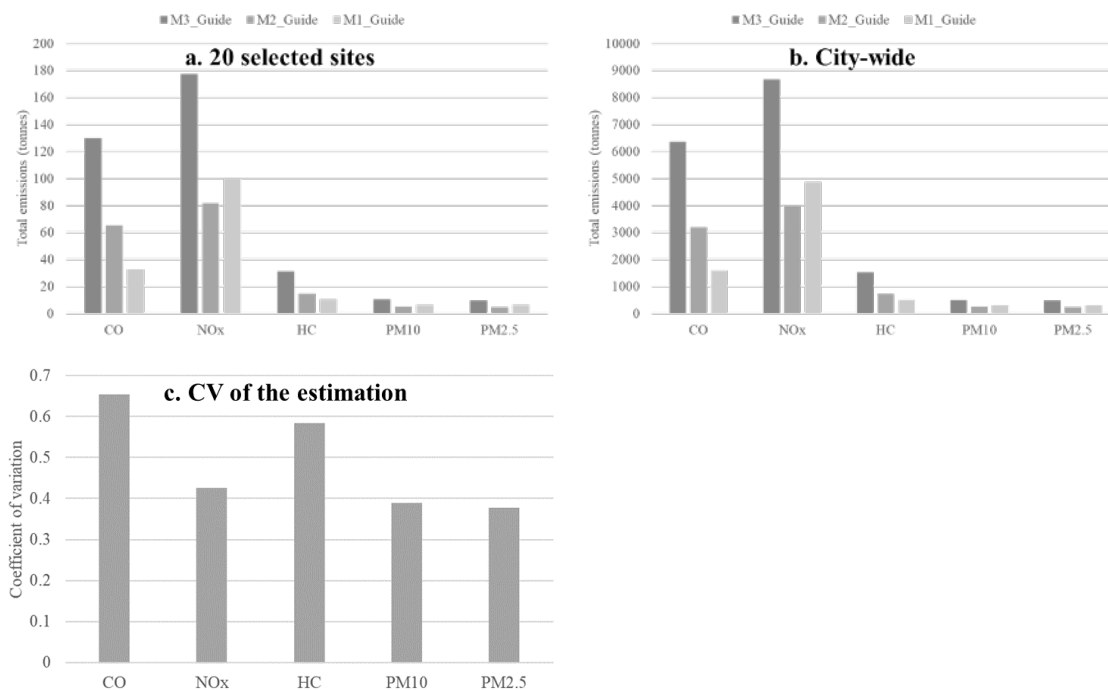


Figure 6: Total annual emissions at 20 selected construction sites (a), the whole city (b), and the coefficient of variation (CV) for three estimation methods (c).

Conclusion

In this study, air pollutant emissions, including CO, HC, NO_x, and PM, from nonroad construction machines were estimated. Fuel-based emission factors (EFs) of 10 construction machines in six machinery types and three activity modes were measured. EFs from the idling activity mode generally have lower average EFs with smaller variations, while the working mode leads to the highest variation with relatively high EFs. From the comparison of EFs among 10 machines, EFs become higher with lower rated power or less stringent emission standard, which is consistent with the trend of the EFs suggested by the Guide. Given similar engine attributes, EFs are varied among different machine types, which possibly results from varied working condition of the machine. Comparing the measured EFs with the Guide-suggest EFs, it is found that in general, the measured EFs are higher than those from the Guide. Consequently, the Guide-based EFs underestimate the amount of all emission types, which can be 10% to 69% lower than those estimated from the measured EFs. Finally, city-wide annual emissions of construction machines are scaled from the total emissions of 20 selected sites with the application of M1, M2, and M3 of the Guide. With the same estimation approach but more specific information on rated power and emission standards, M2 generates higher CO and HC estimations than M1. M3 leads to the highest estimation results among all three methods. The coefficient of variation among the estimation from three methods ranges from 0.38 to 0.65.

The results of this study demonstrate a wide source of uncertainties in the emission estimation for nonroad machines, including the activity mode, the instantaneous EFs, the type of machinery, and the estimation model. The result of this study highlights possible improvements that can be further investigated for the bottom-up nonroad machine emission estimation. From the EF perspective, besides variations on the rated power and emission standards that have been identified by the Guide, different activity modes can also lead to varied EFs and thus should be taken into consideration. Another issue in the Guide is that it classifies all construction machines as a single category. However, due to different workloads, masses, and power, construction machines should be further categorized into different types of use and

the EFs should be provided correspondingly. More real-world measurements covering sufficient samples for different levels of rated power, emission standards, manufacturers, ages, and machine types should be conducted in the future in order to generate more representative EFs and to estimate emissions from a more disaggregated level. Meteorological factors such as temperature and weather conditions may have significant impacts on machine emissions; thus, seasonal EFs should be explored as well. Second, the city-wide emission estimation in this paper is scaled from the selected construction sites. However, large uncertainties exist in terms of the operating hour, the daily fuel usage, and the share of activity modes for different machinery types, which can be varied among construction sites and individual machines. Therefore, regulated surveys and reliable monitoring are needed in the city to establish a more accurate emission estimation result with a high spatio-temporal resolution.

Acknowledgement

The research in this paper was jointly supported by Nanjing Institute of Ecological Environmental Protection (Nanjing, China), the National Natural Science Foundation of China (No. 41877395), the EU-funded project MODALES (grant agreement No 815189), and DYNNOTEQ.

References

- Abolhasani, S., Frey, H.C., 2013. Engine and duty cycle variability in diesel construction equipment emissions. *J. Environ. Eng. (United States)* 139, 261–268. [https://doi.org/10.1061/\(ASCE\)EE.1943-7870.0000548](https://doi.org/10.1061/(ASCE)EE.1943-7870.0000548)
- Abolhasani, S., Frey, H.C., Kim, K., Rasdorf, W., Lewis, P., Pang, S.H., 2008. Real-world in-use activity, fuel use, and emissions for nonroad construction vehicles: A case study for excavators. *J. Air Waste Manag. Assoc.* 58, 1033–1046. <https://doi.org/10.3155/1047-3289.58.8.1033>
- Cao, T., Russell, R.L., Durbin, T.D., Cocker, D.R., Burnette, A., Calavita, J., Maldonado, H., Johnson, K.C., 2018. Characterization of the emissions impacts of hybrid excavators with a portable emissions measurement system (PEMS)-based methodology. *Sci. Total Environ.* 635, 112–119. <https://doi.org/10.1016/j.scitotenv.2018.04.011>
- Desouza, C.D., Marsh, D.J., Beevers, S.D., Molden, N., Green, D.C., 2020. Real-world emissions from non-road mobile machinery in London. *Atmos. Environ.* 223, 117301. <https://doi.org/10.1016/j.atmosenv.2020.117301>
- Devi, L.P., Palaniappan, S., 2017. A study on energy use for excavation and transport of soil during building construction. *J. Clean. Prod.* 164, 543–556.
- Fan, W., Chen, J., Li, Y., Jiang, T., Sun, S., Wang, G., Liao, H., Jiang, T., Wu, K., Qian, J., Ye, H., 2018. Study on the non-road mobile source emission inventory for sichuan province. *China Environ. Sci.* 38, 4460–4468.
- Frey, H.C., Rasdorf, W., Lewis, P., 2010. Comprehensive field study of fuel use and emissions of nonroad diesel construction equipment. *Transp. Res. Rec.* 2158, 69–76.
- Fu, M., Ge, Y., Tan, J., Zeng, T., Liang, B., 2012. Characteristics of typical non-road machinery emissions in China by using portable emission measurement system. *Sci. Total Environ.* 437, 255–261. <https://doi.org/10.1016/j.scitotenv.2012.07.095>
- Guo, X., Wu, H., Chen, D., Ye, Z., Shen, Y., Liu, J., Cheng, S., 2020. Estimation and prediction of pollutant emissions from agricultural and construction diesel machinery in the Beijing-Tianjin-Hebei (BTH) region, China☆. *Environ. Pollut.* 260, 113973. <https://doi.org/10.1016/j.envpol.2020.113973>
- Hou, X., Tian, J., Song, C., Wang, J., Zhao, J., Zhang, X., 2019. Emission inventory research of typical agricultural machinery in Beijing, China. *Atmos. Environ.* 216, 116903. <https://doi.org/10.1016/j.atmosenv.2019.116903>
- Hu, Q., Huang, C., Qiao, L., Ma, Y., Yang, Q., Tang, W., Zhou, M., Zhu, S., Lou, S., Tao, S., Chen, Y., Li, L., 2019. Speciated PM composition and gas and particle emission factors for diesel construction machinery in China. *Aerosol Air Qual. Res.* 19, 1820–1833. <https://doi.org/10.4209/aaqr.2018.07.0272>
- Huanxing, C., Gang, L., Ying, Y., Liang, J., Shunli, L., 2020. Review and outlook of China non-road diesel mobile machinery emission standards stricter emissions standards for better air quality in China. *Johnson Matthey Technol. Rev.* 64, 76–83. <https://doi.org/10.1595/205651320x15730367457486>
- Lewis, P., Frey, H.C., Rasdorf, W., 2009. Development and use of emissions inventories for construction vehicles. *Transp. Res. Rec.* 46–53. <https://doi.org/10.3141/2123-06>
- Lewis, P., Karimi, B., Shan, Y., Rasdorf, W., 2019. Comparing the economic, energy, and environmental impacts of biodiesel versus petroleum diesel fuel use in construction equipment. *Int. J. Constr. Educ. Res.* 15, 276–290. <https://doi.org/10.1080/15578771.2018.1483982>

- Lewis, P., Leming, M., Rasdorf, W., 2012. Impact of engine idling on fuel use and CO₂ emissions of nonroad diesel construction equipment. *J. Manag. Eng.* 28, 31–38. [https://doi.org/10.1061/\(ASCE\)ME.1943-5479.0000068](https://doi.org/10.1061/(ASCE)ME.1943-5479.0000068)
- Marshall, S.K., Rasdorf, W., Lewis, P., Frey, H.C., 2012. Methodology for estimating emissions inventories for commercial building projects. *J. Archit. Eng.* 18, 251–260. [https://doi.org/10.1061/\(ASCE\)AE.1943-5568.0000073](https://doi.org/10.1061/(ASCE)AE.1943-5568.0000073)
- Ministry of Environmental Protection of China, 2014. The Compilation Guide for Non-road Mobile Source Emission Inventory (trial edition).
- Pirjola, L., Rönkkö, T., Saukko, E., Parviainen, H., Malinen, A., Alanen, J., Saveljeff, H., 2017. Exhaust emissions of non-road mobile machine: Real-world and laboratory studies with diesel and HVO fuels. *Fuel* 202, 154–164. <https://doi.org/10.1016/j.fuel.2017.04.029>
- Rasdorf, W., Frey, C., Lewis, P., Kim, K., Pang, S.H., Abolhassani, S., 2010. Field procedures for real-world measurements of emissions from diesel construction vehicles. *J. Infrastruct. Syst.* 16, 216–225. [https://doi.org/10.1061/\(ASCE\)IS.1943-555X.0000027](https://doi.org/10.1061/(ASCE)IS.1943-555X.0000027)
- Rasdorf, W., Lewis, P., Marshall, S.K., Arocho, I., Frey, H.C., 2012. Evaluation of On-Site Fuel Use and Emissions over the Duration of a Commercial Building Project. *J. Infrastruct. Syst.* 18, 119–129. [https://doi.org/10.1061/\(ASCE\)IS.1943-555X.0000071](https://doi.org/10.1061/(ASCE)IS.1943-555X.0000071)
- Sepasgozar, S.M.E., Blair, J., 2019. Measuring non-road diesel emissions in the construction industry: a synopsis of the literature. *Int. J. Constr. Manag.* 0, 1–16. <https://doi.org/10.1080/15623599.2019.1573479>
- Shao, Z., 2016. Non-road emission inventory model methodology. *Int. Counc. Clean Transp.*
- U.S. Environmental Protection Agency, 2014. 2014 National Emissions Inventory Report (Retrieved in May 2020).
- U.S. Environmental Protection Agency, 2005. NONROAD2005 Model.
- Wang, F., Li, Z., Zhang, K., Di, B., Hu, B., 2016. An overview of non-road equipment emissions in China. *Atmos. Environ.* 132, 283–289. <https://doi.org/10.1016/j.atmosenv.2016.02.046>
- Yu, F., Li, C., Liu, J., Liao, S., Zhu, M., Xie, Y., Sha, Q., Huang, Z., Zheng, J., 2020. Characterization of particulate smoke and the potential chemical fingerprint of non-road construction equipment exhaust emission in China. *Sci. Total Environ.* 723, 137967. <https://doi.org/10.1016/j.scitotenv.2020.137967>
- Zhang, Q., Yang, L., Ma, C., Zhang, Y., Wu, L., Mao, H., 2020. Emission characteristics and chemical composition of particulate matter emitted by typical non-road construction machinery. *Atmos. Pollut. Res.* 11, 679–685. <https://doi.org/10.1016/j.apr.2019.12.018>
- Zhang, Y., Lou, D., Tan, P., Hu, Z., 2019. Experimental study on the emission characteristics of a non-road diesel engine equipped with different after-treatment devices. *Environ. Sci. Pollut. Res.* 26, 26617–26627. <https://doi.org/10.1007/s11356-019-05839-y>
- Zhang, Y., Zhou, R., Peng, S., Zhang, X., Mao, H., Zhu, L., Li, X., Zheng, L., Wang, Y., 2020. Study on emission characteristics of non-road mobile source pollutants in Tianjin. *IOP Conf. Ser. Earth Environ. Sci.* 467. <https://doi.org/10.1088/1755-1315/467/1/012163>
- Zhao, Y., Qiu, L.P., Xu, R.Y., Xie, F.J., Zhang, Q., Yu, Y.Y., Nielsen, C.P., Qin, H.X., Wang, H.K., Wu, X.C., Li, W.Q., Zhang, J., 2015. Advantages of a city-scale emission inventory for urban air quality research and policy: The case of Nanjing, a typical industrial city in the Yangtze River Delta, China. *Atmos. Chem. Phys.* 15, 12623–12644. <https://doi.org/10.5194/acp-15-12623-2015>

2.24 A novel real driving emissions mapping model at a road-segment scale

M. Laraki^{1*}, G. De Nunzio¹, L. Thibault¹, P. Dégeilh¹, S. Rodríguez¹, B. Ribstein², F. Mahé²,
B. Rocher³, D. Piga³

¹IFP Energies nouvelles, Solaize, France

²ARIA Technologies, Boulogne-Billancourt, France

³Atmo Sud, Marseille, France

mohamed.laraki@ifpen.fr

Abstract

Road traffic emissions are a major source of atmospheric pollution. Understanding those emissions sources and their impacts on air quality is mainly done by experimental measurements that are often expensive for large-scale usage. In this paper, an approach to estimate road traffic emissions on any road segment and their impact on air quality is proposed. A driving behavior model, calibrated with recorded speed trajectories, is used to generate representative dynamic speed profiles on any road segment. It takes macroscopic and traffic information, available everywhere, as inputs. It is then combined with a microscopic emissions model with different vehicle fleet compositions. The calculation of the overall road traffic emissions on every link of the road network is performed by considering the traffic volume estimated in the network by traffic detectors or traffic models. Finally, estimated road traffic emissions are combined with other emission sources as inputs of an atmospheric dispersion model to quantify the air quality with an increased spatial and temporal resolution on a road network. Each block of the proposed modeling framework is validated independently. Promising results are obtained in terms of reproducing real driving behaviors, validating emissions with experimental data, and getting low pollutants concentration errors while comparing to measured annual averages in different areas. A map of NO_x concentration in a traffic light scenario, with three different fleet compositions, is presented as an application of the proposed framework.

Introduction

According to the World Health Organization (WHO), about 18 000 deaths per day are due to poor air quality (IEA, 2016). The transport sector still represents one of the most important sources of pollutants, it is responsible for around 50% of NO_x emissions and around 10% of PM_{2.5} emissions. The limit values set by the European Commission are repeatedly exceeded by many countries on the European territory. The European Environment Agency recently emphasized (European Environment Agency, 2018) that current air quality monitoring tools are not able to accurately estimate the contribution of real driving emissions or identify critical areas. For large road networks, the estimation of pollutant emissions is usually based on a macroscopic method adapted to large scales, typically road-segments of several kilometers so that the route can be considered as representative of all the traffic conditions. Such methods are not able to accurately take into account real driving conditions, road infrastructure, and the traffic regulation measures on vehicle pollutant emissions.

More and more traffic data are becoming easily available with the recent evolution in Intelligent Transportation Systems. New models and methods for traffic-related predictions can accordingly be introduced. Accurate dynamic speed estimation is of particular interest. It can lead to a better overall understanding of driving behavior and result in learning traffic factors that affect drivers' actions.

In this work, we build on the results of (Laraki, De Nunzio, & Thibault, 2020) and extend the application of the driving behavior model to the road traffic emissions estimation, and air quality evaluation with extensive validation and comparison results. The used driving behavior model constructs speed trajectories on any road-segment even with no recorded trajectories. It takes as inputs macroscopic data (road infrastructure, topology, etc.) that are available through commercial Geographic Information System (GIS). The model is able to reproduce real driving behavior on a high spatial resolution. It has been trained and validated on a large database of 1-Hertz driving recordings. Estimated speed trajectories were compared to these driving recordings and promising results have been obtained in terms of reproducing real driving behavior. An extension of this validation is proposed in this paper.

In order to accurately estimate pollutant emissions from the predicted driving behavior, an adapted microscopic vehicle emissions model should be used. Indeed, the pollutant emissions level is strongly road-segmented to the driving behavior, regardless of the vehicle and its technologies. For the same itinerary, and with the same car, the level of pollutant emissions can be tripled between two drivers, depending on how they drive. Several microscopic models exist but they are mostly designed for offline studies (Ma, Andréasson, & Chen, 2012). They are often coupled with microscopic traffic simulators which provide the 1-Hertz speed profile (Badin, et al., 2017). Unfortunately, there is an important gap between simulated and measured speed profiles and therefore pollutant emissions, as illustrated in

(Nam, Gierczak, & Butler, 2003). Also, most of those microscopic emissions models cannot be used for a large road network due to their computational time. The model proposed in (Thibault, et al., 2016) is used. This microscopic emissions model has been optimized for large-scale usage (road network) and can cover even the most recent pollutants after-treatment technologies. Experiment validation of this model with recent vehicle technologies will be presented in this paper.

The last block of the proposed modeling approach aims to quantify the traffic emissions impact, with a high spatial and temporal resolution, at the air quality level. Most of the easy-to-use models of atmospheric dispersion in built-up areas rely on Gaussian models such as ADMS-Urban (McHugh, Carruthers, & Edmunds, 1997) or PRIME (Schulman, Strimaitis, & Scire). Such models are able to consider the effects of the individual buildings and the global street network on the dispersion. However, they fail to accurately take into account heterogeneous urban structures. On the other hand, Computational Fluid Dynamics (CFD) models provide very accurate solutions by solving the Navier-Stokes equations, thus properly accounting for complex flows in any configuration. These models can be classified according to the range of the modeled and/or resolved scales (Camelli, Hanna, & Lohner, 2004; (Gowardhan, Pardyjak, Senocak, & Brown, 2007)). However, CFD solutions often suffer from extreme computational times. Thus, the Lagrangian stochastic modeling approach can be the best compromise between simple Gaussian models and advanced CFD models. Lagrangian models simulate the dispersion of the airborne pollutant with virtual particles, each representing a mass of the released substance. Their diffusions are respectively influenced by the wind and by the velocities obtained as solution of Langevin stochastic differential equations, able to reproduce the turbulent flow properties.

To accurately take into account the impact of buildings on the dispersion of pollutants with a reasonable computational time and with a high 3D field grid resolution, the Parallel Micro SWIFT SPRAY (PMSS) (Oldrini, Olry, Moussafir, & Armand, 2011) is used as the atmospheric dispersion model. PMSS is the parallel version of the Micro SWIFT SPRAY (MSS) model. MSS is a combination of a mass-consistent diagnostic 3D wind-field model (Micro-Swift) and the Lagrangian Particle Dispersion Model (Micro-Spray). The PMSS has been validated on numerous measurement campaigns carried out by the US Department of Defense as well as on measurements in atmospheric wind tunnels.

The proposed modeling approach focuses on the estimation of vehicular traffic pollutant emissions in each road-segment of a network. Those traffic pollutant emissions are then combined with an atmospheric dispersion model to quantify their impact on the air quality. Firstly, the objective is to exploit and validate a generalized approach for the estimation of vehicle speed trajectory at a road-segment scale. Secondly, a microscopic vehicle and pollutant emissions model is used and adapted to be able to convert the estimated driving behavior into vehicle emissions. In this paper, we propose to validate this microscopic emissions model with recent vehicle technologies. Thirdly, the vehicle emissions are converted into the emissions of an equivalent vehicle representing the vehicle's fleet circulating in the considered area obtained from public statistical studies. The calculation of the overall road traffic emissions on every road-segment of the road network is performed by considering the traffic volume estimated in the network by traffic detectors or traffic models. Lastly, estimated road traffic emissions are combined with other emission sources as inputs of an atmospheric dispersion model to quantify the pollutants atmospheric dispersion with an increased spatial and temporal resolution on a road network. An illustration of the modeling framework is shown in Figure 1. In the next section, the methodology and the main modeling blocks proposed to attain this goal are described in detail.

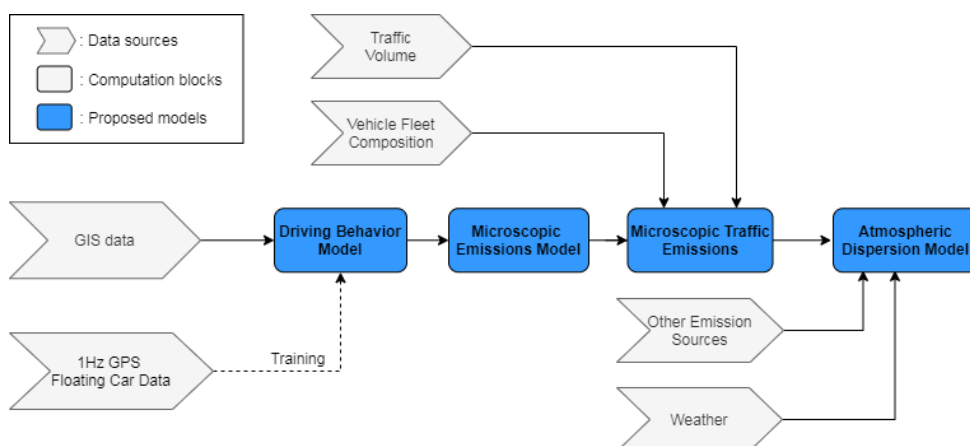


Figure 1: Illustration of the overall approach to translate macroscopic road information into road traffic environmental impact. This work focuses on the central blocks computing the microscopic vehicle emissions from only macroscopic available data.

The contributions of this work are twofold:

- The proposed modeling approach is able to estimate microscopic road traffic emissions and the pollutants atmospheric concentrations, with an increased spatial and temporal resolution, on any road network. Such a resolution is very valuable to identify critical areas in terms of air quality and understand what road-segments should need careful investigation.
- This proposed framework is evaluated with an exhaustive validation of each block. Firstly, the driving behavior model is compared to real-world speed trajectories. Then the used microscopic emissions model is compared to Portable Emissions Measurement System (PEMS) measurements and with other experimental measurements with recent vehicle technologies. Finally, estimated emissions concentrations are compared to measured annual concentrations averages on various locations.

The paper is organized as follows. Section 2 describes the driving behavior model. The employed microscopic emissions model, the meta-modeling approach to convert individual vehicle emissions into road traffic emissions, and the used atmospheric dispersion model are presented in Section 3. Finally, a thorough validation analysis of each constituting block of the proposed model is given in Section 4. Concluding remarks and main results are summarized in Section 5.

Driving behavior model

Real-world driving speed measurements are not available everywhere and generally difficult to obtain. Nowadays, the advent of vehicles connectivity and intelligent transportation systems is making driving data increasingly easy to acquire. However, often, the spatial and temporal coverage of these data is not sufficient to establish an accurate driving behavior model on each road-segment of the road network. Thus, in order to predict driving behavior on any road-segment, even in absence of pre-recorded driving data, the proposed model aims to relate macroscopic road and traffic data available everywhere through commercial GIS (e.g. (HERE MAPS)) to typical dynamic (i.e. time-variant) vehicle speed trajectories. The proposed driving behavior model is defined in a machine learning framework as a sequence of cascaded sub-models which are inspired by empirical observation of real-world driving and traffic data (De Nunzio, Laraki, & Thibault, 2021).

For the design of the model, a data-set of real-world driving Floating Car Data, recorded with the *Geco air* application (Geco air, 2017), is used. This application records automatically the 1-Hertz Global Positioning System (GPS) signal when the user is moving to provide him a feedback on the individual environmental footprint of his mobility. The model is trained in the Greater Paris and Lyon area (France), consisting of approximately 200 thousand road-segments and over 2 million data samples, or observations (i.e. driving profiles). Those data include several information recorded at a high frequency (1Hz):

- Timestamp
- Speed
- Heading and slope angles
- Latitude/Longitude
- GPS data accuracy

The structure of the model is illustrated in Figure 2 and described briefly in the following.

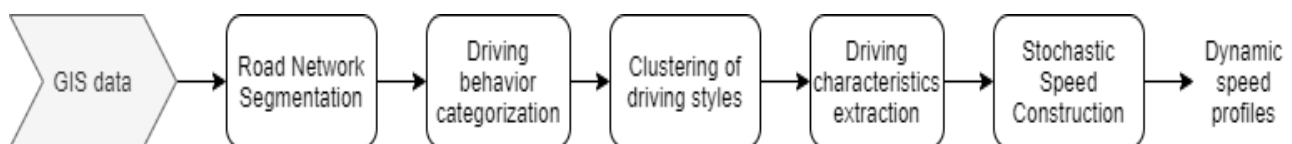


Figure 2: Illustration of the cascaded driving behavior model.

- **GIS data:** These data can be provided by several GIS (Here Maps, Google Maps, OpenStreetMap, etc.). Each GIS proposes a decomposition of the road network into road-segments. A road-segment is defined as an elementary link between two nodes of the network on which there is no variation of the road-segment attributes. Those attributes include traffic signs presence (Stop, yield, traffic light...), functional class (hierarchical classification of the road-segment), number of lanes, speed limit, free flow speed etc...
- **Road network segmentation:** For each road-segment, the speed trajectory for a vehicle heavily varies, depending on where the vehicle comes from and where it is going. Therefore, the first step is to separate the road-segments into road-segment triplets, covering all the origin and destination options for the same road-segment.

- **Driving behavior categorization:** Speed trajectories can share similar shapes and characteristics, depending on macroscopic descriptors of the road features (signalization, curvature...): in the second step of the approach, a heuristic decision tree is built, depending on macroscopic descriptors, to group similar speed characteristics in the same category.
- **Clustering of driving styles:** Speed trajectories dispersion in a category can still be high because there can be several groups of vehicle speed trajectories in the same triplet. A clustering method is therefore used to identify the most representative driving behaviors (class) for each category.
- **Driving characteristics extraction:** Each identified class has a typical speed trajectory. Before being able to construct it, the fourth step is to link road-segment cluster characteristics to macroscopic variables. A supervised learning algorithm is used to estimate speed characteristics (inlet, outlet speed, stopping point) for each class of each road-segment depending on the considered macroscopic variables (signalization, number of connected road-segments, network hierarchy...)
- **Stochastic speed construction:** The last step is to construct for each class of each road-segment a representative speed trajectory depending on the estimated driving characteristics. A probabilistic approach, based on multi-dimensional discrete probability density functions (PDF), is used to approximate the stochastic part of the driving behavior, which deterministic approaches fail to capture. The approach is able to construct dynamic speed trajectories by iteratively estimating the accelerations from the road-segment inlet to the outlet.

Microscopic emissions and dispersion models

Microscopic emissions model

The dynamic speed profiles obtained as an output of the driving behavior model can be now fed into a microscopic energy consumption and emissions model of the vehicle.

The model proposed in (Thibault, et al., 2016) is used as the microscopic emissions model. It has been validated experimentally using PEMS, engine and roller test beds, on a large variety of vehicles from different technologies and emission standards. The model is easy to use and is optimized for large scale usage (road network).

Figure 3 shows the cloud computing architecture used to estimate pollutant emissions from GPS measurements. The four inputs of this calculation, provided by the user smartphone are the registration number of the vehicle (ID) and GPS measurements automatically recorded (i.e. position, speed and altitude).

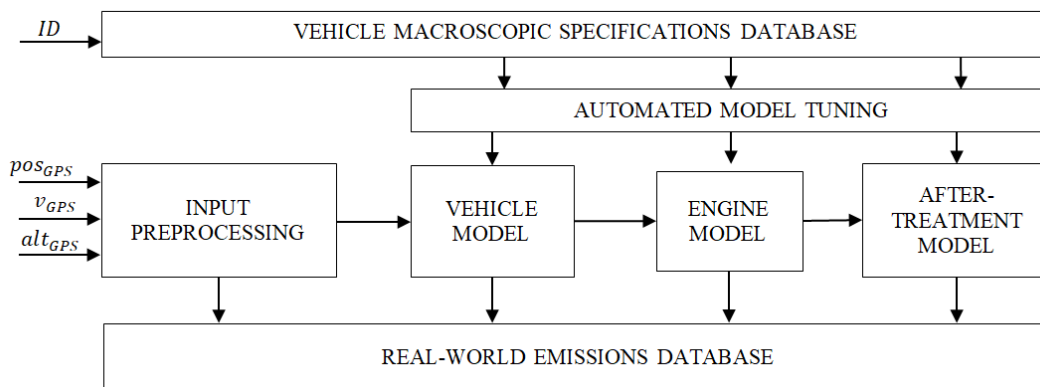


Figure 3: Vehicle pollutant emissions model scheme.

The choice of the right modeling level is a trade-off between precision, number of input parameters, and computation time. The desired models should be able to catch the impact of real-world driving conditions and to identify situations where pollutant emissions are particularly high or low. Moreover, the model has to deal with inputs sampled at low rates, typically 1Hz, as provided by the GPS sensor of most smartphones. This is a critical point because the creation of pollutant emissions occurs during an engine cycle, typically few milliseconds.

An important remark is that the models are not based on the results of a standard driving cycle (such as the New European Driving Cycle (NEDC)), which often fails to represent real on-road conditions. On-road and on-cycle emissions can be widely different for some pollutants and some engine technologies. The models integrate realistic engine and after-treatment calibrations, which is essential for real-world emissions modeling.

In this work, the dynamic speed profiles obtained as an output of the driving behavior are used instead of GPS data. Also, to reduce the computational time, optimal and most representative vehicles of a fleet composition are pre-tuned before being used in the emissions computation.

Microscopic traffic emissions

The third block of the proposed modeling approach aims to combine the driving behavior model and the single-vehicle microscopic emissions model and to extend the results at the traffic level. In other words, once the pollutant emissions of one vehicle are calculated on one road-segment based on the estimated driving behavior, it is necessary to calculate the overall emissions of all the vehicles in the whole road network under analysis.

Vehicle fleet composition

In order to compute the contribution to the overall emissions of all possible vehicle powertrains and after-treatment technologies, the vehicle fleet composition in the considered geographic area needs to be estimated. In this work, the estimation of the vehicle fleet composition is not addressed, and it is considered as a data source. The statistical vehicle fleet composition is constructed from available public reports (CITEPA, 2020). Those reports give an estimate of the fleet composition for each road type: urban, suburban and highway. Vehicle type includes passenger car, light-duty, heavy-duty, bus and two-wheelers.

For each road type, the fleet composition includes statistical proportions according to the vehicle type, powertrain, European standard emission and vehicle segment. Each combination of those variables defines a vehicle category.

- **Vehicle type:** ranging from passenger car, light-duty, heavy-duty, bus and two-wheelers.
- **Powertrain:** Ranging from conventional (Diesel, gasoline), to hybrid and electric vehicles.
- **European standard emissions:** ranging from Euro 0 to Euro 6 emissions standards.
- **Segment:** defining various engine displacement or vehicle weight categories.

Figure 4 illustrates an example of vehicles distribution evolution for passenger car according to different European standards emissions in urban areas. A noticeable decrease in Euro 0 contribution of almost 100% is observed from 1990 to 2019. More recent Euro 6 vehicles start to take an important share of almost 30% in 2019.

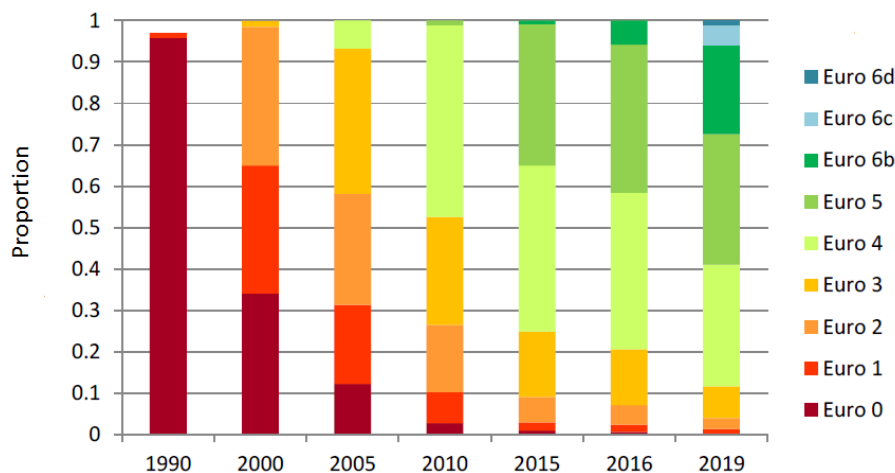


Figure 4: Passenger car distribution evolution for different European standards emissions in urban areas.

Note that all the previously defined vehicle categories are defined in the microscopic emissions model described in the previous section.

The equivalent emissions of a vehicle representing the entire fleet are simply obtained via a weighted sum of the individual emissions of each vehicle category indicated in the fleet composition, where each weight corresponds to the proportion of each vehicle category in the total fleet composition.

Traffic volume

In order to correctly evaluate the impact of traffic volume on the pollutant emissions, the emissions of the equivalent vehicle representing the whole fleet needs to be multiplied by the estimated number of vehicles on every road-segment of the considered road network. Usually, this information is given by macroscopic traffic models calibrated on real-world traffic counts as an average annual daily traffic (AADT). This is also the typical data source and input for other

state-of-the-art macroscopic traffic emission models, such as COPERT (Ntziachristos, Gkatzoflias, Kouridis, & Samaras, 2009), in which the total traffic emission is obtained as the product of AADT and emission factors as a function of an average driving speed. Note that our approach is microscopic because both the driving behavior model and the vehicle emissions model are dynamic and microscopic (i.e. consideration of speed dynamics, road slope, road infrastructure, traffic levels, temperature dynamics of engine and exhaust-line, etc.).

Finally, the microscopic traffic emissions are obtained in this work by multiplying the microscopic emissions of the fleet-equivalent vehicle by the macroscopic traffic volume information AADT.

Dispersion model

The last block of the proposed modeling approach aims to quantify the emissions impact, with a high spatial and temporal resolution, at the air quality level. To do so, PMSS (Oldrini, Olry, Moussafir, & Armand, 2011) is used as the dispersion model. The model is capable of mapping the temporal evolution of concentrations in the considered area with a high fidelity and with at a high grid resolution. It is able to reconstruct 3D fields of concentration, dry and wet deposition from point, linear, surface or volume sources (stacks, road traffic, accidental releases, diffuse sources...). PMSS has been validated on numerous measurement campaigns carried out by the US Department of Defense (Defense and Threat Response Agency) as well as on measurements in atmospheric wind tunnels. Another advantage of such a model is its explicit consideration of the impact of buildings on the dispersion of pollutants.

PMSS is based on the joint implementation of :

- The PSWIFT flow model is the parallel version of the SWIFT flow model. SWIFT is originally a mass consistent flow model that can produce diagnostic wind, temperature, turbulence and humidity fields on complex terrain. It was improved to explicitly take buildings with a RANS solver using an artificial compressibility approach to allow for more accurate, and nonetheless fast, calculation of the velocity and pressure. This more accurate pressure field can be used for example to evaluate infiltration inside the buildings from the pressure on façades.
- The PSPRAY dispersion model is the parallel version of the SPRAY model. It is a Lagrangian particle dispersion model. It simulates the dispersion of an airborne contaminant by following the trajectories of a large number of numerical particles. These trajectories are obtained by integrating in time the sum of a transport component, the local average wind, a stochastic component taking into account the influence of the atmospheric turbulence, and an additional component taking into account the buoyancy effects if any. The PSPRAY model has been improved to be able to simulate dispersion in a built-up area by considering bouncing against the obstacles. More recently, the capability to handle dense gas physics has been integrated in the dispersion model.

In addition to the traffic emissions, the dispersion model takes as inputs weather information and other emissions sources estimation.

Weather information

Weather information is required as inputs of the atmospheric dispersion model. It can be taken from a Weather Research and Forecasting (WRF) model and/or from other available measurements. They include a detailed representation of the wind field (wind speed and direction) at various heights. They should also include temperature, pressure, humidity and rainfall information on the considered area.

Other emissions sources

Emissions sources other than the ones related to traffic are also considered for the pollutants atmospheric concentrations estimation. Most of those other sources are considered as background pollution. They are estimated from measurement stations in the considered area. Large Point Sources (LPS) emissions are considered separately. Their estimations with the thermodynamic parameters of the stacks (height, temperature, and ejection velocity of the discharges at the exit of the stack) are provided by local Air Quality Monitoring service.

Results

In this section, experimental data is used to validate the proposed approach. It overall shows the importance of considering a high spatial and temporal resolution when analyzing the impact of transport emissions on the environment. The validation is performed in three parts:

- The proposed driving behavior model is first evaluated and compared to the real-world speed profile in a test area. The data-set of real-world driving FCD (Floating Car Data) was recorded via the *Geco air* application at 1Hz frequency.
- The microscopic emissions model is validated with experimental data of recent vehicle technologies. Then, the driving behavior model is combined with the aforementioned microscopic emissions model. Results are compared to a macroscopic emission model and to PEMS measurements.
- The proposed approach is then combined with the PMSS dispersion model. Pollutant emissions impact assessment on air quality is discussed.

Driving behavior model validation

The driving behavior model was validated and tested outside of the training data-set. In particular, while the model was trained on real-world driving data recorded in the urban and suburban areas of Paris and Lyon, it was tested in the city of Marseilles. The objective of this validation is to assess the extrapolation capabilities of the model for the dynamic speed profiles construction to be representative even in a different geographical context. The performance of the model was assessed from both a qualitative and quantitative point of view, by evaluating the driving behavior estimation accuracy and the statistical errors with respect to real-world speed profiles recorded in the test area.

Figure 5 shows a comparison example with 1Hz driving speed recordings in a road-segment with traffic light. Qualitatively, the constructed speed trajectories reproduce the dynamic behavior (acceleration and stopping point) of recorded speed trajectories for the considered road-segment. In this traffic light case, two clusters are well identified and reproduced by the approach: the red light cluster with a stopping point and the green light cluster with a rather constant speed. In general, the higher the number of stochastically constructed speed trajectories, the more accurate the estimation. Here, 6 speed trajectories have been constructed for each cluster, which appears to be the best compromise between speed trajectories accuracy and computational time. The driving behavior dispersion level is also well reproduced. The model is able to capture the variations of v_i (inlet speed), v_f (outlet speed) and S (stopping point) that are found in the recorded speed trajectories.

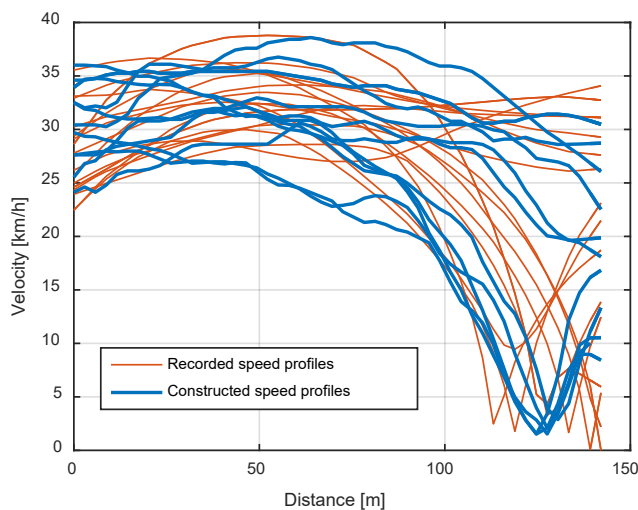


Figure 5: Comparison between constructed and measured vehicle speed trajectories for a road-segment with traffic light.

Figure 6 summarizes the results for more than 500 road-segments in Marseilles, with at least 30 recorded speed trajectories for each road-segment. Results are presented as boxplots showing the median of the mean absolute error distribution for different speed metrics. The median is less than 2km/h for v_i (inlet speed), v_f (outlet speed) and v_m (mean speed). This corresponds to a relative error lower than 10%. Thus, the results show a promising extrapolation potential of the method.

Note that the driving behavior estimation changes overtime as a function of real-time traffic predictions, retrieved every 5 minutes from HERE Maps, but any other digital map webservice could be employed. The proposed speed construction method could also take traffic incidents into account. This can be done by adding new categories to the decision tree related to each incident, for instance road hazard, accidents, etc..

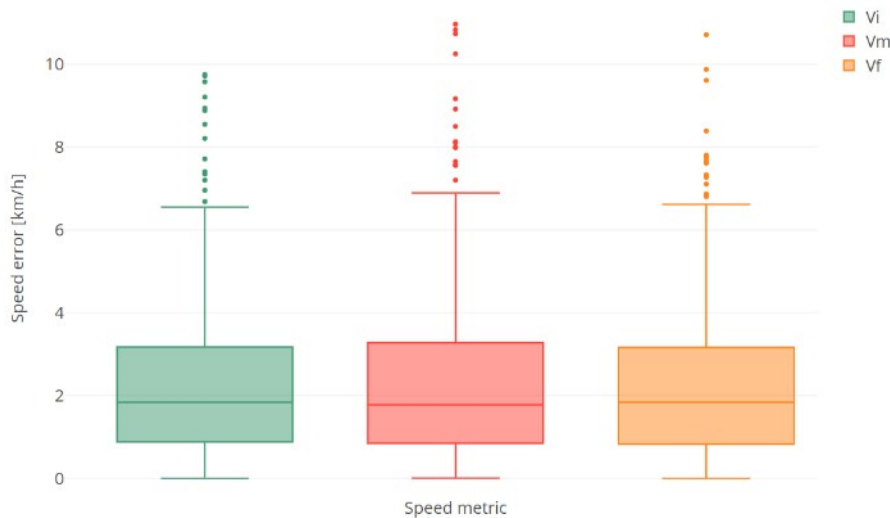


Figure 6: Speed metric errors between modeled and measured speed trajectories for the validation case (Marseilles, France).

Validation at the emissions level

Microscopic emissions model validation

The model proposed in (Thibault, et al., 2016) is used as the microscopic emissions model. It has been validated experimentally using PEMS, engine and roller test beds, on a large variety of vehicles from different technologies and emission standards. This section aims to further extend it and validate it with experimental data from recent vehicle technologies. To do so, experimental data obtained from (IFP Energies nouvelles, 2020) are used. The objective of this study is to evaluate the real-use emissions of Euro 6d-TEMP vehicles. An experimental campaign was carried on 22 vehicles spanning a wide range of segments. For each vehicle, measurements of CO₂ emissions, regulated and non-regulated pollutants (PN₁₀, N₂O, CH₄ and NH₃) are carried out under various conditions of use: Worldwide harmonized Light vehicles Test Cycles (WLTC), compliant and very dynamic RDE tests, climatic conditions from -2 to +35 ° C.

Figure 7 compares the proposed microscopic modelling (Model) with measurements made with PEMS and Copert (Ntziachristos, Gkatzoflias, Kouridis, & Samaras, 2009) Emissions Factors (EFs) for an 6d-TEMP vehicle (details given Table 1). The comparison was made on an RDE compliant test, in terms of instantaneous NO_x emissions. The exhaust emissions are aggregated on road-segments of 500 meters length. EFs are computed by using the measured average speed on each road-segment. The proposed model is able to catch some sensitivity and variations, to different driving conditions, as the measurements, whereas emissions factors, which are only based on the average speed, is not. The estimation of NO_x emissions demonstrates a good precision level and reproduces the significant events responsible for pollutant emissions, while EF gives an estimation around the mean value throughout the trip.

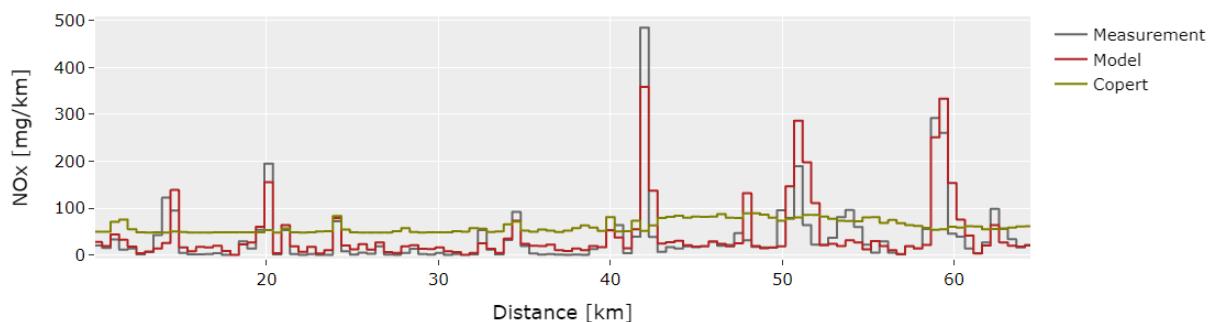


Figure 7: Comparison of the microscopic emission model (“Model”) with measurements (“PEMS”), and emission factors (“EF”) for an RDE test.

Table 1: Vehicle specifications.

Engine Type	Diesel
Classification	Euro 6d-TEMP
Engine Displacement	1461cc
Engine Power	113 hp
Vehicle Mass	1531kg
Aftertreatment	DOC+DPF+SCR

This comparison is extended to 12 6d-TEMP vehicles ranging from Diesel to Gasoline engines. Both the proposed microscopic model and Copert are compared to PEMS measurements for RDE tests (under various conditions) and for WLTC. Figure 8 shows the NO_x error distribution for both the proposed microscopic model (Model) and Copert. The NO_x gap is computed as the difference between the approach (Model or Copert) and PEMS measurements. For low road-segments length (50 meters), the Copert NO_x emissions error median is around 15mg/km and 45mg/km for Gasoline and Diesel vehicles respectively. This median error is significantly reduced with the proposed microscopic model to achieve a median error less than 3mg/km for both engine types. For such a spatial resolution, the microscopic model is more accurate than the macroscopic one. As illustrated in Figure 7, the model is able to reproduce the significant events responsible for pollutant emissions as the measurements. For high road-segment lengths (3000m), Copert accuracy is increased with a NO_x emissions error median around 11mg/km and 46mg/km for Gasoline and Diesel vehicles respectively. For the proposed model, the median is less than 5mg/km for both engine types. For low spatial resolutions, the microscopic model remains more accurate than Copert.

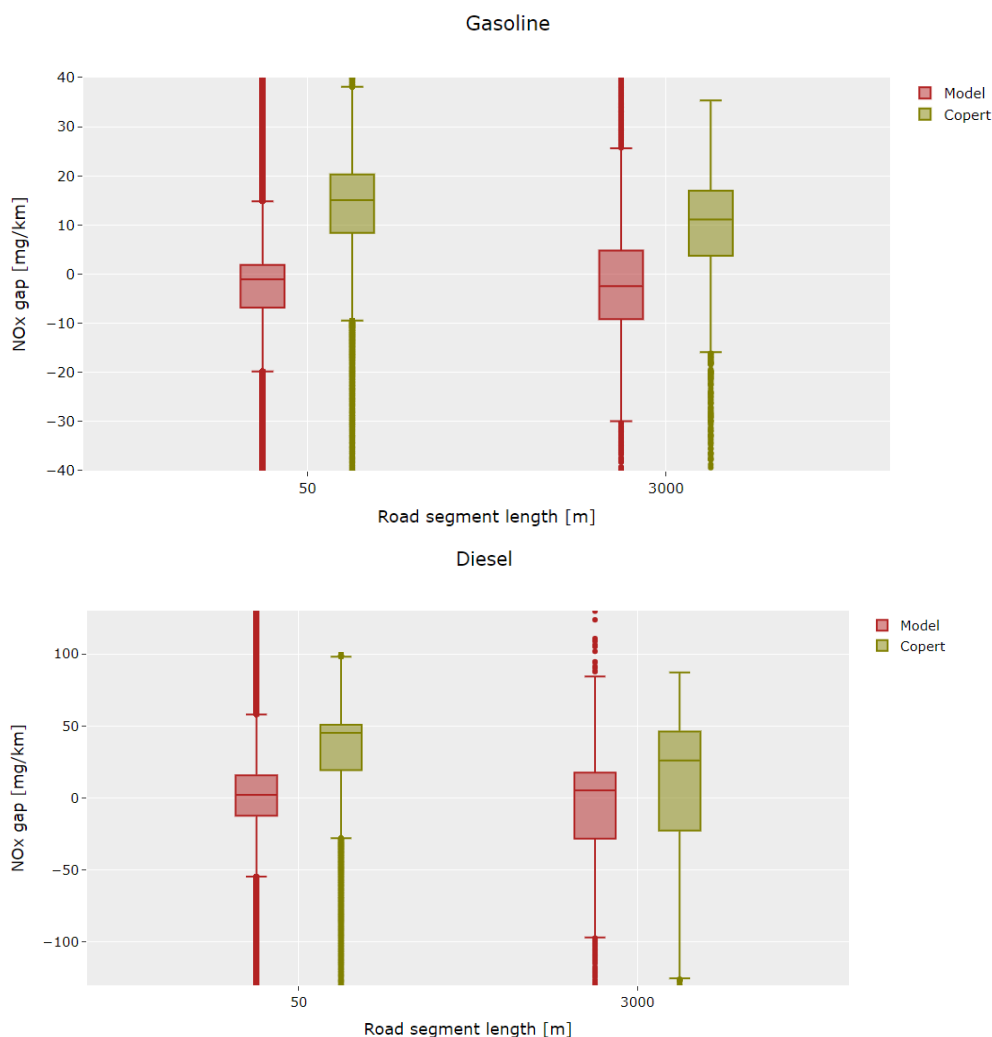


Figure 8: Proposed approach and Copert NO_x estimation errors distribution in comparison to PEMS measurements for Diesel and Gasoline 6d-TEMP vehicles and for low and high road-segment lengths.

Proposed approach validation: combination with the driving behavior model

In this section, the results are aimed at showing the added value of the proposed modeling approach (i.e. driving behavior model and microscopic emissions model) in predicting microscopic traffic emissions over the state-of-the-art methods, such as Copert, merely using emission factors per type of vehicle neglecting the dynamic content of the driving behavior. Both models are first compared to PEMS measurements at a road-segment scale. Then, Since we do not have a true measurement (PEMS) of pollutant emissions in a large area, the reference used in the comparison is the emissions calculated by the microscopic emissions model using as input the *Geco air* real-world speed profiles recorded on the different road-segments of the road network.

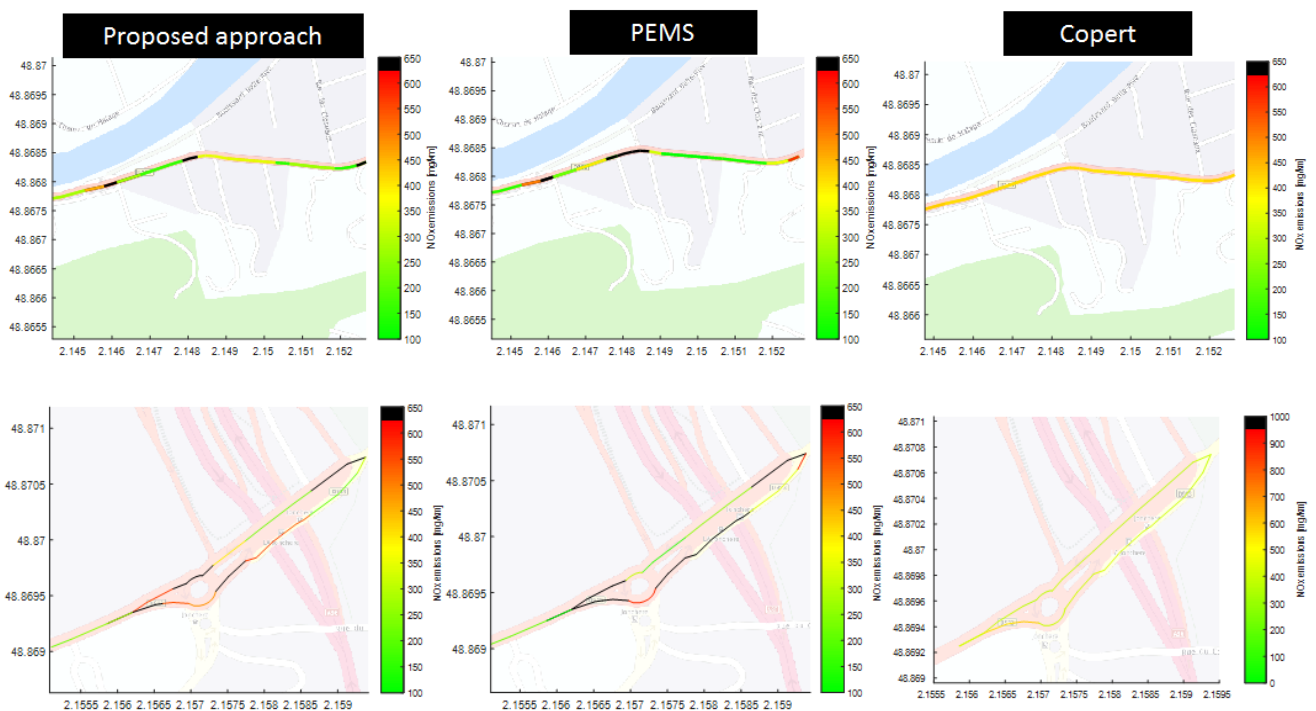


Figure 9: Comparison between the proposed approach, PEMS and COPERT NO_x emissions at a road-segment scale for an Euro 5 Diesel vehicle.

From a qualitative point of view, if we look at the traffic emissions on a map and compare them with the reference PEMS emissions (Figure 9), it can be noted that the proposed models reproduce well the true variability of NO_x emissions as depicted by PEMS, while Copert tends to remain close to the global average around 500mg/km by preventing to clearly highlight the critical areas in terms of emissions. Quantitatively, NO_x estimation error is reduced by more than 55% by the proposed approach in comparison to Copert. 65% of the road-segments have less than 100 mg/km error with the proposed model, compared to less than 25% with Copert.

The comparison between the proposed approach and COPERT has been extended to all road-segments in a neighborhood of Marseilles. This is illustrated as a qualitative comparison of maps for vehicle NO_x emissions. Both Copert and the proposed approach have the same average NO_x emissions. However, the proposed model shows more sensitivity: the infrastructure impact on traffic emissions is better taken into account than with the Copert model.

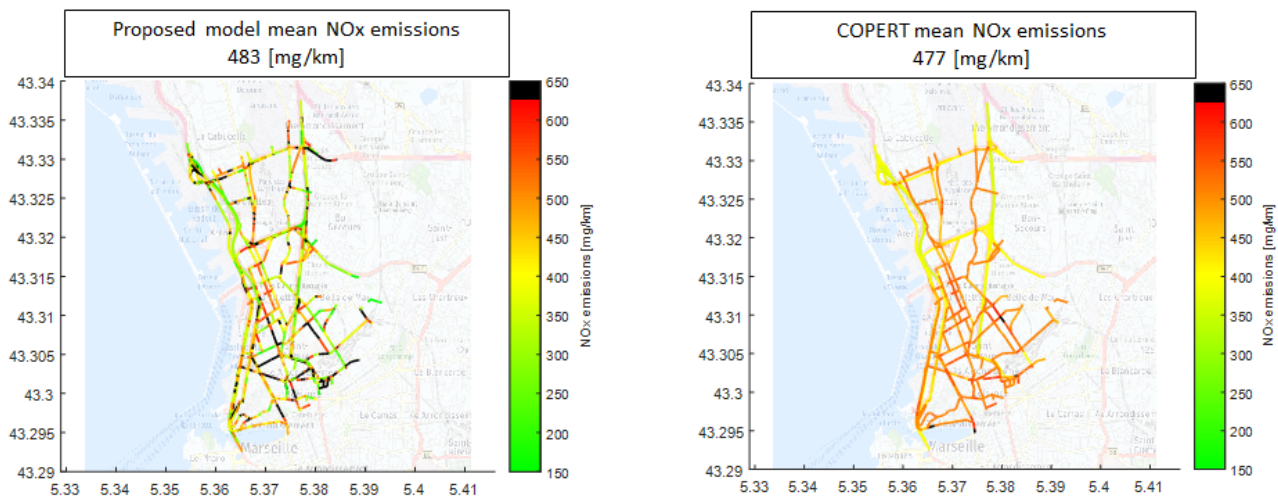


Figure 10: Copert vs proposed model. NO_x emissions map comparison in Marseilles, France. The colorbar color scale is black at 630 mg/km. Above this value, the road-segment is considered highly emitter. The black color saturation is used to identify more easily critical road-segments.

The proposed approach seems to have a higher spatial resolution than Copert. In order to evaluate both models' sensitivity to different spatial resolutions, emissions are computed for road-segments with low length and high length. For each distance bin, road-segments of different lengths have been grouped in order to obtain at least 100 error estimations. Since we do not have a true measurement (PEMS) of pollutant emissions in a large area, the reference used in the comparison is the emissions calculated by the microscopic emissions model using as input the *Geco air* real-world speed profiles recorded on the different road-segments of the road network.

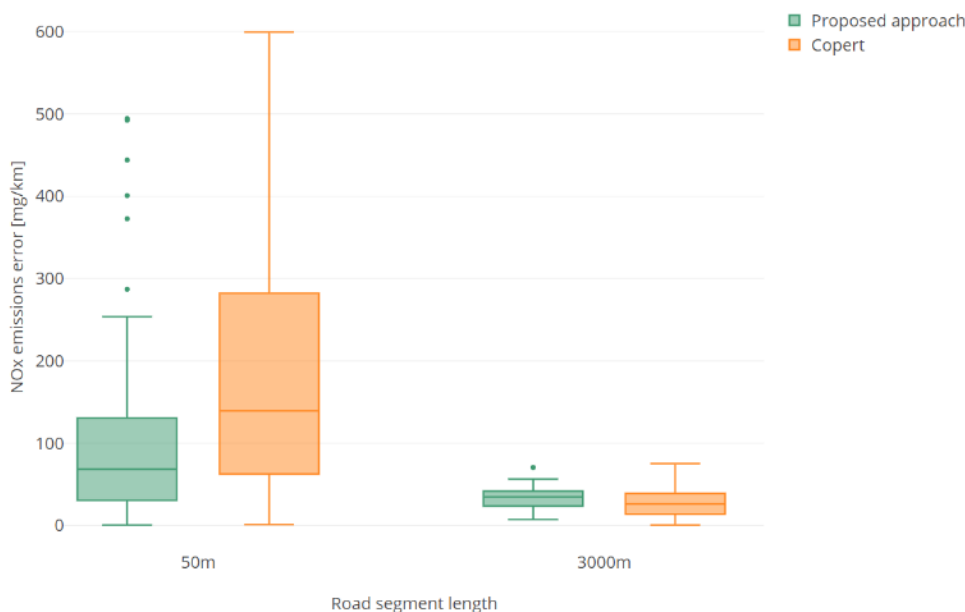


Figure 11: Proposed approach and Copert NO_x estimation errors distribution for road-segments of low and high lengths.

Figure 11 shows the NO_x error distribution for both the microscopic (proposed approach) and macroscopic (Copert) models. For low road-segments length, the NO_x emissions error median is reduced from 150 mg/km for the macroscopic model to 70 mg/km for the microscopic model. For such a spatial resolution, the microscopic model is more accurate than the macroscopic one, with a median error reduction of around 54%. However, for high road-segments lengths, both models show similar NO_x error distribution. For low resolution, the microscopic model does not offer a better NO_x estimation accuracy than the macroscopic model.

This study has been extended to road-segments of different lengths. To do so, road-segments have been artificially grouped together to consider very high segment lengths. Microscopic and macroscopic model sensitivity to various spatial resolutions is presented in Figure 12. The emissions estimation error of both approaches is computed as a function of the road-segment length. For segment lengths lower than 500 meters, the microscopic emission error is reduced by more than 50% in comparison to the macroscopic one. This represents 91% of the road-segments in the studied area, for which the mean length is around 55 meters. For higher distances, the NO_x emission error is reduced, and both approaches converge towards the same NO_x emissions error for a segment length around 2700 meters. In this case, the spatial resolution is relatively low and the microscopic approach presents no contribution over the macroscopic one.

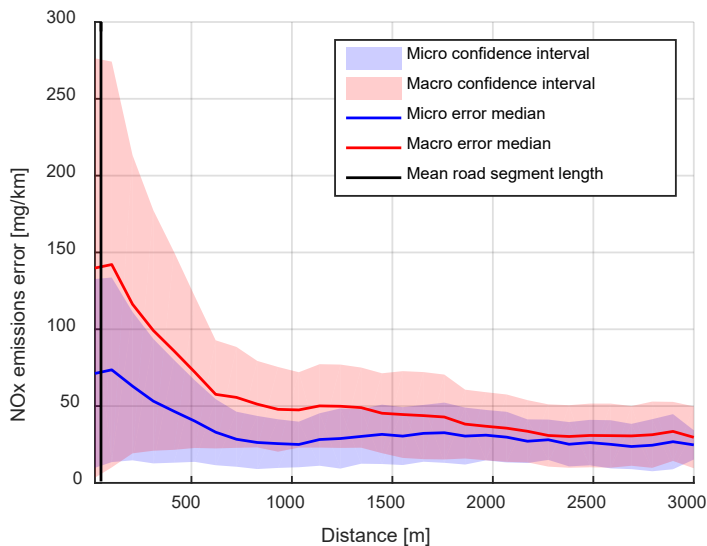


Figure 12: Microscopic and macroscopic NO_x estimation errors as a function of the road-segment length.

Proposed approach simulation at the dispersion level

In this section, the objective is to simulate the proposed workflow at the dispersion level. To do so, as illustrated in Figure 1, microscopic traffic emissions estimations are taken as an input of the atmospheric dispersion model. Microscopic traffic emissions estimations consider the contribution of various vehicle types ranging from two-wheelers to passenger vehicles, to light commercial vehicle, heavy duty vehicles and buses.

Emissions from other sources are considered background pollution. They are measured hourly from a measurement station in the considered area. Weather information (wind speed and direction, humidity, etc..) is also required as inputs of the atmospheric dispersion model. It is taken from a Weather Research and Forecasting (WRF) Model. A second urban station measures hourly NO₂ and NO_x concentrations.

Daily air quality map simulation

This study is performed in the previously defined neighborhood in Marseilles, France. Due to the complex characteristics of the streets, a spatial resolution of 4 m is chosen for this area. A representative day is considered for the simulation. It has been chosen according to various criteria:

- Without rain.
- Low SO₂ concentration. A high SO₂ concentration could mean a nearby marine activity (and therefore may impact the concentrations measured for the other pollutants).
- Data available for the two air quality measurement stations.
- NO₂ daily average concentration close to the annual average.

Accordingly, the 20/06/2019 day has been chosen and simulation results are presented in terms of the daily average NO₂ concentration map in Figure 13. A high NO₂ variation is observed with the proposed spatial resolution. Major road-segments colored in red (point A in the figure) presents high NO₂ concentrations. This is due to a high traffic flow with a major heavy duty vehicles contribution. High NO₂ concentrations are also observed in tunnel exits (point B), high positive slopes, and areas of high congestion (point C).

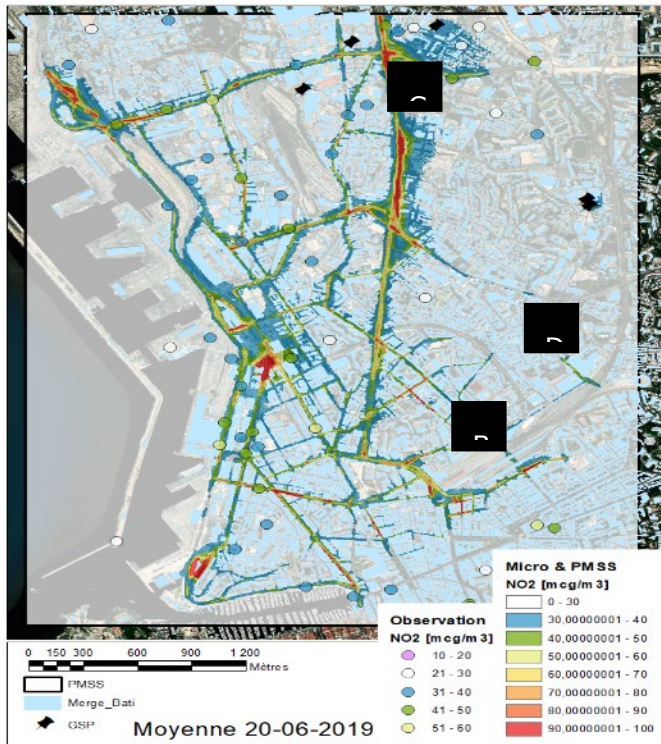


Figure 13: NO₂ daily average concentration map in a Marseilles, France neighborhood, on 20/06/2019.

To evaluate the proposed approach contribution, estimated daily average NO₂ concentrations are compared to the ones estimated by taking Copert as the traffic emissions model. Both estimations are then compared to the measured annual NO₂ average in different locations of the considered area. Table 2 shows a comparison example for two cases. The first case B depicts a downward slope with some decelerations due to a traffic light presence. This induces emissions overestimation by Copert. In contrary to the proposed model, Copert does not take the slope and acceleration evolution in its computation. The NO₂ daily average concentration is overestimated by around 20 µg/m³ for Copert while the mean absolute error is around 1 for the proposed model. The second case D depicts a congested location with an upward slope. In this case, Copert underestimates NO₂ daily average concentration by 7 µg/m³ while the mean absolute error is around 2 for the proposed model.

The comparison is extended to more than 20 locations with annual average NO₂ measurements. For more than 70% of the cases, the proposed approach mean absolute error is less than 5 µg/m³. For Copert less than 60% of those cases have a mean absolute error lower than 5 µg/m³. The proposed approach better takes into account the infrastructure impact on air quality at a high spatial resolution.

Table 2: Estimated daily average NO₂ concentrations compared to measured annual NO₂ average. Both the proposed microscopic traffic emissions and Copert models are used for traffic emissions estimation.

Case	Measured NO ₂ concentrations [µg/m ³]	Proposed approach NO ₂ [µg/m ³]	Copert NO ₂ [µg/m ³]
B	42	43	61
D	41	39	34

Impact of fleet variation on air quality

In this subsection, the impact of fleet variation on air quality is addressed. Air quality maps are simulated at a high spatial and temporal resolution where emissions are updated every 5 seconds and with a spatial resolution of 1 meter. The considered case of study is comprised of a succession of 3 traffic lights. Such a case presents relatively high accelerations which affect local air quality considerably.

Three fleet compositions are considered:

- The default fleet composition is provided from available public reports (CITEPA, 2020). This fleet composition is denoted as FleetA.
- A fleet composition comprised of 100% of petrol vehicles for passenger cars. Light commercial and heavy-duty vehicles fleet composition and proportions are similar to the ones in FleetA. This fleet composition is denoted as FleetE.
- A fleet composition comprised of 100% of recent Euro 6d-TEMPdiesel vehicles for passenger cars. Light commercial and heavy-duty vehicles fleet composition and proportions are similar to the ones in FleetA. This fleet composition is denoted as FleetD.

Figure 14 presents NO_x air quality maps around 3 traffic lights for each fleet composition assumption. They are computed in the acceleration phase where the three traffic lights have just turned to green. This allows us to better take into account the impact of the acceleration on the pollutants atmospheric concentrations for different fleet compositions. In this figure, traffic lights are presented as pink circles with black dots. Relatively high NO_x concentrations are observed around those traffic lights. This is particularly noted for the FleetA case, where average NO_x concentrations are around 85µg/m³ near those traffic lights. Such average is reduced to 73µg/m³ and 67µg/m³ for FleetD and FleetE respectively. FleetD emissions represent on average 68.4% of the NO_x emissions of the CITEPA average passenger car (FleetA). FleetD NO_x emissions are more comparable to FleetE, where the average NO_x concentration difference is around 7µg/m³. The latter (FleetE) emits on average 61.2% of the NO_x emissions of the CITEPA average passenger car (FleetA).

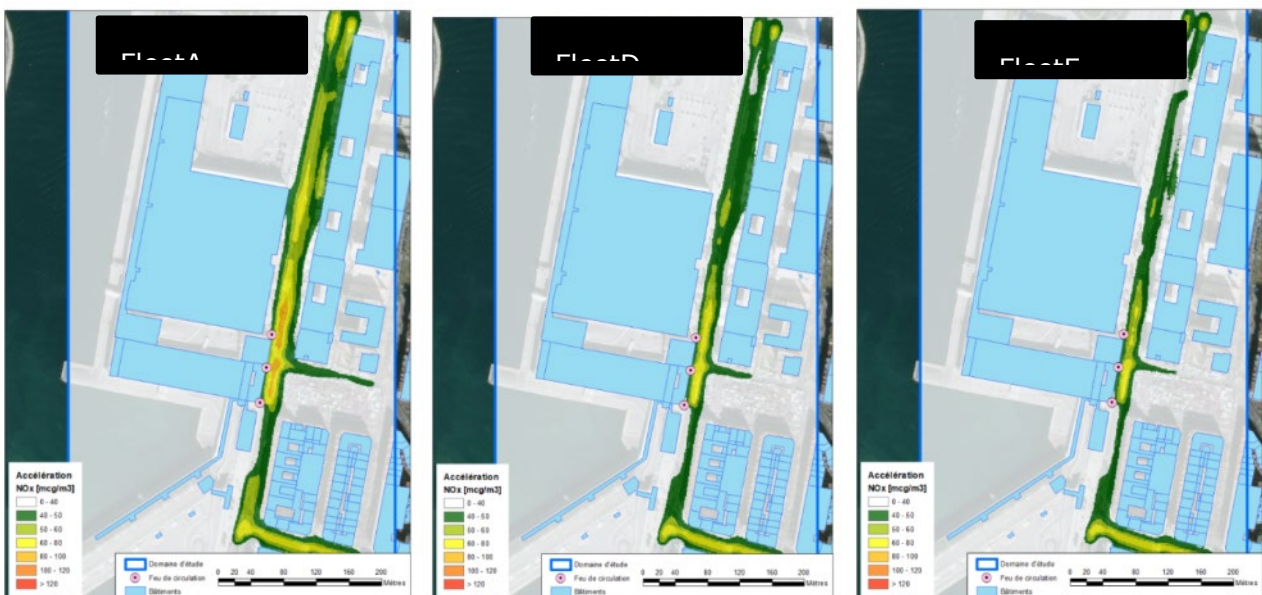


Figure 14: NO_x concentration maps resulting from three fleet compositions where traffic lights have just turned to green.

Conclusions

This paper presents an approach to estimate road traffic emissions on any road-segment and quantifies their impact on air quality. The modeling framework combines a road-segment driving behavior model with a microscopic emissions model and an atmospheric dispersion model. A high temporal and spatial resolution is obtained in terms of pollutants emissions and their estimated concentrations. Results show an increased accuracy in NO_x emissions estimation for small road-segments of hundreds of meters, in comparison to a macroscopic state-of-the-art model such as Copert. The proposed methods are able to take into account the speed variability and the impact of traffic and road infrastructure. Traffic emissions are estimated with a microscopic physics-based emissions model that has been extended and validated with the most recent vehicle after-treatment technologies (e.g. Euro 6d-TEMP). The proposed modeling framework was then used as a more precise road-transport emissions source for atmospheric dispersion. This resulted in a high spatial resolution of the NO₂ concentration map. Several critical areas with relatively high concentrations could be identified. Accordingly, such a tool could be used by cities to detect areas and/or infrastructure elements negatively affecting local air quality. It could be also used by decision-makers to identify the most effective ways to improve air quality. A case study showed that recent vehicle technologies could induce a reduction in NO₂

concentration by more than 15%. Such study will be extended to large road networks and with various fleet compositions.

Acknowledgement

This research was funded by ADEME (French Environment and Energy Management Agency); AIRMES project, PRIMEQUAL 2018, grant number 1866C0013.

References

- Andrieu, C. (2013). Modélisation fonctionnelle de profils de vitesse en lien avec l'infrastructure et méthodologie de construction d'un profil agrégé.
- Badin, A.-L. a., Vittoz, T., Sorand, C., Lejri, D., Leclercq, L., & Olly, X. (2017). Combining microscopic traffic modelling and 3 pollutant emission modellings to assess modifications of traffic supply and demand. *Journal of Earth Sciences and Geotechnical Engineering*.
- Bengio, Y., & Grandvalet, Y. (2004). No unbiased estimator of the variance of k-fold cross-validation. *Journal of machine learning research*, 5(Sep), 1089-1105.
- Breiman, L. (2001). Random forests machine learning. *45*: 5–32.
- Camelli, F. E., Hanna, S., & Lohner, R. (2004). Simulation of the MUST field experiment using the FEFLU-Urban CFD mode. *Computer Science*.
- CITEPA. (2020). Gaz à effet de serre et polluants atmosphériques. Bilan des émissions en France de 1990 à 2018. Technical report.
- De Nunzio, G., Laraki, M., & Thibault, L. (2021). Road Traffic Dynamic Pollutant Emissions Estimation: From Macroscopic Road Information to Microscopic Environmental Impact. *Atmosphere*.
- De Nunzio, G., Thibault, L., & Sciarretta, A. (2017). Model-based eco-routing strategy for electric vehicles in large urban networks. *Comprehensive energy management-eco routing & velocity profiles*.
- European Environment Agency. (2018). Europe's urban air quality – re-assessing implementation challenges in cities.
- Fellendorf, M., & Vortisch, P. (2010). Microscopic traffic flow simulator VISSIM. *Fundamentals of traffic simulation*.
- Geco air. (2017). https://www.gecoair.fr/home_en/.
- Gowardhan, A. A., Pardyjak, E. R., Senocak, I., & Brown, M. J. (2007). Investigation of Reynolds stresses in a 3D idealized urban area using large eddy simulation.
- HERE MAPS. (s.d.). Récupéré sur <https://www.here.com/>
- IEA. (2016). World energy outlook – energy and air pollution. Special report.
- IFP Energies nouvelles. (2020). "Study of Euro 6d-TEMP emissions – IFPEN for DGEC, Summary report,". https://www.ifpenergiesnouvelles.fr/sites/ifpen.fr/files/inline-images/Innovation%20et%20industrie/Motorisations%20thermiques/Study-of-Euro-6d-TEMP-emissions_IFPEN-DGEC_SynthesisReport_Dec2020.pdf.
- Kaufman, L., & Rousseeuw, P. J. (2009). Finding groups in data: an introduction to cluster analysis. (Vol. 344). *John Wiley & Sons*.
- Laraki, M., De Nunzio, G., & Thibault, L. (2020). Vehicle speed trajectory estimation using road traffic and infrastructure information. *IEEE 23rd International Conference on Intelligent Transportation Systems*.
- Laureshyn, A., Astom, K., & Brundell-Freij, K. (2009). From speed profile data to analysis of behaviour: classification by pattern recognition techniques. *IATSS research*.
- Lin, J., & Niemeier, D. A. (2003). Estimating regional air quality vehicle emission inventories: constructing robust driving cycles. *Transportation Science*.
- Ma, X. a., Andréasson, I., & Chen, H. (2012). An Evaluation of Microscopic Emission Models for Traffic Pollution Simulation Using On-board Measurement. *Environmental Modeling & Assessment*.
- McHugh, C. A., Carruthers, D. J., & Edmunds, H. A. (1997). ADMS-Urban: An air quality management system for traffic, domestic and industrial pollution. *International Journal of Environment and Pollution*, 8(3-6), 666-674.

- Min, W., & Wynter, L. (2011). Real-time road traffic prediction with spatio-temporal correlations. *Transportation Research Part C: Emerging Technologies*.
- Minett, C. F., Salomons, A. M., Daamen, W., Van Arem, B., & Kuijpers, S. (2011). Eco-routing: comparing the fuel consumption of different routes between an origin and destination using field test speed profiles and synthetic speed profiles. *2011 IEEE Forum on Integrated and Sustainable Transportation Systems*.
- Nam, E. K., Gierczak, C. A., & Butler, J. W. (2003). A Comparison of real-world and modeled emissions under conditions of variable driver aggressiveness. *82nd Annual Meeting of the Transportation Research Board*.
- Newell, G. F. (1993). A simplified theory of kinematic waves in highway traffic, part I: General theory. *Transportation Research Part B: Methodological*.
- Ntziachristos, L., Gkatzoflias, D., Kouridis, C., & Samaras, Z. (2009). COPERT: a European road transport emission inventory model. *Information technologies in environmental engineering; Springer, 2009; pp. 491–504*.
- Oldrini, O., Olry, C., Moussafir, J., & Armand, P. &. (2011). Development of PMSS, the parallel version of Micro-SWIFT-SPRAY. *In Proc. 14th Int. Conf. on Harmonisation within Atmospheric Dispersion Modelling for Regulatory Purposes.*, pp. 443-447.
- Schulman, L. L., Strimaitis, D. G., & Scire, J. S. (s.d.). Development and evaluation of the PRIME plume rise and building downwash model. *Journal of the Air & Waste Management Association, 50(3), 378-390*.
- Thibault, L., Degeilh, P., Lepreux, O., Voise, L., Alix, G., & Corde, G. (2016). A new GPS-based method to estimate real driving emissions. *In 2016 IEEE 19th International Conference on Intelligent Transportation Systems (ITSC) (pp. 1628-1633). IEEE*.
- Van Hieu, D., & Meesad, P. (2015). Fast k-means clustering for very large datasets based on mapreduce combined with a new cutting method. *In Knowledge and Systems Engineering (pp. 287-298). Springer, Cham*.
- Van Lint, J., & Van der Zijpp, N. (2003). Improving a travel-time estimation algorithm by using dual loop detectors. *Transportation Research Record*.
- Wolfermann, A., & Alhajyaseen, W. K. (2011). Modeling speed profiles of turning vehicles at signalized intersections. *3rd International Conference on Road Safety and Simulation RSS2011, Transportation Research Board TRB, Indianapolis*.

2.25 Lower emissions from existing cars: personalised advice based on emission maps

R. van Gijlswijk¹, J. de Ruiter¹, N. Ligterink¹, A. Indrajana¹, M. Opetnik², C. Matzer²

¹ Netherlands Organisation for Applied Scientific Research TNO, DA Den Haag, The Netherlands

² Technische Universität Graz, Institut für Verbrennungskraftmaschinen und Thermodynamik, Austria

rene.vangijlswijk@tno.nl

Abstract

Pollutant emissions from the passenger car fleet in Europe can not only be reduced by the influx of clean new vehicles, but also by reducing the emission levels of existing vehicles. Since for a number of reasons the average fleet emissions do not decrease as fast as envisaged by policy makers, attempting to reduce the emissions from the present fleet can be an attractive and potentially powerful option, with direct effects.

The exhaust and wear emission levels of an individual vehicle depend among other things on the euro standard, the precise engine and exhaust gas aftertreatment system, weight of the vehicle, brake and tyre composition, the state of maintenance, originality of the technical specs, and age of the vehicle. However, to which extent the potential emissions actually take place, is greatly influenced by driver behaviour, the use case of the vehicle and the local conditions, as emissions vary among different circumstances.

To advise owners and drivers on reducing the emissions of their vehicle, all of the factors need to be taken into consideration. The heart of the present work is the standardisation of the information describing the relationship between vehicles in use and their emissions, on the basis of which the personal or fleet-emission reduction potential can be determined. Individual advice should be based on appropriate measurements, of that particular vehicle or a similar vehicle. Moreover, presenting such information should be transparent, so conclusion and limitations of the underlying data should be clear.

The proposed approach starts from measurement data available at TNO, TU Graz and other institutes in Europe, collected using dynamometers, Portable Emission Measurement Systems (PEMS) and other sensor based devices such as the TNO Smart Emission Measurement System (SEMS). The measurement data is analysed to establish a base emission map for each component. The map in principle covers all instantaneous situations relevant for the emission component.

The emission map layers encompass:

- Tailpipe emissions under hot engine conditions: NO_x (primary focus), PN, CO, HC
- Tailpipe emissions under cold start conditions: NO_x (primary focus), PN, CO, HC
- Tailpipe emissions of non-regulated emissions: NO₂, N₂O, PAH, CH₄, cyanides, NH₃
- Particulate emissions from wear: brakes, tyres, road surface
- Additional tailpipe emissions due to aging/poor maintenance: NO_x, PN, CO, HC, NO₂, N₂O, PAH, CH₄, cyanides, NH₃
- Tampering: additional emissions as a result of tampering: NO_x, PN
- Retrofitting: potential reduction in tailpipe emissions as a result of retrofitting solutions on older vehicles: NO_x, PN

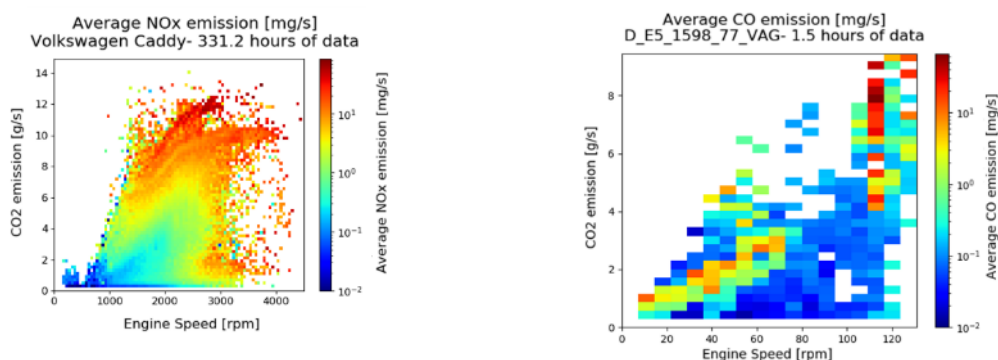


Figure 1: Example CO emission map.

Differences in emission behaviour of vehicles occur on multiple levels, e.g. vehicle model (weight), fuel type, euro standard, or specific engine. To classify vehicles in a logical way, a taxonomy was developed. It has 11 levels, describing the vehicle make and model, and engine characteristics. The emission map layers can be linked to any level, to be attributed to all vehicles sharing that particular part of the taxonomy code.

A data file structure has been developed to facilitate exchange and publication of the map data, as well as to enable the implementation of the maps in multiple third party tools.

Introduction

The improvement of air quality has become one of society's main challenges. Traffic and transport have a large effect on air quality in Europe. In particular passenger cars and commercial vehicles contribute to exposure of inhabitants with nitrogen oxides, particulates, carbon monoxide, hydrocarbons, ammonia and other pollutants. Although technical improvements and more stringent legislation had a significant impact, air quality has not improved correspondingly.

Partially this is related to the long lifespan of vehicles, which makes the renewal rate slow. According to ACEA, the average age of the European passenger car fleet is 11.5 years. 55% of the present European fleet was built before 2010, and since Euro 5a was introduced in September 2009 for new models, this 55% is almost entirely Euro 4 and older. So even though the latest Euro 6d Final vehicles may be very clean, a significant effect can take years.

Efforts to reduce emissions from the existing fleet do not suffer from the slow renewal rate, and can instantly improve air quality. Reducing emissions from existing cars is possible, because the emissions are not only dependent on the technology used by the manufacturer, but also by the way that the vehicle is operated. Dependent on the technology, certain driver behaviour can cause spikes in, or continuous high levels of emissions. This behaviour may be high speed driving, sudden sharp acceleration, heavy braking, frequently changing the throttle pedal, or driving in the wrong gear. Mapping out the emission behaviour of vehicles in a standardized way helps understanding how driver behaviour and emission behaviour are related, and what guidance can be given to drivers to avoid conditions where the emissions of their particular vehicle are high. This should lead to reduced overall emissions from their vehicle. The knowledge captured in the emission maps can be used in driver advice tools.

Vehicle taxonomy

Taxonomy structure

As the emissions from a vehicle are a combination of technical vehicle characteristics and the use of the vehicle, a first step in understanding emissions is to distinguish vehicles by their technical characteristics. Relevant for emissions are the fuel type and the emission standard, but a more refined approach can include also other factors that are specific to certain manufacturers. To characterise and categorise European passenger cars in a logical and controlled way, a taxonomy has been developed. It includes a number of important factors that are needed to distinguish vehicles by emission behaviour (pollutants and CO₂), and is used throughout several Horizon and LIFE+ projects. Emission maps can be attached to any level of the taxonomy. The underlying work is public and can be found on www.project-ucare.eu. Emission maps are a uniform representation of the emissions, suitable for modelling and estimating effects of changes in use of behaviour. The taxonomy has 11 levels, covering two parts: a vehicle part and an engine part. The engine is a 'child' of the vehicle; see Figure 2.

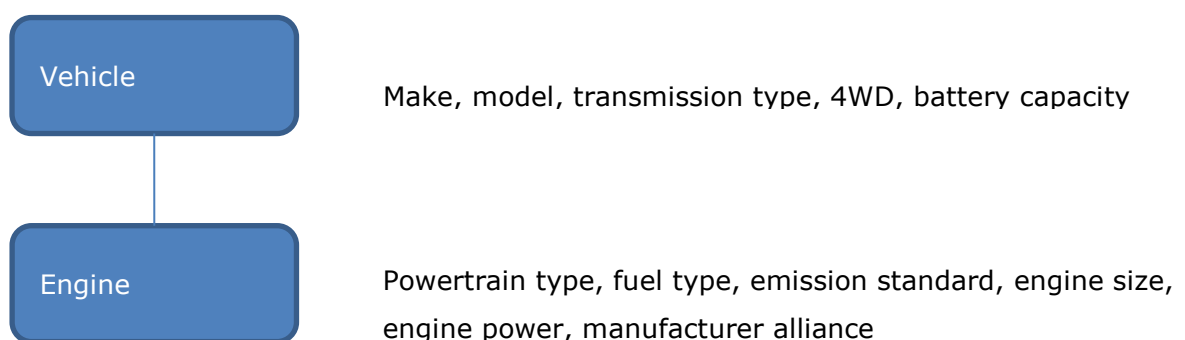


Figure 2: Basic concept of vehicle taxonomy.

The vehicle code contains make, model, transmission type, all-wheel drive capability and the (externally chargeable) battery capacity. Figure 3 shows an example of the vehicle part of the taxonomy.

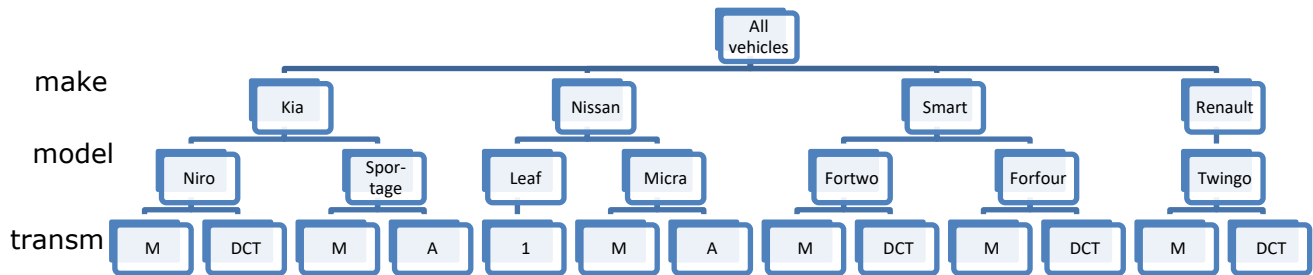


Figure 3: Example of taxonomy. Vehicle part, first three layers: make, model, transmission type (M=manual, A=automatic, DCT=dual clutch transmission, 1=single speed).

The other characteristics of a vehicle, such as the empty mass and dimensions of the vehicle, can be retrieved once the place of a vehicle in the taxonomy is known. Tyre and road wear can be related to these vehicle characteristics. Tailpipe emissions however are related to the engine characteristics.

The engine part of the taxonomy is illustrated in Figure 4.

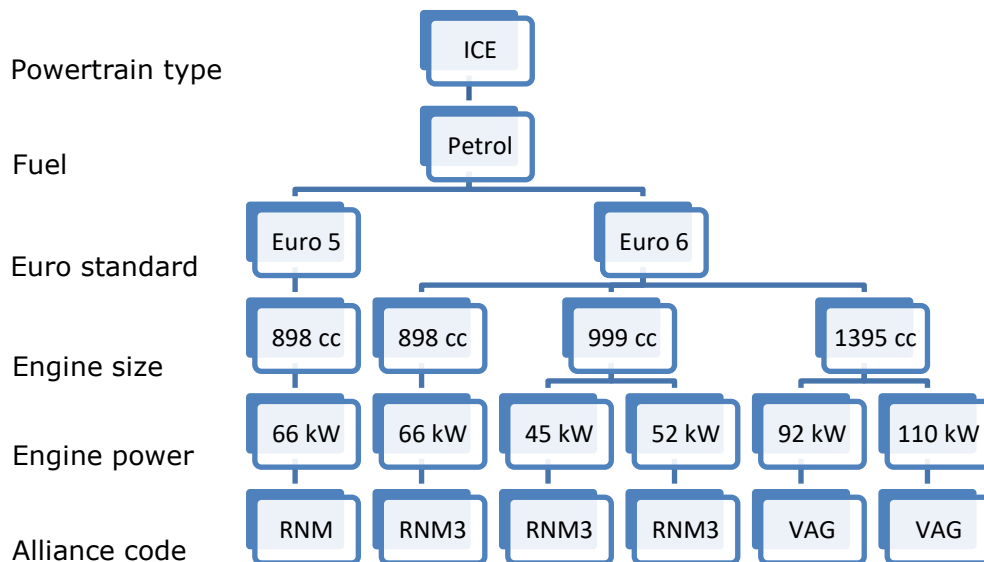


Figure 4 Example of taxonomy. Engine part.

Distinguishing engines: alliance code

As becomes apparent from the graph, what is considered an 'engine' in Figure 2 is actually an engine configuration. Vehicles are often sold with multiple engine configurations: different fuels, different engine sizes and different power ratings. In turn, engines of a certain configuration are often applied in multiple vehicle models, even across brands. The frequently occurring shared development of engines and use of engines from other manufacturers makes the link between the vehicle manufacturer and the engine manufacturer not obvious. To avoid double entries, an 'alliance code' was added as the 11th taxonomy level. The code indicates a group of vehicle brands for which a certain engine was applied. This can be multiple brands of one manufacturer group, e.g. VW and Audi of the Volkswagen Group, but it can also be a combination of brands of different manufacturers that have applied the same engine. In the case of RNM3 in Figure 4, besides within the Renault-Nissan-Mitsubishi alliance, the engine was also applied in Smart vehicles. Together with the other levels: powertrain type, fuel type, emission standard, engine size and engine power, it creates a unique identifier. The underlying assumption is that the emission behaviour of an engine is not different among different car models it has been applied in. Assigning alliance codes to engine configurations was done partially manually, partially automatically using the Dutch vehicle registration database (opendata.rdw.nl). All distinguished alliances can be found on www.project-ucare.eu, under D1.1 – Alliance code.

Naming conventions

Using measurement data, emission maps can be made for a specific engine. A naming convention has been developed to be able to refer to positions in the taxonomy in an abbreviated way. This helps with easy exchange of emission map files, as discussed in chapter 0. The powertrain type is not included in the name, because it is there only for simple communication purposes; it can be derived from the fuel type. All other layers in the engine part of the taxonomy are included as an abbreviation, and separated by underscores. Fuel types are represented with one or two letters. Two fuels are allowed, separated by a double hyphen (--), and in alphabetical order.

Table 1 shows the fuel type naming.

Table 1: Fuel type codes.

Fuel type	Fuel type abbreviation		Fuel type	Fuel type abbreviation
Diesel	D		LPG/Petrol	LP--P
Petrol	P		CNG/Petrol	C--P
Electricity	E		Ethanol/Petrol	A--P
Ethanol (E85)	A		Biodiesel/Diesel	BD--D
CNG	C		Electricity/Hydrogen	E--H
LPG	LP		Electricity/Petrol	E--P
Hydrogen	H		Electricity/Diesel	D--E
Biodiesel	BD			
LNG	LN			

Euro standards are abbreviated by their number (0-5, 6a, 6b, 6c, and 6d). Euro 6d-Temp is denoted as 6dT. Displacement (engine size) is included without unit, in cubic centimetres. Rated power is included without unit, in kilowatts. Last item in the taxonomy code is the alliance code, which is in itself already an abbreviation.

A complete taxonomy code represents a specific engine. It is desirable to be able to generalise emission behaviour as well, for instance describing the average behaviour of vehicles of a certain Euro standard. In the taxonomy this has been foreseen by introducing the 'ALL' code that can replace a specific code at every level.

Example taxonomy codes

Examples of vehicle-specific and generalised ('ALL') engine codes are demonstrated in Table 2. The first one is equal to the leftmost path in Figure 4.

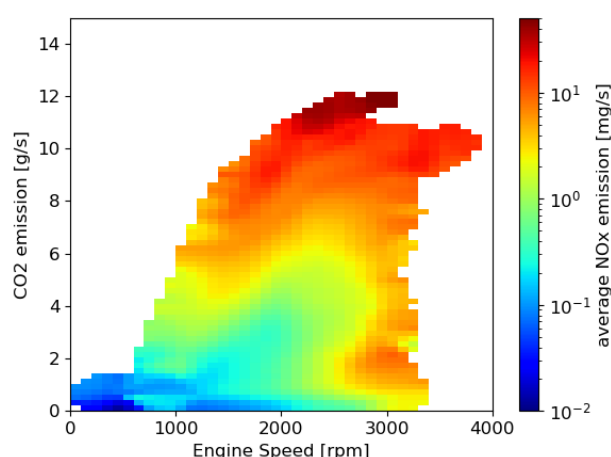
Table 2: Examples of vehicle-specific and generalised engine codes.

Engine code	Explanation
P_5_898_66_RNM	Petrol, Euro 5, 898 cc, 66 kW engine belonging to the RNM (Renault-Nissan-Mitsubishi-Dacia-Datsun-Lada) alliance
D_6dT_1969_140_VOLV	Diesel, Euro 6d-Temp, 1969 cc, 140 kW engine belonging to the VOLV (Volvo) alliance
E--P_6b_1798_73_TOYO	Petrol plug-in hybrid, Euro 6b, 1793 cc, 73 kW engine belonging to the TOYO (Toyota) alliance
D_4_ALL_ALL_ALL	Generalised code referring to all diesel Euro 4 engines
P_6_898-999_ALL_RNM3	Generalised code referring to all petrol, Euro 6 engines with engine displacements between 898 and 999 cc of the RNM3 (Renault-Nissan-Dacia-Smart) alliance

Base emission maps

Design

Emission maps are a concept, as well as the name and structure of the corresponding file format, to exchange pollutant emission data at a detailed level, with the underlying dependencies. It is suitable for all regulated and non-regulated pollutant emissions from the tailpipe. As described in the introduction, emissions are dependent on the vehicle technology as well as the driver input. The emission maps are dimensioned to relate emission levels to driver input. Then, based on measurement data of the key parameters, a map of the emission levels can be made. For nitrogen oxides (NO_x), for example, the map can depict engine speed on the x-axis, CO₂ emissions on the y-axis, and the NO_x emissions in mg/s as a colour. Figure 5 shows an example of such a map for a random vehicle. Note that CO₂ emission is used here as a proxy for power or engine load¹⁸. Dozens of base maps are already available for download, free of charge, via the OpenAire platform Zenodo.

**Figure 5:** Example emission map for average NO_x emission from a Euro 6 diesel engine.

During driving, dependent on the driver input, the engine speed and CO₂ output vary almost continuously. This means that the vehicle ‘runs’ across the map. Average instantaneous emissions can thus be predicted on a second-by-second basis.

¹⁸ The CO₂ flow in g/s is proportional to the fuel flow, i.e. energy delivered per time, i.e. the power content of the fuel.

The map shows that for this vehicle category, if a driver presses the accelerator pedal at mid to high engine speed, the emissions are high (top of the graph). Also driving with high engine speed and relatively low power, the emissions are high (right hand side of the graph).

To be able to create such a map, measurement data is needed for the entire spectrum of engine use, from at least one vehicle representative for the taxonomy code. Furthermore, interpolation algorithms are needed to fill the map if gaps occur. Also it may be necessary to reduce the map resolution if a limited amount of data is available. Generally speaking, boundary conditions have to be set to warrant a minimum quality and usefulness of the emission maps produced.

Emission maps should be fact-based and transparent. It was agreed in the uCARE project to fill the distributable emission map files with data-backed values only. If gaps do occur in the emission map, the end-user has the freedom to choose a suitable interpolation method to fill in the gaps before further analysis or usage of the map. A script will be provided by the uCARE team to process the emission maps. The script will take care of interpolation and smoothing of the maps.

For some map layers, it may be chosen to implement the emission maps as a continuous function instead. Parameter values to insert into the function can then be distributed per vehicle (class) in the same way maps are distributed. The function is then implemented on the tool side.

Interpreting emission maps

Base maps can be used to investigate driver emissions. On a second-by-second basis, relevant driving parameters (e.g. engine load, speed, and/or RPM) can be used to look up the expected instantaneous emissions for a specific vehicle (see Figure 6). The instantaneous emissions can be used to approximate driver emissions over the duration of a trip. Different driving parameters lead to different emissions. In this way, advice can be given as to the driving parameters which can lead to lower emissions.

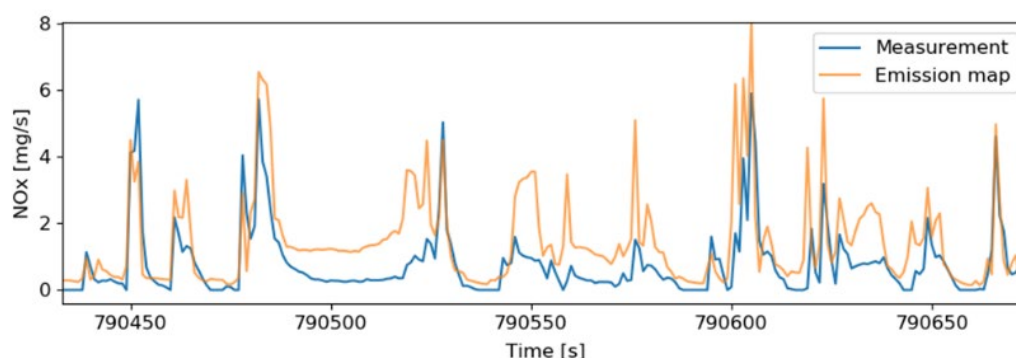


Figure 6: Comparison of NO_x emissions from measurement data and as calculated from an emission base map using vehicle speed and CO₂ emission.

Note that this profile does contain a measure of uncertainty due to the fact that possibly not all factors are included that describe the nature of real-world driving. Emissions may also vary over time and seasons. Such effects are not included, or averaged over (Indrajuana, 2020).

The base layer - hot engine tailpipe emissions

Tailpipe emissions for a given vehicle can generally be related to engine speed and engine load, and, related to the aftertreatment for most Euro 6 diesel vehicles, a historic component describing the temperature level of the SCR system. Vehicles with the same engine/exhaust gas aftertreatment combination should have similar emission behaviour with respect to the hot emissions layer. Therefore, the full engine block code is chosen as the distinguishing identifier. Note that aftertreatment behaviour is highly software dependent which would further investigation.

The emission maps are intended to be used in tools that simulate emissions of trips, e.g. to evaluate the improvement potential by changing driver behaviour. Vehicle speed profiles can be produced in many ways, without the necessity to read data from the vehicle's OBD or CAN bus. In order to also be able to share this data, a second design option will also be implemented for the hot emissions layer, based on vehicle speed instead of engine speed. Note that the actual emissions at a given speed depend on the selected gear, which means that the map based on vehicle speed cannot represent all situations but only driving with "average" gear shift behaviour, where "average" is related to the gear shifting used in the test data for setting up the AEMs.

Engine load, the second parameter to which tailpipe emissions can generally be related, is not always available. The CO₂ emission rate is chosen as the y-axis for NO_x AEMs, as CO₂ is a good proxy for the engine power demand which will vary with acceleration, payload, road slope and wind. In the case of limited data (test cycle data only), the CO₂ emission can be estimated by estimating ‘power’ using payload and test cycle characteristics such as velocity profile with the equations of vehicle longitudinal dynamics.

The first maps depict NO_x and are based on the TNO monitoring program (Spren *et al.* 2016) of a 2018 Volkswagen Caddy (see Figure 7). The map on the left-hand side has engine speed as an x-axis, the one to the right is based on vehicle speed.

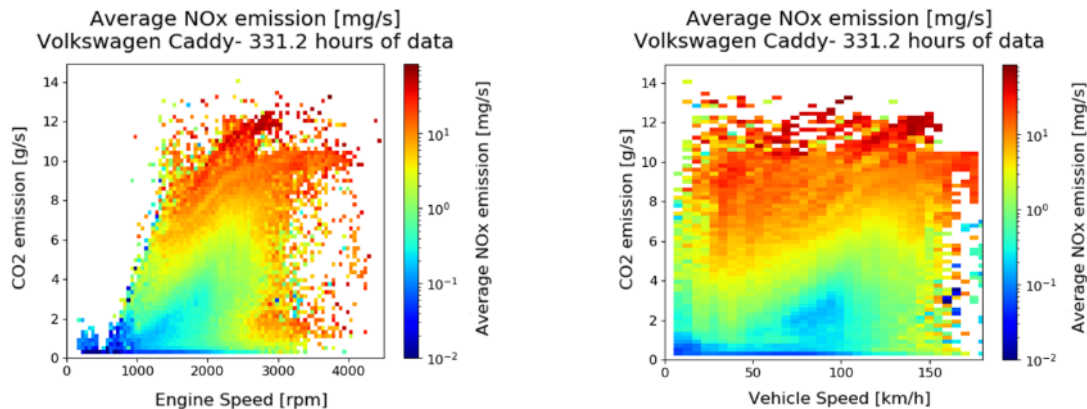


Figure 7: Emission map of average NO_x mass flow of a Euro 6 Volkswagen Caddy with a 1968 cc 55kW engine (D_6_1968_55_VAG), based on over 300 hours of driving data.

Similar maps can be made for PN, CO and HC. Figure 8 shows an example of a CO map.

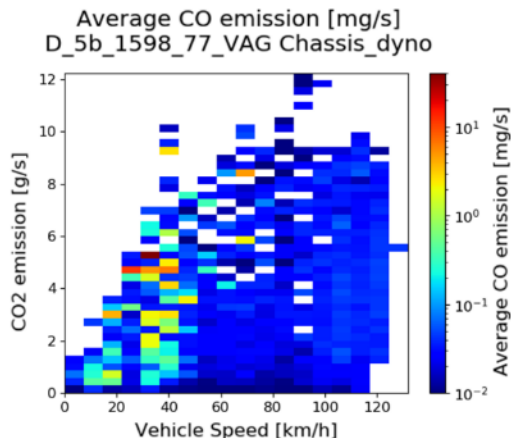


Figure 8: Emission map of average CO emission mass flow of Euro 5b Ford Fiesta with a 1598 cm³ 77 kW engine.

Emission maps of this design can be created for each engine. However, for most engines, less than 300 hours of data is available. This does not have to hamper the usability of the emission maps, as long as map coverage is warranted, and the resolution is adjusted in an appropriate way.

Non-regulated tailpipe emissions

Emissions of NO₂, N₂O, PAH, CH₄, cyanides and NH₃ can be mapped over the most suitable variables, based on chassis dynamometer tests where more extensive analyser equipment is used (e.g. FTIR). PEMS tests usually record, additionally to NO_x, also NO and NO₂ separately. An example NH₃ map (based on CO₂ and vehicle speed) is shown in Figure 9. Note that this may not be the final design for the NH₃ emission maps.

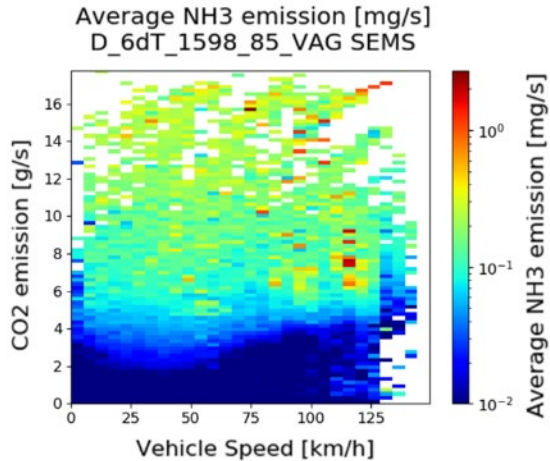


Figure 9: Emission map of average NH₃ mass flow of a Euro 6 diesel vehicle with 1598 cc 85 kW Volkswagen Group engine, based on 67 hours of driving data.

Examples of base emission maps

Monitoring the emissions of vehicles gives a good coverage of the whole operation spectrum of an engine. Figure 10 shows a graph of a NO_x emission map which is based on more than 600 hours of on-road measurement data of a Euro 6 diesel car. The average NO_x emission is shown per bin of vehicle speed and CO₂ emission.

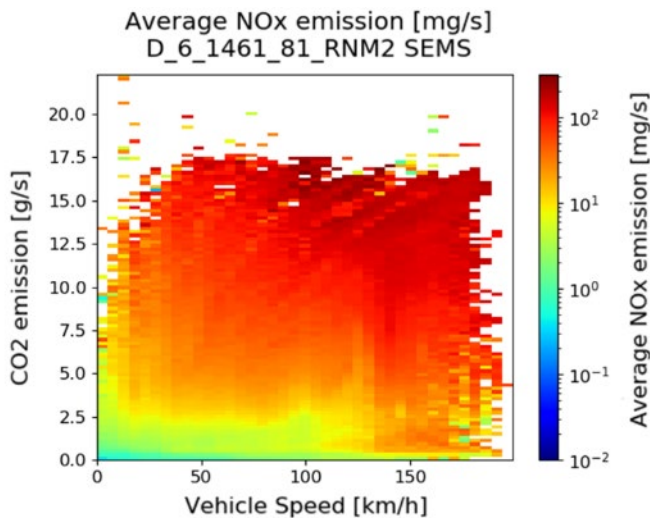


Figure 10: Emission map graph of a 1461cc, 81kW Euro 6 Diesel engine with average NO_x emission [mg/s] per vehicle speed [km/h] and CO₂ [g/s] bin.

Figure 11 shows a NO_x emission graph of a Euro 5a diesel engine with almost 330 hours of monitoring data. In the CO₂ emission range higher than 7 grams per second the effect of shifting gears is visible by the dark red lines.

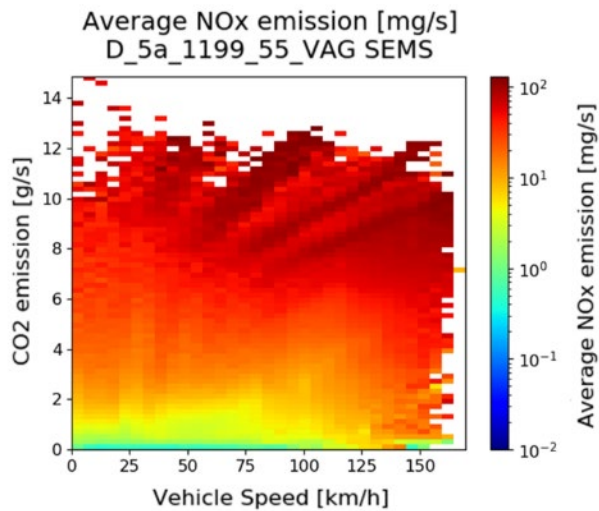


Figure 11: Emission map graph of a 1199cc, 55kW Euro 5a diesel engine with average NOx emission [mg/s] per vehicle speed [km/h] and CO₂ [g/s] bin.

Figure 12 shows the emission plot for a Euro 4 petrol engine. In comparison with Figure 11 this engine emits less NO_x over the whole spectrum. However, the amount of underlying data for Figure 12 is much less than for Figure 11.

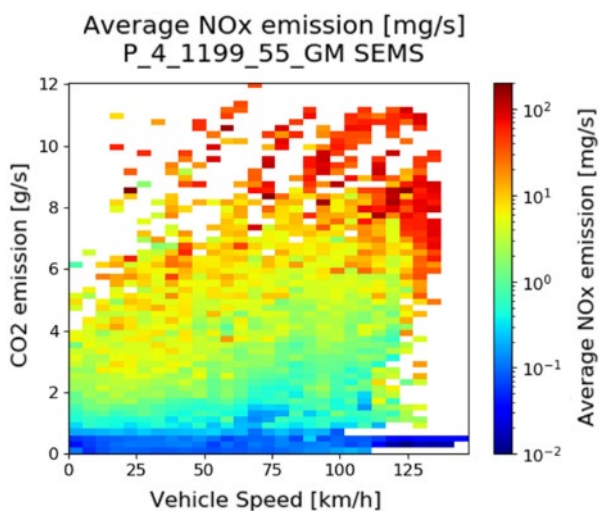


Figure 12: Emission map graph of a 1199cc, 55kW Euro 4 petrol engine with average NOx emissions[mg/s] per vehicle speed [km/h] and CO₂[g/s] bin.

Augmentation layers

The basemap is intended to be used in conjunction with so-called augmentation layers. Where the base layer describes hot engine tailpipe emissions, the augmentation layers describe effects of different driving conditions and emission sources. All layers together characterize parts of the emission behaviour of the vehicle. This is depicted in Figure 13.

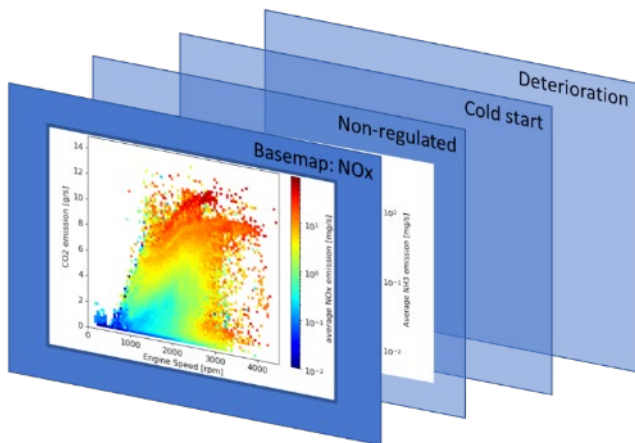


Figure 13: Graphical representation of the different layers that can be included within an augmented emission map.

Current base layers would describe NO_x (primary focus), PN, CO, and HC emissions. Other base layers could include tailpipe emissions of non-regulated emissions: NO₂, N₂O, PAH, CH₄, cyanides, and NH₃.

The following augmentation layers are currently under investigation (de Ruiter, *et al.* 2021):

- Tailpipe emissions under cold start conditions: NO_x (primary focus), PN, CO, HC
- Wear emissions: particulates from brake and tyre wear
- Deterioration: additional tailpipe emissions as a result of ageing and/or poor maintenance: NO_x, PN, CO, HC, NO₂, N₂O, PAH, CH₄, cyanides, NH₃

The initial proposals above address a range of conditions that are influenceable by the user which can affect vehicle emissions. Each map layer can have a different x- and y-axis, a different resolution and a different level in the taxonomy to be attached to.

Map integration and map selection

AEMs have been created for many engines. However, given the vast number of engine types in use (including updates with newer Euro standard compliance), it has not been possible to create a vehicle-specific emission map for every single one of them. Fortunately, dependent on the map layer, there are similarities among certain maps that can be used to make extrapolations to other engines deemed similar in behaviour. Three tools were developed to help tool-builders: fallback maps, a selection tool, and a combining tool (De Ruiter, *et al.* 2021).

Fallback maps

To have an emission map available for every engine that was not specifically measured, a set of fallback maps was created: one for every fuel – Euro standard combination (where data available). The fallback maps have a taxonomy code with the following structure: F_E_ALL_ALL_ALL, whereby F and E stand for the fuel and Euro class parameters. To generate the maps, the raw measurement data of all tested vehicles within a fuel-Euro class-group was combined, and re-processed as were it a single vehicle.

Selection tool

The fallback maps ignore the possible differences in emissions caused by engine displacement, power, and make. Therefore, recently a more sophisticated tool was developed that, for any given untested car/engine, selects the best suitable one among the available maps. So far the tool was implemented for NO_x only. The underlying algorithm analyses the existing available maps using a clustering method and describes their characteristics in 9 coefficients. This model setup activity is flexible and can incorporate new maps as they are added to the collection over time. When the model is run, it uses the untested engine's taxonomy code to rank available maps by their Gower distance, and produces the five most suitable maps for the untested engine (Nooij, S., 2021). A large variation has been observed among for instance Euro 6dT diesel engines. The selection tool can help to find a more representative map than the Euro 6d-Temp fallback map. The work on the tool is in progress. Further criteria to select the best map may be the amount of data (the second best suitable map may have more detail), and engine manufacturer as opposed to alliance

code; various collaborations of one manufacturer have different alliance codes, but may utilize the same exhaust gas treatment equipment.

Combining tool

Emission basemaps of a certain engine may come from different sources, e.g. when vehicles with the same engine were measured by one or more institutes. If there are multiple basemaps for the same uCARE taxonomy code, these basemaps should be combined. A map combination tool was built for this purpose, which works as shown in Figure 14.

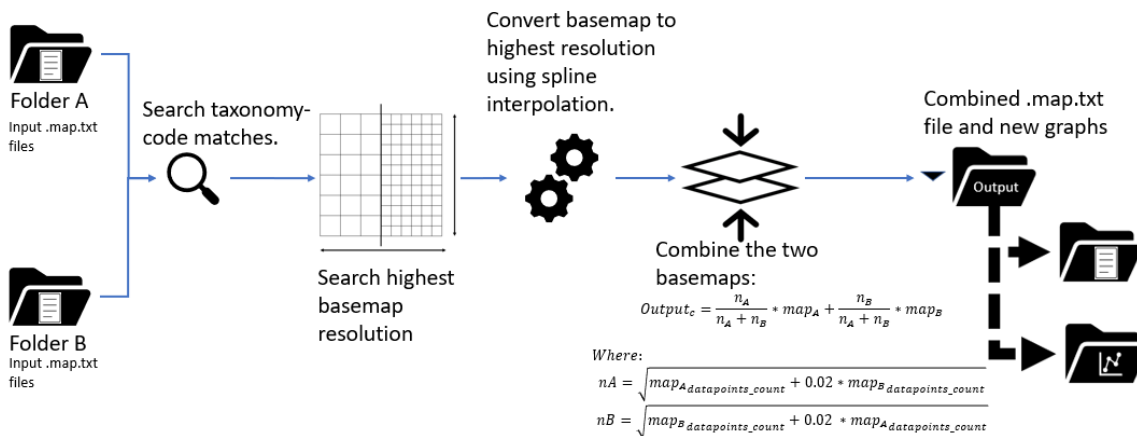


Figure 14: Illustration of basemap combining tool.

The lowest resolution basemap is converted to match the resolution of the more detailed one, using spline interpolation. The maps are combined using a weighting factor based on the square root of the total number of datapoints within the map.

Discussion and conclusions

To characterise, store and distribute emission data of vehicles, an emission map concept has been proposed. Experiment-based understanding of the relationship between the use of a vehicle and the emissions are described in a logical and structured way, be it in the form of a map or in the form of a function. To order vehicles and their engines that the emissions (maps) are attributed to, an 11-level taxonomy has been developed. Maps or functions can be created on any level of the vehicle taxonomy, dependent on distinctiveness and availability of data.

A strict separation of factual data and interpretation has been pursued. Interpolation and smoothing of maps, as well as the implementation of the functions in the augmented emission maps, is considered part of the tools that use the maps/functions.

The dimensions of maps can vary for each layer, dependent on which parameters describe the emission behaviour best. For hot engine tailpipe emissions, vehicle or engine speed, and CO₂ emission mass flow (as a proxy for engine power) were selected. The maps are produced on an engine level: vehicles sharing the same engine are modelled in the same way.

To handle a varying data availability among vehicle types or engine types, maps have a flexible resolution. The map resolution that is selected, complies to minimum standards in terms of coverage.

Although maps are added on a regular basis, for many engines base emission maps are not available yet. Fallback maps and a map selection tool were created to ensure generic applicability of the concept. Finally, a combine tool was created to merge multiple maps for the same engine.

Making emission data of vehicles, in relation to underlying variables, available to this extent and in this detail, brings to light many nuances in emission results. In the past only the average results and the results of standard tests were available and used for comparison. However, with on-road testing as the new standard for emission testing, a large variation is observed in results, partly related to driving behaviour and conditions. Results are not a priori comparable. In order to understand, relate and compare results and to be able to base emission estimations on measurements, a further development is needed. This work intends to provide a suitable basis to use emission measurements more widely and comprehensively.

Acknowledgement

The work on the emission maps and engine taxonomy has been carried out in the H2020 uCARE project under GA 815002.

The deliverable reports and spreadsheets describing the work in this paper are public and can be found on www.project-ucare.eu. The growing collection of emission map files can be downloaded free of charge from: <https://zenodo.org/communities/ucare>

References

Elstgeest, M., Indrajana, A., Ruiters, J. de, Gijlswijk, R. van, Ligterink, N., Tilanus, P., Augmented emission maps, uCARE deliverable D1.2 v2.0, 2020.

ACEA, Vehicles in use – Europe, January 2021.

Spreen, J. S. et al, Assessment of road vehicle emissions: methodology of the Dutch in-service testing programmes - TNO 2016 R11178v2, 2016.

Indrajana, A.P., Ligterink, N.E., van der Mark, P.J., Monitoring-based assessment of the NO_x emissions of a Renault Talisman and a Volkswagen Caddy, TNO Report 2020 R10438, 2020.

Ruiters, J. de, Gijlswijk, R. van, Elser, M., Ligterink, N., Tilanus, P., Augmented emission maps are an essential new tool to give individualised emission feedback, 2021. *Manuscript accepted for presentation at ITS World Congress 2021.*

Nooij, S., Emission map selection tool and driver classification, master thesis, April 2021.

2.26 Portable, on-board FTIR spectrometers: A universal tool for real-world monitoring of greenhouse gases, reactive nitrogen compounds, and other gaseous pollutants?

Michal Vojtíšek¹, Martin Pechout²

¹ Center for Sustainable Mobility, Czech Technical University in Prague, Czech Republic

² Department of Vehicles and Ground Transport, Czech University of Life Sciences, Prague, Czech Republic

michal.vojtisek@fs.cvut.cz

Abstract

Exhaust emissions from internal combustion engines are one of the principal sources of greenhouse gas emissions, and one of the leading sources of air pollution in most metropolitan areas. Outdoor air pollution is associated premature death of about 0.1% population annually and associated economic damages on the order of 5% of the gross domestic product.

In addition to CO₂, the importance of methane (CH₄) and nitrous oxide (N₂O) is emerging as a result of the increased use of natural gas or biogas and of reduction catalysts. Of health relevant pollutants, most of the health effect is associated with particle bound semi-volatile organic compounds and with nitrogen monoxide (NO) and dioxide (NO₂), reported together as nitrogen oxides (NO_x). Ammonia (NH₃), owing to the potential to form secondary particles of ammonium nitrate, and potentially other reactive nitrogen compounds may be of interest. Of volatile organic gases, formaldehyde, acetaldehyde, and other fuel and technology dependent compounds may also be of a concern.

Fourier Transform Infra-Red (FTIR) analyzers have been increasingly used to analyze a wide range of compounds in exhaust gases, including all of the mentioned gases of interest, and have been recognized as a method for type-approval measurement of NH₃. Commercially available laboratory FTIR were shown to produce results comparable to laboratory analyzers for CO, CO₂, NO and NO₂, with the only potential downside being agreement with a flame ionization detector on total hydrocarbons.

Two pathways are suggested to exploit FTIR as a portable on-board instrument. In one, water is removed by cooling of the sample and/or selective membranes, after which greenhouse gases CO₂, CH₄, N₂O, and non-polar, non-water-soluble, highly volatile compounds such as NO and NO₂ can be readily quantified even at mediocre optical resolutions (units of cm⁻¹) and relatively short optical path lengths (on the order of 1 m), allowing small cells and detectors with thermoelectric cooling to be used.

For a more detailed and comprehensive analysis, water is kept in the sample, and the entire sampling train is heated to prevent condensation of water, ammonia, and less volatile compounds. Retaining the water allows for the detection of additional compounds such as ammonia, formaldehyde, or ethanol. Higher optical resolution (0.5 cm⁻¹) is then typically required to resolve the compounds interfering with water and CO₂. Operating at a higher resolution, however, requires a faster detector and tighter tolerances in the optical path, and the increased noise needs to be balanced against the instrument response time. Another critical decision is the selection of the optical path length. Longer path lengths increase the instrument sensitivity, but also increase the occurrence of regions where analysis is prevented due to nearly complete attenuation by water, and typically require larger optical cell volumes, increasing the system response time. Optical path lengths of 2-10 meters have been used.

Several different FTIR systems used by the authors in moving vehicles as portable emissions monitoring systems will be discussed. Overall, FTIR technology may be useful for real-world emissions measurement of all gaseous pollutants of current interest with a single instrument.

Introduction

Internal combustion engines of various types and running on a variety of traditional and experimental fuels remain to be the principal source of motive power for the majority of automobiles and heavy on-road vehicles, as well as for the majority of most types of mobile machinery. The freedom of movement and the tremendous societal and economic benefits realized through mobility and work done by the machinery come at a major cost: Engines are one of the major sources of air pollution in urban areas, and one of the key sources of greenhouse gas emissions. Outdoor air pollution is listed within the top ten health hazards [1] and is associated with severe health and economic damages, including premature death of on the order of 0.1% of population annually (over half a million premature deaths per year in the EU [2], over an order of magnitude more compared to traffic accidents), and economic costs of approximately 5% of the Gross Domestic Product [3,4]. While engine exhaust emissions have improved considerably, and the number of

premature deaths has a gradual downward trend, they remain one of the key problems. The persistence of the emissions problem is attributed not only to the high intensity of motor vehicle traffic and the close proximity of exhaust sources to the population, but also due to the discrepancy between type approval limit values and the actual emissions during everyday operation. The introduction and consequent gradual optimization of highly efficient exhaust aftertreatment has produced a situation where the distributions of emissions along a trip and among the vehicles are increasingly skewed, with large portion of fleet emissions attributed to a relatively small number of vehicles and large portion of trip emissions attributed to relatively short episodes of high emissions. Additionally, the quest to lower the emissions of the key pollutants that become subject of emissions limits (regulated pollutants) had an inadvertent side effects in the form of additional pollutants, which were, at the time, not of a grave concern. A meaningful characterization of the actual emissions from in-use vehicles requires, therefore, measurement under realistic conditions of a range of pollutants on a range of individual engines.

To assess the inherent characteristics of the design and systematic problems, portable, on-board monitoring instruments mounted on selected vehicles tested thoroughly under a variety of realistic conditions can be used during engine design and calibration, evaluation of drop-in fuels and aftermarket NO_x reductions, and independent verification of the in-use performance of vehicle or engine families [5]. To assess high emissions specific to individual vehicles, remote sensing approaches, offering high-volume testing at relatively low cost but at a limited range of operating conditions, can be used to identify individual vehicles with excess emissions due to tampering or malfunctions, and also to identify suspect engine design and calibration issues [6].

In this work, molecular spectroscopy in mid-infrared region, with the use of a Fourier Transform Infra-Red (FTIR) spectrometer, is suggested as a single universal tool for on-road assessment of all principal compounds that are known to be of interest at this time.

Pollutants of interest

Realistic combustion processes yield, in addition to carbon dioxide (CO₂) and water, carbon monoxide (CO), various volatile organic compounds (VOC, also termed HC – hydrocarbons), particulate matter and nitrogen oxides (NO_x). While particulate matter, originating from incomplete combustion of fuel and engine lubricating oil and from uncombustible portion of fuel and oil and engine wear particles, has been viewed as the most critical health-relevant pollutant, its discussion is not within the scope of this work.

Nitric oxide (NO) is formed at high temperatures during the main phase of the combustion from atmospheric nitrogen and oxygen, and form nitric oxide (NO), a process known as Zeldovich mechanism [7,8]. Subsequent oxidation of NO in the atmosphere yields primarily nitrogen dioxide (NO₂), a brownish irritant gas. NO₂ in outdoor air has been associated with mortality and hospital admissions for a range of respiratory and cardiovascular endpoints [8-11]. Other oxides of nitrogen – N₂O₂, N₂O₃, N₂O₄, N₂O₅ – are generated in small concentrations, are unstable and short-lived in the atmosphere. The oxides of nitrogen are summarily referred to as NO_x, although there is no precise definition. Often, NO_x is evaluated as the sum of NO and NO₂. Technically, the sum of NO_x also includes nitrous oxide (N₂O), which is, however, not hazardous to human health, but is a potent greenhouse gas with global warming potential approximately 265 times higher relative to CO₂ [12]. NO_x lead to the formation of nitrous acid (HNO₂) [13,14], nitric acid (HNO₃), and a variety of salts such as ammonium nitrate, present in the atmosphere as particulate matter [15]. Photodissociation of NO₂ under the presence of sunlight produces NO and atomic oxygen, which reacts with molecular oxygen to form ozone [16], a highly reactive compound generally harmful to human health, organisms and plants. NO_x and ground-level (tropospheric) ozone are, together with particulate matter, the principal part of urban air pollution.

CO and VOC are principally a product of incomplete oxidation of fuel and to a lesser extent engine lubricating oil.

On spark ignition engines, CO and VOC, principally a product of incomplete oxidation of fuel and to a lesser extent engine lubricating oil, and NO_x have been successfully abated by the combination of three-way catalysts (TWC) [17] and by maintaining stoichiometric air-fuel ratio through closed-loop control of the quantity of fuel injected [18]. This technology has been remarkably efficient. On some vehicles tested at the turn of the millennium, the concentrations of CO and NO in the exhaust gases were lower than in the surrounding air [19], and even larger automobiles were capable of reaching the total sum of organic compounds and NO_x of less than 10 mg/km [20]. California type approval documentation of a Honda car shows the total emissions of organic compounds and NO_x during the type-approval test (FTP) of approximately 14 mg/km [21].

Larger stationary spark ignition engines fueled by natural gas achieve relatively low engine-out NO_x by operating at a very lean mixture. Such operation is, however, close to the lean limit of the engine, and often results in substantial emissions of methane.

On diesel engines, where three-way catalyst cannot be used due to excess air, some level of reduction of NO_x emissions has been achieved through reducing peak combustion temperatures via delaying injection timing, exhaust gas

recirculation (EGR), and later by advanced combustion strategies such as low temperature combustion (LTC) and partially premixed charge compression ignition combustion [22,23]. Both EGR and advanced combustion concepts are, however, effectively limited to lower engine loads. More recently, various catalytic devices have been explored, of which LNT and SCR have shown relatively high potential [24] and are currently used in production vehicles. LNT (for overview, see [25]) operates alternately in a long (on the order of minute or minutes) “lean” accumulation mode, during which NO_x are stored (i.e., as barium nitrate) in the catalyst, and in a short (on the order of seconds) “rich” regeneration mode, during which the engine operates with excess fuel, NO_x are released, and reduced in a manner similar to a three-way catalyst.

SCR (reviewed in [26]) use a reducing agent, aqueous solution of urea, which is injected upstream of the SCR, is mixed with the exhaust, and thermally decomposes into NH₃, which is used to reduce NO_x; NH₃ is also stored in the SCR. Recently, solid ammonia storage has been demonstrated as an alternative to urea [27]. Except for very low exhaust temperatures associated with cold start and extended low-load operation, SCR catalysts achieve efficiencies over 90%. U.S. federal (EPA) 2010 NO_x limit for heavy vehicle engines of 0.2 g/bhp-h (0.27 g/kWh) and the Euro VI limit of 0.46 g/kWh represent over an order of magnitude reduction over early limits. SCR allows California trucks made after 2010 – and quite possibly also European heavy vehicles – are likely to produce lower NO_x emissions per km per vehicle than most Euro 5 diesel cars, with a further decrease in NO_x limit by additional 90 %, to 0.02 g/bhp-h, proposed [28], and found to be technically feasible by a California Air Resources Board assessment [29].

The most efficient catalytic devices – TWC and SCR rely on precise control of the air-fuel ratio for TWC, and of the dosing of the reducing agent for SCR. Excess air in TWC and insufficient amount of reducing agent in SCR reduce NO_x conversion efficiency, while excess fuel in TWC [30,31] and excess reducing agent in SCR results in the emissions of ammonia (NH₃), an important emerging pollutant. Large portion of NH₃ in urban air in the U.S. and China originate from motor vehicles [32]. NH₃ is a precursor of secondary inorganic aerosol, namely ammonium nitrate and sulfate [33,34] which are the most abundant atmospheric secondary inorganic aerosols in many regions [35,36].

Another emerging pollutant is NO₂, which is intentionally produced in diesel oxidation catalysts, as it aids passive regeneration of diesel particle filters and increases the speed of NO_x conversion in SCR. As a result, NO₂ from new engines accounts for tens of percent of NO_x [37,38]. When high NO₂ is not mitigated by the high efficiency of SCR, such as on many diesel cars operated in the EU, more NO_x is emitted as NO₂ instead of NO, and the concentrations of NO₂ on streets tend to increase.

The list, of course, does not end here. Decomposition of water-urea solution, the most popular SCR reducing agent (also known as Diesel Exhaust Fluid or AdBlue), into ammonia yields isocyanic acid (HCNO) as an intermediate product [39-41], and various nitrogen compounds have been found in diesel exhaust, including 3-nitro-benz[a]benzanthrone, one of the most mutagenic compounds known to date [42].

Limitation of engine design by many manufacturers to the type approval procedures has resulted in marginal design, where catalysts on passenger cars are often properly sized only for low and intermediate loads, and infatuation by high horsepower rating on car engines has resulted in marginal practices to achieve high loads by, for example, disabling exhaust gas recirculation or fuel enrichment on gasoline engines (for examples, see [43-47]). Savings on sophisticated controls of air-fuel ratio or SCR reducing agent dosing have resulted in achieving low NO_x at the expense of considerable emissions of NH₃.

Furthermore, savings of fuel, reducing agent or motorist effort (to replenish diesel exhaust fluid on passenger cars) have motivated, over the last few decades, manufacturers, aftermarket sector, and motorists to modify or adjust their engines to achieve meager savings at the expense of several-fold or even order of magnitude increase of NO_x emissions. Examples of convictions include dual-mapping of engines in 90's on heavy-duty vehicles [48] and later on EU light-duty vehicles (later commonly known as Dieselgate), manufacture of defeat devices (i.e. [49]), disabling of exhaust gas recirculation on cars, and SCR emulators for heavy trucks widely abundant on the internet.

Of all NO_x emissions from passenger cars in Europe, 56% were estimated to be excess emissions, which could be eliminated if the average on-road NO_x emissions were at the level of the respective diesel limit values [50]. These excess emissions represent about 15% of all NO_x emissions in Europe [50] and were associated with about 5000 premature deaths annually [51].

To minimize excess emissions associated with sub-optimal performance of engine and associated exhaust aftertreatment devices, at a minimum, the following compounds should be monitored throughout the operation of the vehicle fleet:

- Principal greenhouse gases CO₂ (all engines), CH₄ (gaseous fuel engines) and N₂O (lean-burn engine aftertreatment)
- Reactive nitrogen species, at the minimum, NO (primary engine-out pollutants from all engines), NO₂ (lean-burn engines with aftertreatment), NH₃ (all engines with NO_x aftertreatment)

- CO and fuel-specific VOC (formaldehyde, acetaldehyde)

Spectroscopic techniques

The absorption spectra of the principal compounds of interest in engine exhaust – water, greenhouse gases CO₂, CH₄, N₂O, health relevant pollutants CO, NO, NO₂, NH₃ – in the spectral range from approximately 4000–600 cm⁻¹ (2.5 – 13.3 μm) are shown in Figure 1; omitted are various organic gases (alkanes, alkenes, aromatics, aldehydes, ...), for which only general regions are shown. This range, useful for molecular spectroscopy measurements, is generally considered mid-infrared range, although some parts of it may be considered near (short wave) or far (long wave) infrared depending on varying classifications. Water is not considered a pollutant but absorbs in many spectral regions and its spectra overlaps with the spectra of many other measured compounds, creating an interference issue. Nitrogen, oxygen and inert gases absorb only minimally in this region.

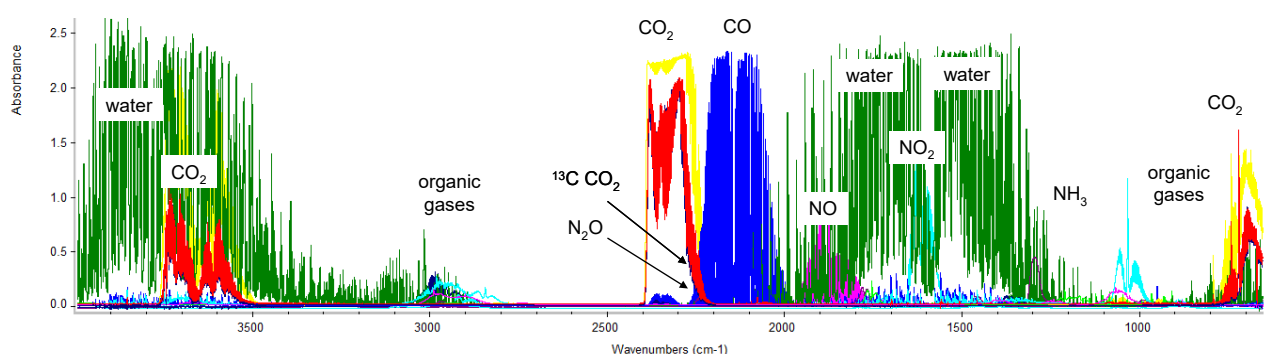


Figure 1: Mid infra-red spectra of principal compounds of interest in vehicular exhaust.

Several spectroscopic techniques are available for quantitative analysis, mostly based on absorption spectroscopy and the Beer-Lambert law. When light of intensity I_0 at specific wavelength is passed through a mixture measured gas and gases not absorbing at this wavelength, the resulting intensity I_r at this wavelength is a function of the absorption properties of this gas (dependent on temperature, pressure, wavelength, and other conditions), its molecular concentration, and the path length:

$$I_r = I_0 \exp(-\epsilon\lambda LC) \quad (1)$$

Where $\epsilon\lambda$ is cross-absorption coefficient in m⁻¹ at wavelength λ , L is path length in m, and C (dimensionless) is the concentration of the measured species. Absorbance A is defined as negative decadic logarithm of transmittance T , defined as the ratio I_r/I_0 :

$$A = -\log T = -\log (I_r/I_0) = k\epsilon\lambda LC \quad (= \epsilon\lambda LC) \quad (2)$$

where constant k is given here only for formal reasons (conversion of logarithm base) and is typically reflected in the constant $\epsilon\lambda$. Typically, constant $\epsilon\lambda$ is determined empirically for each given analyzer and summarily accounts for different additional factors. In reality, the absorption at any wavelength λ is the sum of absorptions of all compounds absorbing at that wavelength. Infrared spectroscopy is therefore prone to interference from other compounds, which need to be accounted for, regardless of whether the knowledge of their concentration is desired.

The simplest technique, used in garage-grade analyzers (used for vehicle diagnostics and repair and for periodic technical inspections) and a variety of inexpensive sensors, is non-dispersive infra-red (NDIR) spectroscopy, where analysis is performed on a wavelength range pre-selected by the choice of source (LED diode), detector, or, most frequently, the source is a glowing element and the wavelength is selected by an optical filter. NDIR requires compensation for interfering gases (quantification at a different wavelength and subtraction), or most frequently, their removal. This is why NDIR is used for CO and CO₂, which have absorption bands generally free of interference, but not for many other gases. In industrial settings, NDIR is also used for NO with the removal of water by thermoelectric cooler. NH₃, and to some extent NO₂, are soluble in, and are removed with, water.

For NO₂, NH₃ and N₂O in vehicular exhaust, "broad band" NDIR cannot be used, due to strong interference of water (NO₂ and NH₃) and CO₂ and CO (N₂O). The analysis regions for these compounds are fairly narrow, with example analysis regions shown in Figure 2. Further, water in the exhaust (typically up to 10% for diesel engines, up to 13% for gasoline engines, up to around 20% on engines running on methane; 4% is shown in Figure 2) leads to nearly complete absorbance (band saturation) at many wavelengths (absorbance 2.0 corresponds to 99% attenuation, 3.0 to 99.9% attenuation). Typically, high-resolution techniques, such as Fourier Transform Infra-Red (FTIR) spectroscopy,

tunable diode laser absorption spectroscopy (TDLAS), or quantum cascade lasers (QCL) are needed, and have been successfully deployed. The example in Figure 2 are calibration spectra used with FTIR analyzer sampling undiluted engine exhaust, representing (except for water, deliberately shown at 4%, relatively low end of the range) values around the upper end of the desired quantification ranges (20 ppm N₂O, 100 ppm NH₃, 200 ppm NO₂, 3000 ppm NO). Often, interference cannot be avoided, and the absorption of the interfering compounds needs to be quantified separately at different wavelengths and subtracted. Fortunately, higher N₂O emissions are typically limited to diesel engines with NO_x aftertreatment (LNT, SCR), which exhibit, thanks to the oxidation catalyst, very low CO emissions, except for LNT regeneration.

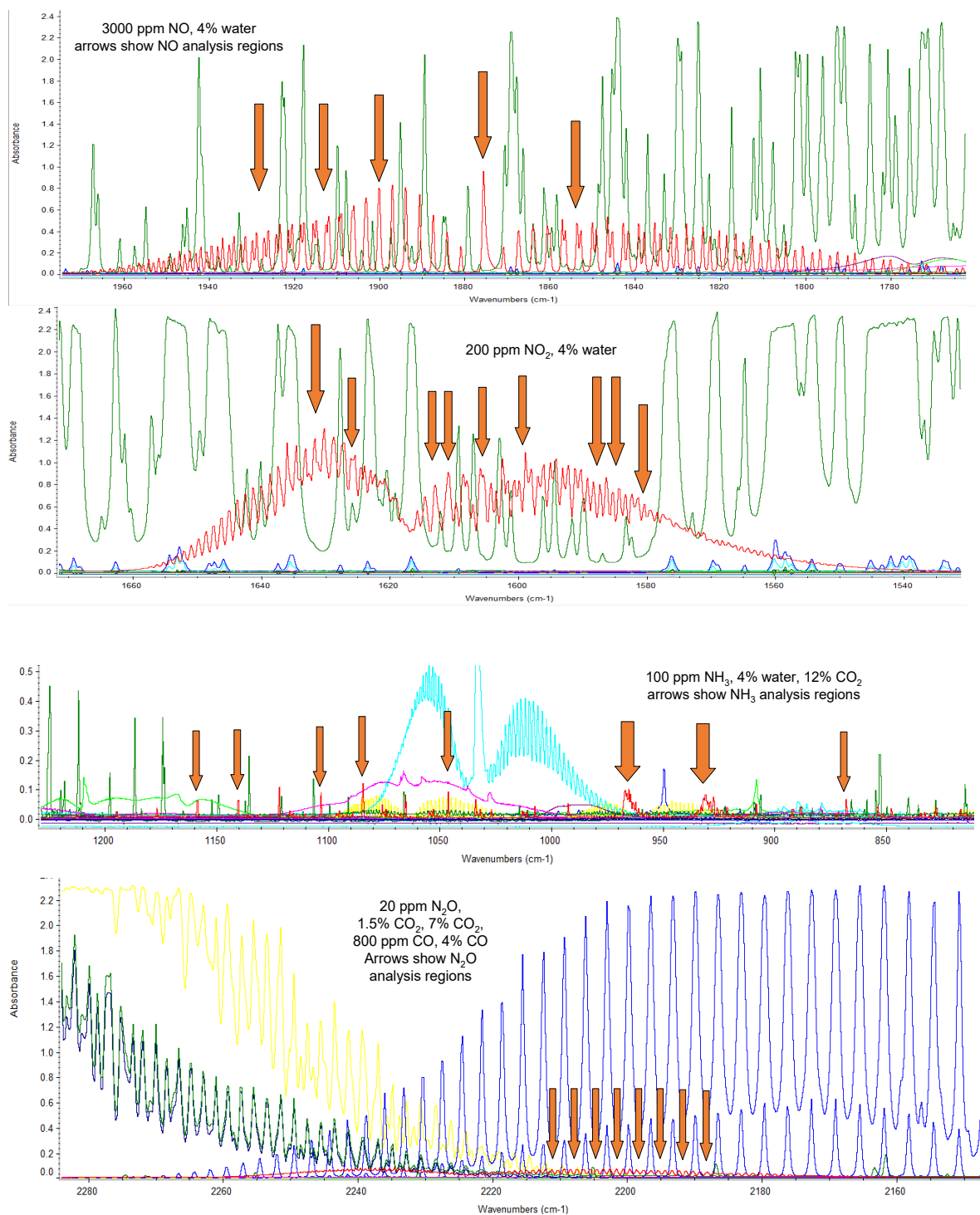


Figure 2: Possible analysis regions for (top to bottom): NO, NO₂, NH₃, N₂O.

FTIR

In an FTIR analyzer, an infrared source producing a wide and continuous range wavelength light, such as a heated tungsten wire, is used. The beam is divided in a Michelson type interferometer by a beam splitter into two beams, one reflecting from a fixed mirror and the other reflecting from a mirror moving along the beam direction. The two beams are then joined, creating, for each difference between the optical path lengths, an interference pattern. The resulting beam is passed through a multi-pass sample cell filled with the analyzed exhaust, and the total intensity recorded, for each difference in optical path lengths, by a detector. The interferogram is transformed by a Fast Fourier Transform into a transmission spectra in the frequency domain. This approach leads to a higher signal to noise ratio than if the transmission at each wavelength was to be measured separately [52].

The use of FTIR for exhaust measurement has been reviewed in [53,54]. The use of FTIR in a moving vehicle has been, so far, limited due to technical challenges. Jeter [55] has used a pair of laboratory FTIR with a membrane sample dryer (a technique not compatible with NH_3 measurement) and a 10 m optical path length mounted in an instrumented vehicle to assess very low emission levels from a passenger car. A smaller but still relatively bulky and relatively slow (30 s time resolution) instrument with a 13 m optical path length was used by Reyes [56]. A portable, fast system has been used by Daham [57], however, the system worked at a relatively low (4 cm^{-1}) optical resolution, while a substantially higher resolution – at least 0.5 cm^{-1} – has been recommended, along with the tunable laser diode approach, for NH_3 measurement [30]. An on-board system built at the Technical University of Liberec using an industrial grade MIDAC FTIR analyzer with a custom optical cell, providing 6 m path length in a relatively low 0.2 liter volume, has been validated for NO and NH_3 measurement in the laboratory and for NO measurements on the road [58]. The limits of detection, calculated assuming 3 times the standard deviation of the background measured, for NH_3 and NO were 1 ppm. The system has been used on a range of vehicles from passenger cars [58] to locomotives [59] (shown in Fig. 3 on the left). A similar setup using faster (1 Hz) industrial FTIR (Nicolet Antaris IGS) with a 0.3 dm^3 , 5 m path length cell, with about double the mass and double power consumption, but a faster time resolution of 1 Hz, has been prepared and validated at the Czech Technical University (shown in Figure 3 on the right) and recently used for evaluation of emissions of compressed natural gas vehicles [60] both on the road and in the laboratory, with laboratory measurements done in parallel using a full-flow dilution tunnel and standard instruments as a reference. A relatively compact setup using a Bruker Matrix FTIR system, with a series of modifications, has been developed and used at the Czech University of Life Sciences [61,62].

The path length and spectral and temporal resolutions are a careful compromise among contradicting goals. A longer path length and longer averaging time decrease the detection limit, but longer path length also increases the regions where the beam is excessively attenuated by carbon dioxide and water. Higher optical resolution increases noise but allows for discrimination of, for example, nitric oxide from order of magnitude higher concentrations of water vapor.

The TU Liberec, Czech Technical University and Czech University of Life Sciences systems used on the road, as well as the reference laboratory FTIR in [58] (MKS 2030), see [63,64] for additional description, used mercury cadmium telluride detectors cooled by liquid nitrogen, heated 5-6 m optical path length multipass cells, and run at the spectral resolution of 0.5 cm^{-1} . The reported sample train and optical cell temperatures ranged from 121 to 191 °C.

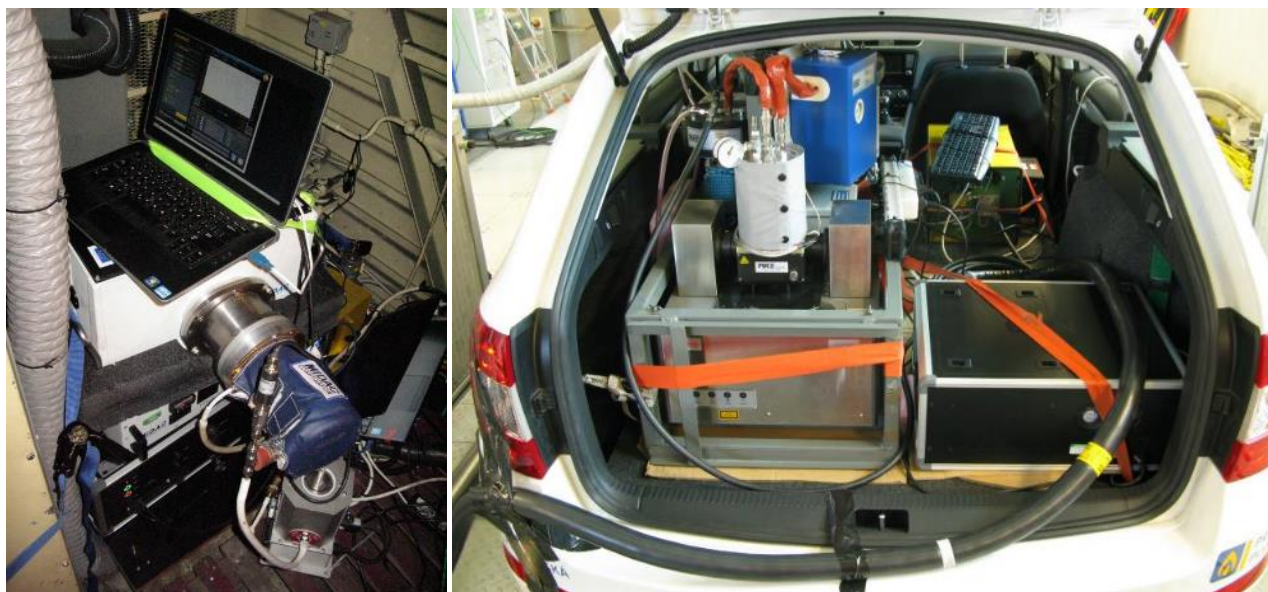


Figure 3: On-road FTIR setups:
 Left: MIDAC, TU Liberec, Czech Republic [58, 59];
 Right: Laboratory grade Nicolet Antaris, Czech Technical University [60].

There are two major caveats with FTIR. One is the possible distortion of the spectra due to contamination of the optics with semi-volatile organic species, excessive vibrations and jolts, fluctuations in various temperatures (instrument internals, optical cell, sample), and other reasons. The quality of the spectra can be checked by evaluating certain regions of the spectra and/or by comparing the concentrations of at least some gases for which reference measurement is available (CO_2 calculated from exhaust gas oxygen sensor, NO_x measured by a sensor in exhaust). This can be, with proper care, minimized, or at least such distortions could be detected.

The second and probably more serious caveat is that the measured absorption spectra is the sum of the absorptions of all absorbing compounds, and that the contributions of each compound are calculated from often overlapping individual absorption spectra obtained by deconvolution of the measured spectra. Therefore, detection limits, uncertainties, or even the capability to obtain a meaningful reading for a given compound, are specific to the composition of the mixture. For example, the detection limit achieved with a mixture of calibration gas with dry nitrogen is unlikely to be achieved in the presence of several orders of magnitude higher concentrations of CO_2 and water vapor. This is, however, a known issue, common to both on-road and laboratory measurement, and is dealt with, to various degree of success, by spectroscopy specialists. It should not, however, be underestimated. For example, in a study by Li et al. [65], multiple commercial FTIR instruments were reported to provide different results. On a positive note, if such problem is discovered and resolved, interpretation of the spectra can be done ex-post.

Conclusions

Several FTIR analyzers have been successfully used on a variety of moving vehicles, from cars to a diesel locomotive, suggesting infrared absorption spectra can be obtained on the road. Combined with the general use of FTIR in laboratory settings to measure a variety of regulated and unregulated compounds, it seems that FTIR analyzers can be, and have been, used to measure the three principal greenhouse gases CO_2 , N_2O and CH_4 , principal reactive nitrogen compounds NO , NO_2 and NH_3 , and a variety of other gases such as CO and formaldehyde, making it a universal instrument for essentially all gaseous pollutants at least of current interest.

Acknowledgement

The manuscript has been prepared as a joint effort of H2020 projects no. 815002 - uCARE – You can also reduce emissions and no. 814966 - CARES – City Air Remote Sensing.

References

1. Health Effect Institute (2018): State of Global Air. <https://www.stateofglobalair.org/sites/default/files/soga-2018-report.pdf>
2. EEA (European Environment Agency): Air quality in Europe – 2020 report. EEA, Copenhagen, 2020.
3. Nam, K.-M., Selin N.E., Reilly J.M., Paltsev S. (2010). Measuring Loss in Human Welfare Caused by Air Pollution: A CGE Analysis for the European Region. *Energy Policy* 38(9): 5059-5071.
4. World Bank and Institute for Health Metrics and Evaluation. 2016. The Cost of Air Pollution: Strengthening the Economic Case for Action. Washington, DC: World Bank.
5. VOJTISEK-LOM, M.; COBB, J. T. (1997). Vehicle mass emissions measurement using a portable 5-gas exhaust analyzer and engine computer data. *Proceedings: Emission Inventory, Planning for the Future, 1997*.
6. BISHOP, G.A.; STARKEY, J.R.; IHLENFELDT, A.; WILLIAMS, W.J.; STEDMAN, D.H. (1989): IR long-path photometry: a remote sensing tool for automobile emissions. *Analytical Chemistry*, 61 (10), 671A–677A.
7. ZELDOVICH, Y. B. (1946): The Oxidation of Nitrogen in Combustion Explosions, *Acta Physicochimica USSR*, 21, 577–628.
8. LAVOIE G.A., HEYWOOD J.B. & KECK J.C. (1970): Experimental and Theoretical Study of Nitric Oxide Formation in Internal Combustion Engines, *Combustion Science and Technology*, 1:4, 313–326.
9. FAUSTINI, A., RAPP, R., FORASTIERE, F., 2014. Nitrogen dioxide and mortality: review and meta-analysis of long-term studies. *Eur. Respir. J.* 44, 744-753.
10. US EPA, 2015. Integrated Science Assessment for Oxides of Nitrogen - Health Criteria (Second External Review Draft), EPA/600/R-14/006. <http://cfpub.epa.gov/ncea/isa/recordisplay.cfm?deid=288043> [Accessed February 2016]. United States Environmental Protection Agency, Washington DC.
11. BRAND, Christian. Beyond 'Dieselgate': Implications of unaccounted and future air pollutant emissions and energy use for cars in the United Kingdom. *Energy Policy*, 2016, 97: 1-12.
12. IPCC (Intergovernmental Panel for Climate Change) Fourth Assessment Report: Climate Change, 2007.
13. GUTZWILLER L., ARENS F., BALTENSPERGER, U., GÄGGELER H.W., AMMANN M. (2002): Significance of Semivolatile Diesel Exhaust Organics for Secondary HONO Formation. *Environmental Science & Technology* 2002 36 (4), 677-682.
14. KURTENBACH, R., et al. (2001). Investigations of emissions and heterogeneous formation of HONO in a road traffic tunnel. *Atmospheric Environment*, 35.20: 3385-3394.
15. HEEB, N.V., et al. (2011). Reactive nitrogen compounds (RNCs) in exhaust of advanced PM–NO_x abatement technologies for future diesel applications. *Atmospheric environment*, 45.18: 3203-3209.
16. SEINFELD J.H., PANDIS S.N. (1998): Atmospheric chemistry and physics: from air pollution to climate change. John Wiley & Sons.
17. MOONEY, J. J.; THOMPSON, C. E.; DETTLING, J. C. (1977). Three-Way Conversion Catalysts Part of the New Emission Control System. *SAE Transactions*, 1553-1562.
18. FALK, C. D., & MOONEY, J. J. (1980). Three—Way Conversion Catalysts: Effect of Closed—Loop Feed—Back Control and Other Parameters on Catalyst Efficiency. *SAE Transactions*, 1822-1832.
19. JETTER, J., MAESHIRO, S., HATCHO, S., AND KLEBBA, R., "Development of an On-Board Analyzer for Use on Advanced Low Emission Vehicles," SAE Technical Paper 2000-01-1140, 2000, doi:10.4271/2000-01-1140.
20. ANTHONY J.; KUBSH, J. (2007). The Potential for Achieving Low Hydrocarbon and NO_x Exhaust Emissions from Large Light-Duty Gasoline Vehicles. SAE Technical Paper 2007-01-1261.
21. California Air Resources Board: Executive Order no. A-023-0683, 2018, https://www.arb.ca.gov/msprog/onroad/cert/plcltdmdv/2018/honda_pc_a0230683_1d5_s3-30.pdf
22. KIMURA, S., AOKI, O., KITAHARA, Y., AND AIYOSHIKAWA, E. (2001). Ultra-Clean Combustion Technology Combining a Low-Temperature and Premixed Combustion Concept for Meeting Future Emission Standards. SAE Technical Paper 2001-01-0200.
23. JACOBS, T.J.; ASSANIS, D.N. (2007). The attainment of premixed compression ignition low-temperature combustion in a compression ignition direct injection engine. *Proceedings of the Combustion Institute*, 31.2: 2913-2920.
24. JOHNSON, T.V. (2002). Diesel emission control: 2001 in Review. SAE Technical paper 2002-01-0285.
25. MRÁČEK D. (2016): Analysis and Modelling of Spatiotemporal Concentration Profiles in NO_x Reduction Automotive Catalytic Converters. Ph.D. dissertation, VŠCHT Praha. <https://repozitar.vscht.cz/theses/phd/fchi/2016/CHINZ4/14126>
26. GUAN, Bin, et al. Review of state of the art technologies of selective catalytic reduction of NO_x from diesel engine exhaust. *Applied Thermal Engineering*, 2014, 66.1: 395-414.
27. GIECHASKIEL, B., SUAREZ-BERTOIA, R., LAHDE, T., CLAIROTTE, M., CARRIERO, M., BONNEL, P., & MAGGIORE, M. (2019). Emissions of a Euro 6b Diesel Passenger Car Retrofitted with a Solid Ammonia Reduction System. *Atmosphere*, 10(4), 180.

28. US EPA, NO_x memorandum – NO_x petition response. <https://www.epa.gov/sites/production/files/2016-12/documents/nox-memorandum-nox-petition-response-2016-12-20.pdf>
29. California Air Resources Board (2015): Draft Technology Assessment: Lower NO_x Heavy Duty Diesel Engines. https://www.arb.ca.gov/msprog/tech/techreport/diesel_tech_report.pdf
30. SUAREZ-BERTO A., ZARDINI, A.A., ASTORGA, C. (2014). Ammonia exhaust emissions from spark ignition vehicles over the New European Driving Cycle. *Atmos. Environ.* 97. doi:10.1016/j.atmosenv.2014.07.050
31. HEEB N.V., et al. (2006): Three-way catalyst-induced formation of ammonia—velocity- and acceleration-dependent emission factors. *Atmospheric Environment*, 40, 31, 5986-5997, doi 10.1016/j.atmosenv.2005.12.035.
32. SUN, K., et al. (2017). Vehicle emissions as an important urban ammonia source in the United States and China. *Environ. Sci. Technol.* 51.4: 2472-2481.
33. FINLAYSON-PITTS, B. J., PITTS J.N. (1999). *Chemistry of the Upper and Lower Atmosphere*, Elsevier, New York.
34. BEHERA, S.N. AND SHARMA M. (2010). Investigating the potential role of ammonia in ion chemistry of fine particulate matter formation for an urban environment. *Science of The Total Environment*, 408(17), 3569-3575.
35. KIM, B.M., TEFFERA, S., ZELDIN, M.D. (2000). Characterization of PM_{2.5} and PM₁₀ in the South Coast Air Basin of Southern California: Part 1—Spatial Variations. *Journal of the Air & Waste Management Association*, 50 (12), 2034-2044.
36. SILLANPÄÄ, M., ET AL. (2006). Chemical composition and mass closure of particulate matter at six urban sites in Europe. *Atmospheric Environment*, 40, Supplement 2 (0), 212-223.
37. CARSLAW, D.C., 2005. Evidence of an increasing NO₂/NO_x emissions ratio from road traffic emissions. *Atmos. Environ.* 39. doi:10.1016/j.atmosenv.2005.06.023
38. OLSEN, D.B., KOHLS, M., ARNEY, G., 2010. Impact of oxidation catalysts on exhaust NO₂/NO_x ratio from lean-burn natural gas engines. *J. Air Waste Manag. Assoc.* 60. doi:10.3155/1047-3289.60.7.867
39. GUTZWILLER L., ARENS F., BALTENSPERGER, U., GÄGGELER H.W., AMMANN M. (2002): Significance of Semivolatile Diesel Exhaust Organics for Secondary HONO Formation. *Environmental Science & Technology* 2002 36 (4), 677-682
40. BAIK, J.H., YIM, S.D., NAM, I.S. et al. *Topics in Catalysis* (2004) 30:37, doi: 10.1023/B:TOCA.0000029725.88068.97
41. KOEBEL M., ELSENER M., KLEEMANN M. (2000). Urea-SCR: a promising technique to reduce NO_x emissions from automotive diesel engines. *Catalysis Today*, 59, 3-4, 2000, 335-345.
42. ENYA T., et al. (1997): 3-Nitrobenzanthrone, a Powerful Bacterial Mutagen and Suspected Human Carcinogen Found in Diesel Exhaust and Airborne Particulates. *Environmental Science and Technology*, 31, 2772-2776.
43. FRANCO, V., SÁNCHEZ, F.P., GERMAN, J., MOCK, P. (2014). Real-world exhaust emissions from modern diesel cars: a meta-analysis of PEMS emissions data from EU (EURO 6) and US (TIER 2 BIN 5/ULEV II) diesel passenger cars. *ICCT Int. Counc. Clean Transp.*
44. LIGTERINK, N., KADIJK, G., MENSCH, P. VAN, HAUSBERGER, S., REXEIS, M. (2013). Investigations and real world emission performance of Euro 6 light-duty vehicles.
45. WEISS, M., et al. (2012). Will Euro 6 reduce the NO_x emissions of new diesel cars? - Insights from on-road tests with Portable Emissions Measurement Systems (PEMS). *Atmos. Environ.* 62, 657-665. doi:10.1016/j.atmosenv.2012.08.056
46. YANG, L., FRANCO, V., MOCK, P., KOLKE, R., ZHANG, S., WU, Y., GERMAN, J. (2015). Experimental Assessment of NO_x Emissions from 73 Euro 6 Diesel Passenger Cars. *Environ. Sci. Technol.* 49, 14409-14415. doi:10.1021/acs.est.5b04242
47. VOJTÍŠEK-LOM, M.; FENKL, M.; DUFEK, M.; MAREŠ, J. (2009). Off-cycle, real-world emissions of modern light-duty diesel vehicles. *Society of Automotive Engineers Technical Paper* 2009-24-0148.
48. United States Department of Justice (2015): Clean Air Act diesel engine cases. [WWW Document]. URL <https://www.justice.gov/enrd/diesel-engines>
49. US EPA (United States Environmental Protection Agency, 2019) : Performance Diesel Inc. Clean Air Act Settlement Sheet. Online at <https://www.epa.gov/enforcement/performance-diesel-inc-clean-air-act-settlement-information-sheet>. In reference to: United States of America v. Performance Diesel, Inc., Civil Action No. 4:19-cv-00075-DN, United States District Court for the District of Utah.
50. JONSON, J.E.; BORKEN-KLEEFELD, J.; SIMPSON, D.; NYÍRI, A.; POSCH, M.; HEYES, C. (2017): Impact of excess NO_x emissions from diesel cars on air quality, public health and eutrophication in Europe. *Environ. Res. Lett.*, 12, 094017, doi 10.1088/1748-9326/aa8850
51. CHOSSIÈRE, G. P., MALINA, R., ALLROGGEN, F., EASTHAM, S. D., SPETH, R. L., & BARRETT, S. R. (2018). Country-and manufacturer-level attribution of air quality impacts due to excess NO_x emissions from diesel passenger vehicles in Europe. *Atmospheric environment*, 189, 89-97.
52. FELLGETT, P. B. (1949). "On the Ultimate Sensitivity and Practical Performance of Radiation Detectors". *J. Opt. Soc. Am.* 39 (11): 970-6. doi:10.1364/JOSA.39.000970

53. ADACHI, M. (2000). Emission measurement techniques for advanced powertrains. *Meas. Sci. Technol.* 11. doi:10.1088/0957-0233/11/10/201
54. REYES, F., et al. (2006). Technical Note: Analysis of non-regulated vehicular emissions by extractive FTIR spectrometry: tests on a hybrid car in Mexico City. *Atmospheric Chemistry and Physics*, 6.12: 5339-5346.
55. JETTER, J., MAESHIRO, S., HATCHO, S., AND KLEBBA, R. (2000). Development of an On-Board Analyzer for Use on Advanced Low Emission Vehicles. SAE Technical Paper 2000-01-1140, doi:10.4271/2000-01-1140.
56. REYES F., GRUTTER M., JAZCILEVICH A., GONZALEZ-OROPEZA R. (2006). Analysis of non-regulated vehicular emissions by extractive FTIR spectrometry: tests on a hybrid car in Mexico City. *Atmospheric Chemistry and Physics Discussions*, European Geosciences Union, 6 (4), pp.5773-5796.
57. DAHAM, B., ANDREWS, G., LI, H., BALLESTEROS, R., BELL M.C., TATE J., ROPKINS K. (2005). Application of a Portable FTIR for Measuring On-road Emissions. SAE Technical Paper 2005-01-0676, doi:10.4271/2005-01-0676.
58. SUAREZ-BERTOIA, R., MENDOZA-VILLAFUERTE, P., RICCOBONO, F., VOJTISEK, M., PECHOUT, M., PERUJO, A., ASTORGA, C. (2017). On-road measurement of NH₃ emissions from gasoline and diesel passenger cars during real world driving conditions, *Atmospheric Environment*, 166, 488-497.
59. VOJTISEK-LOM, M., JIRKŮ, J., PECHOUT, M. (2020). Real-World Exhaust Emissions of Diesel Locomotives and Motorized Railcars during Scheduled Passenger Train Runs on Czech Railroads. *Atmosphere*, 11.6: 582.
60. VOJTÍŠEK M., BERÁNEK V., KLÍR V., JINDRA P., PECHOUT M., VOŘÍŠEK T. (2018): On-road and laboratory emissions of NO, NO₂, NH₃, N₂O and CH₄ from late-model EU light utility vehicles: Comparison of diesel and CNG. *Science of the Total Environment*, 616-617, 774-784.
61. PECHOUT, M., KOTEK, M., JINDRA, P., MACOUN, D., HART, J., & VOJTISEK-LOM, M. (2019). Comparison of hydrogenated vegetable oil and biodiesel effects on combustion, unregulated and regulated gaseous pollutants and DPF regeneration procedure in a Euro6 car. *Science of the Total Environment*, 696, 133748.
62. SUAREZ-BERTOIA, R., PECHOUT, M., VOJTÍŠEK, M., & ASTORGA, C. (2020). Regulated and non-regulated emissions from Euro 6 diesel, gasoline and CNG vehicles under real-world driving conditions. *Atmosphere*, 11(2), 204.
63. CLAIROTTE, M., et al. (2012). Online characterization of regulated and unregulated gaseous and particulate exhaust emissions from two-stroke mopeds: A chemometric approach. *Anal. Chim. Acta* 717:28-38. <https://doi.org/10.1016/j.aca.2011.12.029>.
64. SUAREZ-BERTOIA, R., ZARDINI, A.A., KEUKEN, H., ASTORGA, C., 2015. Impact of ethanol containing gasoline blends on emissions from a flex-fuel vehicle tested over the Worldwide Harmonized Light duty Test Cycle (WLTC). *Fuel* 143:173-182. <https://doi.org/10.1016/j.fuel.2014.10.076>.
65. LI, N., ROBINSON, J., BARRETT, R., WHEATLEY, A., 2016. Nitrogen Species Measurement Investigation Using Two Different Ftir. *Iastem Int. Conf.*, pp. 24-29 (doi:IJASEAT-IRAJ-DOI-4984).

2.27 A virtual PEMS for Eco Driver training

Martin Opetnik^{1*}, Stefan Hausberger¹

Institute of Internal Combustion Engines and Thermodynamics, Graz University of Technology, Graz, Austria

opetnik@ivt.tugraz.at

Introduction

Significant passenger car, light-commercial vehicle (LCV) and heavy-duty vehicle (HDV) emission reductions have been achieved over the last decades. Driving forces behind these accomplishments are various. The emission standards, known in Europe as the 'Euro' classes, led to technological improvements of emission reduction systems. Triggered by emission standards and CO₂ reduction targets, innovations in engine and vehicle technologies (e.g. downsizing) and powertrain optimizations, e.g. through hybridization and electrification, are penetrating the market. Also, conventional fuels have improved while synthetic fuels are in a far stage of development, incrementally bringing down the need for fossil fuels. Another option for achieving further emission reductions for the existing fleet is the driver behaviour including the vehicle maintenance, the loading and especially the driving style with the target of 'eco-driving'.

The project "uCARE – You can always reduce emissions" (<https://www.project-ucare.eu/>) was started in 2019 within the Horizon2020 program. The uCARE project enables campaigns by cities, regions and NGOs to reduce pollutant emissions by changing car user behaviour. During this project, multiple simple feedback solutions and Do-It-Yourself Tests were developed. Our part in this project is to set up a virtual PEMS which can be used for eco driving training. This tool can provide a layman user with a rating of their driving and feedback on how to improve their driving. Also expert users can use the tool to make assessments of emission reduction potentials by changed driver behaviour and/or driving conditions. The virtual PEMS was elaborated based on the tool PHEM (Passenger Car and Heavy Duty emission model) developed by TUG.

Although 'eco-driving' in terms of reducing fuel consumption has been around for more than a decade, this is still a largely uncharted domain when it comes to reducing pollutant emissions. A reduction of CO₂ is directly linked to reduced fuel consumption which means a direct economic benefit to the driver. Therefore the effects of eco-driving on CO₂-emissions can be assessed e.g. by the reading of the on-board fuel consumption indicator. For NO_x, CO, HC, particles etc., the measurement of the impact of the driving style needs PEMS (portable emission measurement systems) and thus is very costly. The idea of the virtual PEMS software is to simulate these emission components from the vehicle speed and engine speed signal read from the OBD interface of the vehicle. The simulation is based on test data collected during the project from many vehicles.

Vehicle emission model PHEM

PHEM is developed at the Institute of Internal Combustion Engines and Thermodynamics (IVT) of TU Graz since the late 1990s. Development is continuously ongoing to include new technologies and to improve simulation methods. A short description is given below. More details can be found e.g. in (Hausberger, 2003), (Rexeis, 2013), (Hausberger, 2012), (Matzer, 2017).

PHEM calculates the fuel consumption and emissions of road vehicles in 1Hz for a given driving cycle based on the vehicle longitudinal dynamics and emission maps. The engine power demand is calculated for each time step in a cycle from the vehicle's driving resistances, losses in the drivetrain and auxiliary power demand. The engine speed is determined based on tyre dimensions and the drivetrain's gear ratios, where an integrated gearshift model operates the transmission. Specific gearshift models for standard test procedures (NEDC, WLTP, etc.) as well as for real-world driving behaviour are included. Base exhaust emissions and fuel flow are then interpolated from engine maps depending on the resulting engine speed and power. To increase the accuracy of the simulated emissions, correction functions applied consider different emission behaviour under transient engine loads. Furthermore, detailed models for the conversion efficiency of different exhaust gas after treatment systems exist. The temperatures of catalytic converters are simulated based on the 0-dimensional heat transfer between exhaust gas and catalyst material as well as between exhaust line and ambient air. This routine is especially important for simulation of SCR (Selective Catalytic Reduction) systems – which cool down at low engine loads.

Since the vehicle longitudinal dynamics model calculates the engine power output and speed from physical interrelations, this approach can depict any driving condition. The model can handle different payloads of vehicles in combination with longitudinal road gradients and variable speeds and accelerations as well as effects of different gear shifting behaviour. The road gradient is calculated from measured GPS altitude using RDE calculation and smoothing routines.

The maps containing fuel consumption, CO₂ and pollutant emissions use normalised formats, for the engine speed between idling (=0) and rated speed (=1) and for the power between 0kw (=0) and rated power (=1). This allows the usage of weighted average engine maps representative for each segment (e.g. EU6 diesel cars). The model PHEM is used e.g. to produce the emission factors for all vehicle categories in the Handbook on Emission factors (HBEFA).

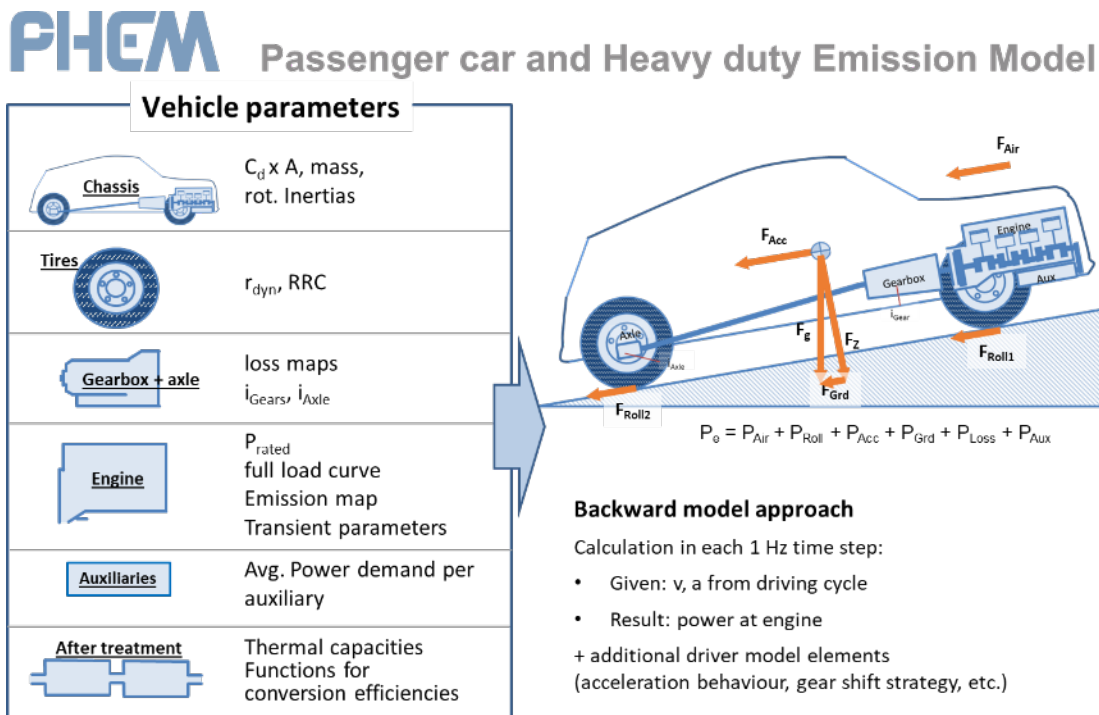


Figure 1: Scheme of the PHEM Model.

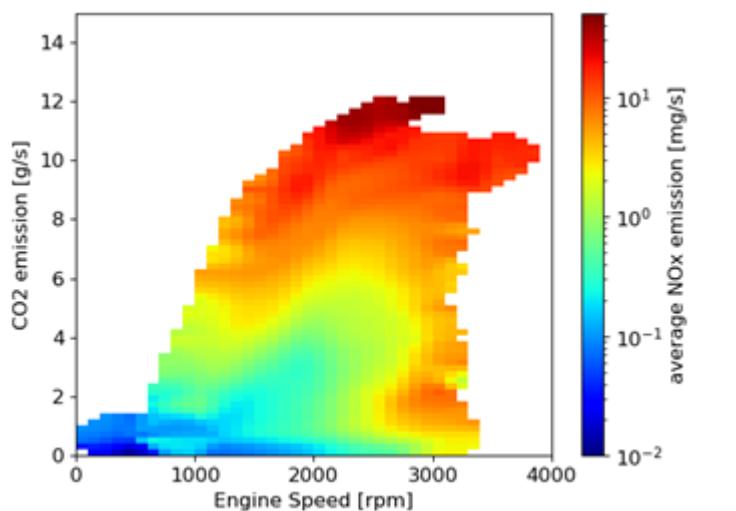


Figure 2: Scheme of augmented emission map.

Augmented emission maps

In the uCARE project so called “augmented emission maps” are created. In these emission maps, the instantaneously recorded emissions are gridded into according to the engine speed and the CO₂ mass flow. Since the maps are gained from vehicle tests, typically no information on the engine power or torque is available. Thus the CO₂ mass flow serves as proxy for the engine load in this map format. Additional “augmented” information contains parameters for the cold start model.

To use these augmented maps, PHEM calculates the engine speed and engine power as described above and interpolates the CO₂ emissions from generic engine maps (CO₂/power/rpm) which were elaborated for a set of engine technologies. Since the fuel maps do not differ very much between vehicle makes and models, the use of these generic CO₂ maps does not add much to the model uncertainty. The generic maps can be calibrated on demand, if chassis dyno or engine test data for the specific engine is available. In the current work flow of PHEM, the exhaust components provided for specific vehicles via the augmented map are converted into the normalised PHEM formats (pollutant/power/rpm) using the generic CO₂ maps. Pollutants not provided in the augmented maps are taken from the average HBEFA PHEM maps for the corresponding engine technology and EURO class.

Model development

Vehicle set-up parameters and their impact

An important requirement in the development of the simulation model is the assessment of impacts of different vehicle settings on the resulting emissions. The physical effects are increasing mass, rolling resistance coefficients and air resistance coefficient x frontal area. To produce the basic data on impacts of possible vehicle settings, a series of coast-down tests with a large number of possible vehicle attachments and tyre modifications were carried out. The resulting driving resistance values were set in relation to the standard settings in order to represent the influence as a factor. These impact-factors of vehicle setup on driving resistances are stored in the model and can be activated by users via GUI to correct the basic vehicle parameters according to the real vehicle set up.

The following variations were considered in the test series:

- Summer/winter tyres
- High/normal/low tyre pressure
- Wind/wet road/rain
- Lower loading (220kg)
- Roof rack without attachments/Roof box/bike rack/trailer
- PEMS in trunk/PEMS on trailer hitch

To illustrate the impacts of resulting changes in rolling resistance and aerodynamic drag, an average RDE cycle (1/3 mix of urban/road/motorway) was simulated with a representative vehicle. The changes of NO_x and CO₂ emissions compared to the base vehicle parameters are shown in the following graph.

E.g. for CO₂, a "low loading" of the car, i.e. by removing all unnecessary 'dead' weights in the vehicle results in a 4.3% reduction compared to the 'standard configuration'. A too low tyre pressure of summer tyres generates a 3.5% extra CO₂, properly inflated winter tyres increase CO₂ by 5.3%. Typical measures, which worsen a cars aerodynamic resistance, such as roof boxes, bike racks and especially trailers, negatively impact CO₂ as well. The highest increase was simulated with trailers, where the increase of CO₂ is more than 30%, for NO_x more than 100%. The effects of each variation on NO_x emissions are higher than the impact on CO₂ for the simulated EURO 6d-temp diesel car by a factor of 3-4.

Gear shift models

Another important goal of the uCARE tool is to rate trips according to their difference from an environmentally friendly (i.e., "SuperEco") driving style. An important step in driver evaluation is to establish a baseline for this evaluation. First, it was necessary to record which measures have a relevant impact on emissions behaviour.

PHEM offers a driver model to simulate the gear change behaviour based inter alia on the vehicle speed and the engine power demand level. The model was parameterized for eco/normal/aggressive shifting behaviour by measuring a large number of eco, normal and aggressive cycles in RDE.

On top of the eco-gear shift model a "SuperEco" shift strategy was implemented, which checks all possible gears for possibly lower emission results at the same power output (including losses for shifting) compared to the pre-selected gear. The best gear which still allows the target acceleration is then selected. This shift strategy can be applied for all exhaust components available in the engine map as well as for a user defined weighted mix of different pollutants. This principle can be seen in Figure 4 as example for a EURO 6d diesel NO_x map. To prevent wild upshifting and downshifting, only one shift is allowed in a given time period.

In addition to the best possible gear selection the virtual super-eco driver also limits his acceleration as function of the current velocity (see chapter 0). Results from the analysis of driver behaviour indicate that emission levels from modern vehicles are not very sensitive against irrational gear shift behaviour (Eco-shift/Normal-shift/Aggr-shift). Higher emission reduction potential was found by optimized acceleration and deceleration strategies (Eco-trip). Figure

5 shows as example the results from the automated analysis of the driver rating. Changing just the gear shift behaviour against the measured one saves ca. 4% NO_x, while an adjustment of acceleration, deceleration and maximum speed could reduce NO_x by 23%.

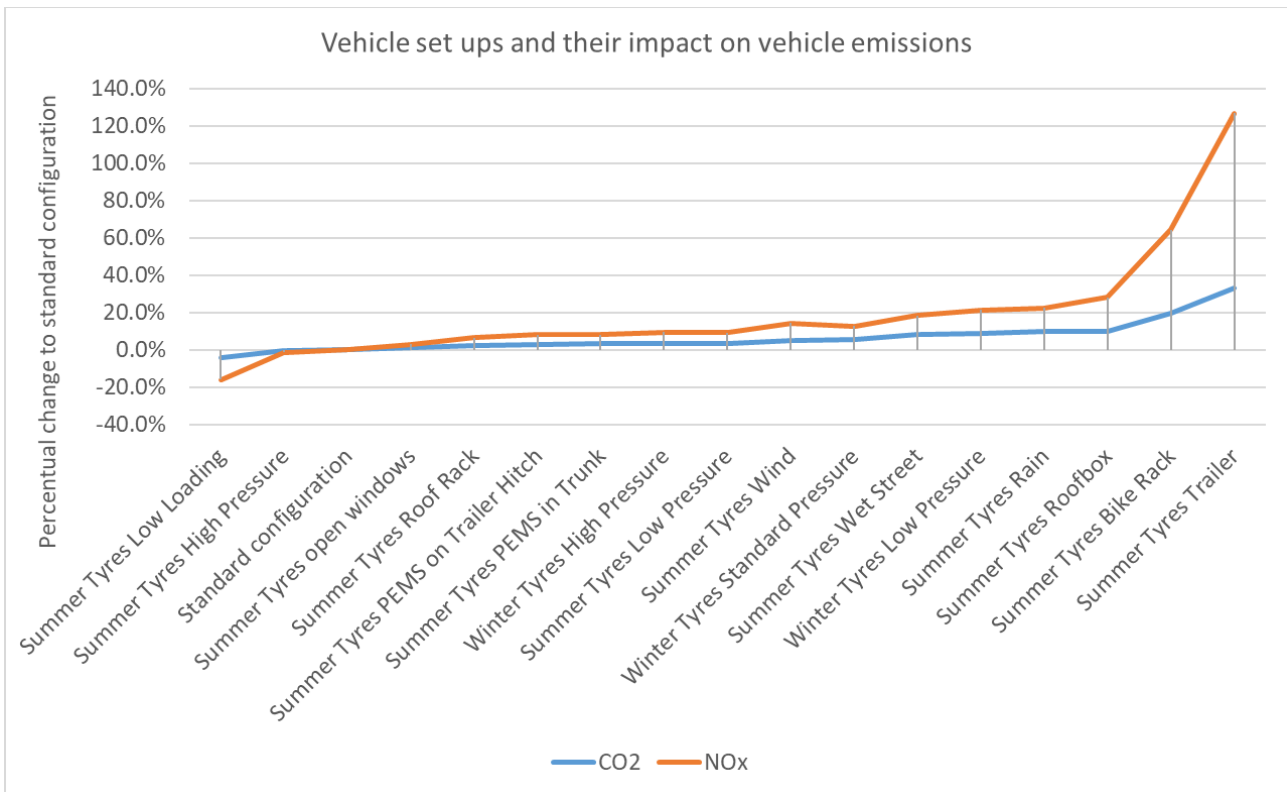


Figure 3: Vehicle set ups and their impact on CO₂- and NO_x-Emissions simulated for a EURO 6d-temp diesel car. High pressure = Front 3.1 bar / Rear 2.9 bar, Standard pressure: Front 2.6 bar / Rear 2.4 bar, Low pressure = Front 2 bar / Rear 1.8 bar

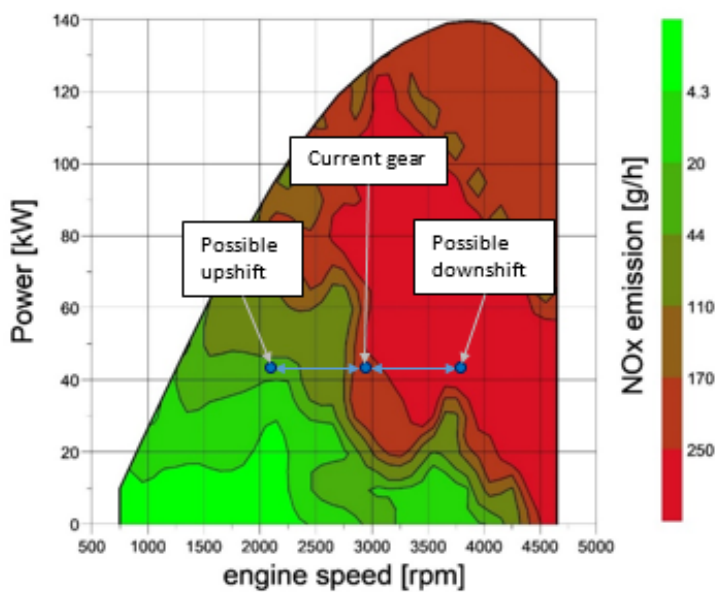


Figure 4: Example of Efficient shift model.

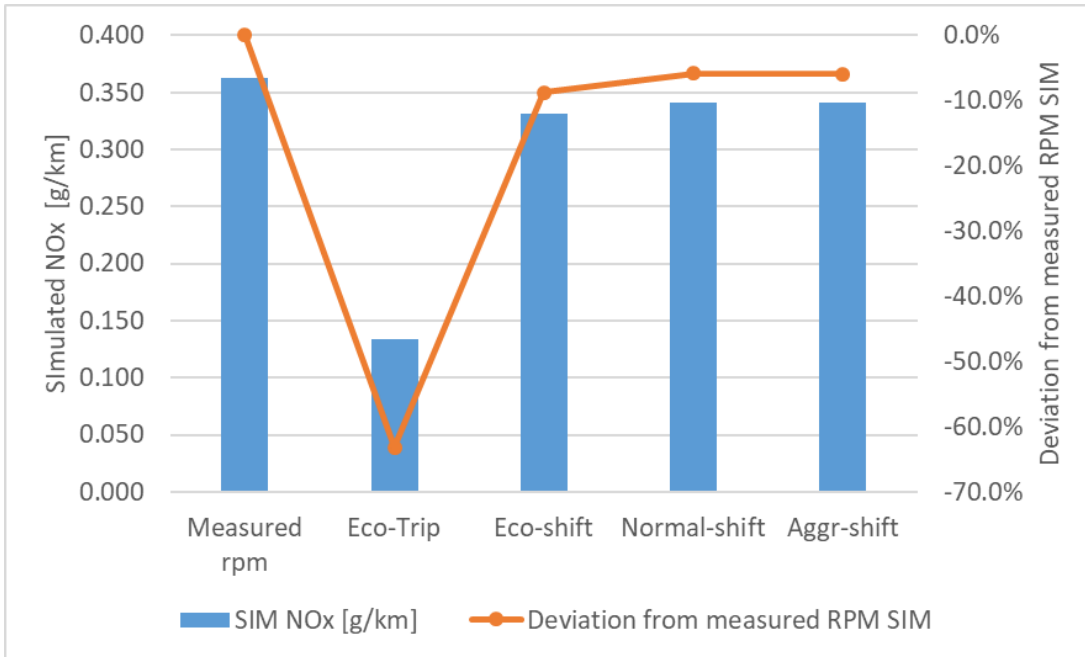


Figure 5: Impacts of gear shift and acceleration on NOx-Emissions simulated for an RDE trip of a EURO 6d-temp car (“DirectRPM.” uses the measured engine speed, the other bars use simulated gear shifts; “SuperEco” uses also a limit function for the acceleration, see chapter 3.3).

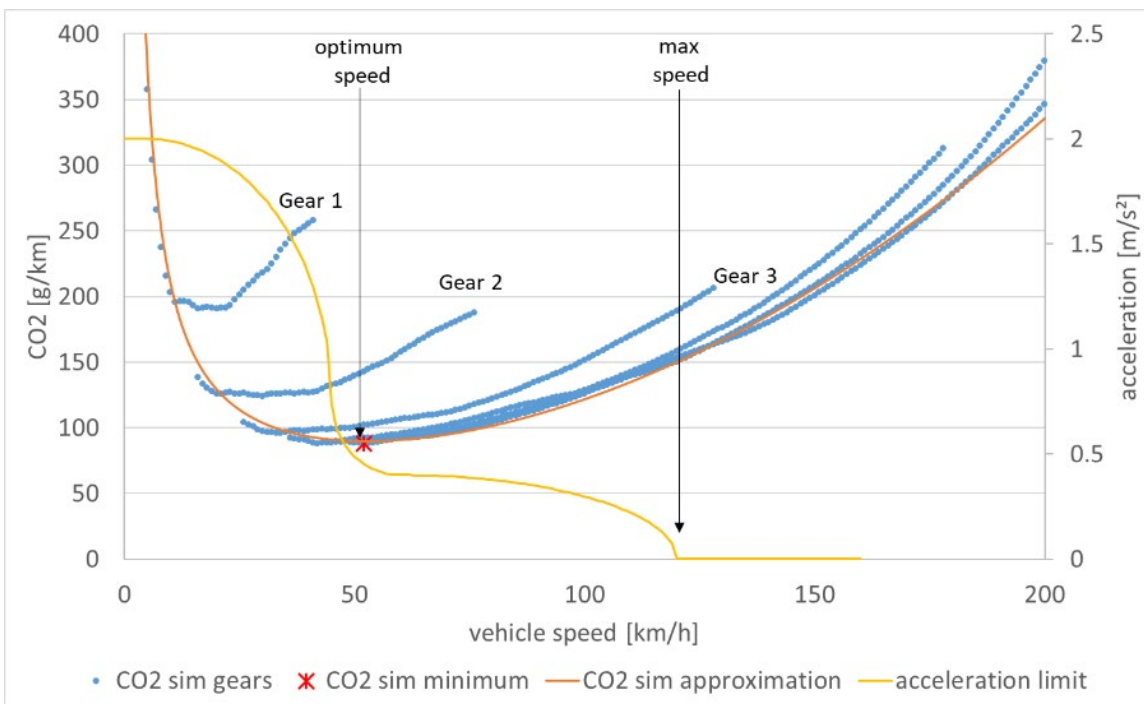


Figure 6: Simulated best point for CO2 at constant speed and derived acceleration limit.

Acceleration limitation

Since limiting the possible acceleration and the maximum speed have a much higher potential for reducing emissions, an acceleration limitation was implemented in the model. In the analysis of a Euro 6d-Temp diesel vehicle, the ideal point for constant speed was discovered by simulating constant speed points. Figure 6 shows the simulated CO2 of

the constant speed points of each gear (blue points). In an approximation (orange line) to the minima of each velocity step, the lowest value was determined (red cross).

This approximation was used as a boundary condition for the creation of an acceleration limit. The acceleration limit default setting currently used for the virtual super-eco driver is marked in yellow in Figure 6. Quick (but not full load) acceleration up to the optimum speed is defined as the driver recommendation and as a parameter in the simulation. From the optimum speed on, acceleration should only be gentle up to a maximum speed.

Reduction potential by an optimised driving style

The uCARE version of the model PHEM automatically simulates the emissions based on the measured vehicle speed and altitude in 1 Hz time resolution for two variants: in the first run the measured engine speed is used while in the second run the engine speed is computed using the super eco shift strategy and also the acceleration and maximum speed limitation described above are applied. Comparing the resulting emissions from the measured engine speed and the results using our virtual super-eco driver shows the reduction potential for all exhaust gas components available in the engine maps.

The model was tested by simulating 250 aggressively driven cycles. The resulting reduction potential, based on the ratio of the two simulation variants for a Euro 6 diesel vehicle, is shown in Figure 7. As can be seen, this results in different reduction potentials for the individual pollutants. While the maximum calculated reduction potential for CO₂ is around 20%, values of 70% are calculated for NO_x, 28% for CO and 36% for PN. The reduction potential shown here is planned to be taken as a reference for an overall ranking of a trip by the model. The lower the reduction potential by the super-eco driver in a cycle, the better it is evaluated. Conversely, the closer a cycle is to the maximum reduction potential, the worse it is rated.

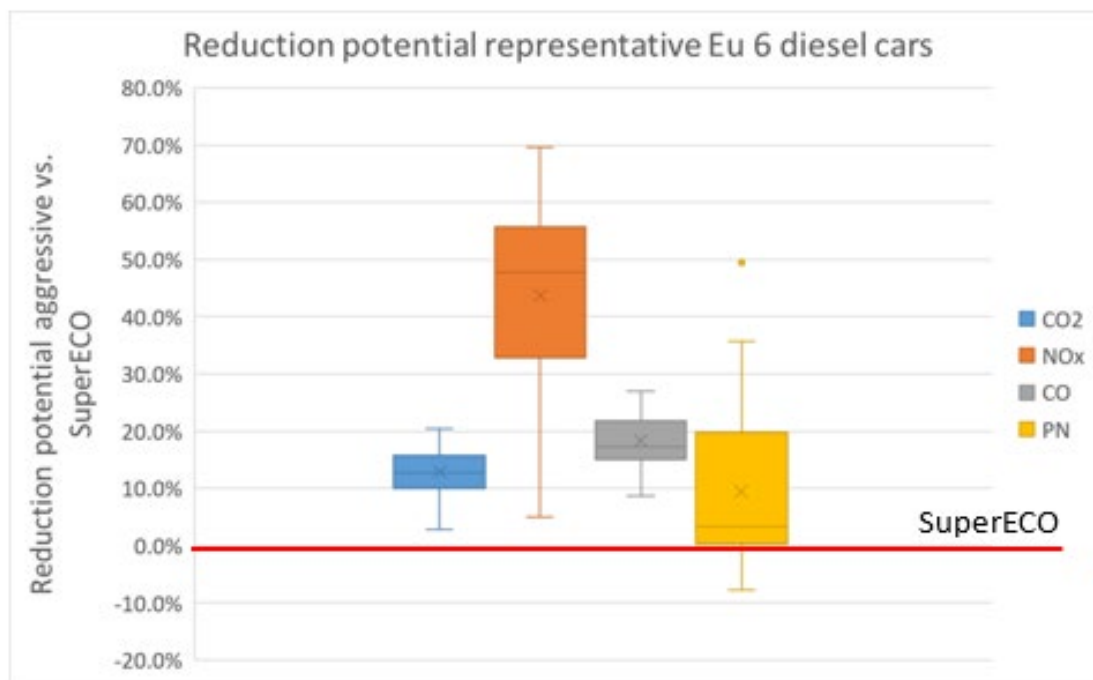


Figure 7: Calculated maximum reduction potential for representative Euro 6 diesel car.

Reduction potential rating results

Figure 8 shows the results of this rating method for CO₂ applied on 20 mostly highly aggressive driven cycles simulated for both, petrol and diesel with Euro 5 and Euro 6 emission standard. Figure 9 shows the corresponding results for NO_x. As can be seen, cycles 1, 3 and 6, for example, are rated as very aggressive (high reduction potential for both CO₂ and NO_x), while cycles 10 and 11 are, at least for CO₂, rated as very eco-style driven (low reduction potential). For petrol vehicles, the relative NO_x reduction potential is in some cases much higher than for diesel vehicles. It should be noted, however, that the base level for NO_x in these aggressive cycles for petrol vehicles is lower by a factor of 3 for gasoline EU5 than for diesel, and by a factor of 15 for EU6. As a result, the same reduction in mg/km produces a much higher reduction potential in %.

As can be seen from the figures, the measures applied achieve quite significant reductions for both CO2 and NOx in aggressive cycles.

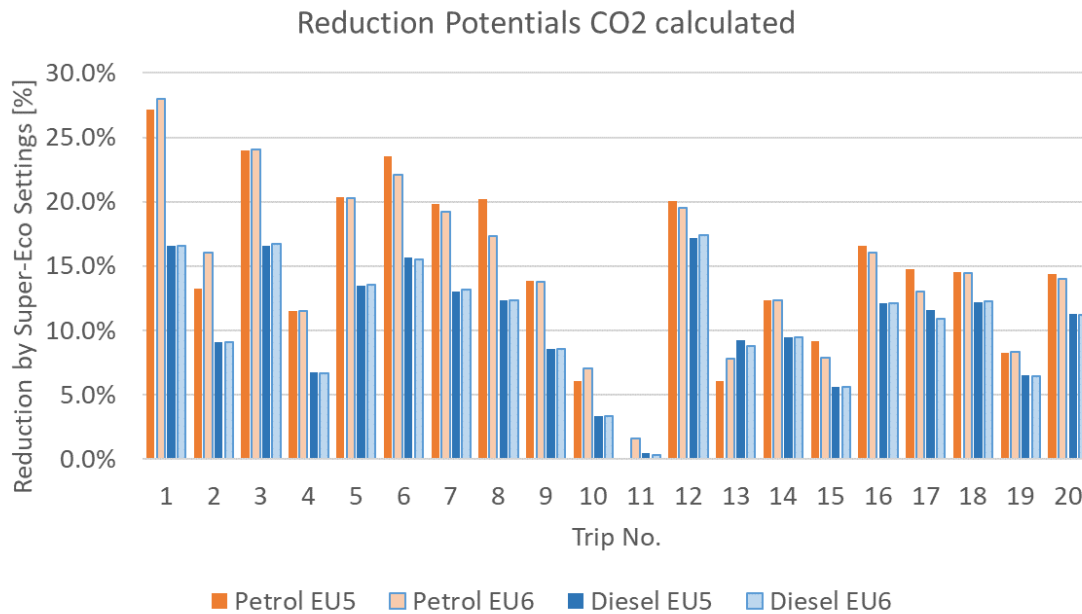


Figure 8: Exemplary CO2 reduction potentials for diesel and petrol both EU5 and EU6.

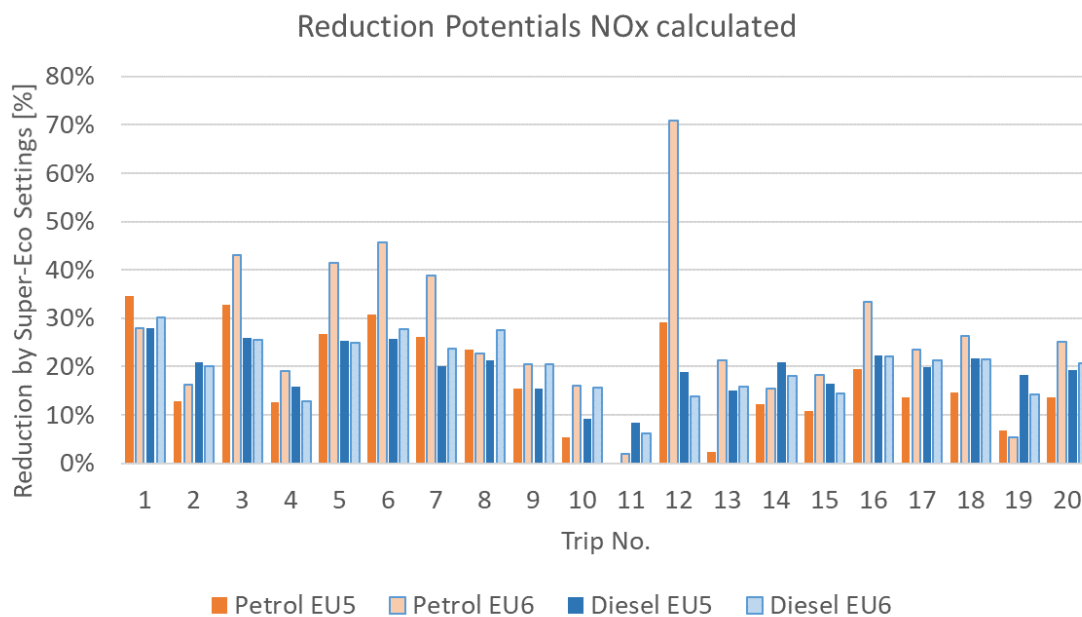


Figure 9: Exemplary NOx reduction potentials for diesel and petrol both EU5 and EU6.

Other rating methods

Furthermore, additional methods were developed which can be integrated into an automated analysis of the driver's driving behaviour to provide better driver feedback with suggestions for improvement.

- Deviation of real selected gears compared to Super Eco results when cruising in certain speed ranges. →
Suggestions for optimal gear ranges
- Deviation of acceleration versus speed compared to Super Eco results →
Suggestions for adjusting acceleration behaviour.
- Distribution of deceleration (or braking power) over speed compared to Super-Eco statistical results →
Suggestions for adjusting deceleration (or braking power)

Summary

In order to create a virtual PEMS for the rating of passenger car trips, several models were combined into one software. The PHEM model developed at TUG served as the basic framework. Subroutines were added in the software to make use of the augmented emission maps produced in the uCARE project and a virtual “super eco-driver” model was implemented to serve as basis for rating the real driver and to automatically produce recommendations for improved driving behaviour. Several attributes were used to represent the super-eco driving behaviour:

- Acceleration limitation based on simulated fuel consumption data from constant speed points.
- Maximum speed limitation
- Efficient-Shift gearshift model, which sets the optimum gear on the basis of characteristic maps

For the evaluation of measured cycles the trip is simulated twice. First, the cycle is simulated unchanged. In the second run all the above-mentioned attributes of super-eco driving are applied. The difference between the simulation as measured and the super-eco model provides the reduction potential by an optimised driving style and shows also the main areas of possible improvements (shift strategy, acceleration, deceleration, maximum speed).

As basis for a ranking of measured cycles, the reduction potentials of the individual emission components were simulated for 250 aggressively driven cycles. For CO₂, reduction potentials of up to 20% were achieved by applying the above-mentioned measures. For NO_x, these values are as high as 70%.

Acknowledgement

We want to thank all partners of the uCARE project for their input during the uCARE model development.

References

Matzer C.: Bestimmung von Kraftstoffverbrauch und Abgasemissionen von Pkw in realen Betriebszuständen mittels Messung und Simulation, Graz, 2020

Mitch Elstgeest, Armando Indrajana, Jessica de Ruiter, René van Gijlswijk, Norbert Ligterink, Paul Tilanus.: uCARE-D1.2-v2.0 - Augmented emission maps, <https://www.project-ucare.eu/>, The Hague, 2020

2.28 Impact on mobility and environment in six European cities due to the introduction of Electrified L-category Vehicles (EL-Vs) – The ELVITEN project

Maria Georgakaki¹, Giannis Papadimitriou¹, Niki Georgiou², Villy Portouli², Giulia Renzi³, Selini Hadjidimitriou³

¹ Emisia S.A., Antoni Tritsi 21, Thessaloniki, GR-57001, Greece

² Institute of Communication & Computer Systems (ICCS), 9, Iroon Politechniou Str. Zografou, Athens, Greece

³ Interuniversity Consortium for Optimization and Operations Research (ICOOR), 42122 Reggio Emilia, Italy

maria.g@emisia.com

Abstract

The aim of the ELVITEN project was to boost the market uptake of Electrified L-category Vehicles (EL-Vs) and increase their use in urban areas. In this context, long demonstrations have run in six European cities: Trikala, Bari, Genoa, Rome, Malaga, and Berlin. The impact of the introduction of EL-Vs on mobility and on the environment has been studied with detailed analyses that have been performed in the framework of the project.

Mobility:

The methods that have been followed in order to study the impact of EL-Vs on mobility, included a microscopic traffic modelling simulation and a scaled-up to the city level analysis. Simulation of Urban Mobility (SUMO – a microscopic, space-continuous road traffic simulation software) has been used to study the impact on mean travel times. With SUMO, the effect of replacing passenger cars with mopeds in urban areas has been examined, under different traffic flow levels and percentages of mopeds in the flow. Then, a scaled-up approach has been followed in order to obtain an overall view at city level. The results, both from the microscopic simulation and the scaled-up analysis, showed that there is no clear evidence that the increased EL-Vs usage can lead to reduced travel times. Future studies should take into account additional parameters, i.e. traffic information in real driving conditions and parking time.

Environment:

Two scenarios were examined, a 'baseline' and a '30% shift' one. The first scenario reflects a business as usual situation, where the activity projection follows the PRIMES EU Reference Scenario and future electric vehicle sales are based on relevant studies. The second scenario assumes gradual increase of EL-Vs sales and activity compared to the 'baseline', reaching in 2050 a 30% shift of internal combustion engine (ICE) vehicles activity to EL-Vs. For emission calculations, the COPERT software tool has been used. The analysis showed that significant environmental benefits can be achieved from the emission savings in urban areas due to the usage of EL-Vs instead of ICE vehicles in the future, i.e. approximately -22% reduction of NO_x and -21% of PM_{2.5} in all ELVITEN cities.

Converting the environmental impact into money, all ELVITEN cities will gain economic benefits from EL-Vs (black column in Table 1). The environmental benefit from air pollutant and greenhouse gas emission savings will be higher in cities which now have lower air quality (Bari, Genoa, Rome, Malaga) compared to other ELVITEN cities. The environmental benefit from sound emission (noise) savings will be higher in cities which have high urban population density (Rome, Berlin) and many conventional motorcycles (Rome). Regarding the upstream (Well-to-Tank) CO₂ for fuel/electricity production, the situation is expected to improve in the future if more renewable energy sources, solar, wind, will be used for electricity production (to charge the EL-Vs).

Table 1: Economic impact per category of emissions and in total for each ELVITEN city, cumulatively until 2050.

Cumulatively from 2021-2050				
Air pollutant and GHG (exhaust)	Noise	Well-to-Tank CO ₂ emissions	Total	ELVITEN city
€ 1,050,537,800	€ 53,975,741	-€ 75,668,573	€ 1,028,844,968	Rome 
€ 498,858,782	€ 15,265,760	-€ 101,892,848	€ 412,231,693	Berlin 
€ 292,352,230	€ 1,900,219	-€ 24,286,730	€ 269,965,720	Bari 
€ 202,236,696	€ 1,278,126	-€ 15,273,570	€ 188,241,252	Genoa 
€ 142,411,527	€ 849,461	-€ 8,072,206	€ 135,188,782	Malaga 
€15,728,315	€ 192,209	-€ 13,578,389	€ 2,342,135	Trikala 

Cost-benefit analysis (CBA):

Comparing the environmental benefits against the costs associated with more EL-Vs, via a CBA model, the outcome showed that shifting to EL-Vs is a justifiable investment on behalf of all ELVITEN cities, except Trikala. Possible explanation for this is the small size of the city and the fact that Trikala is already 'cleaner' than other ELVITEN cities, hence, the costs associated with more EL-Vs are higher than the environmental benefits. For such a small city, an enhanced sharing scheme would be more profitable, so that citizens do not have to buy many EL-Vs by themselves, but use public EL-Vs instead.

Table 2 presents the total cash flow (benefits - costs) of all ELVITEN cities, comparatively for every 5 years. Red cells represent a situation where costs are higher than benefits (negative total cash flow or total loss), while green cells represent a situation where benefits are higher than costs (positive total cash flow or total profit).

Table 2: Comparison of cash flow among ELVITEN cities.

Total Cash Flow (Benefits - Costs)	2021-2025	2026-2030	2031-2035	2036-2040	2041-2045	2046-2050
Bari	-€ 20,376,444	€ 9,500,858	€ 26,037,237	€ 41,115,297	€ 87,330,557	€ 95,218,199
Berlin	-€ 666,652	-€ 2,470,819	-€ 2,176,626	€ 25,584,393	€ 69,536,572	€ 58,592,513
Genoa	-€ 13,593,737	€ 6,662,182	€ 18,289,210	€ 28,883,066	€ 60,996,709	€ 67,142,101
Malaga	-€ 2,786,437	€ 11,731,698	€ 22,596,848	€ 29,381,013	€ 46,820,389	€ 57,214,718
Rome	-€ 67,001,383	€ 39,120,359	€ 103,160,075	€ 161,067,912	€ 331,448,796	€ 366,189,926
Trikala	-€ 4,262,703	-€ 7,486,227	-€ 9,321,915	-€ 8,501,007	-€ 6,432,822	-€ 4,979,079

Acknowledgements:

This abstract has been prepared in the framework of the ELVITEN project, which has received funding from the EU Horizon 2020 under grant agreement No 769926. <https://www.elviten-project.eu/en>

2.29 Emission reduction benefits from PHEVs

René van Gijlswijk^{2*}, Norbert Ligterink², Giorgos Mellios¹, Zacharias Samos¹, Nikos Kapetanios¹

¹ EMISIA SA, Antoni Tritsi 21, Thessaloniki 57001, Greece

² Netherlands Organisation for Applied Scientific Research (TNO), The Hague, the Netherlands

rene.vangijlswijk@tno.nl

Abstract

Road transport plays a significant role in climate change and it contributes to poor air quality, especially in densely populated areas. This is a global problem, which also requires regional solutions. Electrification of vehicles is encouraged by the European Commission for this reason. Many countries and regions, like Flanders investigate the option of stimulating new vehicle technologies to reduce emissions. The present paper examines the likely impact of plug-in hybrid electric vehicles (PHEV) in the Flemish region by combining a small-scale measurement campaign and vehicle simulations for the development of relevant emissions factors.

For one and a half months, SEMS equipment were installed on three PHEVs to measure NO_x and CO₂ emissions, while monitoring the vehicle owners' charging behaviour. An important parameter derived from these data is the utility factor (UF), which is the ratio between driving distance in charge-depleting (CD) and charge-sustaining (CS) mode between two charge cycles.

The real world fuel consumption and CO₂ emissions of PHEVs are generally much higher than the official type-approval CO₂ value. The particularities of the test procedure lies at the basis of this difference, and the new test procedure, the WLTP has not reduced this discrepancy.

Introduction

European legislation requires the CO₂ emissions of passenger cars and light duty commercial vehicles to be determined according to a specific method. In a transition period that started 1st September 2017, the old NEDC method is being replaced by the Worldwide Harmonised Light Vehicle Test Procedure (WLTP). The main goal was to improve the representativeness of official CO₂ values to the real-world CO₂ emissions of a vehicle, while warranting a level playing field for manufacturers. Changes were made to the test cycle, test conditions, vehicle conditions such as test mass. For plug-in hybrids, the test procedure was changed to a large extent, introducing the Utility Factor, which should make the weighting between fuel consumption and electricity consumption more true to real driving.

In this paper we show the developments in real-world fuel consumption and CO₂ emission of passenger cars, while paying particular attention to plug-in hybrid vehicles, and point out if WLTP has closed the gap, and whether WLTP has had influence on the real-world emissions. Part of this paper is a case study on real-world use of plug-in hybrids, and is based on the work carried out for the Flemish government.

Potential effect of WLTP procedures

The WLTP test procedure is compulsory from September 2018 for all newly registered cars. The average velocity of the test cycle is higher, with more driving resistance. However, as the test is 23 kilometres, where it was 11 kilometres, the cold start effect is smaller. Other aspects are the higher test mass and the determination of the driving resistance. In particular the rolling resistance is higher.

Based on physical principles and the previous contribution of the three factors, the expected difference would only be 8-10 g/km (based on [Cuelenaere 2018]). The fact that much higher values, typically 20 – 25 g/km higher, are reported is somewhat surprising. It is unknown if the same levels are retained once the European CO₂ targets are based on the WLTP, for 2025 and 2030.

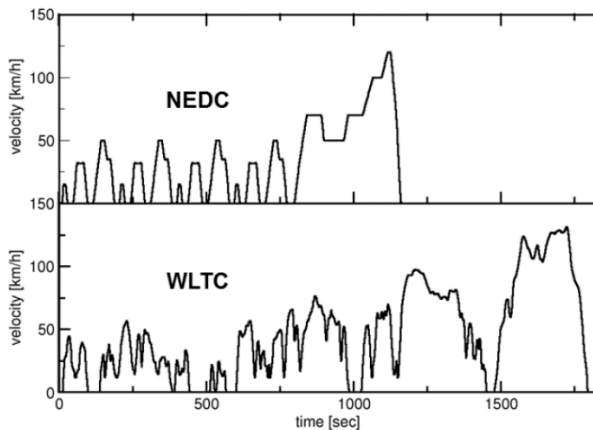


Figure 1: The WLTP is longer and with higher velocities. This reduces the effect of cold start and engine losses, but increases the power demand per kilometre.

Plug-in hybrid vehicles

The WLTP procedure introduces some changes specifically for plug-in hybrids. Most relevant for this paper are the changes in CO₂ calculation. The (direct) CO₂ emission of plug-ins is very much dependent on the ratio between driving on electricity and driving on the combustion engine. The related term in the WLTP procedure is the Utility Factor (UF), which is an estimation of the extent to which the combustion engine is needed in different use patterns of the vehicle.

To explain the UF, first a short introduction of the plug-in driving modes is needed. Plug-in hybrids can operate in different modes, which are normally chosen by the vehicle's software, although a preference can be selected by the user via a button. In charge depleting mode (CD) the vehicle is partially or fully propelled by energy from the battery; in charge sustaining mode (CS) the vehicle behaves similar to a hybrid without a plug: no net energy is extracted from the battery over longer distances, while during acceleration and deceleration energy may be used and stored in the battery.

WLTP introduces three, partially new, partially improved, tests: First, the charge sustaining test, which resembles driving with an empty battery; Second, the charge depleting test, under the condition that the vehicle is propelled fully electrically until the battery is depleted; Third, the range test, to assess the distance a vehicle can cover on a full battery on electricity only.

Note that while plug-ins generally drive in charge depleting mode employing a mix of electric energy and fuel, potentially optimizing the combined efficiency, in the test these are separated. The first part of the charge depleting test is driven fully electrically, the second part after the battery is depleted the vehicle will run in charge sustaining mode.

The UF is determined by the range test. The CO₂ values measured in the charge sustaining test and the charge depleting test are subsequently weighted by the UF, to arrive at the official WLTP CO₂ number. A larger electric range leads to a lower CO₂ value in the charge depleting test, resulting in a lower WLTP CO₂ number. In NEDC the CO₂ value was calculated in a more simple way: the CO₂ value for driving in CS mode was corrected for the ratio between 25 km and the battery range. Figure 2 shows the relation between the electric range in CD mode and the UF.

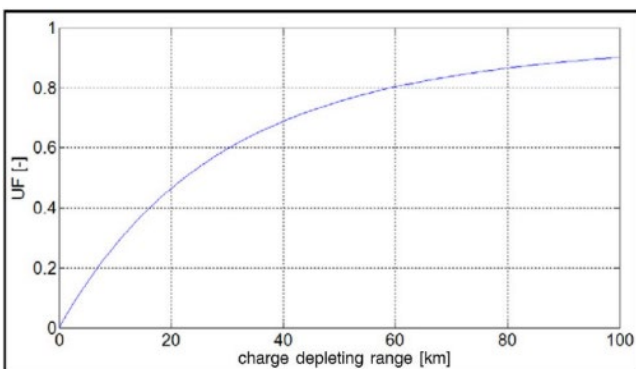


Figure 2: UF (Utility Factor) in EC/2017/1151 provides the assumed electric driving share based on the electric range.

As can be read from the graph, for an electric range of 25 km an electric drive share of over 50% is assumed. The type approval CO₂ emission level is thereby effectively halved. A sample of 8,600 plug-in hybrids in the Netherlands had an average real-world electric drive share of just over 20% [Gijlswijk van, 2020], while the stated electric range is always 25 km or larger. Even if we assume that some older plug-ins (under NEDC) had only enough battery for e.g. 20 km range under WLTP conditions, the real-world electric drive share is significantly smaller than the corresponding UF in the graph suggests.

Underlying cause is likely the overestimation of urban use in WLTP. In the real world most PHEVs are used more extensively, with longer trips, at least in the Netherlands and Flanders, and they are not necessarily charged in between each trip, as implicitly assumed in the development of the regulation. The NEDC and WLTP legislation both assume more shorter trips and recharging in between these trips, leading to a higher UF. The effect is similar, albeit more complex, to the NEDC procedure.

Besides limited motorway driving, other favourable laboratory conditions in the WLTP test also increase the stated electric range, and thereby the UF: cold weather, the use of heating and air-conditioning, lights, etc. (which reduce the electric range in normal use) are not accounted for in the official numbers.

Procedural implications

There is general awareness that the official CO₂ value is not necessarily representative of the fuel consumption and CO₂ emissions in normal use. The gap between the two numbers has increased from 2007 till the introduction of the WLTP. Whether a new gap will grow with the WLTP depends on the independent control by the granting type-approval authorities (GTAA), who have to verify the declared CO₂ value. Two instruments are introduced: First, the On-Board Fuel Consumption Meter (OBFCM) to provide an indication of deviating values. Second, the In-Service Verification (ISV) WLTP tests by the GTAA. These procedures are currently under development.

However, for PHEV the test procedure itself is the major source of the deviation between the real-world CO₂ emissions, and the official test value. There is little to be gained from independent verification of the CO₂ values. Another added complexity is the Certificate of Conformity (CoC) CO₂ values. Each model variant of a PHEV may have a different CO₂ value, based on the tyre label, mass, aerodynamic features, etc. This makes it more complex to address the observed differences. There seems a general trend that most PHEVs have more than 150 g/km in the charge sustaining test, and between 50% and 75% electric driving according to the WLTP UF.

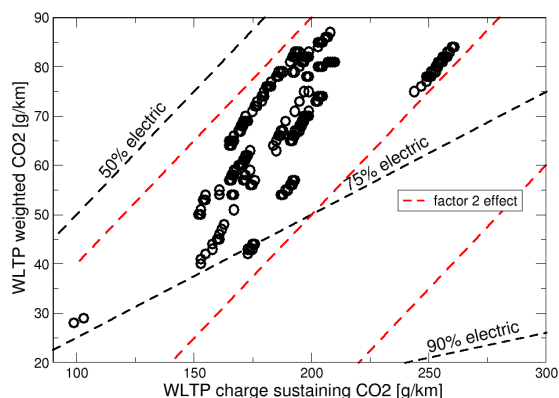


Figure 3: The charge sustaining CO₂ versus the declared CO₂ show trends of different WLTP PHEV models along factor 2 line: roughly half of the CO₂ reduction effect in charge sustaining test is apparent in the declared value, independent of the UF.

The effect of approximately a factor two on the CS test, compared to the declared value seems to suggest a rather artificial relation in the test procedure. The higher power demand decreases the electric range and increase the CS CO₂ at the same time, generating a double effect.

Real-world CO₂ gap

In [Ligterink, 2019] the difference between NEDC and WLTP values were estimated for the same car. Regression analysis pointed to a fuel independent difference of 15 g/km + 10%. Petrol taken separately showed that WLTP values were on average 14.5 g/km + 8% higher than the corresponding NEDC values; for diesel the average WLTP CO₂ value was 15.6 g/km + 12% higher than the NEDC value. A small increase in average weight and engine power was observed to have occurred simultaneously with the NEDC-to-WLTP transition [Cuelenaere 2018 (1), Cuelenaere 2018 (2),

Ligterink 2019], contributing slightly to the increase in type approval CO₂ values. A possible effect of the WLTP procedure is that vehicles may be better tuned for low real world fuel consumption.

The WLTP procedure allows manufacturers to declare a higher value than measured in the test. Insufficient data is available to evaluate if indeed individual vehicle WLTP values increased beyond abovementioned expectations. If so, the (declared) WLTP values would be closer to real-world CO₂ values. An analysis was possible on an average level however. Based on tank pass and charge pass data provided by Travelcard BV, the real-world to WLTP gap could be calculated for approximately 24,000 vehicles (non-plug-in internal combustion engine passenger cars and vans). The actual fuel consumption of the vehicles was monitored by logging tank event data and corresponding odometer readings over the period since they entered the leased car fleet. Figure 4 shows the result. To avoid large scatter on the left side of the graph, the lines start at the moment there are 100 WLTP approved vehicles in the dataset.

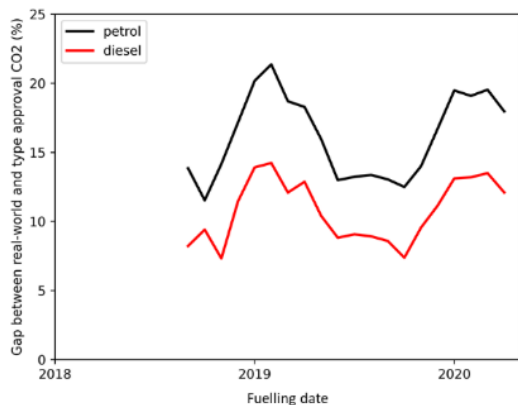


Figure 4: Gap between real-world CO₂ emission and WLTP CO₂ values for conventional petrol and diesel passenger cars.

The graph shows that the gap is smaller for diesels than for petrol cars. On average, for petrol cars the real-world fuel consumption is 16% higher than the declared WLTP values. For diesel the average gap is 10%. By comparison, the NEDC gap for 2019 vehicles was 44 g/km for petrol and diesel alike, which equals 37% and 38%, respectively.

As with NEDC, the gap is generally smaller for vehicles with a high absolute fuel consumption, and comparatively large for economical cars. This effect is illustrated in Figure 5. The vehicles in the test dataset were sorted by WLTP declared value. The real world CO₂ values were averaged for blocks of 100 vehicles, and plotted as a blue line.

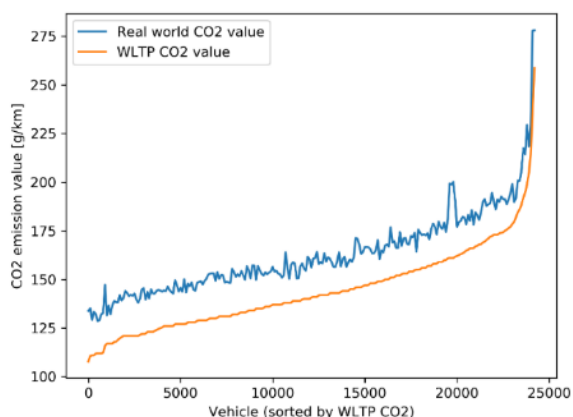


Figure 5: Trend of average real world CO₂ values at increasing WLTP values.

An interesting next step, now more data comes available, is to compare NEDC and WLTP for individual vehicle models.

Plug-in hybrid passenger cars

The dataset described in the previous paragraph revealed that plug-in hybrids with WLTP type approval arrived on the market with a delay: only 52 were registered (average WLTP to real-world gap: 119 g/km). A more solid gap analysis of plug-in hybrid vehicles should for now be based on NEDC. In 2020 more PHEVs were registered. Till March 2021

about 48,000 PHEVs were registered in the Netherlands, which is close to 6% of all registrations. Almost all major brands now have PHEV models available. The average WLTP CO₂ is 47 g/km, and CS CO₂ is 177 g/km, which makes the average UF 0.73. The current TNO dataset does not contain all of these new PHEV models. The entire tank pass dataset contains fueling and odometer records of 8,600 plug-in hybrids: some 6,500 petrol plug-ins and almost 2,000 diesel plug-ins.

Figure 6 shows the evolution of type approval and real-world CO₂ emission averages for these vehicles. For plug-in hybrids, the type approval values have remained fairly constant since 2013. The averages are just below the 50 g CO₂/km threshold for supercredits in EC 443/2009. By contrast, the real-world emission values have increased gradually. This is probably due to a combination of a reduced average electric range and an increased size of plug-in vehicle models. Seasonal effects are larger than for conventional vehicles, but vary also greatly among manufacturers.

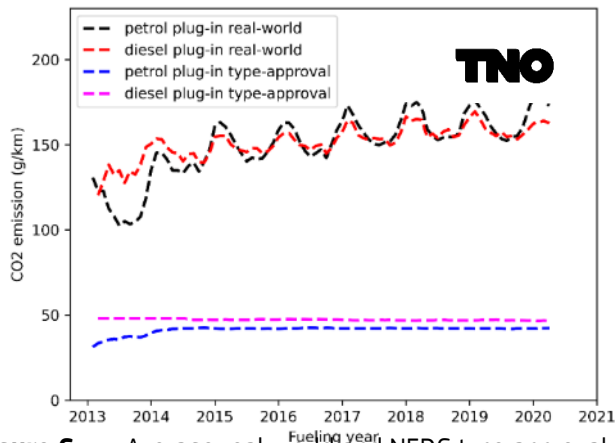


Figure 6: Average real-world and NEDC type approval tailpipe CO₂ emission of all plug-in hybrid vehicles on petrol and diesel in the Travelcard tank pass fleet (approximately 8,600 plug-ins). The real-world CO₂ emissions have increased since 2013, while the type-approval CO₂ emissions remained relatively constant. The increasing real-world emissions lead to an increasing gap.

For PHEVs the determination of the fuel consumption is more complex due to the differences in vehicle and battery size. The electric driving is observed as larger distances driving between certain fueling events. See Figure 7.

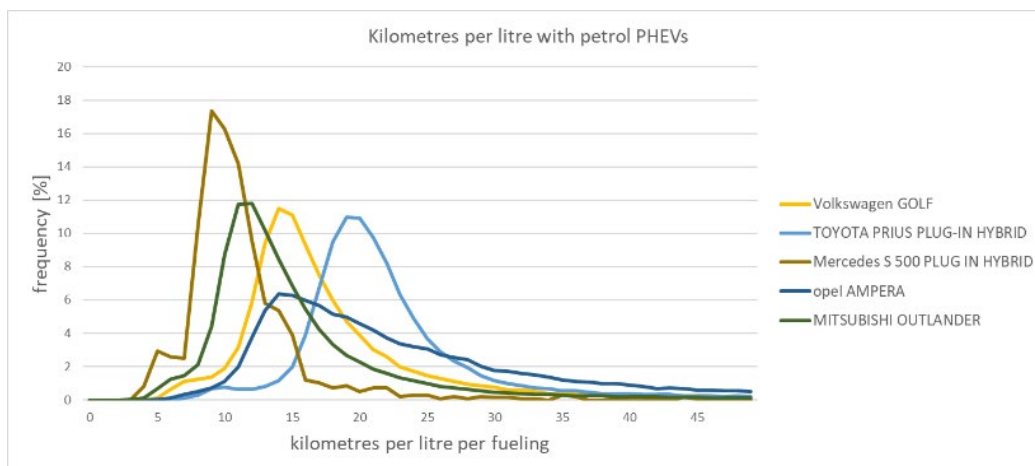


Figure 7: Examples of typical real-world fuel consumption of PHEVs. The PRIUS with the small battery but efficient vehicle, the Ampera with the large battery, and variants of standard PHEVs increasing size and lower fuel efficiencies. The long tail of large distances per litre for the Ampera indicates substantial electric distance fractions. While a symmetric distribution, like the Mercedes, indicate mainly combustion engine driving.

An analysis per vehicle model was done earlier [Gijlswijk van, 2018], for vehicles sold in the year 2016. The results in Figure 8 show that the actual average CO₂ emissions are not much lower than those of non-plug-in passenger cars of a similar size: around 160 g/km. The type-approval values per model confirm the flat line in Figure 6 mostly just below 50 g/km. The gap between type approval and real world is indicated by the dotted lines, and is 90-130 g/km.

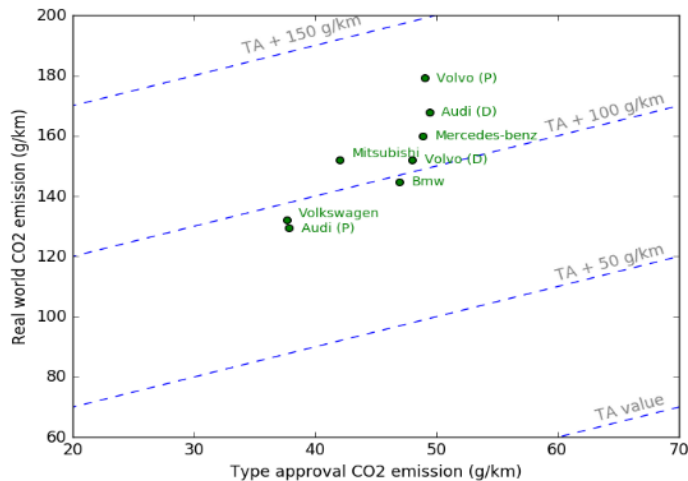


Figure 8 Average type-approval and real-world CO₂ emission of plug-in hybrids sold in 2016 for the 10 most sold brands. P: petrol, D: diesel.

A comparison was made between NEDC and WLTP values of the same vehicle models [Ligterink, 2019]. Figure 9 shows that the replacement of NEDC by WLTP has yielded hardly more realistic values for plug-in hybrids; a 30% increase (at most; see formula in the graph) is a small difference considering the gap with real-world emissions of 200% to 300%.

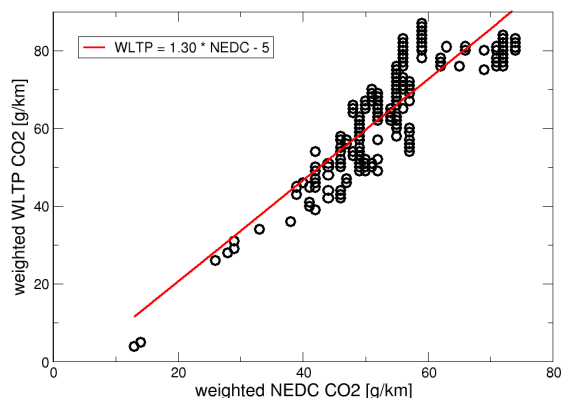


Figure 9: A fit (red line) through WLTP vs. NEDC CO₂ values of plug-in hybrids leads to a difference of 30% - 5 g/km, with a large scatter.

Behaviour of plug-in hybrids: case study Flanders

For the Flemish government a consortium of VUB, TNO, and Emisia have studied the potential contribution of plug-in hybrid vehicles to CO₂ reduction of the vehicle fleet in Flanders, Belgium. The results were used for policy development support [Hooftman, 2020]. To fill hiatuses in literature data, the project involved monitored three plug-in hybrid vehicles in normal use. The Smart Emissions Measurement System (SEMS), developed by TNO, was used to monitor the usage pattern of the three vehicles, as well as the emissions from the tailpipe; see Figure 10.



Figure 10: SEMS sensors fitted to a plug-in hybrid vehicle.

With the second-by-second data collected in the study, including charging data and location, detailed information on the vehicle use and underlying factors of electric driving could be determined. With the detailed data this information the share of electrically driven kilometres can be differentiated for different road types.

This test contained two vehicles with petrol engines, the Mitsubishi Outlander and the Volvo XC90 T8, and one diesel engine driven vehicle, the Volvo V60 Twin Engine, which were selected based on their popularity in Flanders. Fuel consumption has been monitored for all three vehicles, as well as electricity consumption for the two Volvos. To determine the electricity consumption in EV mode, the battery state of charge (SoC) was monitored.

By coupling the SEMS GPS signal to road maps of Open Street Map (OSM, www.openstreetmap.org), the data has been divided into three categories based on the road type. A distinction has been made between city roads, rural roads and motorways. Measurements for which the GPS coordinates could not be matched with a road type in OSM have been omitted from the final sample. For each vehicle about 70% of the raw data has been included in the analysis, which corresponds with a total driven distance of about 3,200, 5,500 and 4,200 kilometres for the Volvo V60, Volvo XC90 and the Mitsubishi Outlander respectively, over a period of two months. Some statistics of the tests are summed up in Table 1.

Table 1: Test data plug-in hybrids.

	Unit	Mitsubishi Outlander (petrol)	Volvo V60 (diesel)	Volvo XC90 (petrol)
Test duration (ignition switch on, SEMS on)	h	108.8	78.5	145.3
Duration vehicle in motion	h	97.3	69.9	116.0
Distance driven	km	6,002	4,270	7,056
Time in hybrid mode	h	58.6	42.7	66.7
Distance in hybrid mode	km	4,487	3,119	5,377
Time in EV mode	h	38.7	27.2	44.9
Distance in EV mode	km	1,515	1,151	1,679
Average speed	km/h	55.2	54.4	48.6

From the average speeds in the table it can already be derived that most of the distance was covered on the highway. Figure 11 confirms that. Furthermore it shows that approximately half the distance driven in EV mode was spent in

urban conditions. For rural and highway situations, the share of full electric driving was 30-50% and 10-20%, respectively.

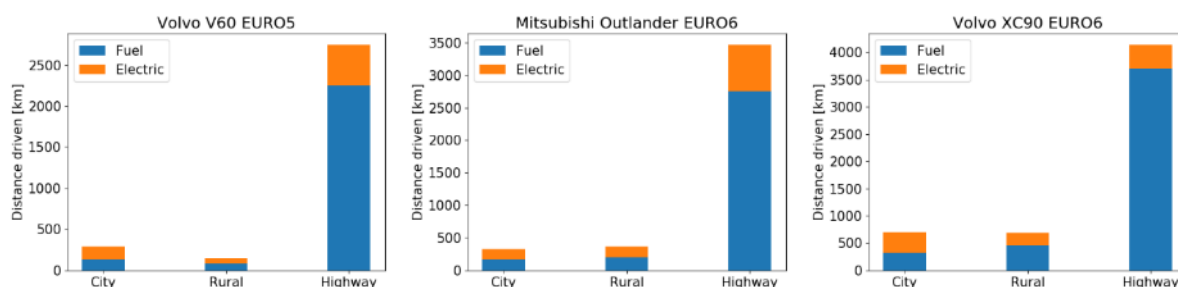


Figure 11: Road type distribution of three plug-in hybrid vehicles, split by drive mode; blue = hybrid mode, orange = EV mode.

Weighted by the shares of the different road types in the travelled distances, the share of electric driving was 25%, 27% and 24% for the Outlander, V60 and XC90, respectively.

Fuel consumption and electricity consumption

For each vehicle the average fuel consumption and average tailpipe CO₂ emission was calculated for driving in hybrid mode (combustion engine running). For the two Volvos also the electricity consumption in kWh/km has been calculated from the battery state-of-charge data. The numbers are in-vehicle results excluding charging losses. Table 2 shows a summary of the results.

Table 2: CO₂ emission, fuel consumption and electricity consumption. Note: the Mitsubishi Outlander does not provide battery details.

	Unit	Mitsubishi Outlander (petrol)	Volvo (diesel) V60	Volvo (petrol) XC90
Tailpipe CO ₂ emission, average incl electric kilometres	g/km	202	163	241
Tailpipe CO ₂ emission in hybrid mode	g/km	270	217	307
Fuel consumption in hybrid mode	l/100 km	11.4	8.2	13.0
Usable battery capacity (estimated)	kWh	9.0	9.9	9.9
Electric energy consumption, average incl fuelled kilometres	kWh/100 km	N/A	3.5	6.1
Electric energy consumption in EV mode	kWh/100 km	N/A	13.0	22.7

Despite the hybrid drivetrain, fuel consumption numbers in hybrid mode (CS mode) are in line with non-hybrids of the same vehicle class.

Conclusions

The PHEV technology has CO₂ reducing potential. However, in practice the official CO₂ emission values are not met, and the test procedure is not a reflection of normal use. To harvest the CO₂ reducing potential further measures are needed. Enforced geofencing could be an option to harvest the potential.

Acknowledgement

Part of this research was sponsored by the Flemish government, and part by the Dutch government.

References

- Gijlswijk, R. van, Paalvast, M., Ligterink, N., Smokers, R., Real-world fuel consumption of passenger cars and light commercial vehicles, TNO 2020 R11664, 2020.
- Ligterink, N., Cuelenaere, R.F.A., Aspects of the transition from NEDC to WLTP – aanvullend rapport: CO₂ waarden van plug-in voertuigen ('supplementary report: CO₂ values of plug-in vehicles), TNO 2019 R11310, 2019.
- Cuelenaere, R.F.A., Heijne, V.A.M., Ligterink, N.E., Aspecten van de NEDC-WLTP overgang in relatie tot CO₂-waarden van personenauto's – fase 1: de probleemschets (Aspects of the transition from NEDC to WLTP for CO₂ values of passenger cars – phase 1: problem definition), TNO 2018 R10732, 2018.
- Cuelenaere, R.F.A., Eijk, E. van, Ligterink, N.E., Stelwagen U., Aspects of the transition from NEDC to WLTP for CO₂ values of passenger cars – phase 2: preliminary findings, TNO 2018 R11145, 2018.
- Ligterink, N.E., Cuelenaere, R.F.A., Stelwagen U., Aspects of the transition from NEDC to WLTP for CO₂ values of passenger cars – phase 3: after the transition, TNO 2019 R10952, 2019.
- Gijlswijk, R. van and Ligterink, N., Real-world fuel consumption of passenger cars based on monitoring of Dutch fuel pass data 2017, TNO 2018 R10371, 2018.
- Hooftman, N., Ligterink, N., Paalvast, M., Gijlswijk, R. van, Voogd, E., Mellios, G., Samos, Z., Verhoeve, W., Emissiereductiepotentieel voor hybride voertuigen bestemd voor de weg, uitgevoerd in opdracht van het Vlaams Planbureau voor Omgeving, 2020.

2.30 Impacts to emissions and air quality of electric vehicles in Denmark in 2030

S.S. Jensen*, J.H. Christensen, L.M. Frohn, J. Brandt, M. Ketzel, O.-K. Nielsen, M.S. Plejdrup, M. Winther, T. Ellermann

Aarhus University, Department of Environmental Science

ssj@envs.au.dk

Abstract

The aim of this paper is to present an impact assessment for selected proposals in the Danish Government's Climate and Air Proposal with focus on three measures for electrification of road transport in Denmark. The three policy options are (1) One million electric cars in 2030 (about one third of all cars in 2030), (2) 100% electric urban buses in 2030 (3) 100% electric taxis in 2030.

Air quality calculations of regional concentrations, urban background concentrations and street concentrations are carried out for NO₂ and PM_{2.5} for 2016 and 2030. Regional background concentrations are calculated with the Danish Eulerian Hemispheric Model (DEHM) with a geographic resolution of 5.6 km x 5.6 km. Urban background concentrations are modelled with the Urban Background Model (UBM) with a spatial resolution of 1 km x 1 km. Street concentrations are calculated with the Operational Street Pollution Model (OSPM) for 98 selected streets in Copenhagen. The starting point is 2016 and the scenario year is 2030. European emissions are based on baseline emission projections and for the climate scenario on the countries' baseline if the NEC-directive for national emission ceilings are met, otherwise the NEC-directive emission ceiling for the country.

Danish emissions are based on the baseline projection of the Danish Energy Agency. The baseline forecast is based on existing policy actions, also named 'frozen policy' and for the climate scenario on With Additional Measures for the energy sector. The development in vehicle emissions is based on the national emission model for road traffic based on the European COPERT V road transport emission model and the development in the vehicle fleet is based on data from the Technical University of Denmark. An exponential growth in the sales of electric cars starting from 2019 is assumed in order to reach one million electric cars in 2030. For the scenarios for taxis and urban buses it is simple assumed that all taxis and all urban buses are electric in 2030. Non-exhaust emissions are assumed to be unchanged when shifting from fossil fuelled cars to electric vehicles (EVs).

Electrification of the Danish road transport sector with one million electric cars (one third of all cars in 2030), 100% electric taxis and 100% urban buses in 2030 is predicted to reduce NO_x emission by 14%, PM_{2.5}-exhaust by 19%, and total PM_{2.5} by 2.3% compared to the baseline in 2030 including all vehicle categories (passenger cars, vans, and heavy-duty vehicles). It leads to reductions in regional background concentrations in Denmark, in urban background concentrations evaluated for the four largest cities and in streets concentrations evaluated for 98 streets in Copenhagen.

Introduction

The aim of this paper is to present an impact assessment for emissions and air quality for selected initiatives in the Government's Climate and Air Proposal from 2018 (Danish Government, 2018) with focus on three measures for road transport and two measures for wood stoves – hereafter named the climate scenario. The impact assessment is described in greater detail in a report to the Ministry of Environmental and Food of Denmark (Jensen et al., 2019).

The focus is on three measures for electrification of road transport. The three policy measures are (1) One million electric cars in 2030 (about one third of all cars in 2030), (2) 100% electric urban buses in 2030 (3) 100% electric taxis in 2030.

The background for the project is the requirements of the EU directive from 2016 on National Emission Ceilings (NEC directive) (EU, 2016). The directive requires development of national programmes for the control of air pollution named NAPCP – National Air Pollution Control Programme. Denmark is committed regularly to evaluate the development of the national emissions and their expected future development, and carry out actions to reduce emissions in order to achieve the reduction targets that have been set for Denmark in the NEC directive.

The NEC directive sets out national commitments for reductions in emissions for 2020 and 2030 for the pollutants: sulphur dioxide (SO₂), nitrogen oxides (NO_x), non-methane volatile organic compounds (NMVOC), ammonia (NH₃), and fine particles (PM_{2.5} - particulate matter less than 2.5 microns). Emissions of these substances are included in the calculations of air quality of NO₂ (nitrogen dioxide), PM_{2.5}, PM₁₀ (mass of particulate matter less than 10 microns), and O₃ (ozone).

Methodology

Emissions of baseline and climate scenarios

The effects of five selected initiatives in the Government's Climate and Air Proposal are estimated (Danish Government, 2018): (1) one million. EVs in 2030 and no sale of new petrol and diesel cars in 2030 and of new plug-in hybrid cars from 2035, (2) no CO₂ emissions and air pollution from urban buses in cities from 2030 interpreted as 100% electric urban buses, (3) no petrol and diesel taxis in 2030 interpreted as 100% electric taxis, (4) old stoves before 2000 scrapped when home ownership is changed, and (5) subsidy to scrap old stoves before 2000.

The baseline scenario for Denmark originates from the baseline projection of the Danish Energy Agency. This is a forecast based on existing policy actions, also named 'frozen policy' and referred to as WM – With Measures. The baseline scenario is described in details in *Nielsen et al. (2018a)* and the projections for 2030 in *Nielsen et al. (2018b)*. The climate scenario uses another projection by the Danish Energy Agency - With Additional Measures for the energy sector (WAM) that has lower emissions than the baseline. The WAM scenario is described in *Nielsen et al. (2018b)*.

The foreign emissions are different in the Danish baseline scenario (WM) and WAM scenario). The WM scenario uses the foreign countries' baseline emissions, and the WAM scenario also uses the countries' baseline if the NEC-directive emission ceilings are met, otherwise the NEC-directive emission ceiling for the country is used.

The starting point is 2016, and 2020 and 2030 are scenario years. For the climate scenario, calculations are only carried out for 2030.

The development in vehicle emissions is based on the national emission model for road traffic (Winther, 2018) based on emission factors from the European COPERT V road transport emission model (EMEP/EEA, 2019) and the development in the vehicle fleet is based on data from the Technical University of Denmark. An exponential growth in the sales of electric cars starting from 2019 is assumed in order to reach one million electric cars in 2030. For the scenarios for taxis and urban buses it is simple assumed that all taxis and all urban buses are electric in 2030. Non-exhaust emissions are assumed to be unchanged when shifting from fossil fuelled cars to EVs, that is, non-exhaust emissions are assumed to be the same for fossil and EVs.

Regional background concentrations

For the baseline and climate scenario the regional background concentrations are calculated with the Danish Eulerian Hemispheric Model (DEHM) with a geographic resolution of 5.6 km x 5.6 km in Denmark. The regional background represents the average concentration in rural areas over a larger area. The regional air pollution represents the contribution of long-range transported air pollution from emissions from abroad and from Denmark.

Background concentrations with high resolution

For the baseline and climate scenario the development in background concentrations with high resolution is calculated with the Urban Background Model (UBM). Urban background pollution represents the average background pollution inside and outside cities calculated with a spatial resolution of 1 km x 1 km. Urban background concentrations correspond in a city to the concentration at roof top level or in a backyard/park. DEHM calculations are input in UBM. For Denmark emissions are available at a spatial resolution of 1 km x 1 km based on the SPREAD model that distributes national emissions based on various geographic variables.

Street concentrations

For the baseline and climate scenario the development in street concentrations is calculated with Operational Street Pollution Model (OSPM) for 98 selected streets in Copenhagen. The selected streets in Copenhagen are the same as those included in the Danish Air Quality Monitoring Program. The development in vehicle emissions is based on the Danish emission model for road traffic and other mobile sources (Winther, 2018).

Air quality calculations of regional concentrations, urban background concentrations and street concentrations are carried out for NO₂, PM_{2.5} and PM₁₀. Results for PM₁₀ are not presented here but available in *Jensen et al. (2019)*. We focus on as PM_{2.5} and NO₂ as they pose the largest health impacts of air pollution. The European Environmental Agency (EEA) estimated the health impacts due to ambient air pollution in Europe (EU-28) in 2018 to approx. 379,000 premature deaths caused by PM_{2.5}, 54,000 deaths caused by NO₂ and 19,400 deaths caused by ozone (EEA, 2020).

All three air quality models are driving by meteorological data from WRF. The model chain is described in *Jensen et al. (2017)* including comprehensive list of references to the individual models. Model results are compared with measurements for the starting year 2016 as part of the Danish Air Quality Monitoring Programme (Ellermann et al., 2017).

The multi-scale air quality modelling approach is illustrated in Figure 1.

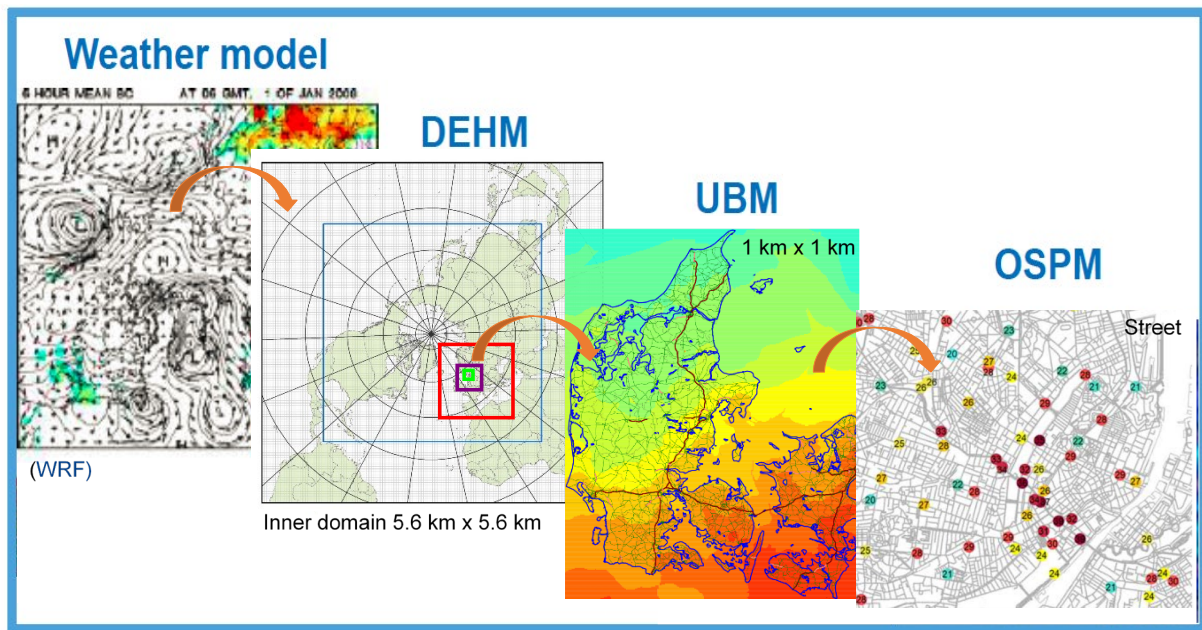


Figure 1: Illustration of multi-scale air quality modelling approach.

Results

Development in fleet of passenger cars

An exponential growth in the new sales of electric cars starting from 2019 is assumed in order to reach one million electric cars in 2030 and no new sales of fossil cars are allowed in 2030. The development in new car sales is illustrated in Figure 2.

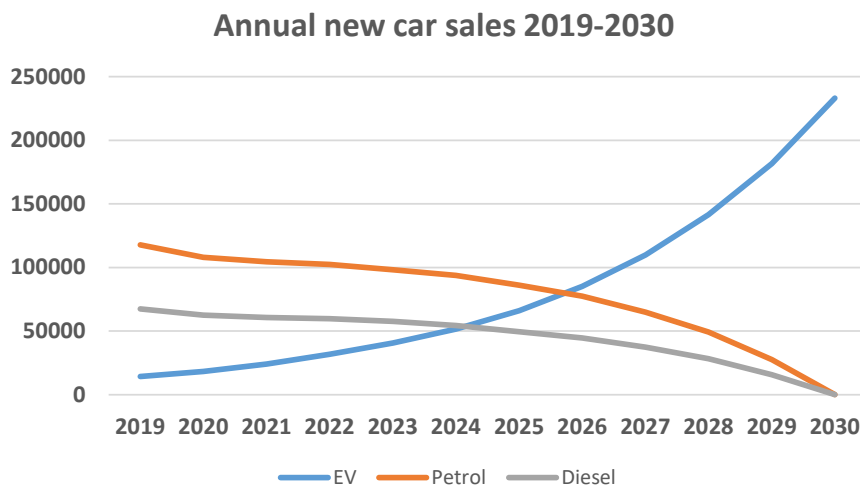


Figure 2: Illustration of multi-scale air quality modelling approach.

The statistics for sales in 2020 is 14,200 for EVs and 18,300 for PHEV. For EVs it is the same magnitude as we assumed 18,200 in the model for 2020. In our climate scenario, we increase EVs to reach one million in 2030 and PHEV has a moderate increase compared to EVs.

The development in the car fleet of passenger cars from 2019 to 2030 by fuel type for the baseline and the one million EV scenario is shown in Table 1.

It is seen that EVs increase by 766% compared to baseline in 2030. It is an increase of 876,000 EVs as the baseline development assumes 114,000 EVs in 2030. Petrol cars decrease by 26% and diesel cars by 27% in the climate scenario compared to the baseline in 2030. Despite a very large increase in EVs and a decrease in fossil cars EVs only constitute 30% of all cars in 2030 as the car fleet increases from 2.7 million in 2019 to 3.3 million in 2030.

The total fleet of fossil and EV cars increases from 2019 to 2030 by 22% or with 604,000 cars. This means that the new EVs of 876,000 exceeds the general increase in cars. However, had the car fleet remained constant from 2019 to 2030, one million EV's would have constituted 37% of all cars in 2030.

Table 1: Car fleet of passenger cars in 2019 and 2030 by fuel type for baseline and one million EV scenario.

Scenario	Petrol	Diesel	EV	PHEV	CNG	Total
Baseline 2019	1,761,208	947,605	11,939	2590	200	2,723,542
Baseline 2030	2,038,595	1,121,571	114,331	52,213	490	3,327,200
One million EVs in 2030	1,500,380	815,533	990,390	20,552	344	3,327,200
Difference, total	-538,215	-306,038	876,059	-31,660	-145	0
Difference, %	-26%	-27%	766%	-61%	-30%	0%

For the scenarios for taxis and urban buses it is simply assumed that all taxis and all urban buses are electric in 2030.

Development in emissions

A reduction in Danish emissions of NO_x, NMVOC, NH₃ and PM_{2.5} is seen from 2016 to 2030 in the baseline scenario (WM). SO₂ is the only pollutant expected to increase from 2016 to 2030 in the baseline scenario due to increased coal consumption. In the alternative scenario for the energy sector (WAM) emissions are slightly lower than in the baseline scenario in 2030.

Foreign emissions are also reduced from 2016 to 2030. The foreign emissions are different in the Danish baseline scenario (WM) and the alternative scenario for the energy sector (WAM). The WM scenario uses the foreign countries' baseline emissions, and the WAM scenario also uses the countries' baseline if the NEC-directive emission ceilings are met, otherwise the NEC-directive emission ceiling for that country is used. The climate scenario uses the same assumptions as the WAM scenario.

Effect on emissions of the climate scenario for road transport

The emission reduction of the three initiatives for electrification of part of the road transport sector in 2030 is shown in Table 2 in relation to the baseline scenario in 2030.

Table 2: Emission reduction of the three initiatives for electrification of part of the road transport sector in 2030.

Pollutant	One million EVs	Electric taxis	Electric urban busses	Total
Units	(Tonnes)	(Tonnes)	(Tonnes)	(Tonnes)
NO _x	1713	77	178	1968
PM _{2.5} -exhaust	26	1	2.5	29
PM _{2.5} -non-exhaust	0	0	0	0
PM _{2.5} -total	26	0.8	2.5	29
Units	(%)	(%)	(%)	(%)
NO _x	12	0.6	1.3	14
PM _{2.5} -exhaust	17	0.5	1.6	19
PM _{2.5} -non-exhaust	0	0	0	0
PM _{2.5} -total	2.0	0.1	0.2	2.3

The largest emission reduction is achieved for the scenario with one million electric cars in 2030, where NO_x emissions are reduced by 12% and PM_{2.5}-exhaust by 17% compared to the baseline in 2030 and including all vehicle categories (passenger cars, vans, and heavy-duty vehicles). The total reduction in PM_{2.5} (exhaust and non-exhaust) is only 2% since PM_{2.5}-non-exhaust is not reduced and non-exhaust constitutes a very large proportion of total PM_{2.5} in 2030. Non-exhaust is tire wear, road wear and brake wear.

The emission reduction for electric urban buses is around a tenth of the scenario of one million electric cars, and for the electric taxis it is only a twentieth. The reason is that there are far fewer urban buses and taxis compared to passenger cars.

Timmers & Achten (2016) reviewed non-exhaust PM emissions from electric cars in comparison with petrol and diesel cars. They found that EVs had higher tyre and road wear and resuspension compared to petrol and diesel cars due to higher weight. EVs had the same total PM emissions as petrol and diesel cars despite EVs have no exhaust and brake wear was assumed to be zero. We assumed no change in non-exhaust when shifting from fossil cars to EVs which seems to underestimate non-exhaust from EVs according to Timmers & Achten.

Total impact of the climate scenario

Total reductions in emissions between the baseline and climate scenarios in 2030 are shown in Table 3.

Table 3: Total reductions in emissions between the baseline and climate scenarios in 2030.

Scenario	NO _x (tonnes)	PM _{2.5} (tonnes)
Transport	-1,968	-29
Woodstoves	+41	-979
Total	-1,927	-1,008

The transport sector reduces NO_x emissions by 1,968 tons, while wood stoves increase emissions by 41 tons due to more modern stoves, which gives the total reduction of approx. 1,900 tons. Wood stoves reduces PM_{2.5} emissions with 979 tons while the reduction of the transport sector only is 29 tons, which in total is approx. 1,000 tons. Hence, the reductions in NO_x emissions is almost entirely determined by reductions in the transport sector, while reductions in PM_{2.5} almost completely are determined by wood stoves.

Scrapping of old stoves before 2000 when home ownership is changed is more effective in reduction of emissions than a subsidy to scrap old wood stoves before 2000.

NO_x emissions are slightly increasing because modern stoves burn at a higher temperature, and thereby increases the formation of NO_x.

The effect of the scrapping subsidy is very uncertain. For example, a scrapping subsidy may have a very limited effect, if it only subsidises replacements, which anyway would be have been carried out.

Development in rural background concentrations with high resolution

The average rural background concentrations for the five regions in Denmark are calculated with DEHM/UBM for the baseline and the climate scenario, see Table 4. In this case, the calculations are based on a geographical resolution of 1 km x 1 km.

For the baseline the rural background concentrations of PM_{2.5} for the five regions are reduced by 18-22% in 2030 compared to 2016, and for NO₂ 20-31%. The interval indicates that the percentage reduction is different from region to region.

In the climate scenario the percentage decreases are slightly larger than in the baseline scenario. In the climate scenario PM_{2.5} is expected to be reduced for the 5 regions with 21-25% in 2030 compared to 2016, and 22-34% for NO₂.

Table 4: Rural background concentrations of NO₂ and PM_{2.5} modelled with DEHM/UBM.

µg/m ³	Location	2016	2030	Difference 2030/2016	2030	Difference 2030/2016
Region			Base	Base	Climate	Climate
NO₂						
North Denmark	Average	5.8	4.6	-20%	4.6	-22%
Central Denmark	Average	6.3	4.6	-27%	4.5	-28%
Southern Denmark	Average	7.0	5.1	-27%	5.0	-29%
Capital	Average	11.2	7.7	-31%	7.4	-34%
Zealand	Average	8.7	6.6	-24%	6.5	-25%
PM_{2.5}						
North Denmark	Average	6.4	5.3	-18%	5.1	-21%
Central Denmark	Average	7.2	5.7	-20%	5.5	-23%
Southern Denmark	Average	8.3	6.4	-22%	6.2	-25%
Capital	Average	8.2	6.5	-20%	6.2	-24%
Zealand	Average	8.4	6.6	-22%	6.3	-25%

Development in urban background concentrations in four cities

Urban background concentrations of NO₂ decrease in the baseline scenario with 22-39% in 2030 compared to 2016 for the same locations as the urban background air quality monitoring stations in the four largest cities of Denmark: Copenhagen, Aarhus, Odense and Aalborg. PM_{2.5} concentrations in the base scenario are expected to be reduced by 18-22% in 2030 compared to 2016 for the four cities.

The decrease is a result of reductions in the regional background calculated with DEHM as well as Denmark's contribution calculated with UBM. For all three pollutants there are a few percentage points additional reduction in urban background concentrations in the climate-scenario compared to the baseline.

Table 5: Urban background concentrations of NO₂ and PM_{2.5} modelled with DEHM/UBM.

µg/m ³	Location	2016	2030	Difference 2030/2016	2030	Difference 2030/2016
City	Monitor station		Base	Base	Climate	Climate
NO₂						
Copenhagen	H.C. Ørsted	13.8	8.5	-39%	8.0	-42%
Odense	Rådhus	12.1	7.9	-35%	7.5	-38%
Aarhus	Botanisk Have	15.8	11.0	-30%	10.6	-33%
Aalborg	Østerbro	13.5	10.5	-22%	10.2	-24%
PM_{2.5}						
Copenhagen	H.C. Ørsted	8.1	6.5	-19%	6.3	-23%
Odense	Rådhus	8.6	6.7	-22%	6.4	-26%
Aarhus	Botanisk Have	8.2	6.6	-20%	6.3	-23%
Aalborg	Østerbro	6.9	5.7	-18%	5.5	-21%

Development in street concentrations for 98 streets in Copenhagen

Development in concentrations of NO₂

The baseline development of vehicle emissions for NO_x is expected to decrease by approx. 61% from 2016 to 2030. Particle exhaust emission is estimated to decrease by 81% from 2016 to 2030. In the climate scenario for road transport exhaust emissions are set to zero in the scenario of one million electric cars, and the same for electric urban buses and electric taxis.

The average NO₂ concentration for the 98 streets in Copenhagen is expected to decrease from 29 µg/m³ in 2016 to 15 µg/m³ in 2030 in the baseline scenario.

In the climate scenario the average street concentration of NO₂ is 1.9 µg/m³ lower than in the baseline scenario. On the other hand, the background concentrations of the climate scenario are only marginally less than the baseline scenario, an average about 0.4 µg/m³. The reduction in street concentrations is therefore dominated by the reduction in emissions from traffic.

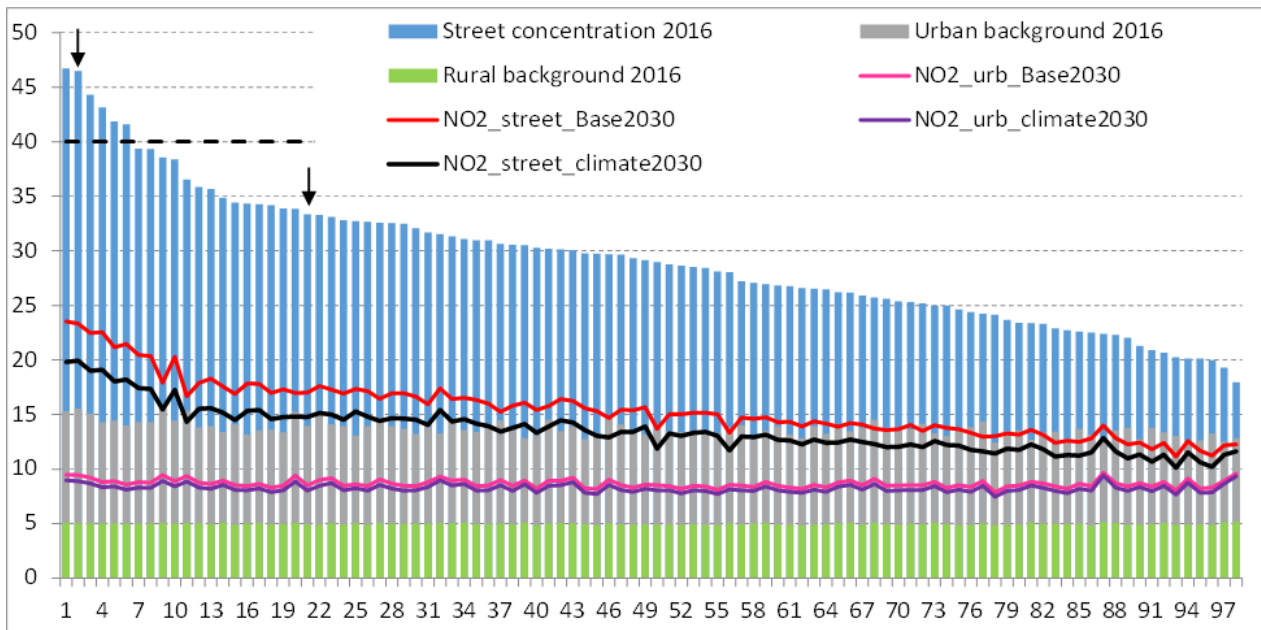


Figure 3: Street concentrations of NO₂ in 2016 and 2030 in baseline and climate scenario for 98 streets in Copenhagen.

Development in concentrations of PM_{2.5}

The average PM_{2.5} street concentration decreases from 13 µg/m³ in 2016 to 10 µg/m³ in 2030 in the baseline scenario. The percentage reduction for PM_{2.5} is not as great as for NO₂, since only particle exhaust emissions are reduced. Non-exhaust emissions - such as road wear, tire wear and brake wear - are unchanged and make up a far greater share than the exhaust emission.

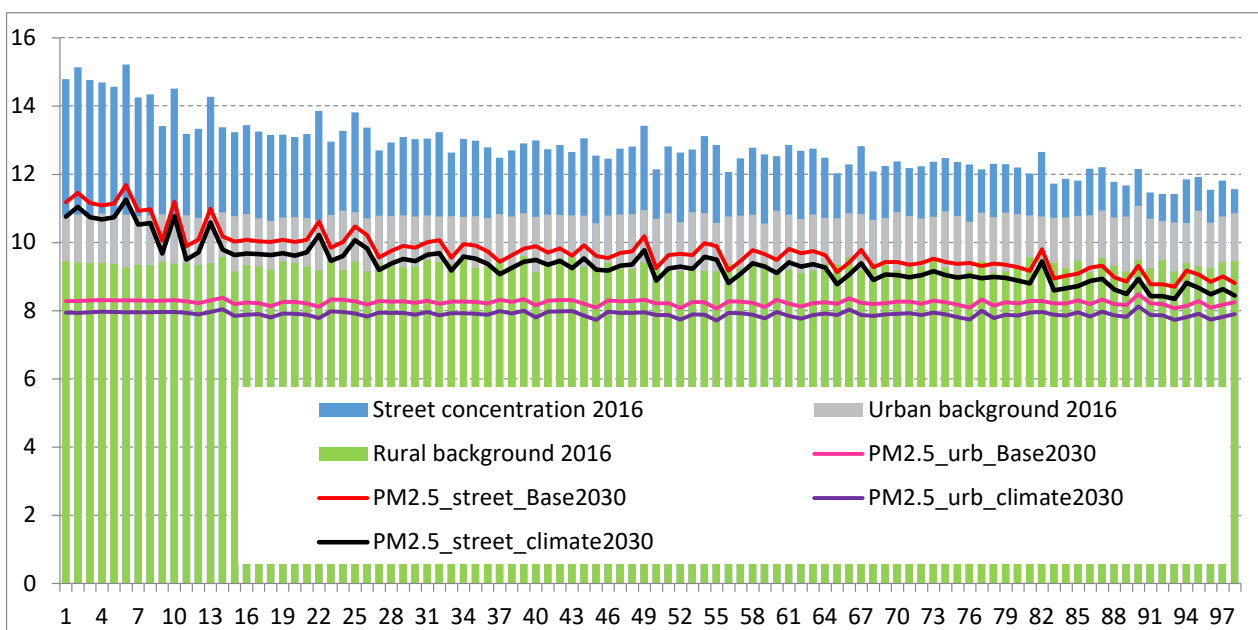


Figure 4: Street concentrations of PM_{2.5} in 2016 and 2030 in baseline and climate scenario for 98 streets in Copenhagen.

For PM_{2.5} there is also a marginal difference between the baseline scenario and the climate scenario. In the climate scenario the average street PM_{2.5} concentration is 0.4 µg/m³ lower than the baseline scenario. For the background concentrations the difference is on average 0.3 µg/m³. Therefore, the lower street concentrations in the climate scenario are mainly dominated by the reduction in background concentrations and to a less degree less emissions from traffic in the streets.

The reason is that exhaust emission represents a very small part of the total emissions from traffic exhaust and non-exhaust in 2030, and electrification of parts of the road sector only reduces exhaust emissions.

Conclusion

Three climate measures were assessed for partly electrification of the Danish road transport sector based on the Danish Government's Climate and Air Proposal. The scenario was named climate scenario and including one million EVs, 100% electric taxis and 100% electric urban buses in 2030. The impact assessment addressed emissions and rural, urban background and street concentrations in 2030 using multi-scale modelling.

In the climate scenario, EV cars were predicted to increase 766% starting from 2019 and constitute 30% of all cars in 2030. The car fleet of fossil and electric cars is projected to increase 22% from 2019 to 2030 and fossil cars remain high in 2030 (70%).

The climate scenario decreases emissions of NO_x by 14%, PM_{2.5}-exhaust by 19%, and total PM_{2.5} by 2.3% compared to the baseline in 2030 and including all vehicle categories (passenger cars, vans, and heavy-duty vehicles).

The baseline development from 2016 to 2030 decrease rural, urban background and street concentrations significantly and the climate scenario adds further decrease in 2030.

A review study suggests that EVs have higher non-exhaust particle emissions of tire and road wear and resuspension compared to petrol and diesel cars due to higher weight. The consequence is that EVs have the same total PM emissions as petrol and diesel cars despite EVs have no exhaust and brake wear was assumed to be zero by the review study. We assumed no change in non-exhaust when shifting from fossil cars to EVs, which seems to underestimate non-exhaust from EVs according to Timmers & Achten (2016). This implies that higher non-exhaust from EVs may jeopardise gains for reduced PM exhaust and brake wear for EVs.

Acknowledgement

The Ministry of Environment and Food of Denmark funded the study.

References

- Danish Government, 2018: Together in greener future. Climate and Air Proposal. October 2018. 42 p. (In Danish).
- EEA (2020): Air quality in Europe – 2020 report. European Environmental Agency. EEA report No. 09/2020. ISSN 1977-8449.
- Ellermann, T., Nygaard, J., Nøjgaard, J.K., Nordstrøm, C., Brandt, J., Christensen, J., Ketzel, M., Massling, A., Bossi, R. & Jensen, S.S. 2017. The Danish Air Quality Monitoring Programme. Annual Summary for 2016. Aarhus University, DCE – Danish Centre for Environment and Energy, 78 pp. Scientific Report from DCE – Danish Centre for Environment and Energy No. 234. <http://dce2.au.dk/pub/SR234.pdf>.
- EMEP/EEA, 2019: Air Pollutant Emission Inventory Guidebook, prepared by the UNECE/EMEP Task Force on Emissions Inventories and Projections (TFEIP). Available at: <https://www.eea.europa.eu/publications/emep-eea-guidebook-2019> (09-12-2019).
- EU, 2016. Directive (EU) 2016/2284 of the European Parliament and of the Council of 14 December 2016 on the reduction of national emissions of certain atmospheric pollutants, amending Directive 2003/35/EC and repealing Directive 2001/81/EC https://eur-lex.europa.eu/legal-content/EN/TXT/?uri=uriserv:OJ.L_.2016.344.01.0001.01.ENG&toc=OJ:L:2016:344:TOC
- Jensen, S.S, Ketzel, M., Becker, T., Christensen, J., Brandt, J., Plejdrup, M.S., Winther, M., Nielsen, O.-K., Hertel, O., Ellermann, T. (2017): High Resolution Multi-scale Air Quality Modelling for All Streets in Denmark. Transportation Research Part D: Transport and Environment 52 (2017) 322–339.
- Jensen, S.S., Christensen, J.H., Frohn, L.M., Brandt, J., Ketzel, M., Nielsen, O.-K., Plejdrup, M.S., Winther, M., Hertel, O., Ellermann, T. 2019. Impacts assessment of selected policy measures within climate and air pollution. Aarhus University, DCE – Danish Center for Environment and Energy, 48 p. – Scientific report No. 315. <http://dce2.au.dk/pub/SR315.pdf>. (In Danish with English summary).
- Nielsen, O-K, Plejdrup, M.S., Winther, M., Mikkelsen, M.H., Nielsen, M., Gyldenkærne, S., Fauser, P., Albrektsen, R., Hjelgaard, K.H., Bruun, H.G. & Thomsen, M. (2018a): Annual Danish Informative Inventory Report to UNECE. Emission inventories from the base year of the protocols to year 2016. Aarhus University, DCE – Danish Centre for Environment and Energy, 495 pp. Scientific Report from DCE – Danish Centre for Environment and Energy No. 267 <http://dce2.au.dk/pub/SR267.pdf>
- Nielsen, O.-K., Plejdrup, M.S., Winther, M., Nielsen, M., Hjelgaard, K., Mikkelsen, M.H., Albrektsen, R. & Thomsen, M. (2018b): Projections of Emissions. SO₂, NO_x, NMVOC, NH₃, PM_{2.5} and soot. Aarhus University, DCE – Danish Centre for Environmental and Energy, 75 p. - Scientific Report Nr. 298 <http://dce2.au.dk/pub/SR298.pdf>.(In Danish with English summary).
- [Timmers, Victor R.J.H. & Achten, Peter A.J. \(2016\): Non-exhaust PM emissions from electric vehicles. Atmospheric Environment 134 \(2016\) 10-17.](#)
- Winther, M. 2018: Danish emission inventories for road transport and other mobile sources. Inventories until the year 2016. Aarhus University, DCE – Danish Centre for Environment and Energy, 127pp. Scientific Re-port from DCE – Danish Centre for Environment and Energy No. 277. <http://dce2.au.dk/pub/SR277.pdf>.

GETTING IN TOUCH WITH THE EU

In person

All over the European Union there are hundreds of Europe Direct information centres. You can find the address of the centre nearest you at: https://europa.eu/european-union/contact_en

On the phone or by email

Europe Direct is a service that answers your questions about the European Union. You can contact this service:

- by freephone: 00 800 6 7 8 9 10 11 (certain operators may charge for these calls),
- at the following standard number: +32 22999696, or
- by electronic mail via: https://europa.eu/european-union/contact_en

FINDING INFORMATION ABOUT THE EU

Online

Information about the European Union in all the official languages of the EU is available on the Europa website at: https://europa.eu/european-union/index_en

EU publications

You can download or order free and priced EU publications from EU Bookshop at: <https://publications.europa.eu/en/publications>. Multiple copies of free publications may be obtained by contacting Europe Direct or your local information centre (see https://europa.eu/european-union/contact_en).

The European Commission's science and knowledge service

Joint Research Centre

JRC Mission

As the science and knowledge service of the European Commission, the Joint Research Centre's mission is to support EU policies with independent evidence throughout the whole policy cycle.



EU Science Hub

ec.europa.eu/jrc



@EU_ScienceHub



EU Science Hub - Joint Research Centre



EU Science, Research and Innovation



EU Science Hub



Publications Office
of the European Union

doi:10.2760/019404

ISBN 978-92-76-43803-8